

# Synthesis and metal complex formation of water soluble derivatives of the iron-chelating ligand deferasirox

Dissertation  
zur Erlangung des Grades  
des Doktors der Naturwissenschaften  
der Naturwissenschaftlich-Technischen Fakultät III  
Chemie, Pharmazie, Bio- und Werkstoffwissenschaften  
der Universität des Saarlandes

von

**Nadine Jane Koch**

Saarbrücken

2011

Tag des Kolloquiums:	16.12.2011
Dekan:	Prof. Dr. Wilhelm F. Maier
Berichterstatter:	Prof. Dr. Kaspar Hegetschweiler Prof. Dr. Gregor Jung
Vorsitz:	Prof. Dr. David Scheschkewitz
Akad. Mitarbeiter:	Dr. Andreas Rammo

## Acknowledgements

The studies for this doctoral thesis have been performed in the research group of Prof. Dr. Kaspar Hegetschweiler at the Saarland University.

First of all I would like to thank Prof. Kaspar Hegetschweiler for the interesting topic of my doctoral thesis and for his advice and helpfulness during my studies.

I would like to thank the current members Matthias Basters, Martin Becker, Sergej Gisbrecht, Anna Goldammer, Silvia Lauria, Günter Merten, Dr. Bernd Morgenstern, Dr. Christian Neis, Sabine Wilbrand and Mandy Wild as well as former members Dr. Mark Bartholomä, Dr. Barbara Kutzky, David Petry, Dr. Thorsten Riebold, Dr. Thomas Schweitzer and Dr. Stefan Stucky of our research group for the great working atmosphere and the great times we had.

Special thanks go to Anna Goldammer for performing several NMR measurements, numerous discussions and the critical revision of this thesis. Special thanks also go to Sabine Wilbrand for performing NMR measurements and preparative HPLC.

I would like to thank our laboratory technician Anton "Toni" Zschka for measuring numerous elemental analyses and for his support with laboratory matters. Thanks also go to our secretary Beate Tiefenbrunner for administrative support and nice talks beyond chemistry.

I would like to especially thank Frank Teucke and Thomas Nicolai for good teamwork and for many valuable discussions during their studies.

Further, I would like to thank Dr. Volker Huch for the collection of the X-ray diffraction data and Dr. Stefan Stucky and Dr. Christian Neis for solving and refining the crystal structures.

Thanks go to Traudl Allgayer for carrying out the ICP-OES measurements. Further, I would like to thank Dr. Matthias Großer for ESI-MS measurements. Thanks also go to Dr. Robert Haberkorn for MXRFA measurements.

Special thanks go to Prof. Dr. Peter Strauch (University of Potsdam) for having me in his lab and for performing and interpreting EPR measurements.

Very special thanks go to my parents Lilian and Hans-Jürgen Koch for endless support throughout my life. Without them I would have never had the chance and the strength to achieve what I have achieved. Further, I want to especially thank my father for his support and for revising this thesis.

Very special thanks go to Lewe Meichsner who has supported me through highs and lows. Thanks for your endless understanding and never ending encouragement.

I would also like to thank my dear friend Carolin Thiele for many great years at university and many talks and wonderful times beyond university life.

## List of abbreviations

[A] <sub>t</sub>	total concentration of all species containing A
AAS	atom absorption spectroscopy
AU	absorption units
BFC	bifunctional chelating agent
BNC	bayonet nut connector
CN	coordination number
conc.	concentrated
CT	X-ray computed tomography
d	day
DMSO	dimethyl sulphoxide
E°	standard electrode potential
EPR	electron paramagnetic resonance
ESI-MS	electrospray ionization mass spectroscopy
FT-IR	Fourier transform infrared
h	hours
HMDE	hanging mercury drop electrode
HPLC	high-performance liquid chromatography
hs	haemosiderin
I	ionic strength
k <sub>ex</sub>	water-exchange rate constant
K <sub>w</sub>	dissociation constant of water
L	ligand or litre
M	central metal ion or molar mass
MDS	myelodysplastic syndrome
MRI	magnetic resonance imaging
N	normality of solutions
NHE	normal hydrogen electrode
NMR	nuclear magnetic resonance
ORTEP	Oak Ridge Thermal Ellipsoid Plot
pD	pH dependent on deuterium

PET	positron emission tomography
Ph	phenyl
$pK_a^D$	acidity constant dependent on deuterium
$pK_w$	$-\log(K_w)$
solv	solvent molecule
T	temperature
$T_{1/2}$	half-life
TMS	tetramethylsilane
UV-VIS	ultraviolet / visible
x	molar fraction

## Ligand abbreviations

deferasirox	ICL670, 4-[3,5-bis(2-hydroxyphenyl)-1 <i>H</i> -1,2,4-triazol-1-yl]-benzoic acid
DCA	dicarboxylic acid derivative of deferasirox 5-[3,5-bis(2-hydroxyphenyl)-1 <i>H</i> -1,2,4-triazol-1-yl]-isophthalic acid
DSA	disulfonic acid derivative of deferasirox 2-[3,5-bis(2-hydroxyphenyl)-1 <i>H</i> -1,2,4-triazol-1-yl]-benzene-1,4-disulfonic acid
MSA	monosulfonic acid derivative of deferasirox 4-[3,5-bis(2-hydroxyphenyl)-1 <i>H</i> -1,2,4-triazol-1-yl]-benzenesulfonic acid
1N-phenyl derivative	1N-phenyl derivative of deferasirox 3,5-bis(2-hydroxyphenyl)-1-phenyl-1,2,4-triazole
DFO	deferoxamine, desferrioxamine-B
DOTA	2,2',2'',2'''-(1,4,7,10-tetraazacyclododecane-1,4,7,10-tetrayl)-tetraacetic acid
dpt	bis(3-aminopropyl) amine
DTPA	diethylenetriaminepentaacetic acid
EDTA	ethylenediamine tetraacetic acid
L1	deferiprone, CP20
NTA	nitrilotriacetic acid
salphen	<i>N,N</i> -bis(salicylidene)-1,2-phenylenediamine
tempt	2,4,6-tris[4-(imidazole-1-ylmethyl)phenyl]-1,3,5-triazine
tren	2,2',2''-triaminotriethylamine
trien	trientine, triethyltetramine dihydrochloride

## Table of contents

1	Short abstract .....	1
2	Kurzzusammenfassung .....	2
3	Abstract.....	3
4	Introduction .....	6
4.1	Iron metabolism in human .....	6
4.2	Iron overload and iron chelation.....	10
4.3	Motivation and objectives .....	15
5	Synthesis of the ligands.....	17
5.1	Synthesis of the ligand deferasirox and its monosulfonic acid derivative (MSA) .....	17
5.2	Synthesis of the dicarboxylic acid (DCA) and disulfonic acid derivative (DSA) of deferasirox .....	19
6	The Ligand DCA .....	25
7	The ligand DSA.....	33
7.1	Determination of the $pK_a$ values of DSA .....	34
7.1.1	Determination of the $pK_{a,2}$ by spectrophotometric batch titration .....	34
7.1.2	Determination of the $pK_{a,3}$ and $pK_{a,4}$ with potentiometric titrations .....	41
7.1.3	Crystal structures of the ligand DSA.....	47
7.2	Complex formation of DSA with iron (III).....	53
7.2.1	Determination of the stability constant of the $[\text{Fe}(\text{DSA})]^-$ complex by spectrophotometric batch titration in pure water .....	53
7.2.2	Continuous potentiometric and spectrophotometric titrations of DSA with iron (III).....	58
7.2.3	The Crystal structure $\text{Cs}_5[\text{Fe}(\text{DSA})_2] \cdot 10.74 \text{ H}_2\text{O}$ .....	73
7.2.4	Investigation of the redox chemistry of the iron (II) / iron (III)-DSA system by cyclic voltammetry .....	79
7.3	Complex formation of DSA with copper (II) .....	89
7.3.1	Investigation of the complex formation of DSA with copper (II) in pure water by potentiometric titrations .....	90
7.3.2	EPR-Experiments with copper (II) complexes of deferasirox and DSA .....	103
7.3.3	The crystal structures $\text{Na}_3[\text{Cu}(\text{DSA})(\text{HCO}_3)] \cdot 2.5 \text{ H}_2\text{O} \cdot 1.5 \text{ MeOH}$ and $\text{Na}_3[\text{Cu}(\text{DSA})(\text{HCO}_3)] \cdot (\text{H}_2\text{O})_{25/6} \cdot 3 \text{ MeOH}$ .....	116

7.4	Complex formation of DSA with nickel (II).....	123
7.5	Complex formation of DSA with zinc (II) .....	132
7.6	Complex formation of DSA with cadmium (II).....	141
7.7	Complex formation of DSA with magnesium (II) .....	150
7.8	Complex formation of DSA with calcium (II) .....	156
7.9	Complex formation of DSA with aluminium (III) .....	162
<b>8</b>	<b>Complex formation of magnesium (II), calcium (II) and aluminium (III) with deferasirox in pure water .....</b>	<b>172</b>
8.1	Investigation of the $pK_a$ values of deferasirox .....	173
8.1.1	Determination of the $pK_a$ values of deferasirox in pure water by continuous potentiometric titrations .....	174
8.1.2	Investigation of the protonation of deferasirox in acidic solutions in pure water by spectrophotometric batch titration .....	179
8.1.3	$^1\text{H-NMR}$ spectroscopic measurements of the ligand deferasirox in acidic $\text{D}_2\text{O}/\text{D}_6\text{-DMSO}$ solution .....	187
8.2	Complex formation of deferasirox with magnesium (II) in pure water solution .....	189
8.3	Complex formation of deferasirox with calcium (II) in pure water solution .....	193
8.4	Complex formation of deferasirox with aluminium (III) in pure water solution .....	197
<b>9</b>	<b>Interaction of deferasirox, MSA and DSA with gadolinium (III) and gallium (III) in contrast agents .....</b>	<b>201</b>
9.1	Complex formation of deferasirox and its water soluble derivatives with gadolinium (III).....	201
9.1.1	Complex formation of deferasirox with gadolinium (III) in water/DMSO solution $x_{\text{DMSO}} = 0.20$ .....	204
9.1.2	Complex formation of MSA with gadolinium (III) and determination of the $pK_a$ values of MSA in pure water .....	206
9.1.3	Complex formation of DSA with gadolinium (III) in pure water .....	214
9.1.4	Summary and discussion .....	219
9.2	Complex formation of deferasirox and its water soluble derivatives with gallium (III) .....	223
9.2.1	Complex formation of deferasirox with gallium (III) in pure water and water/DMSO solution $x_{\text{DMSO}} = 0.20$ .....	226
9.2.2	Complex formation of MSA with gallium (III) in pure water .....	230
9.2.3	Complex formation of DSA with gallium (III) in pure water.....	237
9.2.4	Summary and discussion .....	241

10 Linear free energy relation and discussion .....	249
11 Experimental Section .....	263
11.1 Ligand synthesis .....	263
11.1.1 Synthesis of 2-(2-hydroxyphenyl)-benzo-4 <i>H</i> -[1,3]-oxazin-4-one.....	263
11.1.2 Synthesis of 4-[3,5-bis(2-hydroxyphenyl)-1 <i>H</i> -1,2,4-triazol-1-yl]benzoic acid (deferasirox) .....	265
11.1.3 Synthesis of 4-[3,5-bis(2-hydroxyphenyl)-1 <i>H</i> -1,2,4-triazol-1-yl]benzenesulfonic acid (MSA).....	267
11.1.4 Synthesis of 2-hydrazinylbenzene-1,4-disulfonic acid · HCl (DSH).....	268
11.1.5 Synthesis of 2-[3,5-bis(2-hydroxyphenyl)-1 <i>H</i> -1,2,4-triazol-1-yl]benzene-1,4-disulfonic acid (DSA) .....	270
11.1.6 Synthesis of 5-hydrazinylisophthalic acid hydrochloric acid (DCH).....	272
11.1.7 Synthesis of 5-[3,5-bis(2-hydroxyphenyl)-1 <i>H</i> -1,2,4-triazol-1-yl]isophthalic acid (DCA) .....	274
11.1.8 Crystal growth of [deferasirox] · H <sub>2</sub> O .....	276
11.1.9 Crystal growth of [DSA-H <sub>4</sub> ] · 1.5 MeOH .....	276
11.1.10 Crystal growth of Cs <sub>4</sub> [DSA-H <sub>2</sub> ] <sub>2</sub> · (H <sub>2</sub> O) <sub>13/6</sub> · MeOH .....	277
11.1.11 Crystal growth of Cs <sub>5</sub> [Fe(DSA) <sub>2</sub> ] · 10.74 H <sub>2</sub> O.....	277
11.1.12 Crystal growth of Na <sub>3</sub> [Cu(DSA)(HCO <sub>3</sub> )] · 2.5 H <sub>2</sub> O · 1.5 MeOH (violet) and Na <sub>3</sub> [Cu(DSA)(HCO <sub>3</sub> )] · (H <sub>2</sub> O) <sub>25/6</sub> · 3 MeOH (green).....	278
11.2 Titration experiments .....	280
11.2.1 Potentiometric titration experiments .....	280
11.2.2 Potentiometric titrations in water/DMSO solution mixture.....	282
11.2.3 Spectrophotometric titrations.....	284
11.2.4 Calculation of equilibrium constants .....	286
11.2.5 NMR-titration experiments.....	287
11.3 Instrumentation.....	288
11.3.1 NMR-spectroscopy .....	288
11.3.2 Elemental analysis (C,H,N) .....	288
11.3.3 UV-VIS-spectroscopy .....	288
11.3.4 IR-spectroscopy.....	289
11.3.5 ESI-mass spectroscopy .....	289
11.3.6 Preparative HPLC .....	289
11.3.7 EPR-spectroscopy.....	289
11.3.8 ICP-OES spectroscopy .....	290
11.3.9 Microscopic X-ray fluorescence - MXRFA .....	290
11.3.10 Crystal structure determination .....	290
11.3.11 Cyclic voltammetry .....	290
11.4 Chemicals and preparation of stock solutions .....	291
12 Appendix .....	293
13 References .....	301

## 1 Short abstract

A water soluble model of deferasirox, 2-[3,5-bis(2-hydroxyphenyl)-1*H*-1,2,4-triazol-1-yl]benzene-1,4-disulfonic acid (DSA), was prepared and characterised. The ligands complex formation with the metal ions  $\text{Fe}^{3+}$  ( $\log\beta_{110} = 23.54(4)$ ;  $\log\beta_{120} = 39.50(2)$ ),  $\text{Al}^{3+}$ ,  $\text{Ga}^{3+}$ ,  $\text{Gd}^{3+}$ ,  $\text{Ni}^{2+}$ ,  $\text{Cu}^{2+}$ ,  $\text{Zn}^{2+}$ ,  $\text{Cd}^{2+}$ ,  $\text{Mg}^{2+}$  and  $\text{Ca}^{2+}$  was investigated in pure water by titrations. A crystal structure of the  $[\text{Fe}(\text{DSA})_2]^{5-}$  complex and two structures of the  $[\text{Cu}(\text{DSA})(\text{HCO}_3)]^{3-}$  complex were obtained. The redox chemistry of  $\text{Fe}^{3+}$  with DSA was studied in acidic and alkaline solution. Investigations on the  $\text{Cu}^{2+}$ -DSA and -deferasirox system revealed little to no evidence for polynuclear species. Deferasirox and DSA form rather strong complexes with  $\text{Ga}^{3+}$  and weak with  $\text{Gd}^{3+}$  which have been studied with respect to interactions with contrast agents. The  $\text{p}K_a$  value ( $\text{p}K_a = 0.98(4)$ ,  $\text{H}_2\text{O}$ ) of deferasirox in acidic solution and the stability constants of  $\text{Al}^{3+}$  ( $\log\beta_{120} = 29.0(5)$ ),  $\text{Mg}^{2+}$  ( $\log\beta_{120} = 7.4(6)$ ) and  $\text{Ca}^{2+}$  ( $\log\beta_{110} = 3.28(7)$ ) were estimated for pure water solution. Deferasirox and DSA are correlated in terms of a linear free energy relation for the  $[\text{M}(\text{L})]$  and  $[\text{M}(\text{L})_2]$  complex (equation:  $\log\beta_{120} [\text{deferasirox}] = 0.96(2) \times \log\beta_{120} [\text{DSA}] - 1.5(8)$ ). The estimated  $\log\beta_{120}$  for deferasirox are:  $\text{Ga}^{3+}$  33.8(1),  $\text{Gd}^{2+}$  18.3,  $\text{Cu}^{2+}$  19.4,  $\text{Ni}^{2+}$  15.1,  $\text{Zn}^{2+}$  13.3,  $\text{Cd}^{2+}$  10.3 for pure water. Furthermore, the  $\text{pM}$  values for deferasirox in pure water have been calculated and show that it is a selective iron-chelator with  $\text{pFe} = 22.2$ .

## 2 Kurzzusammenfassung

Eine wasserlösliche Modelverbindung von Deferasirox, 2-[3,5-bis(2-hydroxyphenyl)-1*H*-1,2,4-triazol-1-yl]benzene-1,4-disulfonsäure (DSA), wurde synthetisiert und charakterisiert. Die Komplexbildung von DSA mit  $\text{Fe}^{3+}$  ( $\log\beta_{110} = 23.54(4)$ ;  $\log\beta_{120} = 39.50(2)$ ),  $\text{Al}^{3+}$ ,  $\text{Ga}^{3+}$ ,  $\text{Gd}^{3+}$ ,  $\text{Ni}^{2+}$ ,  $\text{Cu}^{2+}$ ,  $\text{Zn}^{2+}$ ,  $\text{Cd}^{2+}$ ,  $\text{Mg}^{2+}$  und  $\text{Ca}^{2+}$  wurde mit Titrationsen ( $\text{H}_2\text{O}$ ) untersucht. Die Kristallstruktur des  $[\text{Fe}(\text{DSA})_2]^{5-}$  Komplexes sowie zwei Strukturen des  $[\text{Cu}(\text{DSA})(\text{HCO}_3)]^{3-}$  Komplexes wurden erhalten. Die Redox-Eigenschaften von DSA mit  $\text{Fe}^{3+}$  wurden im sauren und alkalischen Medium bestimmt. Untersuchungen der  $\text{Cu}^{2+}$ -DSA und -Deferasirox Komplexe ergaben wenig bis gar keine Beweise für polynukleare Teilchen. Deferasirox und DSA bilden starke Komplexe mit  $\text{Ga}^{3+}$  und eher schwache mit  $\text{Gd}^{3+}$ , welche auf Wechselwirkungen mit Kontrastmitteln untersucht wurden. Der  $\text{p}K_s$  Wert von Deferasirox ( $\text{p}K_s = 0.98(4)$ ,  $\text{H}_2\text{O}$ ) in saurer Lösung, sowie die Stabilitätskonstanten mit  $\text{Al}^{3+}$  ( $\log\beta_{120} = 29.0(5)$ ),  $\text{Mg}^{2+}$  ( $\log\beta_{120} = 7.4(6)$ ) und  $\text{Ca}^{2+}$  ( $\log\beta_{110} = 3.28(7)$ ) wurden für  $\text{H}_2\text{O}$  abgeschätzt. Deferasirox und DSA konnten in Form einer linearen freien Energie-Beziehung für  $[\text{ML}]$  und  $[\text{ML}_2]$  (Gleichung:  $\log\beta_{120} [\text{Deferasirox}] = 0.96(2) \times \log\beta_{120} [\text{DSA}] - 1.5(8)$ ) korreliert werden. Die abgeschätzten  $\log\beta_{120}$  für Deferasirox in Wasser sind:  $\text{Ga}^{3+}$  33.8(1),  $\text{Gd}^{2+}$  18.3,  $\text{Cu}^{2+}$  19.4,  $\text{Ni}^{2+}$  15.1,  $\text{Zn}^{2+}$  13.3,  $\text{Cd}^{2+}$  10.3. Es konnten die  $\text{pM}$  Werte für Deferasirox in  $\text{H}_2\text{O}$  berechnet werden, welche Deferasirox mit einem  $\text{pFe} = 22.2$  als selektiven Eisenchelator bestätigen.

### 3 Abstract

2-[3,5-bis(2-hydroxyphenyl)-1*H*-1,2,4-triazol-1-yl]benzene-1,4-disulfonic acid (DSA) a highly water soluble disulfonic acid derivative of the iron-chelating ligand deferasirox was successfully synthesised on a large scale and characterised in this thesis. The  $pK_a$  values of the fourfold protonated ligand DSA were investigated in pure water and revealed two very acidic  $pK_a$  values  $pK_{a,1} < -2$  and  $pK_{a,2} = 1.33(8)$  ( $T = 298\text{ K}$ ,  $I = 0.1\text{ mol/L HCl/KCl}$ ). The  $pK_{a,1}$  can be assigned to a protonation of one of the sulfonic acids which cannot be determined in aqueous solution. The  $pK_{a,2}$  needed to be determined with a spectrophotometric batch titration in acidic solution ( $\text{pH } 1 - 2$ ) and could be assigned to a protonation of one of the 1,2,4-triazole nitrogen atoms. Two further acidity constants  $pK_{a,3} = 9.35(1)$  and  $pK_{a,4} = 11.32(2)$  of the two hydroxyphenyl rings have been determined by continuous potentiometric titrations. The zwitterionic structure has been confirmed by a crystal structure of the ligand DSA received from a methanol/ethyl acetate solution.

The complex formation of DSA with the metal ion  $\text{Fe}^{3+}$  has been investigated in aqueous solution. Related to the observed strong complex formation the  $[\text{Fe}(\text{DSA})]^-$  complexation constant  $\log\beta_{110} = 23.54(4)$  ( $T = 298\text{ K}$ ,  $I = 0.1\text{ mol/L HCl/KCl}$ ) needed to be determined in acidic solution ( $\text{pH } 1 - 2$ ) with a spectrophotometric batch titration. Additionally, two further stability constants for the  $[\text{Fe}(\text{DSA})_2]^{5-}$  complex with  $\log\beta_{120} = 39.50(2)$  and the  $[\text{Fe}(\text{L})(\text{LH})]^{4-}$  complex with  $\log\beta_{121} = 43.67(3)$  ( $T = 298\text{ K}$ ,  $I = 0.1\text{ mol/L KCl}$ ) have been obtained. Further, a crystal structure of the  $[\text{Fe}(\text{DSA})_2]^{5-}$  complex is reported with the  $\text{Fe}^{3+}$  central ion in a distorted octahedral geometry and both ligands coordinating tridentate meridional. The redox chemistry of DSA with  $\text{Fe}^{3+}$  was investigated in acidic and alkaline solution with cyclic voltammetry in pure water. The reduction potential for the  $[\text{Fe}^{\text{III/II}}(\text{DSA})_2]^{5-/6-}$  couple (vs. NHE) was calculated to  $E_{1/2} = -0.67\text{ V}$ .

The investigation of the complex formation of the divalent metal ions  $\text{Ni}^{2+}$ ,  $\text{Cu}^{2+}$ ,  $\text{Zn}^{2+}$  and  $\text{Cd}^{2+}$  with DSA gave rise to monomeric complexes such as  $[\text{M}(\text{L})]^{2-}$  and  $[\text{M}(\text{LH})]^-$ , bis-complexes like  $[\text{M}(\text{L})_2]^{6-}$  and  $[\text{M}(\text{L})(\text{LH})]^{5-}$  but also to dinuclear complexes such as  $[\text{M}_2(\text{L})_2]^{4-}$  and  $[\text{M}_2(\text{L})_2(\text{OH})]^{5-}$  for the  $\text{Ni}^{2+}$ -DSA sys-

tem and the complexes  $[M_2(L)_2(OH)]^{5-}$  and  $[M_2(L)_2(OH)_2]^{6-}$  for the  $Cu^{2+}$ ,  $Zn^{2+}$  and  $Cd^{2+}$ -DSA systems. Two crystal structures of the  $[Cu(DSA)(HCO_3)]^{3-}$  complex were obtained with the ligand DSA coordinating tridentate meridional and the  $Cu^{2+}$  central ion in a square planar coordination geometry. Further, the nature of the precipitate of the  $Cu^{2+}$ -deferasirox system and the  $Cu^{2+}$ -DSA solutions were studied by EPR spectroscopy. Primarily, monomeric species were detected, however the EPR spectrum at elevated temperatures or of the aged  $Cu^{2+}$ -deferasirox precipitate changed to a broad badly resolved signal which can be interpreted as antiferromagnetic coupling often observed for a polymeric structure. An EPR spectrum of the  $Cu^{2+}$ -DSA system in acidic solution (pH 2.7) may indicate a dinuclear species due to the corresponding half-field signal observed.

The complex formation of the ligands deferasirox, MSA and DSA with the metal ions  $Gd^{3+}$  and  $Ga^{3+}$  was studied with respect to the simultaneous administration of deferasirox in iron-chelation therapy and  $Gd^{3+}$  and  $Ga^{3+}$  preparations as contrast agents and radiopharmaceuticals. In summary, the investigations with potentiometric titrations gave rise to a rather weak complexation of deferasirox ( $pGd = 6.3$ ,  $pFe = 22.2$ ) and its water soluble derivatives with the  $Gd^{3+}$  ion which follows that both pharmaceuticals can be administered simultaneously. The complex formation determined for all three ligands with the  $Ga^{3+}$  ion were very strong (deferasirox  $pGa = 19.1$ ) so that a simultaneous administration could result in a ligand exchange reaction in the body and is therefore not recommended.

Additionally, the protonation of the 1,2,4-triazole unit of deferasirox was studied in acidic solution. The acidity constant  $pK_a = 0.98(4)$  ( $H_2O$ ,  $T = 298$  K,  $I = 1.0$  mol/L HCl/KCl) was determined by spectrophotometric batch titrations with different molar fractions of  $x_{DMSO}$  and extrapolation to pure water. Another approach was carried out by  $^1H$ -NMR titration to determine the  $pK_a = 0.89(2)$  ( $T = 294 \pm 2$  K,  $D_2O$ -DCl/ $D_6$ -DMSO,  $x_{DMSO} = 0.20$ , no supporting electrolyte). The stability constants of  $Al^{3+}$ ,  $Mg^{2+}$  and  $Ca^{2+}$  with deferasirox were determined by potentiometric titrations of different molar fractions ( $x_{DMSO} = 0.20, 0.18, 0.16, 0.14$ ) and extrapolated to pure water  $Al^{3+}$  ( $\log\beta_{110} = 15.9(1)$ ;  $\log\beta_{120} = 29.0(5)$ ),  $Mg^{2+}$  ( $\log\beta_{110} = 5.31(8)$ ;  $\log\beta_{120} = 7.4(6)$ ) and  $Ca^{2+}$  ( $\log\beta_{110} = 3.28(7)$ ). Accord-

ingly, the corresponding potentiometric titrations were performed with  $\text{Al}^{3+}$ ,  $\text{Mg}^{2+}$  and  $\text{Ca}^{2+}$  with DSA in pure water. The stability constants of the  $[\text{M}(\text{L})]$  complex (equation:  $\log\beta_{110} [\text{deferasirox}] = 0.96(5) \times \log\beta_{110} [\text{DSA}] - 1.2(8)$ ) and  $[\text{M}(\text{L})_2]$  complex (equation:  $\log\beta_{120} [\text{deferasirox}] = 0.96(2) \times \log\beta_{120} [\text{DSA}] - 1.5(8)$ ) of deferasirox and DSA can be correlated in terms of a linear free energy relation. With this correlation it was possible to estimate the stability constants  $\log\beta_{110}$ :  $\text{Ga}^{3+}$  19.6,  $\text{Gd}^{2+}$  10.3,  $\text{Cu}^{2+}$  16.0,  $\text{Ni}^{2+}$  10.1,  $\text{Zn}^{2+}$  9.4,  $\text{Cd}^{2+}$  6.4 and  $\log\beta_{120}$ :  $\text{Ga}^{3+}$  33.8(1),  $\text{Gd}^{2+}$  18.3,  $\text{Cu}^{2+}$  19.4,  $\text{Ni}^{2+}$  15.1,  $\text{Zn}^{2+}$  13.3,  $\text{Cd}^{2+}$  10.3 in pure water which cannot be measured directly. In conclusion, the pM values were calculated for all the studied metal ions with deferasirox which confirmed that deferasirox is a selective iron-chelator with the  $\text{pFe} = 22.2$ .

## 4 Introduction

Iron is the second most abundant metal (after aluminium) and the fourth most abundant element of the earth's crust <sup>[1]</sup>. It is a transition metal in two stable oxidation states the rather soluble ferrous state  $\text{Fe}^{2+}$  ( $d^6$  electronic configuration) and the less soluble ferric state  $\text{Fe}^{3+}$  ( $d^5$  electronic configuration) <sup>[2]</sup>. It is one of the elements indispensable for life according to its capability of transporting electrons and oxygen. Iron is especially suitable for its numerous tasks in the human body attributed to its extreme variability of the  $\text{Fe}^{2+}/\text{Fe}^{3+}$  redox potential which can be fine-tuned by the type of chosen ligand <sup>[1]</sup>. Iron-ligand complexes have access to the entire biologically significant range of redox potentials, from -0.5 to about +0.6 V <sup>[1]</sup>. If iron is not properly bound to proteins in the body it may participate in harmful free radical reactions (Fenton and Haber-Weiss) <sup>[3]</sup> or undergo hydrolysis, especially  $\text{Fe}^{3+}$  may precipitate to the highly insoluble  $\text{Fe}(\text{OH})_3$ . Living organisms have adopted efficient iron transport and storage mechanisms for a safe handling of iron, avoiding the toxicity of free unbound iron. <sup>[1-4]</sup>

### 4.1 Iron metabolism in human

The total iron content of the human body is about 40 – 50 mg Fe/kg bodyweight. Men attain typically higher iron values than women. The distribution and iron metabolism of the total iron in the human body of an adult male is illustrated in **Figure 4.1**. A simple overview of the main function of the transport protein transferrin and the storage proteins ferritin and haemosiderin is provided in relation to the distribution of iron in the human body. <sup>[1]</sup>

Iron is mainly absorbed in the upper part of the gut (duodenum) from the diet. The daily intake of iron from the diet is about 12 – 18 mg. However, only 1 – 2 mg/day are absorbed to compensate the daily iron losses of about the same amount. There are two main sources of iron from nutrition, haem iron, which is highly bioavailable and well absorbed in contrast to non-haem iron. Further, the amount of absorbed iron is regulated by the intestinal mucosa cells according to the daily loss. Since the human body has no effective system for

iron excretion the loss is due to exfoliation of mucosa cells and red blood cells to about two-thirds and one-third is a consequence of exfoliation of cells from skin and from the urinary tract. The iron balance is primarily determined by iron absorption, hence as iron stores decline, iron absorption increases. [1, 4-5]

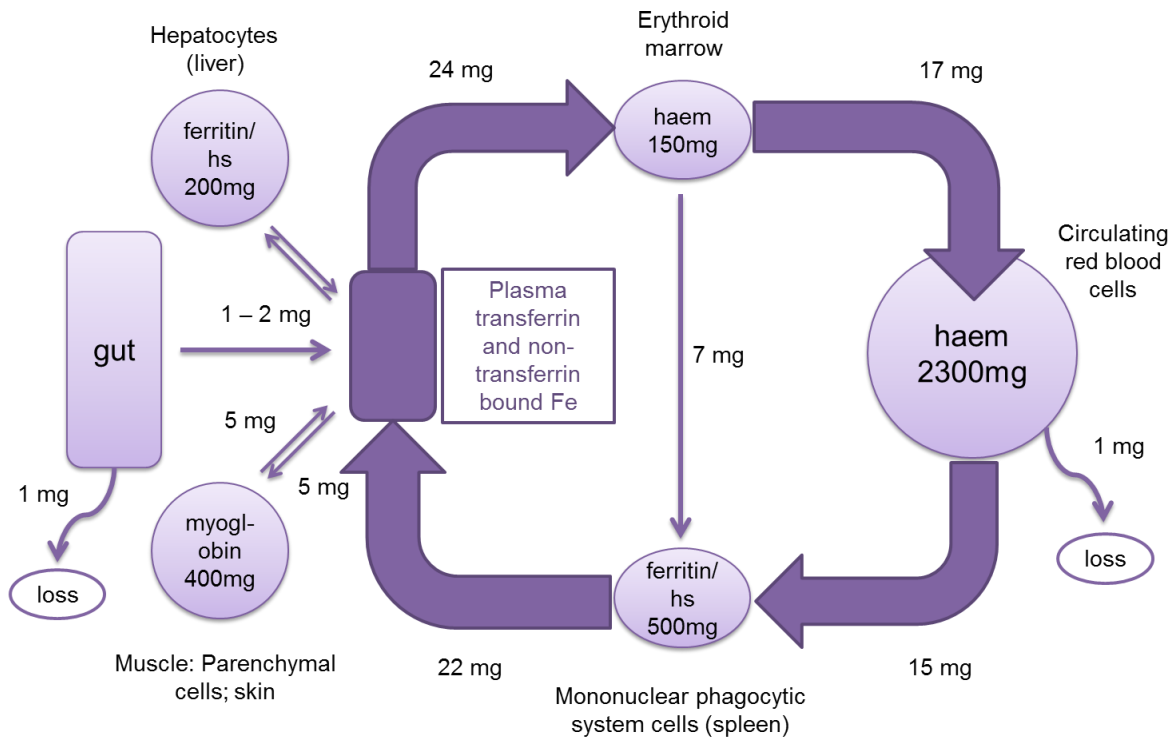


**Figure 4.1:** Simple schematic presentation of iron metabolism in man with regard to iron stores, daily iron exchange and iron movement in the human body of a normal adult male. The values are given in mg per day. The dark violet circulation refers to the plasma iron (transferrin and non-transferrin bound iron) with about 4 mg, yet the daily turnover is about 30 mg. The abbreviation hs stands for haemosiderin. [1]

## Transferrin

Once iron is absorbed it needs to be transported to sites of utilization and storage. The class of iron-binding proteins found in many vertebrates is called transferrins. Serum transferrin is the main iron transport protein, in plasma and extracellular fluids, which distribute iron between the different cellular compartments (depict as dark violet arrows in **Figure 4.1**). Interestingly, only a small fraction of total body iron, about 3 mg Fe/kg, circulates in the plasma and other extracellular fluids bound to the iron transport protein transferrin. It is a glycoprotein with a molecular weight of about 80 kD which is able to bind two ferric ( $\text{Fe}^{3+}$ ) ions coupled with binding of commonly two bidentate carbonate anions, as found for human serotransferrin [6]. A possible role of the anions is

to serve as binding ligands between the protein and the metal ion in vitro. Another role might be to complete the coordination sphere of the ferric ion to prevent hydrolysis of the ferric ion by coordinating water molecules. The half-life of a molecule transferrin is 7.6 days while the bound iron only has a biological half-life of about 1.7 h. Consequently, transferrin undergoes more than one hundred cycles by iron binding, transport and release before it is removed from the circulation and iron itself is cleaved and bound to transferrin about every 2 h. [1, 7-8]

## **Haem**

Most of the body iron 30 mg Fe/kg is contained in the haem prosthetic group (porphyrin) of the oxygen transport protein haemoglobin which is part of the circulating red blood cells (erythrocytes). The iron transported to the bone marrow (erythroid marrow; erythropoiesis is the process of producing red blood cells) by transferrin is incorporated into haem to supply the haemoglobin production. The red blood cells circulate in the peripheral blood stream for about 120 days. Subsequently, they are taken up by the mononuclear phagocytic system in the spleen (to a minor extent by macrophages in the liver) that digests the haemoglobin and recycles the iron to the plasma transferrin circulation. Further, some of the newly formed red blood cells are destroyed within the bone marrow and the iron is released, this is called ineffective erythropoiesis. Additionally, 2 mg Fe/kg is present in various tissues as other haemoproteins, iron-sulphur proteins and non-haem, non-iron-sulphur proteins. [1]

## **Ferritin and haemosiderin (hs)**

The storage proteins ferritin and haemosiderin (hs) store the remaining 10 – 12 mg Fe/kg in men, around 5 mg Fe/kg in women, in the liver, spleen, bone marrow and muscle. Ferritin is an oligomeric protein of 24 similar or identical molecular subunits (apoferritins) with a total molecular weight 500 kD, forming a hollow protein shell (apoferritin protein shell) with an external diameter of 12 – 13 nm and an inside diameter of 7 – 8 nm which consists of a central inorganic ferric oxyhydroxide core. This protein is capable of storing up to

4500 atoms of iron in a water soluble, non-toxic and bioavailable form as ferric hydroxyphosphate micelles. It is proposed that ferrous iron ( $\text{Fe}^{2+}$ ) is oxidised to ferric iron by dinuclear ferrioxidase sites with  $\text{O}_2$  and ferric iron is deposited in the mineral core of the ferritin molecule as amorphous ferrihydrite (proposed formula:  $\text{Fe}_5\text{HO}_8 \cdot 4\text{H}_2\text{O}$  [9]). Ferritin is also a valuable tool for the clinician due to the determination of serum ferritin levels which are used for example for diagnosing and monitoring of hereditary or acquired secondary iron overload conditions. [1, 10-13]

The water-insoluble storage protein haemosiderin also consist of an inorganic iron core, yet the protein part is not well characterised. However, it seems to contain apoferritin or degradation products of apoferritin. A matter of debate is whether haemosiderin may be a degradation product of ferritin itself. The core of haemosiderin can comprehend ferrihydrite iron, like the storage protein ferritin, amorphous ferric oxide iron or crystalline goethite-like ( $\alpha\text{-FeOOH}$ ) iron [14]. The iron stored in haemosiderin is visible as iron-rich golden-yellow intracellular granules in tissue. Usually, iron is first stored in ferritin and after these deposits are full haemosiderin is used as storage protein. Iron from haemosiderin has not such a great bioavailability as ferritin. For this reason, haemosiderin bound iron is only found in small amounts in human tissue. However, in conditions of iron overload the vast majority of excess iron (about 80%) in the body is found as haemosiderin which has a higher content of iron than ferritin. Chelation therapy can help release iron from haemosiderin. [1, 4, 15]

## **Myoglobin**

About 4 mg Fe/kg is found in the muscles bound to the oxygen storage protein myoglobin [1]. Myoglobin is a protein chain of 153 amino acids folded around one single haem molecule. Ferrous iron ( $\text{Fe}^{2+}$ ) is bound to myoglobin with a five-fold pseudo octahedral geometry; the sixth coordination site of the octahedron can be occupied by an oxygen molecule. [16]

It has been reported that iron can be chelated from ferritin and haemosiderin [17-18]. However, there is another source of intracellular iron that seems

to be easily chelated called the labile iron pool (LIP). The labile iron pool was suggested as an intermediate or transitory pool between extracellular iron and cellular iron associated with proteins <sup>[19]</sup>. A synonym of the labile iron pool is chelatable iron pool referring to the assumption that it is probably the major site of iron chelation by chelators such as deferoxamine <sup>[1]</sup>. The iron in this chelatable pool comprises both ferrous and ferric iron which has been taken up into the cell and is “loosely” bound to low-molecular weight organic molecules (e.g. citrate and phosphate), polypeptides and surface components of membranes which all have a low affinity to iron. The intention of the labile iron pool is to provide available iron for haem synthesis and for iron incorporation into iron-dependent enzymes and the storage protein ferritin. The risk of this loosely bound iron is the potential participation in redox-cycling. In conclusion, it seems though that most chelatable iron is present in the labile iron pool. <sup>[1, 19-20]</sup>

This rough overview of the main transport and storage proteins helps understand the major principles of iron metabolism. Nevertheless, iron metabolism is much more complicated and involves many more aspects as discussed in this section <sup>[5, 21]</sup>. The understanding of iron metabolism and especially storage is the basis for the application of iron chelators in iron overload diseases.

## 4.2 Iron overload and iron chelation

The term “iron overload” refers to the condition when too much iron is accumulated in the human body. Excess iron is predominantly deposited into parenchymal tissue in the liver, heart and endocrine system, which leads to damage and, ultimately, to organ failure <sup>[22]</sup>. Two different types of iron overload disorders are distinguished, the primary and the secondary iron overload as demonstrated in **Figure 4.2**. Primary overload disorders are for example caused by hereditary hemochromatosis. Patients with hemochromatosis suffer from an iron-loading disorder resulting from a genetically determined failure to prevent unneeded dietary iron from entering the body which is characterised by progressive parenchymal iron overload with the potential for multiorgan damage <sup>[23]</sup>.

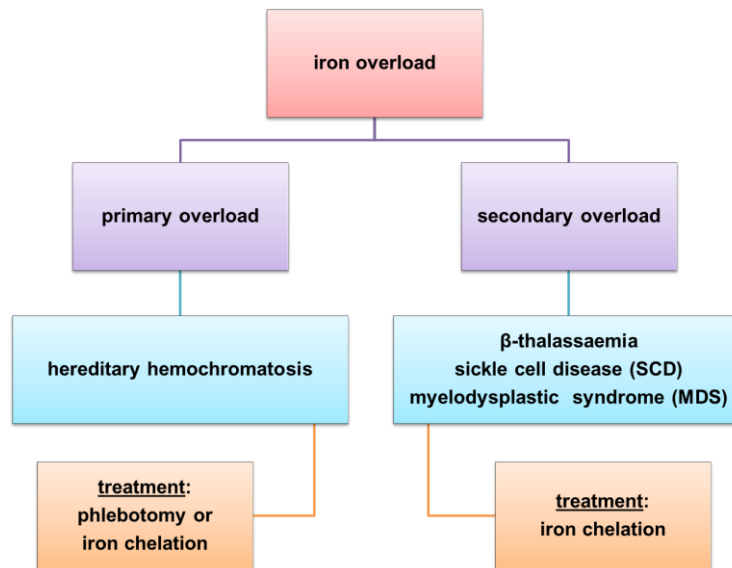


**Figure 4.2:** Overview of the two main causes for iron overload, resulting diseases and treatment <sup>[24]</sup>.

Hemochromatosis is generally treated by phlebotomy which is a safe and effective mode of iron removal when a patient is not anemic (anemia is the lack of haemoglobin, i.e. erythrocytes). However, not all patients show good compliance with phlebotomy for this reason iron chelation may be an alternative treatment. <sup>[25]</sup>

The source for secondary iron overload is not the anemic disease itself, but the treatment of chronic anemias with regular red blood cell transfusions which lead to accumulation of iron in the body. <sup>[26]</sup>

The most common blood transfusion dependent chronic anemia is  $\beta$ -thalassemia. The  $\beta$ -thalassemia syndromes are a group of hereditary blood disorders characterised by the reduced or absent  $\beta$ -globin chain synthesis, resulting in reduced haemoglobin in red blood cells, decreased production of red blood cells and anemia. The  $\beta$ -thalassemias can be classified into the  $\beta$ -thalassemia major (strongly transfusion dependent), intermedia (only occasionally require transfusions) and minor (usually clinically asymptomatic, but sometimes have a mild anemia). <sup>[27]</sup>

Further, patients with sickle cell disease, which is a group of inherited disorders caused by the sickle like mutation affecting the  $\beta$ -globin chain of

haemoglobin, rely on transfusions of red blood cells on a chronic or intermittent basis [26]. Another transfusion dependent class of diseases are the myelodysplastic syndromes, which is a group of heterogeneous disorders characterised by impaired blood cell production by the bone marrow usually by patients of median age 65 – 75 years [26].

All mentioned chronic anemias have in common that long-term blood transfusions lead to iron overload and to organ damage. For the treatment of transfusion dependent iron overload, chelation therapy has been applied for several years by the use of selective and high affinity iron chelators, which mobilise body iron and the iron complexes are excreted by urine and faeces. [25]

Meanwhile three highly specific iron chelators are commercially available: deferoxamine, deferasirox and deferiprone; depict in **Figure 4.3**.

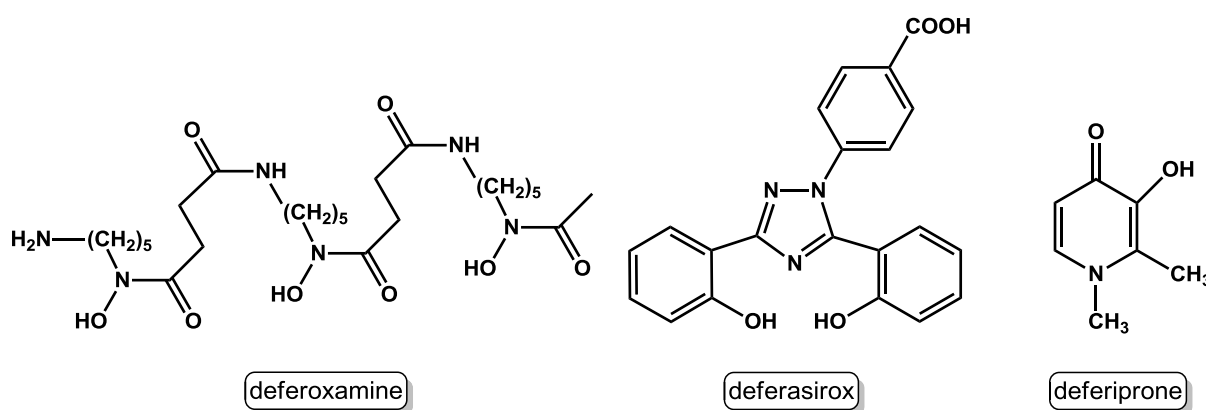


**Figure 4.3:** Chemical structures of the active substances in the pharmaceuticals Desferal® (deferoxamine, DFO), Exjade® (deferasirox, ICL670) and Ferriprox® (deferiprone, L1, CP20).

Deferoxamine (desferrioxamine-B, DFO, Desferal®, Novartis Pharma AG) was first introduced to the market and available for the treatment of secondary iron overload in the early 1960's and marked a breakthrough in the treatment of  $\beta$ -thalassemia [28]. The hexadentate chelator forms a 1:1 complex with the central metal ion  $\text{Fe}^{3+}$  which is coordinated by the three hydroxide and their neighbouring carbonyl oxygen atoms [29]. However, this iron chelator shows some disadvantages. Particularly, it is very hydrophilic which results in a very poor absorption by the gastrointestinal tract [29]. Further, DFO has a very short

plasma half-life of about 20 – 30 min <sup>[22]</sup>. As a consequence of these disadvantages, DFO is orally inactive and needs to be administered as a slow subcutaneous infusion over 8 – 12 h about 5 – 7 days per week for life <sup>[25]</sup>. Even though DFO is a highly specific iron chelator, a poor compliance in a large segment of the patient population was observed due to adverse effects from the long-term infusions <sup>[28]</sup>.

There was soon a great requirement for the development of new orally active iron chelators for the treatment of transfusion dependent iron overload. Deferiprone (L1, CP20, Ferriprox®, ApoPharma, Apotex Inc.) was the first orally active iron chelator which was synthesised and evaluated at University of Essex (UK) in the 1980's <sup>[25, 30]</sup>. The hydrophilic bidentate iron chelator binds iron in a 1:3 iron to ligand ratio by coordination with the hydroxide and carbonyl oxygen atoms <sup>[30]</sup>. Deferiprone was licensed in 1999 in the European Union and a number of countries outside the USA and Canada (total 43 countries) for the second-line treatment of iron overload in adult patients when DFO therapy was contraindicated or inadequate <sup>[26, 31]</sup>. Deferiprone has a short half-life of about 91 – 160 min which makes a three-times-daily dosing necessary <sup>[26, 30-31]</sup>.

Further, deferiprone is a low molecular weight hydrophilic molecule which enters cells and subsequently is able to transfer intracellular chelated iron to the stronger chelator DFO if this is simultaneously present in plasma. Therefore, a combined therapy of deferiprone and DFO has many advantages for example avoiding high doses of each drug with respect to adverse effects and increasing patient compliance due to fewer transfusions and still having daily chelation therapy. The main advantage of deferiprone itself is that it seems to be superior at protecting the heart from iron overload. <sup>[32]</sup>

Combined chelation treatment provides a useful option for patients who are unwilling or unable to maintain the five-times DFO transfusions or for whom the monotherapy is insufficient <sup>[30]</sup>.

Finally, a new orally bioavailable iron chelator was developed by Novartis: deferasirox (ICL670, Exjade®, Novartis Pharma AG). The iron chelator has emerged from an extraordinary large study started at CIBA-Geigy (now Novartis Pharma AG) in 1994. During this chemistry program 700 compounds of vari-

ous chemical classes were synthesised and subjected to a rigorous filtering process which included the determination of iron binding, testing of oral activity and the important testing of subchronic tolerability in animals at a very early stage in research. The tridentate iron chelator deferasirox, a bis-hydroxy-phenyltriazole, was the compound best combining all desired properties. [25]

As a result of extensive clinical studies deferasirox (Exjade®) was approved in November 2005 for the treatment of chronic iron overload due to blood transfusions in patients aged  $\geq 2$  years [25-26]. Deferasirox is highly lipophilic and has a long half-life of 11 – 19 h for the treatment of  $\beta$ -thalassemia. A once-daily dosing maintained deferasirox plasma levels within the therapeutic range over a 24-hour period providing continuous chelation coverage. Studies working on the treatment of cardiac iron accumulation with deferasirox are encouraging for the cardiac efficacy of deferasirox. Further, deferasirox has shown to maintain or reduce body iron in patients with MDS [22, 26, 33]. Studies on the reduction of body iron in sickle cell disease by deferasirox have also been reported [22, 26, 34]. Additionally, studies are being performed on the efficacy and safety of deferasirox as a further treatment of hereditary hemochromatosis [35]. [26]

It has been shown that excess iron is deposited in the form of haemosiderin and ferritin mainly in the liver, spleen and endocrine organs causing organ damage. Iron chelation mobilizes body iron deposits probably by an indirect process where iron is chelated from the labile iron pool of the cell which is in equilibrium with the insoluble haemosiderin. [28, 36]

It is interesting to note that only three iron selective chelators have been developed in the past 40 to 50 years. It seems to be challenging to develop orally active iron chelators for the use of transfusion dependent iron overload with an adequate safety profile. Further, the failure rate during development has been very high. Valuable new iron chelators could be designed in future as very selective iron chelators which show regional selectivity or selectivity for the targeting of iron containing structures. [25]

### 4.3 Motivation and objectives

The complex formation of the iron-chelating ligand deferasirox has been previously investigated with several divalent ( $\text{Cu}^{2+}$ ,  $\text{Zn}^{2+}$ ,  $\text{Mg}^{2+}$  and  $\text{Ca}^{2+}$ ) and trivalent ( $\text{Fe}^{3+}$  and  $\text{Al}^{3+}$ ) metal ions [37-40]. However, the solubility of deferasirox is poor in pure water so that potentiometric titration experiments needed to be carried out in a mixed water/DMSO solution ( $x_{\text{DMSO}} = 0.20$ ). The stability constants with metal ions determined in water/DMSO differ from stability constants in pure water. Further, precipitation was observed with divalent metal ions in water/DMSO solution which constrained the investigations. Since deferasirox is applied as iron-chelating agent in the pharmaceutical Exjade<sup>®</sup> the stability constants with metal ions in pure water would be of special interest. For this reason the water soluble ligand MSA (monosulfonic acid derivative of deferasirox) was developed previously and its complexation chemistry was investigated in pure water [37]. Yet, this ligand was only soluble in low concentrations in pure water so that investigations especially with divalent metal ions were also hampered by precipitation during titration experiments. Accordingly, there was a great necessity for a sufficiently water soluble ligand which can help elucidate the complex behaviour of deferasirox in pure water.

The main objective of this thesis was to synthesise a highly water soluble ligand on the basis of the iron-chelating ligand deferasirox. The new ligand should adopt very similar coordination geometry as deferasirox and similar coordination characteristics. The resulting ligand was a disulfonic acid derivative 2-[3,5-bis(2-hydroxyphenyl)-1*H*-1,2,4-triazol-1-yl]benzene-1,4-disulfonic acid (DSA) of the ligand deferasirox which was easy to synthesise on a large-scale (several grams). Of special importance was to show the high specificity of the new ligand for  $\text{Fe}^{3+}$  and the similar redox-chemistry in accordance with deferasirox. Potentiometric and spectrophotometric titration experiments with the divalent metal ions  $\text{Ni}^{2+}$ ,  $\text{Cu}^{2+}$ ,  $\text{Zn}^{2+}$ ,  $\text{Cd}^{2+}$ ,  $\text{Mg}^{2+}$  and  $\text{Ca}^{2+}$  and the trivalent metal ions  $\text{Fe}^{3+}$ ,  $\text{Al}^{3+}$ ,  $\text{Ga}^{3+}$  and  $\text{Gd}^{3+}$  will confirm that DSA is a selective iron-chelating ligand like deferasirox.

The high water solubility was of great importance to prevent precipitation during titration experiments. In effect, it has been proposed that the precipitate

observed of deferasirox and MSA with divalent metal ions such as  $\text{Cu}^{2+}$  and  $\text{Zn}^{2+}$  is of polymeric nature. A study by Ryabukhin with the 1N-phenyl derivative of deferasirox proposes the formation of polymeric complexes with the divalent metal ions  $\text{Co}^{2+}$ ,  $\text{Ni}^{2+}$  and  $\text{Cu}^{2+}$  [41]. On account of this hypothesis it was our aim to bring insight into the nature of the composition of the precipitate of  $\text{Cu}^{2+}$  with deferasirox. More knowledge should be provided by investigations with EPR spectroscopy on the  $\text{Cu}^{2+}$ -deferasirox precipitate and on  $\text{Cu}^{2+}$ -DSA solutions. Further, potentiometric titration experiments carried out with DSA and divalent metal ions with different molar ratios of metal ion to ligand should also bring new findings on the nature of the species in pure water solution.

It has been assumed that deferasirox can be protonated at the 1,2,4-triazole unit in strong acidic solution [39]. Studies on the ligands deferasirox and DSA in strong acidic solutions with batch titrations and  $^1\text{H-NMR}$  spectroscopy will help contribute to the confirmation of this assumption.

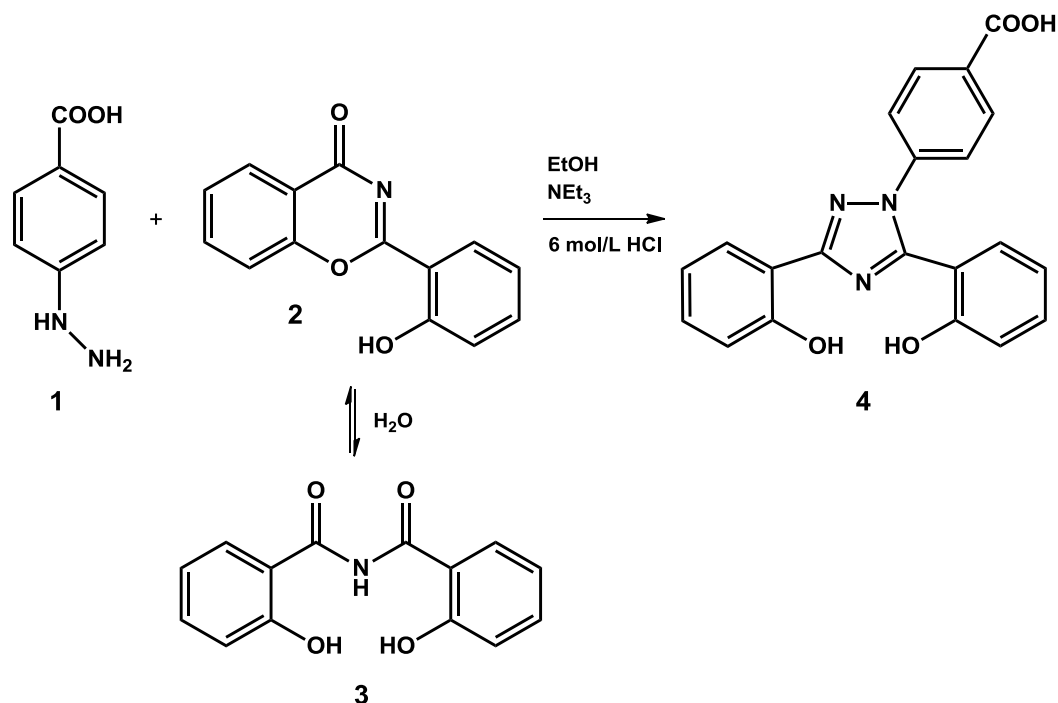
Furthermore, some questions emerged concerning the simultaneous administration of deferasirox with  $\text{Gd}^{3+}$  and  $\text{Ga}^{3+}$  containing contrast agents or radiopharmaceuticals. How strong are  $\text{Gd}^{3+}$  and  $\text{Ga}^{3+}$  complexes with deferasirox, and its water soluble derivatives, in comparison to the  $\text{Fe}^{3+}$  complexes? Moreover, could these complexes be strong enough to cause ligand exchange reactions in the body? The answer to these questions should be found by performing potentiometric titrations with deferasirox, MSA and DSA with  $\text{Gd}^{3+}$  and  $\text{Ga}^{3+}$ .

Most stability constants of deferasirox complexes cannot be measured in pure water, yet they can be estimated by linear extrapolation of constants measured with different molar fractions  $x_{\text{DMSO}}$ . Stability constants of the  $\text{Fe}^{3+}$  ion with deferasirox have successfully been extrapolated to pure water [39-40]. Our aim was to estimate the stability constants of deferasirox with  $\text{Al}^{3+}$ ,  $\text{Mg}^{2+}$  and  $\text{Ca}^{2+}$  in pure water, to generate a correlation between these constants and those measured in pure water for DSA. A correlation in form of a linear free energy relation between the two ligands will allow us to estimate stability constants of deferasirox metal ion complexes in pure water which cannot be determined directly. Accordingly, the ligand DSA will be a valuable tool to help elucidate the complex behavior of deferasirox.

## 5 Synthesis of the ligands

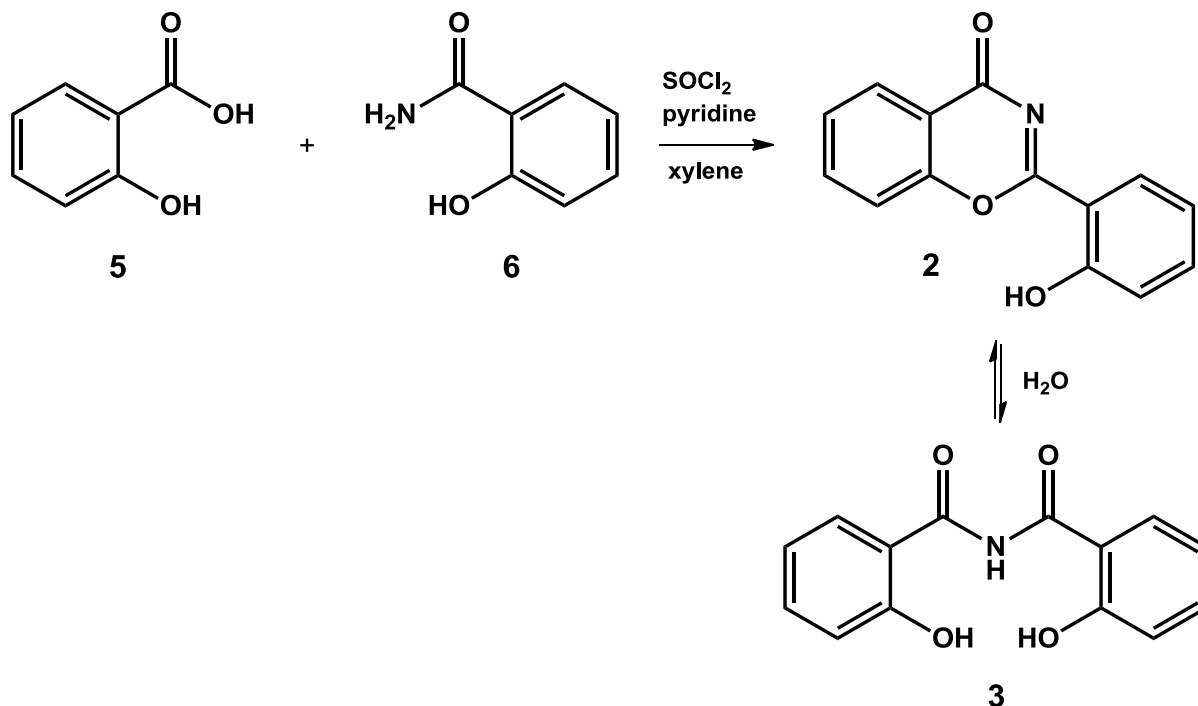
### 5.1 Synthesis of the ligand deferasirox and its monosulfonic acid derivative (MSA)

The synthesis of 3,5-bis(2-hydroxyphenyl)-1-phenyl-1,2,4-triazole, an unsubstituted derivative of deferasirox, was first mentioned in the literature by Ryabukhin <sup>[42]</sup>. The Novartis Pharma AG picked up this synthesis and developed the ligand synthesis of deferasirox from it. The ligand was synthesised according to literature by the reaction of two main building blocks to form the 1,2,4-triazole unit <sup>[40]</sup>. This reaction of a substituted hydrazine with a diacylamine is referred to as the Einhorn-Brunner-Synthesis <sup>[43]</sup>. To receive deferasirox **4** (4-[3,5-bis(2-hydroxyphenyl)-1*H*-1,2,4-triazol-1-yl]benzoic acid) as shown in **Scheme 5.1**, 4-hydrazino-benzoic acid **1** was reacted with 2-(2-hydroxyphenyl)-benzo-4*H*-[1,3]-oxazin-4-one **2** (benzo-oxazin-4-one) or rather with 2-hydroxy-*N*-(2-hydroxybenzoyl)-benzamide **3** which is the hydrolysed form of the benzo-oxazin-4-one. The 4-hydrazino-benzoic acid is commercially available and used as obtained.



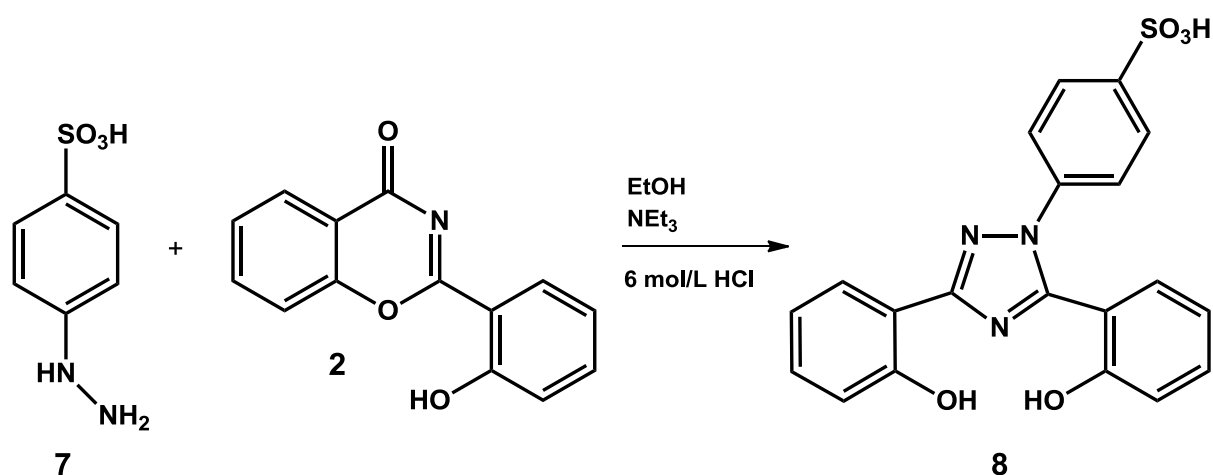
**Scheme 5.1:** Synthesis of deferasirox **4** (4-[3,5-bis(2-hydroxyphenyl)-1*H*-1,2,4-triazol-1-yl]benzoic acid) from 4-hydrazino-benzoic acid **1** and 2-(2-hydroxyphenyl)-benzo-4*H*-[1,3]-oxazin-4-one **2** respectively 2-hydroxy-*N*-(2-hydroxybenzoyl)-benzamide **3**.

The second building block benzo-oxazin-4-one needed to be synthesised from salicylic acid **5** and salicylamide **6** in the presence of thionyl chloride and pyridine in a cyclodehydration as shown in **Scheme 5.2**.



**Scheme 5.2:** Synthesis of 2-(2-hydroxyphenyl)-benzo-4H-[1,3]-oxazin-4-one **2** respectively 2-hydroxy-*N*-(2-hydroxybenzoyl)-benzamide **3** from salicylic acid **5** and salicylamide **6** with thionyl chloride and pyridine in xylene.

The carboxylic acid functional group of deferasirox can be replaced by a sulfonic acid to increase water solubility. **Scheme 5.3** shows the synthesis only differs in the application of 4-hydrazino-benzosulfonic acid **7** which is also commercially available. The preparation of the monosulfonic acid derivative MSA **8** (4-[3,5-bis(2-hydroxyphenyl)-1*H*-1,2,4-triazol-1-yl]benzenesulfonic acid) is otherwise in accordance with the reaction described above for the ligand deferasirox <sup>[40]</sup>.



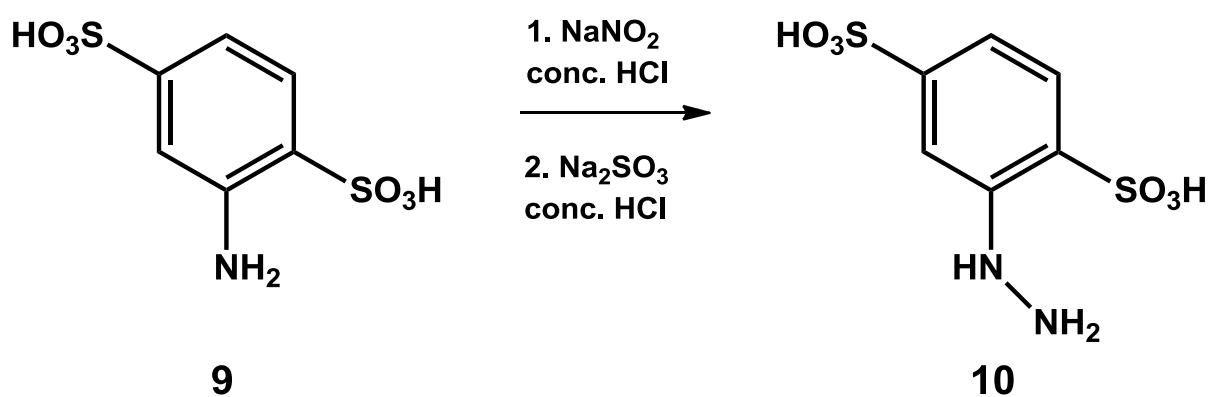
**Scheme 5.3:** Synthesis of the monosulfonic acid derivative MSA **8** (4-[3,5-bis(2-hydroxyphenyl)-1H-1,2,4-triazol-1-yl]benzenesulfonic acid) from 4-hydrazino-benzenesulfonic acid **7** and benzo-oxazin-4-one **2**.

These two ligands were both synthesised in boiling ethanol with stoichiometric amounts of triethylamine. Purification was carried out by precipitating the ligand from the reaction mixture and washing the resulting precipitate with cold water. After drying in vacuum and full characterisation the ligands were employed for further studies.

## 5.2 Synthesis of the dicarboxylic acid (DCA) and disulfonic acid derivative (DSA) of deferasirox

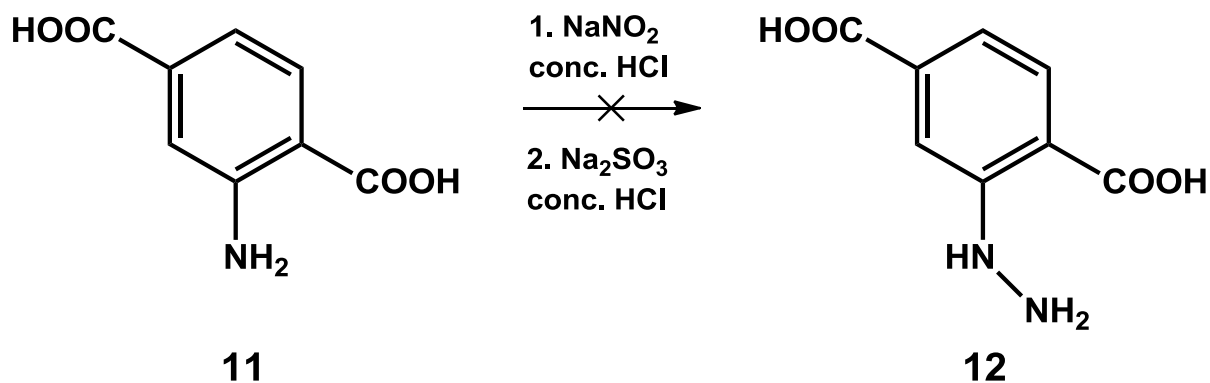
The ligand MSA was soluble in pure water (water solubility 0.7 g/L <sup>[37]</sup>) in contrast to deferasirox (water solubility 0.4 g/L at pH = 7.4 <sup>[38]</sup>) and therefore its complex formation could be investigated in pure water. However, during some titration experiments precipitation was observed. This made the investigation of the complex formation much more difficult. To prevent precipitation during titration experiments we decided to increase water solubility even more. The idea we had was the addition of another functional group to the benzoic acid moiety to enhance water solubility. This was implemented by adding a second carboxylic acid to deferasirox or a second sulfonic acid functional group to MSA. The main region of the ligand where complex formation occurs is not affected by this variation. However, the charge of the ligand changes as a result of the addition of another functional group which can be deprotonated. Consequently,

the hydrazine needed to be modified. The question was to either modify the hydrazine we used in the synthesis for deferasirox and MSA or to buy a modified starting material and synthesise the hydrazine. The second method seemed more promising hence 5-aminoisophthalic acid and aniline-2,5-disulfonic acid were applicable as starting materials. The synthesis is based on a procedure for the preparation of 4-hydrazino-benzosulfonic acid <sup>[44]</sup>. The aniline-2,5-disulfonic acid **9** derivative is suitable for the preparation of the 2-hydrazinylbenzene-1,4-disulfonic acid **10** (DSH) as shown in **Scheme 5.4**. Aniline-disulfonic acids and their diazonium compounds in general have been known very early to the literature <sup>[45-46]</sup>.



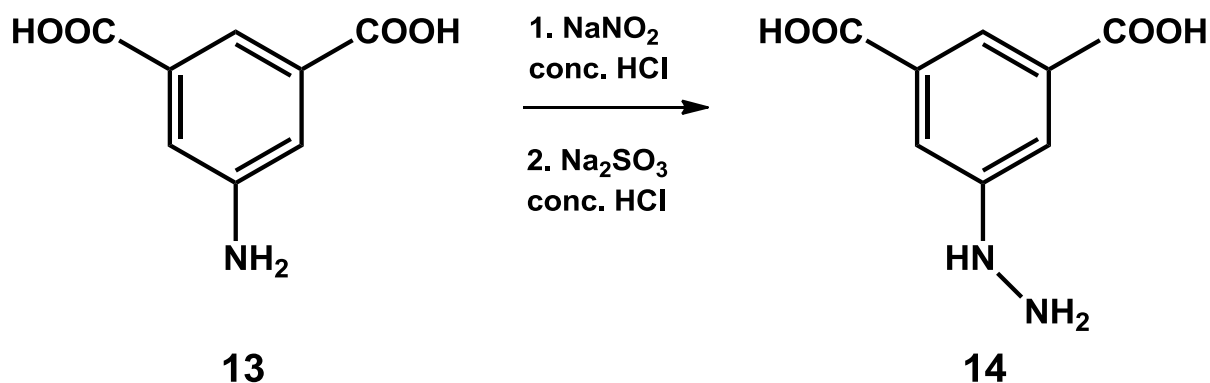
**Scheme 5.4:** Synthesis of 2-hydrazinylbenzene-1,4-disulfonic acid (DSH) **10** from aniline-2,5-disulfonic acid **9**.

At first, we tried to synthesise the dicarboxylic acid hydrazine by using 2-aminoterephthalic acid **11** as demonstrated in **Scheme 5.5**. The 2-hydrazinylterephthalic acid **12** would have been an analogue to the disulfonic acid derivative. The synthesis was carried out on the one hand with the same procedure as for DSH and on the other hand based on a similar procedure from literature with the help of SnCl<sub>2</sub> <sup>[44, 47]</sup>. Both methods failed several times. The diazonium salt was verified but the hydrazine did not form.



**Scheme 5.5:** Attempt to synthesise 2-hydrazinylterephthalic acid **12** from 2-aminoterephthalic acid **11**.

Consequently, we tried the preparation of 5-hydrazinylisophthalic acid (DCH) **14** with two carboxylic acid groups in 1 and 3 positions with 5-aminoisophthalic acid **11** as starting material as presented in **Scheme 5.6**. This synthesis was successful.

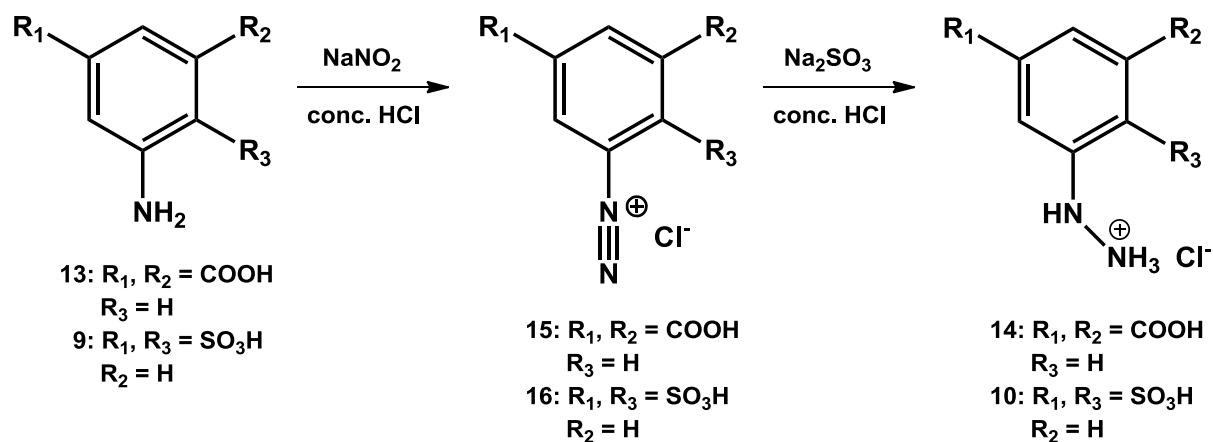


**Scheme 5.6:** Synthesis of 5-hydrazinylisophthalic acid **14** from 5-aminoisophthalic acid **13**.

Both hydrazines 5-hydrazinylisophthalic acid (DCH) and 2-hydrazinylbenzene-1,4-disulfonic acid (DSH) were prepared by the same procedure. It was carried out as a two-step reaction in pure water/HCl as solvent.

As demonstrated in **Scheme 5.7**, in the first step the amine functional group of 5-aminoisophthalic acid **13** and aniline-2,5-disulfonic acid **9** was diazotised in hydrochloric acid with sodium nitrite in an ice bath. The moist diazonium salt **15** or **16** was passed on to the next step without further purification.

To form the hydrazine a reduction with sodium sulphite was performed at low temperature.

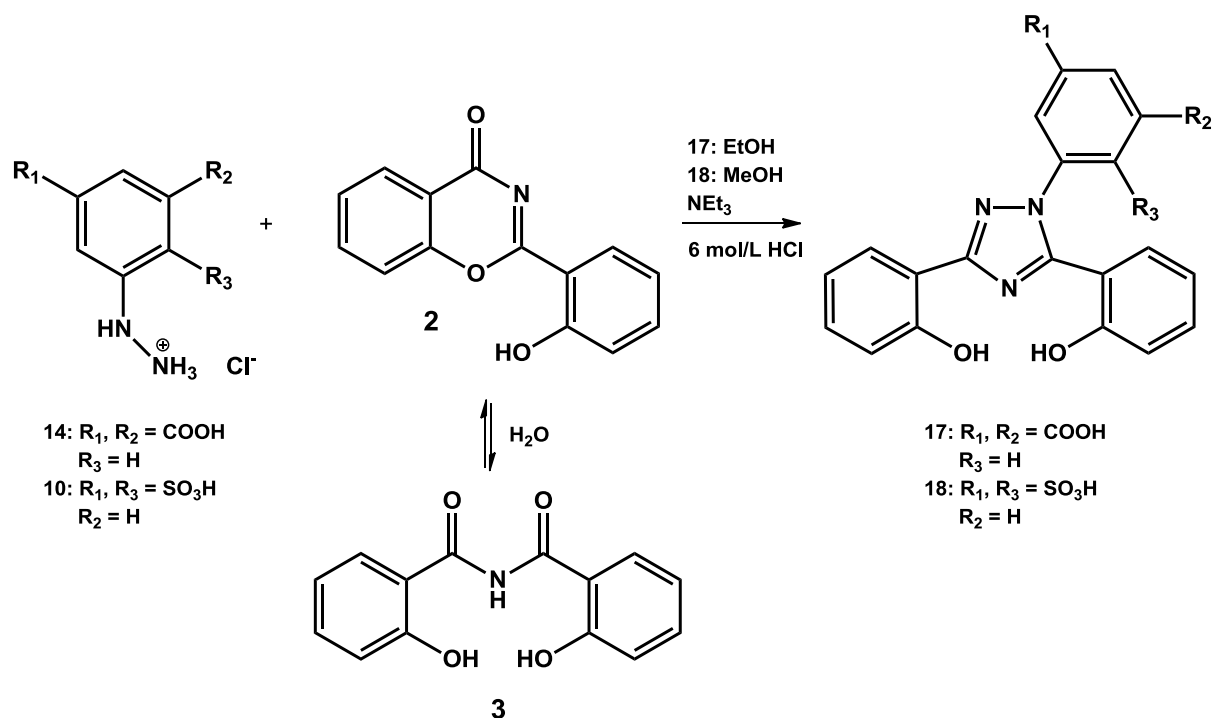


**Scheme 5.7:** The first step shows the diazotation of the 5-aminoisophthalic acid **13** and aniline-2,5-disulfonic acid **9** with sodium nitrite and concentrated HCl to 3,5-dicarboxybenzenediazonium chloride **15** and 2,5-disulfobenzenediazonium chloride **16**. The second step depicts the reduction of the diazonium salt **15** and **16** to 5-hydrazinylisophthalic acid **14** and 2-hydrazinylbenzene-1,4-disulfonic acid **10** with sodium sulphite and concentrated HCl.

The hydrazine **14** and **10** were precipitated with concentrated HCl. As a result of the preparation process the hydrazine was obtained as a hydrochloride. Both hydrazines were not obtained entirely pure. Their preparation with several salts and their good water solubility made it difficult to separate the product from all salt impurities. Attempts to separate the hydrazine from the salts with anion exchanger or size exclusion chromatography (using sephadex for gel permeation chromatography) failed. In effect, the hydrazines applied for the synthesis of the ligands were used with small impurities which could be removed during the workup process of the ligands.

Now having synthesised the hydrazine we could react it with the same compound benzo-oxazin-4-one as in the synthesis of deferasirox and MSA mentioned in section 5.1 to form the desired ligands. **Scheme 5.8** demonstrates the Einhorn-Brunner-Synthesis of the two derivatives of deferasirox DCA **17** (dicarboxylic acid derivative, 5-[3,5-bis(2-hydroxyphenyl)-1*H*-1,2,4-triazol-1-yl]isophthalic acid) and DSA **18** (disulfonic acid derivative, 2-[3,5-bis(2-hydroxyphenyl)-1*H*-1,2,4-triazol-1-yl]benzene-1,4-disulfonic acid). The ligand DCA was prepared in boiling ethanol whereas DSA is prepared in boiling

methanol. Both ligand syntheses were carried out with excess of triethylamine and a slight excess of benzo-oxazin-4-one.



**Scheme 5.8:** Synthesis of the ligand DCA **17** in ethanol and DSA **18** in methanol with the appropriate hydrazine **14** and **10** and 2-(2-hydroxyphenyl)-benzo-4*H*-[1,3]-oxazin-4-one **2** respectively 2-hydroxy-*N*-(2-hydroxybenzoyl)-benzamide **3** by Einhorn-Brunner-Synthesis.

The ligand DCA was isolated from the reaction mixture by precipitation with HCl. Several different ways of reprecipitation failed to remove small impurities. Therefore, the ligand DCA was passed on to preparative HPLC. The separation was performed with a reversed phase column and methanol/water mixtures with 0.1% formic acid as eluent. At first, the separation was carried out with different gradient compositions. Then 90% methanol was kept isocratic until the ligand completely eluted. The ligand was precipitated from pure water. After drying in vacuum the ligand was pure and had absorbed some water which was determined by elemental analysis.

The ligand DSA was precipitated from the reaction mixture with HCl and reprecipitated from methanol with ethyl acetate. After removing all solvent impurities in vacuum the ligand needed to be left standing exposed to the air to absorb water. Usually five molecules of water were obtained and determined by

elemental analysis. Effectively, the ligand could be employed for further investigations.

In conclusion, the variation of both ligands is at the peripheral phenyl group which does not participate in complexation behaviour. Therefore, the ligands DCA and DSA have the same complexation mode as deferasirox. The ligand DCA is not well water soluble (water solubility was not determined) and did not fulfil the requirements of being more water soluble than MSA. Contrary to DCA the ligand DSA (water solubility 8.0 g/L) is much better water soluble than MSA (water solubility 0.7 g/L <sup>[37]</sup>) and therefore titration experiments could be carried out without precipitation.

## 6 The Ligand DCA

The dicarboxylic acid derivative ligand DCA is very closely related to the iron chelating ligand deferasirox. Its structure is presented in **Figure 6.1**. The variation was performed at the peripheral benzocarboxylic acid group. The carboxylic acid in position 1 of deferasirox is replaced by two carboxylic acid groups in positions 1 and 3 of DCA. The intention of the variation was to design a new ligand that is more water soluble than deferasirox. We believe that higher water solubility will prevent precipitation of insoluble complexes during titration experiments.

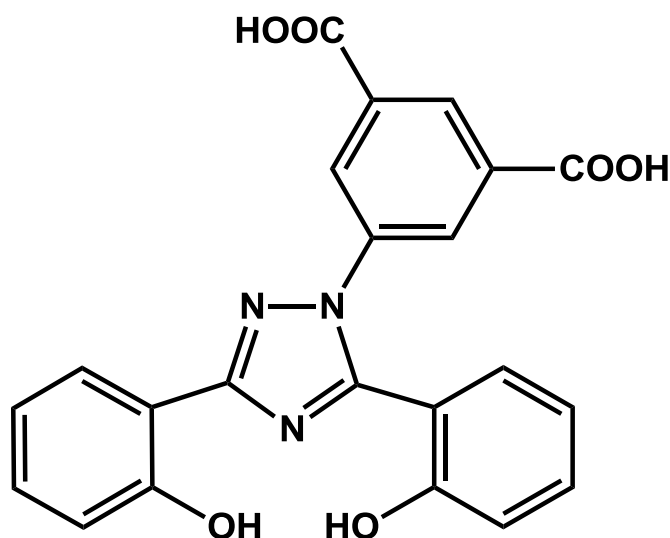


**Figure 6.1:** The structural formula of the ligand 5-[3,5-bis(2-hydroxyphenyl)-1H-1,2,4-triazol-1-yl]isophthalic acid (dicarboxylic acid derivative DCA of deferasirox).

Despite the two carboxylic acid groups the ligand's water solubility was not enhanced enough to carry out titration experiments in pure water. The  $pK_a$  values were studied in a water/DMSO mixture with a molar fraction of  $x_{\text{DMSO}} = 0.20$ . For this ligand four  $pK_a$  values were determined by continuous potentiometric titration. An example titration with titration conditions is given in **Table 6.1**.

**Table 6.1:** An example titration experiment of the ligand DCA with overall protonation constants  $\log\beta_x$  <sup>[a]</sup> and acidity constants  $pK_{a,i}$  <sup>[b]</sup>. The standard deviations of the values are given in brackets <sup>[c]</sup>. The titration conditions are given at T = 298 K.

<b>log<math>\beta</math> and pK<sub>a</sub> values of DCA</b>			
measuring method		potentiometric	
method type		continuous	
solvent		water/DMSO $x_{\text{DMSO}} = 0.20$	
[L] <sub>t</sub>		1.00 mmol/L	
[H] <sub>t</sub>		4.10 mmol/L	
titration volume		50.0 mL	
titrant		0.1 mol/L KOH	
supporting electrolyte		0.1 mol/L KCl	
electrode		Schott IoLine	
pK <sub>w</sub>		15.58	
pH range		3.4 – 12.5	
volume of data points		60	
time for mixing process		150 s	
$\sigma$ <sup>[d]</sup>		0.771	
<b>log<math>\beta_1</math></b>	<b>12.26(1)</b>	<b>pK<sub>a,1</sub></b>	<b>3.91(2)</b>
<b>log<math>\beta_2</math></b>	<b>22.61(2)</b>	<b>pK<sub>a,2</sub></b>	<b>4.95(2)</b>
<b>log<math>\beta_3</math></b>	<b>27.56(2)</b>	<b>pK<sub>a,3</sub></b>	<b>10.35(2)</b>
<b>log<math>\beta_4</math></b>	<b>31.47(2)</b>	<b>pK<sub>a,4</sub></b>	<b>12.26(1)</b>

<sup>[a]</sup> For the ligand L  $\log\beta_x$  is defined as:  $\beta_x = [\text{LH}_x] \times [\text{L}]^{-1} \times [\text{H}]^{-x}$ .

<sup>[b]</sup> For the ligand LH<sub>x</sub> the pK<sub>a,i</sub> is defined as:  $pK_{a,i} = -\log K_{a,i}$  and  $K_{a,i} = [\text{LH}_{x-i}] \times [\text{H}] \times [\text{LH}_{(x+1)-i}]^{-1}$ .

<sup>[c]</sup> The deviations given in brackets correspond to the threefold standard deviation taken from Hyperquad2008.

<sup>[d]</sup> The  $\sigma$  value is taken from Hyperquad2008.

The first two  $pK_a$  values  $pK_{a,1}$  and  $pK_{a,2}$  can be assigned to the deprotonations of the carboxylic acid groups. Accordingly, the  $pK_{a,3}$  and  $pK_{a,4}$  can be assigned to the deprotonations of the two hydroxyphenyl groups. The values of these acidity constants are in the expected range. In **Table 6.2** mean values of 7 titrations were calculated by two methods.

**Table 6.2:** Mean values of the overall protonation constants  $\log\beta_x$  <sup>[a]</sup> and acidity constants  $pK_{a,i}$  <sup>[b]</sup> from potentiometric titrations for the ligand DCA determined by two methods in water/DMSO with  $x_{\text{DMSO}} = 0.20$ ,  $T = 298 \text{ K}$  and  $I = 0.1 \text{ KCl}$ .

<b><math>\log\beta</math> and <math>pK_a</math> values of DCA</b>			
mean values and standard deviations from 7 titrations <sup>[c]</sup>			
$\log\beta_1$	<b>12.27(2)</b>	$pK_{a,1}$	<b>3.90(2)</b>
$\log\beta_2$	<b>22.62(3)</b>	$pK_{a,2}$	<b>4.95(1)</b>
$\log\beta_3$	<b>27.57(4)</b>	$pK_{a,3}$	<b>10.35(1)</b>
$\log\beta_4$	<b>31.46(5)</b>	$pK_{a,4}$	<b>12.27(2)</b>
mean values by simultaneous evaluation of 7 titrations <sup>[d]</sup>			
pH range		3.4 – 12.5	
$\sigma$ <sup>[e]</sup>		0.921	
$\log\beta_1$	<b>12.27(1)</b>	$pK_{a,1}$	<b>3.90(1)</b>
$\log\beta_2$	<b>22.62(1)</b>	$pK_{a,2}$	<b>4.94(1)</b>
$\log\beta_3$	<b>27.56(1)</b>	$pK_{a,3}$	<b>10.35(1)</b>
$\log\beta_4$	<b>31.46(1)</b>	$pK_{a,4}$	<b>12.27(1)</b>

<sup>[a]</sup> For the ligand L  $\log\beta_x$  is defined as:  $\beta_x = [\text{LH}_x] \times [\text{L}]^{-1} \times [\text{H}]^{-x}$ .

<sup>[b]</sup> For the ligand  $\text{LH}_x$  the  $pK_{a,i}$  is defined as:  $pK_{a,i} = -\log K_{a,i}$  and  $K_{a,i} = [\text{LH}_{x-i}] \times [\text{H}] \times [\text{LH}_{(x+1)-i}]^{-1}$ .

<sup>[c]</sup> The standard deviations in brackets were calculated with:  $\sqrt{\frac{\sum_{i=0}^n (x_i - \bar{x})^2}{(n-1)}}$ ;  $x_i$  measured value;  $\bar{x}$  mean value;  $n$  number of values.

<sup>[d]</sup> The titrations were evaluated simultaneously with the program Hyperquad2008. The deviations given in brackets correspond to the threefold standard deviation taken from Hyperquad2008.

<sup>[e]</sup> The  $\sigma$  value is taken from Hyperquad2008.

The first values in **Table 6.2** are arithmetic means calculated from 7 titrations with their calculated standard deviations in brackets. In addition, the second values given in **Table 6.2** are values calculated with the program Hyperquad2008. For this, all 7 titrations were loaded into Hyperquad2008 and were evaluated simultaneously with the same model. By comparing the two methods we could show that the values obtained are in good agreement. They differ only on the second decimal place. Another small difference is that the deviations for the first values calculated with the standard deviation are somewhat higher than those for the second set of values taken from Hyperquad2008. This can be explained by the fact that Hyperquad2008 has 7 sets of data to calculate the second set of values simultaneously. Which makes the values more accurate and therefore the deviation ranges are smaller. Whereas, to obtain the mean value of the first set of data each titration was evaluated separately.

**Figure 6.2** shows a potentiometric titration curve of the  $pK_a$  titration of DCA with a total ligand concentration of 1.00 mmol/L. The titration was carried out in water/DMSO with  $x_{\text{DMSO}} = 0.20$ , with an ionic strength of  $I = 0.1$  mol/L KCl and at  $T = 298$  K. The ligand solution was titrated with 0.1 mol/L potassium hydroxide solution from pH 3.4 to about pH 12.5. The high pH results from the different solvation of protons and hydroxide ions in water/DMSO solution. Accordingly, the ionic product is considerably smaller in the water/DMSO system than in pure water. For the molar fraction  $x_{\text{DMSO}} = 0.20$  the  $pK_w$  is 15.58 and the pH scale is extended to the pH range of 0 – 15.6. Resulting from this, neutral solutions have a pH value of about 7.8 <sup>[40]</sup>.

The titration curve in **Figure 6.2** shows a distinct inflection at 2 equivalents (millimoles of KOH added to millimoles of ligand present). This strong increase in pH can be assigned to the complete deprotonation of the two carboxylic acid groups. If we look carefully at the titration curve at 3 equivalents we can identify a small increase of pH at about pH 11. This can be assigned to the deprotonation of the hydroxyphenyl groups. The deprotonation of the ligand is concluded at 4 equivalents.

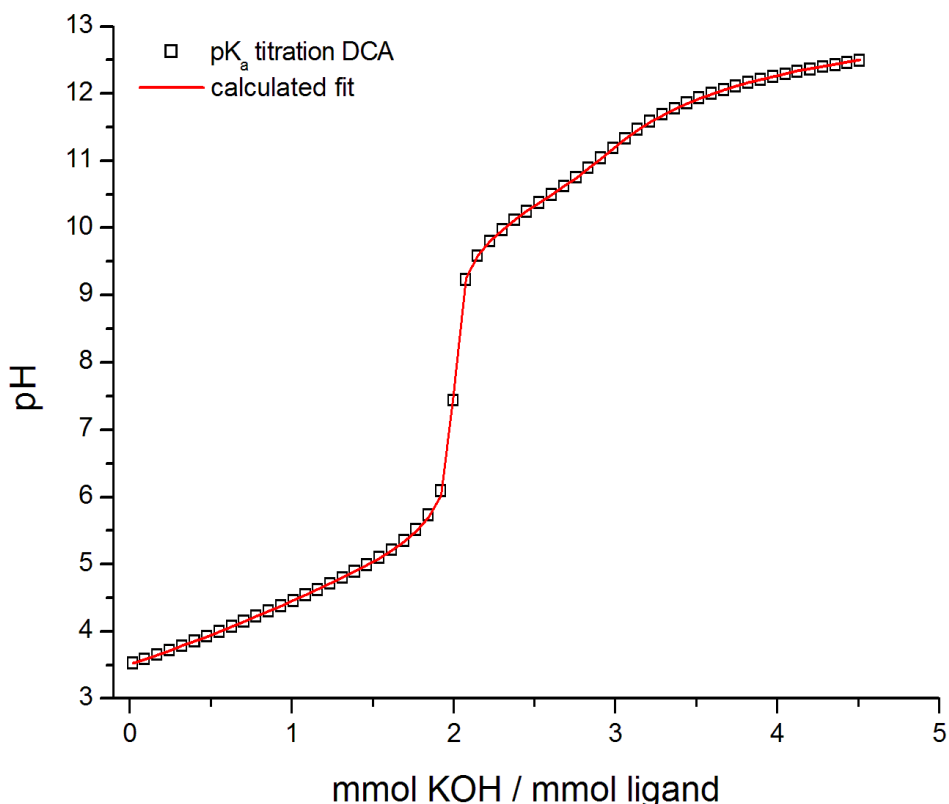


**Figure 6.2:** Potentiometric titration curve of the free ligand DCA and in water/DMSO with  $x_{\text{DM-SO}} = 0.20$ ,  $[\text{L}]_t = 1.00$  mmol/L,  $T = 298$  K and  $I = 0.1$  mol/L KCl. The open squares represent experimental points and the fit (solid line) was calculated from the equilibrium constants with Hyperquad2008.

The species distribution diagram **Figure 6.3** is a representation of all of the identified species during the deprotonation of DCA. At the beginning of the titration at pH 3.4 the fully protonated ligand  $\text{LH}_4$  and its resulting deprotonated species  $\text{LH}_3^-$  are present with a concentration of 75% and 25%, respectively. While the fully protonated ligand decreases in per cent, the species  $\text{LH}_3^-$  gains and reaches its maximum concentration (63%) at pH 4.4. The doubly deprotonated ligand  $\text{LH}_2^{2-}$  is found along the whole titration range investigated. It starts to form just after the titration has started and its concentration reaches 0% at the end of the titration. This species is the predominant species with a higher concentration than any other component between pH 5 and 10. It reaches its highest percentage around pH 7.6 and is present with a maximum concentration of over 90% from pH 6 to 9.4. This observation is in accordance with the

$pK_a$  values determined and the observed inflection at 2 equivalents lasting from pH 6 to 9. At this point both carboxylic acid groups are fully deprotonated and the  $pK_a$  values of the hydroxyl phenyl rings dominate the species distribution. At pH 8 the predominant component  $LH_2^{2-}$  starts to deprotonate to  $LH_3^-$  which reaches its highest peak (82%) at pH 11.3. The titration ends at pH 12.5 where the fully deprotonated ligand  $L^{4-}$  becomes the major species (62%) and the only other species is  $LH^{3-}$  (38%).

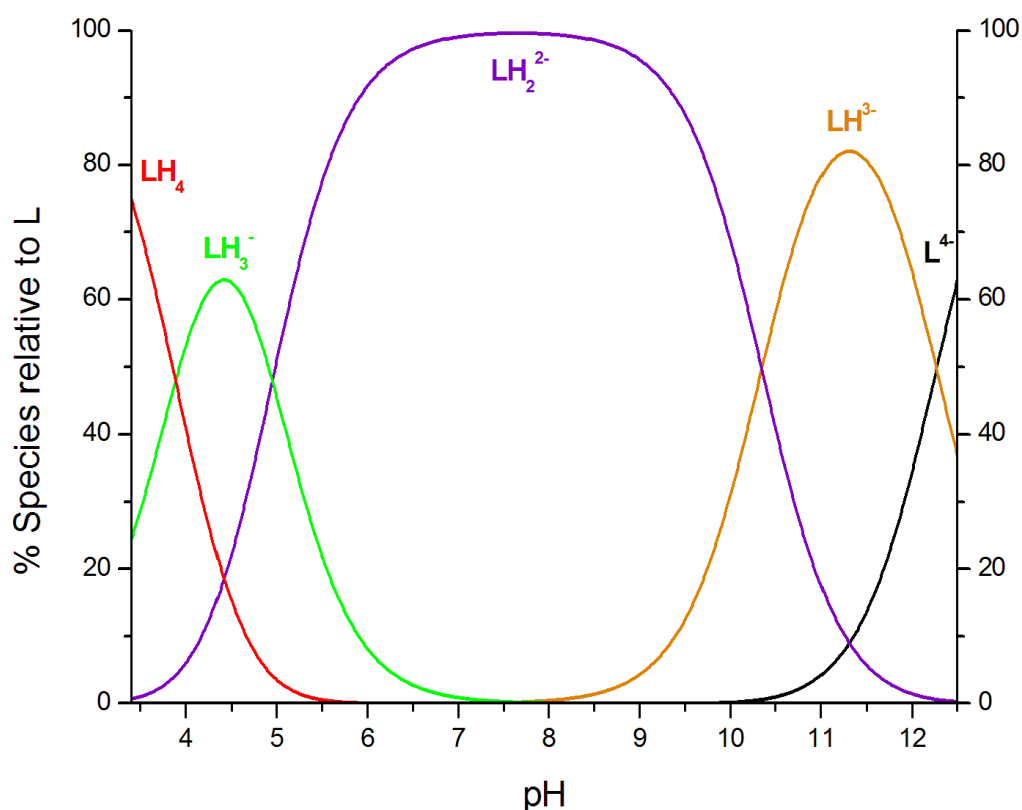


**Figure 6.3:** Species distribution diagram of the ligand DCA indicating the species present as a function of pH with  $x_{DMSO} = 0.20$  at  $T = 298\text{ K}$  and  $I = 0.1\text{ mol/L KCl}$ . % Species relative to L are defined as per cent of total concentration of ligand  $[L]_t = 1.00\text{ mmol/L}$  set at 100%. The species concentrations were calculated from the equilibrium constants listed in **Table 6.2** (mean values and standard deviations from 7 titrations) with the program Hyss2006.

It is vital that these findings need to be compared with the ligand deferasirox. In **Table 6.3**  $\log\beta$  and  $pK_a$  values of DCA and deferasirox are compared. The main difference between both ligands is DCA has four  $pK_a$  values and deferasirox has three. If we look at the  $\log\beta$  values we see that the first three  $\log\beta$

are very similar. The  $\log\beta_4$  of DCA is a deprotonation of the second carboxylic acid group which is missing in deferasirox.

**Table 6.3:** Comparison of the overall protonation constants  $\log\beta_x$  <sup>[a]</sup> and acidity constants  $pK_{a,i}$  <sup>[b]</sup> for the ligand DCA with deferasirox. The constants are all arithmetic means with calculated standard deviations <sup>[c]</sup>. All constants were studied in water/DMSO with  $x_{\text{DMSO}} = 0.20$ ,  $T = 298 \text{ K}$  and  $I = 0.1 \text{ KCl}$ .

DCA		Deferasirox <sup>[d]</sup>	
$\log\beta_1$	12.27(2)	$\log\beta_1$	12.18(2)
$\log\beta_2$	22.62(3)	$\log\beta_2$	22.36(3)
$\log\beta_3$	27.57(4)	$\log\beta_3$	27.00(3)
$\log\beta_4$	31.46(5)	-	-
$pK_{a,1}$	3.90(2)	-	-
$pK_{a,2}$	4.95(1)	$pK_{a,1}$	4.64(1)
$pK_{a,3}$	10.35(1)	$pK_{a,2}$	10.18(1)
$pK_{a,4}$	12.27(2)	$pK_{a,3}$	12.18(2)

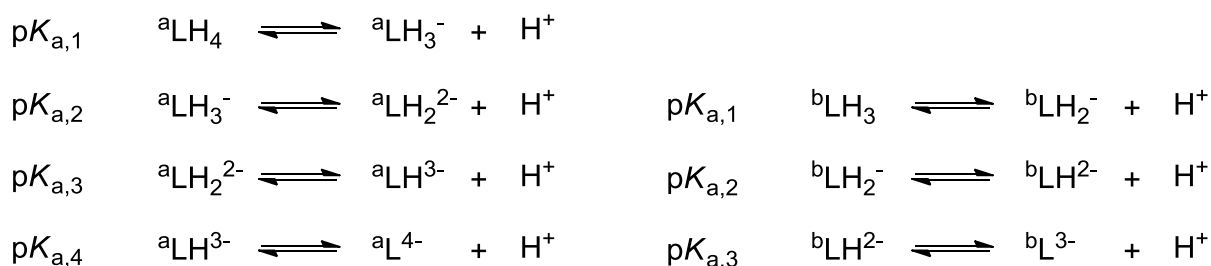
<sup>[a]</sup> For the ligand L  $\log\beta_x$  is defined as:  $\beta_x = [\text{LH}_x] \times [\text{L}]^{-1} \times [\text{H}]^{-x}$ .

<sup>[b]</sup> For the ligand  $\text{LH}_x$  the  $pK_{a,i}$  is defined as:  $pK_{a,i} = -\log K_{a,i}$  and  $K_{a,i} = [\text{LH}_{x-i}] \times [\text{H}] \times [\text{LH}_{(x+1)-i}]^{-1}$ .

<sup>[c]</sup> The standard deviations in brackets were calculated with:  $\sqrt{\frac{\sum_{i=0}^n (x_i - \bar{x})^2}{(n-1)}}$ ;  $x_i$  measured value;  $\bar{x}$  mean value; n number of values.

<sup>[d]</sup> Values from section 8.1.1.

As a result, the  $pK_{a,1} = 3.90$  of DCA is very acidic compared to the  $pK_{a,1} = 4.64$  which is assigned to the deprotonation of the carboxylic acid group of deferasirox. The ligand DCA ( $\text{LH}_4$ ) is neutral in charge and can easily deprotonate as demonstrated on the left side in **Scheme 6.1**. Since deferasirox only has one carboxylic acid group the ligand  $\text{LH}_3$  deprotonates with a higher  $pK_{a,1}$  as shown on the right side of **Scheme 6.1**.



**Scheme 6.1:** Stepwise deprotonation of the ligands DCA ( ${}^a\text{LH}_4$ ) and deferasirox ( ${}^b\text{LH}_3$ ).

Thus, the  $pK_{a,2} = 4.95(1)$  of DCA can be compared to the  $pK_{a,1} = 4.64(1)$  of deferasirox. The second  $pK_a$  of DCA is higher than the corresponding  $pK_{a,1}$  of deferasirox. This can easily be explained by the charge of the ligand. The second deprotonation occurs from the ligand species  $\text{LH}_3^-$  which has a negative charge. This causes a weaker acidity of the second carboxylic proton. Whereas, the ligand species for deferasirox is  $\text{LH}_3$  which is neutral of charge and the deprotonation is caused more easily. The protonation steps of deferasirox are given on the left side in **Scheme 6.1**. Once deprotonated, DCA will always have a higher negative charge than deferasirox and therefore deprotonation is hampered.

Taken together, we state that all comparable  $\log\beta$  and  $pK_a$  values of DCA (except  $pK_{a,1}$ ) are slightly higher than those of deferasirox due to the higher negative charge of DCA.

The complex formation of DCA was not investigated in detail. However, the ligand DCA forms dark violet complexes with  $\text{Fe}^{3+}$  in acidic solution and red complexes in alkaline solution just like deferasirox.

In conclusion, the ligand DCA was not suitable as an auxiliary ligand for further investigations of the complex formation of deferasirox. In essence, the ligand shows the same difficulty as deferasirox, too low water solubility for titration experiments in pure water solution.

## 7 The ligand DSA

The previously discussed ligand DCA was not sufficiently water soluble. As a result, we needed to design a ligand that fulfils the criteria for higher water solubility. The ligand MSA, having a sulfonic acid group instead of a carboxylic acid group, was just soluble enough in pure water to perform titration experiments. Its solubility in water is 0.7 g/L <sup>[37]</sup>. Even though being soluble in pure water precipitation still occurred during titration experiments. If we add a second sulfonic acid group we should enhance water solubility to a great extent. The disulfonic acid ligand DSA presented in **Figure 7.1** has two sulfonic acid groups and a water solubility of about 8 g/L, which is about 10 times higher than MSA and 20 times higher than deferasirox (0.4 g/L at pH 7.4 <sup>[38]</sup>).

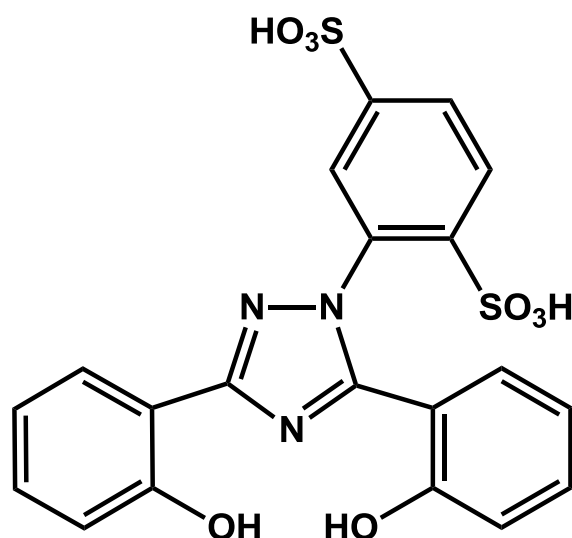


**Figure 7.1:** The structural formula of the ligand 2-[3,5-bis(2-hydroxyphenyl)-1*H*-1,2,4-triazol-1-yl]benzene-1,4-disulfonic acid (disulfonic acid derivative of deferasirox DSA).

Subsequently, the ligand DSA was sufficiently soluble to keep all complexes in solution. We used this ligand as an auxiliary ligand to elucidate the complex formation behaviour of deferasirox in pure water.

## 7.1 Determination of the $pK_a$ values of DSA

The expected  $pK_a$  values of DCA were well determined, as discussed previously. The  $pK_a$ s of the carboxylic acid groups range from 3.5 to 5. For this reason, they can easily be studied by continuous potentiometric titrations which are restricted to the range pH 2 to 12 <sup>[48]</sup>.

The ligands MSA and DSA are featuring sulfonic acid groups which are much more acidic than carboxylic acid groups. Subsequently, the first  $pK_a$  of MSA needed to be determined by a spectrophotometric batch titration between pH 1 and 2 <sup>[37, 40]</sup>. The two  $pK_a$ s of the hydroxyphenyl groups were investigated by continuous potentiometric titrations (see section 8.1.1). According to the studies with MSA we needed to determine the acidity constants of the ligand DSA with both methods mentioned, in pure water. Preliminary studies on the determination of the  $pK_a$  values were performed by F. Teucke, under my guidance <sup>[49]</sup>.

### 7.1.1 Determination of the $pK_{a,2}$ by spectrophotometric batch titration

The ligand DSA was synthesised as a fourfold protonated ligand  $LH_4$ . For titration purposes the ligand was dissolved in pure water. As a consequence of the strong acidity of two sulfonic acid groups the ligand is already partially deprotonated at the beginning of the continuous potentiometric titration. To determine these strong acidic equilibrium constants the pH range needed to be extended to pH < 2. This was carried out by performing a discontinuous spectrophotometric batch titration experiment between pH 1 and 2, hence to maintain the ionic strength 0.1 mol/L HCl/KCl was applied. The batch titrations were carried out by F. Teucke, under my supervision <sup>[49]</sup>. Each titration point was prepared separately in a thermostated double-walled glass vessel ( $T = 298$  K) by the procedure described in section 11.2.3. The determined  $pK_{a,2}$  value and the titration conditions chosen are given in **Table 7.1**.

This deprotonation step of the ligand DSA can be described by the reaction:

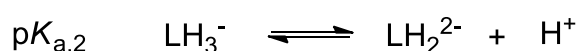


**Table 7.1:** A spectrophotometric batch titration experiment of the ligand DSA for the determination of the acidity constants  $pK_{a,2}$  <sup>[a]</sup>. The standard deviation of the value is given in brackets <sup>[b]</sup>. The titration conditions are given at  $T = 298$  K.

<b><math>pK_{a,2}</math> value of DSA</b>	
measuring method	spectrophotometric
method type	batch titration
solvent	pure water
$[L]_t$	40.0 $\mu\text{mol/L}$
titration volume	10.042 mL
titrant and supporting electrolyte	$c(\text{HCl}) + c(\text{KCl}) = 0.1 \text{ mol/L}$
pH range	1.00 – 2.00
volume of data points	10
equilibration time	24 h
range of wave length	$290 < \lambda < 380 \text{ nm}$
<b><math>pK_{a,2}</math></b>	<b>1.37(5)</b>
$\sigma_{\text{abs}}$ <sup>[c]</sup>	$1.9 \cdot 10^{-3}$
$\sigma_{\text{squares}}$ <sup>[c]</sup>	$1.5 \cdot 10^{-3}$

<sup>[a]</sup> For the ligand  $\text{LH}_x$  the  $pK_{a,i}$  is defined as:  $pK_{a,i} = -\log K_{a,i}$  and  $K_{a,i} = [\text{LH}_{x-i}] \times [\text{H}] \times [\text{LH}_{(x+1)-i}]^{-1}$

<sup>[b]</sup> The deviation given in brackets corresponds to the standard deviation taken from Specfit.

<sup>[c]</sup> The  $\sigma_{\text{abs}}$  and  $\sigma_{\text{squares}}$  values are taken from Specfit.

Furthermore, the experiment was repeated and a mean value calculated from the results of four titration experiments. The mean value is given in **Table 7.2** and compared with the  $pK_{a,1}$  for MSA. U. Heinz has determined the  $pK_{a,1}$  for MSA in his doctoral thesis under similar conditions as DSA: pure water,  $T = 298$  K and  $I = 0.1 \text{ mol/L KCl}$  <sup>[37]</sup>.

**Table 7.2:** Mean value of 4 batch titrations for the acidity constant  $pK_{a,2}$  <sup>[a]</sup> for the ligand DSA in pure water, T = 298 K and I = 0.1 mol/L HCl/KCl. Comparison to the  $pK_{a,1}$  of MSA in pure water, T = 298 K and I = 0.1 mol/L KCl.

Comparison $pK_a$ value of DSA and MSA			
measuring method		spectrophotometric	
method type		batch titration	
solvent		pure water	
supporting electrolyte		0.1 mol/L KCl	
<b>DSA</b>		<b>MSA</b>	
$pK_{a,1}$	<-2	-	-
$pK_{a,2}$ <sup>[b]</sup>	<b>1.33(8)</b>	$pK_{a,1}$ <sup>[b]</sup>	<b>1.12(4)</b> <sup>[c]</sup>

<sup>[a]</sup> For the ligand  $LH_x$  the  $pK_{a,i}$  is defined as:  $pK_{a,i} = -\log K_{a,i}$  and  $K_{a,i} = [LH_{x-i}] \times [H] \times [LH_{(x+1)-i}]^{-1}$

<sup>[b]</sup> The standard deviations in brackets were calculated with:  $\sqrt{\frac{\sum_{i=0}^n (x_i - \bar{x})^2}{(n-1)}}$ ;  $x_i$  measured value;  $\bar{x}$  mean value; n number of values.

<sup>[c]</sup> Value taken from doctoral thesis of U. Heinz <sup>[37]</sup>.

The acidity constant  $pK_{a,2}$  of DSA has a low value indicating the strong acidity of the deprotonation. If we compare the  $pK_{a,1}$  of MSA to this  $pK_{a,2}$  of DSA we recognize that the MSA acidity constant is about 0.2 units smaller. This can be explained by the fact that the ligand MSA is present before deprotonation as the neutral species  $LH_3$  which deprotonates more easily than the already once deprotonated species  $LH_3^-$  of DSA, with a negative charge.

The UV-VIS spectra measured for the determination of the  $pK_{a,2}$  of DSA are given in **Figure 7.2**. The spectra were recorded in the range  $230 < \lambda < 380$  nm. For evaluation we analysed the range  $290 < \lambda < 380$  nm with the program Specfit. The deprotonated ligand species  $LH_2^{2-}$  and the protonated ligand  $LH_3^-$  species were defined as coloured species in Specfit. This method is applicable resulting from the delocalisation of electrons in the aromatic systems of the ligand. Thus, we can ascertain there is a significant change in the spectra due to the deprotonation.

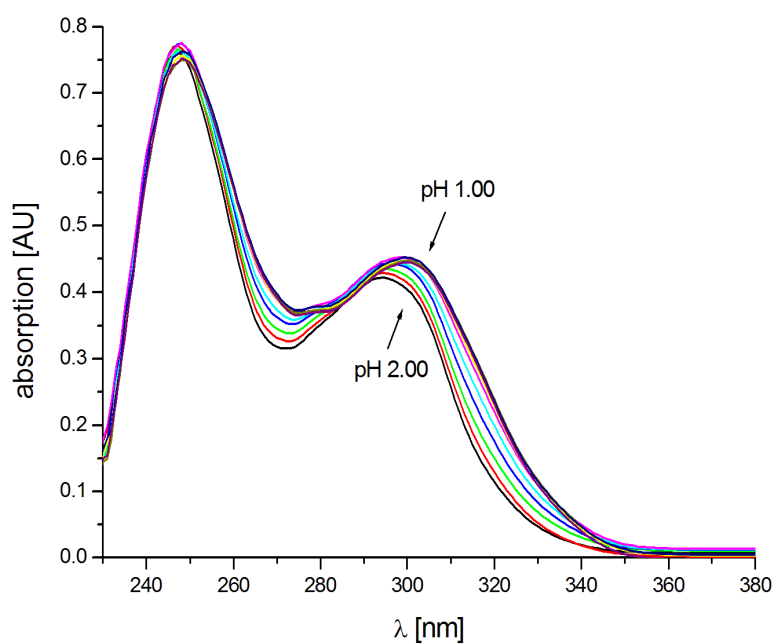


**Figure 7.2:** UV-VIS spectra of the batch titration of DSA collected from pH 1.00 – 2.00 (pure water,  $[\text{DSA}]_t = 40.0 \mu\text{mol/L}$ ,  $T = 298 \text{ K}$ ,  $I = 0.1 \text{ mol/L HCl/KCl}$ ).

The individual spectra for the two species taken from Specfit are presented in **Figure 7.3**.

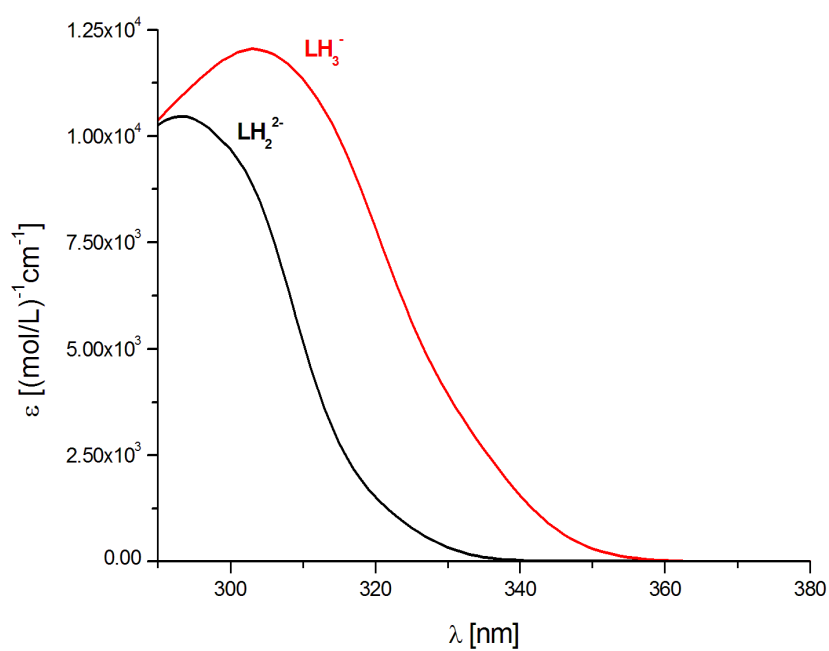


**Figure 7.3:** Individual spectra of the two species  $\text{LH}_3^-$  and  $\text{LH}_2^{2-}$  taken from Specfit.

The question is to which protonation site can this macroscopic protonation constant be assigned to? The two possibilities are either one of the sulfonic acid groups of DSA or one of the triazole nitrogen atoms in either 2 or 4 position of the ligand. The sulfonic acid groups are known to have very acidic protonation constants. Previous studies have reported on the determination of the  $pK_a$  values of arenesulfonic acids. In studies by Cerfontain et al. the  $pK_a$  values of arenesulfonic acids were investigated by UV spectroscopy<sup>[50]</sup> and <sup>1</sup>H-NMR-techniques<sup>[51]</sup>. In later studies by Crumrine et al. <sup>33</sup>S-NMR chemical shifts were employed to verify  $pK_a$  values of arenesulfonic acids<sup>[52-53]</sup>. They made use of the linear relation of the  $pK_a$  values to <sup>33</sup>S-NMR chemical shifts of arenesulfonic acids. In these studies they prepared aqueous solutions of the arenesulfonic acids and their sodium or potassium salts for NMR experiments. The  $pK_a$  values obtained for benzenesulfonic acid and its derivatives by <sup>33</sup>S-NMR technique were verified by  $pK_a$  values calculated from a Hammett plot.

Cerfontain reports have in common that the  $pK_a$  values needed to be examined in almost concentrated sulphuric acid. For this purpose the Hammett acidity function was applied and the Hammett acidity  $H_0$  varied. The  $pK_a$  values are obtained by extrapolation to dilute solution.

A summary of the  $pK_a$  values of benzenesulfonic acid and some derivatives is given in **Table 7.3**. As expected, the  $pK_a$  values are negative and therefore very acidic. The values have been determined with three different methods: UV spectroscopy, <sup>33</sup>S-NMR chemical shifts and with a Hammett Plot as reported by Crumrine et al.<sup>[53]</sup>. As a result these values seem to be very trustworthy.

A report by Benoit et al. also using <sup>13</sup>C-NMR spectroscopy to determine the acidity of benzenesulfonic acid suggests a  $pK_a$  value of -2.5(1) determined in H<sub>2</sub>O-H<sub>2</sub>SO<sub>4</sub> mixtures<sup>[54]</sup>. This value differs from those reported by Cerfontain and Crumrine. Benoit has only determined one arenesulfonic acid and it is not sure if this report is reliable. Nevertheless, Benoit also determined a negative  $pK_a$  value which shows the strong acidity of benzenesulfonic acid.

**Table 7.3:** The  $pK_a$  <sup>[a]</sup> value of benzenesulfonic acid and its derivatives determined with the UV spectroscopy and <sup>33</sup>S-NMR techniques at 312 K.

Substrate	$pK_a$ UV method <sup>[b]</sup>	$pK_a$ <sup>33</sup> S-NMR at 312 K <sup>[c]</sup>
C <sub>6</sub> H <sub>5</sub> SO <sub>3</sub> H	-6.65(5)	-6.66(4)
<i>m</i> -SO <sub>3</sub> -C <sub>6</sub> H <sub>5</sub> SO <sub>3</sub> Na <sub>2</sub>	–	-7.01(4)
<i>p</i> -SO <sub>3</sub> -C <sub>6</sub> H <sub>5</sub> SO <sub>3</sub> K <sub>2</sub>	–	-6.99(4)
<i>o</i> -CH <sub>3</sub> -C <sub>6</sub> H <sub>4</sub> SO <sub>3</sub> H	-6.55(5)	–
<i>m</i> -CH <sub>3</sub> -C <sub>6</sub> H <sub>4</sub> SO <sub>3</sub> H	-6.56(5)	-6.60(4)
<i>p</i> -CH <sub>3</sub> -C <sub>6</sub> H <sub>4</sub> SO <sub>3</sub> H	-6.59(5)	-6.57(4)
<i>p</i> -Br-C <sub>6</sub> H <sub>4</sub> SO <sub>3</sub> H	-6.86(5)	-6.87(4)
<i>m</i> -NO <sub>2</sub> -C <sub>6</sub> H <sub>4</sub> SO <sub>3</sub> H	–	-7.28(4)
<i>o</i> -NO <sub>2</sub> -C <sub>6</sub> H <sub>4</sub> SO <sub>3</sub> H	-6.68(5)	–
<i>p</i> -NO <sub>2</sub> -C <sub>6</sub> H <sub>4</sub> SO <sub>3</sub> Na	-6.57(5)	-7.21(4)
<i>p</i> -NH <sub>2</sub> -C <sub>6</sub> H <sub>4</sub> SO <sub>3</sub> K	–	-6.42(4)

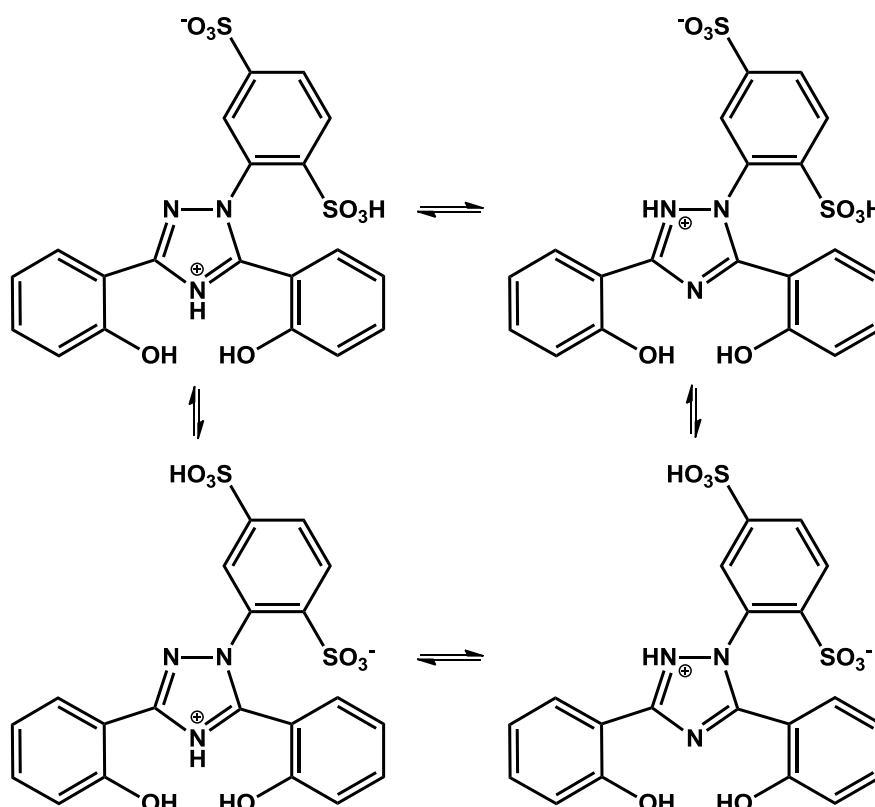
<sup>[a]</sup>  $pK_a$  is defined as  $-\log K_a$  with  $K_a = [\text{ArSO}_3^-] \times [\text{H}] \times [\text{ArSO}_3\text{H}]^{-1}$

<sup>[b]</sup> The  $pK_a$ s were taken from Cerfontain <sup>[50]</sup>. All arenesulfonic acids were employed in the acid form.

<sup>[c]</sup> The  $pK_a$ s were taken from Crumrine <sup>[53]</sup>.

In conclusion, these reports have shown that  $pK_a$  values of aromatic sulfonic acids cannot be determined in dilute aqueous solution. We suppose that the  $pK_{a,2}$  of DSA determined with spectrophotometric batch titration carried out in 0.1 mol/L HCl/KCl can be assigned to the protonation of the triazole unit.

The consequence of this assertion is that DSA is obtained as a zwitterion. An overview of the zwitterions tautomeric forms is presented in **Scheme 7.1**. The triazole ring could be protonated at the nitrogen atoms in position 2 or 4. Additionally, a protonation of the sulfonic acids could occur in position 1 or 4. Which of the tautomeric forms is favoured is not certain.



**Scheme 7.1:** Possible tautomeric forms of DSA as a zwitterion.

However, the protonation constant of the unsubstituted 1,2,4-triazole is known to the literature as  $pK_a = 2.38(5)$  ( $T = 298\text{ K}$ ,  $I = 0.1\text{ mol/L}$ )<sup>[55]</sup>. The benzene-1,4-disulfonic acid substituent at the nitrogen atom in position 1 should have a strong influence on the triazole ring. The sulfonic acid group has electron withdrawing properties (-M resonance effect). In addition, there are two electron withdrawing sulfonic acid groups which cause a decrease in electron density in the triazole unit. Consequently, the  $pK_a$  of the triazole nitrogen should also be decreased. The  $pK_a$  was determined to 1.33(8) for the deprotonation of the triazole unit of DSA. This  $pK_a$  is about 1.0 unit smaller than the  $pK_a$  of the unsubstituted 1,2,4-triazole. The effect of the benzene-1,4-disulfonic acid substituent seems to have influence on the electron density in the triazole unit.

Taken together, we have examined the  $pK_{a,2}$  of DSA in the pH range 1 – 2 in pure water. The  $pK_{a,2}$  value was determined to 1.33(8) and the protonation could be assigned to one of the triazole nitrogen atoms in position 2 or

4. From this confirmation we conclude that the structure of the ligand DSA is that of a zwitterion with one sulfonic acid and one triazole nitrogen protonated. This assumption is confirmed by a crystal structure discussed in section 7.1.3.

### 7.1.2 Determination of the $pK_{a,3}$ and $pK_{a,4}$ with potentiometric titrations

The ligand DSA has two other  $pK_a$  values which could be investigated by continuous potentiometric titrations. Preliminary titrations were carried out by F. Teucke, under my supervision <sup>[49]</sup>. The titration experiments were carried out in pure water at 298 K and with KCl as supporting electrolyte for constant ionic strength  $I = 0.1$  mol/L. Due to difficulties with the electrodes used by F. Teucke new titrations were carried out later with the Schott IoLine electrode.

We have determined the  $pK_{a,2}$  by spectrophotometric batch titration. However, we comprised the  $pK_{a,2}$  into the model used to calculate the  $pK_{a,3}$  and  $pK_{a,4}$  with the program Hyperquad2008. The  $pK_{a,2}$  varied considerably so that the value was obtained to improve the fit of the titration. For the determination of complexation constants the value from the spectrophotometric titration was applied.

An example titration with  $\log\beta$  and  $pK_a$  values is given in **Table 7.4**. Four protons are neutralised during the potentiometric titration. The first proton is already entirely dissociated at the beginning of the titration. The second proton is almost entirely dissociated subsequent the  $pK_{a,2}$  cannot be determined sufficiently. The other two  $pK_a$  values can be assigned to the deprotonations of the hydroxyphenyl rings. These values are in the expected range.

**Table 7.4:** An example titration experiment of the ligand DSA with overall protonation constants  $\log\beta_x$  <sup>[a]</sup> and acidity constants  $pK_{a,i}$  <sup>[b]</sup>. The standard deviations of the values are given in brackets <sup>[c]</sup>. The titration conditions are given at T = 298 K.

<b><math>\log\beta</math> and <math>pK_a</math> values of DSA</b>			
measuring method		potentiometric	
method type		continuous	
solvent		pure water	
[L] <sub>t</sub>		1.00 mmol/L	
[H] <sub>t</sub>		4.00 mmol/L	
titration volume		50.0 mL	
titrant		0.1 mol/L KOH	
supporting electrolyte		0.1 mol/L KCl	
electrode		Schott loLine	
$pK_w$		13.78	
pH range		2.7 – 10.9	
volume of data points		80	
time for mixing process		80 s	
$\sigma$ <sup>[d]</sup>		0.780	
$\log\beta_1$	<b>11.33(2)</b>	$pK_{a,1}$	<-2
$\log\beta_2$	<b>20.70(2)</b>	$[pK_{a,2}]$	1.79(6) <sup>[e]</sup>
$[\log\beta_3]$	22.49(6) <sup>[e]</sup>	<b><math>pK_{a,3}</math></b>	<b>9.37(2)</b>
$\log\beta_4$	–	<b><math>pK_{a,4}</math></b>	<b>11.33(2)</b>

<sup>[a]</sup> For the ligand L  $\log\beta_x$  is defined as:  $\beta_x = [LH_x] \times [L]^{-1} \times [H]^{-x}$ .

<sup>[b]</sup> For the ligand  $LH_x$  the  $pK_{a,i}$  is defined as:  $pK_{a,i} = -\log K_{a,i}$  and  $K_{a,i} = [LH_{x-i}] \times [H] \times [LH_{(x+1)-i}]^{-1}$ .

<sup>[c]</sup> The deviations given in brackets correspond to the threefold standard deviation taken from Hyperquad2008.

<sup>[d]</sup> The  $\sigma$  value is taken from Hyperquad2008.

<sup>[e]</sup> Value refined with Hyperquad2008, but not taken into account.

The calculated mean values for eight titration experiments are presented in **Table 7.5**. These mean values are calculated by arithmetic mean and standard deviation or by simultaneous evaluation of the 8 titrations with the program Hyperquad2008. In this table the value for  $pK_{a,2}$  was taken from the batch titration experiment as explained in section 7.1.1.

**Table 7.5:** Mean values of the overall protonation constants  $\log\beta_x$  <sup>[a]</sup> and acidity constants  $pK_{a,i}$  <sup>[b]</sup> for the ligand DSA determined by two methods in pure water, T = 298 K and I = 0.1 mol/L KCl.

<b>log<math>\beta</math> and p<math>K_a</math> values of DSA</b>			
mean values and standard deviations from 8 titrations <sup>[c]</sup>			
<b>log<math>\beta_1</math></b>	<b>11.32(2)</b>	<b>p<math>K_{a,1}</math></b>	<b>&lt;-2</b>
<b>log<math>\beta_2</math></b>	<b>20.67(3)</b>	<b>p<math>K_{a,2}</math> <sup>[d]</sup></b>	<b>1.33(8)</b>
<b>log<math>\beta_3</math> <sup>[d]</sup></b>	<b>22.00(8)</b>	<b>p<math>K_{a,3}</math></b>	<b>9.35(1)</b>
<b>log<math>\beta_4</math></b>	–	<b>p<math>K_{a,4}</math></b>	<b>11.32(2)</b>
mean values by simultaneous evaluation of 8 titrations <sup>[e]</sup>			
pH range		2.7 – 10.9	
$\sigma$ <sup>[f]</sup>		0.649	
<b>log<math>\beta_1</math></b>	<b>11.31(1)</b>	<b>p<math>K_{a,1}</math></b>	<b>&lt;-2</b>
<b>log<math>\beta_2</math></b>	<b>20.66(1)</b>	<b>p<math>K_{a,2}</math> <sup>[d]</sup></b>	<b>1.33(8)</b>
<b>log<math>\beta_3</math> <sup>[d]</sup></b>	<b>21.99(8)</b>	<b>p<math>K_{a,3}</math></b>	<b>9.35(1)</b>
<b>log<math>\beta_4</math></b>	–	<b>p<math>K_{a,4}</math></b>	<b>11.31(1)</b>

<sup>[a]</sup> For the ligand L  $\log\beta_x$  is defined as:  $\beta_x = [LH_x] \times [L]^{-1} \times [H]^{-x}$ .

<sup>[b]</sup> For the ligand  $LH_x$  the  $pK_{a,i}$  is defined as:  $pK_{a,i} = -\log K_{a,i}$  and  $K_{a,i} = [LH_{x-i}] \times [H] \times [LH_{(x+1)-i}]^{-1}$ .

<sup>[c]</sup> The standard deviations in brackets were calculated with:  $\sqrt{\frac{\sum_{i=0}^n (x_i - \bar{x})^2}{(n-1)}}$ ;  $x_i$  measured value;  $\bar{x}$  mean value; n number of values.

<sup>[d]</sup> The  $pK_{a,2}$  was taken from the batch titration described in section 7.1.1.

<sup>[e]</sup> The titrations were evaluated simultaneously with the program Hyperquad2008. The deviations given in brackets correspond to the threefold standard deviation taken from Hyperquad2008.

<sup>[f]</sup> The  $\sigma$  value is taken from Hyperquad2008.

The calculated arithmetic mean values for  $pK_{a,3} = 9.35(1)$  and  $pK_{a,4} = 11.32(2)$  are in very good agreement with the mean values calculated with Hyperquad2008  $pK_{a,3} = 9.35(1)$  and  $pK_{a,4} = 11.31(1)$ . The low deviations determined for both methods refer to the second decimal place. In addition, the  $\sigma$  value for the Hyperquad2008 calculation is  $< 1$  which demonstrates the good accordance of the measured titration curve with the calculated fit.

The titration curve for the  $pK_a$  titration of DSA is shown in **Figure 7.4**. A distinct inflection appears at 2 equivalents. It ranges from pH 4 to 8 and is initiated by the complete deprotonation of both strong acidic protons of the ligand.

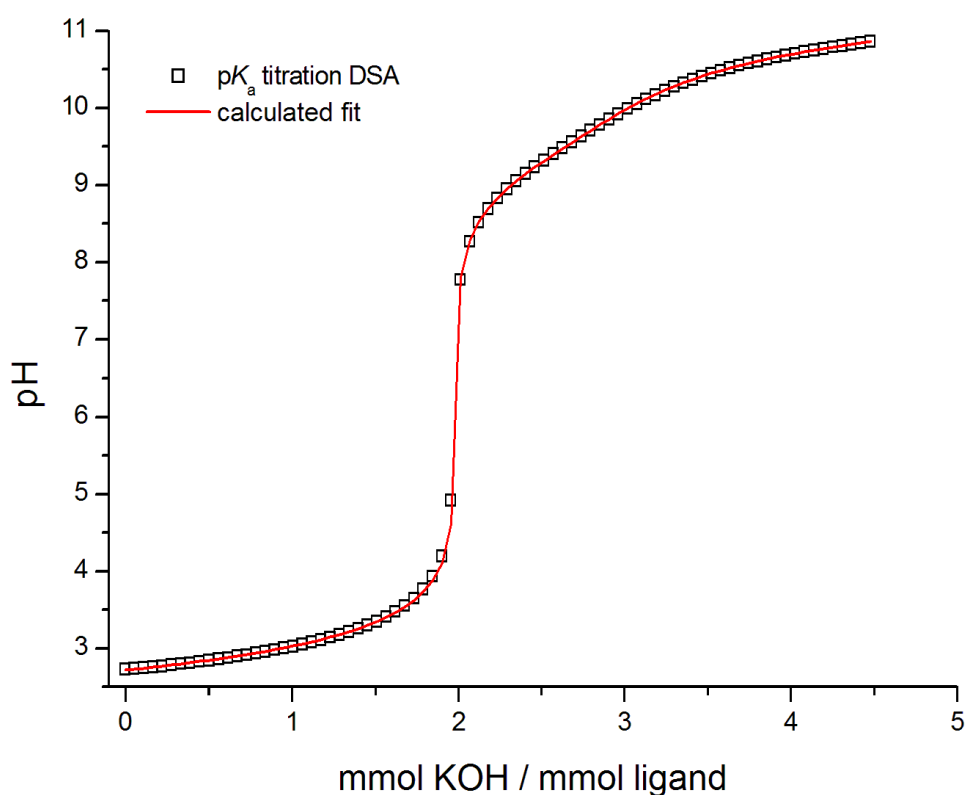


**Figure 7.4:** Potentiometric titration curve of the free ligand DSA in pure water,  $[L]_t = 1.00$  mmol/L,  $T = 298$  K and  $I = 0.1$  mol/L KCl. The open squares represent experimental points and the fit (solid line) was calculated from the equilibrium constants with Hyperquad2008.

The first proton, presumably corresponding to one of the sulfonic acids, was completely dissociated at the beginning of the titration. The second proton ( $pK_{a,2} = 1.33(8)$ ), assigned to one of the triazole nitrogen atoms, is completely deprotonated at pH 4 indicated by this inflection at 2 equivalents.

The two hydroxyphenyl protons of the ligand  $\text{LH}_2^{2-}$  are deprotonated in alkaline solution. Subsequently, at 4 equivalents the ligand is completely deprotonated.

On the basis of the equilibrium constants in **Table 7.5**, the species distribution diagrams of the ligand DSA are calculated as a function of pH, and the results are illustrated in **Figure 7.5**. The pH range from 1.00 to 2.00 depicts the batch titration performed for the determination of the  $\text{p}K_{\text{a},2}$ . The species  $\text{LH}_3^-$  is present at pH 1 by 68%. It is deprotonated to  $\text{LH}_2^{2-}$  which is formed at pH 2 by 83%. The pH range between pH 2.0 and 2.7 was not investigated.

In the continuous potentiometric titration starting at pH 2.7 the twofold protonated ligand  $\text{LH}_2^{2-}$  is predominant species over a long pH range. It reaches its maximum concentration of 100% after the inflection at pH 4 which corresponds to 2 equivalents in the titration curve. At pH 7  $\text{LH}_2^{2-}$  is deprotonated and the species  $\text{LH}^{3-}$  starts to form. This species reaches its highest peak 83% at pH 10.3. As the pH is raised from 9.3 to 10.9 the fully deprotonated ligand  $\text{L}^{4-}$  is formed. In essence, at the end of the titration  $\text{LH}^{3-}$  (72%) and  $\text{L}^{4-}$  (27%) are the dominant species and  $\text{LH}_2^{2-}$  only appears in low abundance.

In summary, for the evaluation of complexation constants of the ligand DSA the  $\text{p}K_{\text{a}}$  values are needed. We used the arithmetic mean values  $\text{p}K_{\text{a},3} = 9.35(1)$  and  $\text{p}K_{\text{a},4} = 11.32(2)$  from the potentiometric titration and the  $\text{p}K_{\text{a},2} = 1.33(8)$  from the batch titration for all further evaluations of DSA titration experiments.

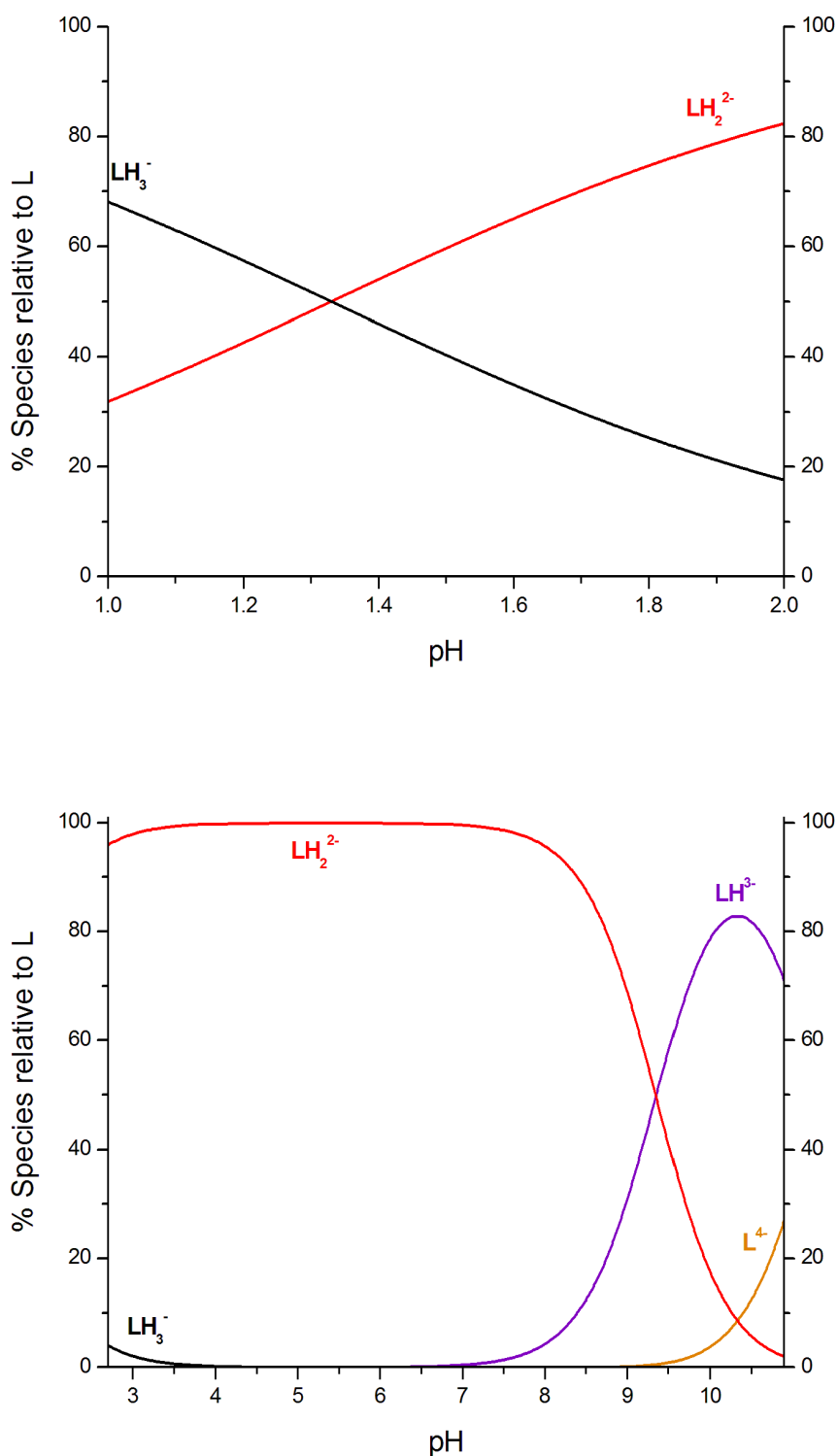


**Figure 7.5:** Species distribution diagram as a function of pH for the ligand DSA, batch titration experiment (top,  $[L]_i = 40.0 \mu\text{mol/L}$ , pure water,  $T = 298 \text{ K}$  and  $I = 0.1 \text{ mol/L KCl}$ ) for pH 1.00 - 2.00 and continuous potentiometric titration (bottom,  $[L]_i = 1.00 \text{ mmol/L}$ , pure water,  $T = 298 \text{ K}$  and  $I = 0.1 \text{ mol/L KCl}$ ) for pH 2.7 to 10.9. The species concentration were calculated from the equilibrium constants listed in **Table 7.5** (mean values from 8 titrations) with the program Hyss2006.

### 7.1.3 Crystal structures of the ligand DSA

The ligand DSA crystallized in two different structures. One structure shows the deprotonated ligand with  $\text{Cs}^+$  as counterions. The other structure shows the zwitterionic form of the ligand in the solid state.

#### The crystal structure $[\text{DSA-H}_4] \cdot 1.5 \text{ MeOH}$ as zwitterion

A crystal structure of the zwitterionic form of the ligand DSA was obtained by crystallization of the fourfold protonated ligand in methanol. The crystal structure was obtained by F. Teucke, under my supervision [49]. For crystallization the solution was kept in an exsiccator over ethyl acetate. Suitable single crystals were employed for X-ray analysis. The crystal structure is presented in **Figure 7.6**.

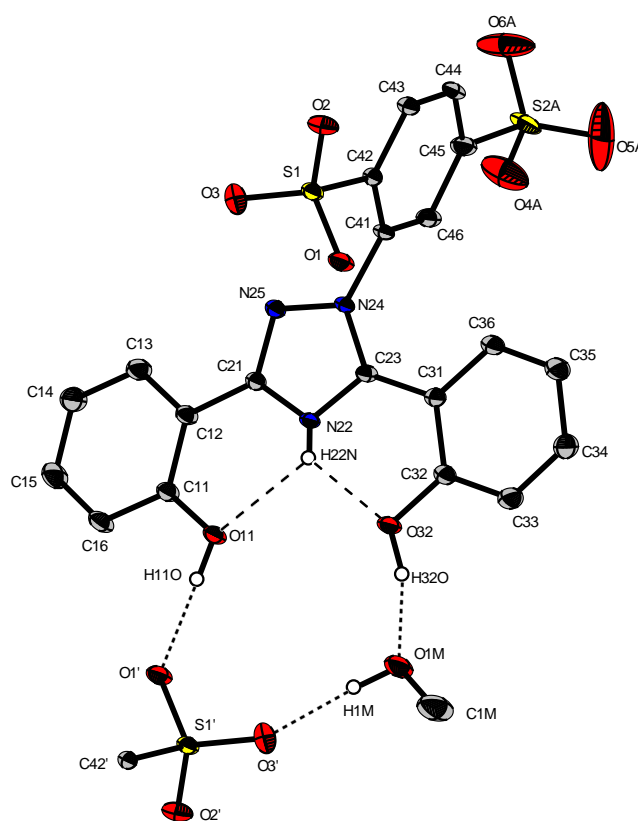


**Figure 7.6:** ORTEP-plot of the crystal structure of  $[\text{DSA-H}_4] \cdot 1.5 \text{ MeOH}$ . The atomic displacement ellipsoids are drawn at the 30% probability level (C = grey, H = white, N = blue, O = red and S = yellow). CH-hydrogen atoms are omitted for clarity. OH- and NH-hydrogen atoms are displayed with defined radius. In addition to the ligand entity the illustration shows an adjacent S1-sulfonic acid group and one molecule methanol. Hydrogen bonding interactions and weak interactions are depicted as dotted lines and dashed lines, respectively.

The ligand crystallizes in the monoclinic space group C2/c. The structure solution was found to be rather difficult attributed to the description of certain solvent molecules that crystallized with the ligand. Accordingly, the X-ray reflexes were revised with the corresponding electron density of the solvent molecules by the Squeeze option of the program Platon<sup>[56-57]</sup>. The subtracted electron density per ligand molecule was 44 electrons. It is difficult to assign these electrons to specific solvent molecules such as H<sub>2</sub>O, methanol or ethyl acetate. Yet, we can confirm that this electron density corresponds to four positions in the unit cell and all four positions note about equal amounts of electrons. The resulting R values ( $R_1 = 6.74\%$  and  $wR_2 = 21.04\%$ ) obtained by refinement without the solvent molecules are acceptable.

The high R values are also associated with the disorder of the S2-sulfonic acid group. For clarity, only the main position (70%) is presented in **Figure 7.6**. Perhaps, this disorder of the S2-sulfonic acid group can be attributed to the absence of hydrogen bonding interactions to stabilize it in a fixed position. In contrast, the position of the sulfonic acid S1 is stabilised by hydrogen bonding interactions between O1' and H-O11 of another DSA ligand molecule as well as between O3' and H1M of methanol. Moreover, the torsional angle (C42-C41-N24-N25) between the benzene-1,4-disulfonic acid moiety and the triazole plane is 91.6%. As a result, their positions are almost perpendicular to each other causing less interaction between the benzene-1,4-disulfonic acid moiety and the triazole plane. Further, the 2p-orbitals of the hydroxyphenyl rings from different ligand molecules in the structure interact with each other. Their arrangement is described by the term  $\pi$ -stacking. For this structure the hydroxyphenyl rings assemble with the spacing between 3.33 and 3.68 Å along the c-axis.

An isotropic refinement was possible for the hydrogen atoms H-O11, H-O32, H-N22 and H1M. The two protons H-O11 and H-O32 stabilize the hydroxyphenyl rings in a downward position by hydrogen bonding to O1' (of a neighbouring S1 sulfonic acid) and to O1M (methanol). Consequently, the hydroxyphenyl rings form a plane with the triazole unit in a torsional angle of maximum 5° from this plane. Further we note weak interactions of O11 and O32 of the hydroxyphenyl rings with H-N22 of the triazole unit also stabilizing

the almost flat geometry. Some bond distances and bond angles for the hydrogen bonding interactions and weak interactions are given in **Table 7.6**.

**Table 7.6:** Selected bond distances and bond angles <sup>[a]</sup> for the hydrogen bonding interactions and weak interactions for the structure of [DSA-H<sub>4</sub>] · 1.5 MeOH.

atom	bond distance [Å]	bond angle [°]
N22 – H22N ... O32	2.53	131.2
N22 – H22N ... O11	2.62	123.4
O32 – H32O ... O1M	2.53	156.7
O1M – H1M ... O3'	2.67	159.1
O11 – H11O ... O1'	2.67	172.5

<sup>[a]</sup> Determined with Diamond.

Special attention is to be paid to the protonation of the triazole nitrogen N22. The protonation at the nitrogen in position 4 of the 1,2,4-triazole unit was found by isotropic refinement. This is consistent with the assignment of the  $pK_{a,2}$  to a protonation at one of the triazole nitrogen atoms. The nitrogen N22 seems to be protonated more easily due to the weak interactions with the hydroxyphenyl rings. As a result, the ligand has a positive charge at this N22 nitrogen atom. Since there are no counterions in solution and the solvent molecule methanol of the structure is also protonated, one of the sulfonic acid groups must also be protonated. We could not refine any proton at either one of the sulfonic acids. We assume this is a result of the disorder of the sulfonic acid group S2.

Taken together, the ligand crystallized as a zwitterion protonated at the 1,2,4-triazole nitrogen N22 in position 4 and at one of the sulfonic acids. This confirms our prediction of the ligands structure in aqueous solution suggested in section 7.1.1.

### The crystal structure $\text{Cs}_4[\text{DSA-H}_2]_2 \cdot (\text{H}_2\text{O})_{13/6} \cdot \text{MeOH}$

The ligand DSA also crystallized as partly deprotonated ligand  $\text{LH}_2^{2-}$  with two  $\text{Cs}^+$  as counterions. The following structure crystallizes in the triclinic space group  $P\bar{1}$  from a methanol solution kept over ethyl acetate in an exsiccator. In the unit cell there are 4 ligand molecules and 8  $\text{Cs}^+$  counterions and in the asymmetric unit presented in **Figure 7.7** two ligand molecules with 4  $\text{Cs}^+$  counterions are displayed.

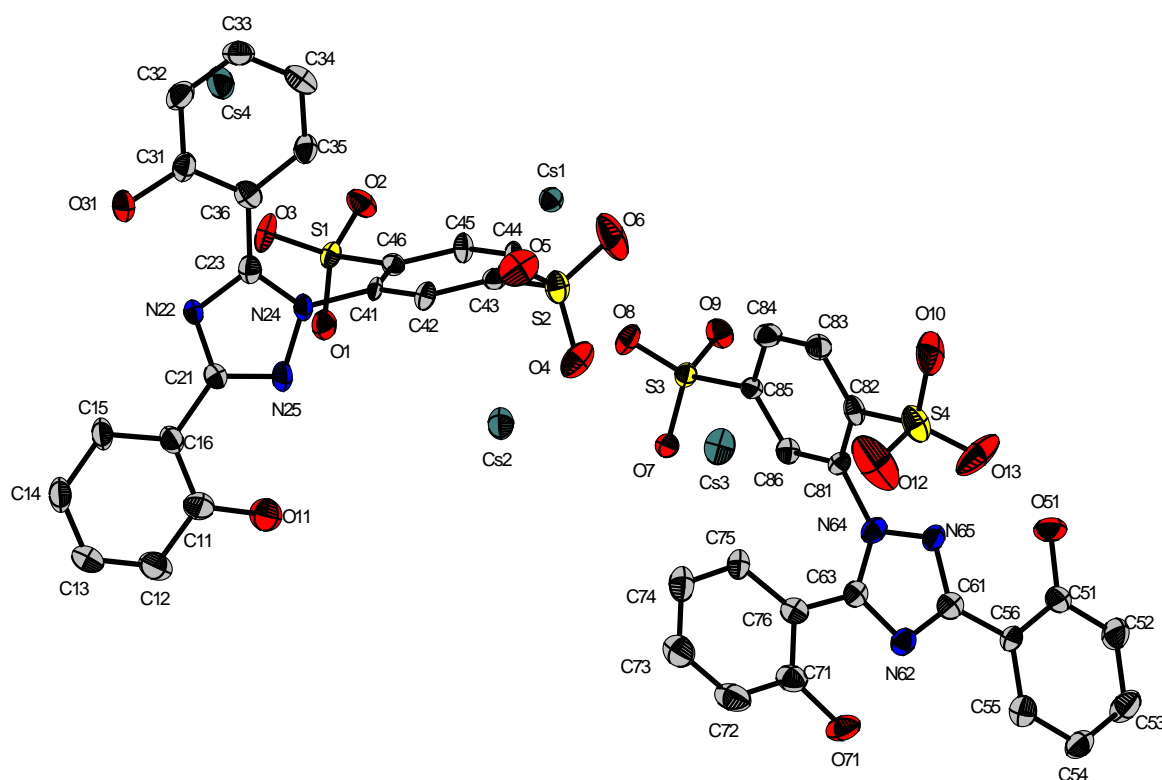


**Figure 7.7:** ORTEP-plot of the crystal structure of  $\text{Cs}_4[\text{DSA-H}_2]_2 \cdot (\text{H}_2\text{O})_{13/6} \cdot \text{MeOH}$ . The atomic displacement ellipsoids are drawn at the 50% probability level (C = grey, N = blue, O = red, S = yellow and Cs = petrol). CH-hydrogen atoms and solvent molecules are omitted for clarity.

The structure was solved and refined with 13/6 water and one methanol solvent molecules embedded into the structure. The R values we received for this solution of the structure with the programs SHELXS-97 and SHELXL-97 were:  $R_1 = 5.79\%$  and  $wR_2 = 15.19\%$ . Despite the good R values, the structure was not satisfying on account of the strong disorder of the solvent molecule

which could only be refined isotropic. For this reason, the X-ray reflexes were revised with the residual electron density in the structure by the Squeeze option of the program Platon. As a result, the new R values improved to  $R_1 = 5.43\%$  and  $wR_2 = 11.83\%$ . The residual electron density subtracted was 104.5 electrons corresponding to two ligand molecules. The solvent molecules mentioned above generate 44 electrons. We assume the remaining 60.5 electrons can be assigned to further solvent molecules which could not be located and refined. **Figure 7.7** shows this new refined crystal structure without the disordered solvent molecules.

In this structure the hydroxyphenyl rings also form a plane with the triazole unit. They are slightly tilted out of the plane by an angle of  $5.0^\circ$  for the ligand with the S1 and S2,  $8.9^\circ$  for the ligand with S3 and S4 sulphur atoms. Looking at the positions of the hydroxylic oxygen of the phenyl rings we will assess that one is pointing to the nitrogen atom in position 4 and one to the nitrogen atom in position 2 of the central 1,2,4-triazole unit at both ligands. According to the total charge of the ligand entities and the amount of  $\text{Cs}^+$  counterions we suggest that all hydroxyphenyl groups are protonated, even though the protons could not be refined. This explains their positions pointing towards the nitrogen atoms of the triazole unit presumably caused by hydrogen bonding interactions. The donor-accepter distances between the hydroxylic oxygen and the triazole nitrogen atoms are as expected for hydrogen bonding interactions and confirm our suggestion. These are summarized in **Table 7.7**.

**Table 7.7:** Donor-accepter distances <sup>[a]</sup> for hydrogen bonding interactions between hydroxyphenyl rings and triazole nitrogen atoms of  $\text{Cs}_4[\text{DSA-H}_2]_2 \cdot (\text{H}_2\text{O})_{13/6} \cdot \text{MeOH}$ .

atom	Donor-accepter distance [Å]
O11 – N25	2.66
O31 – N22	2.54
O51 – N65	2.66
O131 – N62	2.56

<sup>[a]</sup> Determined with Diamond.

The position of the benzene-1,4-disulfonic acid moiety of each of the two ligands is almost perpendicular to the triazole plane. The angle the two rings enclose is  $89.8^\circ$  for the ligand with S1 and S2 sulphur atoms and  $88.7^\circ$  with S3 and S4. Effectively, the rather bulky sulfonic acid groups gain maximum spacing to the hydroxyphenyl rings to inhibit steric interaction. Further the sulfonic acids arrange towards the  $\text{Cs}^+$  counterions since they are all deprotonated and negative in charge. This causes a layer like arrangement in the structure if we look along the b-axis as demonstrated in **Figure 7.8**. The four  $\text{Cs}^+$  counterions align in one layer with the sulfonic acids towards them. The triazole plains form the next layer with two stacked ligands generated by an inversion centre.

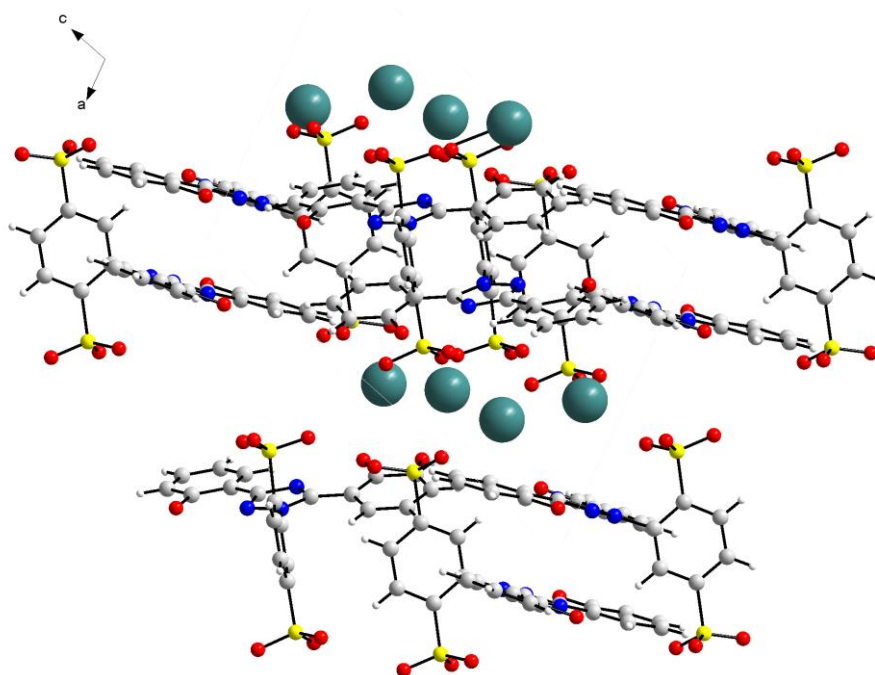


**Figure 7.8:** Layers in the structure  $\text{Cs}_4[\text{DSA-H}_2]_2 \cdot (\text{H}_2\text{O})_{13/6} \cdot \text{MeOH}$  (C = grey, N = blue, O = red, S = yellow and Cs = petrol). View along the b-axis.

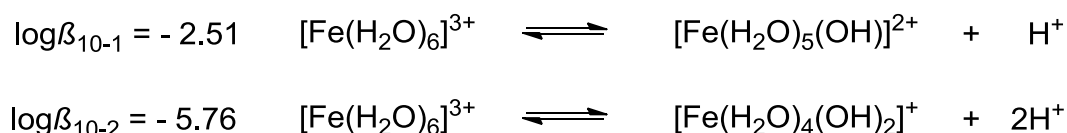
The ligand DSA crystallized as twice deprotonated ligand  $\text{LH}_2^{2-}$  when  $\text{Cs}^+$  is present as counterions. In contrast to the structure without counterions mentioned above, the triazole nitrogen is not protonated, consequently the protonated hydroxyphenyl rings turn towards the nitrogen atoms in position 2 and 4 of the 1,2,4-triazole unit initiated by hydrogen bonding interactions. In both structures the benzene-1,4-disulfonic acid is nearly perpendicular to the triazole plane and achieves less steric hindrance.

## 7.2 Complex formation of DSA with iron (III)

The ligand DSA was designed to resemble the iron chelating ligand deferasirox in all its characteristics yet it is improved regarding water solubility of the ligand itself and its metal complexes. The complexation chemistry of the ligand deferasirox with  $\text{Fe}^{3+}$  has been investigated by U. Heinz and S. Stucky (formerly S. Steinhauser) [37, 39]. Since the ligand was poorly soluble in pure water the complexation constants were first determined by U. Heinz [37] in water/DMSO medium with a molar fraction of  $x_{\text{DMSO}} = 0.20$  and then extrapolated to pure water by S. Stucky [39]. The results of these investigations are summarized in an article in the European Journal of Inorganic Chemistry [40].

### 7.2.1 Determination of the stability constant of the $[\text{Fe}(\text{DSA})]^-$ complex by spectrophotometric batch titration in pure water

The strong complexation of deferasirox with  $\text{Fe}^{3+}$  made it necessary to determine the complexation constant of the mono-complex below pH 2 due to complete complex formation at the beginning of the titrations. The complexation of DSA with  $\text{Fe}^{3+}$  is in accordance with deferasirox. It shows very strong complexation with  $\text{Fe}^{3+}$  and forms a violet 1:1 complex at very low pH. Consequently, this stability constant was determined with spectrophotometric batch titrations from pH 1.00 to 2.03 as described in section 11.2.3. The titration experiments were carried out by F. Teucke, under my guidance [49]. For the determination of the stability constant of the  $[\text{Fe}(\text{L})]^-$  (110) complex of DSA the hydrolysis of the  $[\text{Fe}(\text{H}_2\text{O})_6]^{3+}$  complex was taken into account. The following formation constants presented in **Scheme 7.2** were calculated from values taken from the NIST Database [55].



**Scheme 7.2:** Formation constants  $\log\beta_{10-1}$  ( $\text{H}_2\text{O}$ ,  $T = 298 \text{ K}$ ,  $I = 0.1 \text{ mol/L}$ ) and  $\log\beta_{10-2}$  ( $\text{H}_2\text{O}$ ,  $T = 298 \text{ K}$ ,  $I = 0.5 \text{ mol/L}$  \*) of the hydrolysis products of  $[\text{Fe}(\text{H}_2\text{O})_6]^{3+}$  [55]. (\*  $I = 0.1 \text{ mol/L}$  was not available).

The stability constant of an example batch titration and the titration conditions is summarized in **Table 7.8**.

**Table 7.8:** A spectrophotometric batch titration experiment of  $\text{Fe}^{3+}$  with DSA for the determination of the stability constant  $\log\beta_{xyz}$  <sup>[a]</sup> for the complex  $[\text{Fe}(\text{DSA})]^-$ . The titration conditions are given at  $T = 298 \text{ K}$ .

<b>Stability constant for <math>[\text{Fe}(\text{DSA})]^-</math></b>	
measuring method	spectrophotometric
method type	batch titration
solvent	pure water
molar ratio M:L	1:1
$[\text{M}]_t$	0.20 mmol/L
$[\text{L}]_t$	0.20 mmol/L
titration volume	10.266 mL
Titrant and supporting electrolyte	$c(\text{HCl}) + c(\text{KCl}) = 0.1 \text{ mol/L}$
pH range	1.00 – 2.03
volume of data points	10
equilibration time	24 h
range of wave length	$400 < \lambda < 900 \text{ nm}$
$\log\beta_{10-1}$ <sup>[b]</sup>	-2.51
$\log\beta_{10-2}$ <sup>[b]</sup>	-5.76
<b><math>\log\beta_{110}</math> <sup>[c]</sup></b>	<b>23.54(1)</b>
$\sigma_{\text{abs}}$ <sup>[d]</sup>	$1.7 \cdot 10^{-3}$
$\sigma_{\text{squares}}$ <sup>[d]</sup>	$1.5 \cdot 10^{-2}$

<sup>[a]</sup> For the ligand L  $\log\beta_{xyz}$  is defined as:  $\beta_{xyz} = [\text{M}_x\text{L}_y\text{H}_z] \times [\text{M}]^{-x} \times [\text{L}]^{-y} \times [\text{H}]^{-z}$ .

<sup>[b]</sup> Values were calculated from overall formation constants taken from the NIST Database <sup>[55]</sup>.

<sup>[c]</sup> The deviation given in brackets corresponds to the standard deviation taken from Specfit.

<sup>[d]</sup> The  $\sigma_{\text{abs}}$  and  $\sigma_{\text{squares}}$  values are taken from Specfit.

A mean value of the stability constant was calculated from 5 batch titration experiments all carried out with the same conditions as described above. This mean value is given in the **Table 7.9** and compared to the [Fe(MSA)] (110) complex of the monosulfonic acid derivative MSA.

**Table 7.9:** Mean value of 5 batch titrations for the stability constant  $\log\beta_{xyz}$  <sup>[a]</sup> for [Fe(DSA)]<sup>-</sup> in pure water, T = 298 K and I = 0.1 mol/L HCl/KCl. Comparison to the [Fe(MSA)] complex.

Mean $\log\beta_{110}$ value of the [Fe(DSA)] <sup>-</sup> complex			
measuring method		spectrophotometric	
method type		batch titration	
solvent		pure water	
supporting electrolyte		0.1 mol/L KCl	
<b>DSA</b>		<b>MSA</b>	
$\log\beta_{110}$ <sup>[b]</sup>	<b>23.54(4)</b>	$\log\beta_{110}$ <sup>[c]</sup>	<b>21.30(4)</b>

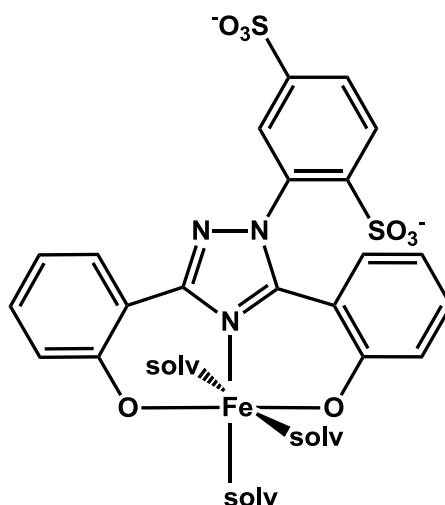
<sup>[a]</sup> For the ligand L  $\log\beta_{xyz}$  is defined as:  $\beta_{xyz} = [M_xL_yH_z] \times [M]^{-x} \times [L]^{-y} \times [H]^{-z}$ .

<sup>[b]</sup> The standard deviations in brackets were calculated with:  $\sqrt{\frac{\sum_{i=0}^n (x_i - \bar{x})^2}{(n-1)}}$ ;  $x_i$  measured value;  $\bar{x}$  mean value; n number of values.

<sup>[c]</sup> Value taken from S. Steinhauser <sup>[40]</sup>.

The stability constant of the 110 complex of DSA is slightly higher and therefore more stable than the 110 complex of MSA. The geometry of the [Fe(DSA)]<sup>-</sup> complex is depicted in **Scheme 7.3**. It has a negative charge in contrast to the [Fe(MSA)] complex. Protonated [Fe(LH)]<sup>2-</sup> (111) complexes were not verified for both ligands. To form a 111 complex both ligands need to be protonated at either a sulfonic acid group or a triazole nitrogen atom. The sulfonic acids are much too acidic and the triazole nitrogen has a protonation constant of  $pK_{a,2} = 1.33(8)$  for DSA and  $pK_{a,1} = 1.12(1)$  for MSA. The favoured coordination mode of the ligand with Fe<sup>3+</sup> is a tridentate meridional coordination mode. Consequently, it is unfavourable to protonate the triazole nitrogen. A model with a 111 complex for DSA could not be calculated for all batch titration

experiments. Possible values for a 1:1 complex were not consistent. As a consequence, we decided not to take this complex into account.



**Scheme 7.3:** Possible tridentate meridional coordination of the  $[\text{Fe}(\text{DSA})]^-$  complex (110; solv = solvent molecule).

If we compare the complexation of DSA with  $\text{Fe}^{3+}$  between pH 1 and 2 with that of deferasirox, the sole species found with deferasirox is a  $[\text{Fe}(\text{LH})]^+$  complex instead of a  $[\text{Fe}(\text{L})]$  complex. The ligand deferasirox has a carboxylic acid functional group which has a  $\text{pK}_{\text{a},1} = 4.64(1)$  ( $x_{\text{DMSO}} = 0.20$ ,  $T = 298$  K,  $I = 0.1$  mol/L KCl, section 8.1.1). Accordingly, the carboxylic acid is protonated between pH 1 – 2. As a result, the ligand species forming the complex with  $\text{Fe}^{3+}$  is  $\text{LH}^{2-}$  which forms the complex in a tridentate meridional coordination mode. Further, all three ligands deferasirox, MSA and DSA arrange in the same coordination mode, yet deferasirox is protonated at the peripheral benzo-carboxylic acid group.

The absorption spectra for the batch titration of  $\text{Fe}^{3+}$  with DSA were collected in the range  $200 < \lambda < 1000$  nm and analysed in the range  $400 < \lambda < 900$  nm as presented in **Figure 7.9**. The  $[\text{Fe}(\text{DSA})]^-$  complex exhibits an absorption maximum at 516 nm. For evaluation with the program Specfit a spectrum of a 0.2 mmol/L  $\text{Fe}^{3+}$  solution was also collected and provided to Specfit as a known spectrum. In Specfit  $\text{Fe}^{3+}$  and the 110 complex were defined as coloured species. All ligand species and the iron hydroxo complexes were defined as non-coloured. The individual spectra of the  $[\text{Fe}(\text{L})]^-$  complex and free  $\text{Fe}^{3+}$  are illustrated in **Figure 7.10**.

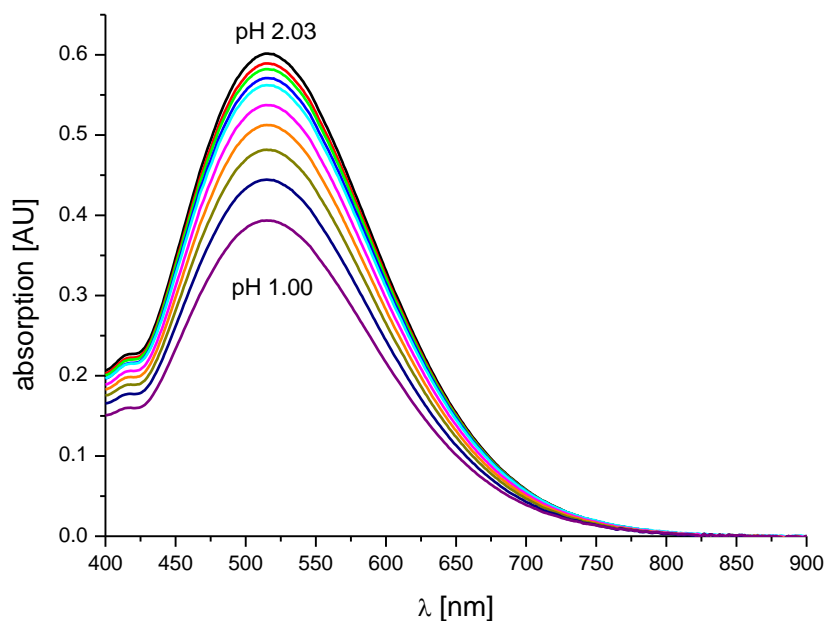


**Figure 7.9:** UV-VIS spectra of the batch titration of the [Fe(DSA)]<sup>-</sup> complex collected from pH 1.00 – 2.03 (pure water, [Fe<sup>3+</sup>]<sub>t</sub> = 0.20 mmol/L, [DSA]<sub>t</sub> = 0.20 mmol/L, T = 298 K, I = 0.1 mol/L HCl/KCl).

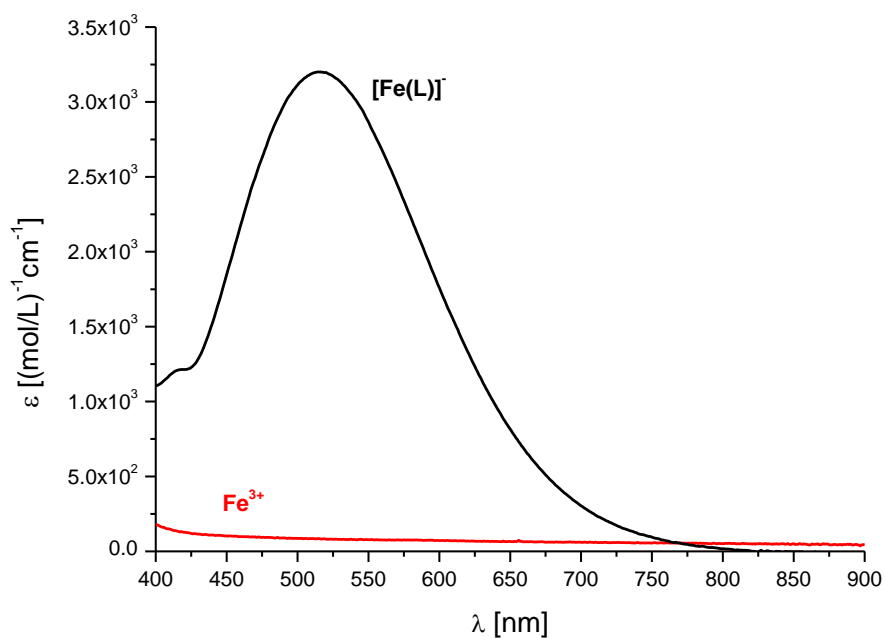


**Figure 7.10:** Individual spectra of the batch titration of the [Fe(DSA)]<sup>-</sup> complex generated with the program Specfit.

The spectra give rise to only one species  $[\text{Fe}(\text{L})]^-$  in solution. Further, the  $\text{Fe}^{3+}$  spectrum with its maximum absorbance at 315 nm has little influence on the spectra of the  $[\text{Fe}(\text{DSA})]^-$  complex.

Taken together, the ligand DSA forms a violet  $[\text{Fe}(\text{DSA})]^-$  complex ( $\lambda_{\text{max}}$  at 516 nm) with  $\text{Fe}^{3+}$  in acidic aqueous solution. Its stability constant is  $\log\beta_{110} = 23.54(4)$ . It forms the 110 complex like MSA, attributed to the unfavourable protonation of this 110 complex. Deferasirox differs from these two ligands only in the protonation at the peripheral carboxylic acid group which forms a  $[\text{Fe}(\text{LH})]^+$  complex in acidic solution. The 110 complex of deferasirox and  $\text{Fe}^{3+}$  is formed above pH 2 in water/DMSO solution with a molar fraction of  $x_{\text{DMSO}} = 0.20$ . Further, the stability constant for this deferasirox complex in pure water is  $\log\beta_{110} = 22.0$  <sup>[40]</sup>, therefore somewhat smaller than the stability constant of the  $[\text{Fe}(\text{DSA})]^-$  complex. In essence, we suggest that all three ligands deferasirox, MSA and DSA adopt the same tridentate meridional coordination mode with  $\text{Fe}^{3+}$  in solution. As a result, DSA is very similar to deferasirox in its complex formation with  $\text{Fe}^{3+}$  in acidic solution.

### 7.2.2 Continuous potentiometric and spectrophotometric titrations of DSA with iron (III)

To investigate the complex formation of DSA with iron (III) above pH 2 continuous potentiometric titrations were performed in aqueous solution. The ligand deferasirox and MSA form bis-complexes with  $\text{Fe}^{3+}$  in which two ligands are bound to one  $\text{Fe}^{3+}$  central ion. As a consequence, titration experiments were carried out with a  $\text{Fe}^{3+}:\text{DSA}$  1:2 and 1:3 molar ratio. Spectrophotometric titration data was collected simultaneously to the potentiometric titrations. Preliminary titrations were carried out by F. Teucke <sup>[49]</sup>. Owing to difficulties with the applied electrodes, the titrations were repeated with a new electrode Schott loLine. For the evaluation of both potentiometric and spectrophotometric titrations the hydrolysis of the  $[\text{Fe}(\text{H}_2\text{O})_6]^{3+}$  complex was taken into account (see **Scheme 7.2**). Titration conditions and values of the potentiometric titrations for both molar ratios are listed in **Table 7.10**.

**Table 7.10:** Example titration experiments of the complexation of Fe<sup>3+</sup> with DSA. Overall stability constants  $\log\beta_{xyz}$ <sup>[a]</sup> are listed. The titration conditions are given at T = 298 K.

<b><math>\log\beta</math> values for the complexation of Fe<sup>3+</sup> with DSA</b>		
molar ratio of M:L	1:2	1:3
measuring method	potentiometric	potentiometric
method type	continuous	continuous
solvent	pure water	pure water
[M] <sub>t</sub>	0.48 mmol/L	0.33 mmol/L
[L] <sub>t</sub>	1.00 mmol/L	1.00 mmol/L
titration volume	50.0 mL	50.0 mL
titrant	0.1 mol/L KOH	0.1 mol/L KOH
supporting electrolyte	0.1 mol/L KCl	0.1 mol/L KCl
electrode	Schott IoLine	Schott IoLine
pK <sub>w</sub>	13.78	13.78
pH range	3.0 – 5.3	3.0 – 4.8
volume of data points	54	50
time for mixing process	900 s	900 s
$\sigma$ <sup>[b]</sup>	0.865	0.656
$\log\beta_{10-1}$ <sup>[c]</sup>	-2.51	-2.51
$\log\beta_{10-2}$ <sup>[c]</sup>	-5.76	-5.76
$\log\beta_{110}$ <sup>[d]</sup>	23.54(4)	23.54(4)
<b><math>\log\beta_{120}</math><sup>[e]</sup></b>	<b>39.51(2)</b>	<b>39.44(2)</b>
<b><math>\log\beta_{121}</math><sup>[e]</sup></b>	<b>43.71(4)</b>	<b>43.50 (4)</b>

<sup>[a]</sup> For the ligand L  $\log\beta_{xyz}$  is defined as:  $\beta_{xyz} = [M_xL_yH_z] \times [M]^{-x} \times [L]^{-y} \times [H]^{-z}$ .

<sup>[b]</sup> The  $\sigma$  value is taken from Hyperquad2008.

<sup>[c]</sup> Values were calculated from overall formation constants taken from the NIST Database <sup>[55]</sup>.

<sup>[d]</sup> Value determined by spectrophotometric batch titration (section 7.1.1).

<sup>[e]</sup> The deviations given in brackets correspond to the threefold standard deviation taken from Hyperquad2008.

The  $[\text{Fe}(\text{DSA})]^-$  complex has already been formed at the beginning of the continuous potentiometric titration for evaluations with the programs Hyperquad2008 and Specfit the known stability constant of the  $[\text{Fe}(\text{DSA})]^-$  complex was set as a constant value. Mean values of the stability constants of each molar ratio were calculated. Additionally, all 12 titrations from both molar ratios were evaluated simultaneously. The mean values are summarized in **Table 7.11**. All mean values are very similar however the values studied by simultaneous evaluation are more precise due to both molar ratios being taken into account. Nevertheless, all evaluations lead to the same model with the two species  $[\text{Fe}(\text{L})_2]^{5-}$  (120 complex) and  $[\text{Fe}(\text{L})(\text{LH})]^{4-}$  (121 complex).

**Table 7.11:** Mean values of the overall stability constants  $\log\beta_{xyz}$  <sup>[a]</sup> from potentiometric titrations of  $\text{Fe}^{3+}$  with DSA determined by two methods in pure water,  $T = 298 \text{ K}$  and  $I = 0.1 \text{ mol/L}$  KCl.

<b><math>\log\beta</math> values for the complexation of <math>\text{Fe}^{3+}</math>: DSA</b>			
1:2		1:3	
mean values of 6 titrations <sup>[b]</sup>		mean values of 6 titrations <sup>[b]</sup>	
$\log\beta_{120}$	39.53(7)	$\log\beta_{120}$	39.5(1)
$\log\beta_{121}$	43.76(7)	$\log\beta_{121}$	43.6(1)
mean values by simultaneous evaluation of all 12 titrations <sup>[c]</sup>			
$\sigma$ <sup>[d]</sup>		1.626	
<b><math>\log\beta_{120}</math></b>		<b>39.50(2)</b>	
<b><math>\log\beta_{121}</math></b>		<b>43.67(3)</b>	

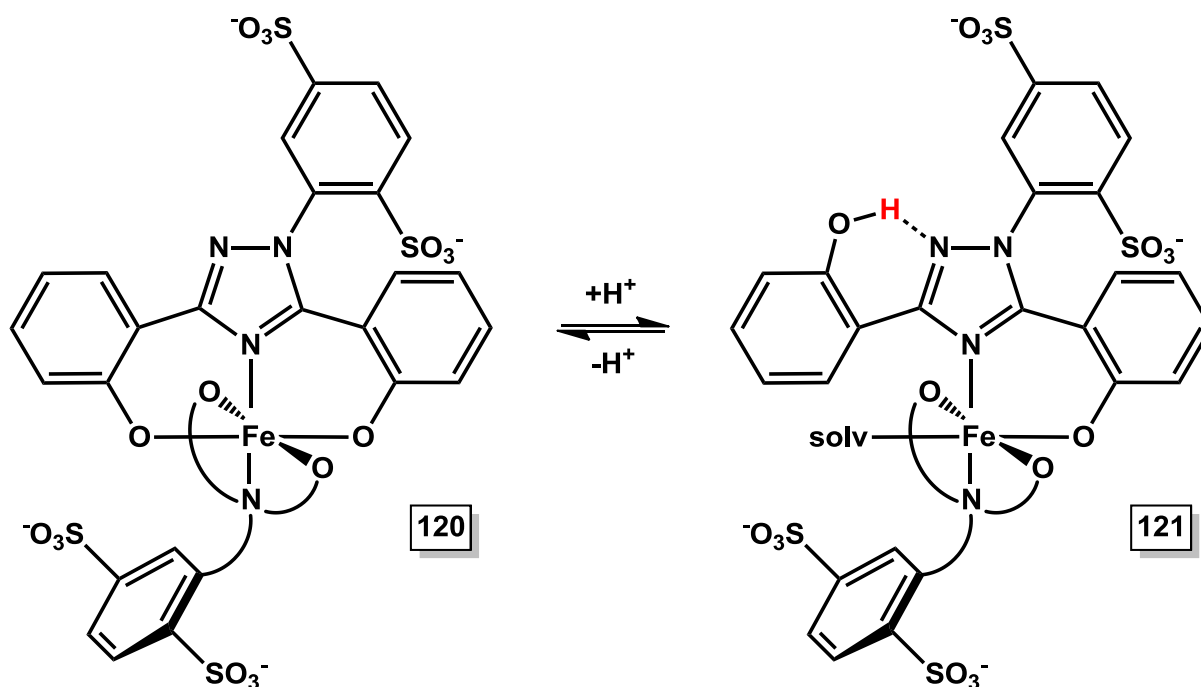
<sup>[a]</sup> For the ligand L  $\log\beta_{xyz}$  is defined as:  $\beta_{xyz} = [\text{M}_x\text{L}_y\text{H}_z] \times [\text{M}]^{-x} \times [\text{L}]^{-y} \times [\text{H}]^{-z}$ .

<sup>[b]</sup> The standard deviations in brackets were calculated with:  $\sqrt{\frac{\sum_{i=0}^n (x_i - \bar{x})^2}{(n-1)}}$ ;  $x_i$  measured value;  $\bar{x}$  mean value; n number of values.

<sup>[c]</sup> The titrations were evaluated simultaneously with the program Hyperquad2008. The deviations given in brackets correspond to the threefold standard deviation taken from Hyperquad2008.

<sup>[d]</sup> The  $\sigma$  value is taken from Hyperquad2008.

The bis-complex  $[\text{Fe}(\text{L})_2]^{5-}$  with two ligands bound to one central  $\text{Fe}^{3+}$  ion and a protonated form  $[\text{Fe}(\text{L})(\text{LH})]^{4-}$  of it were determined. The suggested coordination geometry of these complexes is illustrated in **Scheme 7.4**.



**Scheme 7.4:** Suggested coordination geometries of the  $\text{Fe}^{3+}$ -DSA bis-complexes  $[\text{Fe}(\text{L})_2]^{5-}$  (120) and  $[\text{Fe}(\text{L})(\text{LH})]^{4-}$  (121).

The  $[\text{Fe}(\text{DSA})_2]^{5-}$  complex adopts a tridentate meridional coordination geometry which is consistent with a crystal structure described in section 7.2.3. The protonation of the 120 complex can only occur at one of the phenolate groups thus the sulfonic acids, and the triazole nitrogen are too acidic. An apparent  $\text{p}K_a = 4.17$  value was determined for the deprotonation of the  $[\text{Fe}(\text{L})(\text{LH})]^{4-}$  complex of DSA. It is noteworthy that this is only an apparent  $\text{p}K_a$  owing to the combination of two steps. For once the phenolate group is deprotonated and second the Fe-O bond is formed resulting in a tridentate coordination mode from the bidentate. The apparent  $\text{p}K_a$  value of the deprotonation of the 121 complex comprehends both of these reactions. Further, this type of deprotonation will be referred to as an apparent  $\text{p}K_a$  value in this thesis. We assume that the phenolate group in position 3 of the triazole ring will be favoured by the protonation since it can rotate towards the nitrogen atom in posi-

tion 2 and form hydrogen bonding interactions as depicted above. Consequently, one ligand is bound tridentate and one ligand bidentate to the  $\text{Fe}^{3+}$  central ion. The free binding site is occupied by a solvent molecule.

The strong complexation of DSA with  $\text{Fe}^{3+}$  can also be deduced from the titration curves of both molar ratios compared to the  $\text{p}K_a$  titration curve as demonstrated in **Figure 7.11**. The titrations start at about pH 3 and were carried out to about pH 5 to prevent formation of iron hydroxide in solution.

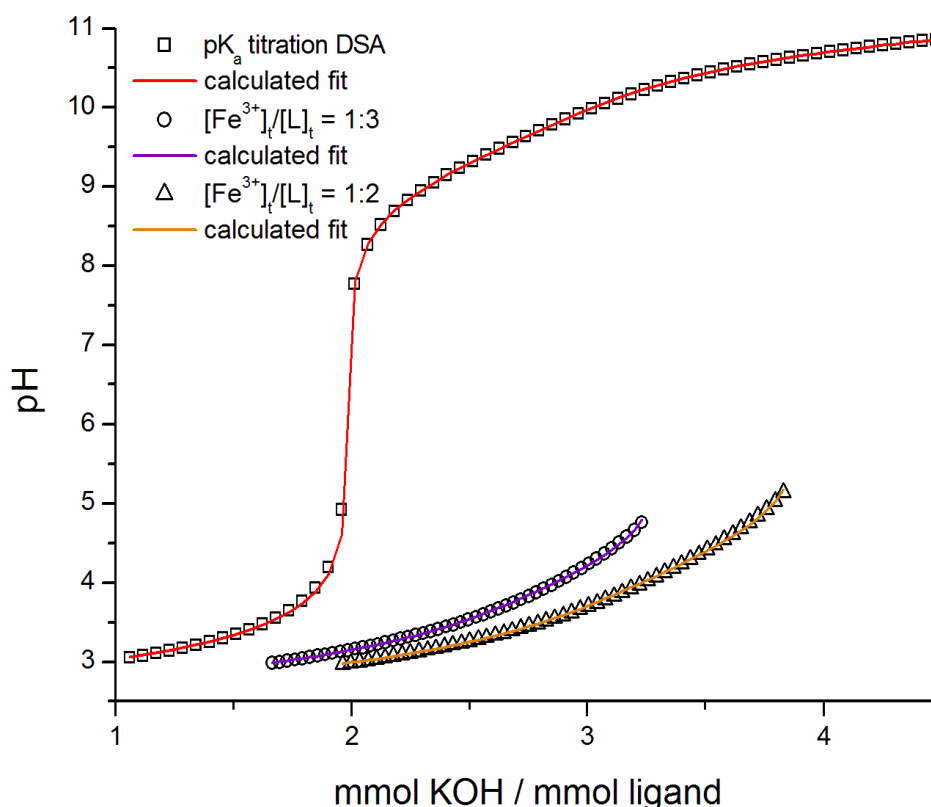


**Figure 7.11:** Potentiometric titration curves of the free ligand DSA and  $\text{Fe}^{3+}$  with DSA with the molar ratios 1:2 ( $[\text{Fe}^{3+}]_t = 0.48$  mmol/L,  $[\text{L}]_t = 1.00$  mmol/L) and 1:3 ( $[\text{Fe}^{3+}]_t = 0.33$  mmol/L,  $[\text{L}]_t = 1.00$  mmol/L) in pure water,  $T = 298$  K and  $I = 0.1$  mol/L KCl. The open squares, circles and triangles represent experimental points and the fit (solid line) was calculated from the equilibrium constants with Hyperquad2008.

The potentiometric titration with a  $\text{Fe}^{3+}$ :DSA 1:2 molar ratio has an inflection point at four equivalents. The inflection points were not evaluated and are not displayed in the graph. The strong pH decrease of the 1:2 molar ratio titration curve compared to the  $\text{p}K_a$  titration curve shows that complexation proceeds throughout the titration. As a consequence, all four protons were re-

leased into solution causing the inflection at four equivalents. The titration with the 1:3 molar ratio has an inflection at 3.33 equivalents also indicating the strong complexation with two ligands bound to one  $\text{Fe}^{3+}$  central ion and one excess ligand in solution. We could not find any evidence for complexes with more than 2 ligands bound to the  $\text{Fe}^{3+}$  central ion.

On the basis of the equilibrium constants of the  $\text{Fe}^{3+}$ :DSA 1:1 molar ratio spectrophotometric batch titration and the 1:2 molar ratio continuous potentiometric titrations the species distributions were calculated as a function of the pH and the results are presented in **Figure 7.12**. The mono-hydroxo complex  $[\text{Fe}(\text{OH})]^{2+}$  is only present in the batch titration as a minor species. Subsequently, the hydroxo complexes of  $\text{Fe}^{3+}$ , taken into account for the calculation, do not play an important role in this species distribution. The batch titration begins at pH 1 with 36% free  $\text{Fe}^{3+}$  and 64% readily formed  $[\text{Fe}(\text{DSA})]^{-}$  complex. This 110 complex becomes the predominant complex to pH 2 with a maximum concentration of 96% at this pH. The pH range between pH 2.0 – 3.0 was not investigated.

The continuous potentiometric titrations were performed beginning at pH 3 and the  $[\text{Fe}(\text{DSA})]^{-}$  complex is present with a concentration of 87%. At this pH a protonated bis-complex  $[\text{Fe}(\text{L})(\text{LH})]^{4-}$  has already formed with a concentration of 12%. As the pH is raised this protonated bis-complex reaches a maximum concentration of 33% at pH 4 and then deprotonates to the bis-complex  $[\text{Fe}(\text{DSA})_2]^{5-}$ . The  $[\text{Fe}(\text{DSA})_2]^{5-}$  complex starts to form at pH 3 and is predominant complex at the end of the evaluated titration at about pH 5.3 with 92% of  $[\text{Fe}(\text{DSA})_2]^{5-}$  complex formed. The species distribution was calculated to pH 9 to show that this complex becomes the sole complex in solution from physiological pH 7.4 to pH 9. Consequently, the  $[\text{Fe}(\text{DSA})_2]^{5-}$  complex is the active complex at physiological pH. If we compare the species distribution of DSA to that calculated for deferasirox extrapolated for pure water (see S. Steinhauser<sup>[40]</sup>), we will find that the 120 complex of both ligands is the sole complex with a concentration of 100% at physiological pH 7.4. As a result, DSA shows the same complex behaviour as deferasirox regarding the iron (III) complex present at physiological pH.

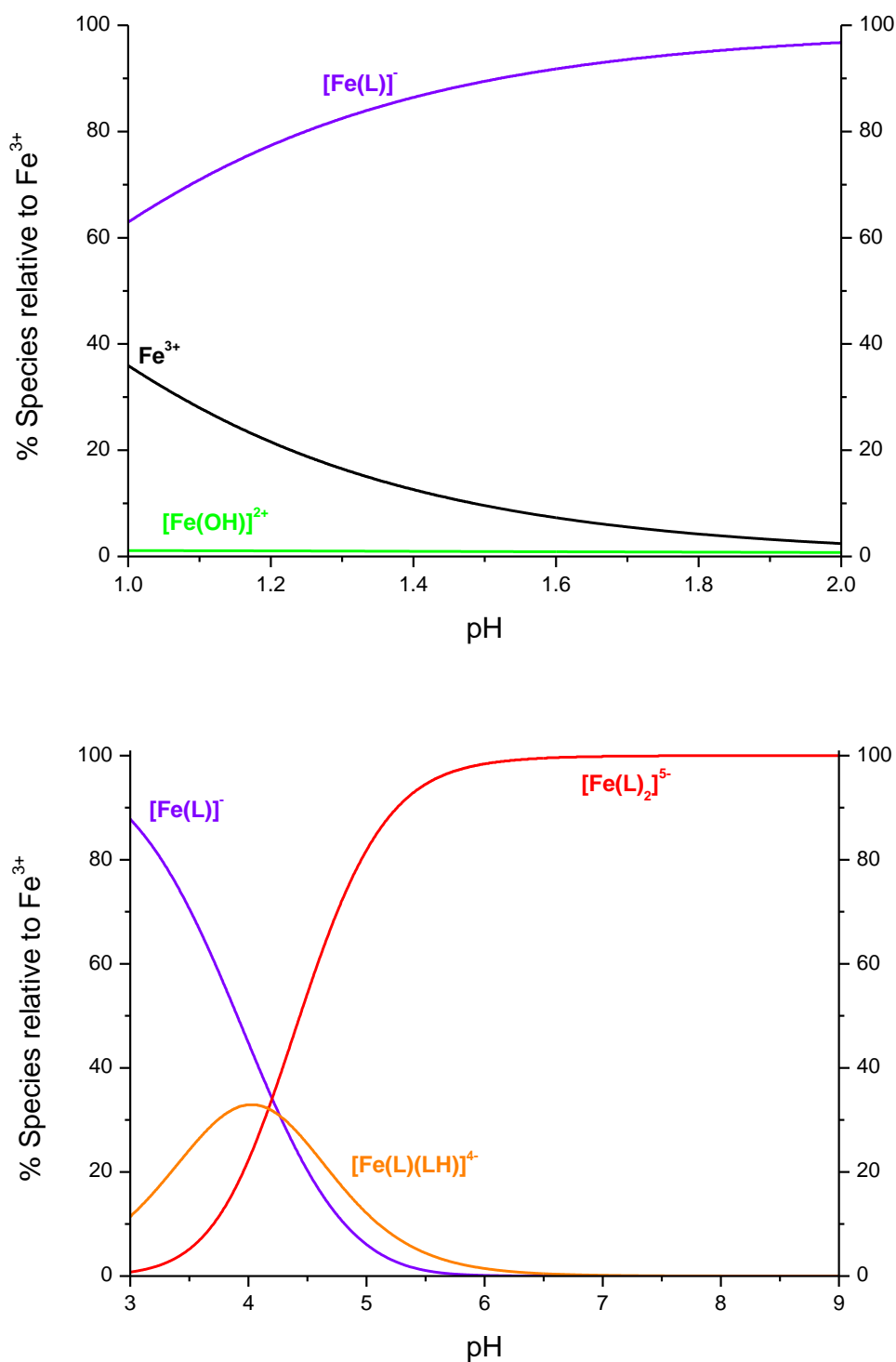


**Figure 7.12:** Species distribution diagrams as a function of pH for  $\text{Fe}^{3+}$  with the ligand DSA, batch titration experiment (top,  $[\text{Fe}^{3+}]_t = 0.20$  mmol/L,  $[\text{L}]_t = 0.20$  mmol/L, pure water,  $T = 298$  K and  $I = 0.1$  mol/L KCl) for pH 1.00 – 2.00 and continuous potentiometric titration (bottom,  $[\text{Fe}^{3+}]_t = 0.48$  mmol/L,  $[\text{L}]_t = 1.00$  mmol/L, pure water,  $T = 298$  K and  $I = 0.1$  mol/L KCl) for pH 3.00 – 9.00. The species concentration were calculated from the equilibrium constants listed in **Table 7.11** (mean values from simultaneous evaluation of 12 titrations) with the program Hyss2006.

**Table 7.12:** Example titration experiments of the complexation of Fe<sup>3+</sup> with DSA. Overall stability constants  $\log\beta_{xyz}$ <sup>[a]</sup> are listed. The titration conditions are given at T = 298 K.

<b>log<math>\beta</math> values for the complexation of Fe<sup>3+</sup> with DSA</b>		
molar ratio of M:L	1:2	1:3
measuring method	spectrophotometric	spectrophotometric
method type	continuous	continuous
solvent	pure water	pure water
[M] <sub>t</sub>	0.48 mmol/L	0.33 mmol/L
[L] <sub>t</sub>	1.00 mmol/L	1.00 mmol/L
titration volume	50.0 mL	50.0 mL
titrant	0.1 mol/L KOH	0.1 mol/L KOH
supporting electrolyte	0.1 mol/L KCl	0.1 mol/L KCl
electrode	Schott IoLine	Schott IoLine
range of wave length	400 < $\lambda$ < 900 nm	400 < $\lambda$ < 900 nm
volume of data points	51	43
time for mixing process	900 s	900 s
$\sigma_{\text{abs}}$ <sup>[b]</sup>	2.3 10 <sup>-3</sup>	1.4 10 <sup>-3</sup>
$\sigma_{\text{squares}}$ <sup>[b]</sup>	1.3 10 <sup>-1</sup>	4.2 10 <sup>-2</sup>
$\log\beta_{10-1}$ <sup>[c]</sup>	-2.51	-2.51
$\log\beta_{10-2}$ <sup>[c]</sup>	-5.76	-5.76
$\log\beta_{110}$ <sup>[d]</sup>	23.54(4)	23.54(4)
<b><math>\log\beta_{120}</math><sup>[e]</sup></b>	<b>39.05(5)</b>	<b>39.39(4)</b>
<b><math>\log\beta_{121}</math><sup>[e]</sup></b>	<b>43.51(4)</b>	<b>43.72 (4)</b>

<sup>[a]</sup> For the ligand L  $\log\beta_{xyz}$  is defined as:  $\beta_{xyz} = [M_xL_yH_z] \times [M]^{-x} \times [L]^{-y} \times [H]^{-z}$ .

<sup>[b]</sup> The  $\sigma_{\text{abs}}$  and  $\sigma_{\text{squares}}$  values are taken from Specfit.

<sup>[c]</sup> Values were calculated from overall formation constants taken from the NIST Database <sup>[55]</sup>.

<sup>[d]</sup> Value determined by spectrophotometric batch titration (section 7.1.1).

<sup>[e]</sup> The deviation given in brackets corresponds to the standard deviation taken from Specfit.

The stability constants of DSA with  $\text{Fe}^{3+}$  were verified by spectrophotometric titrations carried out simultaneously with some of the potentiometric titrations. The determined stability constants and conditions are listed in **Table 7.12**. They were performed in two molar ratios  $\text{Fe}^{3+}$ :DSA 1:2 and 1:3 under the same conditions as the potentiometric titrations described previously. Further, the UV-VIS spectra recorded were evaluated with the program Specfit. The calculated mean values of the stability constants determined by spectrophotometric titrations are summarized in **Table 7.13**. For comparison the potentiometric stability constants are also displayed.

**Table 7.13:** Mean values of the overall stability constants  $\log\beta_{xyz}$  <sup>[a]</sup> of the complexation of  $\text{Fe}^{3+}$  with DSA determined by spectrophotometric titrations in pure water,  $T = 298 \text{ K}$  and  $I = 0.1 \text{ mol/L KCl}$ . Comparison to the overall stability constants determined by potentiometric titration.

<b><math>\log\beta</math> values for the complexation of <math>\text{Fe}^{3+}</math>:DSA</b>			
1:2		1:3	
measuring method		spectrophotometric	
mean values of 4 titrations <sup>[b]</sup>		mean values of 5 titrations <sup>[b]</sup>	
<b><math>\log\beta_{120}</math></b>	<b>39.3(5)</b>	<b><math>\log\beta_{120}</math></b>	<b>39.5(6)</b>
<b><math>\log\beta_{121}</math></b>	<b>43.7 (4)</b>	<b><math>\log\beta_{121}</math></b>	<b>43.8(5)</b>
mean values by simultaneous evaluation of all 12 titrations <sup>[c]</sup>			
measuring method		potentiometric	
$\sigma$ <sup>[d]</sup>		1.626	
<b><math>\log\beta_{120}</math></b>	<b>39.50(2)</b>		
<b><math>\log\beta_{121}</math></b>	<b>43.67(3)</b>		

<sup>[a]</sup> For the ligand L  $\log\beta_{xyz}$  is defined as:  $\beta_{xyz} = [\text{M}_x\text{L}_y\text{H}_z] \times [\text{M}]^{-x} \times [\text{L}]^{-y} \times [\text{H}]^{-z}$ .

<sup>[b]</sup> The standard deviations in brackets were calculated with:  $\sqrt{\frac{\sum_{i=0}^n (x_i - \bar{x})^2}{(n-1)}}$ ;  $x_i$  measured value;  $\bar{x}$  mean value; n number of values.

<sup>[c]</sup> The titrations were evaluated simultaneously with the program Hyperquad2008. The deviations given in brackets correspond to the threefold standard deviation taken from Hyperquad2008.

<sup>[d]</sup> The  $\sigma$  value is taken from Hyperquad2008.

The spectrophotometric method confirmed the suggested two species model examined by potentiometric titrations. With this method only bis-complexes were identified. The stability constants of the spectrophotometric titrations are in very good agreement with those determined by potentiometric titrations. Yet the spectrophotometric constants are a little less accurate as the potentiometric ones. They were determined to one decimal place compared to two. Nevertheless, they are all in accordance with each other regarding their deviations.

The UV-VIS spectra were evaluated with Specfit in the same pH range, between 3.0 and 5.0, as the potentiometric data. Further, they were analysed from  $400 \text{ nm} < \lambda < 900 \text{ nm}$ . These spectra are illustrated in **Figure 7.13**. In Specfit a spectrum of the  $\text{Fe}^{3+}$  stock solution ( $\text{Fe}^{3+}$  concentration according to the  $[\text{Fe}^{3+}]_t$  of the sample solution) was ascertained as a known spectrum and defined as a coloured species. The 120 and 121 complexes were also defined as coloured species. All ligand species and the iron hydroxo complexes were defined as non-coloured species. According to the potentiometric titrations the  $[\text{Fe}(\text{L})]^-$  complexation constant was ascertained as a constant value in Specfit and defined as a coloured species.

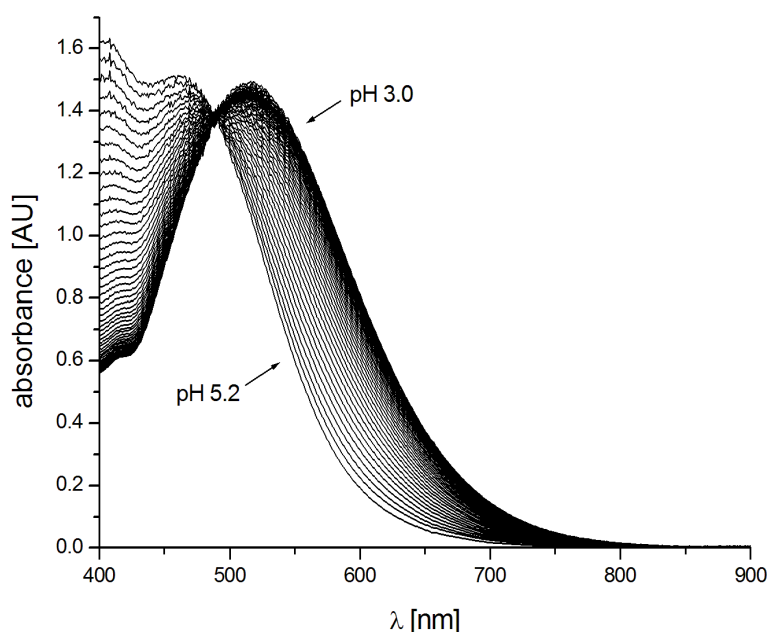


**Figure 7.13:** UV-Vis spectra of the continuous potentiometric titration of  $\text{Fe}^{3+}$  with DSA with a 1:2 molar ratio collected from pH 3.0 – 5.2 ( $[\text{Fe}^{3+}]_t = 0.48 \text{ mmol/L}$ ,  $[\text{DSA}]_t = 1.00 \text{ mmol/L}$ , pure water,  $T = 298 \text{ K}$ ,  $I = 0.1 \text{ mol/L KCl}$ ).

The individual spectra of the examined complexes are shown in **Figure 7.14**. The spectra of all three complexes differ due to changes in the coordination sphere. Thus, the coordination sphere changes when a second ligand is added to the  $[\text{Fe}(\text{L})]^-$  complex. This second ligand is initially protonated at one of the phenolate groups, we presume, to form a  $[\text{Fe}(\text{L})(\text{LH})]^{4-}$  complex. The spectrum of the  $[\text{Fe}(\text{L})(\text{LH})]^{4-}$  complex differs significantly from that of the  $[\text{Fe}(\text{L})_2]^{5-}$  complex indicating again a change in the coordination sphere. As we suggested in **Scheme 7.4**, this would be the case when one phenolate group of the  $[\text{Fe}(\text{L})(\text{LH})]^{4-}$  complex is protonated and the  $\text{Fe}^{3+}$  central ion is coordinated by one tridentate ligand, one bidentate ligand and a solvent molecule that takes the place at the free octahedral binding site. By deprotonation of the  $[\text{Fe}(\text{L})(\text{LH})]^{4-}$  complex the  $[\text{Fe}(\text{L})_2]^{5-}$  complex is formed with both ligands bound in a meridional tridentate coordination mode.

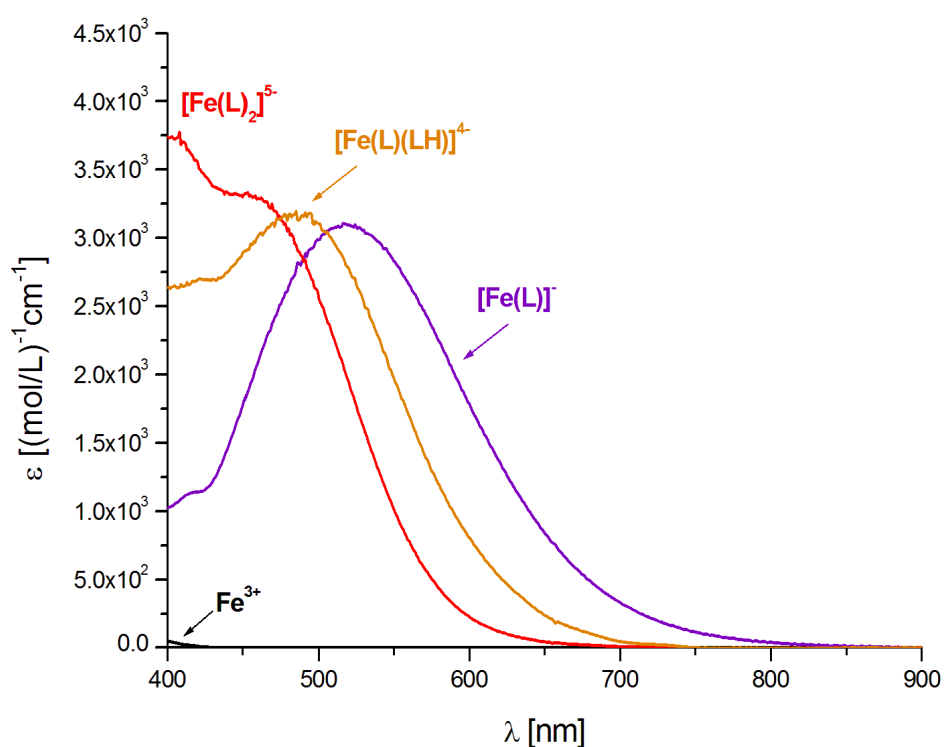


**Figure 7.14:** Individual spectra of the continuous spectrophotometric titration of  $\text{Fe}^{3+}$  with DSA in a 1:2 molar ratio generated with the program Specfit.

The significant change of the individual spectra of the 121 and 120 complex supports our theory on the protonation site at one of the phenolate groups of the ligand DSA.

In summary, the stability constant of the  $[\text{Fe}(\text{DSA})]^-$  complex was determined by spectrophotometric batch titration. Further, two bis-complexes  $[\text{Fe}(\text{L})_2]^{5-}$  and  $[\text{Fe}(\text{L})(\text{LH})]^{4-}$  for the ligand DSA were identified by potentiometric and spectrophotometric titrations. In **Table 7.14** these stability constants of the  $\text{Fe}^{3+}$ -DSA system are compared to stability constants of  $\text{Fe}^{3+}$ -deferasirox complexes extrapolated to pure water.

**Table 7.14:** Comparison of the overall stability constants  $\log\beta_{xyz}$  <sup>[a]</sup> of  $\text{Fe}^{3+}$ -DSA complexes measured in pure water with  $\text{Fe}^{3+}$ -deferasirox complexes extrapolated to pure water.

DSA		deferasirox <sup>[d]</sup>	
solvent		pure water	
supporting electrolyte		0.1 mol/L KCl	
$\log\beta_{110}$ <sup>[b]</sup>	<b>23.54(4)</b>	$\log\beta_{110}$	<b>22.0</b>
$\log\beta_{111}$	-	$\log\beta_{111}$	<b>24.3</b>
$\log\beta_{120}$ <sup>[c]</sup>	<b>39.50(2)</b>	$\log\beta_{120}$	<b>36.9</b>
$\log\beta_{121}$ <sup>[c]</sup>	<b>43.67(3)</b>	$\log\beta_{121}$	<b>41.2</b>
$\log\beta_{122}$	-	$\log\beta_{122}$	<b>43.4</b>

<sup>[a]</sup> For the ligand L  $\log\beta_{xyz}$  is defined as:  $\beta_{xyz} = [\text{M}_x\text{L}_y\text{H}_z] \times [\text{M}]^{-x} \times [\text{L}]^{-y} \times [\text{H}]^{-z}$ .

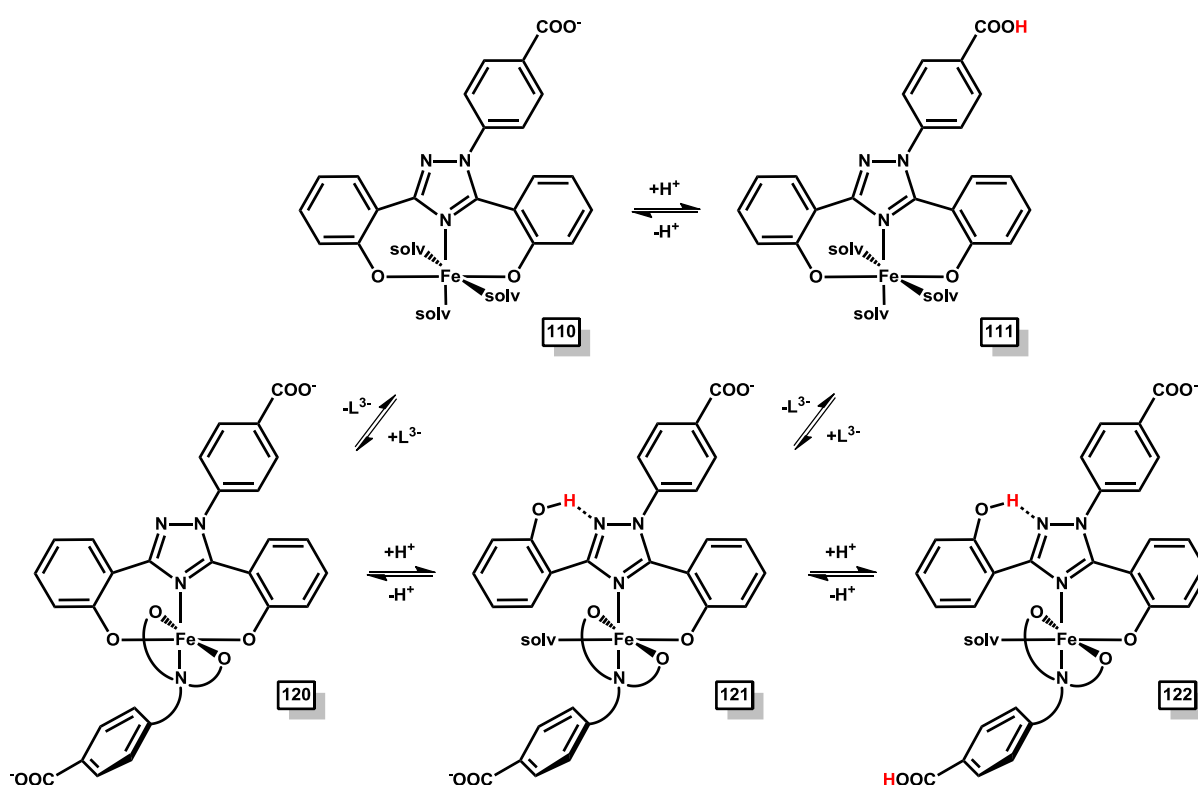
<sup>[b]</sup> The standard deviations in brackets were calculated with:  $\sqrt{\frac{\sum_{i=0}^n (x_i - \bar{x})^2}{(n-1)}}$ ;  $x_i$  measured value;  $\bar{x}$  mean value; n number of values.

<sup>[c]</sup> The titrations were evaluated simultaneously with the program Hyperquad2008. The deviations given in brackets correspond to the threefold standard deviation taken from Hyperquad2008.

<sup>[d]</sup> Values were taken from S. Steinhauser <sup>[40]</sup>.

We note that two complexes formed by deferasirox  $[\text{Fe}(\text{LH})]^+$  (111) and  $[\text{Fe}(\text{LH})_2]^-$  (122) with  $\text{Fe}^{3+}$  are not formed by DSA with  $\text{Fe}^{3+}$ . It has been discussed in section 7.2.1 why the  $[\text{Fe}(\text{LH})]$  complex for DSA was not taken into

account. In summary, the main difference is that the free ligand deferasirox has a carboxylic acid group with a  $pK_a$  of 3.65(6) (pure water,  $T = 298$  K,  $I = 0.1$  mol/L KCl, section 8.1.1) compared to DSA having a protonation constant of  $pK_a = 1.33(8)$  assigned to one of the triazole nitrogen atoms. The sulfonic acids are much too acidic to be protonated in aqueous solution. The  $[\text{Fe}(\text{LH})]^+$  complex of deferasirox can be formed due to a protonation at the carboxylic acid causing a tridentate meridional coordination mode as shown in **Scheme 7.5**. This is very favourable for this ligand system therefore the  $[\text{Fe}(\text{LH})]^+$  complex already forms in acidic solution between pH 1 and 2.



**Scheme 7.5:** Suggested coordination geometries of the deferasirox complexes  $[\text{Fe}(\text{L})]$  (110),  $[\text{Fe}(\text{LH})]^+$  (111),  $[\text{Fe}(\text{L})_2]^{3-}$  (120),  $[\text{Fe}(\text{L})(\text{LH})]^{2-}$  (121) and  $[\text{Fe}(\text{LH})_2]^+$  (122).

To form a  $[\text{Fe}(\text{LH})]$  complex with DSA the ligand can only adopt a bidentate coordination mode with one phenolate group protonated which is unfavourable and could not be verified by the batch titration. As a consequence, the formation of a  $[\text{Fe}(\text{LH})]$  complex of DSA is dependent on the protonation site and its protonation constant.

The other complex not formed by DSA is the 122 complex. The spectrum of the  $[\text{Fe}(\text{LH})_2]^-$  complex of deferasirox shows only a minor difference to that of the  $[\text{Fe}(\text{L})(\text{LH})]^{2-}$  (121) complex, with the consequence that the 122 complex could only be determined by potentiometric not by spectrophotometric titration. In contrast, the spectrum of the  $[\text{Fe}(\text{L})_2]^{3-}$  (120) complex and the 121 complex of deferasirox differ immensely. Accordingly, the coordination sphere must change by protonating the 120 complex. We assume the protonation takes place at one of the phenolate groups causing one of the tridentate meridional ligands to coordinate bidentate as illustrated in **Scheme 7.5**. The hydroxyphenyl group can form hydrogen bonding interaction with a triazole nitrogen atom stabilizing this kind of coordination mode. The same coordination mode has been suggested for the  $[\text{Fe}(\text{L})(\text{LH})]^{2-}$  complex of  $\text{Fe}^{3+}$  with DSA in **Scheme 7.4**. If we take a look at the apparent  $\text{p}K_a$  value of the deprotonation of the 121 complexes for both ligands we can observe they are in the same range. The apparent  $\text{p}K_a$  value for the deprotonation of the 121 complex for DSA is 4.17 and for deferasirox 4.3 (pure water). This supports the assumption that for both ligands the protonation occurs at one of the phenolate rings. It is noteworthy, that this is only an apparent deprotonation constant which originates from two reactions, the formation of the Fe-O bond and the deprotonation of the hydroxyphenyl group, combined in the constant.

Again, only deferasirox forms a 122 complex. The spectra of both protonated complexes 121 and 122 are very similar therefore the coordination sphere should also be very similar. This would imply that the second protonation occurs at one of the carboxylic acid groups of the ligand also shown in **Scheme 7.5**. The  $\text{p}K_a$  value of the deprotonation of the 122 complex of deferasirox is 2.2 (pure water) indicating a more acidic site being deprotonated for example a carboxylic acid. The species distribution of deferasirox with  $\text{Fe}^{3+}$  is given in **Figure 7.15** and shows that the 122 complex is present to less than 5%. This complex is not very relevant for the species distribution.

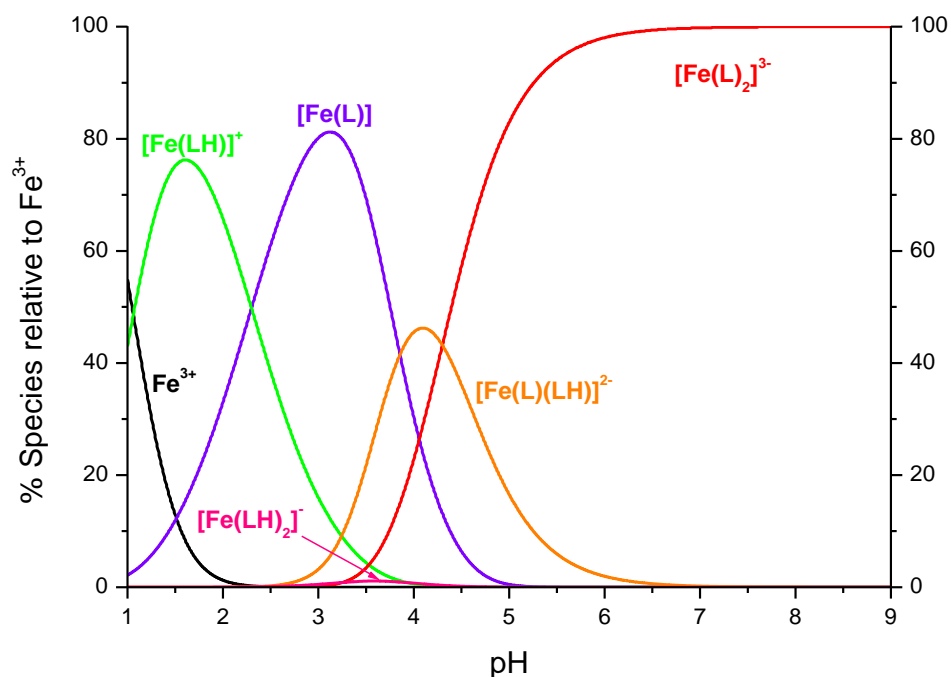


**Figure 7.15:** Species distribution for the  $\text{Fe}^{3+}$ -deferasirox system in pure water calculated with the values from **Table 7.14** with the program Hyss2006 at the following conditions  $[\text{Fe}]_t = 0.48 \text{ mmol/L}$ ,  $[\text{L}]_t = 1.00 \text{ mmol/L}$ ; pure water,  $T = 298 \text{ K}$  and  $I = 0.1 \text{ mol/L KCl}$ .

In conclusion, the 121 complex of the ligands DSA and deferasirox is assumingly protonated at the phenolate group causing a mixed tridentate and bidentate coordination mode of the ligands. If DSA had formed a 122 complex both ligands would need to coordinate bidentate which is clearly not favourable. For this reason, we suppose that the formation of a 122 complex for the  $\text{Fe}^{3+}$ -DSA system was not found.

The important complexes formed by both ligands are the 110 and the 120 complexes. If we compare the complexation constants for the 110 complexes, the DSA constant is slightly higher by 1.54 units. The individual 120 complexation constant is  $\log K_{120} = 15.96$  ( $\log K_{120} = [\text{ML}_2] / [\text{ML}] \times [\text{L}]$ ) for DSA and  $\log K_{120} = 14.9$  for deferasirox which is 1.06 units lower. Accordingly, the complex stability of  $\text{Fe}^{3+}$  with DSA seems to be somewhat higher than with deferasirox. However, the difference is not immense and moreover the complex formation of the 110 and 120 complexes seem to be very similar for both ligands. Taken together, the ligand DSA can be well employed to elucidate the  $\text{Fe}^{3+}$  complexation chemistry of deferasirox.

### 7.2.3 The Crystal structure $\text{Cs}_5[\text{Fe}(\text{DSA})_2] \cdot 10.74 \text{H}_2\text{O}$

A crystal structure of the ligand DSA with  $\text{Fe}^{3+}$  was obtained by T. Nicolai, under my supervision [58]. The dark red crystals were grown from a solution mixture of DSA with iron(III)-acetylacetonate in methanol. Caesium hydroxide functions as a base and provides the necessary counterions. The solution was kept in an exsiccator over ethyl acetate. Suitable single crystals were employed for X-ray analysis. The coordination chemistry of the  $[\text{Fe}(\text{DSA})_2]^{5-}$  complex is presented in **Figure 7.16**.

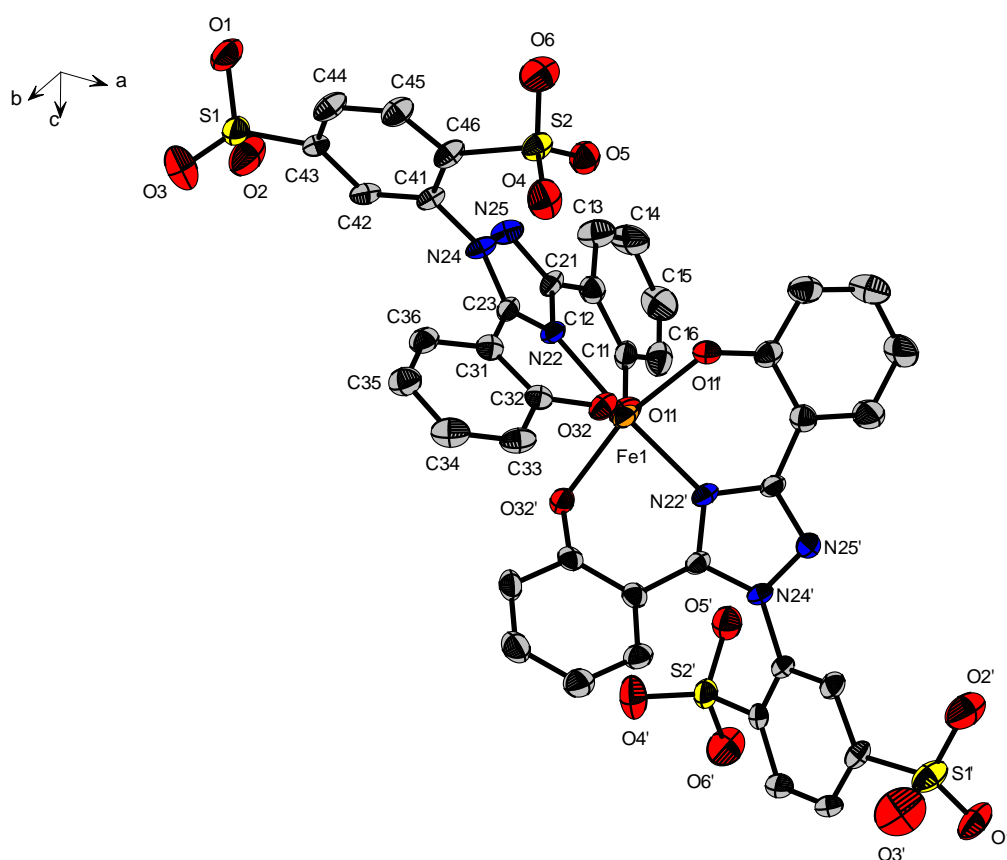


**Figure 7.16:** ORTEP-plot of the  $[\text{Fe}(\text{DSA})_2]^{5-}$  complex of the crystal structure  $\text{Cs}_5[\text{Fe}(\text{DSA})_2] \cdot 10.74 \text{H}_2\text{O}$ . The atomic displacement ellipsoids are drawn at the 50% probability level (C = grey, Fe = orange, N = blue, O = red and S = yellow). CH-hydrogen atoms, solvent molecules and  $\text{Cs}^+$  counterions are omitted for clarity.

The  $[\text{Fe}(\text{DSA})_2]^{5-}$  complex crystallizes in the monoclinic space group  $\text{C}2/c$  with the R values  $R_1 = 6.82\%$  and  $wR_2 = 15.88\%$ . Two completely deprotonated ligands are bound to one  $\text{Fe}^{3+}$  central ion with a tridentate meridional coordina-

tion mode forming a bis-structure. The ligand DSA coordinates as expected with the two phenolate groups O11 and O32 as well as with the triazole nitrogen N22 in an O-N-O coordination mode. The  $\text{Fe}^{3+}$  central ion was located at a special position in the crystal structure. It encloses the crystallographic  $C_2$  axis which generates one ligand molecule from the other by symmetry. The iron central ion is also situated on the edge of the asymmetric unit. There are two whole  $\text{Cs}^+$  counterions and one  $\text{Cs}^+$  situated at the edge of the asymmetric unit. If we take a look at the  $[\text{Fe}(\text{DSA})_2]^{5-}$  complexes charge we will find that altogether there are 5  $\text{Cs}^+$  counterions to compensate it. In **Figure 7.16** the caesium counterions and water molecules were omitted for clarity since one of the caesium ions and some of the 10.74 water molecules are disordered.

Further, the bis-complex with its meridional coordination mode adopts a distorted octahedral coordination geometry as shown in **Figure 7.17**.

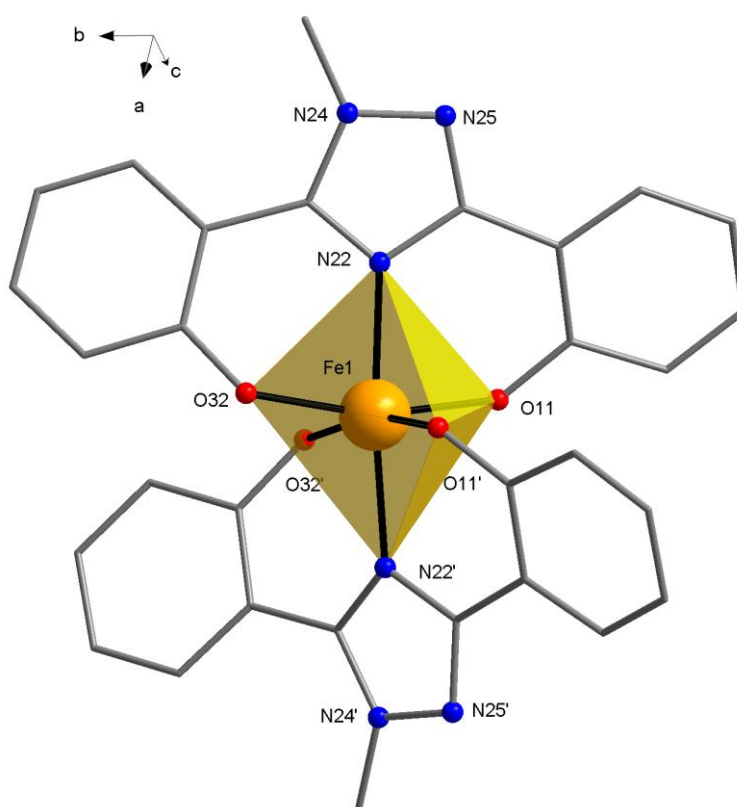
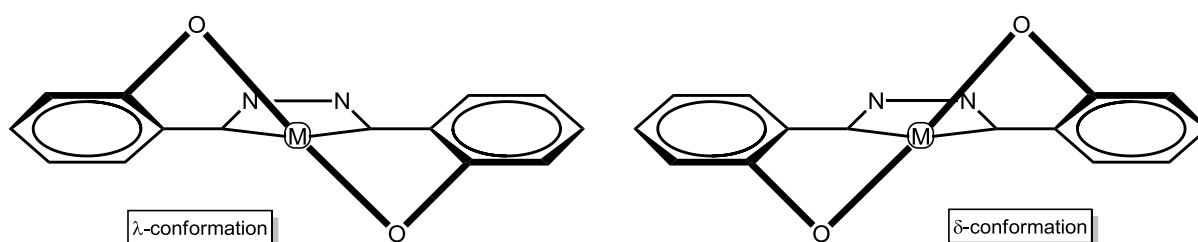


**Figure 7.17:** Coordination polyhedron of the distorted octahedral geometry of the  $\text{Cs}_5[\text{Fe}(\text{DSA})_2] \cdot 10.74 \text{H}_2\text{O}$  structure. Benzene-1,4-disulfonic acids are only indicated.

The distortion of the octahedron is closely related to the possible stereoisomers for a  $ML_2$  complex. When complexing a metal cation the phenolate rings twist out of the plane of the triazole unit. As a consequence, the O11- $Fe^{3+}$ -O32 line formed by the complexation of one ligand entity can cause the two phenolate rings to twist clockwise relative to the central triazole unit forming the  $\lambda$  enantiomer or counter-clockwise forming the  $\delta$  enantiomer as shown in **Scheme 7.6**.



**Scheme 7.6:** Schematic illustration of the two possible ML enantiomers. <sup>[40]</sup>

In the bis-complex the combination of both ligand entities can result in the formation of the  $\lambda\delta$  isomer or the  $\lambda\lambda/\delta\delta$  isomer. The geometry of the isomers differs explicitly. Thus, in the  $\lambda\delta$  conformer the two ligands arrange almost perpendicular to each other. The  $\lambda\lambda/\delta\delta$  conformer usually has a rather flat geometry allowing the phenolate rings to arrange somewhat parallel to each other causing some intermolecular  $\pi$ -stacking interactions. Accordingly, the  $[Fe(DSA)_2]^{5-}$  anion adopts the  $\lambda\lambda/\delta\delta$  conformation. In essence, the rather flat geometry of the structure can be attributed to some intermolecular  $\pi$ -stacking interactions occurring between the phenolate rings of the ligands. <sup>[40]</sup>

Interestingly, the two benzene-1,4-disulfonic acid substituents arrange cisoid in the  $[Fe(DSA)_2]^{5-}$  anion. The crystal structure of the 1N-phenyl derivative ligand of deferasirox with the composition  $Na[Fe(L)]_2 \cdot 4EtOH$  also forms a bis-complex  $[Fe(L)_2]^-$  with a  $\lambda\lambda/\delta\delta$  conformation, yet the phenyl substituents arrange transoid <sup>[40]</sup>.

Further, a crystal structure  $Li_3[Fe(deferasirox)_2] \cdot MeOH$  of the  $Fe^{3+}$ -deferasirox bis-complex has been obtained <sup>[59]</sup>. This  $[Fe(deferasirox)_2]^{3-}$  bis-complex also adopts the  $\lambda\lambda/\delta\delta$  conformation with the benzoic acid substituents

transoid like for the 1N-phenyl derivative. However, the ligands arrange rather perpendicular to each other in the  $[\text{Fe}(\text{deferasirox})_2]^{3-}$  anion causing little to no  $\pi$ -stacking interaction.

The crystal structure of the  $[\text{Fe}(\text{DSA})_2]^{5-}$  complex is concordant with the iron structure of the 1N-phenyl derivative in many characteristics. For example the corresponding bond lengths and angles listed in **Table 7.15** are very similar to those of the 1N-phenyl derivative. The crystal structure of the  $[\text{Fe}(\text{deferasirox})_2]^{3-}$  complex shows many similarities to the  $[\text{Fe}(\text{DSA})_2]^{5-}$  complex, yet differs in some bond lengths and angles.

**Table 7.15:** Selected bond lengths and bond angles for the structure  $\text{Cs}_5[\text{Fe}(\text{DSA})_2] \cdot 10.74 \text{H}_2\text{O}$ .

atom	bond length [Å]	atom	bond length [Å]	atom	bond angle [°]
<b>Fe1 – O11</b>	1.963(6)	<b>Cs1 – O(6W)</b>	3.64(2)	<b>O11 – Fe – O11'</b>	93.7(4)
<b>Fe1 – O32</b>	2.003(7)	<b>Cs1 – O32</b>	3.233(6)	<b>O32 – Fe1 – O32'</b>	88.3(4)
<b>Fe1 – N22</b>	2.109(7)	<b>Cs2 – O1'</b>	3.100(8)	<b>O11 – Fe1 – O32</b>	164.7(2)
<b>Cs1 – O4</b>	3.248(8)	<b>Cs2 – O(1W)</b>	3.207(11)	<b>O11 – Fe1 – O32'</b>	91.0(3)
<b>Cs1 – O5</b>	3.161(7)	<b>Cs2 – O6'</b>	3.241(9)	<b>O11 – Fe1 – N22</b>	83.0(3)
<b>Cs1 – O11'</b>	2.952(6)	<b>Cs2 – O2'</b>	3.254(10)	<b>O11 – Fe1 – N22'</b>	93.0(3)
<b>Cs1 – O3'</b>	3.034(9)	<b>Cs2 – O1''</b>	3.313(9)	<b>O32 – Fe1 – N22</b>	82.2(3)
<b>Cs1 – O6'</b>	3.044(8)	<b>Cs2 – O3'</b>	3.359(11)	<b>O32 – Fe1 – N22'</b>	102.0(3)
<b>Cs1 – O(5A)</b>	3.20(2)	<b>Cs2 – O5'</b>	3.717(7)	<b>N22 – Fe1 – N22'</b>	174.1(4)
<b>Cs1 – O(5B)</b>	3.253(19)	<b>Cs2 – O4</b>	2.922(8)		

The rather short Fe1 – N22 bond length of 2.109(7) for  $[\text{Fe}(\text{DSA})_2]^{5-}$  is in the same range as the Fe1 – N1 bond length for the 1N-phenyl derivative complex  $[\text{Fe}(\text{L})_2]^-$  which is 2.092(5) <sup>[40]</sup> and the Fe1 – N11 for  $[\text{Fe}(\text{deferasirox})_2]^{3-}$  with 2.094(2) or Fe1 – N12 with 2.096(2) <sup>[59]</sup>. Additionally, the Fe – O bond

lengths are at the short end of the range expected for high-spin  $\text{Fe}^{3+}$ . The corresponding Fe – O distances are Fe1 – O11 of DSA with 1.963(6) compared to Fe1 – O11 of the 1N-phenyl derivative with 1.958(4) <sup>[40]</sup> and Fe1 – O11 of deferasirox with 1.962(2) and Fe1 – O22 with 1.985(2) <sup>[59]</sup>. Further, the Fe1 – O32 of DSA with 2.003(7) compared to Fe1 – O1 of the 1N-phenyl derivative with 2.002(4) <sup>[40]</sup> are very similar, while the deferasirox distances Fe1 – O12 with 1.982(2) and Fe1 – O21 with 1.981(2) <sup>[59]</sup> are somewhat smaller.

Another similarity of the three structures: DSA, the 1N-phenyl derivative and deferasirox with  $\text{Fe}^{3+}$  is that the ligands in all complexes are not planar as already discussed. All crystal structures of the complexes adopt the  $\lambda\lambda/\delta\delta$  conformation. If we compare the torsional angles  $12.4^\circ$  and  $23.5^\circ$ , of the phenolate rings with regard to the central triazole unit, of the ligand DSA with those of the 1N-phenyl derivative  $14.1^\circ$  and  $23.5^\circ$  <sup>[40]</sup>, we conclude that they are in good agreement. However, the torsional angles of the  $[\text{Fe}(\text{deferasirox})_2]^{3-}$  complex are different with  $0.03^\circ$ ,  $1.2^\circ$ ,  $33.4^\circ$  and  $30.8^\circ$  <sup>[59]</sup>. These reveal that one phenyl ring is almost planar with the central triazole unit and one is twisted out of the plane. Further, the N22 – Fe1 – N22' angle for DSA is  $174.1^\circ$  and correlates well with the corresponding angle  $172.7^\circ$  <sup>[40]</sup> of the 1N-phenyl derivative. In contrast, the angle for the  $\text{Fe}^{3+}$ -deferasirox structure is  $165.9^\circ$  <sup>[59]</sup>.

The five  $\text{Cs}^+$  counterions in the crystal structure compensate the  $[\text{Fe}(\text{DSA})_2]^{5-}$  anions charge. The Cs1 ion has a sevenfold coordination environment. Accordingly, the Cs1 ion is coordinated to the two phenolate oxygen atoms O11' and O32. Further coordination sites of the Cs1 ion are occupied by four sulfonic acid oxygen atoms and by a distorted water oxygen atom. The Cs2 ion also has a sevenfold coordination environment with 6 sulfonic acid oxygen atoms and one water molecule coordinating. The disordered Cs3 – Cs4 ion binds predominantly to water molecules which are partly disordered.

The sulfonic acid groups orientate towards the  $\text{Cs}^+$  counterions causing a twisting angle of  $69.3^\circ$  between the benzene-1,4-disulfonic acid entity and the triazole unit. Nevertheless, the phenolate groups also coordinate with the  $\text{Cs}^+$  counter ions. As a consequence the  $\text{Cs}^+$  ions arrange on both sides of the rather flat geometry of the  $[\text{Fe}(\text{DSA})_2]^{5-}$  complex forming layers as illustrated in **Figure 7.18**.

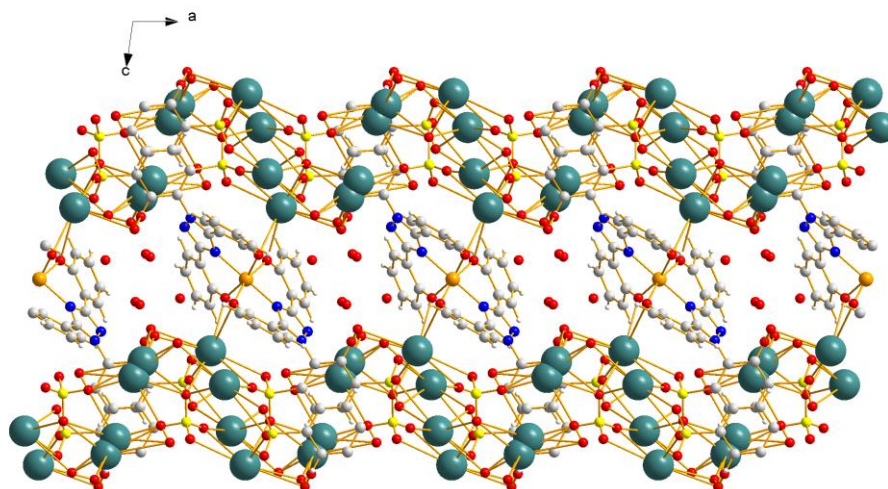


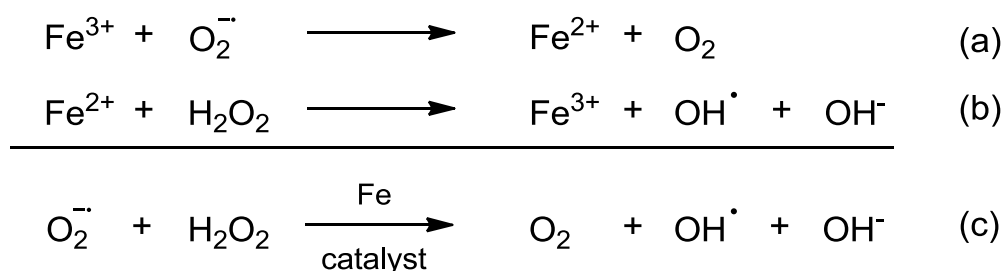
**Figure 7.18:** Formation of layers in the crystal structure  $\text{Cs}_5[\text{Fe}(\text{DSA})_2] \cdot 10.74 \text{H}_2\text{O}$ . View along the b-axis.

Viewing along the b-axis we observe alternating layers of  $\text{Cs}^+$  counterions coordinated to the benzene-1,4-disulfonic acids and layers of the iron central ion coordinating with the triazole unit and its phenolate rings. The benzene-1,4-disulfonic acids rise alternately into the layer, with the  $\text{Cs}^+$  counterions, above and beneath the iron complex. In these layers the benzene-1,4-disulfonic acids are orientated in a way causing some  $\pi$ -stacking interactions. In the layers with the iron complex entities there are cavities between the complexes in which water molecules are intercalated. In fact, the distance between two  $\text{Fe}^{3+}$  atoms on the a-axis is about 12 Å and on the b-axis about 11 Å.

Subsequently, the crystal structure  $\text{Cs}_5[\text{Fe}(\text{DSA})_2] \cdot 10.74 \text{H}_2\text{O}$  gives evidence to the complexes structure in solution. We assumed the dark red bis-complex forms a tridentate meridional coordination mode in alkaline solution. The structure has proven this coordination mode in the solid state. Since this coordination mode seems to be favoured in the solid state we suggest this coordination mode should be also favoured in aqueous solution.

#### 7.2.4 Investigation of the redox chemistry of the iron (II) / iron (III)-DSA system by cyclic voltammetry

The redox chemistry of deferasirox was investigated in detail by S. Stucky (formerly S. Steinhauser) [39]. The results of these investigations have been published in S. Steinhauser 2004 [40]. In that report, the redox behaviour of the two important complexes  $[\text{Fe}(\text{LH})]^+$  and  $[\text{Fe}(\text{L})_2]^{3-}$  of deferasirox has been studied by cyclic voltammetry in acidic and alkaline water/DMSO solution, respectively. It is essential to draw special attention to the redox potential of an iron chelating agent since, depending on the range of the redox potential, it can enhance oxidative stress in the human body. Iron has the catalytic ability to cycle between two stable oxidation states which are the ferric ( $\text{Fe}^{3+}$ ) and the ferrous ( $\text{Fe}^{2+}$ ) iron. Reactive oxygen species (ROS) such as the hydroxyl radical  $\text{OH}^\bullet$  are generated by redox cycling caused by labile and redox-active iron (II) components which originate from a reduction by e.g. the superoxide radicals (equation a) presented in **Scheme 7.7**. The overall oxidation-reduction process is known as the Haber-Weiss reaction (equation c) [60-62]. These ROS which arise from the Fenton reaction (equation b) can be responsible for the induction of cell death by initiating chemical reactions with biomolecules for example mitochondrial damage or oxidation of DNA [29]. For this reason we investigated the redox activity of the important  $\text{Fe}^{3+}$ -DSA complexes  $[\text{Fe}(\text{L})]^-$  and  $[\text{Fe}(\text{L})_2]^{5-}$  to examine whether DSA shows similar redox behaviour as deferasirox.



**Scheme 7.7:** Iron catalysed redox reactions associated with oxidative stress. Equation (a)  $\text{Fe}^{3+}$  is reduced by the superoxide radical. Equation (b)  $\text{Fe}^{2+}$  reduces hydrogen peroxide to the hydroxyl radical and hydroxide anion known as the Fenton reaction. Equation (c) is the iron-catalysed Haber-Weiss reaction.

### 7.2.4.1 Redox chemistry in acidic solutions

The redox chemistry of the ligand DSA with iron (II/III) in acidic solution was investigated in pure water. On account of the species distribution we know that the  $[\text{Fe}(\text{DSA})]^-$  complex is the predominant species in acidic solution and reaches its maximum concentration at pH 2. For this reason, all cyclic voltammograms in acidic solution were recorded at pH 1.9. They were measured in a 0.5 mol/L KCl solution using an Au working electrode and Ag/AgCl as reference electrode. Scanning was always started at about 800 mV. The cyclic voltammograms are presented in **Figure 7.19**.

An irreversible peak from +100 mV to -300 mV (versus Ag/AgCl) was observed in all cyclic voltammograms recorded at different scan rates. This peak can be assigned to the reduction of the ferric complex  $[\text{Fe}^{\text{III}}(\text{DSA})]^-$  to the corresponding ferrous  $[\text{Fe}^{\text{II}}(\text{DSA})]^{2-}$  complex based on the following reaction of equation 1.



Since there is no oxidation peak in the appropriate range, we assert that the ferrous  $[\text{Fe}^{\text{II}}(\text{DSA})]^{2-}$  complex is not stable and decomposes according to the reaction given in equation 2.



This reaction is also a consequence of the low pH. If the ferrous complex is not very stable, as shown in studies of deferasirox with  $\text{Fe}^{2+}$  [39-40], the protons in solution compete against the complexes central metal ion  $\text{Fe}^{2+}$  and protonate the phenolate groups of the ligand DSA at pH 2. Accordingly, the decomposition of the ferrous complex is a pH dependent reaction.

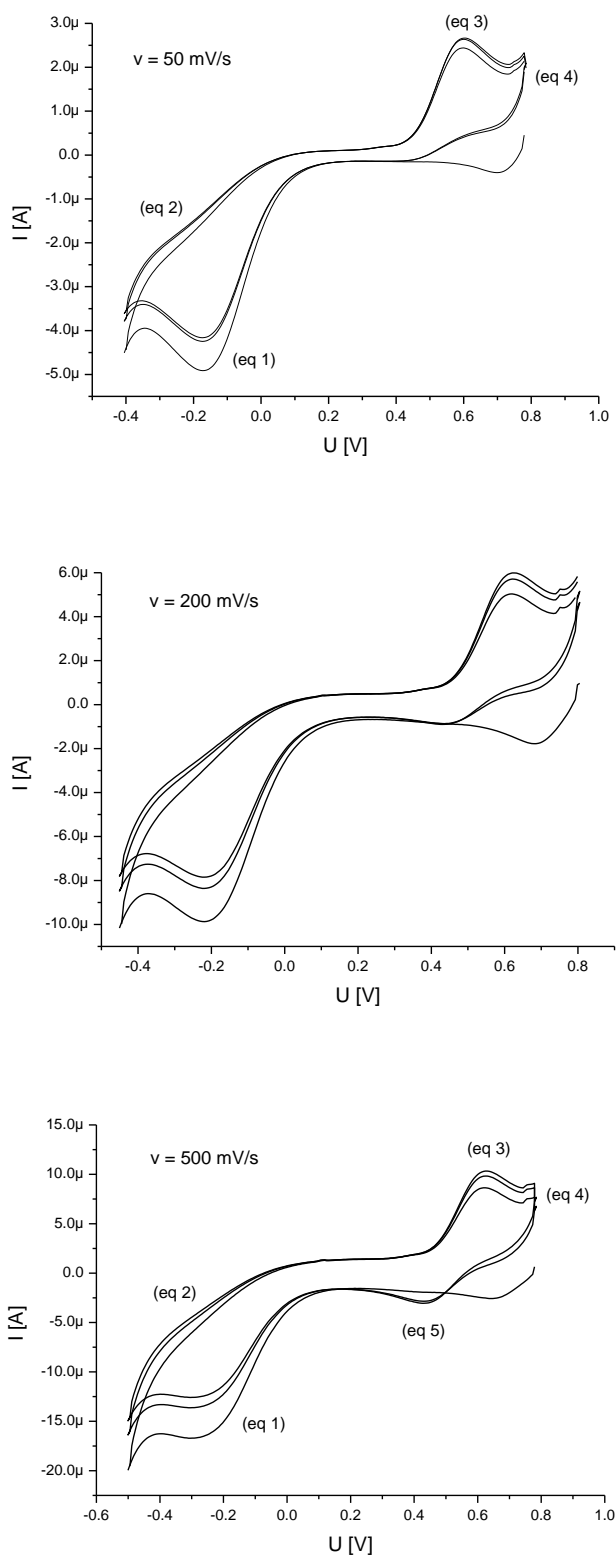


**Figure 7.19:** Cyclic voltammograms of  $[\text{Fe}(\text{DSA})]^-$  at scan rates as indicated measured using an Au working electrode (pure water,  $\text{pH} = 1.9$ ,  $[\text{Fe}]_t = 2.3 \text{ mmol/L}$ ,  $[\text{L}]_t = 5.0 \text{ mmol/L}$  and  $I = 0.5 \text{ mol/L KCl}$ ).

A linear correlation, see **Figure 7.20**, was found between the cathodic peak current of the reduction of the ferric complex  $[\text{Fe}^{\text{III}}(\text{DSA})]^-$  and the square root of the scan rate indicating a diffusion controlled reaction. The potential of the reduction peak shifts towards negative values by increasing the scan rate. This observation is confirmed with an irreversible reaction as we assumed, resulting from equation 2.

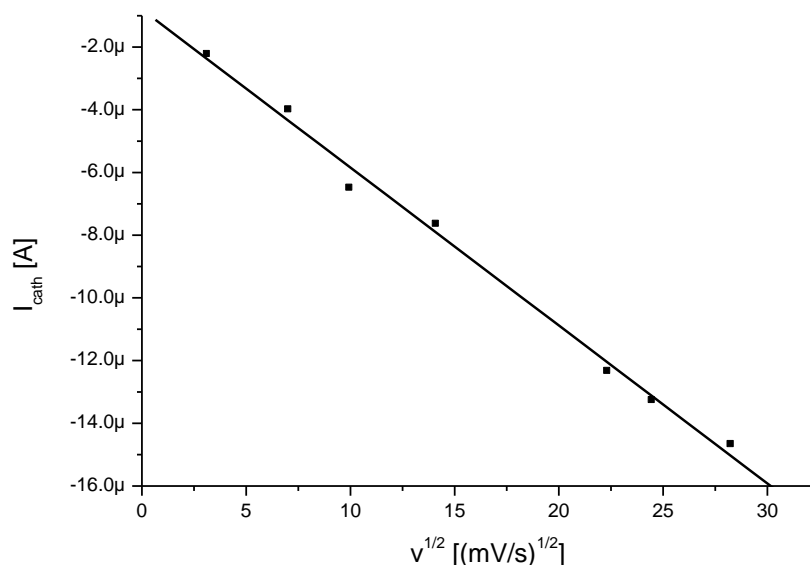


**Figure 7.20:** Linear correlation of the cathodic peak current with the square root of the scan rate for the irreversible diffusion controlled reaction in equation 1 (pH = 1.9).

On account of the complex decomposing to the twofold protonated ligand  $\text{LH}_2^{2-}$  and free  $\text{Fe}^{2+}$  we observe an oxidation peak at about +600 mV (versus Ag/AgCl) during the reverse scan. This oxidation peak can be attributed to the oxidation of  $\text{Fe}^{2+}$  as presented in equation 3.



To confirm this assumption we recorded a cyclic voltammogram of the free  $\text{Fe}^{3+}$  at pH 1.9 which is depicted in **Figure 7.21**. The oxidation peak of the  $\text{Fe}^{2+}/\text{Fe}^{3+}$  system appears at about +600 mV (versus Ag/AgCl) which is in accordance with the peak observed in the Fe-DSA voltammograms.

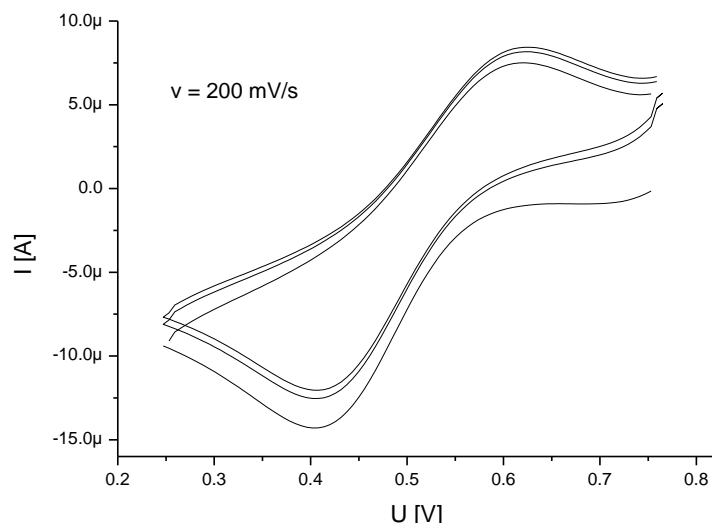


**Figure 7.21:** Cyclic voltammogram of  $\text{FeCl}_3$  at  $\text{pH} = 1.9$  with a scan rate of  $200 \text{ mV/s}$  measured using an Au working electrode (pure water,  $[\text{Fe}]_t = 2.3 \text{ mmol/L}$ ,  $[\text{I}] = 0.5 \text{ mol/L KCl}$ ).

After  $\text{Fe}^{2+}$  has been re-oxidised to  $\text{Fe}^{3+}$  the complex formation is favoured due to the strong complex affinity of ferric iron to DSA. When a new scan begins the ferric complex is re-formed (equation 4).



This interpretation of the cyclic voltammograms is supported by measurements at different scan rates. At slow scan rate ( $50 \text{ mV/s}$ ) the ferric complex has enough time for complete reformation. However, if the scan rate is increased to  $200 \text{ mV/s}$  and  $500 \text{ mV/s}$  an additional reduction peak appears at about  $+400 \text{ mV}$  (versus  $\text{Ag/AgCl}$ ). At these higher scan rates the ferric complex is not entirely formed subsequently remaining free  $\text{Fe}^{3+}$  still in solution is reduced to  $\text{Fe}^{2+}$  (equation 5).



The first cycle at a scan rate of  $500 \text{ mV/s}$  shows no reduction peak of free  $\text{Fe}^{3+}$ . Whereas, in the following cycles the ferric complex is not completely

formed the reduction peak of  $\text{Fe}^{3+}$  is observed. The intensities of the two observed reduction peaks are closely related. If less ferric complex is formed by equation 4 the reduction peak at +100 to -300 mV decreases while the other reduction peak at +400 mV increases caused by more free  $\text{Fe}^{3+}$  in solution. Further cycles are very well reproduced. The reduction peak at about +400 mV assigned to equation 5 is therefore only observed at higher scan rates it disappears at low scan rates. Further, the comparison to the cyclic voltammogram in **Figure 7.21** of the free  $\text{Fe}^{3+}$  confirms this observation. Accordingly, the reduction peak of the  $\text{Fe}^{2+}/\text{Fe}^{3+}$  system is also located at +400 mV.

This redox behaviour of the  $[\text{Fe}(\text{DSA})]^-$  complex is generally in very good agreement with that observed for deferasirox. The cyclic voltammograms are very similar. Even though, one needs to distinguish between the two different ligand complexes active in redox cycling. The  $\text{Fe}^{2+}/\text{Fe}^{3+}$ -deferasirox system was measured in a water/DMSO mixture at  $\text{pH} = 2.9$  which means that the active complex is  $[\text{Fe}(\text{LH})]^+$ . This is a protonated form of the 1:1 complex. The complex studied in this work by cyclic voltammetry is the 1:1 complex  $[\text{Fe}(\text{DSA})]^-$ . Yet, the coordination geometry of both complexes is tridentate meridional and since the proton does not take part in any reactions concerning the redox chemistry, we suggest that both complexes are suitable for comparison. All reactions discussed above in equations 1 – 5 were also found for the corresponding deferasirox complex  $[\text{Fe}(\text{LH})]^+$ . Yet, we have to take into consideration that oxidation and reduction peak potentials of the Fe-DSA system are shifted enormously in comparison to the Fe-deferasirox system. The reduction peak assigned to equation 1 appears at about -200 mV for DSA and about -100 mV <sup>[39]</sup> for deferasirox. A possible explanation could be attributed to the significant difference in charge of the two 1:1 complexes of the ligands. The DSA complex  $[\text{Fe}(\text{DSA})]^-$  has a negative charge while the deferasirox complex  $[\text{Fe}(\text{LH})]^+$  has a positive charge. Accordingly, the Fe-deferasirox complex is much easier to reduce than the Fe-DSA complex causing its reduction peak to shift to more negative potential. However, the oxidation and reduction peaks assigned to equation 3 and 5 are also shifted. We observed the oxidation peak at +600 mV and the reduction peak at +400 mV for the DSA measurements. For the deferasirox system this oxidation peak was found at +400 mV and the

corresponding reduction peak at +300 mV <sup>[39]</sup>. To confirm these oxidation and reduction peaks in the DSA measurements we performed a comparative measurement with the free Fe<sup>2+</sup>/Fe<sup>3+</sup> system which verified the oxidation and reduction peaks of the free Fe<sup>2+</sup>/Fe<sup>3+</sup> system found in the Fe-DSA cyclic voltammograms. To explain the shifting of the peaks we also need to take the experimental conditions into account. The cyclic voltammetric investigations of both ligands have been performed in different solvent media, at different pH and for the Fe-DSA system potassium chloride was used as a supporting electrolyte.

In summary, we note that DSA shows very similar redox behaviour in comparison to deferasirox, despite the different protonation state and charge of the 1:1 complexes of both ligands. Fact is however the values of the oxidation and reduction peaks differ significantly. Nevertheless, all characteristic reactions found in the Fe-deferasirox system are also found in the Fe-DSA system hence we conclude that the redox behaviour of the Fe-DSA system in acidic solution is closely related to that of the Fe-deferasirox system.

### 7.2.4.2 Redox chemistry in alkaline solutions

Investigations of the  $[\text{Fe}^{\text{III/II}}(\text{DSA})_2]^{5-/6-}$  system were carried out in alkaline solution. This bis-complex is the sole species in solution from  $\text{pH} > 7$ . Its redox behaviour was studied at  $\text{pH} 11.1$  in pure water with KCl as supporting electrolyte with a concentration of  $0.5 \text{ mol/L}$ . The cyclic voltammograms needed to be studied with a hanging mercury drop electrode (HMDE) as working electrode. Accordingly, investigations of the  $[\text{Fe}^{\text{III/II}}(\text{L})_2]^{3-/4-}$  system of deferasirox also needed to be determined with the HMDE. S. Stucky (formerly S. Steinhauser) reports in his doctoral thesis that the determination of the stability constant of the  $[\text{Fe}^{\text{II}}(\text{L})_2]^{4-}$  complex of MSA and deferasirox is in particular hampered by the strong reductive effect of the ferrous complex <sup>[39]</sup>. Thus, the ferrous complex seems to be a better reducing agent than  $\text{H}_2$ . The use of a HMDE enables the investigation of strongly negative reduction potentials by suppressing the formation of hydrogen.

The cyclic voltammogram recorded for the  $[\text{Fe}^{\text{III/II}}(\text{DSA})_2]^{5-/6-}$  system is presented in **Figure 7.22**.

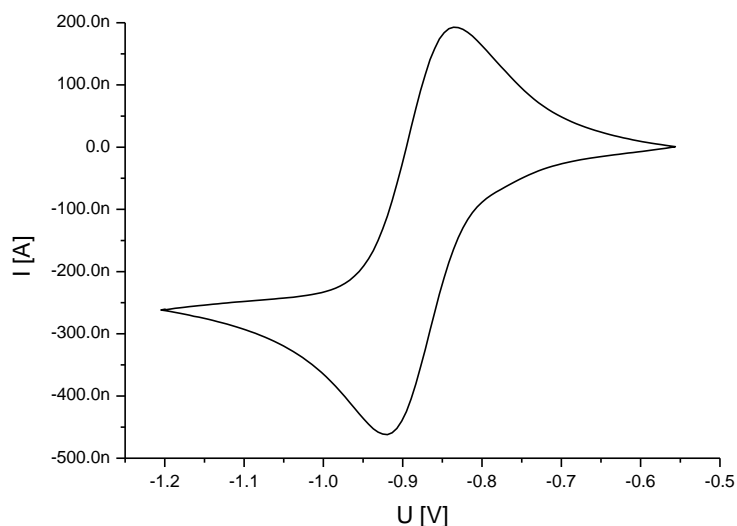


**Figure 7.22:** Cyclic voltammogram of the  $[\text{Fe}^{\text{III/II}}(\text{DSA})_2]^{5-/6-}$  system with a scan rates of  $50 \text{ mV/s}$  measured using a HMDE working electrode (pure water,  $\text{pH} = 11.1$ ,  $[\text{Fe}]_t = 2.3 \text{ mmol/L}$ ,  $[\text{L}]_t = 5.0 \text{ mmol/L}$  and  $I = 0.5 \text{ mol/L KCl}$ ).

The reduction of the ferric complex  $[\text{Fe}^{\text{III}}(\text{DSA})_2]^{5-}$  is a quasi-reversible reduction reaction. As expected, the reaction is not pH dependent as demonstrated in equation 6.



The redox cycling can be attributed to a purely diffusion-controlled process confirmed by the linear relation between the cathodic peak current and the square root of the scan rate illustrated in **Figure 7.23**.

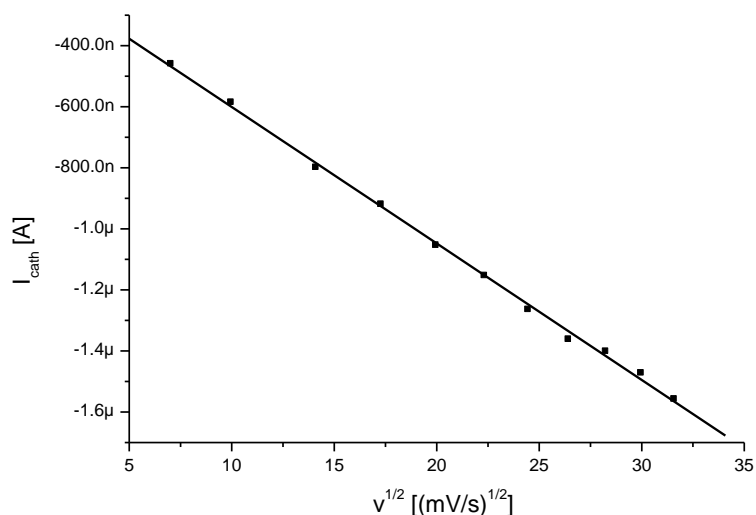


**Figure 7.23:** Linear correlation of the cathodic peak current with the square root of the scan rate for the quasi-reversible diffusion controlled reaction in equation 6 (pH = 11.1).

The peak separation  $\Delta E_p$  found was 83 mV (for comparison deferasirox 93 mV and MSA 102 mV <sup>[40]</sup>). The reduction potential for the  $[\text{Fe}^{\text{III/II}}(\text{DSA})_2]^{5-/6-}$  couple versus NHE was calculated, related to the potential of the Ag/AgCl reference electrode, to be -0.67 V. Further, the reduction potential calculated in relation to the iron(III/II)-hexacyanoferrate system <sup>[63]</sup> has the same value: -0.67 V.

The redox chemistry observed for the  $[\text{Fe}(\text{DSA})_2]^{5-}$  complex is consistent with the investigations of the  $[\text{Fe}(\text{L})_2]^{3-}$  complex of deferasirox. Yet, the reduction potential of the  $[\text{Fe}^{\text{III}}(\text{L})_2]^{3-}$  deferasirox complex determined in pure water is

-0.58 V <sup>[40]</sup>. The reduction potential found for the  $[\text{Fe}^{\text{III/II}}(\text{DSA})_2]^{5-/6-}$  couple is more negative than the one found for the deferasirox  $[\text{Fe}^{\text{III/II}}(\text{L})_2]^{3-/4-}$  couple. This finding can be explained by the fact that the  $\text{Fe}^{\text{III}}$ -DSA complex has a negative charge of 5- and the  $\text{Fe}^{\text{III}}$ -deferasirox of 3- which hampers the reduction of the  $\text{Fe}^{\text{III}}$ -DSA complex causing the reduction potential to shift towards a more negative value.

It is of great importance that the reduction potential of the ferric  $[\text{Fe}(\text{L})_2]^{x-}$  complexes of deferasirox and DSA are found to be in the negative range past about -0.4 V with regard to oxidative stress and redox cycling. With the reduction potentials in this range,  $\text{Fe}^{3+}$  cannot be reduced to  $\text{Fe}^{2+}$  in physiological medium and the ligand complexes used as iron chelating agents cannot induce oxidative stress in the human body <sup>[40]</sup>.

### 7.3 Complex formation of DSA with copper (II)

Copper (II) is one of 11 essential trace elements indispensable to life. Trace elements are present in low concentrations in the human body associated with their main function as catalysts in enzymatic processes in cells. Accordingly, copper (II) is important for protein enzymes such as the metalloenzymes copper oxidases. Further the divalent transition metal has the ability to change its oxidation state easily and thereof the coordination geometry with the protein ligand changes between copper (I) and copper (II) complexes. Proteins use the dependence of the geometry on the oxidation state to control the redox potential of specific Cu-protein complexes. [4]

An important copper-protein and enzyme is caeruloplasmin which is a ferrioxidase. Caeruloplasmin plays a key role in iron metabolism. It converts  $\text{Fe}^{2+}$  to  $\text{Fe}^{3+}$  and increases the rate of loading onto transferrin [64]. Consequently, there is a strong connection between iron and copper metabolism.

The trace element copper is found in all tissues in the human body. High levels of copper concentration are found in the liver and brain. Absorbed copper is immediately bound to the amino acid histidine or the proteins albumin and transcuprin. Intracellular so called “chaperones” escort copper to specific cellular sites and enzymes. Since free copper is toxic in high concentrations ATPase-dependent copper transport proteins in the liver help regulate the copper level in the human body. In fact, the human body has about 40 – 80 mg of total copper. The human diet provides about 2 – 5 mg which covers the daily requirements of 2.5 mg. [4, 64-65]

A genetic defect of a copper transport protein in the liver causes copper overload resulting in a disease called Morbus Wilson. The redox properties of the copper I/II system in excess are responsible for crucial cellular malfunctions which result in liver cirrhosis and brain damage. Patients need a lifelong treatment in form of chelation therapy with D-penicillamine or trien · 2HCl (trientine) to excrete excessive copper. The structure of the chelating ligands is given in **Figure 7.24**. D-Penicillamine forms a purple coloured complex with copper (I) and copper (II) in form of a cluster with chloride as central ion. The cluster anion has the formula  $[\text{Cu}^{\text{I}}_8\text{Cu}^{\text{II}}_6(\text{D-Pen})_{12}\text{Cl}]^{5-}$  [66]. In addition, Morbus

Wilson is treated with zinc salts which are applied to block the intestinal copper uptake [65]. The copper overload caused by Morbus Wilson disease has severe consequences to life expectancy comparable to iron overload caused by haemochromatosis or regular blood transfusions.

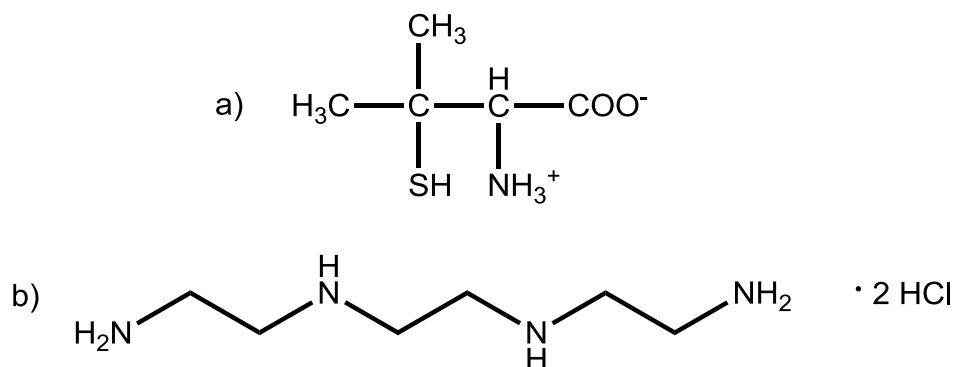


**Figure 7.24:** Copper chelating ligands a) D-penicillamin ( $\beta,\beta$ -dimethylcysteine) and b) trientine (Triethyltetramine dihydrochloride, trien  $\cdot$  2HCl) applied in copper overload therapy.

In summary, copper (II) is an important biometal thus it is of great interest to know the complexation properties of deferasirox and  $\text{Cu}^{2+}$  to identify any interference in chelation therapy of iron overload. Continuous potentiometric titration experiments were performed to identify the species of the  $\text{Cu}^{2+}$ -DSA system in solution. EPR experiments were carried out on deferasirox and DSA  $\text{Cu}^{2+}$  complexes to underline results found by potentiometric titrations. The main question to be clarified is whether deferasirox and its derivatives form dimer or even polymer species with divalent metals such as copper (II).

### 7.3.1 Investigation of the complex formation of DSA with copper (II) in pure water by potentiometric titrations

The deferasirox-copper (II) system was studied by U. Heinz in his doctoral thesis [37]. The determination of stability constants of the copper (II) deferasirox complexes was difficult due to precipitation during the titration experiments. For this reason, he carried out competitive titrations in water/DMSO solution ( $x_{\text{DMSO}} = 0.20$ ) with nitrilotriacetic acid (NTA) as competitive ligand to

keep all complexes in solution. The ligand DSA showed no precipitation for the  $\text{Cu}^{2+}$ :DSA 1:1 and 1:2 titrations in pure water and therefore its complexation chemistry could be successfully investigated by potentiometric titrations.

Preliminary studies on the  $\text{Cu}^{2+}$ -DSA system were performed by F. Teucke, under my surveillance <sup>[49]</sup>. Further studies were necessary due to measurement difficulties resulting from the previously applied electrodes. New titration experiments in pure water were carried out with 3 different  $\text{Cu}^{2+}$ :DSA molar ratios with the electrode Schott IoLine. Conditions for the titration experiments are given in **Table 7.16**.

**Table 7.16:** Titration experiment conditions of the complexation of  $\text{Cu}^{2+}$  with DSA given at  $T = 298 \text{ K}$ .

<b>Conditions for the <math>\text{Cu}^{2+}</math>-DSA titrations</b>			
molar ratio of M:L	1:1	1:2	2:1
measuring method	potentiometric	potentiometric	potentiometric
method type	continuous	continuous	continuous
solvent	pure water	pure water	pure water
$[\text{M}]_t$	1.00 mmol/L	0.50 mmol/L	2.00 mmol/L
$[\text{L}]_t$	1.00 mmol/L	1.00 mmol/L	1.00 mmol/L
titration volume	50.0 mL	50.0 mL	50.0 mL
titrant	0.1 mol/L KOH	0.1 mol/L KOH	0.1 mol/L KOH
supporting electrolyte	0.1 mol/L KCl	0.1 mol/L KCl	0.1 mol/L KCl
electrode	Schott IoLine	Schott IoLine	Schott IoLine
$\text{p}K_w$	13.78	13.78	13.78
pH range	2.7 – 11.0	2.6 – 10.9	2.6 – 3.7
volume of data points	100	90	30
time for mixing process	600 s	600 s	600 s

The titrations performed in the ratios 1:1 and 1:2 showed no precipitation over the whole pH range. Yet, during titration experiments carried out at a 2:1 ratio a green/grey precipitate was observed above pH 4. The composition of the precipitate was not identified.

The purpose of performing titration experiments in different molar ratios is to identify a species model that fits all titrations. Equilibrium constants should be independent from the molar ratio applied. The model and mean values determined are listed in **Table 7.17**.

**Table 7.17:** Mean values of the overall stability constants  $\log\beta_{xyz}$  <sup>[a]</sup> from potentiometric titrations of  $\text{Cu}^{2+}$  with DSA determined by simultaneous evaluation with Hyperquad2008 in pure water,  $T = 298 \text{ K}$  and  $I = 0.1 \text{ mol/L KCl}$ .

<b><math>\log\beta</math> values for the complexation of <math>\text{Cu}^{2+}</math>:DSA</b>	
four 1:1 titrations	four 1:2 titrations
mean values by simultaneous evaluation of 8 titrations <sup>[b]</sup>	
$\sigma$ <sup>[c]</sup>	1.770
pH range	2.7 – 11.0
<b><math>\log\beta_{110}</math></b>	<b>17.93(2)</b>
<b><math>\log\beta_{111}</math></b>	<b>20.4(1)</b>
<b><math>\log\beta_{120}</math></b>	<b>21.8(2)</b>
<b><math>\log\beta_{121}</math></b>	<b>32.7(1)</b>
<b><math>\log\beta_{22-1}</math></b>	<b>29.01(5)</b>
<b><math>\log\beta_{22-2}</math></b>	<b>17.3(1)</b>

<sup>[a]</sup> For the ligand L  $\log\beta_{xyz}$  is defined as:  $\beta_{xyz} = [M_xL_yH_z] \times [M]^{-x} \times [L]^{-y} \times [H]^{-z}$ .

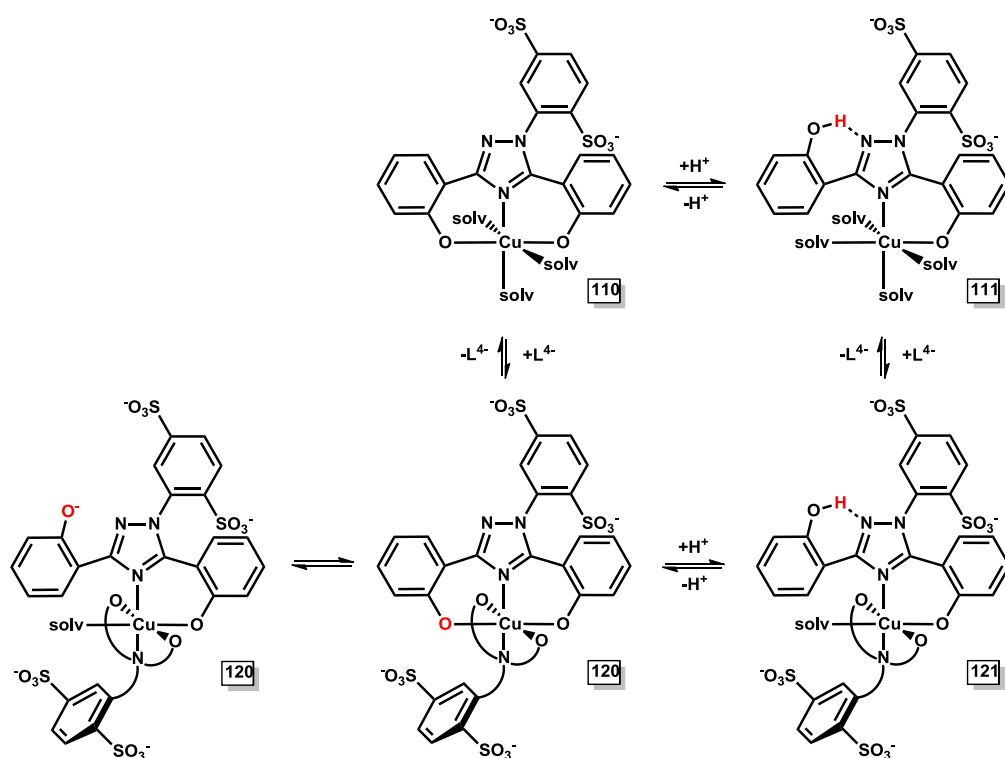
<sup>[b]</sup> The titrations were evaluated simultaneously with the program Hyperquad2008. The deviations given in brackets correspond to the threefold standard deviation taken from Hyperquad2008.

<sup>[c]</sup> The  $\sigma$  value is taken from Hyperquad2008.

At first, titrations of all three molar ratios were evaluated simultaneously with Hyperquad2008. The titration data of the 2:1 molar ratio, before precipita-

tion occurred, was used for evaluation with the other ratios. Unfortunately, the fit was not satisfactory applying the 2:1 data. We assume the pH range from 2.6 to 3.7 was too small for evaluation. Therefore, only the titrations with 1:1 and 1:2 ratios were implemented for evaluation of the stability constants of the  $\text{Cu}^{2+}$ -DSA complexes. Four titration data sets of each molar ratio were used for simultaneous evaluation of the overall stability constants.

Two mononuclear complexes  $[\text{Cu}(\text{L})]^{2-}$  (110 complex) and a protonated complex  $[\text{Cu}(\text{LH})]^{-}$  (111 complex) were identified. In contrast to the  $\text{Fe}^{3+}$  complexes of DSA a 111 complex is formed with  $\text{Cu}^{2+}$ . We assume the protonation occurs at the hydroxyphenyl ring in position 3 which can rotate and form hydrogen bonding interactions with the triazole nitrogen atom in position 2 as illustrated in **Scheme 7.8**. The copper central ion adopts an octahedral environment with a bidentate coordination mode with DSA and solvent molecules taking the place at the free coordination sites.



**Scheme 7.8:** Suggested coordination geometries of the complexes  $[\text{Cu}(\text{L})]^{2-}$  (110),  $[\text{Cu}(\text{LH})]^{-}$  (111),  $[\text{Cu}(\text{L})_2]^{6-}$  (120) and  $[\text{Cu}(\text{L})(\text{LH})]^{5-}$  (121).

The hydrogen bonding interaction contributes to the stabilisation of this coordination, yet the apparent  $\text{p}K_a$  value (deprotonation and formation of  $\text{Cu}-\text{O}$

bond) for the deprotonation of the  $[\text{Cu}(\text{LH})]^-$  complex is 2.5 which originates from the low negative charge of the complex and shows that the tridentate coordination of the 110 complex is the favoured coordination sphere for this kind of ligand. The  $\log\beta_{110} = 17.93(2)$  for the  $[\text{Cu}(\text{DSA})]^{2-}$  complex is evidence for a strong complexation. Yet, the stability constant of the  $[\text{Fe}(\text{DSA})]^-$  was still much stronger with a value of 23.54(4).

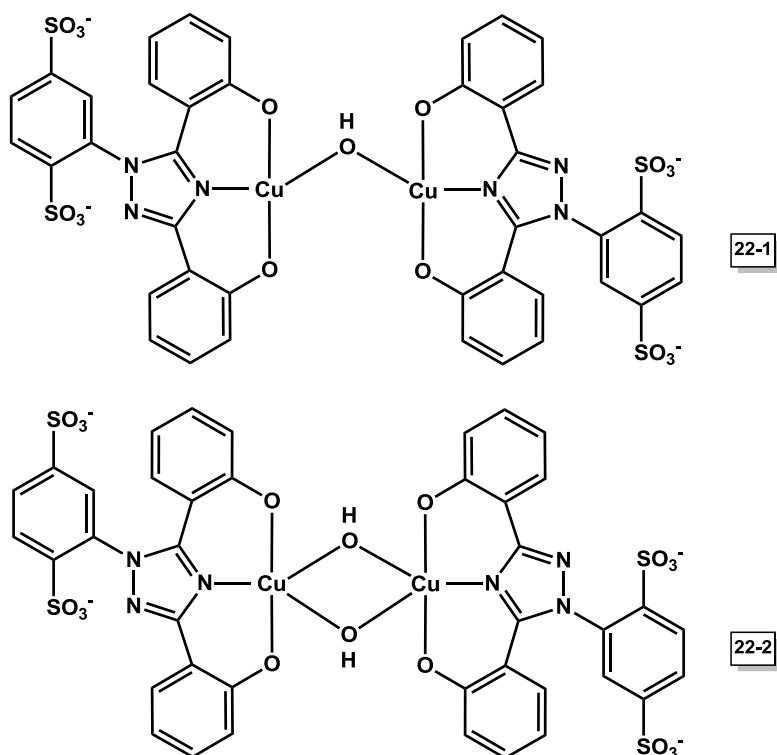
The bis-complexes  $[\text{Cu}(\text{L})_2]^{6-}$  (120 complex) and  $[\text{Cu}(\text{L})(\text{LH})]^{5-}$  (121 complex) determined for  $\text{Cu}^{2+}$ -DSA system are at first sight similar to the complexes found for the  $\text{Fe}^{3+}$ -DSA system. They only differ in charge. Suggestions for the coordination geometry are given in **Scheme 7.8**. The stability constant  $\log K_{120}$  is 3.9 ( $\log K_{120} = [\text{ML}_2] / [\text{ML}] \times [\text{L}]$ ) which is very low and indicates that this complex is not very stable (vs. stability constant  $\log K_{120}$  for  $[\text{Fe}(\text{DSA})_2]^{5-}$  is 15.96). This is not surprising since copper (II) has a  $d^9$  electronic configuration which is known for geometrical distortion by the Jahn-Teller effect. Accordingly, the elongation of the bonds lying axial can occur for the two mononuclear complexes 110 and 111. However, when a second ligand is bound to the  $\text{Cu}^{2+}$  ion a strain of the Cu-O and/or Cu-N distances needs to occur if the complex follows the Jahn-Teller effect. Consequently, the mononuclear complexes experience an energetic stabilisation through the Jahn-Teller effect, in contrast to the bis-complexes which are destabilised by either bond strain through the Jahn-Teller effect or by not distorting the octahedron. For this reason the 120 complex has a very low stability constant and its formation is not favoured.

The apparent  $\text{p}K_a$  value of the deprotonation of the  $[\text{Cu}(\text{L})(\text{LH})]^{5-}$  complex is 10.9. This deprotonation value is higher in contrast to the apparent  $\text{p}K_a = 4.17$  for the previously discussed  $[\text{Fe}(\text{L})(\text{LH})]^{4-}$  complex. In fact, the apparent  $\text{p}K_a$  value (10.9) for the  $[\text{Cu}(\text{L})(\text{LH})]^{5-}$  lies between the two  $\text{p}K_a$  values of the hydroxyphenyl groups of the ligand DSA  $\text{p}K_{a,3} = 9.35(1)$  and  $\text{p}K_{a,3} = 11.32(2)$ . This means that the Cu-O bond of the second ligand in the 120 complex is very weak, if it exists at all. As a consequence, the  $[\text{Cu}(\text{L})_2]^{6-}$  complex consists most probably of a tridentate and a bidentate coordinated ligand rather than of two ligands bound tridentate, as illustrated in **Scheme 7.8**. This result differs from the bis-tridentate coordination mode observed for

$[\text{Fe}(\text{DSA})_2]^{5-}$ . An EPR spectrum in section 7.3.2.3 at pH 10.8 (**Figure 7.38**) gives some evidence for the weak Cu-O coordination in the 120 complex.

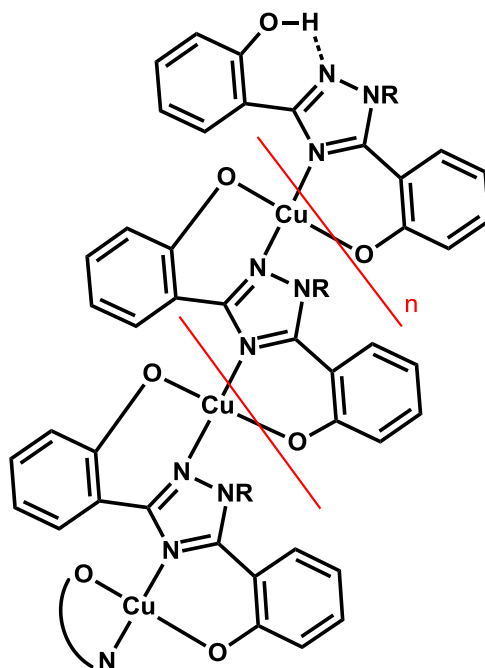
Further, these titration experiments were carried out to bring clarity to the question whether the ligand deferasirox and its derivatives forms dimers or polymers with divalent metal ions as asserted for the 1N-phenyl derivative of deferasirox in literature by Ryabukhin <sup>[41]</sup>. The best possible fit in Hyperquad2008 was found by adding two complexes of the composition  $[\text{Cu}_2(\text{L})_2(\text{OH})_x]$  (22-X complexes) to the species model. The  $\sigma$  value of the fit with a  $[\text{Cu}_2(\text{L})_2(\text{OH})]^{5-}$  (22-1) and a  $[\text{Cu}_2(\text{L})_2(\text{OH})_2]^{6-}$  (22-2) complex was  $\sigma = 1.770$ . In contrast, if these two complexes were excluded from the model the  $\sigma$  value increased to 11.171 indicating a strong contradiction of the model and the experimental titrations. Another model included a  $[\text{Cu}_2(\text{L})_2]^{4-}$  (220 complex) and a 22-1 complex with a  $\sigma$  value of 1.937 (values of the simultaneous evaluation of the 8 titrations as described above:  $\log\beta_{110} = 17.89(3)$ ,  $\log\beta_{111} = 20.5(1)$ ,  $\log\beta_{120} = 21.8(2)$ ,  $\log\beta_{121} = 32.6(1)$ ,  $\log\beta_{220} = 38.0(4)$ ,  $\log\beta_{22-1} = 29.13(6)$ ). A 220 complex would most probably adopt a phenoxo-bridged coordination geometry. Yet, the visual verification of the fit was better for the 22-1 and 22-2 model.

Hydroxo-bridged copper (II) dinuclear complexes of the composition 22-X have been reported in literature. Structures of mono-hydroxo-bridged dicopper(II) complexes of the composition 22-1 are found in literature for example with the ligand tren as a  $[\text{Cu}_2(\text{tren})_2(\text{OH})](\text{ClO}_4)_3 \cdot \text{H}_2\text{O}$  complex <sup>[67]</sup> or with diamino-bis(2-methylpyridyl) and diamino-bis(2-methylbenzimidazolyl) ligands <sup>[68]</sup>. Di-bridged-hydroxo dinuclear copper(II) complexes like the 22-2 complex are also reported in literature for example for the ligand 1,10-phenanthroline <sup>[69]</sup> or the ligands tetramethylethylenediamine and 2,2'-bipyridine <sup>[70]</sup>. Yet, we should note that these ligands all coordinate by nitrogen atoms in contrast to DSA which has an O-N-O coordination. Nevertheless, the principle molecular structure with the hydroxo-bridges should be similar to the ones reported as the structure suggestions in **Scheme 7.9** show.



**Scheme 7.9:** Molecular structure suggestions for the  $[\text{Cu}_2(\text{DSA})_2(\text{OH})]^{5-}$  (22-1) and the  $[\text{Cu}_2(\text{DSA})_2(\text{OH})_2]^{6-}$  (22-2) complexes.

In general these structures should be regarded as suggestions as a consequence of too little experimental evidence for their assignment. The 22-X complexes found can originate from  $[\text{Cu}(\text{L})(\text{OH})_x]$  (11-X) complexes that combine to dinuclear copper (II) complexes. We assume that these complexes do not originate from bidentate coordinating dimers as reported by Ryabukhin. He claims that precipitation observed by adding the divalent metal ions  $\text{Co}^{2+}$ ,  $\text{Ni}^{2+}$  and  $\text{Cu}^{2+}$  to the 1N-phenyl derivative of deferasirox are caused by polymeric structures as illustrated in **Scheme 7.10**<sup>[41]</sup>. In this polymeric structure the ligands would coordinate bidentate and two  $\text{Cu}^{2+}$  ions can coordinate to one ligand molecule forming a  $[\text{Cu}_2(\text{DSA})]$  (210) species monomer. One  $\text{Cu}^{2+}$  ion coordinates to the nitrogen atom in position 2 of the 1,2,4-triazole unit and with the phenolate ring in position 3 twisted towards the copper ion coordinating it. The other  $\text{Cu}^{2+}$  ion is coordinated to the nitrogen atom in position 4 of the 1,2,4-triazole unit and the phenolate in position 5.



**Scheme 7.10:** Possible polymeric structure of deferasirox (R = Ph-COOH) and its derivatives (R = Ph, Ph-SO<sub>3</sub>H, Ph-(SO<sub>3</sub>H)<sub>2</sub>) with divalent metal ions such as copper (II).

The 22-X complexes differ from this kind of polymeric structure since they are presumably aggregation compounds of 11-X complexes. In contrast to the polymeric structure, 22-X compounds adopt a tridentate coordination mode of the ligands and the Cu<sup>2+</sup> ions are connected by hydroxo-bridges. We assume, the twisting of the phenolate group in position 3 is not favoured and therefore the formation of polymeric structures is hampered.

The simultaneous evaluation of the titrations with a molar ratio of Cu<sup>2+</sup>:DSA 1:1 and 1:2 could not be evaluated with 210 or 21-X complexes. However, the individual evaluation of each titration of the three molar ratios showed that a 210 complex could be calculated into the model if the 111 complex was excluded. Yet, not all titrations with the 1:1 molar ratio could be evaluated with the 210 complex. Further, the mean value for the overall stability constant (about  $\log\beta_{210} \approx 21.7$ ) obtained for this 210 complex varied up to 1.2 units between the molar ratios. However, the species distribution calculated for the model with the 210 complex for a 1:2 molar ratio shows that the 210 complex reaches a maximum concentration (< 40%) at about pH 2.8 and is present from the beginning of the titration until pH 4.5. As a result, this complex is not present at physiological pH 7.4.

Consequently, we have decided in favour of the model with the hydroxo-bridged 22-1 and 22-2 dinuclear copper (II) complexes. Accordingly, 8 titrations with two different molar ratios were successfully evaluated simultaneously with this model with the best achieved  $\sigma$  value of 1.770. Nevertheless, we cannot exclude the possibility that 21X complexes exist in solution.

The titration curves performed in two molar ratios  $\text{Cu}^{2+}$ :DSA 1:1 and 1:2 are illustrated in **Figure 7.25**. They are depicted in comparison to the ligand titration curve. All titration curves with  $\text{Cu}^{2+}$  show a pH decrease compared to the  $\text{p}K_a$  titration curve of DSA. This can be attributed to the complexation of the ligands with  $\text{Cu}^{2+}$  which is also observed in the light green colour of the solution prior to the titration. During the titration the solutions colour turns to bright green and at the end to dark green.

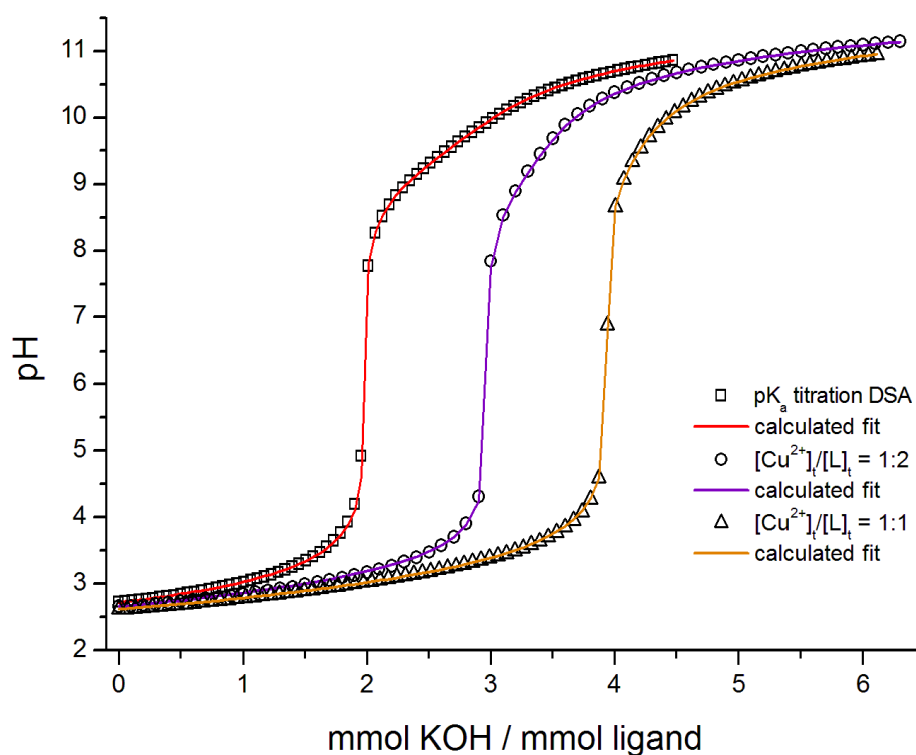


**Figure 7.25:** Potentiometric titration curves of the free ligand DSA and  $\text{Cu}^{2+}$  with DSA with the molar ratios 1:2 ( $[\text{Cu}^{2+}]_t = 0.50$  mmol/L,  $[\text{L}]_t = 1.00$  mmol/L) and 1:1 ( $[\text{Cu}^{2+}]_t = 1.00$  mmol/L,  $[\text{L}]_t = 1.00$  mmol/L) in pure water,  $T = 298$  K and  $I = 0.1$  mol/L KCl. The open squares, circles and triangles represent experimental points and the fit (solid line) was calculated from the equilibrium constants with Hyperquad2008.

The titration performed in a  $\text{Cu}^{2+}$ :DSA 1:2 molar ratio shows an inflection point at 3 equivalents revealing that the  $[\text{Cu}(\text{L})]^{2-}$  complex has formed to its maximum concentration (100% at pH 6) as illustrated in the species distribution diagram in **Figure 7.26**. This complex is the predominant complex from pH 3 to 10 which is found in the whole titration range investigated. At the beginning of the titration about 62% free  $\text{Cu}^{2+}$  ion is present in solution, yet 24%  $[\text{Cu}(\text{L})]^{2-}$  complex and 14%  $[\text{Cu}(\text{LH})]^{-}$  complex have already formed causing the light green colour of the solution. From pH 5 to 7 we observe a completion of the  $[\text{Cu}(\text{L})]^{2-}$  complex formation. In alkaline solution the two dinuclear hydroxo-bridged copper (II) complexes are present. The mono-hydroxo-bridged  $[\text{Cu}_2(\text{L})_2(\text{OH})]^{5-}$  complex starts to form at pH 7.5 and reaches its highest concentration of 45% at the end of the titration at pH 11.

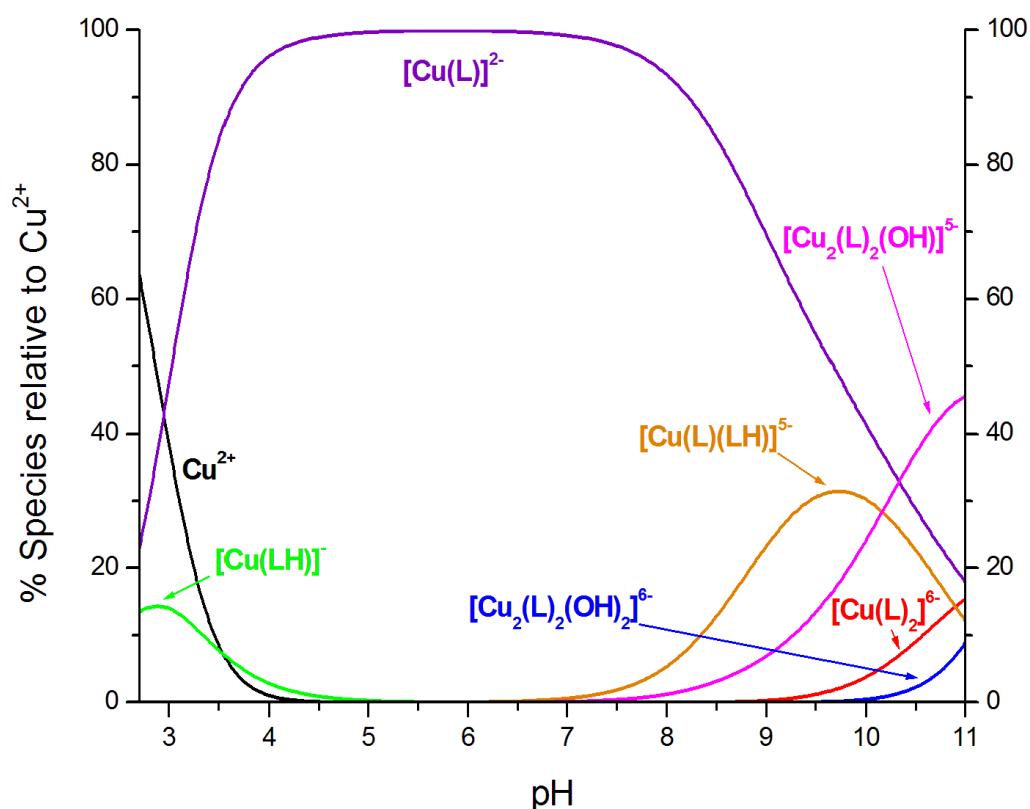


**Figure 7.26:** Species distribution diagram as a function of pH for  $\text{Cu}^{2+}$  with the ligand DSA. Calculated for the continuous potentiometric titration performed with a 1:2 molar ratio ( $[\text{Cu}^{2+}]_t = 0.50$  mmol/L,  $[\text{L}]_t = 1.00$  mmol/L, pure water,  $T = 298$  K and  $I = 0.1$  mol/L KCl) from pH 2.7 to 11.0. The species concentration were calculated from the equilibrium constants listed in **Table 7.17** (mean values from simultaneous evaluation of 8 titrations) with the program Hyss2006.

Further, the di-bridged  $[\text{Cu}_2(\text{L})_2(\text{OH})_2]^{6-}$  complex is only present at pH 10 to 11 with a concentration of 9% at the end of the titration. Accordingly, the  $[\text{Cu}_2(\text{L})_2(\text{OH})]^{5-}$  complex plays a dominant role in alkaline solution. At physiological pH 7.4 hardly any dinuclear complexes exist. Whereas, the  $[\text{Cu}_2(\text{L})_2(\text{OH})_2]^{6-}$  complex is only present in strong alkaline solution with a concentration less than 10%. This complex plays no role at physiological pH. A considerable amount of the bis-complex  $[\text{Cu}(\text{L})(\text{LH})]^{5-}$  starts forming at pH 7 and reaches a maximum concentration of 31% at pH 9.7. It then deprotonates to the bis-complex  $[\text{Cu}(\text{L})_2]^{6-}$  which is only formed to a concentration of 15% at the end of the titration. The low concentration of the  $[\text{Cu}(\text{L})_2]^{6-}$  complex at high pH underlines our prediction that these 1:2 complexes are not favoured due to the impact of the Jahn-Teller effect.

Another titration curve illustrated in **Figure 7.25** was performed with a 1:1 molar ratio. The inflection point appears at 4 equivalents also indicating the completion of the formation of the  $[\text{Cu}(\text{L})]^{2-}$  complex. The species distribution diagram for the 1:1 molar ratio is given in **Figure 7.27**.

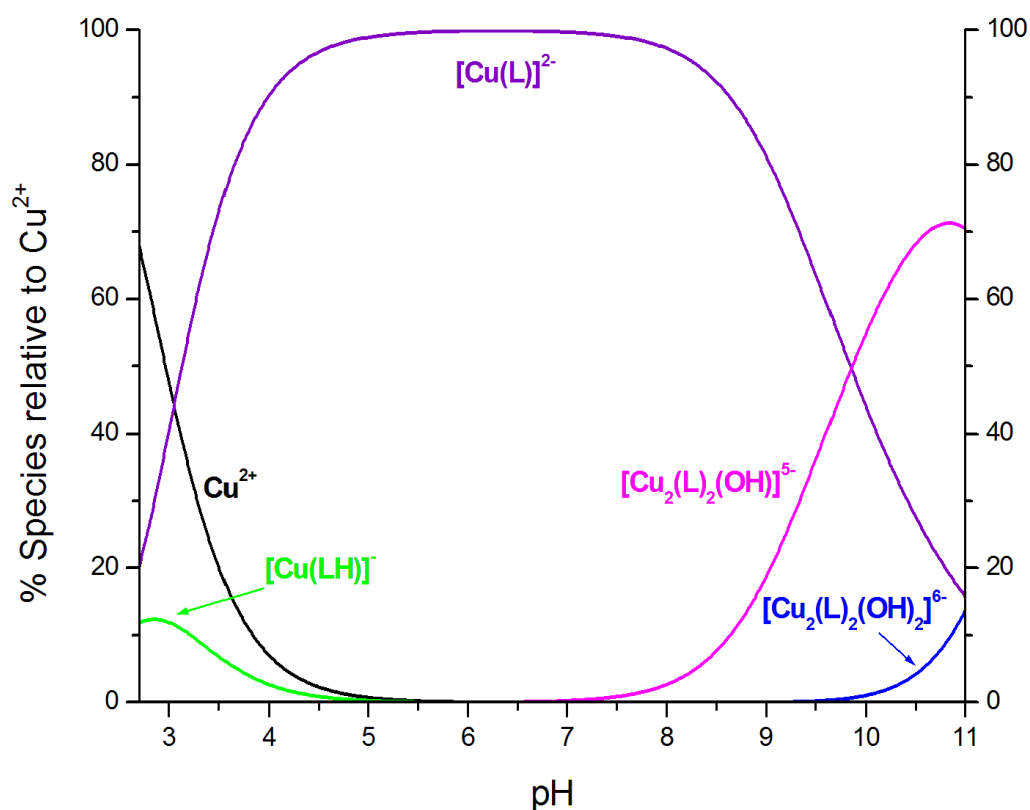


**Figure 7.27:** Species distribution diagram as a function of pH for  $\text{Cu}^{2+}$  with the ligand DSA. Calculated for the continuous potentiometric titration performed with a 1:1 molar ratio ( $[\text{Cu}^{2+}]_t = 1.00 \text{ mmol/L}$ ,  $[\text{L}]_t = 1.00 \text{ mmol/L}$ , pure water,  $T = 298 \text{ K}$  and  $I = 0.1 \text{ mol/L KCl}$ ) from pH 2.7 to 11.0. The species concentration were calculated from the equilibrium constants listed in **Table 7.17** (mean values from simultaneous evaluation of 8 titrations) with the program Hyss2006.

At the start pH 2.7 of the titration 66% free  $\text{Cu}^{2+}$  ion, 21%  $[\text{Cu}(\text{L})]^{2-}$  complex and 12%  $[\text{Cu}(\text{LH})]^{-}$  complex are present. The  $[\text{Cu}(\text{L})]^{2-}$  complex in this species distribution is the major component throughout the whole titration range. It is predominant species from pH 3 to 9.7. The bis-complexes  $[\text{Cu}(\text{L})_2]^{6-}$  and  $[\text{Cu}(\text{L})(\text{LH})]^{5-}$  are not present in this species distribution. Instead, the dinuclear hydroxo-bridged  $\text{Cu}^{2+}$  complexes are more present. The  $[\text{Cu}_2(\text{L})_2(\text{OH})]^{5-}$  complex begins to form at pH 7.5 and reaches its highest concentration of 71% at pH 10.8.

The  $[\text{Cu}_2(\text{L})_2(\text{OH})_2]^{6-}$  complex begins to form at pH 9.5 and reaches a concentration of 13.3% at the end of the titration. Thus, the 1:2 complexes are not favoured by the given molar ratio in contrast to the 22-1 and 22-2 dinuclear

complexes which are the dominant species in alkaline solution. This observation correlates with the hypothesis that 22-X complexes are aggregation compounds of 11-X complexes since these are favoured in a  $\text{Cu}^{2+}$ :DSA 1:1 molar ratio titration.

Taken together, the model found for the  $\text{Cu}^{2+}$ :DSA 1:2 and 1:1 molar ratio titrations with the best minimized  $\sigma$  value comprehends a  $[\text{Cu}_2(\text{L})_2(\text{OH})]^{5-}$  and a  $[\text{Cu}_2(\text{L})_2(\text{OH})_2]^{6-}$  complex in addition to the expected mono and bis-complexes. We need to point out that we cannot exclude that any 21X or 220 species also exist in solution. Of special importance is the complexation of  $\text{Cu}^{2+}$  with DSA at physiological pH 7.4. A possible 210 complex would only be found in acidic solution and not at pH 7.4. The  $[\text{Cu}_2(\text{L})_2(\text{OH})]^{5-}$  complex just begins to form at pH 7.4 and is therefore not relevant since its concentration is below 2%. Additionally, the  $[\text{Cu}_2(\text{L})_2(\text{OH})_2]^{6-}$  complex is only found in alkaline solution pH > 10. If we regard the model with the 220 and  $[\text{Cu}_2(\text{L})_2(\text{OH})]^{5-}$  complexes the 220 complex is present at pH 7.4 with 12%. The dominant complex at physiological pH in all models is however the  $[\text{Cu}(\text{L})]^{2-}$  complex which is present to more than 80%.

It was a great achievement to be able to investigate copper (II) complexes of the ligand DSA in pure water. These investigations have brought more insight into the complex behaviour of the deferasirox system with the help of a related water soluble ligand.

### 7.3.2 EPR-Experiments with copper (II) complexes of deferasirox and DSA

Electron paramagnetic resonance (EPR) spectroscopy is a high-frequency method used to study compounds with one or more unpaired electrons. Hence, this method is only applicable to paramagnetic substances for example organic or inorganic free radicals or complexes with transition metal ions. The basic physical principle is similar to that of NMR spectroscopy, yet in this case electron spins are excited instead of nuclear spins. In EPR spectroscopy the g-factor corresponds to the chemical shift  $\delta$  in NMR spectroscopy and the hyperfine coupling constant to the internuclear coupling constant J. All EPR spectra were performed by Prof. P. Strauch at the University of Potsdam. [71]

#### 7.3.2.1 EPR-spectra of the powdered deferasirox copper (II) precipitate

The attempt to study deferasirox complexes with  $\text{Cu}^{2+}$  in water/DMSO solutions with potentiometric titrations resulted in precipitation of a green solid throughout the whole titration range. The green precipitate started to form at pH 2 and did not dissolve until pH 12.5 (water/DMSO  $x_{\text{DMSO}} = 0.20$ ). The stability constants determined by U. Heinz were obtained by competitive titration experiments with nitrilotriacetic acid (NTA) as competitive ligand [37].

For clarity, it is still of interest to study the composition of the green precipitate. For this reason, EPR spectroscopy was performed with the isolated and dried green precipitate. The EPR spectrum of a freshly prepared sample is given in **Figure 7.28**. In the EPR spectrum we can identify four lines on the left assigned to the parallel part of the spectrum and one large line pointing downwards which is the perpendicular part of the spectrum. This splitting of the spectrum is typical for an isolated  $\text{Cu}^{2+}$  centre with axial symmetry. This is not unlikely, since  $\text{Cu}^{2+}$  is known for Jahn-Teller distortion of the octahedron causing a tetragonal environment. The four lines of the parallel section contribute to the hyperfine coupling of the copper (II) nuclear spin  $I = 3/2$  with the electron spin  $S = 1/2$ . Further, parameters of the spectrum could be evaluated as for example the hyperfine coupling constant for the parallel section is

$A_{\parallel} = 121(2)$  G and the g-factor is  $g_{\parallel} = 2.325(5)$ . The g-factor for the perpendicular section is  $g_{\perp} = 2.06(1)$  and the hyperfine coupling constant is  $A_{\perp} \approx 10$  G.

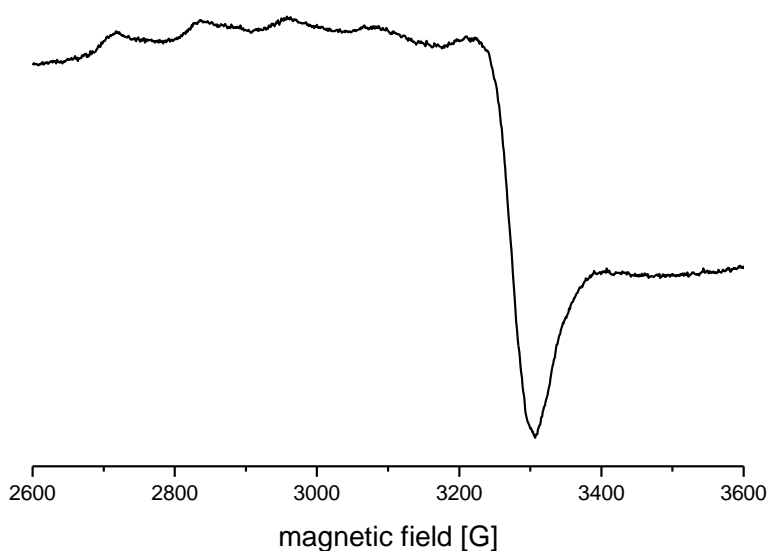


**Figure 7.28:** X-band EPR-spectrum of the freshly prepared sample of the green  $\text{Cu}^{2+}$ -deferasirox precipitate with  $A_{\parallel} = 121(2)$  G,  $g_{\parallel} = 2.325(5)$ ,  $g_{\perp} = 2.06(1)$  and  $A_{\perp} \approx 10$  G.

A hypothesis for the composition of the green insoluble solid is that it might be a solvated  $[\text{Cu}(\text{LH})]$  complex. This complex is neutral in charge which hampers solubility. In addition, it is a mononuclear complex with tendency to axial geometry which is in agreement with the EPR spectrum. A simulated EPR spectrum generated with the given parameters, by Prof. P. Strauch, and the experimental spectrum are shown in **Figure 7.29**. The simulated spectrum correlates very well with the measured spectrum.

Effectively, after a period of about two months the samples EPR spectrum begins to undergo changes. The signal observed at 3250 G is replaced by a new broad and badly resolved signal at 3110 G of lower intensity. Accordingly, this broad signal with its low intensity is coupled with the changes within the solid we might attribute to copper (II) – copper (II) interactions with significant antiferromagnetic coupling <sup>[72]</sup>.

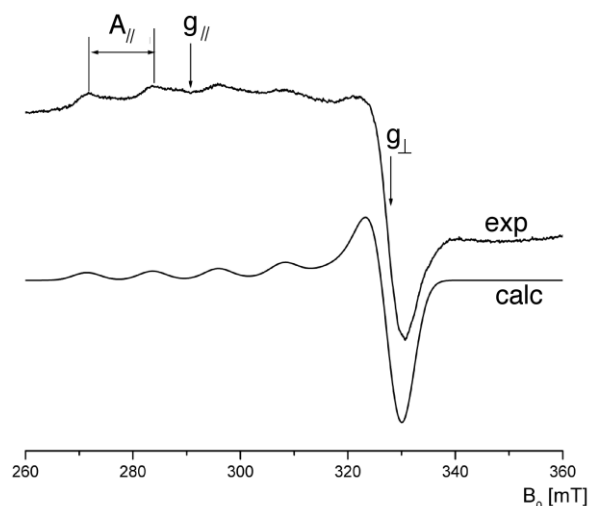


**Figure 7.29:** Experimental and simulated spectrum of the freshly prepared sample of the green  $\text{Cu}^{2+}$ -deferasirox precipitate. The simulated spectrum was calculated with the given experimental parameters ( $A_{||}$  hyperfine coupling constant,  $g_{||}$  and  $g_{\perp}$  g-factors for the parallel and perpendicular part of the spectrum, exp is the experimental spectrum and calc the simulated spectrum,  $B_0$  magnetic field in mT) <sup>[72]</sup>.

The changes in the solid can also be induced by raising the temperature during EPR measurements. Spectra collected at variable temperatures between 296 K and 434 K show a strong decrease of the signal as illustrated in **Figure 7.30**.

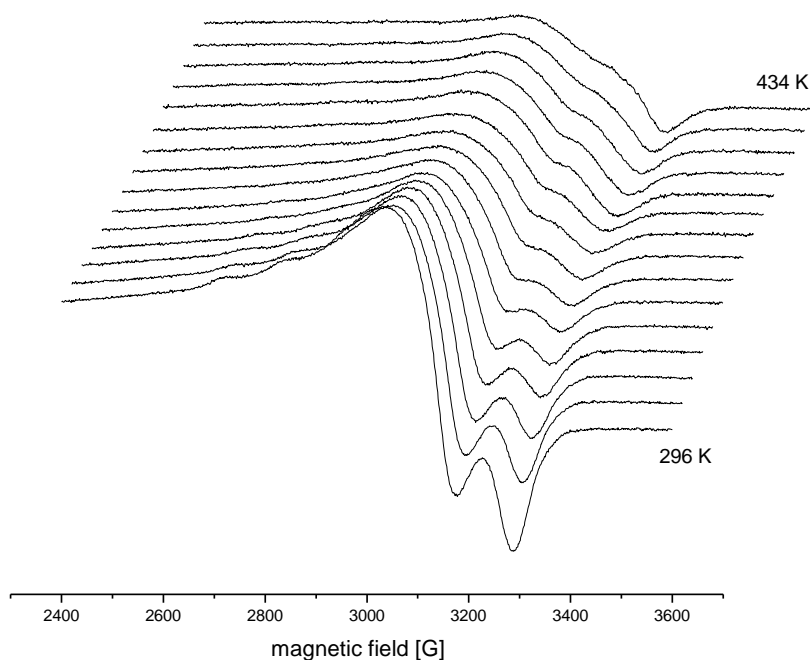


**Figure 7.30:** EPR spectra of the freshly prepared sample of the green  $\text{Cu}^{2+}$ -deferasirox precipitate at variable temperatures.

In conclusion, the green precipitate is a mononuclear species with axial geometry, presumably the [Cu(LH)] complex. This complex seems to age which causes a significant change in the EPR spectrum. The badly resolved broad signal can be explained by an increase in antiferromagnetic coupling as expected for a polymeric structure as shown in **Scheme 7.10** with copper (II) – copper (II) interactions. It is noteworthy, that this is just one interpretation of these spectra. Yet, there is no definite proof to confirm the formation of a polymeric structure.

### 7.3.2.2 EPR-spectra of the deferasirox copper (II) complexes in frozen solutions

The green precipitate was observed from pH 2 until about pH 12.5 in a water/DMSO solution ( $x_{\text{DMSO}} = 0.20$ ). Accordingly, the precipitate dissolves again in alkaline solution. For this reason, the pH of a freshly prepared solution ( $[\text{Cu}^{2+}]_{\text{t}} = 2.0$  mmol/L and  $[\text{L}]_{\text{t}} = 2.0$  mmol/L) was adjusted to pH 13.0 until all precipitate was dissolved and an EPR spectrum was measured of the dark green solution frozen at 126 K. Unfortunately, the spectra were badly resolved and no hyperfine coupling could be identified. The sample was to dilute, consequently a doubly concentrated sample ( $[\text{Cu}^{2+}]_{\text{t}} = 4.0$  mmol/L and  $[\text{L}]_{\text{t}} = 4.0$  mmol/L) was prepared with a molar fraction of  $x_{\text{DMSO}} = 0.22$  to ensure solubility. The EPR spectrum recorded at 126 K and pH 13.9 is presented in **Figure 7.31**. In this spectrum one component seems to predominate. One defined set of 4 lines is observed for the parallel part of the spectrum indicating one isolated copper (II) centre. The EPR parameters of this species are  $A_{\parallel} = 156(3)$ ,  $g_{\parallel} = 2.285(5)$ . In comparison to the spectrum of the green solid in **Figure 7.28** this is a different species according to the different EPR parameters. Further, the perpendicular line of the signal is split. This can be explained by a reduction of the axial symmetry to rhombic symmetry. This spectrum indicates a mononuclear copper (II) complex with rhombic symmetry.

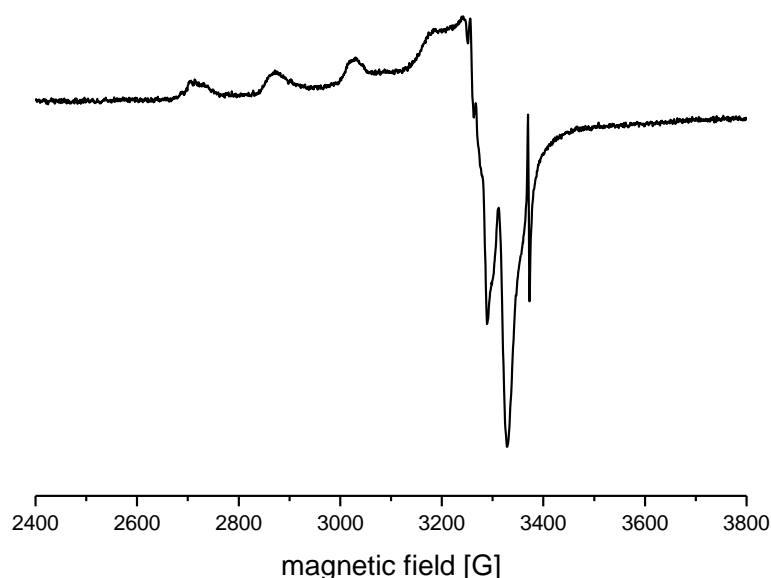


**Figure 7.31:** EPR spectrum of the frozen solution of the  $\text{Cu}^{2+}$ -deferasirox system at pH 13.9 ( $T = 126 \text{ K}$ ,  $[\text{Cu}^{2+}]_t = 4.0 \text{ mmol/L}$ ,  $[\text{L}]_t = 4.0 \text{ mmol/L}$  and  $x_{\text{DMSO}} = 0.22$ ). The parameters are  $A_{\parallel} = 156(3)$ ,  $g_{\parallel} = 2.285(5)$ .

Another spectrum collected at 126 K, from a second sample of the solution at pH 13.9 is given in **Figure 7.32**. This EPR spectrum seems to contain the same species observed in the spectrum in **Figure 7.31**. Curiously, it also reveals the set of lines for at least one or even two other species. These species also have isolated  $\text{Cu}^{2+}$  centres, unfortunately their spectra strongly interfere with each other. Two sets of lines are marked with black and blue arrows. Additionally, the perpendicular line also splits up. The green marked splitting of this line may originate from a hyperfine coupling interaction caused by molecular orbitals formed with the p-orbital of a nitrogen atom ( $S = 1$ , expecting 3 lines in the spectrum) interacting with the electron density of  $\text{Cu}^{2+}$ . The other splitting may again refer to the decrease of symmetry to rhombic symmetry. Unfortunately, the spectra all overlies each other consequently their parameters cannot be identified.

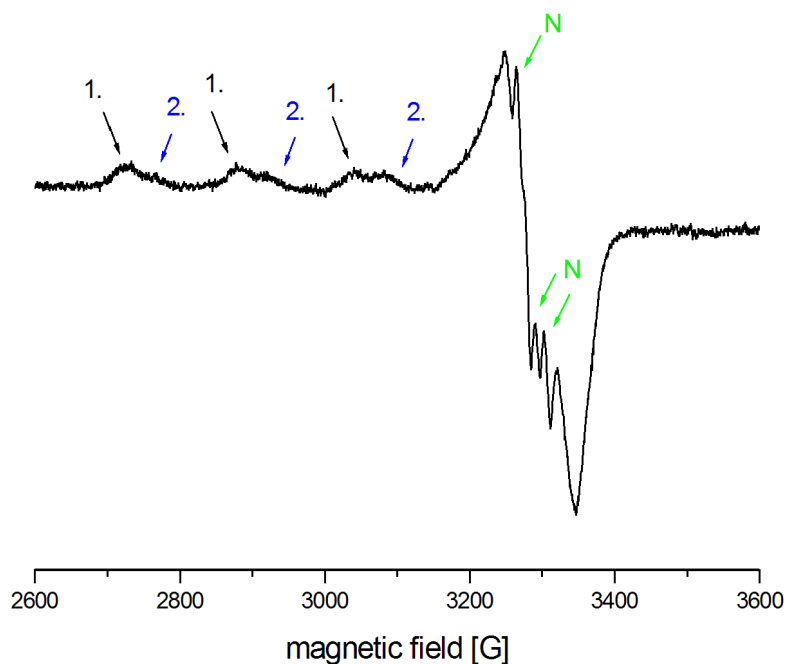


**Figure 7.32:** EPR spectrum of the frozen solution of the  $\text{Cu}^{2+}$ -deferasirox system at pH 13.9 ( $T = 126 \text{ K}$ ,  $[\text{Cu}^{2+}]_t = 4.0 \text{ mmol/L}$ ,  $[\text{L}]_t = 4.0 \text{ mmol/L}$  and  $x_{\text{DMSO}} = 0.22$ ).

Taken together, the EPR spectra of a frozen solution of  $\text{Cu}^{2+}$  and deferasirox at pH 13.9 in water/DMSO ( $x_{\text{DMSO}} = 0.22$ ) revealed one dominant species with different EPR parameters than the species found in the powdered precipitate. A second spectrum showed that at least one other species is present in solution. We deduce from both spectra that the copper (II) centres of all species are isolated. However the parameters of these additional species could not be identified due to overlapping of the spectra. Despite the above, the spectra indicate that the axial symmetry is decreased to a slightly rhombic distortion of the symmetry which is evidence for the change in the coordination sphere of the copper (II) centres of the complexes in solution.

It seems that the precipitate consisting of an insoluble complex (or polymeric structure) dissolves in alkaline solution by changing its coordination environment from axial to rhombic. At least two mononuclear copper (II) complexes form and are significantly soluble in the water/DMSO solution at pH 13.9.

### 7.3.2.3 EPR-spectra of the DSA copper (II) complexes in frozen solutions

A sample of a  $\text{Cu}^{2+}$  and DSA solution with a 1:2 molar ratio was prepared in pure water for EPR measurements. EPR spectra collected at ambient temperature were unsuitable due to strong interactions between the molecules in solution. To suppress intermolecular interactions the EPR spectra were recorded in frozen solutions. Since these samples were diluted by the solvent the solution needed to be more concentrated. The sample solutions were prepared with a concentration of 5.0 mmol/L of  $\text{Cu}^{2+}$  and 10.0 mmol/L of the ligand DSA. Four samples of the given concentration at selected pH values were prepared and their EPR spectra recorded.

A species distribution diagram calculated with the stability constants determined in section 7.3.1 for the given concentrations is presented in **Figure 7.33**.

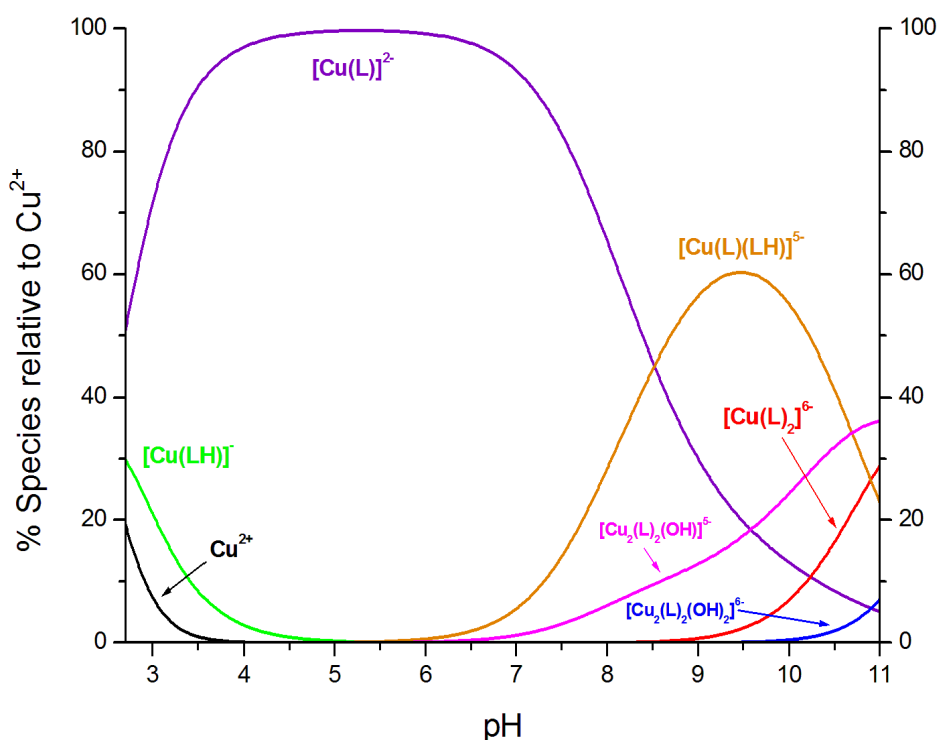


**Figure 7.33:** Species distribution diagram as a function of pH for  $\text{Cu}^{2+}$  with the ligand DSA. Calculated for a 1:2 molar ratio ( $[\text{Cu}^{2+}]_t = 5.0$  mmol/L,  $[\text{L}]_t = 10.0$  mmol/L, pure water,  $T = 298$  K and  $I = 0.1$  mol/L KCl) from pH 2.7 to 11.0. The species concentration were calculated from the equilibrium constants listed in **Table 7.17** (mean values from simultaneous evaluation of 8 titrations) with the program Hyss2006.

The first EPR spectrum was recorded at pH 2.7 as a frozen sample at 180 K. The EPR spectrum is illustrated in **Figure 7.34**.

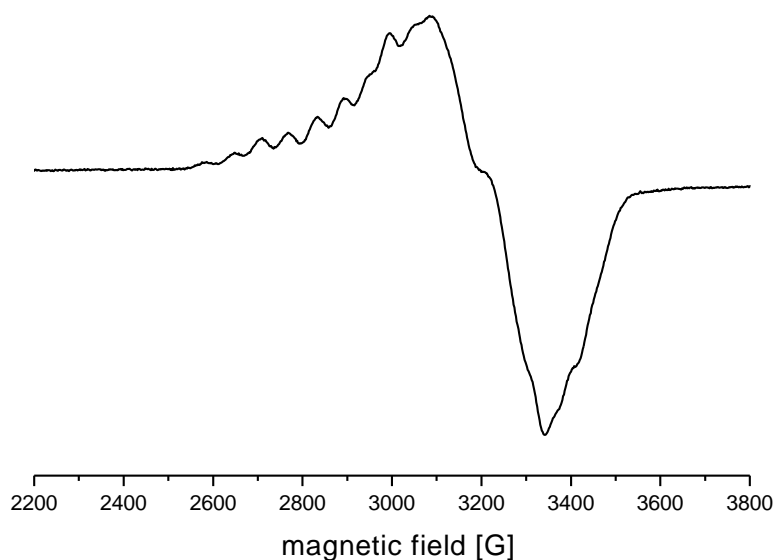


**Figure 7.34:** EPR spectrum of the  $\text{Cu}^{2+}$ -DSA system at pH 2.7 in frozen solution at 180 K (pure water,  $[\text{Cu}^{2+}]_t = 5.0 \text{ mmol/L}$  and  $[\text{L}]_t = 10.0 \text{ mmol/L}$ ).

The hyperfine coupling observed in this spectrum shows at least 7 or 8 lines in the parallel part. These lines do not seem to be equally spaced. For an isolated  $\text{Cu}^{2+}$  centre we would expect four equally spaced lines with a distinct hyperfine coupling constant. For the attempt to interpret this spectrum there are two theories. One is that at least two species are present in this spectrum forming two sets of the expected four lines for isolated  $\text{Cu}^{2+}$  centres. A look at the species distribution in **Figure 7.33** shows that at pH 2.7, the very beginning of the species distribution, two predominant complexes  $[\text{Cu}(\text{L})]^{2-}$  (52%) and  $[\text{Cu}(\text{LH})]^-$  (29%) and about 19% free  $\text{Cu}^{2+}$  (aq) ion are present. The spectrum could be explained by these two complexes present in solution forming two sets of four lines. However, a clear determination of the EPR parameters  $g$ -factor and  $A_{\parallel}$  was not possible since these lines overlap and cannot be allocated. The free  $\text{Cu}^{2+}$  ion should also induce a set of lines in the EPR spectrum. A possible explanation is that this set of lines overlaps with those of the complexes and cannot be identified separately. The perpendicular part of the spec-

trum shows strong line broadening and is badly resolved. Consequently, a prediction of the geometry of the species is hindered. The broad line in the perpendicular part does not distinctly split which may be evidence for axial geometry or only very little rhombic distortion.

A second interpretation for this multi-lined spectrum could be the presence of two neighbouring  $\text{Cu}^{2+}$  centres interacting. If two  $\text{Cu}^{2+}$  centres are coordinated to the same complex their nuclear spins  $S = 3/2$  will interact with each other causing a hyperfine coupling observed as a septet signal in the EPR spectrum. Seven lines of the observed EPR spectrum at pH 2.7 could fulfil this criterion. An additional half field signal assigned to the forbidden transition  $\Delta m_s = \pm 2$  was observed as shown in **Figure 7.35**. This badly resolved signal could be evidence for a  $\text{Cu}^{2+}$ - $\text{Cu}^{2+}$  interaction.

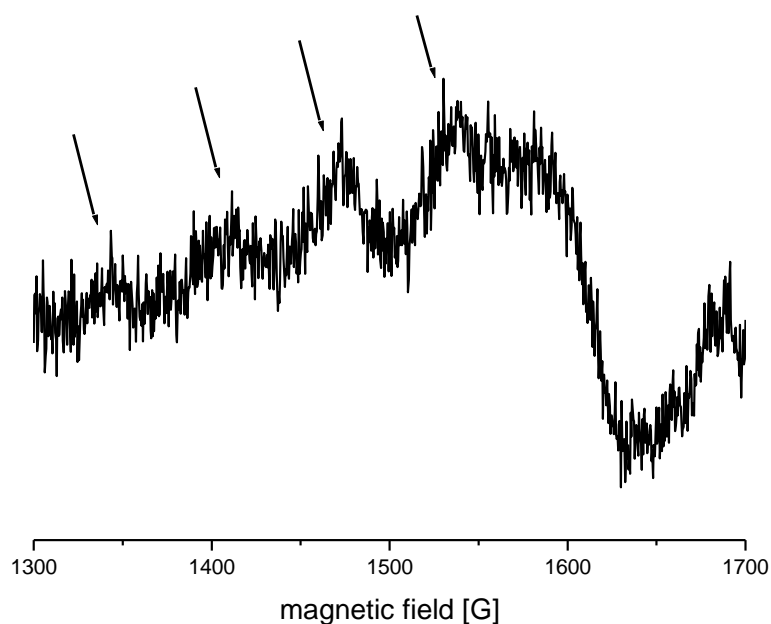


**Figure 7.35:** Half field EPR spectrum observed for the EPR spectrum at pH 2.7.

In section 7.3.1 a possible  $[\text{Cu}_2(\text{DSA})]$  complex was discussed which, if existent, would be present in acidic solution. We cannot exclude that this signal could be assigned to a dimeric  $[\text{Cu}_2(\text{DSA})]$  complex.

A second sample of the  $\text{Cu}^{2+}$ -DSA system was prepared at pH 5.8. The EPR spectrum is given in **Figure 7.36**.

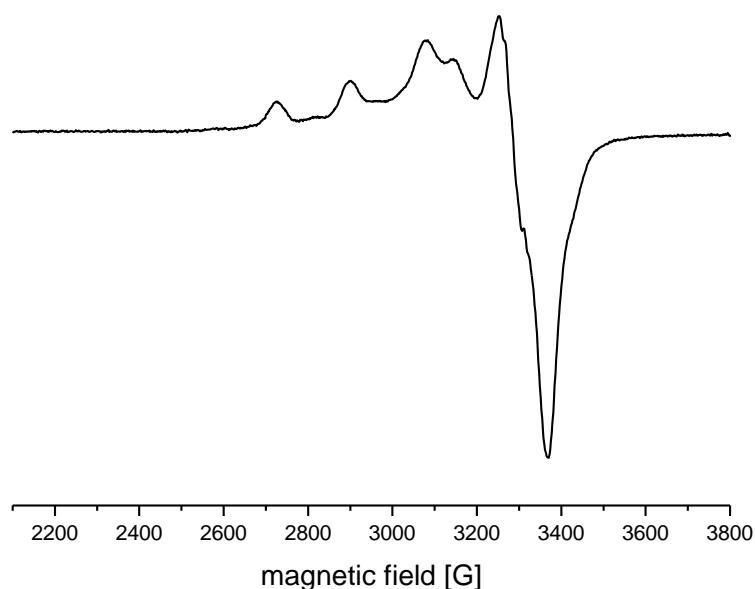


**Figure 7.36:** EPR spectrum of the  $\text{Cu}^{2+}$ -DSA system at pH 5.8 in frozen solution at 127 K (pure water,  $[\text{Cu}^{2+}]_t = 5.0$  mmol/L and  $[\text{L}]_t = 10.0$  mmol/L).

The EPR spectrum shows one dominating species generating three distinctive lines in the parallel part of the EPR spectrum. The fourth line seems to overlap with the perpendicular part of the spectrum. At this pH value the  $[\text{Cu}(\text{DSA})]^{2-}$  complex is major component (99%) in the species distribution. It is likely that the observed lines in the EPR spectrum are caused by the mononuclear  $[\text{Cu}(\text{DSA})]^{2-}$  complex. The perpendicular part of the spectrum gives rise to a mainly axial symmetry in the complex.

In **Figure 7.37** the EPR spectrum at pH 9.6 is illustrated. This spectrum is not very well resolved. The perpendicular part of the spectrum gives evidence for axial symmetry of the complexes. The parallel part shows one minor set of 4 lines, indicated by the black arrows, and one hardly visible set of four lines indicated by the blue arrows. The species observed in this spectrum seem to contain isolated copper (II) centres, yet these lines are of minor quality so that it is difficult to make a statement on how many species are present at this pH. In the species distribution we find one predominant component which is the  $[\text{Cu}(\text{L})(\text{LH})]^{5-}$  complex to 60%. Further, a mono-hydroxo-bridged dicopper (II) complex of the composition  $[\text{Cu}_2(\text{L})_2(\text{OH})]^{5-}$  is observed with a concentration of

18%, also the  $[\text{Cu}(\text{L})]^{2-}$  complex is present with 18%. A di-bridged hydroxo dinuclear copper (II) complex of the composition  $[\text{Cu}_2(\text{L})_2(\text{OH})_2]^{6-}$  is not of relevance since it just begins to form at pH 9.6.

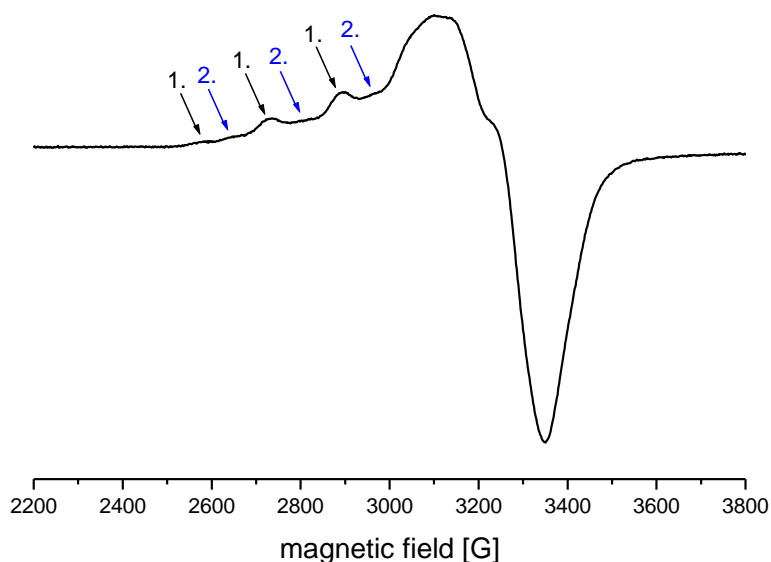


**Figure 7.37:** EPR spectrum of the  $\text{Cu}^{2+}$ -DSA system at pH 9.6 in frozen solution at 180 K (pure water,  $[\text{Cu}^{2+}]_t = 5.0$  mmol/L and  $[\text{L}]_t = 10.0$  mmol/L).

If we speculate on the EPR spectrum containing two species with isolated copper (II) centres we could assign these to the  $[\text{Cu}(\text{L})(\text{LH})]^{5-}$  complex as major species and the  $[\text{Cu}(\text{L})]^{2-}$  complex as a minor species. According to literature hydroxo-bridged dinuclear copper (II) complexes can be EPR silent on account of strong  $\text{Cu}^{2+}$ - $\text{Cu}^{2+}$  interactions resulting from antiferromagnetic interactions (Lee2005, Kawata1987) <sup>[73-74]</sup>. Subsequently, the  $[\text{Cu}_2(\text{L})_2(\text{OH})]^{5-}$  complex might be silent in the EPR spectrum.

A final EPR spectrum of the  $\text{Cu}^{2+}$ -DSA system was recorded at pH 10.8. The spectrum is given in **Figure 7.38**. There are three lines in the parallel part of the spectrum. The fourth line seems to overlap with the perpendicular part. Further, the spectrum indicates only one species as dominating species in solution. EPR parameters for this species were calculated to  $A_{\parallel} = 166(5)$  G and  $g_{\parallel} = 2.257(5)$ . In addition, the perpendicular part gives evidence for an axial geometry.

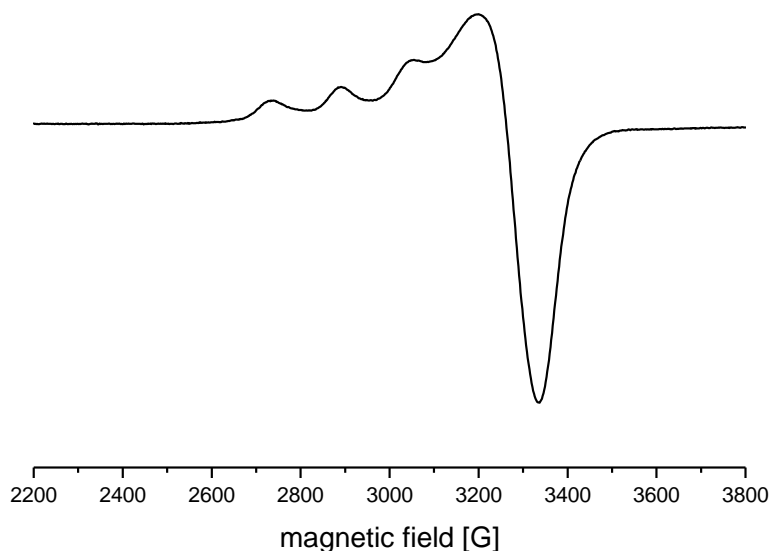


**Figure 7.38:** EPR spectrum of the  $\text{Cu}^{2+}$ -DSA system at pH 10.8 in frozen solution at 180 K (pure water,  $[\text{Cu}^{2+}]_t = 5.0 \text{ mmol/L}$  and  $[\text{L}]_t = 10.0 \text{ mmol/L}$ ).

The species distribution reveals that three complexes coexist in solution at pH 10.8. The concentration of the  $[\text{Cu}(\text{L})(\text{LH})]^{5-}$  complex decreased to 30% while the formation of the  $[\text{Cu}_2(\text{L})_2(\text{OH})]^{5-}$  has increased to 35%. The 1:2 complex  $[\text{Cu}(\text{L})_2]^{6-}$  has also been formed to 24%. We assume the EPR signal of the hydroxo-bridged complex is silent. Still two bis-complexes coexist in solution but only one set of lines has been identified in the spectrum. In **Scheme 7.8** in section 7.3.1 two coordination geometries are suggested for the  $[\text{Cu}(\text{L})_2]^{6-}$  complex. Due to the high apparent  $\text{p}K_a$  (10.9) of the 121 complex it has been assumed that the phenolate group, resulting from the deprotonation of the 121 complex, does not coordinate to the  $\text{Cu}^{2+}$  central ion in the 120 complex. As a consequence, the coordination geometry of the  $\text{Cu}^{2+}$  central ion does not change by deprotonating the 121 complex to the 120 complex. Accordingly, the EPR spectrum of both the 121 and the 120 complex might not differ. The observation of only one species in the EPR spectrum at pH 10.8 may be evidence for the bidentate coordination mode of one ligand DSA in the  $[\text{Cu}(\text{L})_2]^{6-}$  complex as suggested in **Scheme 7.8**.

In summary, we note that most of the EPR spectra of the  $\text{Cu}^{2+}$ -DSA system are not very well resolved, especially in the perpendicular part. As a consequence, it is difficult to determine the Spin Hamiltonian Parameters of the individual species. In conclusion, the first spectrum at pH 2.7 showed seven lines which may be assigned to a dimeric copper (II) complex. The half field signal could be assigned to the forbidden transition  $\Delta m_s = \pm 2$  which would support this hypothesis. Yet, the lines are not equidistant and another eighth line is also present in the spectrum. This might be evidence for the generation of two sets of four lines each assigned to the two main complexes  $[\text{Cu}(\text{L})]^{2-}$  and  $[\text{Cu}(\text{LH})]^-$  of DSA in acidic solution found by potentiometric titrations. The other spectra give rise to only mononuclear isolated copper (II) centres of mostly more than one species in each of the samples. The spectra should be seen as fingerprint spectra only indicating the kind of species in solution, yet a specific assignment of the complexes in the species distribution, calculated from stability constants of potentiometric titrations, to the observed lines was not possible.

### 7.3.3 The crystal structures $\text{Na}_3[\text{Cu}(\text{DSA})(\text{HCO}_3)] \cdot 2.5 \text{H}_2\text{O} \cdot 1.5 \text{MeOH}$ and $\text{Na}_3[\text{Cu}(\text{DSA})(\text{HCO}_3)] \cdot (\text{H}_2\text{O})_{25/6} \cdot 3 \text{MeOH}$

The  $\text{Cu}^{2+}$ -DSA system forms green complexes in aqueous solution. Green complexes are also formed in methanol as solvent which is more pertinent for crystal growth. Two different coloured single crystals were separated from a dark green methanol/ethyl acetate solution to which sodium hydroxide was added as a base. The violet and green small plate shaped prisms were both passed on to single crystal X-ray analysis. To affirm both the violet and the green crystals containing copper (II) as central ion microscopic X-ray fluorescence was performed. The spectra revealed only the element copper as central metal ions present in both crystals.

#### The crystal structure $\text{Na}_3[\text{Cu}(\text{DSA})(\text{HCO}_3)] \cdot 2.5 \text{H}_2\text{O} \cdot 1.5 \text{MeOH}$

The structure of the violet coloured crystals  $\text{Na}_3[\text{Cu}(\text{DSA})(\text{HCO}_3)] \cdot 2.5 \text{H}_2\text{O} \cdot 1.5 \text{MeOH}$  is depicted in **Figure 7.39**. These crystals consist of the  $[\text{Cu}(\text{DSA})]^{2-}$  complex which crystallizes in the triclinic space group  $P\bar{1}$  with the following R values:  $R_1 = 5.75\%$  and  $wR_2 = 15.89\%$ . The coordination environment of the  $\text{Cu}^{2+}$  central ion is square planar. In essence, the ligand DSA is coordinated as the fourfold deprotonated ligand  $\text{L}^{4-}$  in a tridentate ONO-coordination mode occupying three coordination sites of the square plane. Further, one oxygen atom of a bicarbonate molecule completes the square plane. The bicarbonate was presumably formed by  $\text{CO}_2$  from the air in basic solution. Moreover, three sodium counterions, of which one is disordered, complete the structure in addition with 2.5 water molecules and 1.5 molecules of methanol.

Interestingly, for every second  $\text{Cu}^{2+}$  central ion a water molecule is placed almost perpendicularly above the centre of the square plane. Accordingly, the water molecule could form the apex of a square pyramid. However, only every second  $\text{Cu}^{2+}$  central ion would be coordinated by a square pyramidal coordination environment. For the other 50% of the  $\text{Cu}^{2+}$  centres the water molecule is replaced by a molecule methanol. The coordination of the methanol molecule would cause a distorted “4+1” square pyramidal geometry.

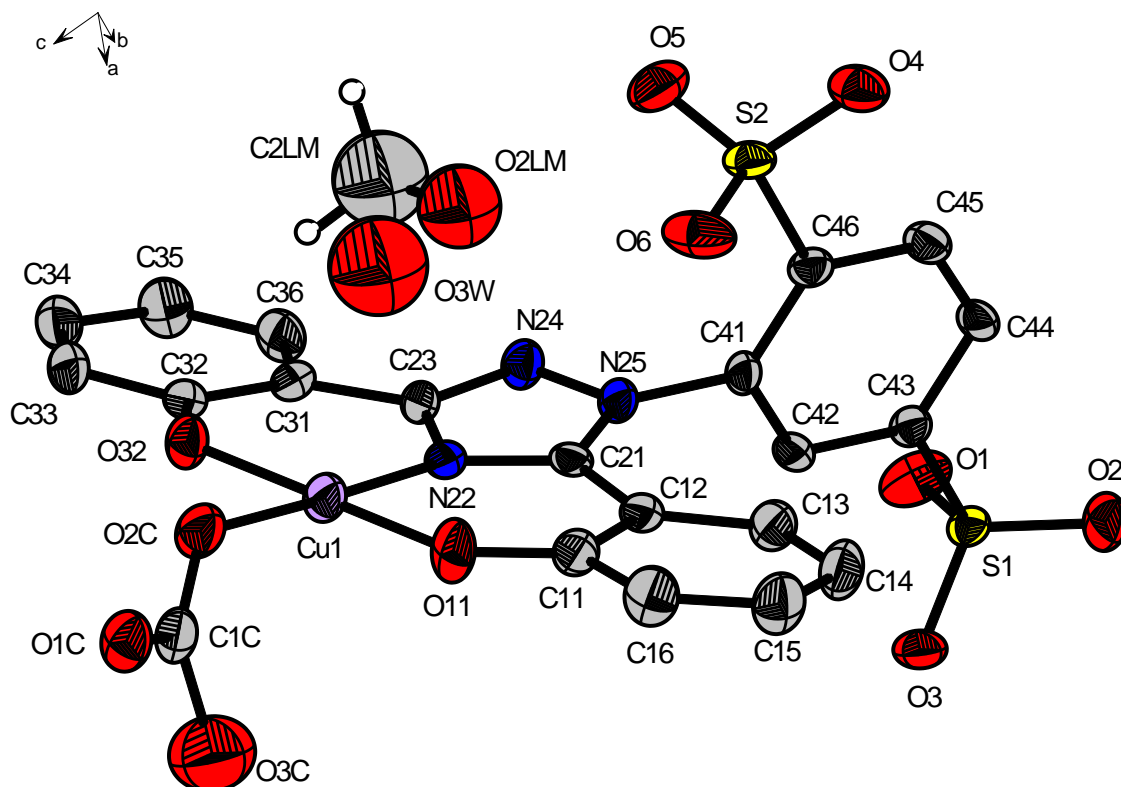


**Figure 7.39:** ORTEP-plot of the main  $[\text{Cu}(\text{DSA})(\text{HCO}_3)]^{3-}$  complex of the crystal structure  $\text{Na}_3[\text{Cu}(\text{DSA})(\text{HCO}_3)] \cdot 2.5 \text{H}_2\text{O} \cdot 1.5 \text{MeOH}$ . The atomic displacement ellipsoids are drawn at the 50% probability level (C = grey, Cu = violet, N = blue, O = red and S = yellow). CH-hydrogen atoms, solvent molecules and  $\text{Na}^+$  counterions are omitted for clarity.

The angles enclosed by the water molecule as apex with the square plane are  $\text{O3W} - \text{Cu} - \text{O11} = 84.92^\circ$ ,  $\text{O3W} - \text{Cu} - \text{N22} = 84.15^\circ$ ,  $\text{O3W} - \text{Cu} - \text{O32} = 93.26^\circ$  and  $\text{O3W} - \text{Cu} - \text{O2C} = 94.12^\circ$ . The distance between the water molecule at the apical position and the  $\text{Cu}^{2+}$  central ion is  $\text{Cu1} - \text{O3W} 2.715 \text{ \AA}$ . According to the literature, typical examples for Cu-OH<sub>2</sub> bond lengths for a square pyramidal coordination of the  $\text{Cu}^{2+}$  central ion by N,O coordinating ligands are  $2.141 \text{ \AA}$  [75] and  $2.276 \text{ \AA}$  [76] or  $2.294 \text{ \AA}$  [77]. The distance in this structure here is significantly elongated by at least  $0.4 \text{ \AA}$ . Despite the nearly perpendicularly centred position of the water molecule, the  $\text{Cu1} - \text{O3W}$  distance is too long for a common square pyramidal coordination. However, it is evident that there are interactions between the water molecule and the copper (II) centre, due to the nearly perpendicular position of the water molecule.

Further, the distance to the oxygen atom of the methanol molecule is even longer 3.590 Å and the square pyramid would be strongly distorted. A square pyramidal Cu<sup>2+</sup> coordination geometry with methanol in apical position is known in the literature though the bond lengths are much shorter, for instance 2.168 Å<sup>[78]</sup> or 2.275 Å<sup>[79]</sup>.

As a consequence the coordination environment of the copper (II) central ion in this structure is considered as square planar. Some selected bond lengths and angles for the corresponding structure are summarized in **Table 7.18**.

**Table 7.18:** Selected bond lengths and bond angles for the structure Na<sub>3</sub>[Cu(DSA)(HCO<sub>3</sub>)] · 2.5 H<sub>2</sub>O · 1.5 MeOH.

atom	bond length [Å]	atom	bond angle [°]
<b>Cu1 – O32</b>	1.914(3)	<b>O32 – Cu1 – O2C</b>	85.54(15)
<b>Cu1 – N22</b>	1.923 (4)	<b>O32 – Cu1 – N22</b>	93.86(15)
<b>Cu1 – O11</b>	1.916(4)	<b>O11 – Cu1 – N22</b>	91.08(16)
<b>Cu1 – O2C</b>	1.972(4)	<b>O11 – Cu1 – O2C</b>	89.46(16)
<b>C1C – O1C</b>	1.236(6)	<b>O32 – Cu1 – O11</b>	174.53(14)
<b>C1C – O2C</b>	1.283(6)	<b>N22 – Cu1 – O2C</b>	178.10(13)
<b>C1C – O3C</b>	1.514(7)		

The bond angles are close to an ideal angle of 90° forming a square planar coordination environment. The square plane is slightly distorted with a twisting angle of maximum 3°. The bond lengths of Cu<sup>2+</sup> with the ligand DSA are in the expected range. Of special interest is the coordinating bicarbonate molecule. The coordination occurs by only one of the oxygen atoms of the bicarbonate causing a monodentate coordination mode which is rarely observed in literature<sup>[80-81]</sup>. The Cu1 – O2C bond with a length of 1.972 Å is a normal value for a Cu – O bond. Supporting the monodentate coordination mode are the too long distances between the Cu<sup>2+</sup> ion and the other bicarbonate oxygen

atoms O1C and O3C which are 4.049 Å and 3.251 Å, respectively. Unfortunately, the hydrogen atom of the bicarbonate molecule could not be refined. A comparison of the bond lengths in the bicarbonate molecule shows that two bonds are very similar with a length of 1.236 Å and 1.283 Å and one is longer with 1.514 Å. We presume this elongated bond is protonated. The proton is also essential for the total charge of the complex since there are only three sodium ions as counterions.

The fully deprotonated L<sup>4-</sup> ligand DSA in this structure adopts a rather flat geometry referring to the central triazole unit with the two phenolate rings. Accordingly, the angles between the phenolate planes and the triazole unit are 10.7° and 11.6°. The benzene-1,4-disulfonic acid moiety is aligned rather perpendicular to the triazole unit with a twisting angle of 81.0°.

All sodium counterions coordinate exclusively with oxygen atoms in their near coordination environment. Only the Na1 and Na2 counterions adopt defined coordination geometries. Na1 arranges towards five oxygen atoms forming a distorted square pyramidal coordination with O1C, O1LM, O3 and O1 in the square plane and O4 of a sulfonic acid as apex. However, Na2 adopts a strongly distorted octahedral geometry with O1W, O32, O3 and O2 in the equatorial positions and O2C and O5 in axial positions. The disordered ions Na3 and Na4 are coordinated by 4 oxygen atoms and 5 oxygen atoms, respectively.

Furthermore, the square planar complexes form layers which are generated by the inversion centres. The space between two layers is occupied by the alternating water O3W and methanol O2LM molecules forming the nearly square pyramidal coordination. The layer beneath the complex does not contain any lattice solvent molecules so that the phenolate rings arrange closer to form some  $\pi$ -stacking interactions with distances of 3.6 Å – 4.4 Å between the rings.

### The crystal structure $\text{Na}_3[\text{Cu}(\text{DSA})(\text{HCO}_3)] \cdot (\text{H}_2\text{O})_{25/6} \cdot 3 \text{ MeOH}$

Besides the violet crystals, green plate shaped prisms were also isolated from the dark green solution in single crystalline form. These green crystals consist of the  $[\text{Cu}(\text{DSA})]^{2-}$  complex crystalizing in the monoclinic space group  $P2_1/c$ . The main complex is depicted in **Figure 7.40**. The complex adopts a square planar coordination geometry with the fully deprotonated  $\text{L}^{4-}$  ligand DSA coordinating in a tridentate ONO-coordination mode. The fourth position is occupied by an oxygen atom of a bicarbonate molecule (the hydrogen atom of the bicarbonate molecule could not be refined).

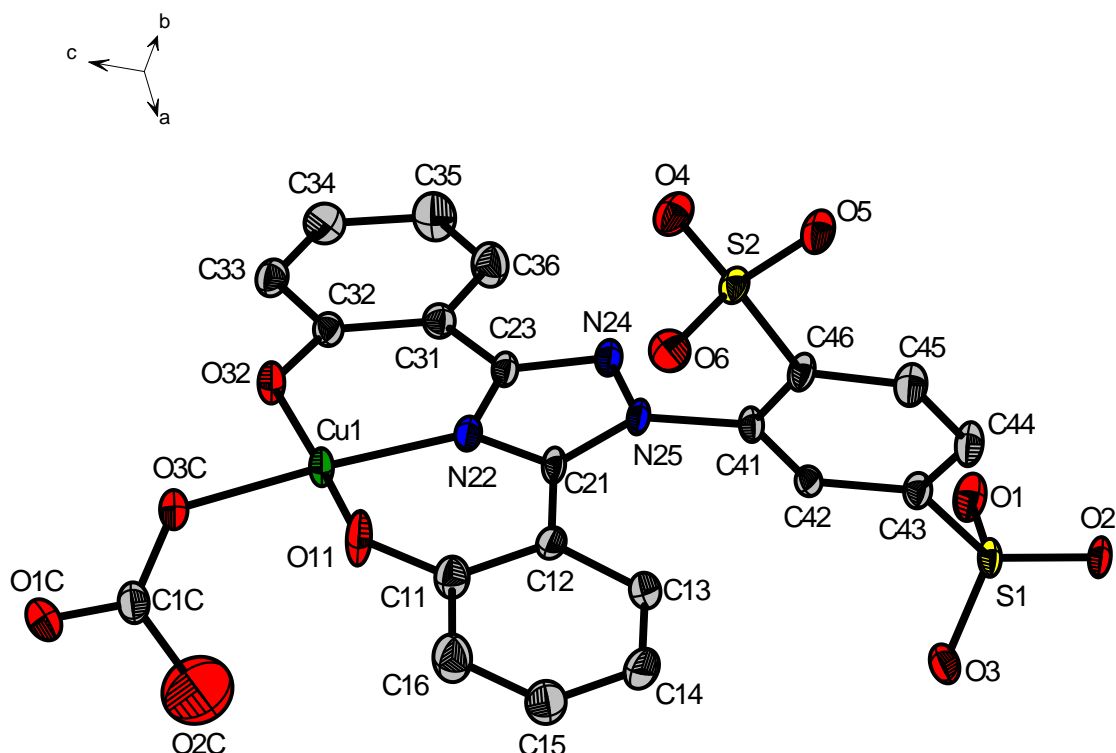


**Figure 7.40:** ORTEP-plot of the main  $[\text{Cu}(\text{DSA})(\text{HCO}_3)]^{3-}$  complex of the crystal structure  $\text{Na}_3[\text{Cu}(\text{DSA})(\text{HCO}_3)] \cdot (\text{H}_2\text{O})_{25/6} \cdot 3 \text{ MeOH}$ . The atomic displacement ellipsoids are drawn at the 50% probability level (C = grey, Cu = green, N = blue, O = red and S = yellow). CH-hydrogen atoms, solvent molecules and  $\text{Na}^+$  counterions are omitted for clarity.

The crystal structure comprehends three sodium counterions to compensate the charge of the complex. Additionally, 25/6 water molecules and three molecules of methanol are enclosed within the crystal lattice which are partially

disordered. These disordered molecules contribute to the higher  $wR_2$  value of 23.72%. The  $R_1$  value is 7.50%. Further, bond lengths and angles of special interest are given in **Table 7.19**.

**Table 7.19:** Selected bond lengths and bond angles for the structure  $\text{Na}_3[\text{Cu}(\text{DSA})(\text{HCO}_3)] \cdot (\text{H}_2\text{O})_{25/6} \cdot 3 \text{ MeOH}$ .

atom	bond length [Å]	atom	bond angle [°]
<b>Cu1 – O32</b>	1.898(4)	<b>O32 – Cu1 – O3C</b>	87.27(15)
<b>Cu1 – N22</b>	1.926(4)	<b>O32 – Cu1 – N22</b>	94.08(16)
<b>Cu1 – O11</b>	1.905(4)	<b>O11 – Cu1 – N22</b>	90.31(17)
<b>Cu1 – O3C</b>	1.961(4)	<b>O11 – Cu1 – O3C</b>	88.75(16)
<b>C1C – O1C</b>	1.246(6)	<b>O32 – Cu1 – O11</b>	171.23(17)
<b>C1C – O2C</b>	1.486(9)	<b>N22 – Cu1 – O3C</b>	176.79(17)
<b>C1C – O3C</b>	1.281(6)		

In both the violet and the green crystals the copper (II) central ion is coordinated square planar with bicarbonate to complete the geometry. In accordance with the violet crystals the bicarbonate molecule coordinates monodentate in this structure which seems to be an infrequent way of coordination as mentioned for the violet crystal structure above. The bond lengths in the bicarbonate molecule are similar to those found for the violet crystals. Two bond lengths in the green crystal structure are shorter 1.246 Å and 1.281 Å and one is longer with 1.486 Å, which gives rise to this oxygen atom being protonated.

Further, the square plane in this structure is slightly distorted with a twisting angle of maximum 8°. The bond lengths and angles of both structures are in good agreement.

By way of comparison the ligand DSA adopts a rather flat geometry in both structures. In this structure the twisting angles between the phenolate planes and the central triazole unit are 5.2° and 13.2°. These differ slightly from those observed for the violet crystals (10.7° and 11.6°). The benzene-1,4-

disulfonic acid moiety twists against the triazole plane by an angle of  $72.4^\circ$ . In the violet structure this angle was closer to a perpendicular position ( $81.0^\circ$ ). In general, all three sodium counterions are surrounded by oxygen atoms of the solvent molecules, the sulfonic acids or the ligand DSA.

One difference between the violet and the green crystals is the violet ones have either a water molecule or a molecule of methanol interacting with the square plane of the complex. The comparison of the Cu-O distances from the plane to the apex of a possible square pyramidal coordination mode with other square pyramidal copper (II) complexes, however showed that the distance in the violet crystals are too long. Yet, a square pyramidal coordination environment would explain the difference in colour since a change in the coordination mode would imply a colour change. The violet crystals are somewhere between a square planar and a square pyramidal coordination. Particularly, the square pyramidal coordination would be rather special since every second  $\text{Cu}^{2+}$  complex has either a water molecule or a molecule of methanol in apical position. We presume this might be the cause for the difference in colour.

In conclusion, both crystal structures obtained from the same solution show a very similar square planar coordination geometry of the  $[\text{Cu}(\text{DSA})]^{2+}$  complex with bicarbonate coordinating monodentate. The main difference between the crystals is the possible square pyramidal coordination interaction observed for the violet crystals. It is of special interest that the  $[\text{Cu}(\text{DSA})]^{2+}$  complex crystallized from an alkaline solution with a square planar coordination environment. This coordination mode can be considered as a consequence of the Jahn-Teller effect. The square planar coordination is an extreme example of the Jahn-Teller distorted octahedral coordination environment of the  $\text{Cu}^{2+}$  complex. In this coordination the ligand DSA is able to coordinate in the favoured tridentate meridional mode in equatorial position of the distorted octahedron. The axial positions seem to be elongated in such a way that the coordination changes from a distorted octahedron to a square planar geometry. The  $[\text{Cu}(\text{DSA})]^{2+}$  is the preferred copper (II) complex which is consistent with the species distributions of the potentiometric titration studies where it is the dominant species throughout almost the whole titration range.

## 7.4 Complex formation of DSA with nickel (II)

The transition metal ion nickel (II) might be a potentially essential trace element though it is not one of the 11 essential trace elements important for human life <sup>[4]</sup>. The question whether nickel is of importance to higher organisms is still to be answered <sup>[82]</sup>.

However, it has been reported that nickel is required by microorganisms which need nickel-dependent enzymes for their existence <sup>[83-84]</sup>. At least nine nickel-containing enzymes are known of which some have been structurally characterised <sup>[84]</sup>. For instance, some NiFe-hydrogenases have been characterised which catalyse the reversible oxidation of hydrogen gas which is a central reaction in microbial energy metabolism <sup>[85]</sup>. In addition, subgroups such as NiFeSe-hydrogenases have been studied in which a selenocysteine ligand coordinates the nickel atom at the active site <sup>[86]</sup>.

On the contrary, nickel is better known for its harmfulness to health. An allergy to nickel can cause contact dermatitis. This is a major issue since nickel is present in everyday life for example in drinking water, food, jewellery, buttons and much more. Further, it is commonly present in implanted medical devices, dental fillings and prostheses. <sup>[87]</sup>

Nickel can be toxic and carcinogenic depending on exposure and the type of nickel compound being exposed to <sup>[82]</sup>. There are reports on nickel compounds inducing oxidative stress in the human body <sup>[88]</sup> for example causing DNA damage in human lymphocytes <sup>[89]</sup>.

Despite the fact that nickel is harmful to health, it is found in the human body serum/plasma (0.14 – 0.63 µg/L), in urine (0.9 – 3.2 µg/L) and in the blood (< 0.05 – 3.8 µg/L) in low concentrations <sup>[90]</sup>. For this reason, it was of interest for us to study the complex formation of DSA with Ni<sup>2+</sup>. Previously, Ryabukhin has reported the formation of polymeric structures of an 1N-phenyl derivative of deferasirox with divalent nickel in solution <sup>[41]</sup>. Indeed, the complex formation of deferasirox or MSA with Ni<sup>2+</sup> has not yet been investigated presumably due to possible insoluble compounds in solution. However, preliminary studies with potentiometric titration experiments were carried out with Ni<sup>2+</sup> and the ligand DSA in pure water by T. Nicolai, under my supervision <sup>[58]</sup>. As a re-

sult, no precipitation was observed during titration experiments with the Ni<sup>2+</sup>-DSA system. Further potentiometric titrations of the Ni<sup>2+</sup>-DSA system needed to be performed with a new electrode (Schott IoLine) in three different molar ratios Ni<sup>2+</sup>:DSA 1:1, 1:2 and 2:1 to investigate the formation of dimeric species. The titration conditions are given in **Table 7.20**.

**Table 7.20:** Titration experiment conditions of the complexation of Ni<sup>2+</sup> with DSA given at T = 298 K.

<b>Conditions for the Ni<sup>2+</sup>-DSA titrations</b>			
molar ratio of M:L	1:1	1:2	2:1
measuring method	potentiometric	potentiometric	potentiometric
method type	continuous	continuous	continuous
solvent	pure water	pure water	pure water
[M] <sub>t</sub>	1.00 mmol/L	0.50 mmol/L	2.00 mmol/L
[L] <sub>t</sub>	1.00 mmol/L	1.00 mmol/L	1.00 mmol/L
titration volume	50.0 mL	50.0 mL	50.0 mL
titrant	0.1 mol/L KOH	0.1 mol/L KOH	0.1 mol/L KOH
supporting electrolyte	0.1 mol/L KCl	0.1 mol/L KCl	0.1 mol/L KCl
electrode	Schott IoLine	Schott IoLine	Schott IoLine
pK <sub>w</sub>	13.78	13.78	13.78
pH range	2.7 – 11.1	2.7 – 11.2	2.7 – 10.6
volume of data points	50	60	60
time for mixing process	400 s	400 s	400 s

Four titration data sets were used of each of the three molar ratios. Unfortunately, we could not find a species model consistent with all titration curves. The largest deviation was observed for the Ni<sup>2+</sup>:DSA 2:1 molar ratio.

Therefore, we obtained a major improvement of the fit by omitting the 2:1 ratio titration curves. Simultaneous evaluation of the 1:1 and 1:2 titrations resulted in the mean values presented in **Table 7.21**.

**Table 7.21:** Mean values of the overall stability constants  $\log\beta_{xyz}$  <sup>[a]</sup> from potentiometric titrations of  $\text{Ni}^{2+}$  with DSA determined by simultaneous evaluation with Hyperquad2008 in pure water,  $T = 298 \text{ K}$  and  $I = 0.1 \text{ mol/L KCl}$ .

<b>log<math>\beta</math> values for the complexation of <math>\text{Ni}^{2+}</math>:DSA</b>	
four 1:1 titrations	four 1:2 titrations
mean values by simultaneous evaluation of 8 titrations <sup>[b]</sup>	
$\sigma$ <sup>[c]</sup>	1.807
pH range	2.7 – 11.2
<b>log<math>\beta_{110}</math></b>	<b>11.76(9)</b>
<b>log<math>\beta_{111}</math></b>	<b>18.28(4)</b>
<b>log<math>\beta_{120}</math></b>	<b>17.24(6)</b>
<b>log<math>\beta_{121}</math></b>	<b>27.15(9)</b>
<b>log<math>\beta_{220}</math></b>	<b>26.8(2)</b>
<b>log<math>\beta_{22-1}</math></b>	<b>15.5(1)</b>

<sup>[a]</sup> For the ligand L  $\log\beta_{xyz}$  is defined as:  $\beta_{xyz} = [\text{M}_x\text{L}_y\text{H}_z] \times [\text{M}]^{-x} \times [\text{L}]^{-y} \times [\text{H}]^{-z}$ .

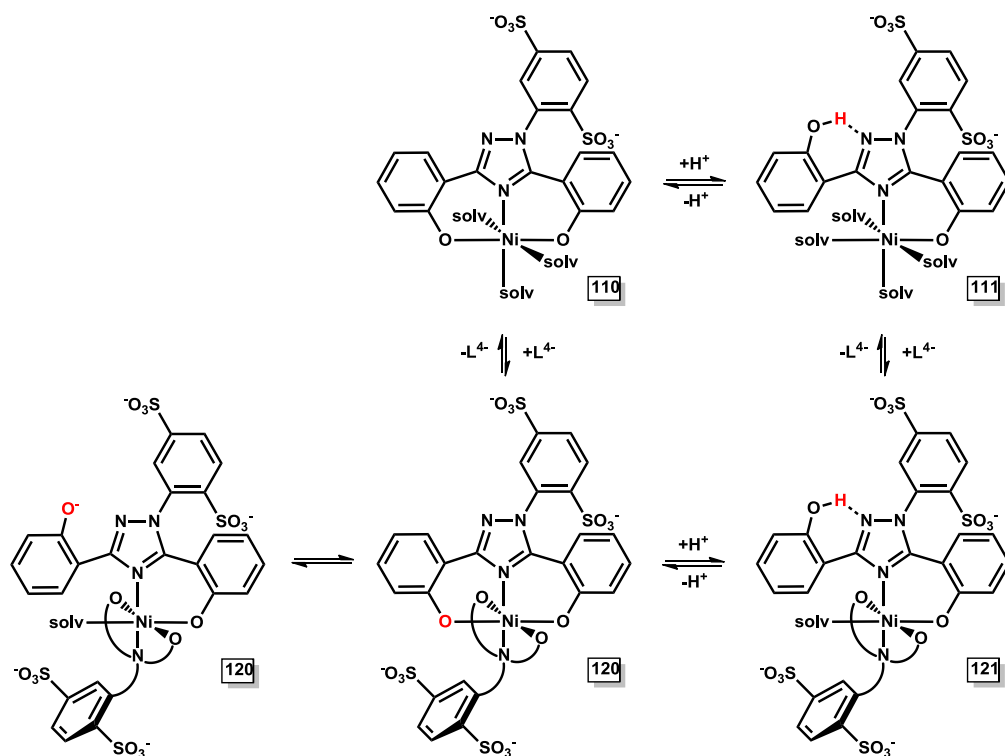
<sup>[b]</sup> The titrations were evaluated simultaneously with the program Hyperquad2008. The deviations given in brackets correspond to the threefold standard deviation taken from Hyperquad2008.

<sup>[c]</sup> The  $\sigma$  value is taken from Hyperquad2008.

The species model comprises two mononuclear complexes  $[\text{Ni}(\text{L})]^{2-}$  (110 complex) and  $[\text{Ni}(\text{LH})]^-$  (111 complex) and two bis-complexes  $[\text{Ni}(\text{L})_2]^{6-}$  (120 complex) and  $[\text{Ni}(\text{L})(\text{LH})]^{5-}$  (121 complex). These complexes were also observed in  $\text{Cu}^{2+}$ -DSA titration experiments. They can adopt a regular octahedral coordination environment since there is no Jahn-Teller effect in the  $\text{Ni}^{2+} d^8$  electronic state. As expected the  $[\text{Ni}(\text{DSA})]^{2-}$  complex with a stability constant of  $\log\beta_{110} = 11.76(9)$  is less stable as the  $[\text{Cu}(\text{DSA})]^{2-}$  complex with a

$\log\beta_{110} = 17.93(2)$ . The apparent  $pK_a = 6.52$  of the  $[\text{Ni}(\text{LH})]^-$  complex is significantly higher than the apparent  $pK_a$  for the corresponding  $\text{Cu}^{2+}$  complex ( $pK_a = 2.5$ ). The equilibrium constant of the  $[\text{Ni}(\text{DSA})_2]^{6-}$  complex is  $\log K_{120} = 5.48$  ( $\log K_{120} = [\text{ML}_2] / [\text{ML}] \times [\text{L}]$ ) and therefore higher than the value determined for the corresponding  $[\text{Cu}(\text{DSA})_2]^{6-}$  complex ( $\log K_{120} = 3.9$ ). This observation can be attributed to the Jahn-Teller effect which destabilises the  $[\text{Cu}(\text{DSA})_2]^{6-}$  complex. Whereas, the  $[\text{Ni}(\text{DSA})_2]^{6-}$  complex is not influenced by the Jahn-Teller effect.

Suggestions for the favoured coordination geometries are given in **Scheme 7.11**. The coordination of the  $[\text{Ni}(\text{LH})]^-$  complex is bidentate with one phenolate group protonated. It can form hydrogen bonding interactions with the triazole nitrogen atom in position 2. Through deprotonation of the  $[\text{Ni}(\text{LH})]^-$  complex the ligand coordinates tridentate meridional and the  $[\text{Ni}(\text{L})]^{2-}$  complex is formed. The suggested protonation of the  $[\text{Ni}(\text{L})(\text{LH})]^{5-}$  complex of DSA occurs at one of the hydroxyphenyl rings causing it to coordinate bidentate. The other ligand in this complex is coordinated tridentate.

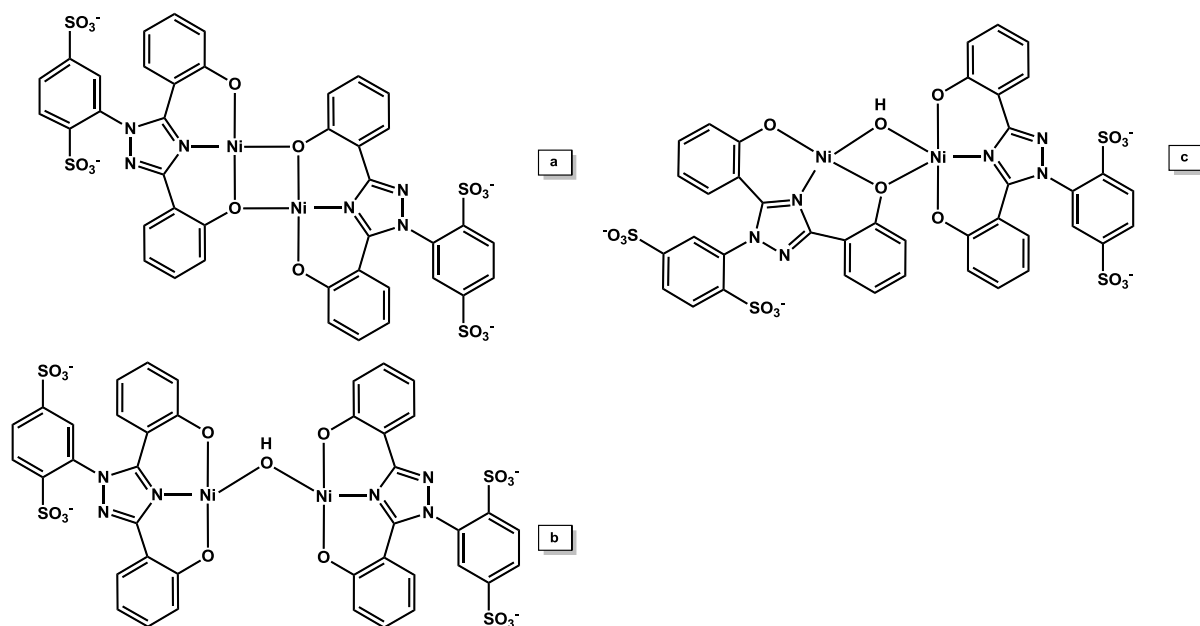


**Scheme 7.11:** Suggested coordination geometries of the complexes  $[\text{Ni}(\text{L})]^{2-}$  (110),  $[\text{Ni}(\text{LH})]^-$  (111),  $[\text{Ni}(\text{L})_2]^{6-}$  (120) and  $[\text{Ni}(\text{L})(\text{LH})]^{5-}$  (121).

The apparent  $pK_a = 9.91$  of the 121 complex is rather high, which is similar to the corresponding apparent deprotonation of the  $[\text{Cu}(\text{L})(\text{LH})]^{5-}$  complex. This high apparent  $pK_a$  value gives evidence for a weak Ni-O bond of the phenolate group in the resulting 120 complex. The bis-complex  $[\text{Ni}(\text{L})_2]^{6-}$  with two fully deprotonated DSA ligands  $\text{L}^{4-}$  bound to one  $\text{Ni}^{2+}$  central ion might rather coordinate with one ligand bidentate and one tridentate meridional forming an octahedral geometry as depicted in **Scheme 7.11**.

The species model applicable for the simultaneous evaluation of both molar ratios  $\text{Ni}^{2+}:\text{DSA}$  1:1 and 1:2 was best with two further complexes  $[\text{Ni}_2(\text{L})_2]^{4-}$  (220 complex) and  $[\text{Ni}_2(\text{L})_2(\text{OH})]^{5-}$  (22-1 complex). In contrast to the copper (II) titrations a  $[\text{Ni}_2(\text{L})_2(\text{OH})_2]^{6-}$  (22-2) complex was not present in this evaluation. We note that the single evaluation of each titration with a 1:2 molar ratio could be evaluated with a  $[\text{Ni}_2(\text{L})]$  (210) species instead of the 220 and 22-1 complexes. Yet the 210 complex could not be evaluated in the single titrations of the 1:1 molar ratio and also not in the simultaneous evaluations of both molar ratios.

Structure suggestions for the  $[\text{Ni}_2(\text{L})_2]^{4-}$  and  $[\text{Ni}_2(\text{L})_2(\text{OH})]^{5-}$  complexes are illustrated in **Scheme 7.12**.



**Scheme 7.12:** Molecular structure suggestions for the  $[\text{Ni}_2(\text{DSA})_2]^{4-}$  (a) and the  $[\text{Ni}_2(\text{DSA})_2(\text{OH})]^{5-}$  (b,c) complex. Possible coordinating solvent molecules are omitted for clarity.

The most likely coordination of the fully deprotonated ligand DSA in a 220 complex is tridentate meridional to one  $\text{Ni}^{2+}$  ion with one phenolate group functioning as phenoxo-bridge. Two entities of this coordination mode combine to form the di-phenoxo-bridged dinuclear  $\text{Ni}^{2+}$  complex 220 as depicted in **Scheme 7.12** complex **a**. This type of coordination has been observed for Schiff base ligands which show a similar O-N-O tridentate coordination forming di-phenoxo-bridged dinuclear  $\text{Ni}^{2+}$  complexes <sup>[91-92]</sup>. The covalency of the nickel ion in the  $[\text{Ni}_2(\text{DSA})_2]^{4-}$  complex is not certain, yet it is likely that some solvent molecules could be coordinated as well.

Further, the coordination sphere of the 22-1 complex **b** (**Scheme 7.12**) is most probably not complete. Both  $\text{Ni}^{2+}$  ions are each coordinated by one tridentate ligand molecule DSA and connected by one hydroxo-bridge. This type of complex is very rarely found in the literature. Another rare coordination would be a combination of a phenoxo-bridge and a hydroxo-bridge as shown in **Scheme 7.12** complex **c**. This would be a new coordination for a  $\text{Ni}^{2+}$ -DSA complex as observed for example for a sevenfold coordinating ligand forming a hydroxo- and phenoxo-bridged dinuclear  $\text{Ni}^{2+}$  complex reported by Gultneh <sup>[93]</sup>. These coordination modes have been observed for 21-1 complexes of at least hexadentate ligands. This differs from the ligand DSA which coordinates tridentate with two ligands forming dinuclear  $\text{Ni}^{2+}$  complexes. However, the complexes reported in the literature give evidence to the possible geometry of the  $[\text{Ni}_2(\text{DSA})_2(\text{OH})]^{5-}$  complex. Which geometry is favoured in solution is just speculation since it cannot be determined by potentiometric titrations.

The potentiometric titration curves of the evaluated molar ratios for the  $\text{Ni}^{2+}$ -DSA system are illustrated in **Figure 7.41**. In comparison to the ligand titration curve the complex titration curves differ after two equivalents have been added. After the inflection at 2 equivalents a considerable pH decrease is observed. The titration curve carried out with a molar ratio of  $\text{Ni}^{2+}$ :DSA 1:2 has an inflection at 2 equivalents and at 3 equivalents. The first inflection indicates that only the very acidic protons, forming the ligand species  $\text{LH}_2^{2-}$ , are present in solution prior to pH 4.

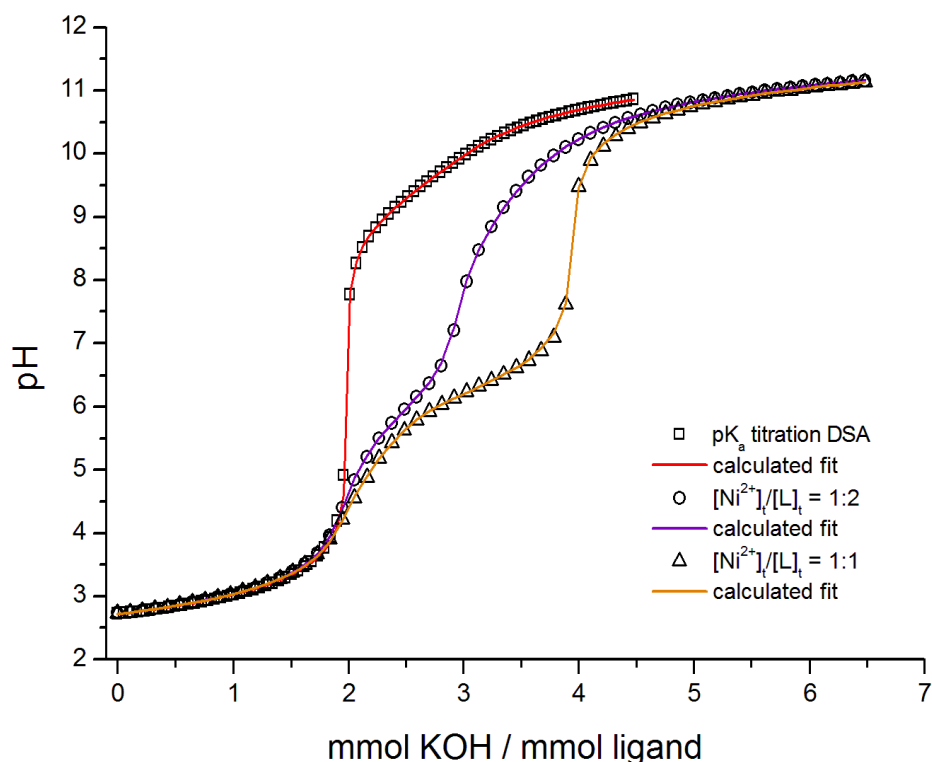


**Figure 7.41:** Potentiometric titration curves of the free ligand DSA and  $\text{Ni}^{2+}$  with DSA with the molar ratios 1:2 ( $[\text{Ni}^{2+}]_t = 0.50 \text{ mmol/L}$ ,  $[\text{L}]_t = 1.00 \text{ mmol/L}$ ) and 1:1 ( $[\text{Ni}^{2+}]_t = 1.00 \text{ mmol/L}$ ,  $[\text{L}]_t = 1.00 \text{ mmol/L}$ ) in pure water,  $T = 298 \text{ K}$  and  $I = 0.1 \text{ mol/L KCl}$ . The open squares, circles and triangles represent experimental points and the fit (solid line) was calculated from the equilibrium constants with Hyperquad2008.

The inflection at three equivalents at about pH 7.5 corresponds to the formation of the  $[\text{Ni}(\text{DSA})]^{2-}$  and  $[\text{Ni}_2(\text{DSA})_2]^{4-}$  complexes. This can be concluded from the species distribution diagram in **Figure 7.42**. The 110 and 220 complexes reach their highest concentrations 48% and 43% at about pH 7.5. At the beginning of the titration 100%  $\text{Ni}^{2+}$  is present and complex formation has not yet occurred.

The  $[\text{Ni}(\text{LH})]^-$  complex begins to form at about pH 3.5 and reaches its maximum concentration (56%) at pH 5.9. In alkaline solution the bis-complexes  $[\text{Ni}(\text{L})(\text{LH})]^{5-}$  and  $[\text{Ni}(\text{L})_2]^{6-}$  are formed with a maximum of 41% at pH 9.4 and 82% at pH 11.2, respectively. The dinuclear  $[\text{Ni}_2(\text{L})_2(\text{OH})]^{5-}$  complex appears in the species distribution with a 1:2 molar ration in low abundance as a minor species.

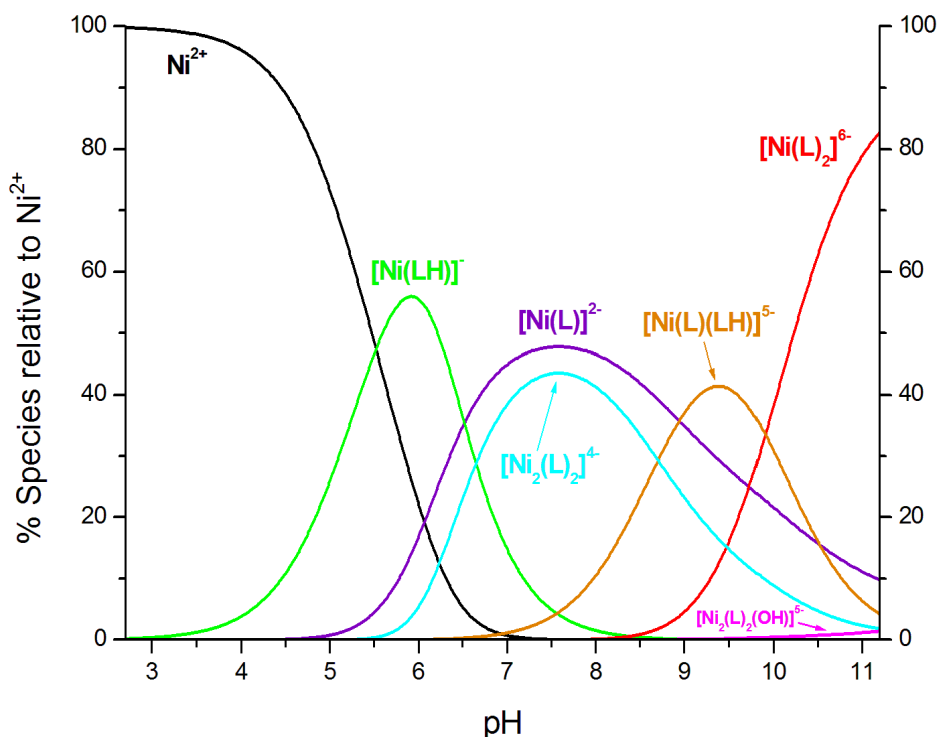


**Figure 7.42:** Species distribution diagram as a function of pH for Ni<sup>2+</sup> with the ligand DSA. Calculated for the continuous potentiometric titration performed with a 1:2 molar ratio ( $[\text{Ni}^{2+}]_t = 0.50$  mmol/L,  $[\text{L}]_t = 1.00$  mmol/L, pure water,  $T = 298$  K and  $I = 0.1$  mol/L KCl) from pH 2.7 to 11.2. The species concentration were calculated from the equilibrium constants listed in **Table 7.21** (mean values from simultaneous evaluation of 8 titrations) with the program Hyss2006.

The species distribution diagram for the Ni<sup>2+</sup>-DSA system with a 1:1 molar ratio in **Figure 7.43** differs from the 1:2 molar ratio diagram. Conspicuous is that no bis-complexes appear in this diagram. They are clearly not favoured by the 1:1 molar ratio. Accordingly, at the beginning of the titration the Ni<sup>2+</sup> ion is again present to 100%. In the titration curve in **Figure 7.41** for the 1:1 molar ratio an inflection appears at 2 equivalents indicating that no complex has been formed at this pH. This is in accordance with the species distribution diagram.

The [Ni(LH)]<sup>2-</sup> complex reaches its highest concentration 46% at pH 5.9. Further, the complexes [Ni(L)]<sup>2-</sup> and [Ni<sub>2</sub>(L)<sub>2</sub>]<sup>4-</sup> start to form at about pH 5 and are present until pH 11.2. Due to the absence of bis-complexes the dinuclear [Ni<sub>2</sub>(L)<sub>2</sub>]<sup>4-</sup> complex is the predominant complex with a maximum concentration of 60% in the titration range from pH 7 to 11.2.

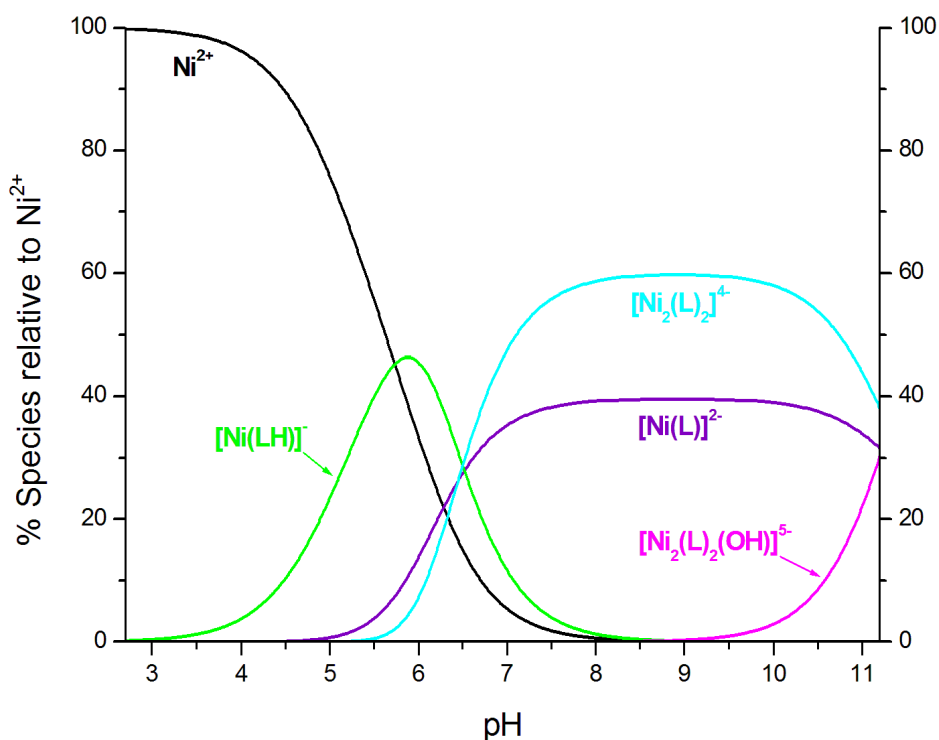


**Figure 7.43:** Species distribution diagram as a function of pH for  $\text{Ni}^{2+}$  with the ligand DSA. Calculated for the continuous potentiometric titration performed with a 1:1 molar ratio ( $[\text{Ni}^{2+}]_i = 1.00 \text{ mmol/L}$ ,  $[\text{L}]_i = 1.00 \text{ mmol/L}$ , pure water,  $T = 298 \text{ K}$  and  $I = 0.1 \text{ mol/L KCl}$ ) from pH 2.7 to 11.2. The species concentration were calculated from the equilibrium constants listed in **Table 7.21** (mean values from simultaneous evaluation of 8 titrations) with the program Hyss2006.

The  $[\text{Ni}(\text{L})]^{2-}$  complex coexists in the same titration range with a maximum concentration of 40%. Moreover the inflection at four equivalents reveals the maximum formation of the two complexes  $[\text{Ni}(\text{L})]^{2-}$  and  $[\text{Ni}_2(\text{L})_2]^{4-}$ . In contrast to the species distribution diagram of the  $\text{Ni}^{2+}$ :DSA 1:2 molar ratio the  $[\text{Ni}_2(\text{L})_2(\text{OH})]^{5-}$  complex is not a minor species and is formed to 30% at pH 11.2.

The complex formation of  $\text{Ni}^{2+}$  with DSA has been investigated by potentiometric titrations with the molar ratios 1:1 and 1:2. A model used to evaluate both molar ratios comprehends a 220 and 22-1 complex. These complexes are dinuclear nickel (II) complexes with presumably either phenoxo- and/or hydroxo-bridges. All complexes during the evaluated titration experiments stayed in solution. We could not find any evidence for polymeric structures as reported by Ryabukhin. However, we cannot exclude the possible existence of polymeric structures at different experimental conditions.

## 7.5 Complex formation of DSA with zinc (II)

Zinc (II) is one of the 11 essential trace elements vital for humans. It is of great importance due to its role as cofactor for more than 300 enzymes <sup>[94-96]</sup>.

A healthy adult has about 2 – 3 g of zinc in the body. High concentrations of zinc are found in the pancreas where insulin is stored, in the iris and retina in the eye, as well as in the liver, lungs and teeth. Further, zinc is part of DNA binding proteins such as zinc finger proteins that coordinate zinc with the help of cysteine and histidine residues for example the steroid hormone receptor superfamily. <sup>[4]</sup>

Zinc is incorporated in the intestine by an unknown mechanism. Re-sorbed zinc is bound to serum proteins such as albumin which represents about 22% of the zinc in the blood. The other 75% are bound to the erythrocytes and 3% to leukocytes. The daily uptake of zinc is 10 – 15 mg. In contrast to iron there is an active mechanism for excreting zinc through the intestine. <sup>[4]</sup>

The investigations of zinc enzymes in the past were hampered by the poor spectroscopic properties of  $Zn^{2+}$ . As a result, the design of ligands as functional mimics and the investigation of their  $Zn^{2+}$  complexes is of great interest as they are useful synthetic analogues that imitate the active sites of enzymes which are difficult to study. <sup>[97-98]</sup>

As a consequence of the obvious importance of  $Zn^{2+}$  for the human body, we investigated the complex formation of DSA with zinc (II) in aqueous solution. Former studies of the stability constants of zinc (II) with deferasirox and MSA were hampered by precipitation during potentiometric titration experiments. U. Heinz carried out competitive titration experiments to determine the stability constants of the  $Zn^{2+}$ -deferasirox system in water/DMSO solution with nitrilotriacetic acid as competitive ligand to keep all complexes in solution <sup>[37]</sup>.

Preliminary studies with potentiometric titrations of the  $Zn^{2+}$ -DSA system carried out by F. Teucke <sup>[49]</sup>, under my supervision, were hampered due to difficulties with the applied electrodes. Titration experiments were performed with a new electrode (Schott IoLine) to further investigate the  $Zn^{2+}$ -DSA system. During titration experiments with a molar ratio  $Zn^{2+}$ :DSA of 1:1 and 1:2 no precipitation occurred. Yet, during titrations with a 2:1 molar ratio greyish-white precip-

itate was observed starting at pH 7 to alkaline solution. All three molar ratios were applicable for simultaneous evaluations. However, only the pH region of the 2:1 titrations before precipitation occurred was used for evaluation. The titration conditions for all molar ratios are listed in **Table 7.22**.

**Table 7.22:** Titration experiment conditions of the complexation of  $Zn^{2+}$  with DSA given at  $T = 298$  K.

<b>Conditions for the <math>Zn^{2+}</math>-DSA titrations</b>			
molar ratio of M:L	1:1	1:2	2:1
measuring method	potentiometric	potentiometric	potentiometric
method type	continuous	continuous	continuous
solvent	pure water	pure water	pure water
$[M]_t$	0.90 mmol/L	0.48 mmol/L	2.00 mmol/L
$[L]_t$	1.00 mmol/L	1.00 mmol/L	1.00 mmol/L
titration volume	50.0 mL	50.0 mL	50.0 mL
titrant	0.1 mol/L KOH	0.1 mol/L KOH	0.1 mol/L KOH
supporting electrolyte	0.1 mol/L KCl	0.1 mol/L KCl	0.1 mol/L KCl
electrode	Schott IoLine	Schott IoLine	Schott IoLine
$pK_w$	13.78	13.78	13.78
pH range	2.7 – 11.0	2.7 – 11.1	2.7 – 6.8
volume of data points	70	70	46
time for mixing process	150 s	150 s	150 s

Four titration experiments of each molar ratio  $Zn^{2+}$ :DSA 1:1, 1:2 and 2:1 were applied for simultaneous evaluation with the program Hyperquad2008. The mean values of this evaluation are summarized in **Table 7.23**. A proper species model with a very good  $\sigma$  value of 1.207 was found to fit all molar rati-

os. The model comprises the mononuclear complexes  $[\text{Zn}(\text{L})]^{2-}$  (110) and  $[\text{Zn}(\text{LH})]^-$  (111) as well as the two bis-complexes  $[\text{Zn}(\text{L})_2]^{6-}$  (120) and  $[\text{Zn}(\text{L})(\text{LH})]^{5-}$  (121). These complexes have also been obtained for the ligand DSA with the divalent metal ions  $\text{Cu}^{2+}$  and  $\text{Ni}^{2+}$ .

**Table 7.23:** Mean values of the overall stability constants  $\log\beta_{xyz}$  <sup>[a]</sup> from potentiometric titrations of  $\text{Zn}^{2+}$  with DSA determined by simultaneous evaluation with Hyperquad2008 in pure water,  $T = 298 \text{ K}$  and  $I = 0.1 \text{ mol/L KCl}$ .

<b><math>\log\beta</math> values for the complexation of <math>\text{Zn}^{2+}</math>:DSA</b>		
four 1:1 titrations	four 1:2 titrations	four 2:1 titrations
pH 2.7 – 11.0	pH 2.7 – 11.1	pH 2.7 – 6.8
mean values by simultaneous evaluation of 12 titrations <sup>[b]</sup>		
$\sigma$ <sup>[c]</sup>	1.207	
<b><math>\log\beta_{110}</math></b>	<b>11.00(1)</b>	
<b><math>\log\beta_{111}</math></b>	<b>16.36(8)</b>	
<b><math>\log\beta_{120}</math></b>	<b>15.37(6)</b>	
<b><math>\log\beta_{121}</math></b>	<b>25.90(6)</b>	
<b><math>\log\beta_{22-1}</math></b>	<b>14.47(6)</b>	
<b><math>\log\beta_{22-2}</math></b>	<b>3.61(4)</b>	

<sup>[a]</sup> For the ligand L  $\log\beta_{xyz}$  is defined as:  $\beta_{xyz} = [\text{M}_x\text{L}_y\text{H}_z] \times [\text{M}]^{-x} \times [\text{L}]^{-y} \times [\text{H}]^{-z}$ .

<sup>[b]</sup> The titrations were evaluated simultaneously with the program Hyperquad2008. The deviations given in brackets correspond to the threefold standard deviation taken from Hyperquad2008.

<sup>[c]</sup> The  $\sigma$  value is taken from Hyperquad2008.

An overall stability constant of  $\log\beta_{110} = 11.00(1)$  was determined for the mononuclear complex with  $\text{Zn}^{2+}$  and the fully deprotonated ligand DSA (cp.  $[\text{Ni}(\text{DSA})]^{2-}$ ,  $\log\beta_{110} = 11.76(9)$ ). The apparent deprotonation constant for the  $[\text{Zn}(\text{LH})]^-$  complex is  $\text{p}K_a = 5.36$  and slightly more acidic than the  $\text{p}K_a$  determined for the corresponding  $[\text{Ni}(\text{LH})]^-$  complex ( $\text{p}K_a = 6.52$ ). Further, the equi-

librium constant for the  $[\text{Zn}(\text{DSA})_2]^{6-}$  complex was determined to  $\log K_{120} = 4.37$  ( $\log K_{120} = [\text{ML}_2] / [\text{ML}] \times [\text{L}]$ ). The value for the corresponding  $[\text{Ni}(\text{DSA})_2]^{6-}$  complex ( $\log K_{120} = 5.48$ ) was somewhat higher. This is not surprising since  $\text{Ni}^{2+}$  complexes are stabilized by the ligand-field stabilization energy. These octahedral zinc (II) complexes experience no stabilisation by the ligand-field theory since  $\text{Zn}^{2+}$  is one of the divalent transition metal ions with a  $d^{10}$  electronic configuration.

The apparent  $\text{p}K_a$  value found for the  $[\text{Zn}(\text{L})(\text{LH})]^{5-}$  complex is  $\text{p}K_a = 10.53$  which is somewhat higher than for the  $[\text{Ni}(\text{L})(\text{LH})]^{5-}$  complex ( $\text{p}K_a = 9.91$ ) and slightly lower than for the  $[\text{Cu}(\text{L})(\text{LH})]^{5-}$  complex ( $\text{p}K_a = 10.9$ ). This apparent  $\text{p}K_a$  value for the deprotonation of the 121 complex of  $\text{Zn}^{2+}$  implies a rather weak  $\text{Zn}^{2+}$ -O bond in the 120 complex. Therefore the bidentate coordination mode of one of the ligands of the  $[\text{Zn}(\text{L})_2]^{6-}$  complex is assumingly more favourable, in accordance with the corresponding  $\text{Cu}^{2+}$  and  $\text{Ni}^{2+}$  complex (**Scheme 7.11**). The coordination mode for the other three complexes should be very similar to the  $\text{Ni}^{2+}$  complexes of DSA, depicted in **Scheme 7.11**. The  $[\text{Zn}(\text{DSA})]^{2-}$  complex adopts the favoured tridentate meridional coordination mode while the protonated  $[\text{Zn}(\text{LH})]^-$  complex coordinates bidentate with the hydroxyphenyl group twisted towards the 1,2,4-triazole nitrogen atom in position 2 of the ring. The  $[\text{Zn}(\text{L})(\text{LH})]^{5-}$  complex has one ligand coordinating tridentate and one ligand molecule bidentate.

Additionally, the species model employed to evaluate all titrations simultaneously contains two dinuclear complexes of the composition  $[\text{Zn}_2(\text{DSA})_2(\text{OH})]^{5-}$  (22-1 complex) and  $[\text{Zn}_2(\text{DSA})_2(\text{OH})_2]^{6-}$  (22-2 complex). These complexes have also been determined for the  $\text{Cu}^{2+}$ -DSA system. The most likely coordination geometry is by hydroxo-bridges between the two zinc (II) ions as suggested for copper (II) in **Scheme 7.9**. The dinuclear mono-hydroxo-bridged complex with two ligands and two  $\text{Zn}^{2+}$  metal ions forming a complex is a common coordination in the literature. For example the tridentate nitrogen coordinating ligands dpt (bis(3-aminopropyl) amine) <sup>[99]</sup> and tempt (2,4,6-tris[4-(imidazole-1-ylmethyl)phenyl]-1,3,5-triazine) <sup>[100]</sup> form  $\text{Zn}_2\text{L}_2(\text{OH})$  complexes. However, also a derivative of the mixed tetradentate N,N,O,O-coordinating ligand salphen (*N,N'*-bis(salicylidene)-1,2-phenylenediamine) <sup>[101]</sup> is known to

form mono-hydroxo-bridged dinuclear complexes of the composition  $Zn_2L_2(OH)$ .

A similar coordination mode as suggested for the di-bridged dinuclear hydroxo complex  $[Zn_2(DSA)_2(OH)_2]^{6-}$  (cp. **Scheme 7.9**) has been discussed in the literature. For instance, a complex of the tridentate nitrogen coordinating ligand 1,4,7-trimethyl-1,4,7-triazacylononane with  $Zn^{2+}$  with the composition  $Zn_2L_2(OH)_2$  has been reported <sup>[102]</sup>. Further, also a bidentate <sup>[103]</sup> and a tetradentate <sup>[104]</sup> nitrogen coordinating ligands are known to form this type of  $Zn_2L_2(OH)_2$  complex. The synthesis of hydroxo-bridged  $Zn^{2+}$  complexes with specially designed ligands has gained importance particularly because these complexes are used as model components for the study of the active site of  $Zn^{2+}$  containing enzymes <sup>[102]</sup>. Consequently, the 22-1 and 22-2 complexes of the ligand DSA with  $Zn^{2+}$  are very reasonable complexes.

The titration curves of the  $Zn^{2+}$ -DSA system for all three molar ratios are depicted in **Figure 7.44** in comparison to the  $pK_a$  titration curve of the ligand.

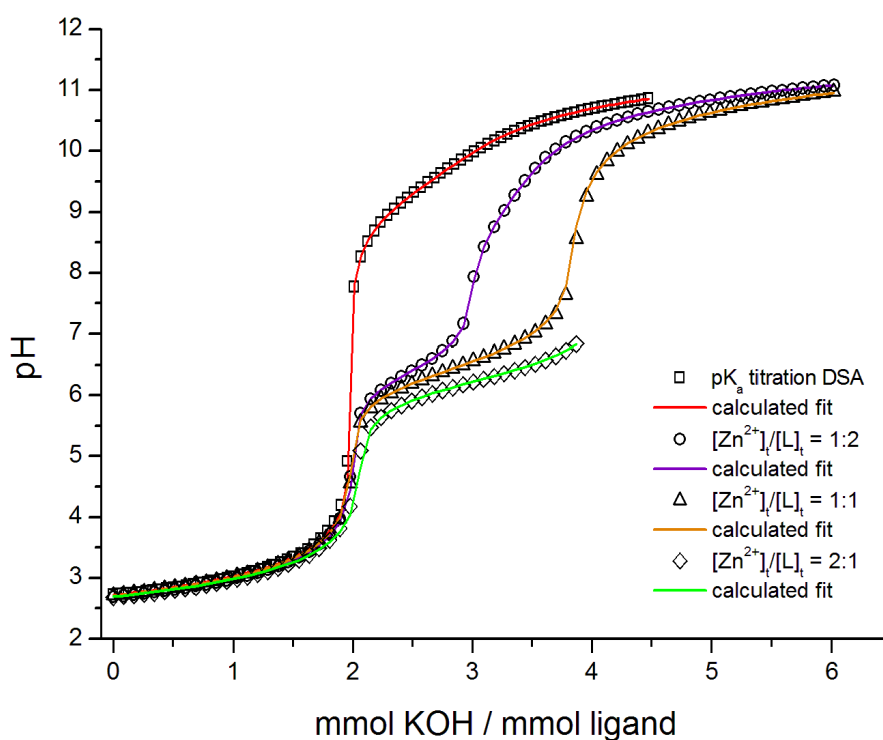


**Figure 7.44:** Potentiometric titration curves of the free ligand DSA and  $Zn^{2+}$  with DSA with the molar ratios 1:2 ( $[Zn^{2+}]_i = 0.48$  mmol/L,  $[L]_i = 1.00$  mmol/L), 1:1 ( $[Zn^{2+}]_i = 0.90$  mmol/L,  $[L]_i = 1.00$  mmol/L) and 2:1 ( $[Zn^{2+}]_i = 2.00$  mmol/L,  $[L]_i = 1.00$  mmol/L) in pure water,  $T = 298$  K and  $I = 0.1$  mol/L KCl. The open squares, circles and triangles represent experimental points and the fit (solid line) was calculated from the equilibrium constants with Hyperquad2008.

The  $\text{Zn}^{2+}$ -DSA titrations show a decrease in pH as a consequence of the complex formation in comparison to the  $\text{p}K_{\text{a}}$  titration curve. All three molar ratios show an inflection at 2 equivalents caused by the two very acidic protons of the ligand DSA which are cleaved immediately after dissolving the ligand. The titration curve with the 1:2 molar ratio has another inflection at 3 equivalents which can be attributed to the complete formation of the complex  $[\text{Zn}(\text{DSA})]^{2-}$ . The second inflection of the 1:1 titration curve appears at about 4 equivalents marking the complete formation of the  $[\text{Zn}(\text{DSA})]^{2-}$  complex. For the 2:1 titrations precipitation occurred during the inflection at 4 equivalents. For this reason the inflection is not depicted in **Figure 7.44**.

The species distribution diagrams of all three molar ratios were calculated with the program Hyss2006. The calculated pH range starts at pH 4.0 since the complex formation of  $\text{Zn}^{2+}$  has not started at this point. In **Figure 7.45** the species distribution diagram with a 1:2 molar ratio is illustrated. The  $[\text{Zn}(\text{L})]^{2-}$  complex starts to form at pH 5 and reaches its highest concentration (96%) at pH 7.5. It is predominant species from pH 6.4 to 10.5.

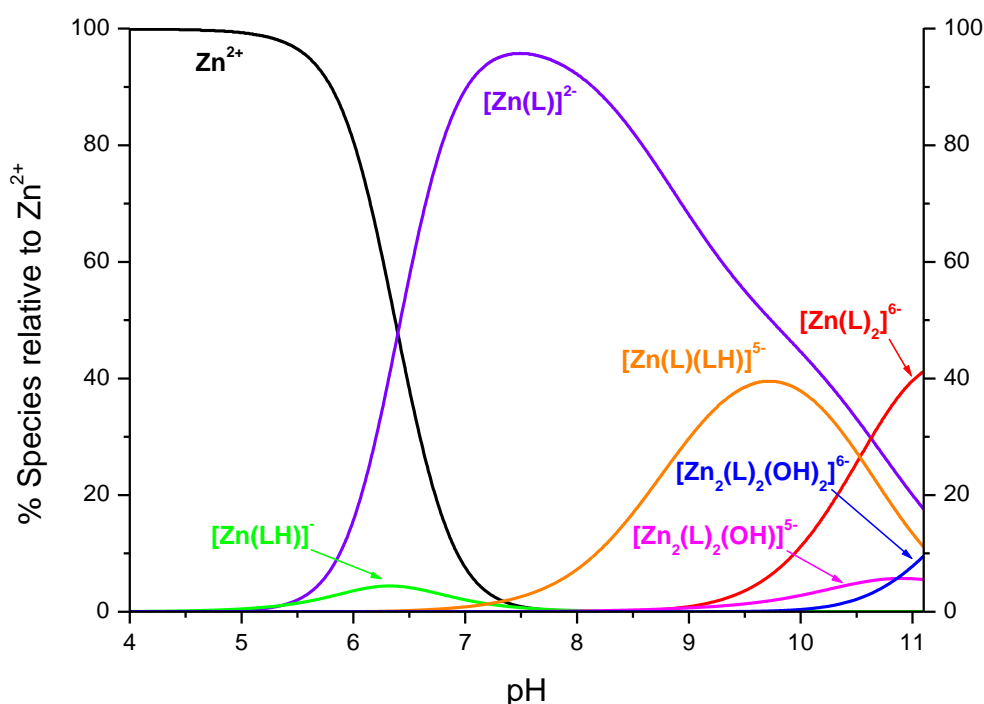


**Figure 7.45:** Species distribution diagram as a function of pH for  $\text{Zn}^{2+}$  with the ligand DSA. Calculated for the continuous potentiometric titration performed with a 1:2 molar ratio ( $[\text{Zn}^{2+}]_{\text{i}} = 0.48 \text{ mmol/L}$ ,  $[\text{L}]_{\text{i}} = 1.00 \text{ mmol/L}$ , pure water,  $T = 298 \text{ K}$  and  $I = 0.1 \text{ mol/L KCl}$ ) from pH 4.0 to 11.1. The species concentration were calculated from the equilibrium constants listed in **Table 7.23** (mean values from simultaneous evaluation of 12 titrations) with the program Hyss2006.

The  $[\text{Zn}(\text{LH})]^-$  complex is a minor species which is present to a maximum content of 4.5% at pH 6.3. The bis-complex  $[\text{Zn}(\text{L})(\text{LH})]^{5-}$  starts to form at about pH 7 and reaches its highest concentration 39% at pH 9.7. At the end of the titration this complex is still present with 11%. The formation of the  $[\text{Zn}(\text{L})_2]^{6-}$  complex starts at pH > 9 and reaches its highest concentration (41%) at the end of the titration. Moreover, the hydroxo-bridged dinuclear complexes  $[\text{Zn}_2(\text{L})_2(\text{OH})]^{5-}$  (22-1) and  $[\text{Zn}_2(\text{L})_2(\text{OH})_2]^{6-}$  (22-2) are present only in strong alkaline solution. The formation of the 22-1 complex starts at pH > 9 while the 22-2 complex forms at pH > 10. At pH 11.1 the 22-1 complex reaches a concentration of 9% and the 22-2 complex of 6%.

The species distribution diagram of the 1:1 molar ratio is presented in **Figure 7.46**.

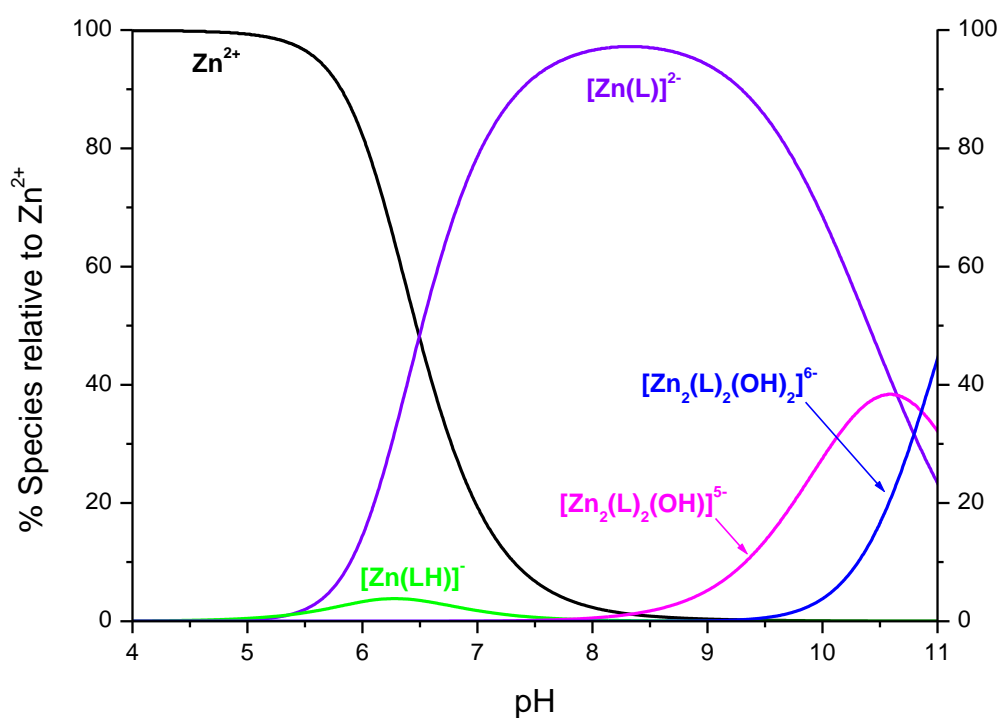


**Figure 7.46:** Species distribution diagram as a function of pH for  $\text{Zn}^{2+}$  with the ligand DSA. Calculated for the continuous potentiometric titration performed with a 1:1 molar ratio ( $[\text{Zn}^{2+}]_t = 0.90$  mmol/L,  $[\text{L}]_t = 1.00$  mmol/L, pure water,  $T = 298$  K and  $I = 0.1$  mol/L KCl) from pH 4.0 to 11.0. The species concentration were calculated from the equilibrium constants listed in **Table 7.23** (mean values from simultaneous evaluation of 12 titrations) with the program Hyss2006.

In accordance to the 1:2 molar ratio diagram the  $[\text{Zn}(\text{LH})]^-$  complex is a minor species (4% at pH 6.3) and the  $[\text{Zn}(\text{L})]^{2-}$  complex is present throughout almost the whole titration range from pH 5 to 11.1. The 1:1 complex reaches a maximum concentration of 97% at pH 8.3 as predominant species.

A significant difference to the diagram of the 1:2 molar ratio is that the bis-complexes  $[\text{Zn}(\text{L})(\text{LH})]^{5-}$  and  $[\text{Zn}(\text{L})_2]^{6-}$  are not present. Therefore, the hydroxo-bridged dinuclear complexes have taken their place forming at pH > 8  $[\text{Zn}_2(\text{L})_2(\text{OH})]^{5-}$  and pH > 9.5  $[\text{Zn}_2(\text{L})_2(\text{OH})_2]^{6-}$ . The mono-hydroxo-bridged  $[\text{Zn}_2(\text{L})_2(\text{OH})]^{5-}$  complex reaches a maximum concentration (38%) at pH 10.6 and has a concentration of 31% at the end of the titration. The  $[\text{Zn}_2(\text{L})_2(\text{OH})_2]^{6-}$  complex reaches its highest concentration 44% at pH 11.1.

**Figure 7.47** shows the species distribution diagram of the 2:1 molar ratio titrations of the  $\text{Zn}^{2+}$ -DSA system.

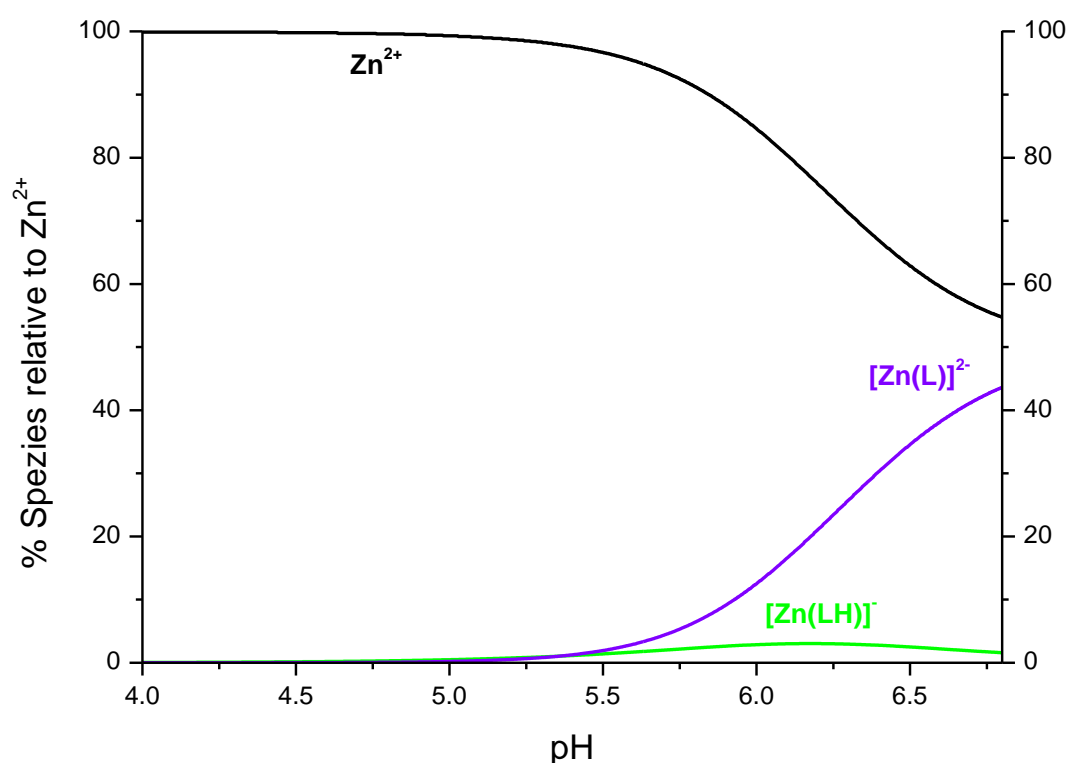


**Figure 7.47:** Species distribution diagram as a function of pH for  $\text{Zn}^{2+}$  with the ligand DSA. Calculated for the continuous potentiometric titration performed with a 2:1 molar ratio ( $[\text{Zn}^{2+}]_t = 2.00 \text{ mmol/L}$ ,  $[\text{L}]_t = 1.00 \text{ mmol/L}$ , pure water,  $T = 298 \text{ K}$  and  $I = 0.1 \text{ mol/L KCl}$ ) from pH 4.0 to 6.8. The species concentration were calculated from the equilibrium constants listed in **Table 7.23** (mean values from simultaneous evaluation of 12 titrations) with the program Hyss2006.

The pH range is only displayed to pH 6.8 due to precipitation occurring at higher pH. Hence, only the two mononuclear species are present. The  $[\text{Zn}(\text{LH})]^-$  complex is still minor species with a maximum concentration of 3% at pH 6.2. The  $[\text{Zn}(\text{DSA})]^{2-}$  complex appears at about pH 5 and reaches its highest concentration (44%) at pH 6.8.

The best fit for the evaluation of the  $\text{Zn}^{2+}$ -DSA system was achieved with the species model in **Table 7.23**. The species model was suitable for the simultaneous evaluation of all titrations of the three molar ratios  $\text{Zn}^{2+}$ :DSA 1:1, 1:2 and 2:1 with a very good  $\sigma$  value of 1.207. It needs to be noted that a  $[\text{Zn}_2(\text{L})_2]^{4-}$  (220) complex could be added to the model, yet this complex appeared only as a minor species with less than 3% concentration in the 1:2 species distribution and < 1% for the 1:1 and 2:1 molar ratios.

The question accompanied by this study is always whether polymeric or dimeric complexes of the composition  $[\text{Zn}_2(\text{L})]$  (210 complex) are present in solutions with divalent transition metal ions. The simultaneous evaluation of the three molar ratio titrations could not be evaluated with a 210 complex. However, we note that only the titrations with 1:2 molar ratio could be evaluated with this type of complex, when the titrations were evaluated separately. In addition, the  $[\text{Zn}(\text{LH})]^-$  complex needed to be excluded to be able to add the 210 complex to the model. Taken together, we could not confirm the existence of any polymeric structures in our titration experiments. This does not mean that dimeric or polymeric species do not exist under these or different conditions.

In conclusion, we suggest the presented species model with the two dinuclear  $[\text{Zn}_2(\text{L})_2(\text{OH})]^{5-}$  (22-1) and  $[\text{Zn}_2(\text{L})_2(\text{OH})_2]^{6-}$  (22-2) complexes is the most likely for the complexation of  $\text{Zn}^{2+}$  with DSA. The hydroxo-bridged coordination of  $\text{Zn}^{2+}$ -ligand complexes is of importance in mimicking the active site of metalloenzymes <sup>[105-106]</sup>. Consequently, the common appearance of hydroxo-bridged complexes in nature confirms our suggested model. However, these complexes are only present in alkaline solution. At physiological pH 7.4 the  $[\text{Zn}(\text{DSA})]^-$  complex is predominant species (1:2 molar ratio 95%, 1:1 molar ratio 91%) in solution.

## 7.6 Complex formation of DSA with cadmium (II)

Cadmium (II) is a group 12 element like zinc (II). We might expect cadmium (II) is also a biological relevant transition metal ion, yet the toxicity and carcinogenicity are regarded as main causes by exposure to cadmium. It is evident that cadmium can cause tumours in the lung and kidney. <sup>[107]</sup>

Uptake of cadmium is contributed to environmental pollution. A reason for the toxicity of cadmium is its interaction with the metabolism of three essential trace elements: calcium, zinc and iron. The main interaction with calcium is in the kidney and in bones resulting in the decrease in bone density, multiple bone fractures and pain as observed for osteoporosis <sup>[108]</sup>. The latter symptoms have been reported as the Itai-itai disease in Japan by mainly middle aged and elderly women in the late 1940's living in the rural Jinzu basin <sup>[109]</sup>. The basin was polluted by cadmium waste from a zinc mine contaminating the rice fields which was the main source of nutrition.

In addition, the interference with the zinc metabolism is attributed to the binding of cadmium to metallothionein, a low-molecular-weight protein that binds zinc and copper. <sup>[4, 108]</sup>

Despite the toxic impact of cadmium, the substitution of zinc in proteins and enzymes by cadmium resulted in a new opportunity for research to investigate the spectroscopic inactive zinc complex sites in these proteins by for example <sup>113</sup>Cd-NMR and <sup>111</sup>Cd-PAC (perturbed angular correlation of  $\gamma$ -rays) <sup>[110]</sup>. Surprisingly, the discovery of the first cadmium enzyme, in marine diatoms, has been reported <sup>[111]</sup>.

It has been reported that iron deficiency increases cadmium absorption from the gastrointestinal tract, yet the mechanism for this relationship is not known <sup>[108]</sup>. However, a study by Saljooghi has been published 2010 concerning the administration of deferasirox to cadmium loaded Wistar rats <sup>[112]</sup>. The results of the study seem to show that "iron concentration after administration of cadmium was significantly decreased". The iron chelating ligand deferasirox seems to have reduced serum cadmium levels and led to a normal iron level. As a consequence, Saljooghi states the "use of deferasirox as a chelator is a potential treatment for complication of cadmium intoxication".

Accordingly, the interaction of cadmium (II) and deferasirox is a topic in current literature. For this reason, we investigated the complex formation of DSA with  $\text{Cd}^{2+}$  in aqueous solution. The complex formation of deferasirox or MSA with  $\text{Cd}^{2+}$  has not been investigated. Titration experiments of the  $\text{Cd}^{2+}$ -DSA system have been carried out in potassium chloride medium. The titration conditions for all three molar ratios  $\text{Cd}^{2+}$ :DSA 1:1, 1:2 and 2:1 are summarized in **Table 7.24**. For the 1:1 and 1:2 molar ratios no precipitation was observed during titration experiments.

**Table 7.24:** Titration experiment conditions of the complexation of  $\text{Cd}^{2+}$  with DSA given at  $T = 298 \text{ K}$ .

<b>Conditions for the <math>\text{Cd}^{2+}</math>-DSA titrations</b>			
molar ratio of M:L	1:1	1:2	2:1
measuring method	potentiometric	potentiometric	potentiometric
method type	continuous	continuous	continuous
solvent	pure water	pure water	pure water
$[\text{M}]_t$	1.00 mmol/L	0.50 mmol/L	2.00 mmol/L
$[\text{L}]_t$	1.00 mmol/L	1.00 mmol/L	1.00 mmol/L
titration volume	50.0 mL	50.0 mL	50.0 mL
titrant	0.1 mol/L KOH	0.1 mol/L KOH	0.1 mol/L KOH
supporting electrolyte	0.1 mol/L KCl	0.1 mol/L KCl	0.1 mol/L KCl
electrode	Schott loLine	Schott loLine	Schott loLine
$\text{p}K_w$	13.78	13.78	13.78
pH range	2.7 – 11.0	2.7 – 11.1	2.7 – 8.0
volume of data points	70	70	48
time for mixing process	120 s	120 s	120 s

However, the titrations with a  $\text{Cd}^{2+}$ :DSA 2:1 molar ratio showed a greyish-white precipitation above pH 8.5. As a consequence, only the pH range  $2.7 < \text{pH} < 8.0$  was employed for evaluation.

To elucidate the complex behaviour of deferasirox related ligands like DSA with  $\text{Cd}^{2+}$  different molar ratios were applied to find a species model compatible with all titrations. Four titrations of all three molar ratios were evaluated simultaneously with the program Hyperquad2008. The mean values for the complexes found are given in **Table 7.25**.

**Table 7.25:** Mean values of the overall stability constants  $\log\beta_{xyz}$  <sup>[a]</sup> from potentiometric titrations of  $\text{Cd}^{2+}$  with DSA determined by simultaneous evaluation with Hyperquad2008 in pure water,  $T = 298 \text{ K}$  and  $I = 0.1 \text{ mol/L KCl}$ .

<b><math>\log\beta</math> values for the complexation of <math>\text{Cd}^{2+}</math>:DSA</b>		
four 1:1 titrations	four 1:2 titrations	four 2:1 titrations
pH 2.7 – 11.0	pH 2.7 – 11.1	pH 2.7 – 8.0
mean values by simultaneous evaluation of 12 titrations <sup>[b]</sup>		
$\sigma$ <sup>[c]</sup>	1.035	
<b><math>\log\beta_{110}</math></b>	<b>7.87(1)</b>	
<b><math>\log\beta_{111}</math></b>	<b>14.78(6)</b>	
<b><math>\log\beta_{120}</math></b>	<b>12.24(3)</b>	
<b><math>\log\beta_{121}</math></b>	<b>22.16(9)</b>	
<b><math>\log\beta_{22-1}</math></b>	<b>7.1(1)</b>	
<b><math>\log\beta_{22-2}</math></b>	<b>-3.65(4)</b>	

<sup>[a]</sup> For the ligand L  $\log\beta_{xyz}$  is defined as:  $\beta_{xyz} = [\text{M}_x\text{L}_y\text{H}_z] \times [\text{M}]^{-x} \times [\text{L}]^{-y} \times [\text{H}]^{-z}$ .

<sup>[b]</sup> The titrations were evaluated simultaneously with the program Hyperquad2008. The deviations given in brackets correspond to the threefold standard deviation taken from Hyperquad2008.

<sup>[c]</sup> The  $\sigma$  value is taken from Hyperquad2008.

The titrations were carried out in a potassium chloride medium with the concentration  $I = 0.1 \text{ mol/L KCl}$ . We need to note that the  $\text{Cd}^{2+}$  ion has a possibly stronger tendency to form chlorocomplexes than some of the other metal ions. Especially the  $[\text{CdCl}]^+$  complex with a formation constants of  $\log K_{110} = 1.52(7)$  ( $T = 298 \text{ K}$ ,  $I = 0.1 \text{ mol/L}$ )<sup>[55]</sup> could take influence on the  $\text{Cd}^{2+}$ -DSA system resulting from the average 100-fold excess of the chloride ion caused by the KCl supporting electrolyte. However, the formation of possible mixed DSA and chlorocomplexes was not taken into account. The determination of the stability constants of the  $\text{Cd}^{2+}$ -DSA system are therefore conditional stability constants even more dependent on the chloride medium. This should be kept in mind while comparing the  $\text{Cd}^{2+}$ -DSA system to other metal ion DSA systems.

Nevertheless, the model calculated for the  $\text{Cd}^{2+}$ -DSA system is in accordance with the model found for the  $\text{Zn}^{2+}$ -DSA system. Two mono complexes are present with a stability constant of  $\log \beta_{110} = 7.87(1)$  for the  $[\text{Cd}(\text{L})]^{2-}$  (110) complex and  $\log \beta_{111} = 14.78(6)$  for the protonated complex  $[\text{Cd}(\text{LH})]^-$  (111). The apparent  $\text{p}K_a$  value for the deprotonation is 6.91. Further, two bis-complexes were determined a  $[\text{Cd}(\text{L})_2]^{6-}$  (120) and a  $[\text{Cd}(\text{L})(\text{LH})]^{5-}$  (121) complex. The  $[\text{Cd}(\text{L})_2]^{6-}$  complex has an overall stability constant of  $\log \beta_{120} = 12.24(3)$  and a  $\log K_{120} = 4.37$  ( $\log K_{120} = [\text{ML}_2] / [\text{ML}] \times [\text{L}]$ ). The apparent deprotonation of the  $[\text{Cd}(\text{L})(\text{LH})]^{5-}$  complex occurs at the hydroxyphenyl group and results in an apparent  $\text{p}K_a$  value of 9.92. This value implicates a rather weak  $\text{Cd}^{2+}$ -O bond of the 120 complex which might result in a bidentate coordination mode for one ligand. The principle coordination geometry of these four  $\text{Cd}^{2+}$  complexes is in accordance with those described for the  $\text{Ni}^{2+}$ -DSA system in **Scheme 7.11**.

To complete the species model for all three molar ratio titrations  $\text{Cd}^{2+}$ :DSA 1:1, 1:2 and 2:1 the dinuclear complexes  $[\text{Cd}_2(\text{L})_2(\text{OH})]^{5-}$  (22-1) and  $[\text{Cd}_2(\text{L})_2(\text{OH})_2]^{6-}$  (22-2) were included. The calculated fit improved from a value  $\sigma > 3$  to  $\sigma = 1.035$ . These two complexes concur with those found for the  $\text{Zn}^{2+}$ -DSA model. The hydroxo-bridged coordination geometry as described for the corresponding  $\text{Cu}^{2+}$ -DSA complexes in **Scheme 7.9** is suggested. The overall stability constants determined for the  $[\text{Cd}_2(\text{L})_2(\text{OH})]^{5-}$  complex is  $\log \beta_{22-1} = 7.1(1)$  and for the  $[\text{Cd}_2(\text{L})_2(\text{OH})_2]^{6-}$  complex  $\log \beta_{22-2} = -3.65(4)$ . The

mono-hydroxo-bridged complex is not common in literature, yet the di-bridged hydroxo complex is found, however for ligands coordinating with nitrogen atoms and sulphur atoms as described by Allred<sup>[113-114]</sup>. In these complexes a  $\text{Cd}_2\text{L}_2(\text{OH})_2$  moiety with two hydroxo bridges between the  $\text{Cd}^{2+}$  ions as we proposed is reported.

The titration curves of all three molar ratios are plotted with the  $\text{pK}_a$  titration curve of DSA in **Figure 7.48**. The inflection at two equivalents can be attributed to the two strong acidic protons of the ligand DSA. In the titration curve with a 2:1 molar ratio an inflection appears at three equivalents which can be assigned to the complete formation of the  $[\text{Cd}(\text{L})]^{2-}$  complex. Accordingly, the inflection of the 1:1 molar ratio titration at 4 equivalents is also assigned to the maximum formation of the  $[\text{Cd}(\text{L})]^{2-}$  complex. Due to precipitation above pH 8.5 no further inflection appears in the 2:1 molar ratio titration curve.

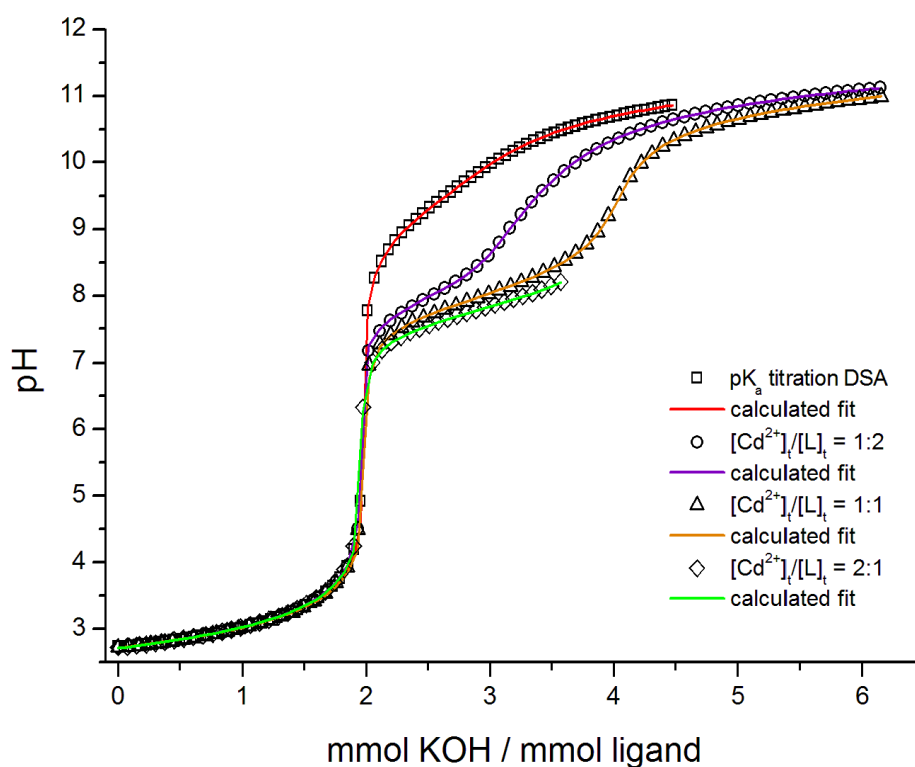


**Figure 7.48:** Potentiometric titration curves of the free ligand DSA and  $\text{Cd}^{2+}$  with DSA with the molar ratios 1:2 ( $[\text{Cd}^{2+}]_t = 0.50$  mmol/L,  $[\text{L}]_t = 1.00$  mmol/L), 1:1 ( $[\text{Cd}^{2+}]_t = 1.00$  mmol/L,  $[\text{L}]_t = 1.00$  mmol/L) and 2:1 ( $[\text{Cd}^{2+}]_t = 2.00$  mmol/L,  $[\text{L}]_t = 1.00$  mmol/L) in pure water,  $T = 298$  K and  $I = 0.1$  mol/L KCl. The open squares, circles and triangles represent experimental points and the fit (solid line) was calculated from the equilibrium constants with Hyperquad2008.

The species distribution diagram of the 1:2 molar ratio titrations is depicted in **Figure 7.49**. Formation of the  $[\text{Cd}(\text{L})]^{2-}$  complex begins at about pH 7 and the complex reaches a maximum concentration (86%) at pH 8.8. The  $[\text{Cd}(\text{L})]^{2-}$  complex is predominant species in the pH range  $8.0 < \text{pH} < 10.5$ . At the end of the titration at pH 11 the complex is still present with 34%. The protonated  $[\text{Cd}(\text{LH})]^-$  complex only appears between pH 7 and 9 with a maximum concentration of 4%. It is a minor species of little relevance. The protonated bis-complex  $[\text{Cd}(\text{L})(\text{LH})]^{5-}$  is present from pH 8 to 11 with a highest concentration (17%) at pH 9.7. The bis-complex  $[\text{Cd}(\text{L})_2]^{6-}$  begins to form at pH 9 its concentration rises with increase of pH to a maximum concentration of 53% at the end of the titration.

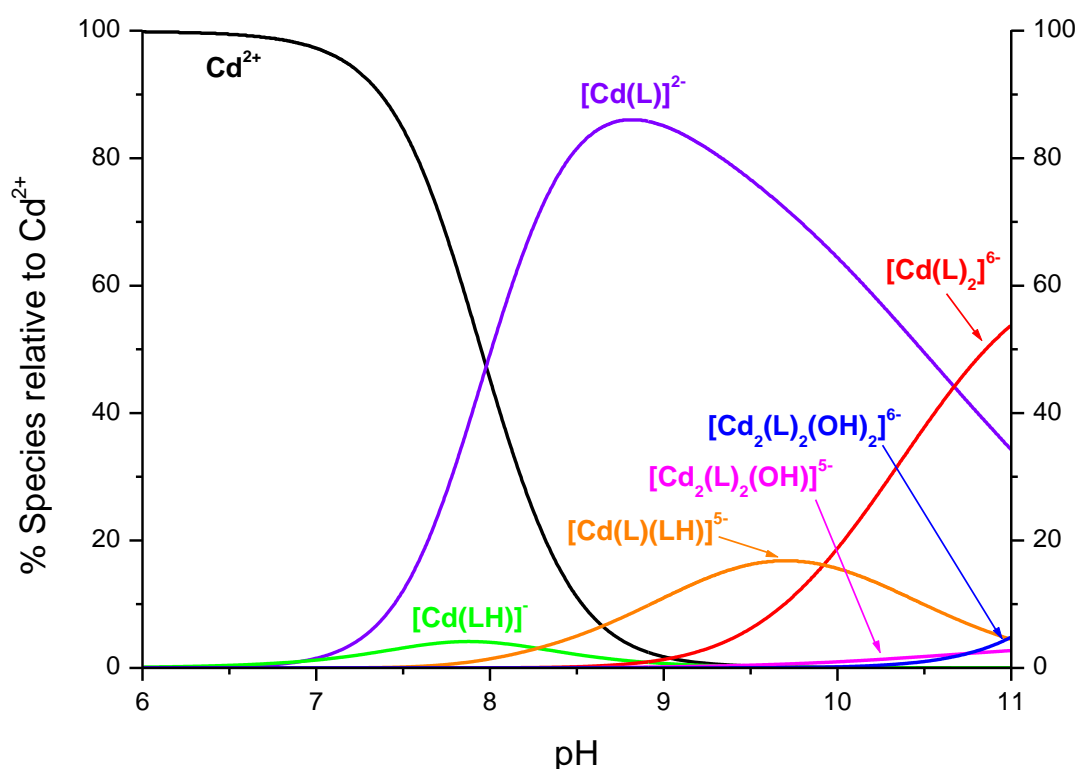


**Figure 7.49:** Species distribution diagram as a function of pH for  $\text{Cd}^{2+}$  with the ligand DSA. Calculated for the continuous potentiometric titration performed with a 1:2 molar ratio ( $[\text{Cd}^{2+}]_t = 0.50 \text{ mmol/L}$ ,  $[\text{L}]_t = 1.00 \text{ mmol/L}$ , pure water,  $T = 298 \text{ K}$  and  $I = 0.1 \text{ mol/L KCl}$ ) from pH 6.0 to 11.0. The species concentration were calculated from the equilibrium constants listed in **Table 7.25** (mean values from simultaneous evaluation of 12 titrations) with the program Hyss2006.

The two dinuclear hydroxo-bridged complexes  $[\text{Cd}_2(\text{L})_2(\text{OH})]^{5-}$  and  $[\text{Cd}_2(\text{L})_2(\text{OH})_2]^{6-}$  appear only in strong alkaline solution with concentrations less than 5% as minor species.

In **Figure 7.50** the species distribution is illustrated for the titrations with a 1:1 molar ratio. In the diagram for this molar ratio the  $[\text{Cd}(\text{DSA})]^{2-}$  complex is predominant species from pH 7 to 11. It reaches its highest concentration of 92% at pH 9.7. At the end of the titration it is still the dominating species with 56%. Again, the  $[\text{Cd}(\text{LH})]^-$  complex is only present as a minor species with less than 5%. The two bis-complexes  $[\text{Cd}(\text{L})_2]^{6-}$  and  $[\text{Cd}(\text{L})(\text{LH})]^{5-}$  are clearly not favoured by this molar ratio. As a result, they only appear as minor species with a concentration less than 5%.

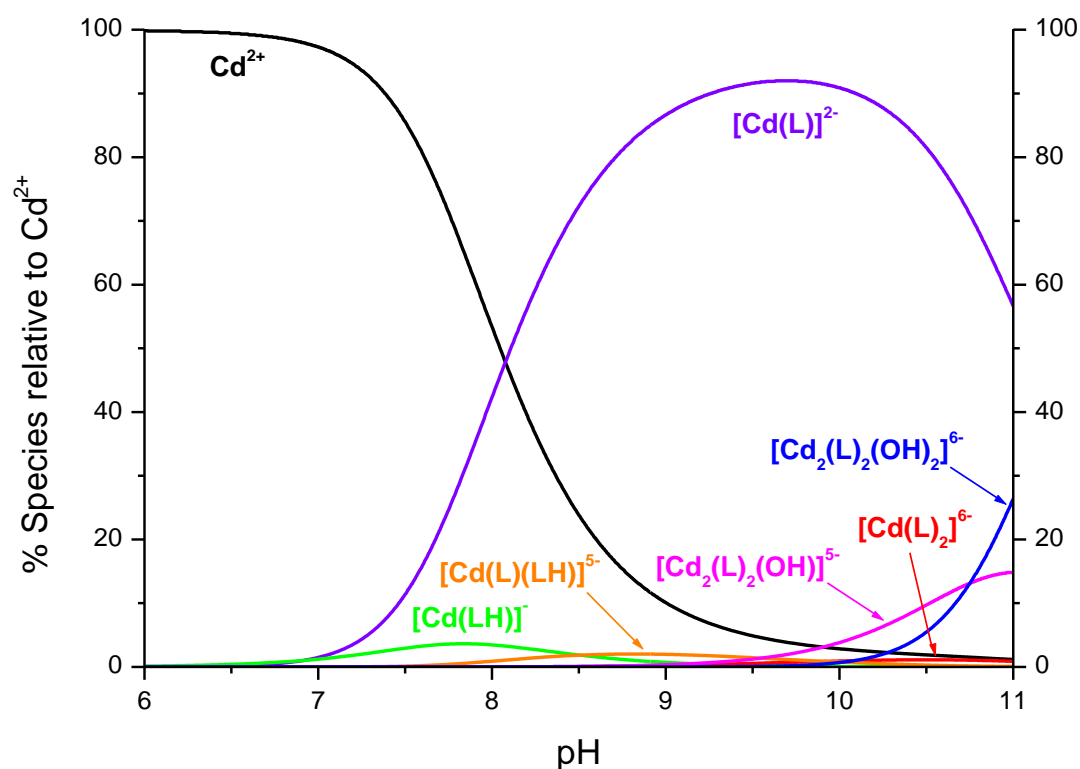


**Figure 7.50:** Species distribution diagram as a function of pH for  $\text{Cd}^{2+}$  with the ligand DSA. Calculated for the continuous potentiometric titration performed with a 1:1 molar ratio ( $[\text{Cd}^{2+}]_t = 1.00 \text{ mmol/L}$ ,  $[\text{L}]_t = 1.00 \text{ mmol/L}$ , pure water,  $T = 298 \text{ K}$  and  $I = 0.1 \text{ mol/L KCl}$ ) from pH 6.0 to 11.0. The species concentration were calculated from the equilibrium constants listed in **Table 7.25** (mean values from simultaneous evaluation of 12 titrations) with the program Hyss2006.

The dinuclear hydroxo-bridged complexes form in alkaline solution and appear in higher concentrations for the 1:1 molar ratio than for the 1:2 molar ratio. The mono-hydroxo-bridged complex  $[\text{Cd}_2(\text{L})_2(\text{OH})]^{5-}$  begins to form at pH 9.5 and reaches a concentration of 15% at the end of the titration. Further, the di-hydroxo bridged complex  $[\text{Cd}_2(\text{L})_2(\text{OH})_2]^{6-}$  starts to form at pH 10 and is present with a concentration of 27% at pH 11.

The species distribution diagram of the 2:1 molar ratio titrations is illustrated in **Figure 7.51**. The pH range is given from pH 6 to 8. In this pH range only the two mononuclear complexes  $[\text{Cd}(\text{L})]^{2-}$  and  $[\text{Cd}(\text{LH})]^-$  are present. The  $[\text{Cd}(\text{LH})]^-$  complex is still a minor species. The  $[\text{Cd}(\text{L})]^{2-}$  complex appears with a concentration of 31% at pH 8.

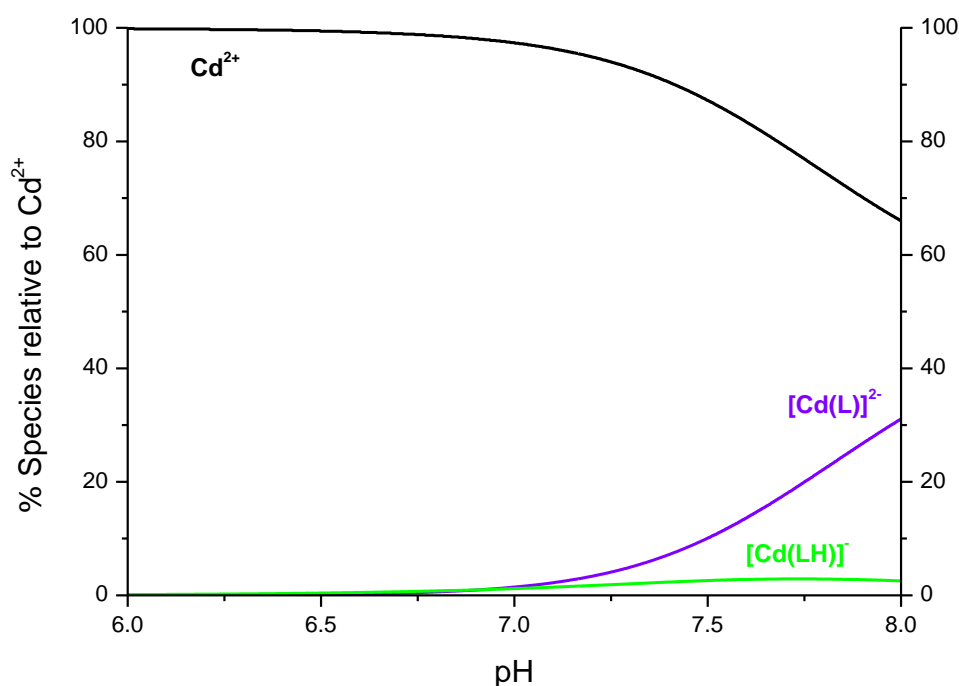


**Figure 7.51:** Species distribution diagram as a function of pH for  $\text{Cd}^{2+}$  with the ligand DSA. Calculated for the continuous potentiometric titration performed with a 2:1 molar ratio ( $[\text{Cd}^{2+}]_t = 2.00 \text{ mmol/L}$ ,  $[\text{L}]_t = 1.00 \text{ mmol/L}$ , pure water,  $T = 298 \text{ K}$  and  $I = 0.1 \text{ mol/L KCl}$ ) from pH 6.0 to 8.0. The species concentration were calculated from the equilibrium constants listed in **Table 7.25** (mean values from simultaneous evaluation of 12 titrations) with the program Hyss2006.

In conclusion, the species model presented in **Table 7.25** was the model with the best fit ( $\sigma$  1.035). A  $[\text{Cd}_2(\text{L})_2]^{4-}$  (220) complex could not be added to this model. The titrations with a 1:2 molar ratio could be evaluated with a  $[\text{Cd}_2(\text{L})]$  (210) complex by single evaluation of each titration experiment. A  $[\text{Cd}_2(\text{L})]$  complex could not be determined by simultaneous evaluation of all three molar ratios.

The recent report by Saljooghi suggests the removal of cadmium (II) in rats by the iron-chelator deferasirox <sup>[112]</sup>. Our investigations with the ligand DSA show a rather weak complexation of  $\text{Cd}^{2+}$  in comparison to  $\text{Fe}^{3+}$ . Complex formation in the  $\text{Cd}^{2+}$ -DSA system begins at pH 7 and at physiological pH 7.4 only 8%  $[\text{Cd}(\text{L})]^{2-}$  and 3%  $[\text{Cd}(\text{LH})]^-$  complex are present in solution. In contrast to the  $\text{Fe}^{3+}$ -DSA system where at pH 7.4 the  $[\text{Fe}(\text{DSA})_2]^{5-}$  has completely formed. Our results would not support a preferential coordination of the cadmium (II) ion to the iron (III) ion. The reported decrease of cadmium concentration in rats by administration of deferasirox might be attributed to a more complicated mechanism in vitro than to the unlikely preferential complexation of  $\text{Cd}^{2+}$  to  $\text{Fe}^{3+}$  by the ligand deferasirox.

## 7.7 Complex formation of DSA with magnesium (II)

Magnesium is an important biometal as a result of its high concentration 11.5 – 16.5 mmol/kg in the human body (an adult with a body weight of 70 kg has a total of 25 g magnesium). The high abundance is attributed to magnesium taking an active part in more than 300 reactions concerning the transfer of phosphate groups and the cleavage and formation of phosphate esters. This can be explained by the fact that the substrate of the enzymes involved in these reaction processes is an  $\text{ATP}^{2-}\text{-Mg}^{2+}$  complex (ATP = adenosine triphosphate).<sup>[4]</sup>

Magnesium is incorporated through the intestine by an unknown mechanism. Yet, the uptake is only 30% while 70% is excreted without incorporation. Further, 95% of the total magnesium in the human body is in the intracellular space. High magnesium concentrations are found in proteins in the skeleton and in organs with high metabolic activity such as the heart, liver, central nervous system and muscles. In plasma only 7% of the total magnesium is bound in complex form. Most of the magnesium bound in plasma is bound to proteins. In addition, there is an active mechanism to excrete excessive magnesium by renal excretion (3 – 6 mmol/d).<sup>[4]</sup>

Due to the high abundance of magnesium in the human body it was of interest to know the affinity of deferasirox towards this biometal ion. U. Heinz investigated the complex formation of deferasirox with  $\text{Mg}^{2+}$  in water/DMSO solutions ( $x_{\text{DMSO}} = 0.20$ ). Deferasirox and MSA form rather weak complexes with  $\text{Mg}^{2+}$ , as one might expect.<sup>[37]</sup>

First investigations of the complex formation of the ligand DSA with  $\text{Mg}^{2+}$  were carried out in pure water by T. Nicolai, under my guidance<sup>[58]</sup>. He carried out potentiometric titrations in a  $\text{Mg}^{2+}:\text{DSA}$  1:2 and 1:4 molar ratio. Models applied for the evaluation of the 1:2 molar ratio titrations were always lacking a  $[\text{Mg}(\text{DSA})_2]^{6-}$  (120) complex. This was rather surprising to us, since titrations of deferasirox and MSA by U. Heinz revealed this type of complex<sup>[37]</sup>. To favour the formation of this  $[\text{Mg}(\text{DSA})_2]^{6-}$  complex the ligand concentration in the titration experiments was increased further to a 1:6 molar ratio. An evaluation of all three molar ratios 1:2, 1:4 and 1:6 was difficult. As a consequence, only titra-

tions with a  $\text{Mg}^{2+}$ :DSA 1:4 and 1:6 molar ratio were evaluated and the determination of a  $[\text{Mg}(\text{DSA})_2]^{6-}$  complex was successful. The titration conditions for these experiments are given in **Table 7.26**.

**Table 7.26:** Titration experiment conditions of the complexation of  $\text{Mg}^{2+}$  with DSA given at  $T = 298 \text{ K}$ .

Conditions for the $\text{Mg}^{2+}$ -DSA titrations				
molar ratio of M:L	1:4		1:6	
measuring method	potentiometric		potentiometric	
method type	continuous		continuous	
solvent	pure water		pure water	
$[\text{M}]_t$ in mmol/L	0.50	0.25	0.25	0.17
$[\text{L}]_t$ in mmol /L	2.00	1.00	1.50	1.00
titration volume	50.0 mL		50.0 mL	
titrant	0.1 mol/L KOH		0.1 mol/L KOH	
supporting electrolyte	0.1 mol/L KCl		0.1 mol/L KCl	
electrode	Sen Tix / Schott IoLine		Schott IoLine	
$\text{p}K_w$	13.78		13.78	
pH range	2.3 – 11.2	2.6 – 11.2	2.5 – 11.3	
volume of data points	100	70	70	
time for mixing process	120 s		160 s	

The overall stability constants determined by simultaneous evaluation of the 1:4 and 1:6 molar ratio titrations are presented in **Table 7.27**. The species model consists of mononuclear complexes of the composition  $[\text{Mg}(\text{L})]^{2-}$  (110) and  $[\text{Mg}(\text{LH})]^-$  (111) in addition to the desired  $[\text{Mg}(\text{L})_2]^{6-}$  (120) complex and a protonated  $[\text{Mg}(\text{L})(\text{LH})]^{5-}$  (121) complex (for geometry see **Scheme 7.11**).

**Table 7.27:** Mean values of the overall stability constants  $\log\beta_{xyz}$  <sup>[a]</sup> from potentiometric titrations of  $\text{Mg}^{2+}$  with DSA determined by simultaneous evaluation with Hyperquad2008 in pure water,  $T = 298 \text{ K}$  and  $I = 0.1 \text{ mol/L KCl}$ .

<b><math>\log\beta</math> values for the complexation of <math>\text{Mg}^{2+}</math>:DSA</b>	
six titrations 1:4	six titrations 1:6
pH 2.3 (or 2.6) – 11.2	pH 2.5 – 11.3
mean values by simultaneous evaluation of 12 titrations <sup>[b]</sup>	
$\sigma$ <sup>[c]</sup>	1.415
<b><math>\log\beta_{110}</math></b>	<b>6.74(2)</b>
<b><math>\log\beta_{111}</math></b>	<b>14.7(1)</b>
<b><math>\log\beta_{120}</math></b>	<b>9.1(2)</b>
<b><math>\log\beta_{121}</math></b>	<b>20.7(8)</b>

<sup>[a]</sup> For the ligand L  $\log\beta_{xyz}$  is defined as:  $\beta_{xyz} = [\text{M}_x\text{L}_y\text{H}_z] \times [\text{M}]^{-x} \times [\text{L}]^{-y} \times [\text{H}]^{-z}$ .

<sup>[b]</sup> The titrations were evaluated simultaneously with the program Hyperquad2008. The deviations given in brackets correspond to the threefold standard deviation taken from Hyperquad2008.

<sup>[c]</sup> The  $\sigma$  value is taken from Hyperquad2008.

The stability constant for the  $[\text{Mg}(\text{L})]^{2-}$  complex is  $\log\beta_{110} = 6.74(2)$ . The apparent  $\text{p}K_a$  value for the deprotonation of the  $[\text{Mg}(\text{LH})]^-$  complex is 8.0. In comparison to other apparent  $\text{p}K_a$  values of the 111 complexes with the divalent transition metal ions discussed before, this apparent  $\text{p}K_a$  for the  $\text{Mg}^{2+}$ -DSA system is higher. With excess ligand provided in the titration experiments, we were able to determine an overall stability constant of  $\log\beta_{120} = 9.1(2)$  for the  $[\text{Mg}(\text{L})_2]^{6-}$  complex. The corresponding  $\log K_{120} = 2.4$  ( $\log K_{120} = [\text{ML}_2] / [\text{ML}] \times [\text{L}]$ ) indicates the rather weak complexation of a second ligand bound to the  $\text{Mg}^{2+}$  central ion. The apparent deprotonation constant of the  $[\text{Mg}(\text{L})(\text{LH})]^{5-}$  complex is quite high with a  $\text{p}K_a$  of 11.6 implicating that the bidentate coordination of one ligand might be favoured (see **Scheme 7.11**). The  $\text{Mg}^{2+}$ -DSA titration curves compared to the  $\text{p}K_a$  titration curve of DSA are illustrated in **Figure 7.52**.

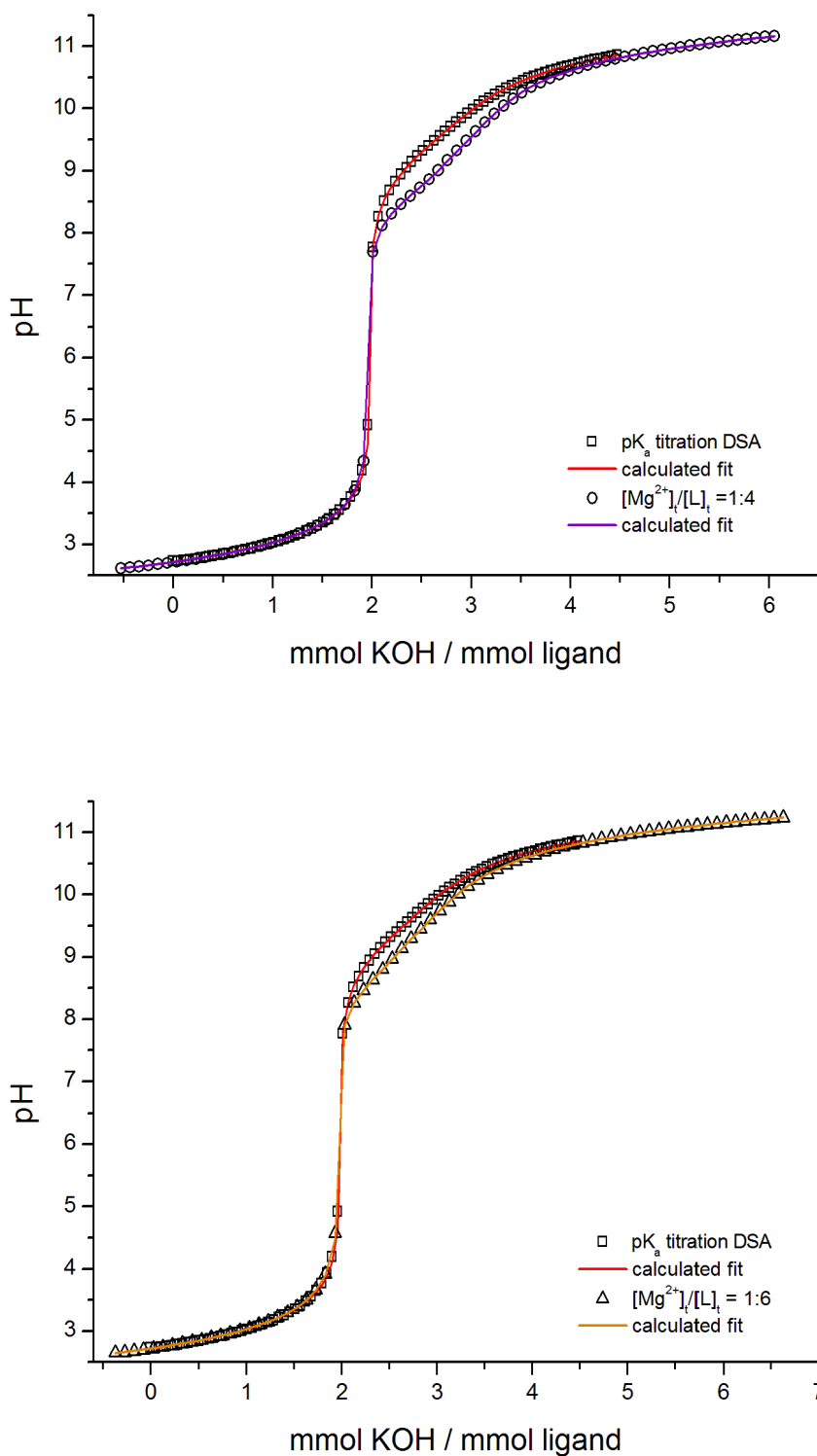


**Figure 7.52:** Potentiometric titration curves of the free ligand DSA and  $\text{Mg}^{2+}$  with DSA with the molar ratios 1:4 ( $[\text{Mg}^{2+}]_t = 0.25$  mmol/L,  $[\text{L}]_t = 1.00$  mmol/L) and 1:6 ( $[\text{Mg}^{2+}]_t = 0.17$  mmol/L,  $[\text{L}]_t = 1.00$  mmol/L) in pure water,  $T = 298$  K and  $I = 0.1$  mol/L KCl. The open squares, circles and triangles represent experimental points and the fit (solid line) was calculated from the equilibrium constants with Hyperquad2008.

The low affinity of the ligand DSA to the metal ion  $\text{Mg}^{2+}$  is evident in the small pH decrease observed for the  $\text{Mg}^{2+}$ -DSA titrations. The inflection at two equivalents can be attributed to the two strong acidic protons of the ligand DSA. At this inflection little complex has been formed.

Only minor changes in concentration distinguish between the 1:4 and 1:6 molar ratio species distributions. As a consequence, only the 1:6 molar ratio species diagram is illustrated in **Figure 7.53**. The complex  $[\text{Mg}(\text{LH})]^-$  begins to form at pH 7 and reaches its highest concentration 12% at pH 8.5.

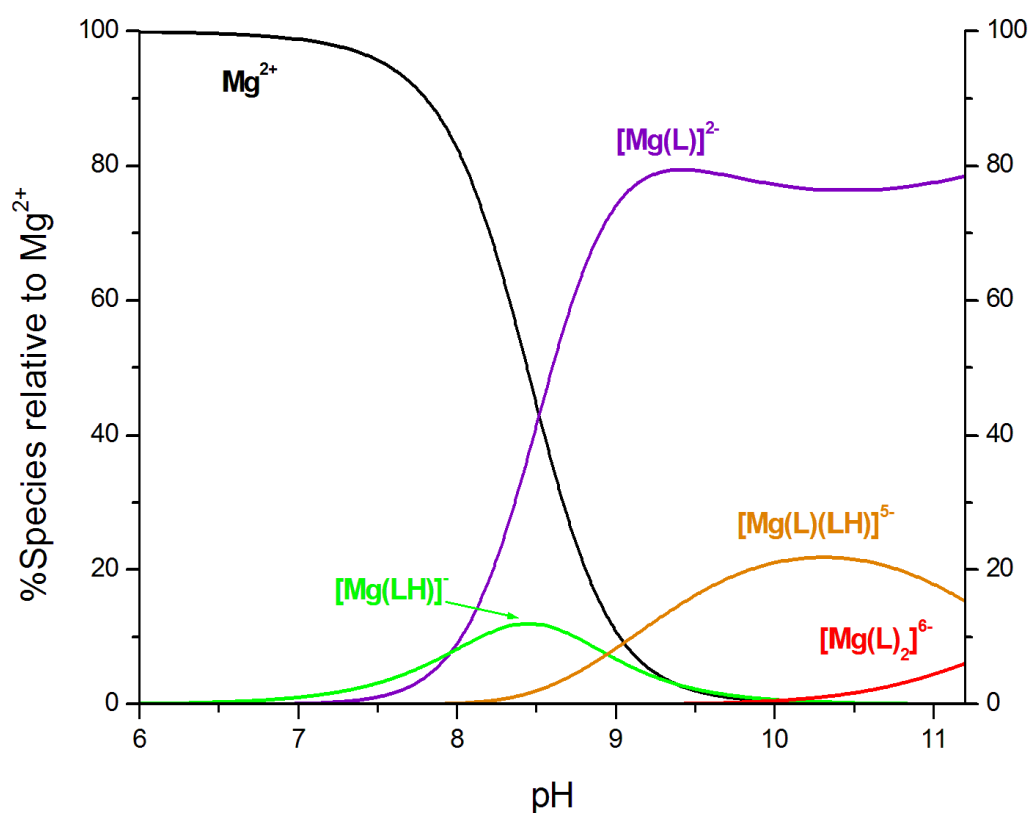


**Figure 7.53:** Species distribution diagram as a function of pH for  $\text{Mg}^{2+}$  with the ligand DSA. Calculated for the continuous potentiometric titration performed with a 1:6 molar ratio ( $[\text{Mg}^{2+}]_t = 0.17 \text{ mmol/L}$ ,  $[\text{L}]_t = 1.00 \text{ mmol/L}$ , pure water,  $T = 298 \text{ K}$  and  $I = 0.1 \text{ mol/L KCl}$ ) from pH 6.0 to 11.2. The species concentration were calculated from the equilibrium constants listed in **Table 7.27** (mean values from simultaneous evaluation of 12 titrations) with the program Hyss2006.

The  $[\text{Mg}(\text{L})]^{2-}$  complex is a major component which is present at a higher concentration than any other species from pH 8 to 11.2. It reaches a maximum concentration of 80% at pH 9.4 and maintains a concentration above 75% to

the end of the titration range. A considerable amount of the protonated bis-complex  $[\text{Mg}(\text{L})(\text{LH})]^{5-}$  is formed in the solution from pH 8.5 to 11.2 with a maximum concentration of 22% at pH 10.3. The  $[\text{Mg}(\text{L})_2]^{6-}$  complex is only present from pH 10 to 11.2. At the end of the titration range this  $[\text{Mg}(\text{L})_2]^{6-}$  complex has a concentration of 7%.

In conclusion, the species distribution shows that the  $[\text{Mg}(\text{L})_2]^{6-}$  complex only forms in strong alkaline solution with a very low abundance which explains the difficulty we had to determine its stability constant. However, by enhancing the equilibrium conditions towards the bis-complexes with increasing ligand concentrations, a stability constant of  $\log K_{120} = 2.4$  was determined for this  $\text{Mg}^{2+}$ -DSA complex. In comparison, the  $[\text{Mg}(\text{DSA})]^{2-}$  has a higher stability constant  $\log \beta_{110} = 6.74(2)$  than its corresponding  $[\text{Mg}(\text{MSA})]^-$  complex with  $\log \beta_{110} = 5.25(1)$  (pure water,  $T = 298 \text{ K}$  and  $I = 0.1 \text{ mol/L KCl}$ ) [37]. In contrast, the  $[\text{Mg}(\text{DSA})_2]^{6-}$  complex has a lower stability constant  $\log K_{120} = 2.4$  compared to the  $\log K_{120} = 3.68$  for  $[\text{Mg}(\text{MSA})_2]^{4-}$  (pure water,  $T = 298 \text{ K}$  and  $I = 0.1 \text{ mol/L KCl}$ ) [37]. It seems that the formation of the 120 complex with magnesium (II) and DSA is not favoured which might be attributed to the higher charge (6-) of the  $\text{Mg}^{2+}$ -DSA 120 complex. The geometry of these complexes should be like those suggested for the  $\text{Ni}^{2+}$ -DSA system in **Scheme 7.11**.

In essence, at physiological pH 7.4 hardly any complex formation has occurred. The only complexes present are the mononuclear  $[\text{Mg}(\text{L})]^{2-}$  and  $[\text{Mg}(\text{LH})]^-$  complexes with concentrations below 5%. Accordingly, the complex formation of  $\text{Fe}^{3+}$  at pH 7.4 should not be influenced by the presents of magnesium (II) ions.

## 7.8 Complex formation of DSA with calcium (II)

It is evident that calcium is a biometal vital for the human body. It is well known that 99% of the total body calcium is in our bones. Calcium is together with phosphate the inorganic material bones and teeth are made of. One per cent of the calcium in our bones provides calcium as a mobile pool which can be activated in case of deficiency. Therefore, bones function as a storage organ for calcium. The daily requirement of calcium for an adult is about 0.8 g and the incorporation of calcium by the intestine has been very well investigated. For example, the key position of vitamin-D and its metabolites in the regulation of intestinal calcium uptake. Between 25% and 40% of by nutrition provided calcium is incorporated. Excessive calcium is excreted by the kidneys or the intestine. The human body is able to excrete 1.0 g/d. As a consequence, if higher amounts are transported to the kidneys over a longer period they can cause renal calculi. <sup>[4]</sup>

Besides the accumulation of calcium in the bones, 1% of the total body calcium is in the blood plasma in either ionised form, bound to proteins or in small amounts in complex form with citrate or phosphate. Calcium in the ionised form plays an important role in the activation of extra- and intravascular systems of the blood coagulation by forming complexes with phospholipids and coagulation factors. <sup>[4]</sup>

Calcium has a signal function in cell activation. In numerous processes calcium can act as a transmitter for information from the activated cell membrane to the receptor molecule in the cell. An example for such a receptor protein is troponin C (part of the protein troponin) in the myocardial muscle and skeletal muscles. Troponin C is a calcium-receptor responsible for the regulation of muscle contractions. <sup>[4, 115]</sup>

To confirm very little to no interaction of the biometal ion  $\text{Ca}^{2+}$  with the iron chelating ligand deferasirox, titration experiments were carried out with deferasirox in water/DMSO ( $x_{\text{DMSO}} = 0.20$ ,  $T = 298 \text{ K}$ ,  $I = 0.1 \text{ mol/l KCl}$ ) and with MSA in pure water ( $T = 298 \text{ K}$ ,  $I = 0.1 \text{ mol/L KCl}$ ) by U. Heinz in his doctoral thesis <sup>[37]</sup>. In accordance, first investigations on the complex formation of DSA with  $\text{Ca}^{2+}$  in pure water were performed by T. Nicolai, under my supervision <sup>[58]</sup>.

The titration curves differ not much from the  $pK_a$  titration curve, revealing a very weak complexation of  $Ca^{2+}$  with DSA. On account of the weak complexation only a  $[Ca(L)]^{2-}$  (110) complex was found in, the difficult to evaluate, 1:2 molar ratio titrations. To enhance the formation of bis-complexes titrations were performed by T. Nicolai in a 1:4 molar ratio. Only the protonated bis-complex  $[Ca(L)(LH)]^{5-}$  (121) and not the desired  $[Ca(L)_2]^{6-}$  (120) complex was determined. Later titration experiments with a 1:6 molar ratio were performed to enhance the formation of the  $[Ca(L)_2]^{6-}$  complex. The conditions for these two molar ratios applied for evaluation are given in **Table 7.28**.

**Table 7.28:** Titration experiment conditions of the complexation of  $Ca^{2+}$  with DSA given at  $T = 298$  K.

Conditions for the $Ca^{2+}$ -DSA titrations				
molar ratio of M:L	1:4		1:6	
measuring method	potentiometric		potentiometric	
method type	continuous		continuous	
solvent	pure water		pure water	
$[M]_t$ in mmol/L	0.50	0.25	0.25	0.17
$[L]_t$ in mmol /L	2.00	1.00	1.50	1.00
titration volume	50.0 mL		50.0 mL	
titrant	0.1 mol/L KOH		0.1 mol/L KOH	
supporting electrolyte	0.1 mol/L KCl		0.1 mol/L KCl	
electrode	Sen Tix / Schott IoLine		Schott IoLine	
$pK_w$	13.78		13.78	
pH range	2.3 – 11.3	2.5 – 11.2	2.6 – 11.2	2.5 – 11.0
volume of data points	100	70	70	
time for mixing process	120 s		120 s	

The simultaneous evaluation of both molar ratios 1:4 and 1:6 is presented in **Table 7.29**. The two species found to fit the titration curves were the  $[\text{Ca}(\text{DSA})]^{2-}$  complex and the protonated bis-complex  $[\text{Ca}(\text{L})(\text{LH})]^{5-}$ .

**Table 7.29:** Mean values of the overall stability constants  $\log\beta_{xyz}$  <sup>[a]</sup> from potentiometric titrations of  $\text{Ca}^{2+}$  with DSA determined by simultaneous evaluation with Hyperquad2008 in pure water,  $T = 298 \text{ K}$  and  $I = 0.1 \text{ mol/L KCl}$ .

<b><math>\log\beta</math> values for the complexation of <math>\text{Ca}^{2+}</math>:DSA</b>			
six titrations 1:4		six titrations 1:6	
pH 2.3 – 11.3	2.5 – 11.2	pH 2.6 – 11.2	2.5 – 11.0
mean values by simultaneous evaluation of 12 titrations <sup>[b]</sup>			
$\sigma$ <sup>[c]</sup>		1.873	
<b><math>\log\beta_{110}</math></b>		<b>4.53(6)</b>	
<b><math>\log\beta_{121}</math></b>		<b>18.3(2)</b>	

<sup>[a]</sup> For the ligand L  $\log\beta_{xyz}$  is defined as:  $\beta_{xyz} = [\text{M}_x\text{L}_y\text{H}_z] \times [\text{M}]^{-x} \times [\text{L}]^{-y} \times [\text{H}]^{-z}$ .

<sup>[b]</sup> The titrations were evaluated simultaneously with the program Hyperquad2008. The deviations given in brackets correspond to the threefold standard deviation taken from Hyperquad2008.

<sup>[c]</sup> The  $\sigma$  value is taken from Hyperquad2008.

The overall stability constant  $\log\beta_{110} = 4.53(6)$  for the  $[\text{Ca}(\text{DSA})]^{2-}$  complex was very well determined. Further, the overall stability constant of the protonated bis-complex was determined to  $\log\beta_{121} = 18.3(2)$ .

A protonated  $[\text{Ca}(\text{LH})]^-$  (111) complex could be added to the model without any change in the  $\sigma$  value of the fit. This can be explained by the fact that this 111 complex appeared as a minor species with a maximum concentration less than 3%. The overall stability constant of this complex was  $\log\beta_{111} = 12.9(8)$ . A stability constant of a minor species is very unsure. This is the reason why we decided to omit this complex from the species model.

Further, a  $[\text{Ca}(\text{L})_2]^{6-}$  (120) complex could also be added to the species model, yet this complex appeared to less than 1%. The estimated overall stability constant  $\log\beta_{120}$  would have been about 6, however the deviation calculated

by Hyperquad2008 was higher than the value itself. The determination of a stability constant for the 120 complex is not possible with our method. It is indeed unsure if this complex forms at all. If we compare the stability constants of the 110 complex of the  $\text{Mg}^{2+}$ -DSA system  $\log\beta_{110} = 6.74(2)$  to the one determined with the  $\text{Ca}^{2+}$ -DSA system  $\log\beta_{110} = 4.53(6)$  we conclude that the complexation with  $\text{Ca}^{2+}$  is about 2 units weaker. The equilibrium constant for the formation of a 120 complex with  $\text{Mg}^{2+}$  was  $\log K_{120} = 2.4$  ( $\log K_{120} = [\text{ML}_2] / [\text{ML}] \times [\text{L}]$ ), indicating the instability of this complex. Consequently, the equilibrium constant for the 120 complex with  $\text{Ca}^{2+}$  will be even smaller than 2.4. We assume that a  $[\text{Ca}(\text{DSA})_2]^{6-}$  complex with such a small formation constant will be too unstable and for this reason this complex was not found in our titrations.

The possibility of calculating an overall stability constant for the  $[\text{Ca}(\text{DSA})_2]^{6-}$  complex with less than 1% in Hyperquad2008 may be a calculation artefact of the program due to the low pH decrease in comparison to the  $\text{p}K_a$  titration curve. This minor difference of the 1:4 molar ratio titration curve of  $\text{Ca}^{2+}$ -DSA to the  $\text{p}K_a$  titration curve of DSA is shown in **Figure 7.54**.

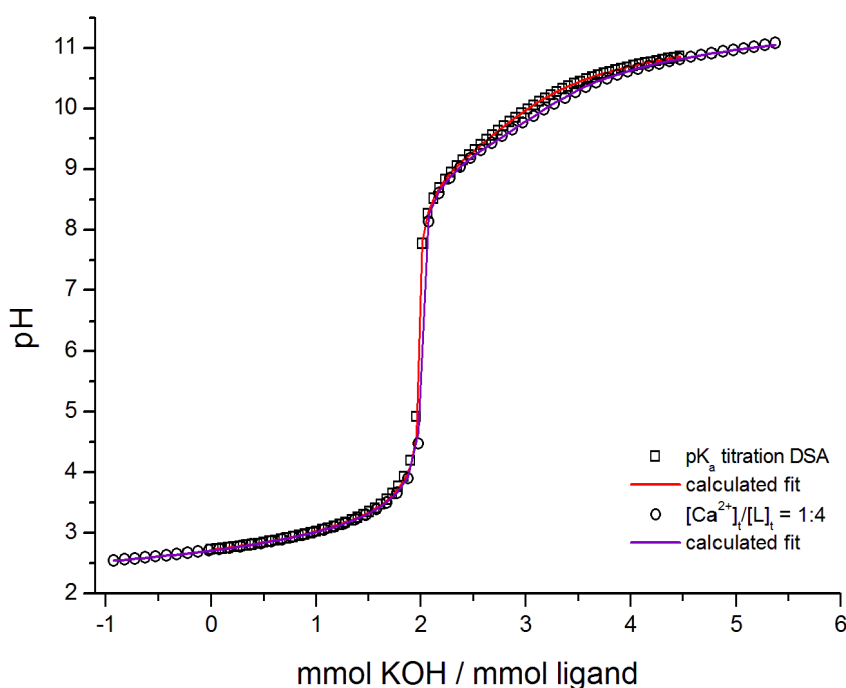


**Figure 7.54:** Potentiometric titration curves of the free ligand DSA and  $\text{Ca}^{2+}$  with DSA with the molar ratio 1:4 ( $[\text{Ca}^{2+}]_i = 0.25$  mmol/L,  $[\text{L}]_i = 1.00$  mmol/L) in pure water,  $T = 298$  K and  $I = 0.1$  mol/L KCl. The open squares and circles represent experimental points and the fit (solid line) was calculated from the equilibrium constants with Hyperquad2008.

Further, **Figure 7.55** shows the titration curve with a 1:6 molar ratio in comparison to the  $pK_a$  titration curve of DSA.

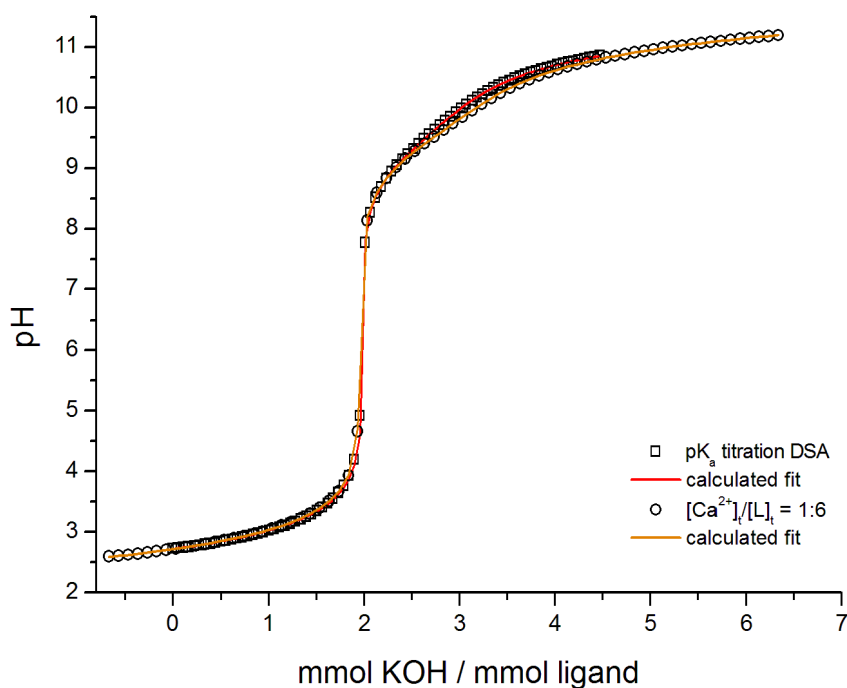


**Figure 7.55:** Potentiometric titration curves of the free ligand DSA and  $\text{Ca}^{2+}$  with DSA with the molar ratio 1:6 ( $[\text{Ca}^{2+}]_t = 0.17 \text{ mmol/L}$ ,  $[\text{L}]_t = 1.00 \text{ mmol/L}$ ) in pure water,  $T = 298 \text{ K}$  and  $I = 0.1 \text{ mol/L KCl}$ . The open squares and circles represent experimental points and the fit (solid line) was calculated from the equilibrium constants with Hyperquad2008.

It is evident that these titrations depict a low complex behaviour between  $\text{Ca}^{2+}$  and the ligand DSA. The pH decrease begins between pH 8 – 9 and is a degree for the weak complexation.

The species distribution diagram in **Figure 7.56** for the 1:6 molar ratio titrations confirms that the complex formation for the  $\text{Ca}^{2+}$ -DSA system begins at pH 8.5. The species distribution for the 1:4 molar ratio is not displayed since it differs only in the concentrations to a minor degree. The  $[\text{Ca}(\text{L})]^{2-}$  complex is formed in the pH range from 8.5 to 11.0 and reaches a maximum concentration of 79% at the end of the titration. The only other complex present in solution is the  $[\text{Ca}(\text{L})(\text{LH})]^{5-}$  complex which begins to form at pH 9.0 and reaches its highest concentration 13% at pH 10.7.

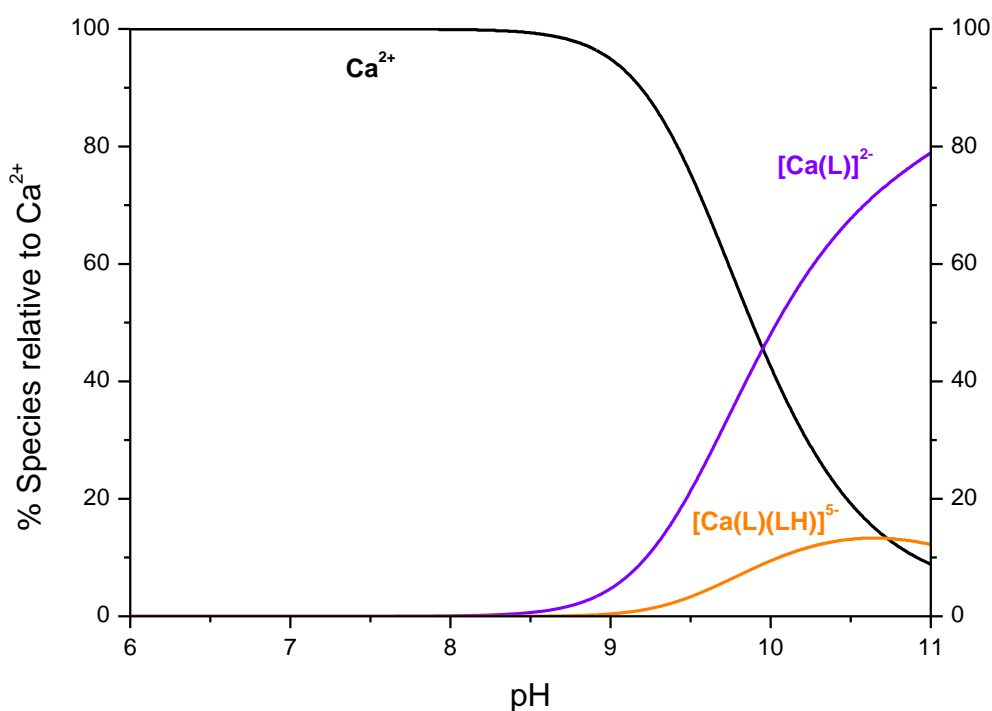


**Figure 7.56:** Species distribution diagram as a function of pH for  $\text{Ca}^{2+}$  with the ligand DSA. Calculated for the continuous potentiometric titration performed with a 1:6 molar ratio ( $[\text{Ca}^{2+}]_t = 0.17 \text{ mmol/L}$ ,  $[\text{L}]_t = 1.00 \text{ mmol/L}$ , pure water,  $T = 298 \text{ K}$  and  $I = 0.1 \text{ mol/L KCl}$ ) from pH 6.0 to 11.0. The species concentration were calculated from the equilibrium constants listed in **Table 7.29** (mean values from simultaneous evaluation of 12 titrations) with the program Hyss2006.

The stability constant  $\log\beta_{110} = 4.53(6)$  of the  $[\text{Ca}(\text{DSA})]^{2-}$  complex is higher than the stability constant  $\log\beta_{110} = 3.42(2)$  of the  $[\text{Ca}(\text{MSA})]^-$  complex (pure water,  $T = 298 \text{ K}$ ,  $I = 0.1 \text{ mol/L KCl}$ )<sup>[37]</sup>, by means of comparison. Further, the  $[\text{Ca}(\text{L})(\text{LH})]^{5-}$  bis-complex was determined for the  $\text{Ca}^{2+}$ -DSA system. In contrast, only the 110 complex was determined for the  $\text{Ca}^{2+}$ -MSA (pure water) and the  $\text{Ca}^{2+}$ -deferasirox systems (water/DMSO,  $x_{\text{DMSO}} = 0.20$ ) and no bis-complexes could be determined<sup>[37]</sup>.

In conclusion, the complex formation of  $\text{Ca}^{2+}$  with DSA is only relevant in alkaline solution above pH 8.5. There is no complex formation at physiological pH 7.4. As a consequence, the biometal ion  $\text{Ca}^{2+}$  will not interfere with complex formation with  $\text{Fe}^{3+}$  and the ligand DSA.

## 7.9 Complex formation of DSA with aluminium (III)

Aluminium is the most abundant metal in the earth's crust. Interestingly, even though it is omnipresent in nature it is a non-essential trace element for human life <sup>[116]</sup>. Consequently, aluminium has no known biological function <sup>[117]</sup>.

Yet, the chemical properties of aluminium show the affinity of  $\text{Al}^{3+}$  towards negatively charged oxygen-donor ligands which are commonly found in biological processes. For example,  $\text{Al}^{3+}$  can bind to phosphate groups of the DNA and RNA inducing topological changes to the DNA and affecting gene transcription. Further,  $\text{Al}^{3+}$  can also bind to nucleoside di- and triphosphates, such as adenosine triphosphate (ATP) which results in  $\text{Al}^{3+}$  affecting the energy metabolism. Aluminium (III) and iron (III) both have a three-fold charge yet rather different ionic radii when comparing the  $\text{Al}^{3+}$  ion (CN:6,  $r = 0.535 \text{ \AA}$ ) <sup>[118]</sup> to the  $\text{Fe}^{3+}$  ion (high-spin, CN: 6,  $r = 0.645 \text{ \AA}$ ) <sup>[118]</sup>. However, it is well investigated that  $\text{Al}^{3+}$  can also bind to the iron-binding protein transferrin and affect iron-homeostasis <sup>[116]</sup>. In fact, approximately 90% of the total aluminium in the human body is bound to transferrin and the other 10% is believed to be associated with low molecular mass biocompounds such as citrate. <sup>[117]</sup>

Further,  $\text{Al}^{3+}$  has a rather slow water exchange rate constant ( $k_{\text{ex}} = 1.29 \text{ s}^{-1}$ ,  $T = 298 \text{ K}$ ) <sup>[2]</sup> compared to important biometals such as  $\text{Ca}^{2+}$  ( $k_{\text{ex}} \approx 10^8 \text{ s}^{-1}$ ) <sup>[2]</sup> and  $\text{Mg}^{2+}$  ( $k_{\text{ex}} = 5.3 \times 10^5 \text{ s}^{-1}$ ) <sup>[2]</sup>. Apparently,  $\text{Al}^{3+}$  can replace  $\text{Mg}^{2+}$  in many biological systems causing for example inhibition of enzymes with  $\text{Mg}^{2+}$  cofactors on account of the slow ligand-exchange rate. As mentioned above  $\text{Al}^{3+}$  has an affinity to phosphate groups which can result in the inhibition of biological processes involving a rapid  $\text{Ca}^{2+}$  exchange. As a consequence, it has been reported that aluminium (III) affects more than 200 biologically important reactions. <sup>[116, 119]</sup>

The daily intake of aluminium by the human body can proceed by foods and beverages. However, even higher quantities (several grams) are consumed by common over-the-counter medications containing aluminium compounds such as antacids and buffered analgesics (for example, aspirin, diclofenac and ibuprofen). <sup>[119]</sup>

However, the effectively absorbed percentage of  $\text{Al}^{3+}$  by the human body from these sources is not known. The uptake is dependent on the composition and the acidity of the diet which influences the availability of aluminium (III). The major route of excretion of normal dietary levels of incorporated  $\text{Al}^{3+}$  seems to be by the biliary system. <sup>[117]</sup>

The toxicity of aluminium (III) is attributed to its capability of crossing the blood-brain barrier. Additionally, the clearance of aluminium from the brain seems to be very slow with a calculated elimination half-life of seven years. <sup>[117]</sup> Aluminium plays a role in dialysis encephalopathy disease which is a progressive brain disease that occurs in some patients who undergo chronic haemodialysis. The sources of the elevated aluminium levels found in the brain of long-term dialysis patients were presumably the use of unpurified water for dialysis and the administration of aluminium containing phosphate binders. <sup>[119-120]</sup>

Further, in the literature there is a controversy whether aluminium plays a role in the pathogenesis of Alzheimer's disease. <sup>[117]</sup>

As a consequence of the similar coordination characteristics of  $\text{Al}^{3+}$  and  $\text{Fe}^{3+}$  it was of interest to investigate complex formation of  $\text{Al}^{3+}$  with deferasirox. U. Heinz has determined the overall stability constants of  $\text{Al}^{3+}$  with deferasirox in water/DMSO medium ( $x_{\text{DMSO}} = 0.20$ ,  $T = 298 \text{ K}$ ,  $I = 0.1 \text{ mol/L KNO}_3$ ) as well as the overall stability constants of  $\text{Al}^{3+}$  with MSA in pure water ( $T = 298 \text{ K}$ ,  $I = 0.1 \text{ mol/L KCl}$ ) <sup>[37]</sup>. His investigations demonstrated a strong complexation of deferasirox and MSA towards  $\text{Al}^{3+}$ , yet not as strong as towards  $\text{Fe}^{3+}$ . In contrast to the potentiometric titrations of  $\text{Fe}^{3+}$  with deferasirox and MSA those with  $\text{Al}^{3+}$  still showed free  $\text{Al}^{3+}$  ion at the beginning of the titrations. Consequently, discontinuous batch titrations were not required.

Some preliminary titration experiments with  $\text{Al}^{3+}$  and the ligand DSA were performed in pure water by T. Nicolai, under my supervision <sup>[58]</sup>. Due to some variance between the values determined with the WTW electrode, Further titration experiments were performed with two molar ratios  $\text{Al}^{3+}$ :DSA 1:2 and 1:4 with the new electrode Schott IoLine. These titrations showed very little variance.

The  $\text{Al}^{3+}$  aqua ion  $[\text{Al}(\text{H}_2\text{O})_6]^{3+}$  has a very slow water exchange rate ( $k_{\text{ex}} = 1.29 \text{ s}^{-1}$ ,  $T = 298 \text{ K}$ ) [2], as described above. Nevertheless, the equilibrium needed to perform continuous potentiometric titrations with the  $\text{Al}^{3+}$ :DSA system was achieved rather fast. Further, in aqueous solutions the  $[\text{Al}(\text{H}_2\text{O})_6]^{3+}$  aqua ion is a strong Lewis acid which hydrolysis easily. For this reason, we took the hydrolysis constants of  $\text{Al}^{3+}$  into account for the evaluation of the potentiometric titrations. The formation constants for the hydrolysis products of  $\text{Al}^{3+}$  in aqueous solution are given in **Table 7.30**. These  $\log\beta_{x,y}$  values were added to the model in Hyperquad2008 as constant values.

**Table 7.30:** Formation constants of the  $\text{Al}^{3+}$  hydrolysis products at 298 K. [121]

<b><math>\log\beta</math> values for the <math>\text{Al}^{3+}</math> hydrolysis products</b>	
species $[\text{Al}_x(\text{OH})_y]^{3x-y}$	$\log\beta_{x,y}$ [a]
$[\text{Al}(\text{OH})]^{2+}_{(\text{aq})}$ [c]	<b>-4.97</b>
$[\text{Al}(\text{OH})_2]^{+}_{(\text{aq})}$ [d]	<b>-9.3</b>
$[\text{Al}(\text{OH})_4]^{-}_{(\text{aq})}$ [c]	<b>-23.0</b>
$[\text{Al}_2(\text{OH})_2]^{4+}_{(\text{aq})}$ [d]	<b>-7.7</b>
$[\text{Al}_3(\text{OH})_4]^{5+}_{(\text{aq})}$ [d]	<b>-13.94</b>
$[\text{Al}_{13}\text{O}_4(\text{OH})_{24}]^{7+}_{(\text{aq})}$ [b] [d]	<b>-98.73</b>

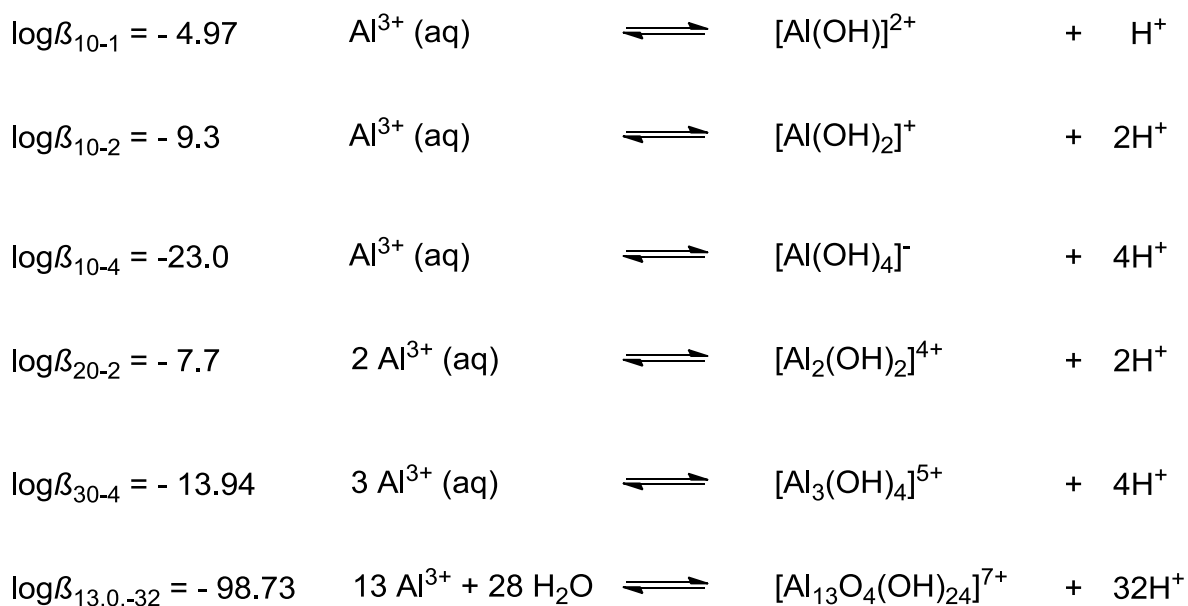
[a]  $\log\beta_{x,y}$  is defined as:  $\beta_{x,y} = [\text{Al}_x(\text{OH})_y]^{3x-y} \times [\text{H}]^y \times [\text{Al}]^{-x}$

[b]  $\log\beta_{x,y}$  is defined as:  $\beta_{13,32} = [\text{Al}_{13}\text{O}_4(\text{OH})_{24}]^{7+} \times [\text{H}]^{32} \times [\text{Al}]^{-13}$

[c] For ionic strength  $I = 0.0 \text{ mol/L}$ .

[d] Ionic strength not defined.

The hydrolysis formation constants of  $\text{Al}^{3+}$  are associated with the reactions in **Scheme 7.13**.



**Scheme 7.13:** Reaction equations for the overall formation constants of the hydrolysis of  $\text{Al}^{3+}$  in aqueous solution. <sup>[121]</sup>

To investigate the types of complexes formed in aqueous solution by  $\text{Al}^{3+}$  with the ligand DSA we performed potentiometric titrations with two molar ratios 1:2 and 1:4 of  $\text{Al}^{3+}$ :DSA. The conditions for the continuous potentiometric titrations of both molar ratios are listed in **Table 7.31**.

**Table 7.31:** Titration experiment conditions of the complexation of  $\text{Al}^{3+}$  with DSA given at  $T = 298 \text{ K}$ .

<b>Conditions for the <math>\text{Al}^{3+}</math>-DSA titrations</b>		
molar ratio of M:L	1:2	1:4
measuring method	potentiometric	potentiometric
method type	continuous	continuous
solvent	pure water	pure water
$[\text{M}]_t$	0.48 mmol/L	0.25 mmol/L
$[\text{L}]_t$	1.00 mmol/L	1.00 mmol/L
titration volume	50.0 mL	50.0 mL
titrant	0.1 mol/L KOH	0.1 mol/L KOH
supporting electrolyte	0.1 mol/L KCl	0.1 mol/L KCl
electrode	Schott IoLine	Schott IoLine
$\text{p}K_w$	13.78	13.78
pH range	2.5 – 5.8	2.6 – 5.3
volume of data points	100	100
time for mixing process	600 s	600 s

The overall stability constants of two complexes were determined by simultaneous evaluation of 12 titrations, six from each molar ratio, with the program Hyperquad2008. The resulting stability constants are summarized in **Table 7.32**.

**Table 7.32:** Mean values of the overall stability constants  $\log\beta_{xyz}$  <sup>[a]</sup> from potentiometric titrations of  $\text{Al}^{3+}$  with DSA determined by simultaneous evaluation with Hyperquad2008 in pure water,  $T = 298 \text{ K}$  and  $I = 0.1 \text{ mol/L KCl}$ .

<b><math>\log\beta</math> values for the complexation of <math>\text{Al}^{3+}</math>:DSA</b>	
six titrations 1:2	six titrations 1:4
pH 2.5 – 5.8	pH 2.6 – 5.3
mean values by simultaneous evaluation of 12 titrations <sup>[b]</sup>	
$\sigma$ <sup>[c]</sup>	0.663
<b><math>\log\beta_{110}</math></b>	<b>18.77(1)</b>
<b><math>\log\beta_{120}</math></b>	<b>32.45(1)</b>

<sup>[a]</sup> For the ligand L  $\log\beta_{xyz}$  is defined as:  $\beta_{xyz} = [\text{M}_x\text{L}_y\text{H}_z] \times [\text{M}]^{-x} \times [\text{L}]^{-y} \times [\text{H}]^{-z}$ .

<sup>[b]</sup> The titrations were evaluated simultaneously with the program Hyperquad2008. The deviations given in brackets correspond to the threefold standard deviation taken from Hyperquad2008.

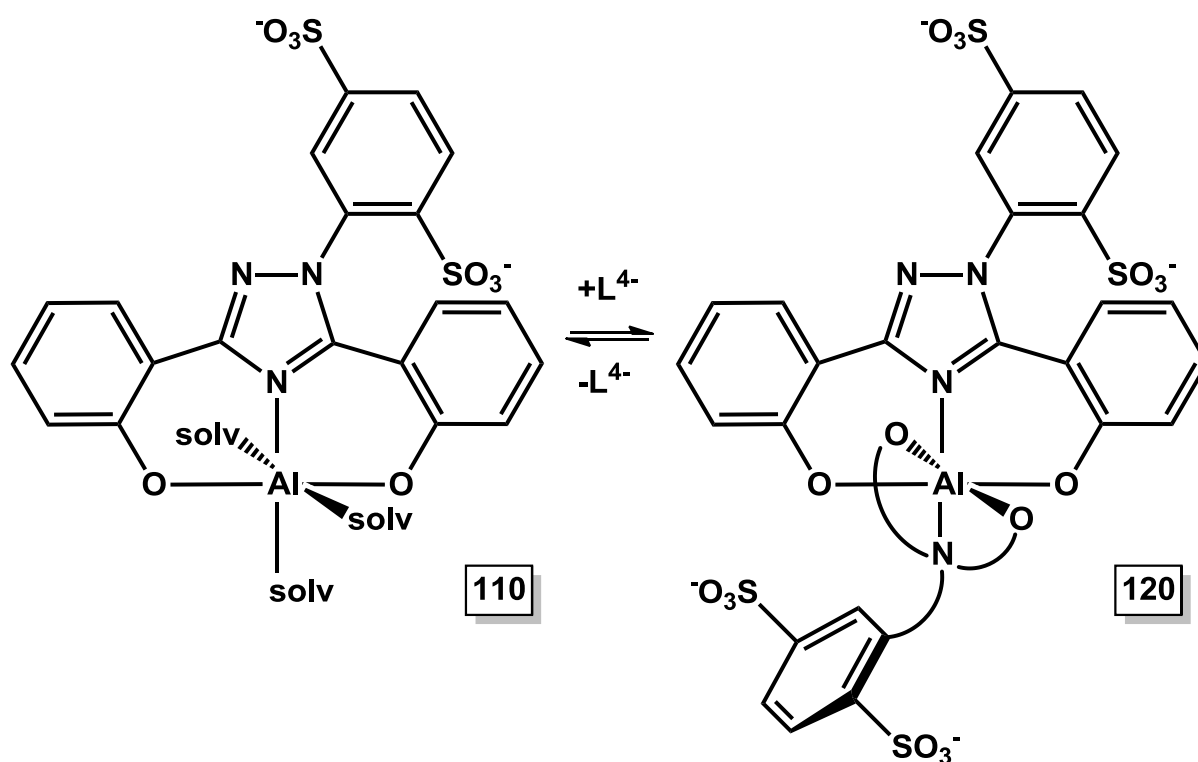
<sup>[c]</sup> The  $\sigma$  value is taken from Hyperquad2008.

The two complexes identified by potentiometric titrations are an  $[\text{Al}(\text{L})]^-$  (110) complex with  $\log\beta_{110} = 18.77(1)$  and a bis-complex of the composition  $[\text{Al}(\text{L})_2]^{5-}$  (120) with  $\log\beta_{120} = 32.45(1)$  which reveals a  $\log K_{120} = 13.68$  ( $\log K_{120} = [\text{ML}_2] / [\text{ML}] \times [\text{L}]$ ). Aluminium (III) forms very strong complexes with DSA in aqueous solution. However, the stability constants of the corresponding  $\text{Fe}^{3+}$ -DSA complexes were still higher with  $\log\beta_{110} = 23.54(4)$  (see **Table 7.9**) and  $\log\beta_{120} = 39.50(2)$  (see **Table 7.11**). The formation constant  $\log K_{120}$  ( $\log K_{120} = [\text{ML}_2] / [\text{ML}] \times [\text{L}]$ ) for the  $[\text{Fe}(\text{DSA})_2]^{5-}$  complex is also more stable with a value of 15.96. The  $\text{Fe}^{3+}$  ion and the  $\text{Al}^{3+}$  ion have the same charge, yet different ionic radii. The  $\text{Fe}^{3+}$  ionic radius (high-spin, CN: 6,  $r = 0.645 \text{ \AA}$ ) <sup>[118]</sup> is significantly larger than the  $\text{Al}^{3+}$  ionic radius (CN: 6,  $r = 0.535 \text{ \AA}$ ) <sup>[118]</sup>. The stability constants show a higher affinity to the  $\text{Fe}^{3+}$  ion. The mixed ONO- coordination mode of the ligand DSA comprehends the oxygen atoms as hard donor atoms, according to the HSAB principle, and the nitrogen atom resembling a rather soft than hard donor atom character. The  $\text{Al}^{3+}$  ion is a particularly hard cation compared to the  $\text{Fe}^{3+}$  ion which is considered

as a hard cation with soft characteristics. As a consequence, the partly soft character of the ligand matches the partly soft character of the  $\text{Fe}^{3+}$  as central ion.

As for the  $\text{Al}^{3+}$ -DSA system, the two complexes 110 and 120 were also found for the  $\text{Al}^{3+}$ -MSA system investigated by U. Heinz. The  $[\text{Al}(\text{MSA})]$  complex had a  $\log\beta_{110} = 16.27(2)$  and a  $\log\beta_{120} = 29.62(6)$  (pure water,  $T = 298\text{ K}$ ,  $I = 0.1\text{ mol/L KCl}$ )<sup>[37]</sup>. The formation constant  $\log K_{120} = 13.35$  ( $\log K_{120} = [\text{ML}_2] / [\text{ML}] \times [\text{L}]$ ) for the  $[\text{Al}(\text{MSA})_2]^{3-}$  complex is only 0.33 units smaller than the corresponding value  $\log K_{120}$  value of 13.68 for the  $\text{Al}^{3+}$ -DSA system. However, the difference in the stability constants of the 110 complexes of MSA and DSA with  $\text{Al}^{3+}$  is much higher with 2.5 units.

Interestingly, no protonated complexes such as a  $[\text{Al}(\text{LH})]$  (111 complex) and  $[\text{Al}(\text{L})(\text{LH})]$  (121 complex) were found for  $\text{Al}^{3+}$  with the sulfonic acid derivatives MSA and DSA by potentiometric titrations. The 110 and 120 complexes found with  $\text{Al}^{3+}$ -DSA adopt the favoured meridional tridentate coordination mode as depicted in **Scheme 7.14**.



**Scheme 7.14:** Suggested coordination geometries of the DSA complexes  $[\text{Al}(\text{L})]^-$  (110) and  $[\text{Al}(\text{L})_2]^{5-}$  (120).

To form a 111 or 121 complex one of the phenolate oxygen atoms would need to be protonated since the sulfonic acid groups and the triazole nitrogen atoms are too acidic. The tendency to form bidentate complexes with one hydroxyphenyl ring not coordinating to  $\text{Al}^{3+}$  seems to be not favoured for either complex. In contrast, the 121 species was found for  $\text{Fe}^{3+}$  complexes of both sulfonic acid derivatives. A possible explanation could be the smaller ionic radius of  $\text{Al}^{3+}$  which causes less strain in the tridentate coordination than  $\text{Fe}^{3+}$ . As seen in the crystal structure of the  $[\text{Fe}(\text{DSA})_2]^{5-}$  anion (see section 7.2.3) the phenolate rings are slightly twisted out of the plain for an optimal coordination of the  $\text{Fe}^{3+}$  ion. As a consequence, some strain occurs to the complex and a protonation of the phenolate ring and with it a bidentate coordination mode will take the strain. We assume the smaller  $\text{Al}^{3+}$  ion might reduce the twisting of the phenolate groups in the tridentate coordination mode and apparently there is no need to form a bidentate protonated species. The titration curves of both molar ratios are given in **Figure 7.57**.

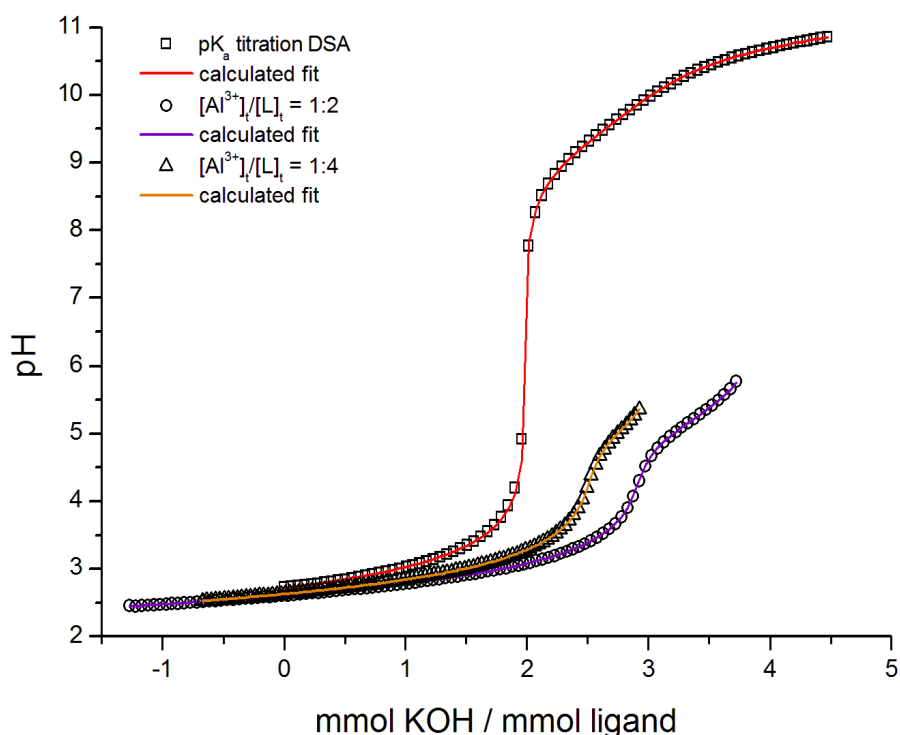


**Figure 7.57:** Potentiometric titration curves of the free ligand DSA and  $\text{Al}^{3+}$  with DSA with the molar ratios 1:2 ( $[\text{Al}^{3+}]_t = 0.48$  mmol/L,  $[\text{L}]_t = 1.00$  mmol/L) and 1:4 ( $[\text{Al}^{3+}]_t = 0.25$  mmol/L,  $[\text{L}]_t = 1.00$  mmol/L) in pure water,  $T = 298$  K and  $I = 0.1$  mol/L KCl. The open squares, circles and triangles represent experimental points and the fit (solid line) was calculated from the equilibrium constants with Hyperquad2008.

The strong complexation of  $\text{Al}^{3+}$  by the ligand DSA is displayed by the considerable decrease in pH of the  $\text{Al}^{3+}$ -DSA titration curves in comparison to the  $\text{p}K_a$  titration curve of DSA. The titration curve with a 1:2 molar ratio  $\text{Al}^{3+}$ :DSA exhibits an inflection at 3 equivalents at pH 4 owing to the completion of the formation of the  $[\text{Al}(\text{L})]^-$  complex. Accordingly, one equivalent of the doubly protonated ligand  $\text{LH}_2^{2-}$  is still present in solution. Further, an inflection appears in the titration curve with a 1:4 molar ratio at 2.5 equivalents also indicating the complete complex formation of the  $[\text{Al}(\text{L})]^-$  complex.

The species distribution diagram of the 1:2 molar ratio in **Figure 7.58** gives rise to the species in solution in relation to the pH scale. The species distribution for the 1:4 molar ratio changes only to a minor degree and is not displayed.

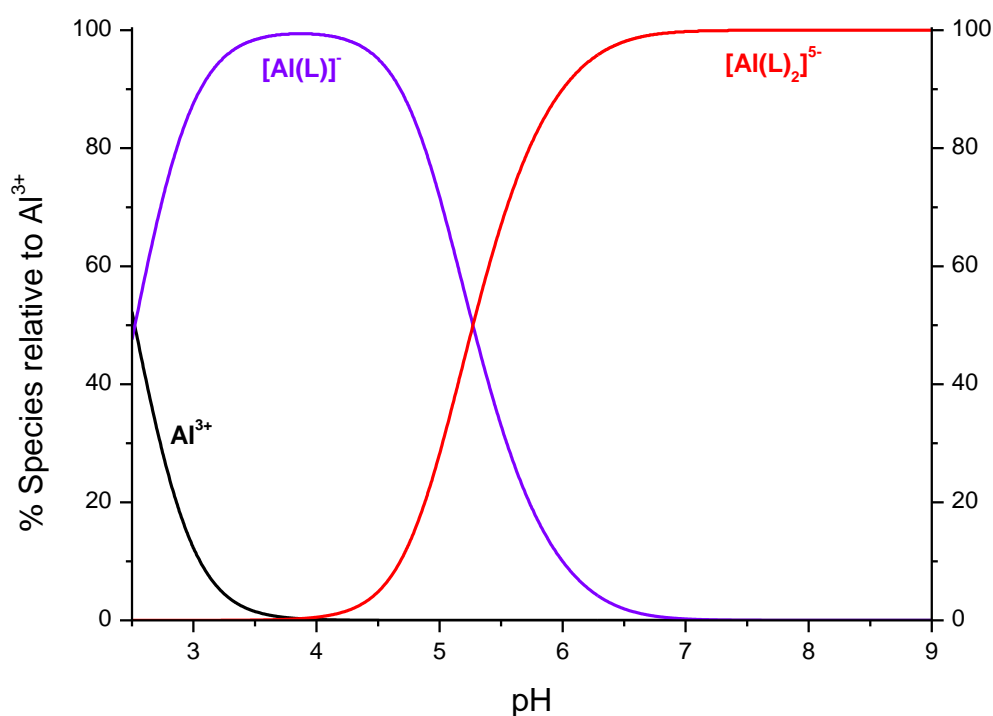


**Figure 7.58:** Species distribution diagram as a function of pH for  $\text{Al}^{3+}$  with the ligand DSA. Calculated for the continuous potentiometric titration performed with a 1:2 molar ratio ( $[\text{Al}^{3+}]_t = 0.48 \text{ mmol/L}$ ,  $[\text{L}]_t = 1.00 \text{ mmol/L}$ , pure water,  $T = 298 \text{ K}$  and  $I = 0.1 \text{ mol/L KCl}$ ) from pH 2.5 to 9.0. The species concentration were calculated from the equilibrium constants listed in **Table 7.29** (mean values from simultaneous evaluation of 12 titrations) with the program Hyss2006.

The hydrolysis products of  $\text{Al}^{3+}$  in **Table 7.30** were employed for the calculation of the species distribution diagram however they do not appear in the species distribution. At the beginning of the titration at pH 2.5 the  $[\text{Al}(\text{DSA})]^-$  (110) complex has been formed to 50% and 50% free  $\text{Al}^{3+}$  is present in solution. The species distribution shows that at pH 3.9, where the inflection is observed, the  $[\text{Al}(\text{DSA})]^-$  complex is formed to 99%. As the pH is raised above pH 4 the  $[\text{Al}(\text{DSA})_2]^{5-}$  (120) complex starts to form. At pH 5.3 both the 110 and the 120 complex coexist to equal amounts. Above pH 5.3 the 120 complex becomes the predominant species and reaches a maximum concentration of 100% from pH > 7.2. As a consequence, the sole species at physiological pH 7.4 is the  $[\text{Al}(\text{DSA})_2]^{5-}$  complex.

In conclusion, we have shown that the ligand DSA forms rather strong complexes with  $\text{Al}^{3+}$ . However, the ligand DSA forms stronger complexes with the metal ion  $\text{Fe}^{3+}$  as demonstrated by the formation constants and species distribution. The  $[\text{Fe}(\text{DSA})]^-$  complex needed to be determined in acidic solution between pH 1 – 2 and was formed to 96% at pH 2. In contrast, the  $[\text{Al}(\text{DSA})]^-$  complex has only formed to 50% at pH 2.5. The  $[\text{Al}(\text{DSA})_2]^{5-}$  complex is the only species in solution at physiological pH 7.4. Even though the ligand DSA forms stronger complexes with  $\text{Fe}^{3+}$ ,  $\text{Al}^{3+}$  might also compete against  $\text{Fe}^{3+}$  for complex formation. However, since  $\text{Al}^{3+}$  is a non-essential trace element and should be found in low abundance in the body the ligand DSA should preferably complex  $\text{Fe}^{3+}$ . However, due to the possible toxic effects of  $\text{Al}^{3+}$ , DSA might also function as a ligand for detoxification of  $\text{Al}^{3+}$  in the body.

## **8 Complex formation of magnesium (II), calcium (II) and aluminium (III) with deferasirox in pure water**

The complex formation of the iron-chelating ligand deferasirox has been investigated with several biometal ions by U. Heinz in his doctoral thesis <sup>[37]</sup>. Unfortunately, the ligand deferasirox is not sufficiently soluble in pure water. Consequently, titration experiments needed to be carried out in a water/DMSO mixture with a molar fraction  $x_{\text{DMSO}} = 0.20$ . The water/DMSO solution medium was appropriate to keep the ligand deferasirox in solution. However, the values determined in water/DMSO solution are somewhat different than the values in pure water. U. Heinz has investigated the relation between the molar fraction of DMSO and the equilibrium constants measured. As a result, the overall stability constants have a roughly linear relation to the molar fraction of DMSO present in solution. Determination of stability constants of the ligand deferasirox in pure water is hampered by the poor solubility. Yet, they can be estimated by measuring the stability constants in solutions with different molar fractions of DMSO and extrapolating the linear relation to pure water.

In this study, the  $pK_a$  values of deferasirox as well as the overall stability constants of the ligand with  $\text{Mg}^{2+}$ ,  $\text{Ca}^{2+}$  and  $\text{Al}^{3+}$  were investigated in water/DMSO solution with four molar ratios ( $x_{\text{DMSO}} = 0.20, 0.18, 0.16$  and  $0.14$ ). The values of the stability constants in pure water were estimated by linear extrapolation.

## 8.1 Investigation of the $pK_a$ values of deferasirox

The  $pK_a$  values of the ligand deferasirox in pure water have been investigated in the past by potentiometric titrations ( $T = 298\text{ K}$ ,  $I = 0.1\text{ KCl/ or KNO}_3$ ) with different molar fractions of DMSO and extrapolation to pure water [37, 39-40]. In this study the determination has been repeated for four molar fractions of DMSO ( $x_{\text{DMSO}} = 0.20, 0.18, 0.16$  and  $0.14$ ). The structural formula of the ligand deferasirox is illustrated in **Figure 8.1**. The three  $pK_a$  values found were assigned to the carboxylic acid group and the two hydroxyphenyl groups. In this study, investigations in acidic solution revealed another  $pK_a$  value which could be assigned to the protonation of a nitrogen atom of the triazole unit. The determination of this acidic protonation constant of the ligand deferasirox was performed with spectrophotometric batch titrations in acidic solution and  $^1\text{H-NMR}$  spectroscopy. Further, a kinetic study, revealing precipitation of the ligand deferasirox, was performed in water/DMSO solution with the rather low molar fraction  $x_{\text{DMSO}} = 0.06$ .

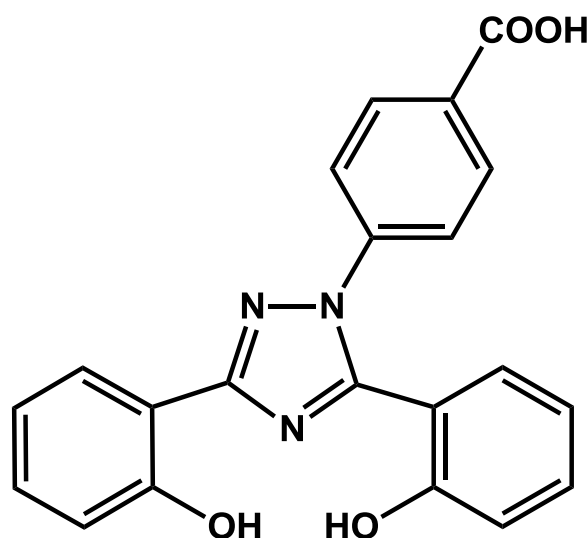


**Figure 8.1:** The structural formula of the ligand 4-[3,5-bis(2-hydroxyphenyl)-1H-1,2,4-triazol-1-yl]benzoic acid (deferasirox, ICL670).

### 8.1.1 Determination of the $pK_a$ values of deferasirox in pure water by continuous potentiometric titrations

The determination of the  $pK_a$  values of deferasirox in pure water is difficult due to the low solubility of the ligand in pure water. However, the  $pK_a$  values in pure water can be estimated by a linear extrapolation of values measured at different molar fractions of DMSO in pure water. The  $pK_a$  values have been determined for the molar fractions  $x_{\text{DMSO}} = 0.20, 0.18, 0.16$  and  $0.14$  at  $T = 298 \text{ K}$  and with potassium chloride ( $0.1 \text{ mol/L KCl}$ ) as supporting electrolyte. The ligand deferasirox was applied with a concentration of  $0.50 \text{ mmol/L}$  based on a better solubility in all molar fractions. The molar fractions  $x_{\text{DMSO}} = 0.20$  and  $0.18$  can be titrated with a  $1.00 \text{ mmol/L}$  concentration of deferasirox. Whereas occasionally a slight turbidity, caused by ligand precipitation, was observed for the solutions prepared with the  $x_{\text{DMSO}} = 0.16$  and  $0.14$  molar fractions. To prevent the ligand from precipitating overnight a small volume of potassium hydroxide  $0.1 \text{ mol/L}$  was added to the flask to raise the pH.

It is important to note that the  $pK_w$  differs in water/DMSO solutions with different molar fractions <sup>[122-123]</sup>. Based on the procedure described in section 11.2.4 the  $pK_w$  values for each molar fraction were determined by potentiometric titrations. Dependent on the  $pK_w$  value the pH scale is extended for  $x_{\text{DMSO}} = 0.20$  to range from pH 0 to 15.6 <sup>[40]</sup>.

The overall stability constants  $\log\beta_x$  and acidity constants  $pK_a$  values in **Table 8.1** were calculated as mean values with standard deviations from at least 6 titrations. The titration conditions are also listed in **Table 8.1**.

**Table 8.1:** Determination of the mean values of the overall protonation constants  $\log\beta_x$  <sup>[a]</sup> and acidity constants  $pK_{a,i}$  <sup>[b]</sup> with standard deviations <sup>[d]</sup> of the ligand deferasirox in water/DMSO solution with different molar fractions  $x_{\text{DMSO}}$  at  $T = 298 \text{ K}$  and  $I = 0.1 \text{ mol/L KCl}$ .

$x_{\text{DMSO}}$	<b>0.20</b>	<b>0.18</b>	<b>0.16</b>	<b>0.14</b>
$[L]_t$	0.50 mmol/L	0.50 mmol/L	0.50 mmol/L	0.50 mmol/L
$pK_w$	15.58	15.39	15.20	15.01
pH range	4.0 – 12.6	3.9 – 12.5	4.3 – 12.0	4.6 – 11.9
No. of titrations	7	6	6	6
No. data points	50	50	40 / 60	50
time mixing [s]	120	120	120	120
$\sigma$ <sup>[c]</sup>	0.781	0.687	0.265	0.408
<b><math>\log\beta_1</math></b>	<b>12.18(2)</b>	<b>12.05(3)</b>	<b>11.94(4)</b>	<b>11.80(2)</b>
<b><math>\log\beta_2</math></b>	<b>22.36(3)</b>	<b>22.12(4)</b>	<b>21.93(4)</b>	<b>21.66(1)</b>
<b><math>\log\beta_3</math></b>	<b>27.00(3)</b>	<b>26.65(3)</b>	<b>26.35(4)</b>	<b>26.01(2)</b>
<b><math>pK_{a,1}</math></b>	<b>4.64(1)</b>	<b>4.53(3)</b>	<b>4.42(1)</b>	<b>4.35(2)</b>
<b><math>pK_{a,2}</math></b>	<b>10.18(1)</b>	<b>10.07(1)</b>	<b>9.99(1)</b>	<b>9.86(1)</b>
<b><math>pK_{a,3}</math></b>	<b>12.18(2)</b>	<b>12.05(3)</b>	<b>11.94(4)</b>	<b>11.80(2)</b>

<sup>[a]</sup> For the ligand L  $\log\beta_x$  is defined as:  $\beta_x = [LH_x] \times [L]^{-1} \times [H]^{-x}$ .

<sup>[b]</sup> For the ligand  $LH_x$  the  $pK_{a,i}$  is defined as:  $pK_{a,i} = -\log K_{a,i}$  and  $K_{a,i} = [LH_{x-i}] \times [H] \times [LH_{(x+1)-i}]^{-1}$ .

<sup>[c]</sup> The  $\sigma$  value is taken from the titration with the highest  $\sigma$  value in Hyperquad2008.

<sup>[d]</sup> The standard deviations in brackets were calculated with:  $\sqrt{\frac{\sum_{i=0}^n (x_i - \bar{x})^2}{(n-1)}}$ ;  $x_i$  measured value;  $\bar{x}$  mean value; n number of values.

The mean  $pK_a$  values from **Table 8.1** were plotted against the molar fraction and the linear regression was calculated for the four  $pK_a$  values. Extrapolation of the linear regression to  $x_{\text{DMSO}} = 0.00$  resulted in the estimated  $pK_a$  values for deferasirox in pure water. **Figure 8.2** shows the linear regression and extrapolation as calculated.

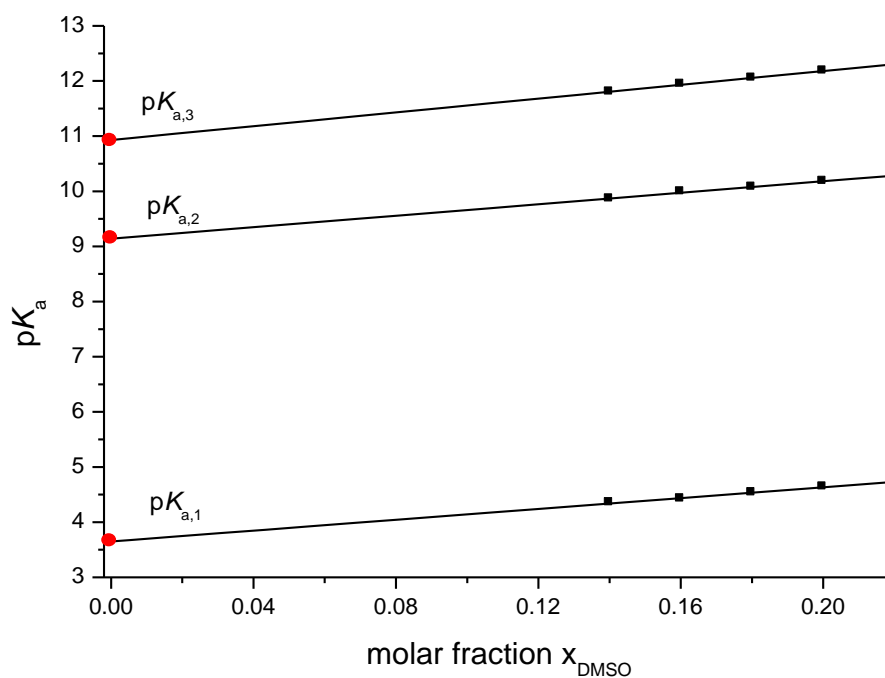


**Figure 8.2:** Dependence of the  $pK_a$  values of deferasirox on the molar fraction  $x_{\text{DMSO}}$ . Linear regression (solid line) of the mean  $pK_a$  values (black squares) listed in **Table 8.1** and extrapolation to  $x_{\text{DMSO}} = 0.00$ . The red circles indicate the extrapolated values at  $x_{\text{DMSO}} = 0.00$ .

The red circles in **Figure 8.2** show the estimated three  $pK_a$  values by linear extrapolation of the in different molar fractions measured  $pK_a$  values of deferasirox.

The estimated  $pK_a$  values for the ligand deferasirox in pure water, the linear regression equation and the regression coefficient are presented in **Table 8.2**.

**Table 8.2:** Estimated  $pK_{a,i}$  <sup>[a]</sup> values of deferasirox in pure water calculated by linear regression of the  $pK_{a,i}$  values measured in four molar fractions and extrapolation to  $x_{\text{DMSO}} = 0.00$  (T = 298 K).

Estimated $pK_{a,i}$ values of deferasirox in pure water			
solvent		pure water	
supporting electrolyte		0.1 mol/L KCl	
$x_{\text{DMSO}} = 0.00$		R <sup>[c]</sup>	regression equation <sup>[b]</sup>
$pK_{a,1}$ <sup>[d]</sup>	<b>3.65(6)</b>	0.99504	$pK_{a,1} = 4.9(3) \times [x_{\text{DMSO}}] + 3.65(6)$
$pK_{a,2}$ <sup>[d]</sup>	<b>9.14(6)</b>	0.99614	$pK_{a,2} = 5.2(3) \times [x_{\text{DMSO}}] + 9.14(6)$
$pK_{a,3}$ <sup>[d]</sup>	<b>10.93(3)</b>	0.99904	$pK_{a,3} = 6.25(2) \times [x_{\text{DMSO}}] + 10.93(3)$

<sup>[a]</sup> For the ligand  $LH_x$  the  $pK_{a,i}$  is defined as:  $pK_{a,i} = -\log K_{a,i}$  and  $K_{a,i} = [LH_{x-i}] \times [H] \times [LH_{(x+1)-i}]^{-1}$

<sup>[b]</sup> Linear regression equation was taken from the program Origin 6.0G.

<sup>[c]</sup> R is the regression coefficient taken from Origin 6.0G.

<sup>[d]</sup> The deviations in brackets were taken from the regression equation from Origin 6.0G.

The linear dependence of the  $pK_a$  value on the molar fraction  $x_{\text{DMSO}}$  is good with respect to the linear regression coefficient R. The  $pK_{a,1} = 3.65(6)$  and  $pK_{a,2} = 9.14(6)$  are in good agreement with those ( $pK_{a,1} = 3.7(1)$  and  $pK_{a,2} = 9.0(1)$ ) reported by S. Steinhauser <sup>[40]</sup>. The  $pK_{a,3} = 10.93(3)$  is somewhat higher than the one reported by S. Steinhauser  $pK_{a,3} = 10.6(1)$  <sup>[40]</sup>.

With the decrease of the molar fraction of DMSO the  $pK_a$  values also decrease. As a result, the estimated  $pK_a$  values in pure water are smaller than the measured  $pK_a$  values in water/DMSO. This observation is in accordance to the determination of the  $pK_a$  values in pure water by U. Heinz and S. Stucky (formerly S. Steinhauser) <sup>[37, 39-40]</sup>. It is known, that DMSO solvates cations better than anions <sup>[124]</sup>. S. Stucky has discussed the solvation of different functional groups according to their charge before and after the deprotonation in pure water compared to DMSO, in his doctoral thesis <sup>[39]</sup>. He has shown that the deprotonation of a neutral functional group forming an anion after deprotonation often causes the  $pK_a$  values in DMSO solution to rise compared to those in pure

8 Complex formation of magnesium (II), calcium (II) and aluminium (III) with deferasirox in pure water

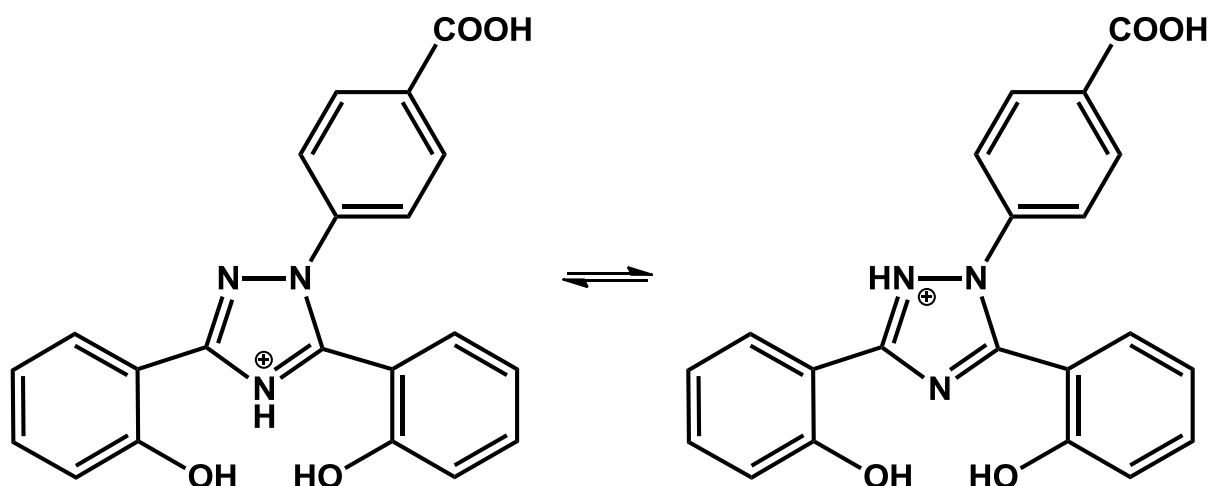
---

water. Further, the  $pK_a$  value is also higher in DMSO when anions are deprotonated to a higher negative charge. An explanation for this observation is that the solvation of anions by DMSO is rather weak causing the proton to be less acidic.

In conclusion, the  $pK_a$  values in **Table 8.1** measured with the four molar fractions of DMSO  $x_{\text{DMSO}} = 0.20, 0.18, 0.16$  and  $0.14$  were used for the calculation of the stability constants of  $\text{Mg}^{2+}$ ,  $\text{Ca}^{2+}$  and  $\text{Al}^{3+}$  with deferasirox in the particular molar fraction.

### 8.1.2 Investigation of the protonation of deferasirox in acidic solutions in pure water by spectrophotometric batch titration

The three  $pK_a$  values assigned to the carboxylic acid and the two hydroxyphenyl groups were successfully determined by potentiometric titrations in the pH range 4 – 12. However, the batch titration in acidic solution with the disulfonic acid derivative DSA in section 7.1 has shown that the  $pK_{a,2}$  value is very acidic 1.33(8) and can be assigned to a protonation of one of the nitrogen atoms of the 1,2,4-triazole unit. Accordingly, it should be possible to protonate the 1,2,4-triazole unit of the ligand deferasirox at one of the nitrogen atoms in position 2 or 4 in acidic solution as shown in **Scheme 8.1**. The results presented and discussed in this section have been published in Stucky 2008 <sup>[125]</sup>.

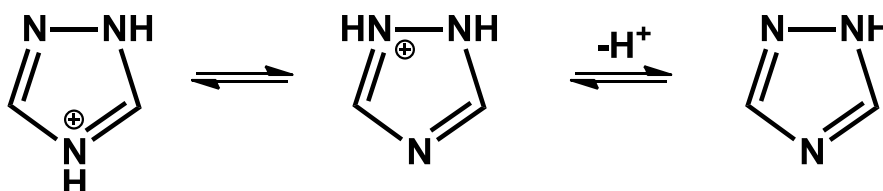


**Scheme 8.1:** Protonation sites of the 1,2,4-triazole unit of deferasirox in acidic solution.

S. Stucky (formerly S. Steinhauser) reported in his doctoral thesis of a significant shift of the absorption maximum in the UV-VIS spectra of deferasirox measured in water/DMSO with a molar fraction of  $x_{\text{DMSO}} = 0.06$  in acidic solutions with increasing acidity <sup>[39]</sup>. This observation is evidence for a protonation at the 1,2,4-triazole unit in acidic solution. The  $pK_a$  value for the protonation of the unsubstituted 1,2,4-triazole as shown in **Scheme 8.2** is 2.38(5) ( $T = 298 \text{ K}$ ,  $I = 0.1 \text{ mol/L}$ ) <sup>[55]</sup>. The ligand deferasirox is a 1,2,4-triazole ligand substituted by two hydroxyphenyl substituents in position 3 and 5 and a benzoic acid moiety-

ty in position 1. The benzoic acid withdraws electron density from the triazole ring (-M resonance effect) and will probably cause the  $pK_a$  value to decrease.

S. Stucky (formerly S. Steinhauser) estimated the  $pK_a$  to be  $< 1$  due to a significant shift of the absorption maximum occurring in very acidic HCl (3.6 mol/L) solution <sup>[39]</sup>.



**Scheme 8.2:** Deprotonation of the unsubstituted 1,2,4-triazole.

To determine the  $pK_a$  value estimated  $< 1$  of this deprotonation a pH range from  $0.0 < \text{pH} < 2.0$  was needed which was implemented by a 1.0 mol/L HCl/KCl medium with a molar fraction of  $x_{\text{DMSO}} = 0.06$ . The determination in this pH range needs to be carried out as a spectrophotometric batch titration.

Further, the  $pK_a$  value in pure water was of interest. For this reason, batch titrations with different molar ratios  $x_{\text{DMSO}} = 0.20, 0.18, 0.16, 0.10$  and  $0.06$  were to be performed and an extrapolation to pure water should be calculated to estimate the  $pK_a$  value. However, solutions prepared with an ionic strength of 1.0 mol/L KCl with a high amount of DMSO such as the molar fractions with  $x_{\text{DMSO}} = 0.20$  and  $0.18$  showed crystallization of the KCl. Potassium chloride is not soluble enough in these molar fractions to keep a 1.0 mol/L KCl concentration in solution. Consequently, only the molar fractions  $x_{\text{DMSO}} = 0.16, 0.10$  and  $0.06$  were applied for the extrapolation to pure water.

The preparation of the samples was performed differently to the batch titrations described previously. The samples were prepared in 25.0 mL volumetric flasks which were thermostated to  $T = 298 \text{ K}$ . The calculated amount of 1.0 mol/L HCl, with the appropriate molar fraction DMSO, was weighed into the flask instead of adding it by means of the needed volume. This procedure was applied to achieve a more precise regulation of the pH values which could only be calculated and not measured. The ligand deferasirox was added as a pre-

8 Complex formation of magnesium (II), calcium (II) and aluminium (III) with deferasirox in pure water

cise volume with a micropipette. Then the flasks were filled with a 1.0 mol/L KCl solution with the appropriate molar fraction. The UV-VIS spectra were evaluated with the program Specfit. The determined  $pK_a$  values and batch titration conditions are given in **Table 8.3**.

**Table 8.3:** Spectrophotometric batch titration experiments of the ligand deferasirox for the determination of the acidity constants  $pK_a$  <sup>[a]</sup> in acidic water/DMSO solution with three molar ratios  $x_{DMSO}$ . The standard deviation of the value is given in brackets <sup>[b]</sup>. The titration conditions are given at T = 298 K.

$x_{DMSO}$	<b>0.16</b>	<b>0.10</b>	<b>0.06</b>
$[L]_t$	40.0 $\mu\text{mol/L}$	20.0 $\mu\text{mol/L}$	40.0 $\mu\text{mol/L}$
pH range	0.10 – 2.00	0.10 – 1.30	0.10 – 2.00
No. of titrations	1	1	2
No. data points	9	8	9
titration volume	25.0 mL	25.0 mL	25.0 mL
titrant and supp. electrolyte	$c(\text{HCl}) + c(\text{KCl}) = 1.0 \text{ mol/L}$		
equilibration time	1h	1h	5 min
$pK_a$ <sup>[b]</sup>	<b>0.3(1)</b>	<b>0.5(1)</b>	<b>0.72(4)</b>
$\sigma_{\text{abs}}$ <sup>[c]</sup>	$2.8 \cdot 10^{-3}$	$1.4 \cdot 10^{-3}$	$1.7 \cdot 10^{-3}$
$\sigma_{\text{squares}}$ <sup>[c]</sup>	$8.6 \cdot 10^{-3}$	$1.2 \cdot 10^{-3}$	$3.2 \cdot 10^{-3}$

<sup>[a]</sup> For the ligand  $\text{LH}_x$  the  $pK_{a,i}$  is defined as:  $pK_{a,i} = -\log K_{a,i}$  and  $K_{a,i} = [\text{LH}_{x-i}] \times [\text{H}] \times [\text{LH}_{(x+1)-i}]^{-1}$

<sup>[b]</sup> The deviation given in brackets corresponds to the standard deviation taken from Specfit.

<sup>[c]</sup> The  $\sigma_{\text{abs}}$  and  $\sigma_{\text{squares}}$  values are taken from Specfit.

The linear dependence of the  $pK_a$  value on the molar fraction  $x_{DMSO}$  was calculated in form of a linear regression for the given values. The linear regression and extrapolation to  $x_{DMSO} = 0.00$  is illustrated in **Figure 8.3**.

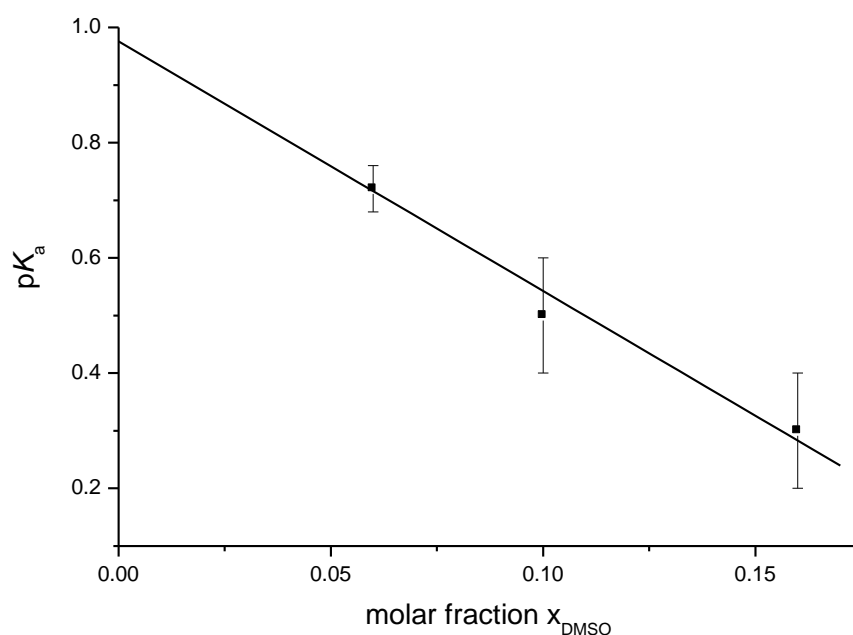


**Figure 8.3:** Plot of the dependence of the  $pK_a$  value of deferasirox on the molar fraction  $x_{\text{DMSO}}$ . Linear regression (solid line) of the  $pK_a$  values (black squares) listed in **Table 8.3** and extrapolation to  $x_{\text{DMSO}} = 0.00$ .

The estimated  $pK_a$  values for the ligand deferasirox in pure water, the regression equation and the regression coefficient  $R$  are given in **Table 8.4**.

**Table 8.4:** Estimated  $pK_a$  <sup>[a]</sup> value of deferasirox in pure water calculated by linear regression of the  $pK_a$  values measured in three molar fractions and extrapolation to  $x_{\text{DMSO}} = 0.00$  ( $T = 298 \text{ K}$ ). <sup>[125]</sup>

Estimated $pK_a$ value of deferasirox in pure water			
solvent		pure water	
titrant and supporting electrolyte		$c(\text{HCl}) + c(\text{KCl}) = 1.0 \text{ mol/L}$	
$x_{\text{DMSO}} = 0.00$		$R$ <sup>[c]</sup>	regression equation <sup>[b]</sup>
$pK_a$ <sup>[d]</sup>	<b>0.98(4)</b>	0.99364	$pK_a = -4.3(9) \times [x_{\text{DMSO}}] + 0.98(4)$

<sup>[a]</sup> For the ligand  $\text{LH}_x$  the  $pK_{a,i}$  is defined as:  $pK_{a,i} = -\log K_{a,i}$  and  $K_{a,i} = [\text{LH}_{x-i}] \times [\text{H}] \times [\text{LH}_{(x+1)-i}]^{-1}$

<sup>[b]</sup> Linear regression equation was taken from the program Origin 6.0G.

<sup>[c]</sup>  $R$  is the regression coefficient taken from Origin 6.0G.

<sup>[d]</sup> The deviations in brackets were taken from the regression equation from Origin 6.0G.

The estimated  $pK_a$  value in pure water is 0.98(4) <sup>[125]</sup>. We note that this value is higher than the values in the water/DMSO mixtures. The resulting  $pK_a$  values decrease with increase of the molar fraction of DMSO. This observation is contradictory to the determined  $pK_a$  values in section 8.1.1 by potentiometric titrations. A possible explanation is associated with the different solvation of cations and anions in DMSO in contrast to pure water. The protonation of the 1,2,4-triazole unit of deferasirox results in a positive charge at the nitrogen atom. The ligand is now a cation  $LH_4^+$  in solution which deprotonates to the neutral ligand  $LH_3$ . Protons are well solvated by DMSO and withdrawn from the equilibrium. This effect influences the  $pK_a$  value by increasing the acidity with the higher molar fraction of DMSO. Additionally, the neutral organic ligand deferasirox resulting from the deprotonation is probably better soluble in DMSO. S. Stucky has shown, in his doctoral thesis <sup>[39]</sup>, examples of ligand deprotonations from a cation to a neutral ligand with a smaller  $pK_a$  value in DMSO than in pure water.

Additionally, U. Heinz has investigated the protonation constants of the ligand MSA in water/DMSO solution with increasing molar fractions of DMSO <sup>[37]</sup>. He found, that the  $pK_{a,1} = 1.12(1)$  of MSA determined in pure water by spectrophotometric batch titration ( $T = 298\text{ K}$ ,  $0.1\text{ mol/L KCl}$ ) decreases with increase of the molar fraction of DMSO in solution. Accordingly, the  $pK_{a,1}$  could only be determined with the lowest molar fraction  $x_{\text{DMSO}} = 0.06$  to a value of 0.9(2). Determination of the  $pK_{a,1}$  in any higher molar fraction resulted in a too low  $pK_{a,1}$  value which could not be studied in a  $0.1\text{ mol/L HCl/KCl}$  medium. This observation is consistent with the decrease of the  $pK_a$  in strong acidic solution for deferasirox by increasing DMSO concentration in this work. As discussed in section 7.1 the  $pK_{a,2}$  of DSA was assigned to a protonation of the 1,2,4-triazole unit nitrogen atom. Consequently, the  $pK_{a,1}$  of MSA can most probably also be assigned to a deprotonation of the 1,2,4-triazole unit. This would explain the concordant behaviour of both the deferasirox  $pK_a$  value in acidic solution and the  $pK_{a,1}$  of MSA decreasing with higher DMSO concentration in contrast to the hydroxyphenyl  $pK_a$  values which increase with higher concentration of DMSO.

The solubility of the  $\text{LH}_4^+$  species in the water/DMSO mixtures plays an essential role. The measured UV-VIS spectra of the batch titration with a molar fraction of  $x_{\text{DMSO}} = 0.10$  are given in **Figure 8.4**.

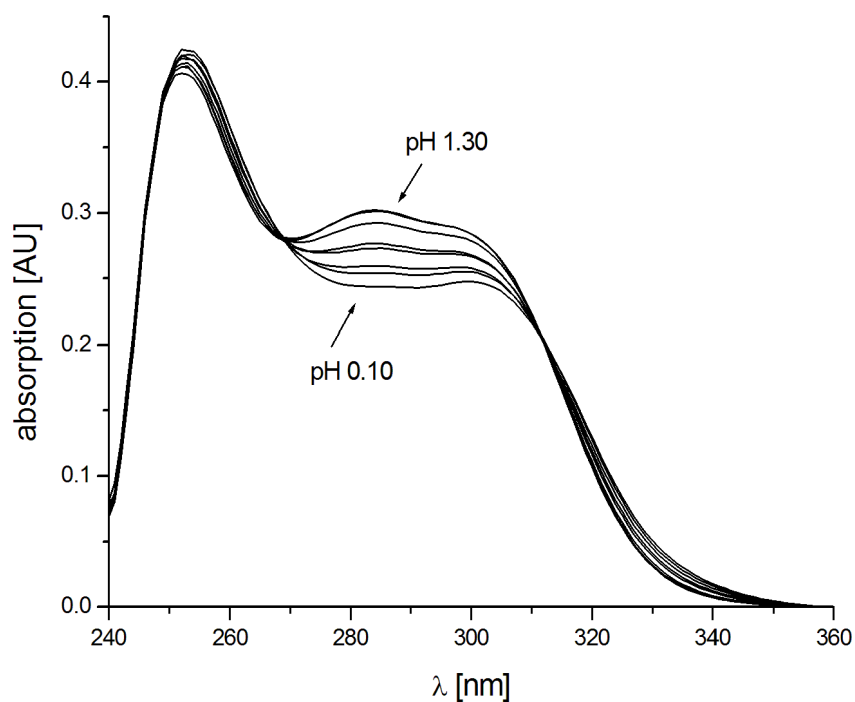


**Figure 8.4:** UV-VIS spectra of the batch titration of deferasirox collected from pH 0.10 – 1.30 ( $x_{\text{DMSO}} = 0.10$ ,  $[\text{L}]_t = 20.0 \mu\text{mol/L}$ ,  $T = 298 \text{ K}$ ,  $I = 1.0 \text{ mol/L HCl/KCl}$ ).

The individual spectra, of this molar fraction  $x_{\text{DMSO}} = 0.10$ , of the two deferasirox species  $\text{LH}_4^+$  and  $\text{LH}_3$  are presented in **Figure 8.5**.

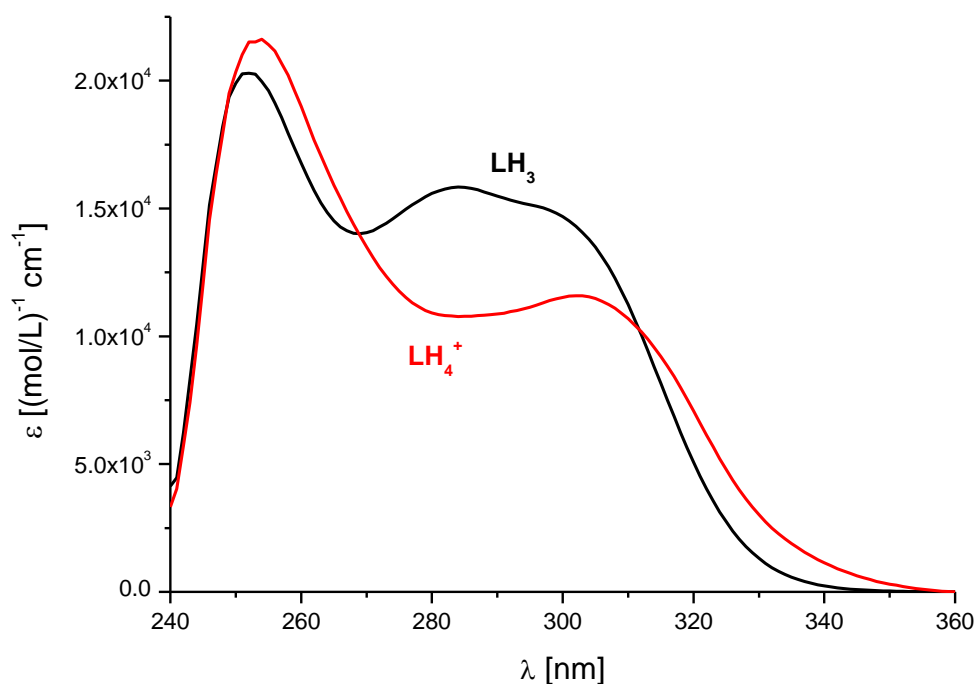


**Figure 8.5:** Individual spectra of the two species  $\text{LH}_4^+$  and  $\text{LH}_3$  (L = deferasirox) taken from Specfit ( $x_{\text{DMSO}} = 0.10$ ,  $T = 298 \text{ K}$ ,  $I = 1.0 \text{ mol/L HCl/KCl}$ ).

Usually, the UV-VIS spectra were measured about an hour after preparing the solutions. However, some of the prepared samples with a molar fraction of  $x_{\text{DMSO}} = 0.06$  showed a decrease of the absorption after about one day which was attributed to the precipitation of deferasirox due to solubility problems in the low molar fraction. This observation was investigated by measuring the absorption at 290 nm as a function of time. The absorption is dependent on the concentration of the ligand deferasirox in solution. The samples were prepared with a total ligand concentration of  $40.0 \mu\text{mol/L}$ . The diagram in **Figure 8.6** illustrates the absorption  $A_{290}$  measured at 290 nm as a function of time for four measured pH values pH = 0.26, 0.70, 1.00 and 2.00.

Apparently, in strong acidic solution the absorption remains nearly constant. However, the absorption decreases even more as the pH rises. The protonated form  $\text{LH}_4^+$  of the ligand is mainly present at pH 0.26 and is responsible for enhanced solubility in acidic solution. At higher pH the ligand is deprotonated and precipitates to form solid  $\text{LH}_3$  after a few days.

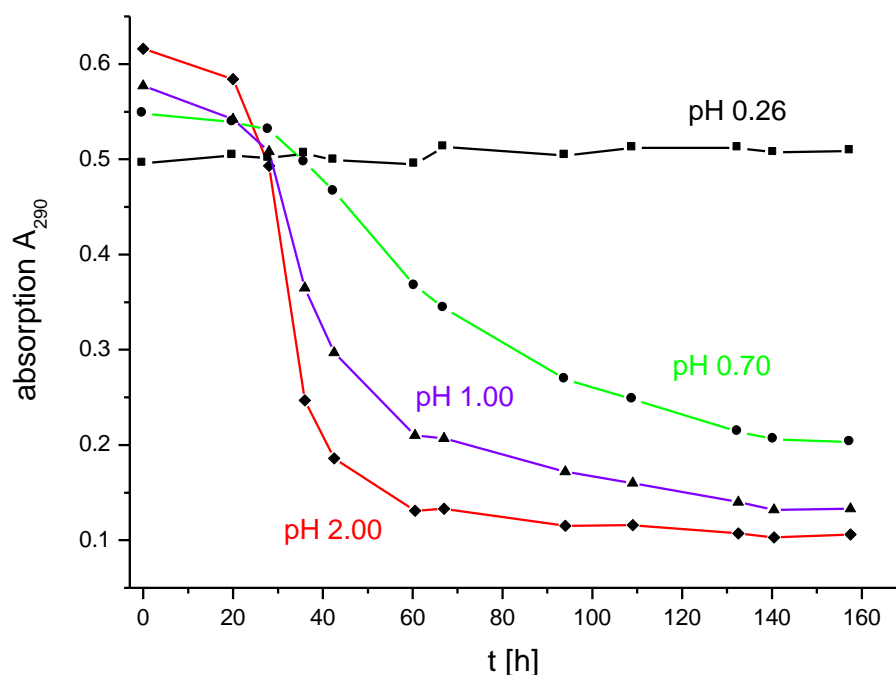


**Figure 8.6:** Measured absorption  $A_{290}$  at 290 nm as a function of time for four samples of the batch titration of deferasirox with  $x_{\text{DMSO}} = 0.06$  ( $[L]_t = 40.0 \mu\text{mol/L}$ ,  $T = 298 \text{ K}$ ,  $I = 1.0 \text{ mol/L HCl/KCl}$ ). Squares, circles and triangles represent the experimental data. The solid lines are added only for illustration.

In summary, a further protonation to  $\text{LH}_4^+$  of the ligand deferasirox in strong acidic solution was elucidated. Related to the weak solubility of deferasirox in acidic solution the new  $pK_a$  value could not be determined directly in pure water, yet it was estimated to 0.98(4) by extrapolation to pure water. Low molar fractions of DMSO such as  $x_{\text{DMSO}} = 0.16$ , 0.10 and 0.06 were chosen to perform the linear regression and extrapolation. The investigation was restricted to low molar fractions of DMSO by the solubility of a 1.0 mol/L KCl in the water/DMSO mixtures. The new  $pK_a$  value could only be assigned to a protonation of one of the 1,2,4-triazole nitrogen atoms since there is no other functional group in deferasirox which could be protonated. The  $pK_a$  value 0.98(4) ( $T = 298 \text{ K}$ ,  $I = 1.0 \text{ mol/L HCl/KCl}$ ) for deferasirox is smaller than the corresponding deprotonation for MSA  $pK_{a,1} = 1.12(1)$  ( $T = 298 \text{ K}$ ,  $I = 0.1 \text{ mol/L KCl}$ ) and DSA  $pK_{a,2} = 1.33(8)$  ( $T = 298 \text{ K}$ ,  $I = 0.1 \text{ mol/L HCl/KCl}$ ) which were determined in pure water.

### 8.1.3 <sup>1</sup>H-NMR spectroscopic measurements of the ligand deferasirox in acidic D<sub>2</sub>O/D<sub>6</sub>-DMSO solution

The ligand deferasirox was investigated in acidic solution by <sup>1</sup>H-NMR spectroscopy. A NMR-titration experiment was performed in the range  $0 \leq \text{pD} \leq 1$ . Six samples were prepared according to the procedure described in section 11.2.5. Small shifts in the expected six NMR signals of the benzocarboxylic acid and the two hydroxyphenyl groups were observed, allowing the calculation of a  $\text{p}K_{\text{a}}^{\text{D}}$  value for the protonation of one of the 1,2,4-triazole nitrogen atoms with the help of the program NMR-Tit<sup>[126]</sup>. The results presented and discussed in this section have been published in Stucky 2008<sup>[125]</sup>. The conditions of the NMR-titration and the determined  $\text{p}K_{\text{a}}^{\text{D}}$  value are given in **Table 8.5**.

**Table 8.5:** Determination of the  $\text{p}K_{\text{a}}^{\text{D}}$ <sup>[a]</sup> value of the system  $\text{LH}_4^+/\text{LH}_3$  for the ligand deferasirox in acidic D<sub>2</sub>O-DCI/D<sub>6</sub>-DMSO solution mixture at  $T = 294 \pm 2$  K.<sup>[125]</sup>

<b><math>\text{p}K_{\text{a}}^{\text{D}}</math> value of deferasirox</b>	
measuring method	<sup>1</sup> H-NMR titration
solvent	D <sub>2</sub> O-DCI/D <sub>6</sub> -DMSO
molar fraction	$x_{\text{DMSO}} = 0.20$
supporting electrolyte	none
pD range	0.0 – 1.0
No. of samples	6
<b><math>\text{p}K_{\text{a}}^{\text{D}}</math><sup>[b]</sup></b>	<b>0.89(2)</b>

<sup>[a]</sup> For the ligand  $\text{LH}_4^+$  the  $\text{p}K_{\text{a}}^{\text{D}}$  is defined as:  $\text{p}K_{\text{a}}^{\text{D}} = -\log K_{\text{a}}^{\text{D}}$  and  $K_{\text{a}}^{\text{D}} = [\text{LD}_3] \times [\text{D}] \times [\text{LD}_4]^{-1}$

<sup>[b]</sup> The  $\text{p}K_{\text{a}}^{\text{D}}$  value was calculated with the program NMR-Tit<sup>[126]</sup>.

The dependence of the measured <sup>1</sup>H-NMR resonances on the pD for the ligand system  $\text{LH}_4^+/\text{LH}_3$  is illustrated in **Figure 8.7**.

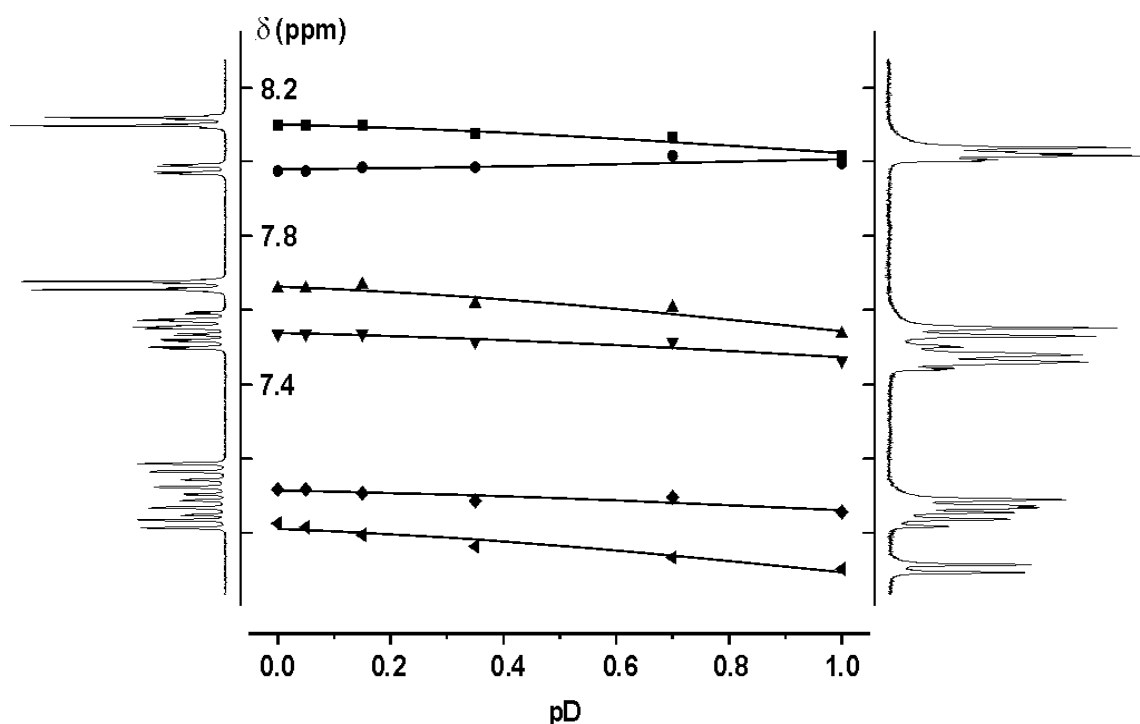


**Figure 8.7:** Shifts of the  $^1\text{H}$ -NMR resonances dependent on pD for the ligand species  $\text{LH}_4^+/\text{LH}_3$  of deferasirox ( $T = 294 \pm 2 \text{ K}$ , no supporting electrolyte,  $\text{D}_2\text{O}$ - $\text{DCl}/\text{D}_6$ -DMSO mixture with  $x_{\text{DMSO}} = 0.20$ , TMS = 0 ppm). Squares, triangles and circles represent experimental values, the solid lines were calculated with the program NMR-Tit<sup>[126]</sup>.

The  $\text{p}K_{\text{a}}^{\text{D}} = 0.89(2)$  determined by  $^1\text{H}$ -NMR-titration with a molar fraction of  $x_{\text{DMSO}} = 0.20$  is smaller than the  $\text{p}K_{\text{a}} = 0.98(4)$  calculated for  $x_{\text{DMSO}} = 0.00$  by spectrophotometric titration in section 8.1.2<sup>[125]</sup>. This is in accordance with the previously discussed solvation differences of anions and cations in DMSO compared to water. The  $\text{p}K_{\text{a}}^{\text{D}}$  value was measured in a water/DMSO medium with a high molar ratio  $x_{\text{DMSO}} = 0.20$  causing it to decrease. However, one needs to keep in mind that the  $\text{p}K_{\text{a}}^{\text{D}}$  value was also measured without supporting electrolyte.

In summary, both methods reveal a  $\text{p}K_{\text{a}}$  value  $< 1$  for the protonation of the 1,2,4-triazole nitrogen atom of the ligand deferasirox in strong acidic solution.

## 8.2 Complex formation of deferasirox with magnesium (II) in pure water solution

The complex behaviour of  $\text{Mg}^{2+}$  with deferasirox in water/DMSO with  $x_{\text{DMSO}} = 0.20$  ( $T = 298 \text{ K}$ ,  $I = 0.1 \text{ mol/L KNO}_3$ ) has been investigated by U. Heinz in his doctoral thesis with potentiometric titrations [37]. As expected he found a rather weak complexation of deferasirox with the biometal ion  $\text{Mg}^{2+}$ . Attributed to the low solubility of deferasirox in pure water the stability constants with  $\text{Mg}^{2+}$  could only be measured in water/DMSO mixtures.

In this study the stability constants of the  $\text{Mg}^{2+}$ -deferasirox system was determined with potentiometric titrations ( $T = 298 \text{ K}$ ,  $I = 0.1 \text{ mol/L KCl}$ ) in water/DMSO medium with four molar fractions  $x_{\text{DMSO}} = 0.20, 0.18, 0.16$  and  $0.14$ . These values for the stability constants showed a linear relation and as a result we could estimate a value for the  $[\text{Mg}(\text{L})]^-$  and the  $[\text{Mg}(\text{L})_2]^{4-}$  complex with deferasirox in pure water. The experiment was limited by the solubility of the  $\text{Mg}^{2+}$ -deferasirox complexes. Titration experiments with a molar fraction of DMSO  $x_{\text{DMSO}} < 0.14$  were not performed due to precipitation of deferasirox owing to its poor solubility. The samples were prepared by the procedure described in section 11.2.2 and were left standing over night for equilibration of the water/DMSO mixture. However, the solutions prepared with a molar ratio  $< x_{\text{DMSO}} = 0.20$  often showed precipitation of the ligand deferasirox overnight and were discarded. The amount of DMSO seems to be not high enough to keep the ligand in solution. To circumvent precipitation these flasks were prepared with a higher pH value by adding a small precise amount of  $0.1 \text{ mol/L KOH}$  to the flasks. The added aliquot  $\text{KOH}$  was taken into account for the evaluation. Consequently, the start pH value of the titrations with each molar fraction rises while the pH value at the end of the titration decreases as expected by lowering the molar fraction of DMSO.

The titration conditions and stability constants for the three complexes  $[\text{Mg}(\text{L})]^-$  (110),  $[\text{Mg}(\text{L})(\text{LH})]^{3-}$  (121) and  $[\text{Mg}(\text{L})_2]^{4-}$  (120) are given in **Table 8.6**. The  $\log\beta_{110}$  was well determined in all four molar fractions. Its value decreases with decreasing the molar fraction  $x_{\text{DMSO}}$ .

**Table 8.6:** Mean values of the overall stability constants  $\log\beta_{xyz}$  <sup>[a]</sup> with standard deviations <sup>[b]</sup> from potentiometric titrations of  $Mg^{2+}$  with deferasirox in water/DMSO solution with different molar fractions  $x_{DMSO}$  at  $T = 298$  K and  $I = 0.1$  mol/L KCl.

$x_{DMSO}$	<b>0.20</b>	<b>0.18</b>	<b>0.16</b>	<b>0.14</b>
$[L]_t$	0.50 mmol/L	0.50 mmol/L	0.50 mmol/L	0.50 mmol/L
$[M]_t$	0.23 mmol/L	0.23 mmol/L	0.23 mmol/L	0.23 mmol/L
$pK_w$	15.58	15.39	15.20	15.01
pH range	3.3 – 12.2	4.3 – 12.1	4.4 – 12.0	4.8 – 11.8
No. of titrations	4	5	4	6
No. data points	70	70	70	70
time mixing [s]	160	120/160	120	160
$\sigma$ <sup>[c]</sup>	0.752	0.436	0.492	0.371
<b><math>\log\beta_{110}</math></b>	<b>7.68(3)</b>	<b>7.41(1)</b>	<b>7.21(2)</b>	<b>6.96(1)</b>
<b><math>\log\beta_{120}</math></b>	<b>11.2(1)</b>	<b>11.25(5)</b>	<b>10.7(1)</b>	<b>10.4(2)</b>
<b><math>\log\beta_{121}</math></b>	<b>22.3(2)</b>	<b>22.5(1)</b>	<b>22.1(3)</b>	<b>21.0(4)</b>

<sup>[a]</sup> For the ligand L  $\log\beta_{xyz}$  is defined as:  $\beta_{xyz} = [M_xL_yH_z] \times [M]^{-x} \times [L]^{-y} \times [H]^{-z}$ .

<sup>[b]</sup> The  $\sigma$  value is taken from the titration with the highest  $\sigma$  value in Hyperquad2008.

<sup>[c]</sup> The standard deviations in brackets were calculated with:  $\sqrt{\frac{\sum_{i=0}^n (x_i - \bar{x})^2}{(n-1)}}$ ;  $x_i$  measured value;  $\bar{x}$  mean value; n number of values.

Contrary to our expectations, the  $\log\beta_{120}$  and  $\log\beta_{121}$  values for the molar fraction  $x_{DMSO} = 0.20$  are smaller than expected. The values should increase in comparison to  $x_{DMSO} = 0.18$ , yet they decrease. Yet, all titrations with the molar fraction  $x_{DMSO} = 0.20$  showed lower values. Further, not all titrations with the molar fraction  $x_{DMSO} = 0.20$  could be evaluated with the  $[Mg(L)(LH)]^{3-}$  complex. Though excluding the 121 complex from the model did not change the stability constant for the  $[Mg(L)_2]^{4-}$  complex. The two stability constants of the  $[Mg(L)(LH)]^{3-}$  and  $[Mg(L)_2]^{4-}$  complexes with a molar ratio  $x_{DMSO} = 0.20$  deviate

strongly from the expected values in comparison with the other molar fractions of DMSO. We have no apparent explanation for this deviation.

Consequently, only the three molar fractions  $x_{\text{DMSO}} < 0.20$  were applied for the linear regression of the stability constants of the  $[\text{Mg}(\text{L})_2]^{4-}$  complex. The linear regression calculated from the stability constants in **Table 8.6** for the  $[\text{Mg}(\text{L})]^-$  and the  $[\text{Mg}(\text{L})_2]^{4-}$  complex and the extrapolation to  $x_{\text{DMSO}} = 0.00$  is presented in **Figure 8.8**.

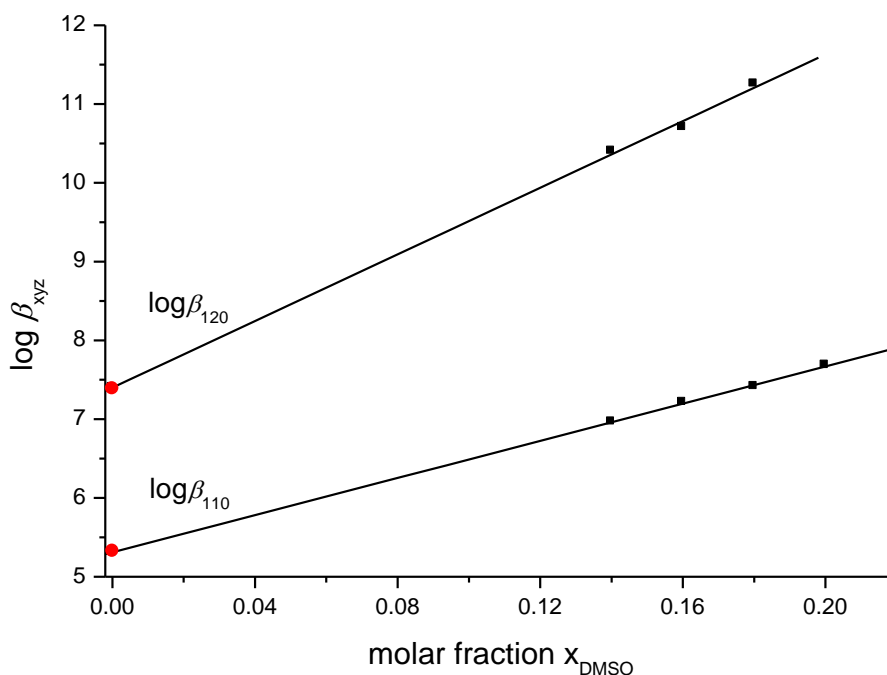


**Figure 8.8:** Dependence of the overall stability constants  $\log \beta_{xyz}$  of the  $[\text{Mg}(\text{L})]^-$  and  $[\text{Mg}(\text{L})_2]^{4-}$  complexes on the molar fraction  $x_{\text{DMSO}}$ . Linear regression (solid line) of the mean  $\log \beta_{xyz}$  values (black squares) listed in **Table 8.1** and extrapolation to  $x_{\text{DMSO}} = 0.00$ . The red circles indicate the extrapolated values at  $x_{\text{DMSO}} = 0.00$ .

The stability constants of the two complexes estimated for pure water are highlighted with red circles. The estimated stability constants and corresponding regression equations and R values for the  $[\text{Mg}(\text{L})]^-$  and the  $[\text{Mg}(\text{L})_2]^{4-}$  complex are presented in **Table 8.7**. The stability constant of the  $[\text{Mg}(\text{L})]^-$  complex is estimated to  $\log \beta_{110} = 5.31(8)$  with a good R value. Whereas, the R value of the calculated regression equation for the  $[\text{Mg}(\text{L})_2]^{4-}$  complex is not as good due to only three values being applied for the linear regression.

**Table 8.7:** Estimated  $\log\beta_{xyz}$  <sup>[a]</sup> values of  $Mg^{2+}$ -deferasirox in pure water calculated by linear regression of the  $\log\beta_{xyz}$  values measured in three (120 complex) and four (110 complex) molar fractions and extrapolation to  $x_{DMSO} = 0.00$  (T = 298 K).

<b>Estimated <math>\log\beta_{xyz}</math> <sup>[a]</sup> values for <math>Mg^{2+}</math>-deferasirox in pure water</b>			
solvent		pure water	
supporting electrolyte		0.1 mol/L KCl	
<b><math>x_{DMSO} = 0.00</math></b>		<b>R <sup>[c]</sup></b>	<b>regression equation <sup>[b]</sup></b>
<b><math>\log\beta_{110}</math> <sup>[d]</sup></b>	<b>5.31(8)</b>	0.99853	$\log\beta_{110} = 11.8(5) \times [x_{DMSO}] + 5.31(8)$
<b><math>\log\beta_{120}</math> <sup>[d]</sup></b>	<b>7.4(6)</b>	0.98589	$\log\beta_{120} = 21.3(36) \times [x_{DMSO}] + 7.4(6)$

<sup>[a]</sup> For the ligand L  $\log\beta_{xyz}$  is defined as:  $\beta_{xyz} = [M_xL_yH_z] \times [M]^{-x} \times [L]^{-y} \times [H]^{-z}$ .

<sup>[b]</sup> Linear regression equation was taken from the program Origin 6.0G.

<sup>[c]</sup> R is the regression coefficient taken from Origin 6.0G.

<sup>[d]</sup> The deviations in brackets were taken from the regression equation from Origin 6.0G.

In conclusion, the stability constants of the  $[Mg(L)]^-$  and the  $[Mg(L)_2]^{4-}$  complex were estimated by linear regression and extrapolation. Complex formation of deferasirox with  $Mg^{2+}$  begins in alkaline solution but is rather weak. Therefore, the stability constant of the 120 complex was more difficult to determine than the one for the 110 complex. The rather weak formation of the  $[Mg(L)_2]^{4-}$  complex with an individual stability constant of  $\log K_{120} = 2.1$  ( $\log K_{120} = [ML_2] / [ML] \times [L]$ ) in pure water renders the determination difficult.

### 8.3 Complex formation of deferasirox with calcium (II) in pure water solution

The first determination of the stability constants of deferasirox with  $\text{Ca}^{2+}$  by potentiometric titration experiments ( $x_{\text{DMSO}} = 0.20$ ,  $T = 298 \text{ K}$ ,  $I = 0.1 \text{ mol/L KNO}_3$ ) were performed by U. Heinz, in his doctoral thesis [37]. He reports that the complex formation of the  $\text{Ca}^{2+}$ -deferasirox system is even weaker than the  $\text{Mg}^{2+}$  complexes with deferasirox. To estimate the stability constants of the  $\text{Ca}^{2+}$ -deferasirox system in pure water we further investigated the complex formation with potentiometric titrations ( $T = 298 \text{ K}$ ,  $I = 0.1 \text{ mol/L KCl}$ ) in four molar ratios  $x_{\text{DMSO}} = 0.20, 0.18, 0.16$  and  $0.14$ .

Accordingly, in this study the complex formation of  $\text{Ca}^{2+}$  with deferasirox begins in strong alkaline solution. However, the evaluation of the titration experiments resulted in two complexes a  $[\text{Ca}(\text{L})]^-$  and a  $[\text{Ca}(\text{L})_2]^{4-}$  complex. The stability constant of the  $[\text{Ca}(\text{L})_2]^{4-}$  complex estimated by extrapolation to pure water ( $x_{\text{DMSO}} = 0.00$ ) however adopted a higher  $\log K_{120}$  value (of  $\approx 4$ ,  $\log K_{120} = [\text{ML}_2] / [\text{ML}] \times [\text{L}]$ ) than the estimated value  $\log \beta_{110} = 3.3$  for the  $[\text{Ca}(\text{L})]^-$  complex in pure water. All investigations of the complexation of the ligand and deferasirox with metal ions in the past have shown that the 120 complex is less stable than the 110 complex owing to steric and statistic effects. We could not find any reason why the  $[\text{Ca}(\text{L})_2]^{4-}$  complex in pure water should be more stable than the  $[\text{Ca}(\text{L})]^-$  complex. The rather weak complexation of the  $\text{Ca}^{2+}$ -deferasirox system is evident in the low pH decrease of the titration curve in comparison to the ligand  $\text{p}K_a$  titrations curve. Yet, in strong alkaline solution above pH 11 a further significant pH decrease is detected in all titrations. We assume this pH decrease is an artefact caused by some other reaction, maybe due to carbon dioxide in alkaline solution, rather than complex formation. Consequently, we only used the titration curve prior to pH 11.5 for evaluation where a pH decrease was detected and assigned to the formation of the  $[\text{Ca}(\text{L})]^-$  complex.

The titration conditions and stability constant of the  $[\text{Ca}(\text{L})]^-$  complex are presented in **Table 8.8**. The titrations with a molar fraction  $x_{\text{DMSO}} < 0.20$  showed precipitation after preparation and standing overnight. To prevent the

8 Complex formation of magnesium (II), calcium (II) and aluminium (III) with deferasirox in pure water

ligand from precipitating from the samples with a lower molar fraction a precise volume of 0.1 mol/L KOH was added to raise the pH. Accordingly, the start pH of each molar fraction rises with decrease of the molar fraction  $x_{\text{DMSO}}$ . The added aliquot KOH was taken into account for the evaluation.

**Table 8.8:** Mean values of the overall stability constants  $\log\beta_{xyz}$  <sup>[a]</sup> with standard deviations <sup>[b]</sup> from potentiometric titrations of  $\text{Ca}^{2+}$  with deferasirox in water/DMSO solution with different molar fractions  $x_{\text{DMSO}}$  at  $T = 298 \text{ K}$  and  $I = 0.1 \text{ mol/L KCl}$ .

$x_{\text{DMSO}}$	<b>0.20</b>	<b>0.18</b>	<b>0.16</b>	<b>0.14</b>
$[\text{L}]_t$	0.50 mmol/L	0.50 mmol/L	0.50 mmol/L	0.50 mmol/L
$[\text{M}]_t$	0.23 mmol/L	0.23 mmol/L	0.23 mmol/L	0.23 mmol/L
$\text{p}K_w$	15.58	15.39	15.20	15.01
pH range	3.0 – 10.9	3.8 – 10.9	4.4 – 11.2	4.7 – 10.8
No. of titrations	8	6	6	6
No. data points	37	29/40	35	35
time mixing [s]	120	120	120	120
$\sigma$ <sup>[c]</sup>	1.256	0.590	0.614	0.490
<b><math>\log\beta_{110}</math></b>	<b>5.62(2)</b>	<b>5.36(3)</b>	<b>5.16(1)</b>	<b>4.91(1)</b>

<sup>[a]</sup> For the ligand L  $\log\beta_{xyz}$  is defined as:  $\beta_{xyz} = [\text{M}_x\text{L}_y\text{H}_z] \times [\text{M}]^{-x} \times [\text{L}]^{-y} \times [\text{H}]^{-z}$ .

<sup>[b]</sup> The  $\sigma$  value is taken from the titration with the highest  $\sigma$  value in Hyperquad2008.

<sup>[c]</sup> The standard deviations in brackets were calculated with:  $\sqrt{\frac{\sum_{i=0}^n (x_i - \bar{x})^2}{(n-1)}}$ ;  $x_i$  measured value;  $\bar{x}$  mean value; n number of values.

As observed for the stability constants of the  $\text{Mg}^{2+}$ -deferasirox system, the stability constants determined for the  $[\text{Ca}(\text{L})]^-$  complex decrease with decreasing molar fraction of DMSO. The linear dependence of the overall stability constant  $\log\beta_{110}$  on the molar fraction is illustrated in **Figure 8.9**. The red circle indicates the estimated  $\log\beta_{110}$  value for pure water.

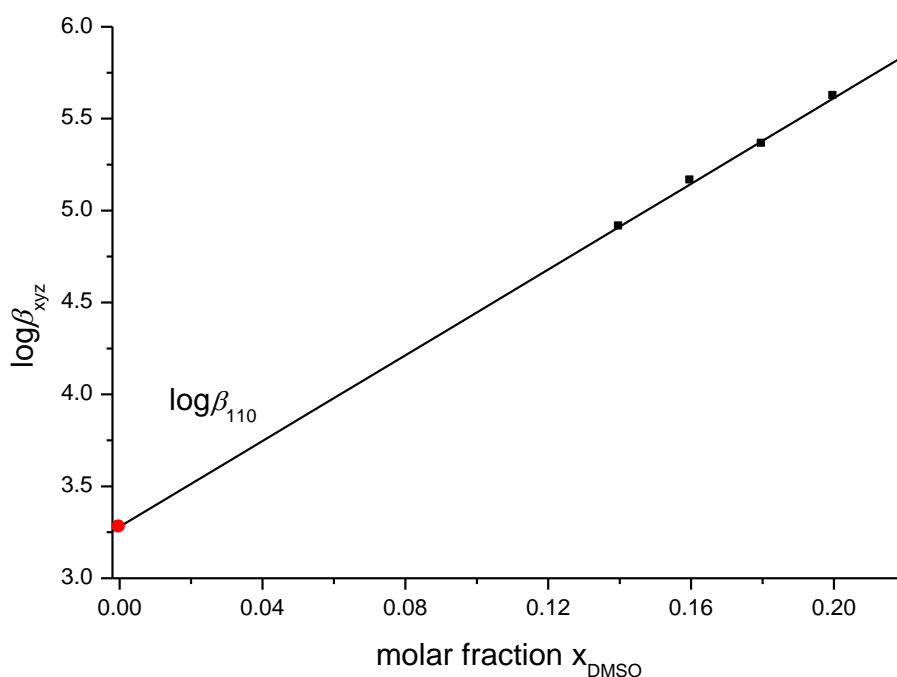


**Figure 8.9:** Dependence of the overall stability constants  $\log \beta_{xyz}$  of the  $[\text{Ca}(\text{L})]^-$  complex on the molar fraction  $x_{\text{DMSO}}$ . Linear regression (solid line) of the mean  $\log \beta_{xyz}$  values (black squares) listed in **Table 8.8** and extrapolation to  $x_{\text{DMSO}} = 0.00$ . The red circles indicate the extrapolated values at  $x_{\text{DMSO}} = 0.00$ .

Based on the plot in **Figure 8.9** the linear regression was calculated. The regression equation and regression coefficient  $R$  are given together with the estimated  $\log \beta_{110}$  value for the  $[\text{Ca}(\text{L})]^-$  complex for pure water in **Table 8.9**. The regression coefficient  $R$  reflects the good agreement of the linear dependence between the  $\log \beta_{110}$  value and the molar fractions  $x_{\text{DMSO}}$ . The estimated  $\log \beta_{110}$  value for the  $[\text{Ca}(\text{L})]^-$  complex is 3.28(7) in pure water. As U. Heinz previously reported the complex formation of  $\text{Ca}^{2+}$  with deferasirox is very weak which is obviously also reflected in the low stability constant estimated for pure water.

**Table 8.9:** Estimated  $\log\beta_{xyz}$  <sup>[a]</sup> values of  $\text{Ca}^{2+}$ -deferasirox in pure water calculated by linear regression of the  $\log\beta_{xyz}$  values measured in four molar fractions and extrapolation to  $x_{\text{DMSO}} = 0.00$  (T = 298 K).

<b>Estimated <math>\log\beta_{xyz}</math> <sup>[a]</sup> values for <math>\text{Ca}^{2+}</math>-deferasirox in pure water</b>			
solvent		pure water	
supporting electrolyte		0.1 mol/L KCl	
<b><math>x_{\text{DMSO}} = 0.00</math></b>		<b>R <sup>[c]</sup></b>	<b>regression equation <sup>[b]</sup></b>
<b><math>\log\beta_{110}</math> <sup>[d]</sup></b>	<b>3.28(7)</b>	0.99884	$\log\beta_{110} = 11.7(4) \times [x_{\text{DMSO}}] + 3.28(7)$

<sup>[a]</sup> For the ligand L  $\log\beta_{xyz}$  is defined as:  $\beta_{xyz} = [\text{M}_x\text{L}_y\text{H}_z] \times [\text{M}]^{-x} \times [\text{L}]^{-y} \times [\text{H}]^{-z}$ .

<sup>[b]</sup> Linear regression equation was taken from the program Origin 6.0G.

<sup>[c]</sup> R is the regression coefficient taken from Origin 6.0G.

<sup>[d]</sup> The deviations in brackets were taken from the regression equation from Origin 6.0G.

Taken together, the stability constant of the  $[\text{Ca}(\text{L})]^-$  complex has been estimated in pure water. In accordance with the study by U. Heinz, a  $[\text{Ca}(\text{L})_2]^{4-}$  complex was not determined with the applied potentiometric titration experiments.

## 8.4 Complex formation of deferasirox with aluminium (III) in pure water solution

The complex formation of  $\text{Al}^{3+}$  with deferasirox reveals a strong affinity of the ligand for the trivalent metal ion. The complex formation was first studied by potentiometric titrations in water/DMSO solution with a molar fraction  $x_{\text{DMSO}} = 0.20$  ( $T = 298 \text{ K}$ ,  $I = 0.1 \text{ mol/L KNO}_3$ ) by U. Heinz in his doctoral thesis [37]. A strong pH decrease of the  $\text{Al}^{3+}$ -deferasirox titration curve in comparison to the  $\text{p}K_a$  titration curve displayed the strong complex formation.

In accordance with the previously discussed results for  $\text{Mg}^{2+}$  and  $\text{Ca}^{2+}$  we examined the complex formation of the  $\text{Al}^{3+}$ -deferasirox system by potentiometric titrations ( $T = 298 \text{ K}$ ,  $I = 0.1 \text{ mol/L KCl}$ ) with water/DMSO mixtures with four molar fractions  $x_{\text{DMSO}} = 0.20, 0.18, 0.16$  and  $0.14$ . Of special interest were the  $[\text{Al}(\text{L})]$  (110) and  $[\text{Al}(\text{L})_2]^{3-}$  (120) complexes with the ligand deferasirox. The stability constants determined by potentiometric titrations with different molar fractions showed a roughly linear relation which was extrapolated to  $x_{\text{DMSO}} = 0.00$  to estimate the value for the stability constants of the two complexes  $[\text{Al}(\text{L})]$  and  $[\text{Al}(\text{L})_2]^{3-}$  in pure water.

The solubility of the ligand deferasirox in pure water increases with increasing pH. The ligand precipitated from the samples prepared with a molar fraction of DMSO  $< 0.20$  after preparation and standing over night. These molar fractions seem to have not enough DMSO to keep the ligand and its complexes entirely in solution. To prevent precipitation in these samples a precise volume of  $0.1 \text{ mol/L KOH}$  was added to the flasks with  $x_{\text{DMSO}} < 0.20$  to raise the pH. The added aliquot KOH was taken into account for the evaluation.

The titration conditions and mean values of the overall stability constants are given in **Table 8.10**. The titrations with a molar fraction  $x_{\text{DMSO}} = 0.20$  were performed without any difficulties. They were evaluated with the program Hyperquad2008 without problems. As the molar fraction was decreased to  $x_{\text{DMSO}} = 0.18$  and  $0.16$  the stability constants of the single titrations varied stronger than for  $x_{\text{DMSO}} = 0.20$ . Despite of the higher variance of the single titrations, the evaluations with Hyperquad2008 were still good. Yet, as a result, the mean values can only be determined to one decimal point.

**Table 8.10:** Mean values of the overall stability constants  $\log\beta_{xyz}$  <sup>[a]</sup> with the standard deviations <sup>[b]</sup> from potentiometric titrations of  $\text{Al}^{3+}$  with deferasirox in water/DMSO solution with different molar fractions  $x_{\text{DMSO}}$  at  $T = 298 \text{ K}$  and  $I = 0.1 \text{ mol/L KCl}$ .

$x_{\text{DMSO}}$	<b>0.20</b>	<b>0.18</b>	<b>0.16</b>	<b>0.14</b>
$[\text{L}]_t$ in mmol/L	0.50	0.50	0.	0.50
$[\text{M}]_t$ in mmol/L	0.25	0.24/0.25	0.24/0.25	0.24/0.25
$\text{p}K_w$	15.58	15.39	15.20	15.01
pH range	3.0 – 6.5	3.3 – 6.3	3.3 – 6.3	3.3 – 10.8
No. of titrations	6	6	4	-
No. data points	63	69	72	63
time mixing [s]	1200	1200	1200	1200
$\sigma$ <sup>[c]</sup>	0.648	0.349	0.329	-
$\log\beta_{110}$	<b>20.14(9)</b>	<b>19.7(1)</b>	<b>19.3(2)</b>	-
$\log\beta_{111}$	<b>24.29(4)</b>	<b>23.9(1)</b>	<b>23.5(1)</b>	-
$\log\beta_{120}$	<b>35.0(1)</b>	<b>34.3(2)</b>	<b>33.8(4)</b>	-
$\log\beta_{121}$	<b>40.3(2)</b>	<b>39.7(1)</b>	<b>39.2(6)</b>	-
$\log\beta_{122}$	<b>46.1(1)</b>	<b>45.3(2)</b>	<b>44.7(6)</b>	-

<sup>[a]</sup> For the ligand L  $\log\beta_{xyz}$  is defined as:  $\beta_{xyz} = [\text{M}_x\text{L}_y\text{H}_z] \times [\text{M}]^{-x} \times [\text{L}]^{-y} \times [\text{H}]^{-z}$ .

<sup>[b]</sup> The  $\sigma$  value is taken from the titration with the highest  $\sigma$  value in Hyperquad2008.

<sup>[c]</sup> The standard deviations in brackets were calculated with:  $\sqrt{\frac{\sum_{i=0}^n (x_i - \bar{x})^2}{(n-1)}}$ ;  $x_i$  measured value;  $\bar{x}$  mean value; n number of values.

In contrast to the prior molar fractions the titration experiments performed with a molar fraction  $x_{\text{DMSO}} = 0.14$  showed precipitation already during the first 20 titration points. The greyish-white precipitate dissolved again in alkaline solution leaving a clear solution at the end of the titration. As the titration proceeds to higher pH the neutral  $[\text{Al}(\text{L})]$  complex is increasingly being formed. We assume this complex is not sufficiently soluble in water and precipitates when

the DMSO concentration in solution is reduced to  $x_{\text{DMSO}} = 0.14$ . In alkaline solution the concentration of the  $[\text{Al}(\text{L})]$  complex decreases and the  $[\text{Al}(\text{L})_2]^{3-}$  complex becomes the dominant species in solution. The  $[\text{Al}(\text{L})_2]^{3-}$  complex is presumably much better soluble in water. As a consequence, a clear solution is observed at the end of the titration at pH 10.8.

Accordingly, the stability constants of the  $[\text{Al}(\text{L})]$  and  $[\text{Al}(\text{L})_2]^{3-}$  complexes determined with the three molar fractions  $x_{\text{DMSO}} = 0.20, 0.18$  and  $0.16$  were applied for the linear regression and extrapolation to pure water as illustrated in **Figure 8.10**.

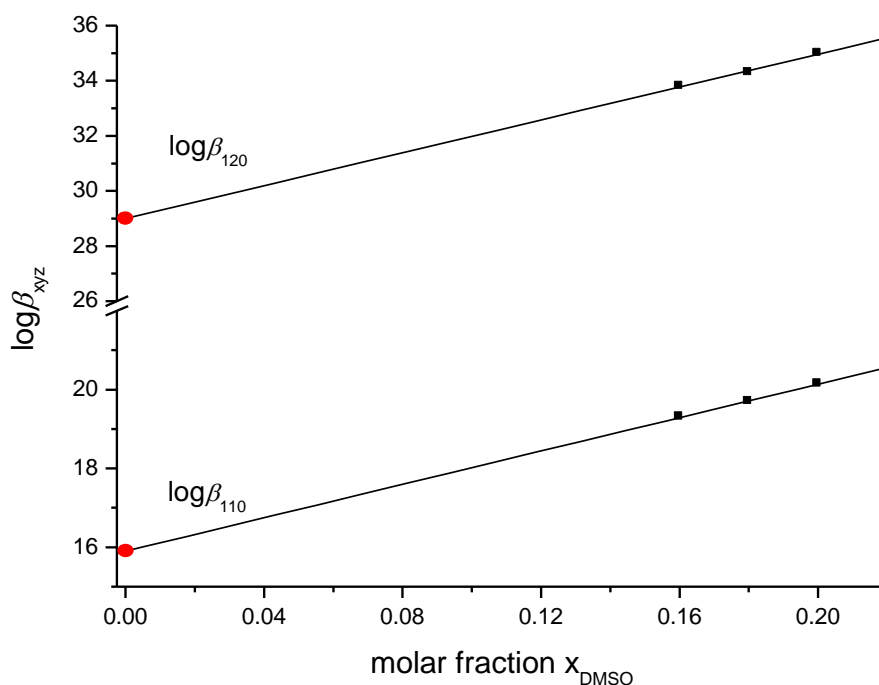


**Figure 8.10:** Dependence of the overall stability constants  $\log \beta_{xyz}$  of the  $[\text{Al}(\text{L})]$  and  $[\text{Al}(\text{L})_2]^{3-}$  complex on the molar fraction  $x_{\text{DMSO}}$ . Linear regression (solid line) of the mean  $\log \beta_{xyz}$  values (black squares) listed in **Table 8.8** and extrapolation to  $x_{\text{DMSO}} = 0.00$ . The red circles indicate the extrapolated values at  $x_{\text{DMSO}} = 0.00$ .

The linear regression equations, regression coefficients  $R$  and the stability constants for all complexes calculated by extrapolation of the linear regression to  $x_{\text{DMSO}} = 0.00$  are given in **Table 8.11**.

**Table 8.11:** Estimated  $\log\beta_{xyz}$  <sup>[a]</sup> values of  $\text{Al}^{3+}$  with deferasirox in pure water calculated by linear regression of the  $\log\beta_{xyz}$  values measured in three molar fractions and extrapolation to  $x_{\text{DMSO}} = 0.00$  (T = 298 K).

<b>Estimated <math>\log\beta_{xyz}</math> <sup>[a]</sup> values for <math>\text{Al}^{3+}</math>-deferasirox in pure water</b>			
solvent		pure water	
supporting electrolyte		0.1 mol/L KCl	
<b><math>x_{\text{DMSO}} = 0.00</math></b>		<b>R <sup>[c]</sup></b>	<b>regression equation <sup>[b]</sup></b>
<b><math>\log\beta_{110}</math> <sup>[d]</sup></b>	<b>15.9(1)</b>	0.99962	$\log\beta_{110} = 21.0(6) \times [x_{\text{DMSO}}] + 15.9(1)$
<b><math>\log\beta_{111}</math> <sup>[d]</sup></b>	<b>20.34(3)</b>	0.99997	$\log\beta_{111} = 19.8(1) \times [x_{\text{DMSO}}] + 20.34(3)$
<b><math>\log\beta_{120}</math> <sup>[d]</sup></b>	<b>29.0(5)</b>	0.99540	$\log\beta_{120} = 30.0(29) \times [x_{\text{DMSO}}] + 29.0(5)$
<b><math>\log\beta_{121}</math> <sup>[d]</sup></b>	<b>34.8(3)</b>	0.99863	$\log\beta_{121} = 27.5(14) \times [x_{\text{DMSO}}] + 34.8(3)$
<b><math>\log\beta_{122}</math> <sup>[d]</sup></b>	<b>39.1(5)</b>	0.99662	$\log\beta_{122} = 35.0(29) \times [x_{\text{DMSO}}] + 39.1(5)$

<sup>[a]</sup> For the ligand L  $\log\beta_{xyz}$  is defined as:  $\beta_{xyz} = [\text{M}_x\text{L}_y\text{H}_z] \times [\text{M}]^{-x} \times [\text{L}]^{-y} \times [\text{H}]^{-z}$ .

<sup>[b]</sup> Linear regression equation was taken from the program Origin 6.0G.

<sup>[c]</sup> R is the regression coefficient taken from Origin 6.0G.

<sup>[d]</sup> The deviations in brackets were taken from the regression equation from Origin 6.0G.

The stability constants of the complexes formed by the  $\text{Al}^{3+}$ -deferasirox system have been investigated with three molar ratios  $x_{\text{DMSO}} = 0.20, 0.18$  and  $0.16$ . By extrapolation of the linear regression the stability constants of the complexes were estimated in pure water. The overall stability constants of the  $[\text{Al}(\text{L})]$  complex  $\log\beta_{110} = 15.9(1)$  and of the  $[\text{Al}(\text{L})_2]^{3-}$  complex  $\log\beta_{120} = 29.0(5)$  were of special interest.

## 9 Interaction of deferasirox, MSA and DSA with gadolinium (III) and gallium (III) in contrast agents

### 9.1 Complex formation of deferasirox and its water soluble derivatives with gadolinium (III)

Gadolinium (III) is one of the most widely used metal ions in paramagnetic complexes for magnetic resonance imaging (MRI) in clinical practice. The technique of MRI is applied for visualising the soft tissues for diagnostic purposes [127]. The images are generated by the lipid and water protons in the tissue of a patient introduced into a magnetic field [127-128]. To receive a good image contrast the relaxation time  $T_1$  and  $T_2$  of the different tissues are of importance as well as the proton density [127]. Tissue types vary in their relaxation properties, which in fact is used by MRI to reconstruct images of organ structures [129]. To improve image contrast,  $T_1$ -agents such as gadolinium (III) compounds have been introduced [130]. These contrast agents are paramagnetic ions that decrease the proton relaxation time of bound water molecules enhancing the contrast of the images [129]. As a result, the dipolar interaction between the water molecule protons and the unpaired electrons of the metal ion is responsible for the paramagnetic efficacy [127].

The interest in the trivalent lanthanide ion  $Gd^{3+}$  is due to its seven unpaired electrons promising a strong paramagnetic character [127]. It is the lanthanide with the largest number of unpaired electrons. Further, it has a relatively long electronic relaxation time [128]. Yet, gadolinium (III) is very toxic and needs to be strongly bound to a chelating agent to avoid toxicity in the human body [131]. The two ligands DOTA (2,2',2'',2'''-(1,4,7,10-tetraazacyclododecane-1,4,7,10-tetrayl)-tetraacetic acid) and DTPA (diethylenetriaminepentaacetic acid) are commonly used as  $Gd^{3+}$  complexes in contrast agents. The structures of the ligands are given in **Figure 9.1**.

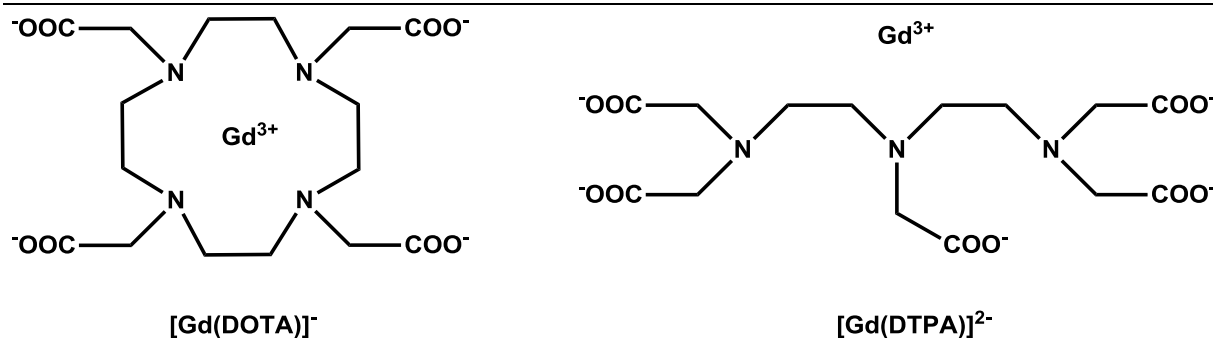


**Figure 9.1:** Structures of the Gd<sup>3+</sup> complexing agents DOTA and DTPA.

These ligands are examples of two classes of complexing agents. DOTA is a macrocyclic ligand and DTPA has an acyclic structure. The ligand classes are further differentiated by charge: ionic or neutral complexes. The contrast agent Gd-DOTA known by the trade mark Dotarem<sup>®</sup> (Guerbet, France) and Gd-DTPA by the trade mark Magnevist<sup>®</sup> (Bayer Schering, Germany) are commonly used contrast agents applied in clinical practice <sup>[131]</sup>. Both ligands are octadentate ligands and therefore occupy eight coordination sites of the Gd<sup>3+</sup> ion leaving one coordination site for the necessary coordinating water molecule. Currently there are 8 approved gadolinium (III) based MRI contrast agents commercially available. Two are derivatives of DOTA and four other Gd<sup>3+</sup>-complexes are derivatives of DTPA <sup>[129]</sup>. All Gd<sup>3+</sup>-complexes have high thermodynamic stability constants, however the macrocyclic complexes such as DOTA are more stable than the acyclic <sup>[132]</sup>. At physiological pH 7.4 the ionic complexes are more stable than the neutral complexes <sup>[127]</sup>. The stability of the complexes is of great importance since the free metal ion Gd<sup>3+</sup> and the free ligand DOTA are both very toxic <sup>[127]</sup>. The toxicity is attributed for example to the similar ionic radii of Gd<sup>3+</sup>  $r = 1.107 \text{ \AA}$  (CN 9) <sup>[118]</sup> and Ca<sup>2+</sup>  $r = 1.18 \text{ \AA}$  (CN 9) <sup>[118]</sup>. As a consequence, free gadolinium (III) can interfere with calcium (II) mediated processes in the human body <sup>[132]</sup>. The Gd-DOTA and Gd-DTPA complexes are very stable and are excreted unaltered <sup>[130]</sup>. However, there are discussions about the possibility of transmetallation of Gd<sup>3+</sup>-complexes in the human body for example by zinc (II) <sup>[133]</sup>, copper (II), calcium (II) and iron(II/III) <sup>[132]</sup>.

In general, Gd-DOTA and Gd-DTPA are called “non-specific” compounds as they are very hydrophilic, they do not bind to proteins or receptors and are excreted unmetabolized in urine <sup>[127]</sup>. These contrast agents are considered as extracellular fluid markers, meaning they distribute nonspecifically throughout the plasma and interstitial space of the body (space that surrounds the cells of a given tissue) <sup>[130]</sup>. Gadolinium (III) complexes do not diffuse through plasma membranes and are therefore unable to cross the intact blood-brain-barrier <sup>[132]</sup>. An application resulting from this is the detection of tumours in the brain <sup>[130]</sup>.

There are an increasing number of reports on the development of contrast agents for specific applications <sup>[129]</sup>. Most of these new compounds are macromolecules binding the known mononuclear complexes such as Gd-DTPA or Gd-DOTA. For instance the targeting of tumours by gadolinium(III)-conjugated dendrimer nanoclusters (Gd-DTPA based) <sup>[134]</sup> or cell imaging with the help of cyclodextrin-based bimodal fluorescence/MRI contrast agents (Gd-DOTA based) <sup>[135]</sup>.

Our interest was to provide an insight into a possible simultaneous administration of a gadolinium (III) containing MRI contrast agent with the iron-chelating ligand deferasirox. The question we asked ourselves is how strong are the complexes formed by Gd<sup>3+</sup> with deferasirox and could deferasirox prefer complexation with Gd<sup>3+</sup> vs. Fe<sup>3+</sup>?

In this study we investigated the complex formation of deferasirox with gadolinium (III) with potentiometric titrations in a water/DMSO solution mixture. Unexpectedly, the titration experiments were hampered by precipitation. On account of these difficulties we also investigated the complex formation of the water soluble derivatives MSA and DSA to elucidate the complex formation of this ligand class in pure water. With these water soluble ligands no precipitation occurred during the titration experiments and stability constants were determined for the Gd<sup>3+</sup> complexes.

### 9.1.1 Complex formation of deferasirox with gadolinium (III) in water/DMSO solution $x_{\text{DMSO}} = 0.20$

On account of the low solubility of deferasirox in pure water solution the potentiometric titration experiments needed to be performed in a water/DMSO mixture with a molar fraction of  $x_{\text{DMSO}} = 0.20$ . Unfortunately, greyish-white precipitation occurred during the titration experiment in the pH range from about 4 – 8. As a result, the main titration range including the physiological pH 7.4 could not be investigated. To receive at least little information about the complex formation of deferasirox with  $\text{Gd}^{3+}$  we carried out acidimetric titrations with 0.1 mol/L HCl (containing  $x_{\text{DMSO}} = 0.20$ ) in the pH range 12.5 – 9. Yet, we could not find a proper species model to evaluate these titrations, which is not surprising. Usually, in alkaline solution the bis-complexes  $[\text{M}(\text{LH})_2]^-$ ,  $[\text{M}(\text{L})(\text{LH})]^{2-}$  or  $[\text{M}(\text{L})_2]^{3-}$  are formed for trivalent metal ions, as observed for the  $\text{Al}^{3+}$ - and  $\text{Fe}^{3+}$ -deferasirox system [37, 39]. To determine the overall stability constants with acidimetric titrations we need a known stability constant in alkaline solution, for example of a soluble hydroxo complex, as known value. For the metal ion  $\text{Gd}^{3+}$  we do not know any soluble hydroxo complexes in water/DMSO solution. This implicates a nearly impossible determination of the stability constants, with potentiometric titrations, of the bis-complexes because they have presumably already sufficiently been formed in alkaline solution.

The investigation of the acidic pH range from 3.1 – 4.6 was very difficult leaving only one pH unit for evaluation. However, evaluation of a titration experiment performed with the conditions described in **Table 9.1** resulted in a model with two complexes  $[\text{Gd}(\text{LH})]^+$  (111) and  $[\text{Gd}(\text{LH}_2)]^{2+}$  (122) calculated with Hyperquad2008. These stability constants given in **Table 9.1** should be regarded as roughly determined values since the pH range was only one unit. Unfortunately, the  $[\text{Gd}(\text{L})]$  complex which would have been of special interest was not determined. The pH range was assumingly too acidic. We suppose that the uncharged mononuclear complex  $[\text{Gd}(\text{L})]$  might be less soluble in solution and could be the cause for precipitation throughout the pH range. Yet, we have no evidence for this proposal since the analysis of the precipitate was not successful.

**Table 9.1:** Titration experiment in acidic solution with  $Gd^{3+}$  and deferasirox. Titration conditions and the overall protonation constants  $\log\beta_x$  <sup>[a]</sup> used for the evaluation with Hyperquad2008 are given as well as the overall stability constants  $\log\beta_{xyz}$  <sup>[b]</sup> at  $T = 298$  K.

<b>Gd<sup>3+</sup>-deferasirox titration in acidic solution</b>			
molar ratio of M:L	1:2		
measuring method	potentiometric		
method type	continuous		
solvent	water/DMSO $x_{DMSO} = 0.20$		
[M] <sub>t</sub>	0.50 mmol/L		
[L] <sub>t</sub>	1.00 mmol/L		
titration volume	50.0 mL		
titrant	0.1 mol/L KOH/DMSO		
supporting electrolyte	0.1 mol/L KCl/DMSO		
electrode	Möller		
pK <sub>w</sub>	15.59		
pH range	3.1 – 4.6		
volume of data points	30		
time for mixing process	500 s		
$\log\beta_x$ <sup>[d]</sup>	$\log\beta_1 = 12.18(2)$	$\log\beta_2 = 22.36(3)$	$\log\beta_3 = 27.00(3)$
$\sigma$ <sup>[c]</sup>	0.239		
$\log\beta_{111}$ <sup>[d]</sup>	<b>19.4(3)</b>		
$\log\beta_{112}$ <sup>[d]</sup>	<b>25.05(4)</b>		

<sup>[a]</sup> For the ligand L  $\log\beta_x$  is defined as:  $\beta_x = [LH_x] \times [L]^{-1} \times [H]^{-x}$ .

<sup>[b]</sup> For the ligand L  $\log\beta_{xyz}$  is defined as:  $\beta_{xyz} = [M_xL_yH_z] \times [M]^{-x} \times [L]^{-y} \times [H]^{-z}$ .

<sup>[c]</sup> The  $\sigma$  value is taken from Hyperquad2008.

<sup>[d]</sup> The deviations given in brackets correspond to the threefold standard deviation taken from Hyperquad2008.

In conclusion, the two protonated complexes  $[\text{Gd}(\text{LH})]^+$  and  $[\text{Gd}(\text{LH}_2)]^{2+}$  are formed to less than 20% and the stability constants should be considered as only roughly determined and judged critically.

### 9.1.2 Complex formation of MSA with gadolinium (III) and determination of the $\text{p}K_{\text{a}}$ values of MSA in pure water

On account of the difficulties with precipitation during titration experiments with the  $\text{Gd}^{3+}$ -deferasirox system we employed the water soluble derivative MSA to elucidate the complex behaviour of this class of hydroxyphenyl-1,2,4-triazole ligands with  $\text{Gd}^{3+}$ . With the help of water soluble derivatives we have the opportunity to determine stability constants with  $\text{Gd}^{3+}$  in pure water. No precipitation was observed during the potentiometric titration experiments with  $\text{Gd}^{3+}$  and MSA. Consequently, the entire pH range was investigated with potentiometric titrations in three molar ratios  $\text{Gd}^{3+}:\text{MSA}$  1:2, 1:3 and 1:5. Gadolinium (III) has the tendency to form complexes not only with the coordination number six but also with eight or nine. By providing excess ligand in titration experiments we investigated whether only two ligands are bound to one  $\text{Gd}^{3+}$  central ion or if a third ligand can be bound.

Essential for the evaluation of the stability constants of the  $\text{Gd}^{3+}$ -MSA system are the  $\text{p}K_{\text{a}}$  values of the ligand MSA (previously determined by U. Heinz [37, 40]). However, we decided to determine the  $\text{p}K_{\text{a}}$  values by potentiometric titrations due to the application of a new pH electrode (Ross Ultra). Accordingly, all potentiometric studies of MSA have been performed with this pH electrode. The  $\text{p}K_{\text{a},1}$  for MSA has been determined by U. Heinz with a discontinuous spectrophotometric batch titration [37]. This value was used for our evaluations and was not redetermined. The  $\text{p}K_{\text{a}}$  values of MSA used for all calculations with Hyperquad2008 are presented in **Table 9.2**.

The determined  $\text{p}K_{\text{a}}$  values for MSA are in good agreement with those determined previously. The  $\text{p}K_{\text{a},2} = 8.75(5)$  is very close to the previously published  $\text{p}K_{\text{a},2} = 8.74(1)$  [40] and the  $\text{p}K_{\text{a},3} = 10.75(7)$  is also in the same range as the  $\text{p}K_{\text{a},3} = 10.63(1)$  [40].

**Table 9.2:** Mean values of the overall protonation constants  $\log\beta_x$  <sup>[a]</sup> and acidity constants  $pK_{a,i}$  <sup>[b]</sup> for the ligand MSA in pure water, T = 298 K and I = 0.1 mol/L KCl.

<b>log<math>\beta</math> and pK<sub>a</sub> values of MSA</b>			
measuring method	potentiometric		
method type	continuous		
solvent	pure water		
[L] <sub>t</sub>	0.50 mmol/L		
[H] <sub>t</sub>	1.50 mmol/L		
titration volume	50.0 mL		
titrant	0.1 mol/L KOH		
supporting electrolyte	0.1 mol/L KCl		
electrode	Ross Ultra		
pK <sub>w</sub>	13.78		
pH range	3.3 – 10.7		
volume of data points	100		
time for mixing process	120 s		
<b>mean values and standard deviations <sup>[c]</sup> from 7 titrations</b>			
<b>log<math>\beta_1</math> <sup>[c]</sup></b>	<b>10.75(7)</b>	<b>pK<sub>a,1</sub> <sup>[d]</sup></b>	<b>1.12(4)</b>
<b>log<math>\beta_2</math> <sup>[c]</sup></b>	<b>19.50(7)</b>	<b>pK<sub>a,2</sub> <sup>[c]</sup></b>	<b>8.75(5)</b>
<b>log<math>\beta_3</math> <sup>[d]</sup></b>	<b>20.62(4)</b>	<b>pK<sub>a,3</sub> <sup>[c]</sup></b>	<b>10.75(7)</b>

<sup>[a]</sup> For the ligand L  $\log\beta_x$  is defined as:  $\beta_x = [\text{LH}_x] \times [\text{L}]^{-1} \times [\text{H}]^{-x}$ .

<sup>[b]</sup> For the ligand LH<sub>x</sub> the pK<sub>a,i</sub> is defined as:  $pK_{a,i} = -\log K_{a,i}$  and  $K_{a,i} = [\text{LH}_{x-i}] \times [\text{H}] \times [\text{LH}_{(x+1)-i}]^{-1}$ .

<sup>[c]</sup> The standard deviations in brackets were calculated with:  $\sqrt{\frac{\sum_{i=0}^n (x_i - \bar{x})^2}{(n-1)}}$ ;  $x_i$  measured value;  $\bar{x}$  mean value; n number of values.

<sup>[d]</sup> Value taken from doctoral thesis of U. Heinz <sup>[37]</sup>.

The titrations of MSA were performed with slightly lower concentrations than the titrations with DSA which is associated with the lower solubility (0.7 g/L <sup>[37]</sup>) of MSA in pure water. Titrations with a total ligand concentration of 1.00 mmol/L were performed for a better comparison of the titration curves, yet at lower concentration the ligand was easier to solubilize. The applied titration conditions for all three molar ratios are given in **Table 9.3**.

**Table 9.3:** Titration experiment conditions of the complexation of Gd<sup>3+</sup> with MSA given at T = 298 K.

<b>Conditions for the Gd<sup>3+</sup>-MSA titrations</b>			
molar ratio of M:L	1:2	1:3	1:5
measuring method	potentiometric	potentiometric	potentiometric
method type	continuous	continuous	continuous
solvent	pure water	pure water	pure water
[M] <sub>t</sub>	0.25 mmol/L	0.25 mmol/L	0.20 mmol/L
[L] <sub>t</sub>	0.50 mmol/L	0.75 mmol/L	1.00 mmol/L
titration volume	50.0 mL	50.0 mL	50.0 mL
titrant	0.1 mol/L KOH	0.1 mol/L KOH	0.1 mol/L KOH
supporting electrolyte	0.1 mol/L KCl	0.1 mol/L KCl	0.1 mol/L KCl
electrode	Ross Ultra	Ross Ultra	Ross Ultra
pK <sub>w</sub>	13.78	13.78	13.78
pH range	3.1 – 10.7	2.9 – 11.0	2.9 – 9.5
volume of data points	80	48	73
time for mixing process	360 s	380 s	550 s

Three individual titrations were performed for each of the three molar ratios and evaluated simultaneously with the program Hyperquad2008. Interestingly, we found two species models which both deliver a good  $\sigma$  value. The stability constants calculated for both models are summarized in **Table 9.4**.

**Table 9.4:** Mean values of the overall stability constants  $\log\beta_{xyz}$  <sup>[a]</sup> from potentiometric titrations of  $Gd^{3+}$  with MSA determined by simultaneous evaluation with Hyperquad2008 in pure water,  $T = 298$  K and  $I = 0.1$  mol/L KCl.

<b><math>\log\beta</math> values for the complexation of <math>Gd^{3+}</math>:MSA</b>			
three 1:2 titrations	three 1:3 titrations	three 1:5 titrations	
mean values by simultaneous evaluation of 9 titrations <sup>[b]</sup>			
<b>model 1</b>		<b>model 2</b>	
$\sigma$ <sup>[c]</sup>	1.161	$\sigma$ <sup>[c]</sup>	1.210
<b><math>\log\beta_{110}</math></b>	<b>10.38(3)</b>	<b><math>\log\beta_{110}</math></b>	<b>10.36(5)</b>
<b><math>\log\beta_{111}</math></b>	<b>16.0(2)</b>	<b><math>\log\beta_{122}</math></b>	<b>32.1(5)</b>
<b><math>\log\beta_{120}</math></b>	<b>18.9(3)</b>	<b><math>\log\beta_{120}</math></b>	<b>18.85(3)</b>
<b><math>\log\beta_{121}</math></b>	<b>25.8(1)</b>	<b><math>\log\beta_{121}</math></b>	<b>25.6(1)</b>

<sup>[a]</sup> For the ligand L  $\log\beta_{xyz}$  is defined as:  $\beta_{xyz} = [M_xL_yH_z] \times [M]^{-x} \times [L]^{-y} \times [H]^{-z}$ .

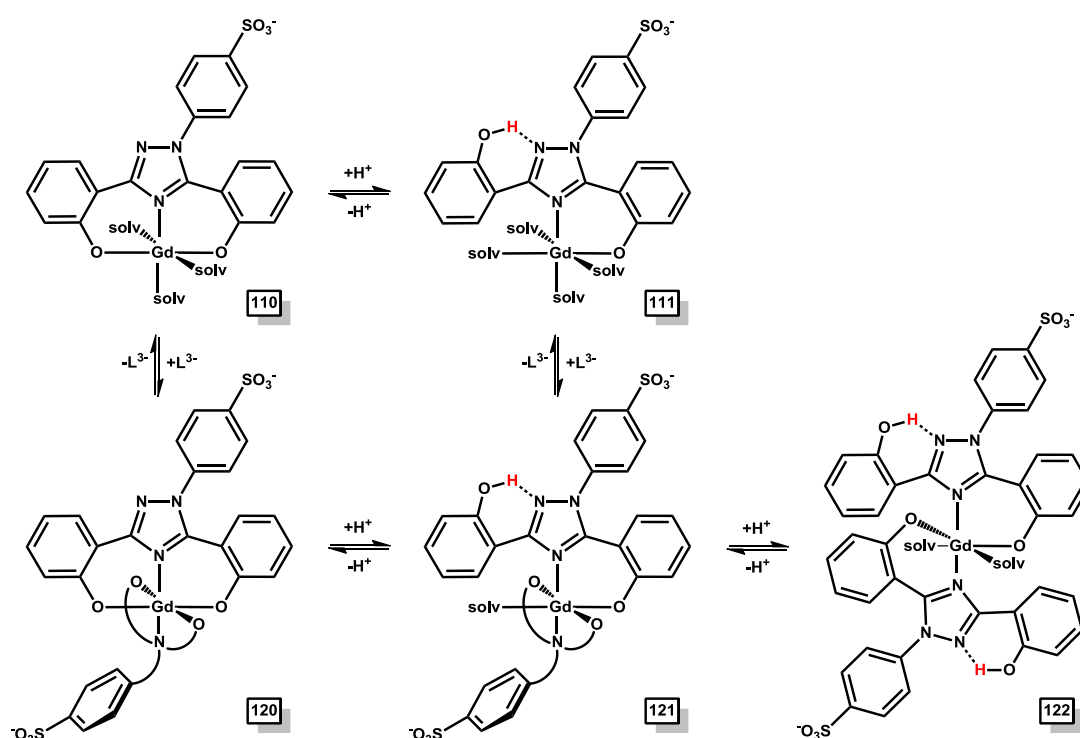
<sup>[b]</sup> The titrations were evaluated simultaneously with the program Hyperquad2008. The deviations given in brackets correspond to the threefold standard deviation taken from Hyperquad2008.

<sup>[c]</sup> The  $\sigma$  value is taken from Hyperquad2008.

The evaluation of the titration experiments did not result in one distinct species model as we had expected. Instead, we were able to calculate two quite similar species models. Both model 1 and model 2 comprehend a  $[Gd(L)]$  (110), a  $[Gd(L)_2]^{3-}$  (120) and a  $[Gd(L)(LH)]^{2-}$  (121) complex. The models differentiate by a  $[Gd(LH)]^+$  (111) complex for model 1 and a  $[Gd(LH)_2]^-$  (122) complex for model 2. An evaluation of the titrations with both a 111 and a 122 complex was not possible. The  $\sigma$  value of the model 1 is slightly smaller which implies a somewhat more suitable fit calculated with these stability constants. A

$[\text{Gd}(\text{L})_3]^{6-}$  (130) complex could be calculated with both models resulted in a formation of the complex to less than 1% and was discarded.

The complex formation of the trivalent metal ions  $\text{Fe}^{3+}$  and  $\text{Al}^{3+}$  with the ligand MSA has been investigated previously in pure water ( $T = 298 \text{ K}$ ,  $I = 0.1 \text{ mol/L KCl}$ ) [37]. The complexes found in solution were a 110, 120 and 121 complex for  $\text{Fe}^{3+}$  with MSA and a 110 and 120 complex for  $\text{Al}^{3+}$  with MSA. Thus a 111 and a 122 complex is not favoured by these trivalent metal ions. It might be though that these protonated complexes are favoured by the somewhat larger  $\text{Gd}^{3+}$  ion which has an ionic radius of  $0.938 \text{ \AA}$  (CN 6) in comparison to  $\text{Fe}^{3+}$  with  $0.645 \text{ \AA}$  (CN 6) and  $\text{Al}^{3+}$   $0.535 \text{ \AA}$  (CN 6) [118]. Structure suggestions for the possible complexes found in both models are illustrated in **Scheme 9.1**. The  $\text{pK}_{\text{a},1} = 1.12(4)$  of the ligand MSA is very acidic and causes deprotonation already in acidic solution. This protonation will not play any role in protonated species of the  $\text{Gd}^{3+}$ -MSA complexes. As a consequence, protonated species such as a 111, 121 and 122 complex are most probably protonated at one of the phenolate groups.



**Scheme 9.1:** Suggested coordination geometries of the MSA complexes  $[\text{Gd}(\text{L})]$  (110),  $[\text{Gd}(\text{LH})]^+$  (111),  $[\text{Gd}(\text{L})_2]^{3-}$  (120),  $[\text{Gd}(\text{L})(\text{LH})]^{2-}$  (121) and  $[\text{Gd}(\text{LH})_2]^-$  (122).

The protonated ligand MSA coordinates bidentate with the phenolate group and the triazole nitrogen atom in position 4. The hydroxyphenyl group can form hydrogen bonding interactions with the triazole nitrogen in position 2 which gives rise to the structure suggestions in **Scheme 9.1**. The ligand can coordinate bidentate in all three protonated complexes 111, 121 and 122.

The titration curves of all three molar ratios are depicted in **Figure 9.2**. The inflection at one equivalent is caused by the deprotonation of the very acidic proton with a  $pK_{a,1} = 1.12(4)$ . After this inflection a significant pH decrease is observed in comparison to the  $pK_a$  titration curve of the ligand MSA. The titration curves were all obtained with a total ligand concentration of 1.00 mmol/L for comparison.

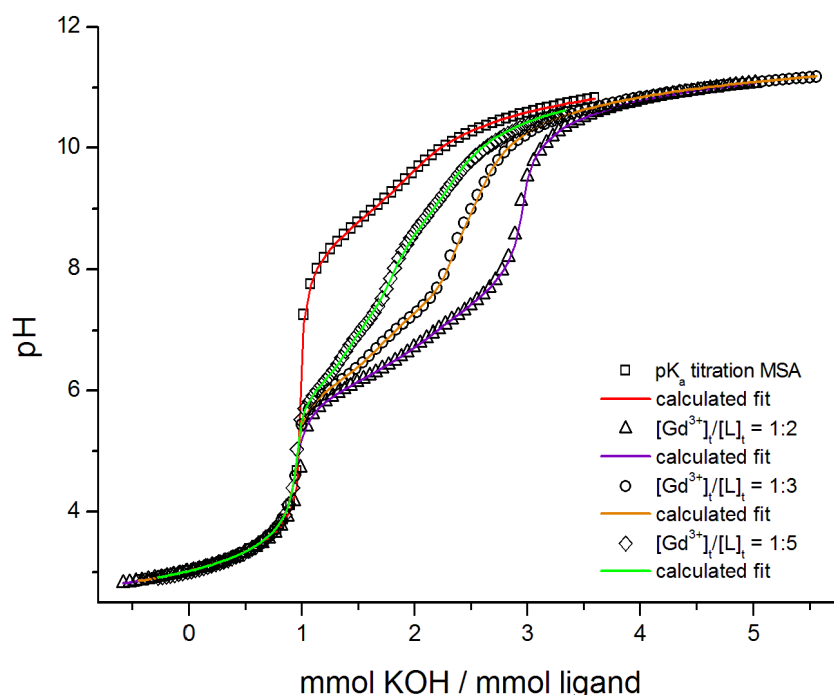


**Figure 9.2:** Potentiometric titration curves of the free ligand MSA and  $Gd^{3+}$  with MSA with the molar ratio 1:2 ( $[Gd^{3+}]_t = 0.50$  mmol/L,  $[L]_t = 1.00$  mmol/L), 1:3 ( $[Gd^{3+}]_t = 0.33$  mmol/L,  $[L]_t = 1.00$  mmol/L) and 1:5 ( $[Gd^{3+}]_t = 0.20$  mmol/L,  $[L]_t = 1.00$  mmol/L) in pure water,  $T = 298$  K and  $I = 0.1$  mol/L KCl. The open squares, circles and triangles represent experimental points and the fit (solid line) was calculated from the equilibrium constants with Hyperquad2008.

In example, the species distributions for both models in the molar ratio 1:3 are illustrated in **Figure 9.3**.

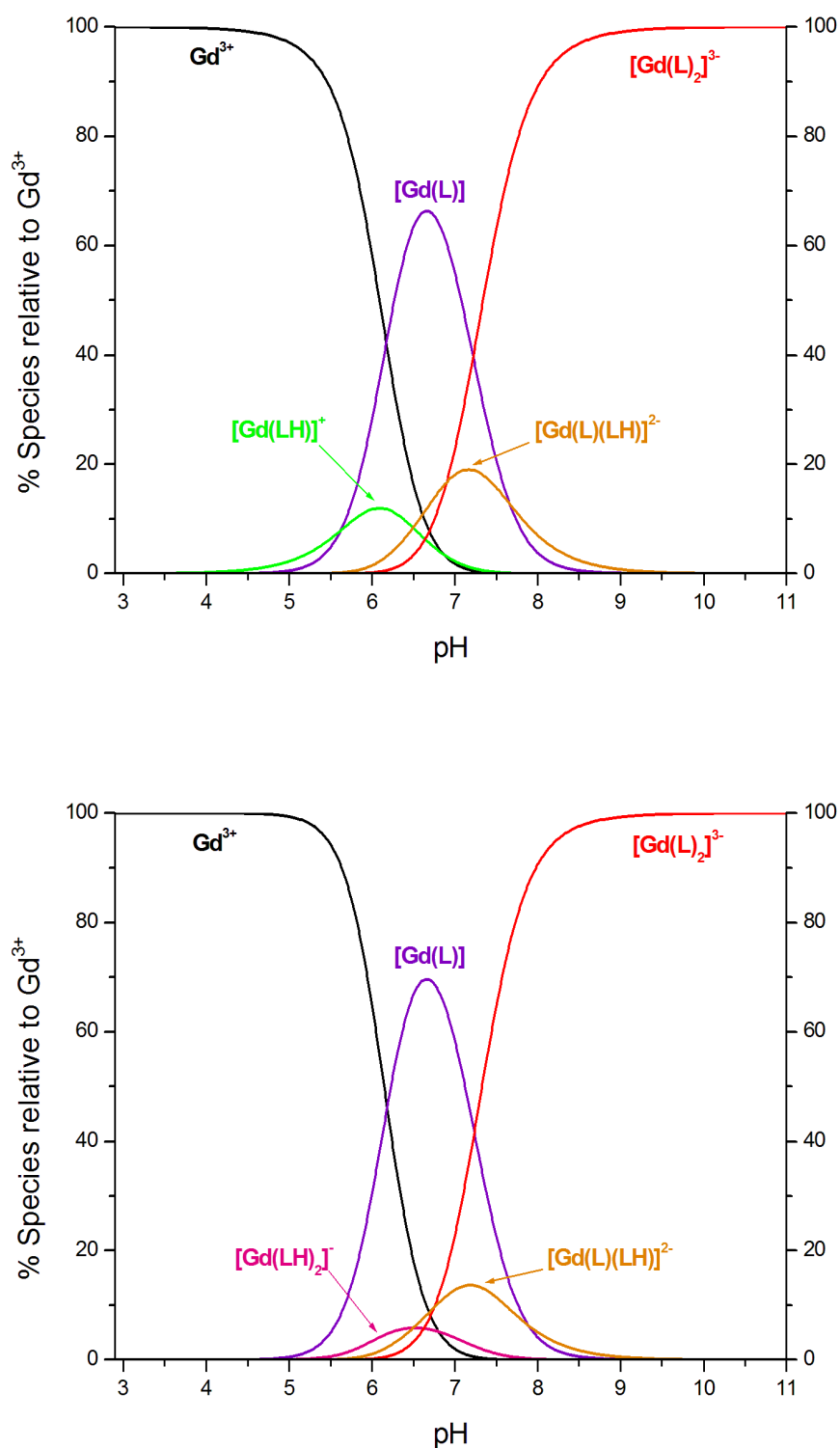


**Figure 9.3:** Species distribution diagram as a function of pH for Gd<sup>3+</sup> with the ligand MSA. Calculated for the continuous potentiometric titrations performed with a 1:3 molar ratio for model 1 (top) and model 2 (bottom) ([Gd<sup>3+</sup>]<sub>t</sub> = 0.25 mmol/L, [L]<sub>t</sub> = 0.75 mmol/L, pure water, T = 298 K and I = 0.1 mol/L KCl). The species concentration were calculated from the equilibrium constants listed in **Table 9.4** (mean values from simultaneous evaluation of 9 titrations) with the program Hyss2006.

Complex formation begins in solution at about pH 5. The dominating species in both models are the  $[\text{Gd}(\text{L})]$  (110) and the  $[\text{Gd}(\text{L})_2]^{3-}$  (120) complex. The mononuclear 110 complex appears with a maximum concentration of 66% at pH 6.7 in the model 1 species distribution and to 69% at pH 6.7 in the model 2. Further, the 120 complex is predominant species from pH 7.3 with a concentration of 44% (model 1) and 46% (model 2). In alkaline solution (pH 9 – 11) the 120 complex is the only complex present. The protonated complexes appear to less than 20% in both models. They do not play a dominant role in the species distribution which indicates that the bidentate coordination mode is not the favourable coordination mode and that these complexes rather deprotonate to form the tridentate 110 and 120 complexes. In addition, the  $[\text{Gd}(\text{LH})_2]^-$  (122) complex only reaches a maximum concentration of 6% at pH 6.5 and can be considered as a minor species. In this 122 complex two ligands MSA would both be coordinated bidentate which is clearly not favoured and therefore the existence of the 122 complex is questionable.

Taken together, only minor differences are found for the stability constants of the  $[\text{Gd}(\text{MSA})]$  (110),  $[\text{Gd}(\text{MSA})_2]^{3-}$  (120) and  $[\text{Gd}(\text{L})(\text{LH})]^{2-}$  (121) complexes both models have in common. Model 1 has a better calculated fit ( $\sigma = 1.161$ ) and the formation of the  $[\text{Gd}(\text{LH})]^+$  complex reaches at least a highest concentration of 12% at pH 6.1. The  $[\text{Gd}(\text{L})]$  complex has a  $\log\beta_{110} = 10.38(3)$  and the  $[\text{Gd}(\text{L})_2]^{3-}$  complex an individual stability constant  $\log K_{120} = 8.5$  ( $\log K_{120} = [\text{ML}_2] / [\text{ML}] \times [\text{L}]$ ) which shows a weaker complexation of the  $\text{Gd}^{3+}$  ion in comparison to the  $\text{Fe}^{3+}$ -MSA system ( $\log\beta_{110} = 21.30(4)$  and  $\log K_{120} = 14.65$ ;  $T = 298 \text{ K}$ ,  $I = 0.1 \text{ mol/L KCl}$ ) [40] or the  $\text{Al}^{3+}$ -MSA system ( $\log\beta_{110} = 16.3$  and  $\log K_{120} = 13.4$ ;  $T = 298 \text{ K}$ ,  $I = 0.1 \text{ mol/L KCl}$ ) [37]. Further, there was only little but not convincing evidence for the complexation of more than two ligands to one  $\text{Gd}^{3+}$  central ion found by this potentiometric study.

### 9.1.3 Complex formation of DSA with gadolinium (III) in pure water

Potentiometric titration experiments were performed by T. Nicolai, under my guidance, with the ligand DSA and  $Gd^{3+}$  in three molar ratios  $Gd^{3+}$ :DSA 1:2, 1:3 and 1:5 to investigate the complex formation <sup>[58]</sup>. The ligand DSA is far more soluble in pure water than MSA and thus titrations could be performed with sufficiently higher concentrations. Further, all complexes formed were soluble and no precipitation was observed. The titration conditions are presented in **Table 9.5**.

**Table 9.5:** Titration experiment conditions of the complexation of  $Gd^{3+}$  with DSA given at  $T = 298$  K.

Conditions for the $Gd^{3+}$ -DSA titrations					
molar ratio of M:L	1:2	1:3		1:5	
measuring method	potentiometric	potentiometric		potentiometric	
method type	continuous	continuous		continuous	
solvent	pure water	pure water		pure water	
$[M]_t$ in mmol/L	0.50	0.33	0.50	0.20	0.40
$[L]_t$ in mmol/L	1.00	1.00	1.50	1.00	2.00
titration volume	50.0 mL	50.0 mL		50.0 mL	
titrant	0.1 mol/L KOH	0.1 mol/L KOH		0.1 mol/L KOH	
supporting electrolyte	0.1 mol/L KCl	0.1 mol/L KCl		0.1 mol/L KCl	
electrode	SenTix / IoLine	SenTix / IoLine		SenTix / IoLine	
$pK_w$	13.78	13.78		13.78	
pH range	2.8 – 11.2	2.5 – 10.8		2.9 – 10.8	
volume of data points	86	80		80	
time for mixing process	550 s /350 s	350 s		350 s	

One combined species model was calculated through simultaneous evaluation of all three molar ratios with the program Hyperquad2008. The overall stability constants of the determined complexes are given in **Table 9.6**.

**Table 9.6:** Mean values of the overall stability constants  $\log\beta_{xyz}$  <sup>[a]</sup> from potentiometric titrations of  $Gd^{3+}$  with DSA determined by simultaneous evaluation with Hyperquad2008 in pure water,  $T = 298$  K and  $I = 0.1$  mol/L KCl.

<b><math>\log\beta</math> values for the complexation of <math>Gd^{3+}</math>:DSA</b>		
five 1:2 titrations	five 1:3 titrations	five 1:5 titrations
mean values by simultaneous evaluation of 15 titrations <sup>[b]</sup>		
$\sigma$	1.717	
<b><math>\log\beta_{110}</math></b>	<b>12.01(3)</b>	
<b><math>\log\beta_{111}</math></b>	<b>17.1(1)</b>	
<b><math>\log\beta_{120}</math></b>	<b>20.61(2)</b>	
<b><math>\log\beta_{121}</math></b>	<b>27.7(1)</b>	
<b><math>\log\beta_{122}</math></b>	<b>34.6(4)</b>	
<b><math>\log\beta_{130}</math></b>	<b>23.2(2)</b>	

<sup>[a]</sup> For the ligand L  $\log\beta_{xyz}$  is defined as:  $\beta_{xyz} = [M_xL_yH_z] \times [M]^{-x} \times [L]^{-y} \times [H]^{-z}$ .

<sup>[b]</sup> The titrations were evaluated simultaneously with the program Hyperquad2008. The deviations given in brackets correspond to the threefold standard deviation taken from Hyperquad2008.

<sup>[c]</sup> The  $\sigma$  value is taken from Hyperquad2008.

The model found for the simultaneous evaluation of all three molar ratios is a model containing the expected  $[Gd(L)]^-$  (110) and  $[Gd(L)_2]^{5-}$  (120) complex as well as all three protonated complexes  $[Gd(LH)]$  (111),  $[Gd(L)(LH)]^{4-}$  (121) and  $[Gd(LH)_2]^{3-}$  (122). Additionally, a  $[Gd(L)_3]^{9-}$  (130) complex was also calculated with this model.

The titration curves of all three molar ratios in comparison to the  $pK_a$  titration curve of DSA are illustrated in **Figure 9.4**.

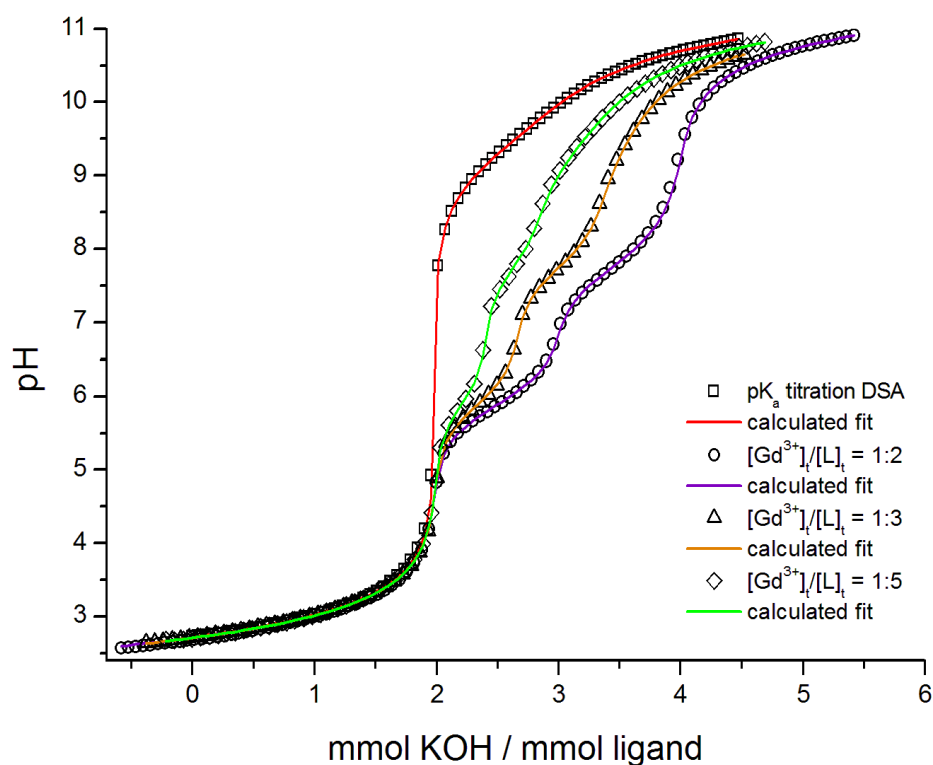


**Figure 9.4:** Potentiometric titration curves of the free ligand DSA and  $\text{Gd}^{3+}$ -DSA with the molar ratio 1:2 ( $[\text{Gd}^{3+}]_t = 0.50$  mmol/L,  $[\text{L}]_t = 1.00$  mmol/L), 1:3 ( $[\text{Gd}^{3+}]_t = 0.33$  mmol/L,  $[\text{L}]_t = 1.00$  mmol/L) and 1:5 ( $[\text{Gd}^{3+}]_t = 0.20$  mmol/L,  $[\text{L}]_t = 1.00$  mmol/L) in pure water,  $T = 298$  K and  $I = 0.1$  mol/L KCl. The open squares, circles and triangles represent experimental points and the fit (solid line) was calculated from the equilibrium constants with Hyperquad2008.

The  $\text{Gd}^{3+}$ -DSA titration curves (**Figure 9.4**) show three inflections. The first inflection at two equivalents is caused by the two very acidic protons of DSA. In the 1:2 molar ratio titrations further inflections appear at three and four equivalents. A look at the species distributions in **Figure 9.5** gives rise to the presence of the determined complexes. The dominant species in solution are the  $[\text{Gd}(\text{L})]^-$  (110) complex and the  $[\text{Gd}(\text{L})_2]^{5-}$  (120) complex. The inflection at three equivalents is caused by the maximum formation of the 110 complex with a concentration of 89% at pH 6.8. Further the third inflection at four equivalents is caused by the formation of the 120 complex in alkaline solution. The 120 complex is the sole complex in alkaline solution.

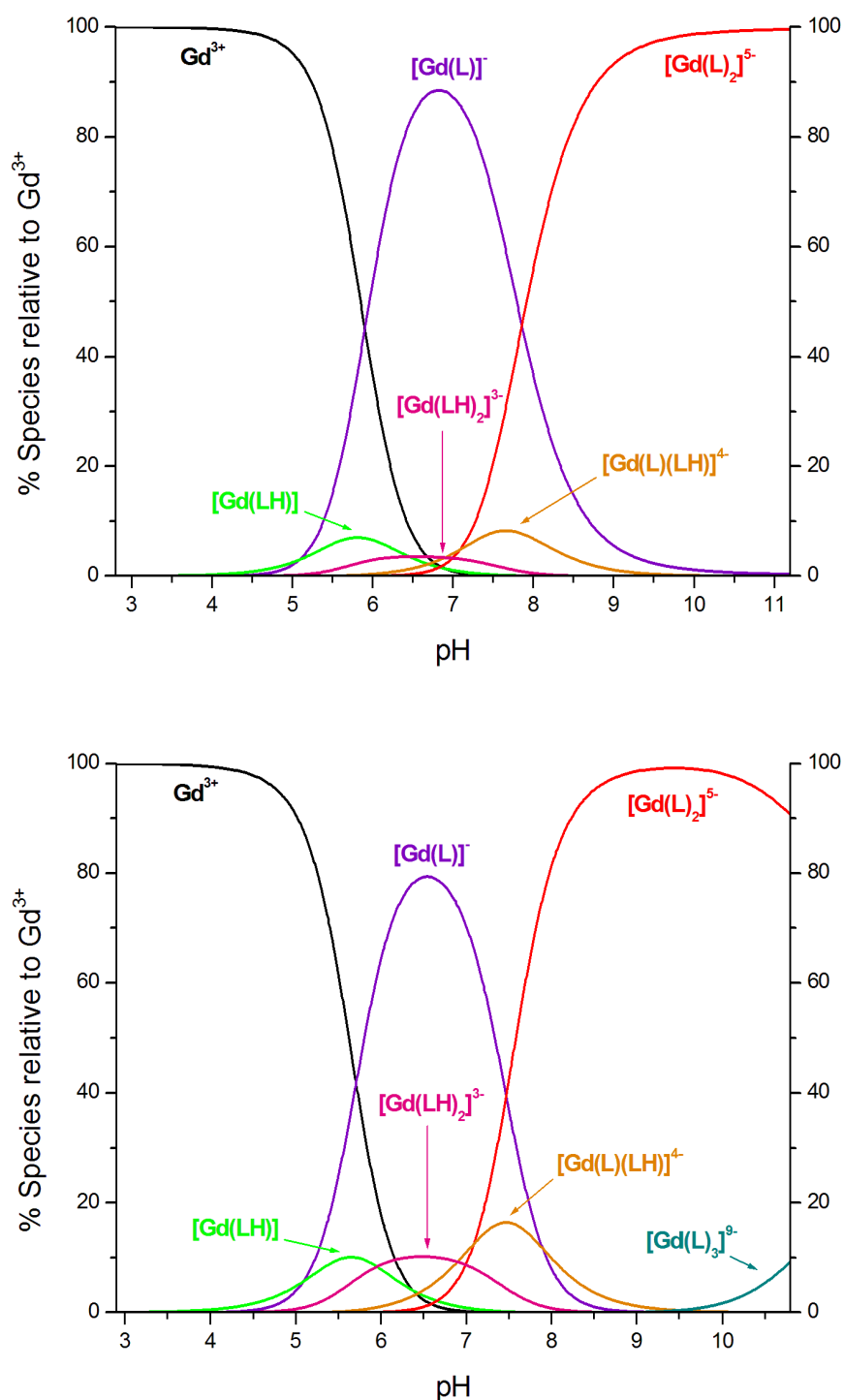


**Figure 9.5:** Species distribution diagram as a function of pH for  $Gd^{3+}$  with the ligand DSA. Calculated for the continuous potentiometric titrations performed with a 1:2 molar ratio (top diagram,  $[Gd^{3+}]_t = 0.50$  mmol/L,  $[L]_t = 1.00$  mmol/L,  $T = 298$  K and  $I = 0.1$  mol/L KCl) and 1:5 (bottom diagram,  $[Gd^{3+}]_t = 0.40$  mmol/L,  $[L]_t = 2.00$  mmol/L,  $T = 298$  K and  $I = 0.1$  mol/L KCl) in pure water. The species concentration were calculated from the equilibrium constants listed in **Table 9.6** (mean values from simultaneous evaluation of 15 titrations) with the program Hyss2006.

According, to the species distribution of the 1:2 molar ratio the protonated complexes  $[\text{Gd}(\text{LH})]$ ,  $[\text{Gd}(\text{L})(\text{LH})]^{4-}$  and  $[\text{Gd}(\text{LH})_2]^{3-}$  appear with less than 10%. These species are minor species and should be regarded critically. The calculated fit of the model improves by adding these minor species. Yet, one needs to keep in mind that the existence of minor species may also result from the compensation of protons by the program Hyperquad2008 which might have been caused by measurement artefacts. The possible existence of the protonated complexes would implicate a bidentate coordination mode of the ligand DSA with one phenoxo group protonated owing to the strong acidity of the  $pK_{a,2}$  1.33(8). The geometry of the complexes would be similar to those previously discussed for  $\text{Gd}^{3+}$ -MSA and illustrated in **Scheme 9.1**

Additionally, the  $[\text{Gd}(\text{L})_3]^{9-}$  (130) complex appears in strong alkaline solution in the species distribution with a 1:3 (not displayed since very similar to 1:2) and 1:5 molar ratio. A 130 complex is imaginable when either all ligands coordinate bidentate to form a  $\text{Gd}^{3+}$  ion with a coordination number of six or with the ligands bound tridentate and  $\text{Gd}^{3+}$  having a coordination number of nine. However, the complex reaches 9% at the end of the titration at pH 10.8. Accordingly, this complex needs to be seen as a minor species. The pH decrease observed in strong alkaline solution can be assigned to the formation of a 130 complex by calculations with the program Hyperquad2008. Yet, this complex needs to be viewed critically.

Taken together, we have determined the stability constants of two dominant complexes in solution. The stability constant of the  $[\text{Gd}(\text{L})]^-$  complex was determined to  $\log\beta_{110} = 12.01(3)$  which is higher than the corresponding value for the  $\text{Gd}^{3+}$ -MSA system ( $\log\beta_{110} = 10.38(3)$ ). Further, the dominating complex from pH 7.5 to alkaline solution is the  $[\text{Gd}(\text{L})_2]^{5-}$  complex with a  $\log K_{120} = 8.60$  ( $\log K_{120} = [\text{ML}_2] / [\text{ML}] \times [\text{L}]$ ). This value is very similar to the  $[\text{Gd}(\text{MSA})_2]^{3-}$  complex with  $\log K_{120} = 8.52$ . The 110 and 120  $\text{Gd}^{3+}$ -DSA complexes have been very well determined. The formation of all other complexes should be judged with critically.

#### 9.1.4 Summary and discussion

Gadolinium (III) complexes such as  $\text{Gd}^{3+}$ -DOTA are often used as contrast agents for MRI examinations on patients. We were interested in the question whether a simultaneous administration of a contrast agents containing  $\text{Gd}^{3+}$  and chelation therapy with deferasirox causes interactions between the complex formations. The ligand deferasirox is a specific ligand for  $\text{Fe}^{3+}$  chelation, however the stability of the  $\text{Gd}^{3+}$  complexes have, to our knowledge, not been investigated. Accordingly, our aim was to determine the stability of the complexes formed by the iron-chelating ligand deferasirox with gadolinium (III). Unfortunately, the determination of the stability constants by potentiometric titrations in water/DMSO ( $x_{\text{DMSO}} = 0.20$ ) were extremely hampered by precipitate throughout most of the titration range (pH 4 – 8). Two protonated complexes of the composition  $[\text{Gd}(\text{LH})]^+$  and  $[\text{Gd}(\text{LH}_2)]^{2+}$  were identified in a very small titration range (pH 3.1 – 4.6) with the overall stability constants  $\log\beta_{111} = 19.4(3)$  and  $\log\beta_{112} = 25.05(4)$ . These stability constants were determined with great difficulties and need to be judged critically.

The water soluble derivatives MSA and DSA of the iron-chelating ligand deferasirox were used to elucidate the complex behaviour with metal ions that have caused precipitation with deferasirox. Potentiometric titration experiments with the mono- and disulfonic acid derivatives MSA and DSA showed no precipitation during the experiments and stability constants of the complexes formed with  $\text{Gd}^{3+}$  in solution were determined in pure water. These can now be compared to the complexes of  $\text{Gd}^{3+}$ -DOTA. The overall stability constants of the  $\text{Gd}^{3+}$  complexes determined in this thesis and the overall stability constants of  $\text{Gd}^{3+}$ -DOTA from Clarke and Martell <sup>[136]</sup> are summarized in **Table 9.7**. All stability constants were investigated at  $T = 298$  K and an ionic strength of  $I = 0.1$  mol/L KCl. Consequently, we may use them for means of comparison.  $\text{Gd}^{3+}$ -DOTA only forms a  $[\text{Gd}(\text{DOTA})]^-$  (110) and  $[\text{Gd}(\text{DOTA-H})]$  (111) complex which were both taken into account. It is apparent, that the stability constant of the  $[\text{Gd}(\text{DOTA})]^-$  complex is at least double the value of the 110 stability constant of MSA or DSA.

**Table 9.7:** Overall stability constants  $\log\beta_{xyz}$  <sup>[a]</sup> of  $Gd^{3+}$  complexes with the listed ligands (T = 298 K, I = 0.1 mol/L KCl).

<b>Overall stability constants <math>\log\beta_{xyz}</math> <sup>[a]</sup> of <math>Gd^{3+}</math> complexes</b>				
	deferasirox	MSA	DSA	DOTA <sup>[b]</sup>
solvent	$x_{DMSO} = 0.20$	pure water	pure water	pure water
$\log\beta_{110}$	-	<b>10.38(3)</b>	<b>12.01(3)</b>	<b>24.0(1)</b>
$\log\beta_{111}$	19.4(3)	16.0(2)	17.1(1)	<b>26.3</b>
$\log\beta_{112}$	25.05(4)	-	-	-
$\log\beta_{120}$	-	<b>18.9(3)</b>	<b>20.61(2)</b>	-
$\log\beta_{121}$	-	25.8(1)	27.7(1)	-
$\log\beta_{122}$	-	-	34.6(4)	-
$\log\beta_{130}$	-	-	23.2(2)	-

<sup>[a]</sup> For the ligand L  $\log\beta_{xyz}$  is defined as:  $\beta_{xyz} = [M_xL_yH_z] \times [M]^{-x} \times [L]^{-y} \times [H]^{-z}$ .

<sup>[b]</sup> Values taken from Clarke and Martell <sup>[136]</sup>.

Species distribution diagrams have been calculated for the  $Gd^{3+}$  complexes of DOTA and MSA, respectively DSA, with the stability constants listed in **Table 9.7**. Species distributions calculated for about equal amounts of the metal ion  $Gd^{3+}$ , MSA or DSA with DOTA showed only Gd-DOTA complexes with  $[Gd(DOTA)]$  as dominant species with a concentration 80 – 100% throughout the pH range. In conclusion, DOTA forms much stronger complexes with  $Gd^{3+}$  than MSA or DSA. If both ligands MSA (or DSA) and DOTA are present in solution in about equal amounts with  $Gd^{3+}$  metal ions the  $Gd^{3+}$  will always prefer the DOTA ligand forming the  $[Gd(DOTA)]^-$  complex to 100% at physiological pH 7.4. The iron-chelating ligands will still be free to bind excess  $Fe^{3+}$ .

Species distribution diagrams calculated with a large excess of MSA or DSA in comparison to DOTA and  $Gd^{3+}$  are shown in **Figure 9.6**.

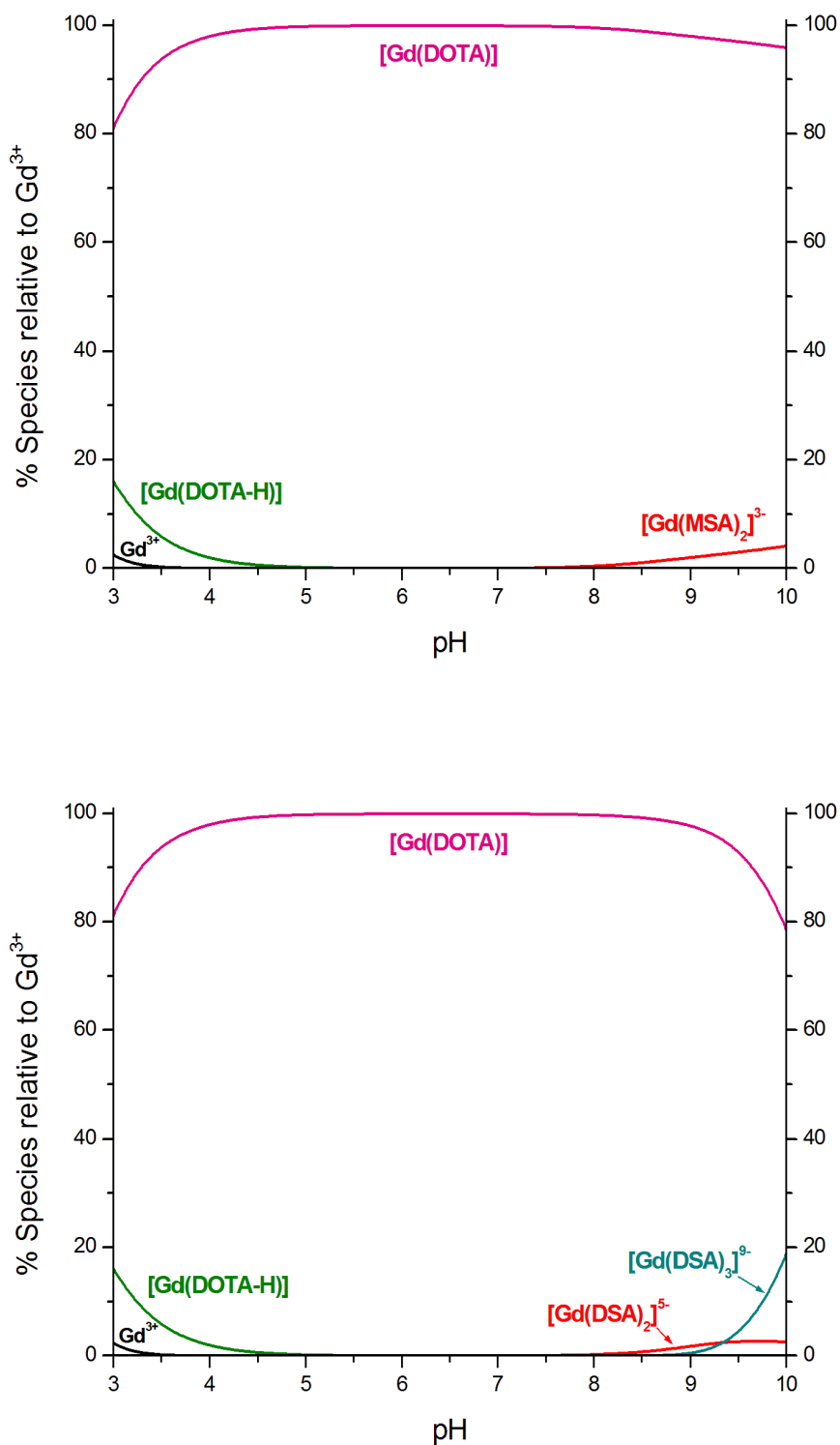


**Figure 9.6:** Species distribution diagrams as a function of pH for  $Gd^{3+}$  with the ligands MSA and DOTA (top,  $[Gd^{3+}]_t = 0.50$  mmol/L,  $[DOTA]_t = 0.50$  mmol/L,  $[MSA]_t = 0.5$  mol/L,  $T = 298$  K and  $I = 0.1$  mol/L KCl) and DSA and DOTA (bottom,  $[Gd^{3+}]_t = 0.50$  mmol/L,  $[DOTA]_t = 0.50$  mmol/L,  $[DSA]_t = 0.5$  mol/L,  $T = 298$  K and  $I = 0.1$  mol/L KCl) in pure water. The species concentration were calculated from the equilibrium constants listed in **Table 9.7** with the program Hyss2006.

An interesting question is whether MSA or DSA complexes appear if the ligand is present in excess. Calculations have shown that MSA and DSA complexes begin to appear with very low concentrations at an excess 1:200 ( $[Gd]_t = 0.5 \text{ mmol/L}$ ,  $[DOTA]_t = 0.5 \text{ mmol/L}$ ,  $[MSA/DSA]_t = 0.2 \text{ mol/L}$ ). The species distribution diagrams in **Figure 9.6** are calculated for a 1:1000 ratio ( $[Gd]_t = 0.5 \text{ mmol/L}$ ,  $[DOTA]_t = 0.5 \text{ mmol/L}$ ,  $[MSA/DSA]_t = 0.5 \text{ mol/L}$ ) to achieve sufficient  $[Gd(MSA)_2]^{3-}$  complex which is the only Gd-MSA complex. It is only present at  $\text{pH} > 8$  with a maximum concentration of 4%. The Gd-DSA distribution diagram is somewhat different due to the presence of a  $[Gd(DSA)_2]^{5-}$  and a  $[Gd(DSA)_3]^{9-}$  complex. Both complexes appear at  $\text{pH} > 8.5$  with a maximum concentration of 3%  $[Gd(DSA)_2]^{5-}$  and 19%  $[Gd(DSA)_3]^{9-}$  at  $\text{pH} 10$ . The  $[Gd(DOTA)]$  complex has a maximum concentration of 78% at  $\text{pH} 10$ . As a consequence, the  $[Gd(DSA)_3]^{9-}$  complex has gained importance in alkaline solution, yet at physiological  $\text{pH} 7.4$  still no Gd-DSA or Gd-MSA complexes appear. Even a 1:1000 excess MSA or DSA to DOTA cannot cause these ligand complexes to appear at  $\text{pH} = 7.4$ .

This result is in good agreement to the following characteristics of  $Gd^{3+}$ -DOTA complexes. Accordingly, the  $Gd^{3+}$ -DOTA complex has a high thermodynamic stability constant ( $\log\beta_{110} = 24.0$ ) and a very high kinetic stability. The kinetic stability has been estimated through the half-life  $T_{1/2}$  of the dissociation of the complex which is  $T_{1/2} > \text{one month}$  ( $T = 298 \text{ K}$ ,  $0.1 \text{ N HCl}$ ) for the  $Gd^{3+}$ -DOTA complex <sup>[132]</sup>. These two factors make the  $Gd^{3+}$ -DOTA complex almost inert once formed. Further, one needs to keep in mind that  $Gd^{3+}$ -DOTA is administered to the patient as the ready formed complex, which will probably not decompose. In conclusion, the investigations with MSA and DSA have shown that a simultaneous administration of the iron-chelating ligand deferasirox and a  $Gd^{3+}$  containing contrast agent, from a chemist point of view, should be without any problems. The  $Gd^{3+}$ -DOTA complex is much too stable to decompose and form complexes with deferasirox. Further, even if  $Gd^{3+}$  is free in solution and DOTA and deferasirox are competing ligands, the  $Gd^{3+}$ -DOTA complexes will preferably form, owing to their high stability, compared to  $Gd^{3+}$ -deferasirox complexes.

## 9.2 Complex formation of deferasirox and its water soluble derivatives with gallium (III)

The radio isotope  $^{68}\text{Ga}$  (III) is gaining presence as a promising radionuclide in radiopharmaceuticals in positron emission tomography (PET) which is often combined with X-Ray computed tomography (CT). Radiopharmaceuticals consist of two main compounds: a molecular structure (ligand, biomolecule) which is designed for specific targeting within the organism and a positron-emitting radionuclide which is responsible for a signal detectable outside of the patient. In some cases a spacer is added between radionuclide and the molecular structure. <sup>[137]</sup>

In PET the molecular structure is implemented as a targeting group which is meant to interact with a specific target surface receptor on the surface of a cell. The radionuclide attached to the targeting molecule decays by emitting a positron. The positron travels through the electron-rich tissue until it recombines with an electron by annihilation. Through the annihilation process the mass of the electron and positron are converted into two high-energy photons with 511 keV in form of  $\gamma$ -rays. These  $\gamma$ -rays are energetic enough to leave the organism and are detected by a PET scanner. <sup>[138]</sup>

Important factors that need to be taken into consideration for the design of radiometal-based radiopharmaceuticals are the half-life of the radionuclide, the mode of decay, cost and availability of the isotope <sup>[139]</sup>. The radionuclides usually have rather short half-lives ( $T_{1/2} = 2 - 110 \text{ min}$  <sup>[137]</sup>) which makes it necessary to produce them only a short time before administration.

Gallium-68 has a half-life of  $T_{1/2} = 67.71 \text{ min}$  and is easily produced by a  $^{68}\text{Ge}/^{68}\text{Ga}$  generator. The germanium-68 parent nuclide has a much longer half-life  $T_{1/2} = 270.95 \text{ days}$  and can be stored up to 1 year in clinics and applied to the  $^{68}\text{Ga}$  generator when needed. There are numerous commercial compact generator systems available. <sup>[138]</sup>

The daughter nuclide  $^{68}\text{Ga}$  can be efficiently separated from the parent nuclide  $^{68}\text{Ge}$  with ion exchange chromatography which has been optimized with many variations <sup>[140]</sup>.

The complex formation of  $\text{Ga}^{3+}$  also needs to be taken into account when applying the trivalent metal ion as a radiopharmaceutical. The free metal ion  $\text{Ga}^{3+}$  is toxic and can only be applied as radionuclide when bound to a ligand which forms strong complexes with the metal ion. Two requirements deserve special attention when designing a  $\text{Ga}^{3+}$  radiopharmaceutical. For once the  $\text{Ga}^{3+}$ -complex should be stable to hydrolysis. The ion  $\text{Ga}^{3+}$  prefers to form soluble, for example  $[\text{Ga}(\text{OH})_4]^-$ , and insoluble  $\text{Ga}(\text{OH})_3$  compounds with hydroxide ions throughout the pH region which should be suppressed as far as possible. The other requirement in vivo is the complexes should be more stable than the  $\text{Ga}^{3+}$ -transferrin complex. Transferrin is an iron-transport plasma protein which forms very stable  $\text{Ga}^{3+}$  complexes with a very high thermodynamic stability constant  $\log K_1 = 20.3$  [141]. In fact the  $\text{Ga}^{3+}$  ion has similar complexation characteristics as the  $\text{Fe}^{3+}$  ion, such as the ionic radius of  $\text{Ga}^{3+}$   $r = 0.620 \text{ \AA}$  (CN 6) [118] compared to  $\text{Fe}^{3+}$   $r = 0.645 \text{ \AA}$  (CN 6) [118]. Thus, the high plasma concentration of transferrin (0.25 g/100 mL) and the large formation constant of the  $\text{Ga}^{3+}$ -transferrin complex could induce that radiopharmaceutical  $\text{Ga}^{3+}$ -complexes could be labile to transferrin ligand exchange in vivo. However, most multidentate ligands form strong complexes with  $\text{Ga}^{3+}$  which are kinetically stable and do not exchange with transferrin. The determination of high thermodynamic stability constants does not necessarily indicate that the complexes formed are also stable in vivo. However, they are often used as a first criterion for suitable radiopharmaceuticals. [139]

The multidentate ligand DOTA forms very stable complexes with the trivalent metal ion  $\text{Ga}^{3+}$  which makes it an ideal complex for PET imaging. Whereas Gd-DOTA complexes, previously discussed in section 9.1, were readily used as non-specific contrast agents for MRI, in PET more specific molecules are needed to yield special targeting agents. As a consequence, so called bifunctional chelating agents (BFC) were developed which consist of a ligand which complexes the radiometal ion, and a functional group for attachment to the biomolecule which functions as targeting agent [139]. Further, peptides such as somatostatin, a peptide involved in the regulation and release of a number of hormones, were attached to the  $^{68}\text{Ga}$ -DOTA complexes to generate specific tumour targeting agents [139]. Tumours that have receptors for the-

se added peptides can be targeted by  $^{68}\text{Ga}$ -DOTA-peptide compounds and therefore detected by PET.

A well-known peptide derivative of the  $^{68}\text{Ga}$ -DOTA system is the complex [ $^{68}\text{Ga}$ -DOTA-Tyr<sup>3</sup>]octreotide called DOTA-TOC which targets subtypes of the somatostatin receptors of tumours <sup>[140]</sup>. Several other radiopeptides have been developed for receptor targeting and tumour localisation <sup>[142]</sup>.

Curiously, the iron-chelating ligand deferoxamine (desferrioxamine-B, DFO) forms very stable complexes with  $\text{Ga}^{3+}$  and has been used to complex  $^{68}\text{Ga}$  (III) and to connect the peptide octreotide as a tumour targeting receptor. This  $^{68}\text{Ga}$ -DFO-octreotide complex was stable in vivo and showed high affinity to the somatostatin receptors. <sup>[139-140, 142]</sup>

On account of the similar characteristics of  $\text{Ga}^{3+}$  and  $\text{Fe}^{3+}$  we investigated the complex behaviour of the iron-chelating ligand deferasirox and its water soluble derivatives with  $\text{Ga}^{3+}$  by potentiometric titrations. The determination of the stability constants is of special interest with regard to the question whether the simultaneous administration of deferasirox in chelation therapy and a  $^{68}\text{Ga}^{3+}$  containing radiopharmaceutical might cause interaction in form of transmetalation or ligand exchange reactions.

### 9.2.1 Complex formation of deferasirox with gallium (III) in pure water and water/DMSO solution $x_{\text{DMSO}} = 0.20$

The complex formation of the iron-chelating ligand deferasirox with the trivalent metal ion  $\text{Ga}^{3+}$  is expected to be strong since deferasirox forms strong complexes with the similar trivalent metal ion  $\text{Fe}^{3+}$ . Due to the low solubility of the ligand deferasirox in pure water the titration experiments needed to be carried out in a water/DMSO solution with a molar fraction of  $x_{\text{DMSO}} = 0.20$ . The first titrations in the water/DMSO medium revealed some precipitation occurring in the pH range 3.5 – 4.5. However, above pH 4.6 the precipitate had dissolved and titrations could be evaluated. The evaluations showed a very strong complexation between deferasirox and  $\text{Ga}^{3+}$  resulting in almost 100%  $[\text{Ga}(\text{LH})]^+$  complex formation already in acidic solution. As a consequence, the first complexes formed in acidic solution could not be determined. In contrast to the  $\text{Fe}^{3+}$ -deferasirox system these complexes cannot be investigated by spectrophotometric batch titrations due to the lack of a coloured solution.

A method introduced by Motekaitis and Martell <sup>[143]</sup> is based on the strong tendency of  $\text{Ga}^{3+}$  to hydrolyse in aqueous solution. Instead of using competitive ligands to determine the stability constants the displacement of the ligand from  $\text{Ga}^{3+}$  by hydroxide ions in alkaline solution is used. In aqueous solution the constants of some well-defined mononuclear hydroxo complexes of the composition  $[\text{Ga}(\text{OH})_n]^{3-n}$  ( $1 \leq n \leq 4$ ) are known and with acidimetric titrations the stability constants of any  $\text{Ga}^{3+}$ -ligand system can be investigated.

Unfortunately, this method can only be applied to pure water solutions since the constants of  $\text{Ga}^{3+}$  are not known in water/DMSO solution. Therefore, the determination of the stability constants of the  $\text{Ga}^{3+}$ -deferasirox system was limited. A possibility was to define the stability constants that could be calculated with the program Hyperquad2008 on the basis of the unknown monomeric complex in strong acidic solution.

The determination of these individual stability constants has been performed previously and the results were summarised in a Final Report for the Novartis Pharma AG. <sup>[72]</sup>

The equilibrium reactions and the resulting stability constants are presented in **Table 9.8**.

**Table 9.8:** Individual stability constants  $\log K_{xyz}$  for the complex formation of the ligand deferasirox with  $\text{Ga}^{3+}$  in water/DMSO solution ( $x_{\text{DMSO}} = 0.20$ ,  $T = 298 \text{ K}$ ,  $I = 0.1 \text{ KCl}$ ).<sup>[72]</sup>

individual equilibrium constants for $\text{Ga}^{3+}$ -deferasirox		
equilibrium		$\log K_{xyz}$
$[\text{Ga}(\text{LH})]^+$	$\rightleftharpoons [\text{Ga}(\text{L}) + \text{H}^+$	4.1
$[\text{Ga}(\text{L}) + \text{L}^{3-}$	$\rightleftharpoons [\text{Ga}(\text{L})_2]^{3-}$	14.8
$[\text{Ga}(\text{LH})_2]^-$	$\rightleftharpoons [\text{Ga}(\text{L})(\text{LH})]^{2-} + \text{H}^+$	4.8
$[\text{Ga}(\text{L})(\text{LH})]^{2-}$	$\rightleftharpoons [\text{Ga}(\text{L})_2]^{3-} + \text{H}^+$	5.9

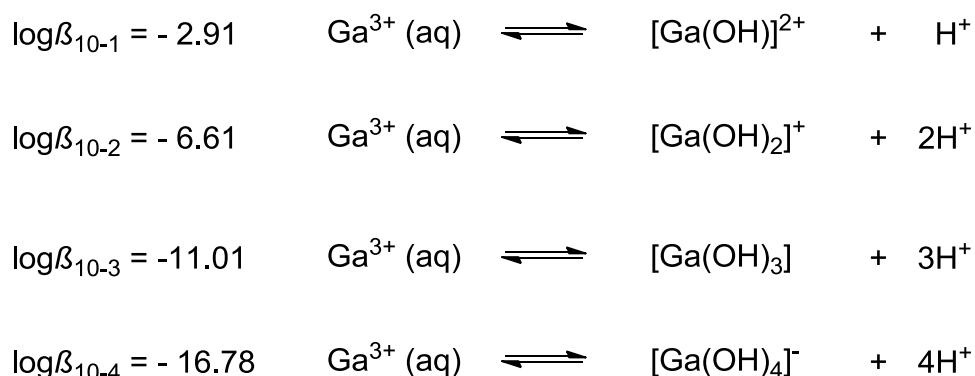
Mostly deprotonation constants were determined by this method, yet also an individual stability constant of the  $[\text{Ga}(\text{L})_2]^{3-}$  complex was calculated with a value of  $\log K_{120} = 14.8$  ( $\log K_{120} = [\text{ML}_2] / [\text{ML}] \times [\text{L}]$ ). In water/DMSO solution the hydrolysis constants of  $\text{Ga}^{3+}$  are not known so the advantage of a calculation on the basis of the  $[\text{Ga}(\text{OH})_4]^-$  complex with its known constant could not be applied. In acidic solution precipitation of a white solid occurred which could be isolated and analysed by  $\text{ESI}^+$  mass spectroscopy. The spectra revealed characteristic peaks in the range of  $m/z = 518 - 520$ ,  $m/z = 596 - 598$  and  $m/z = 624 - 626$  which could be assigned to the ions  $[\text{Ga}(\text{LH})(\text{DMSO})]^+$ ,  $[\text{Ga}(\text{LH})(\text{DMSO})_2]^+$  and  $[\text{Ga}(\text{L})\text{K}(\text{DMSO})(\text{H}_2\text{O})(\text{CH}_3\text{OH})]^+$ , respectively<sup>[72]</sup>. The characteristic pattern of the  $^{69}\text{Ga}/^{71}\text{Ga}$  ratio of 1.0 to 0.66 was observed. Further, a very weak signal at  $m/z = 813$  could be assigned to  $[\text{Ga}(\text{LH}_2)_2]^+$ <sup>[72]</sup>.

In conclusion, the precipitate consists mostly of mononuclear  $\text{Ga}^{3+}$ -deferasirox species that seem to have a lower solubility in solution than the corresponding  $\text{Fe}^{3+}$  and  $\text{Al}^{3+}$  complexes, since no precipitation was observed during these titrations. However, the  $\text{Ga}^{3+}$ -deferasirox stability constants in **Table 9.8** should be viewed critically, due to: i) the difficulties with precipitate in

acidic solution, ii) readily formed 100% complex at the beginning of the titration and iii) the fact that these constants could not be calculated on the basis of the  $[\text{Ga}(\text{OH})_4]^-$  complex.

### The $\text{Ga}^{3+}$ -deferasirox system in pure water

Despite the low solubility of deferasirox on pure water the ligand is reasonably soluble in strong alkaline aqueous solution. A titration experiment of a strong alkaline  $\text{Ga}^{3+}$ -deferasirox solution with hydrochloric acid has been previously performed in pure water [72]. Since this experiment was carried out in pure water the hydroxo complexes of  $\text{Ga}^{3+}$  as described by Motekaitis and Martell [143] can be applied for the calculation of the equilibrium constant of  $\text{Ga}^{3+}$ -deferasirox complexes. The overall stability constants and corresponding reaction equations of the gallium (III) hydroxo complexes implemented in the calculation with Hyperquad2008 are depicted in **Scheme 9.2**



**Scheme 9.2:** Reaction equations for the overall formation constants of the gallium (III) hydroxo complexes in aqueous solution [143].

These hydroxo complexes were applied as constant values for the calculation. The constant values for the gallium (III) hydroxo complexes and the determined overall stability constant for the  $[\text{Ga}(\text{L})_2]^{3-}$  complex of deferasirox are given in **Table 9.9**.

**Table 9.9:** Acidimetric titration experiment for the determination of the complex formation of  $\text{Ga}^{3+}$  with deferasirox in strong alkaline solution, pH range 10.3 – 11.3. [72]

<b>log<math>\beta</math> value for <math>\text{Ga}^{3+}</math>-deferasirox in pure water</b>		
<b>species</b>	<b>log<math>\beta_{xyz}</math> [a]</b>	<b>value</b>
$[\text{Ga}(\text{OH})]^{2+}$	log $\beta_{10-1}$ [b]	-2.91
$[\text{Ga}(\text{OH})_2]^+$	log $\beta_{10-2}$ [b]	-6.61
$[\text{Ga}(\text{OH})_3]$	log $\beta_{10-3}$ [b]	-11.01
$[\text{Ga}(\text{OH})_4]^-$	log $\beta_{10-4}$ [b]	-16.78
<b><math>[\text{Ga}(\text{L})_2]^{3-}</math></b>	<b>log<math>\beta_{120}</math> [c]</b>	<b>33.8(1)</b>

[a] For the log $\beta_{xyz}$  is defined as:  $\beta_{xyz} = [\text{M}_x\text{L}_y\text{H}_z] \times [\text{M}]^{-x} \times [\text{L}]^{-y} \times [\text{H}]^{-z}$ .

[b] Values were taken from Motekaitis and Martell [143] and defined as constant values.

[c] Value taken from the Novartis Pharma AG Final Report [72].

The overall stability constant of the  $[\text{Ga}(\text{L})_2]^{3-}$  complex was determined to log $\beta_{120} = 33.8(1)$  according to the equation:



In conclusion, some individual stability constants of the  $\text{Ga}^{3+}$ -deferasirox system in water/DMSO ( $x_{\text{DMSO}} = 0.20$ ) were determined on the basis of the unknown  $[\text{Ga}(\text{LH})]^+$  complex. The individual constant of the  $[\text{Ga}(\text{L})_2]^{3-}$  complex was determined to log $K_{120} = 14.8$  (log $K_{120} = [\text{ML}_2] / [\text{ML}] \times [\text{L}]$ , water/DMSO  $x_{\text{DMSO}} = 0.20$ ). In pure water the overall stability constant of this  $[\text{Ga}(\text{L})_2]^{3-}$  complex has been determined to log $\beta_{120} = 33.8(1)$  by acidimetric titrations with the help of the stability constant of the known gallium (III) tetrahydroxo complex  $[\text{Ga}(\text{OH})_4]^-$ .

### 9.2.2 Complex formation of MSA with gallium (III) in pure water

The titration experiments with the ligand deferasirox and  $\text{Ga}^{3+}$  revealed very strong complex behaviour with 100% complex formation at the beginning of the titration. To be able to investigate the stability constants of this system the method described by Motekaitis and Martell <sup>[143]</sup> needs to be applied. The method takes advantage of the conversion of almost all complexes in alkaline solution to the known gallium (III) hydroxo complexes. This was rather difficult with  $\text{Ga}^{3+}$ -deferasirox since the method can only be applied in pure water where the gallium (III) hydroxo complexation constants are known. The ligand MSA however is sufficiently soluble in pure water and therefore this method carried out with acidimetric titrations was performed with the  $\text{Ga}^{3+}$ -MSA system. We use the ligand MSA to elucidate the complex behaviour of the deferasirox ligand system, which is often difficult to investigate due to its poor solubility in pure water.

Acidimetric titrations with HCl (0.1 mol/L) were carried out with  $\text{Ga}^{3+}$  and the ligand MSA in pure water with two different molar ratios  $\text{Ga}^{3+}$ :MSA 1:2 and 1:4. The evaluation of the titrations with a 1:4 molar ratio was better than the 1:2 titrations. The titration experiments were evaluated simultaneously with the program Hyperquad2008 to find a suitable species model for all titrations. No precipitation was observed during these titration experiments. The titration conditions for both molar ratios are given in **Table 9.10**.

**Table 9.10:** Titration conditions for the acidimetric titration experiments of  $\text{Ga}^{3+}$  with MSA, given at  $T = 298 \text{ K}$ .

<b>Conditions for the <math>\text{Ga}^{3+}</math>-MSA acidimetric titrations</b>		
molar ratio of M:L	1:2	1:4
measuring method	potentiometric	potentiometric
method type	continuous	continuous
solvent	pure water	pure water
$[\text{M}]_t$	0.50 mmol/L	0.50 mmol/L
$[\text{L}]_t$	1.00 mmol/L	2.00 mmol/L
titration volume	50.0 mL	50.0 mL
titrant	0.1 mol/L HCl	0.1 mol/L HCl
supporting electrolyte	0.1 mol/L KCl	0.1 mol/L KCl
electrode	Ross Ultra	Ross Ultra
$\text{p}K_w$	13.78	13.78
pH range	10.8 – 2.1	11.1 – 2.3
volume of data points	100	100
time for mixing process	550 s	600 s

The  $\text{Ga}^{3+}$ -MSA titrations with the molar ratios 1:2 and 1:4 were evaluated simultaneously with the program Hyperquad2008. Further, the determined  $\text{p}K_a$  values of MSA in **Table 9.2** (section 9.1.2) were used for the calculation as well as the known gallium (III) hydroxo overall stability constants from **Table 9.9**.

The mean values for the overall stability constants of the  $\text{Ga}^{3+}$ -MSA system are presented in **Table 9.11**.

**Table 9.11:** Mean values of the overall stability constants  $\log\beta_{xyz}$  <sup>[a]</sup> from acidimetric titrations of  $\text{Ga}^{3+}$  with MSA determined by simultaneous evaluation with Hyperquad2008 in pure water,  $T = 298 \text{ K}$  and  $I = 0.1 \text{ mol/L KCl}$ .

<b><math>\log\beta</math> values for the complexation of <math>\text{Ga}^{3+}</math>:MSA</b>	
two titrations 1:2	four titrations 1:4
pH 10.8 – 2.1	pH 11.1 – 2.1
mean values by simultaneous evaluation of 6 titrations <sup>[b]</sup>	
$\sigma$ <sup>[c]</sup>	3.284
<b><math>\log\beta_{110}</math></b>	<b>19.8(1)</b>
<b><math>\log\beta_{111}</math></b>	<b>22.2(3)</b>
<b><math>\log\beta_{120}</math></b>	<b>33.8(3)</b>
<b><math>\log\beta_{121}</math></b>	<b>39.1(3)</b>
<b><math>\log\beta_{11-2}</math></b>	<b>9.3(3)</b>

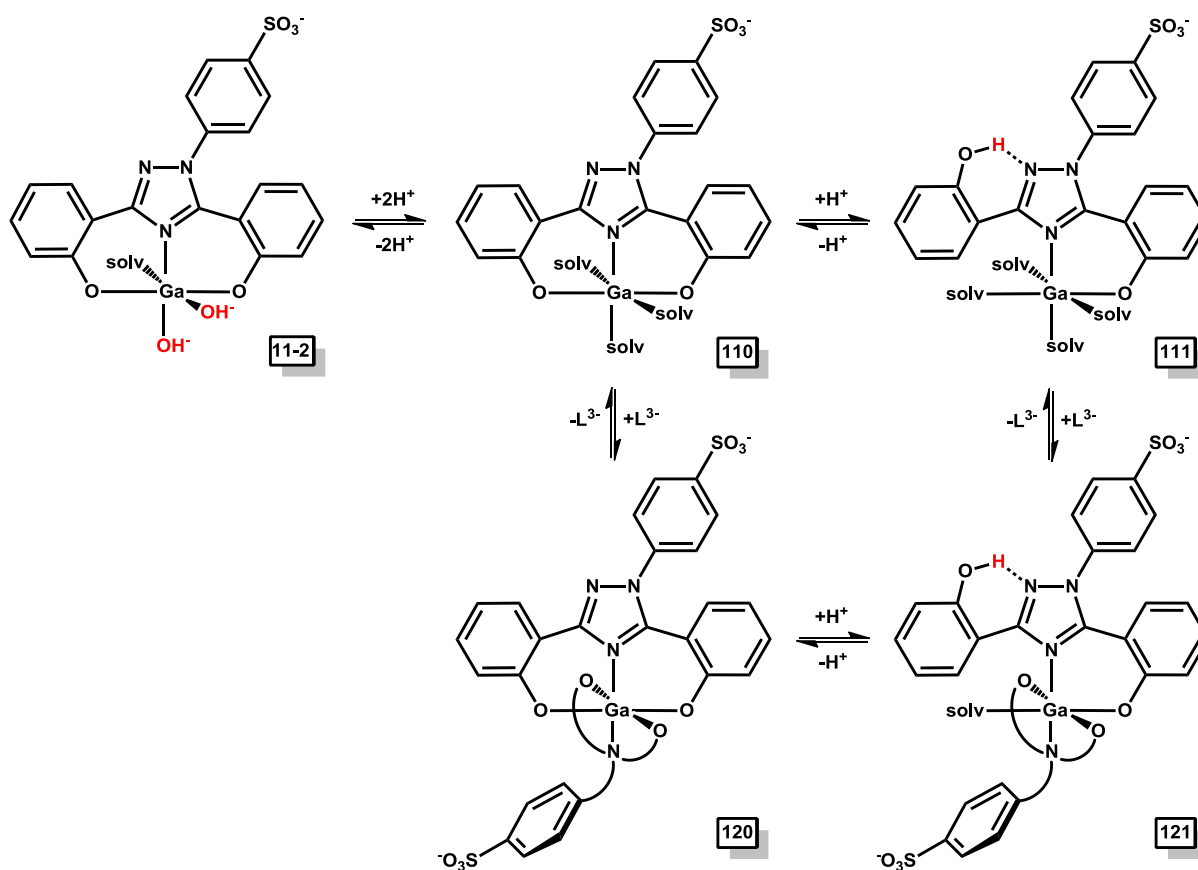
<sup>[a]</sup> For the ligand L  $\log\beta_{xyz}$  is defined as:  $\beta_{xyz} = [\text{M}_x\text{L}_y\text{H}_z] \times [\text{M}]^{-x} \times [\text{L}]^{-y} \times [\text{H}]^{-z}$ .

<sup>[b]</sup> The titrations were evaluated simultaneously with the program Hyperquad2008. The deviations given in brackets correspond to the threefold standard deviation taken from Hyperquad2008.

<sup>[c]</sup> The  $\sigma$  value is taken from Hyperquad2008.

The species model comprehends the expected  $[\text{Ga}(\text{L})]$  (110) complex with a  $\log\beta_{110} = 19.8(1)$  and a protonated complex  $[\text{Ga}(\text{LH})]^+$  (111) with a very acidic apparent  $\text{p}K_a = 2.4$ . The  $[\text{Ga}(\text{L})_2]^{3-}$  (120) complex has an individual stability constant of  $\log K_{120} = 14.0$  ( $\log K_{120} = [\text{ML}_2] / [\text{ML}] \times [\text{L}]$ ). Further, a protonated bis-complex  $[\text{Ga}(\text{L})(\text{LH})]^{2-}$  (121) was determined with an apparent  $\text{p}K_a = 5.3$ . These are all complexes well known for this type of ligand system. Yet, in alkaline solution there was still a complex missing besides the gallium (III) hydroxo complexes to ensure a good fit of the measured titration curve. The complex found to improve the fit was a  $[\text{Ga}(\text{L})(\text{OH})_2]^{2-}$  (11-2) complex. The  $\sigma$  value with 3.284 of the simultaneous evaluation of all six titrations was higher than expected. However, this was the model with the best  $\sigma$  value.

**Scheme 9.3** illustrates the possible coordination geometries of the determined complexes. The 11-2 complex is presumably a monomeric complex of  $\text{Ga}^{3+}$  with MSA where two water molecules coordinated to  $\text{Ga}^{3+}$  are deprotonated. Gallium (III) has a strong tendency to form hydroxo complexes and it is not unlikely that this mixed ligand and hydroxo complex forms in solution.



**Scheme 9.3:** Suggested coordination geometries of the MSA complexes  $[\text{Ga}(\text{L})]$  (110),  $[\text{Ga}(\text{LH})]^+$  (111),  $[\text{Ga}(\text{L})_2]^{3-}$  (120),  $[\text{Ga}(\text{L})(\text{LH})]^{2-}$  (121) and  $[\text{Ga}(\text{L})(\text{OH})_2]^{2-}$  (11-2).

The titration curves of both molar ratios are depicted in **Figure 9.7**. The  $\text{Ga}^{3+}$ :MSA 1:4 titrations were also carried out with a total concentration of  $[\text{Ga}^{3+}]_t = 0.25 \text{ mmol/L}$  to  $[\text{MSA}]_t = 1.00 \text{ mmol/L}$  to be able to compare both titration curves. However, for better evaluations, titrations with higher total concentrations ( $[\text{Ga}^{3+}]_t = 0.50 \text{ mmol/L}$  and  $[\text{MSA}]_t = 2.00 \text{ mmol/L}$ ) were performed for the determination of the stability constants.

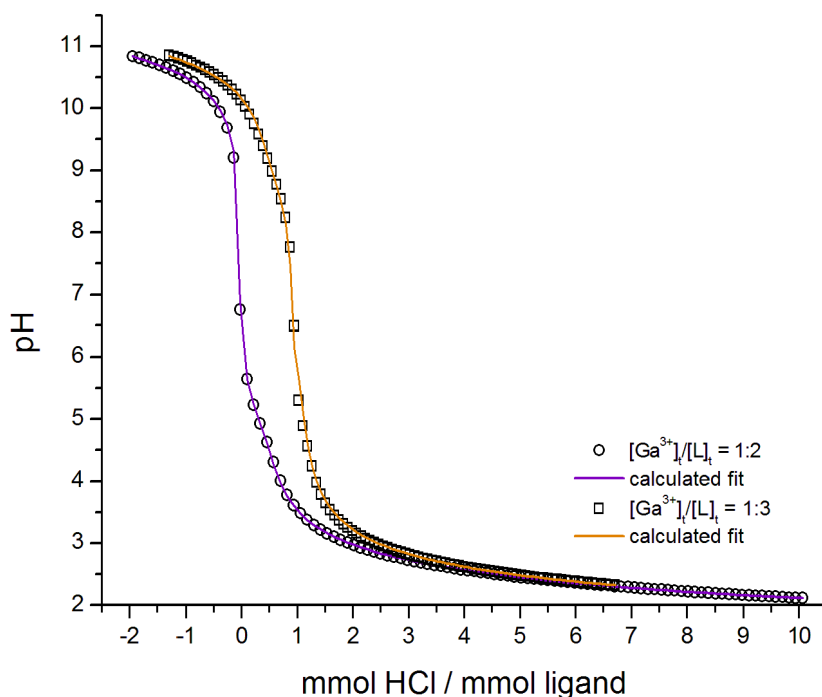


**Figure 9.7:** Acidimetric potentiometric titration curves of  $\text{Ga}^{3+}$  with MSA with the molar ratio 1:2 ( $[\text{Ga}^{3+}]_t = 0.50 \text{ mmol/L}$ ,  $[\text{L}]_t = 1.00 \text{ mmol/L}$ ) and 1:4 ( $[\text{Ga}^{3+}]_t = 0.25 \text{ mmol/L}$ ,  $[\text{L}]_t = 1.00 \text{ mmol/L}$ ) in pure water,  $T = 298 \text{ K}$  and  $I = 0.1 \text{ mol/L KCl}$ . The open squares and circles represent experimental points and the fit (solid line) was calculated from the equilibrium constants with Hyperquad2008.

For a better understanding of the inflections we need to note that the ligand MSA when titrated alkalimetric is applied as  $\text{LH}_3$  with three protons. In the acidimetric titration the pH of the sample solution with MSA and  $\text{Ga}^{3+}$  is adjusted to pH 11.1 with 0.1 mol/L KOH and titrated with 0.1 mol/L HCl. Owing to the very acidic  $\text{p}K_{a,1} = 1.12(4)$  only the phenolate groups of the ligand MSA will be protonated. Further, most of the ligand MSA is complexed and the protons often are added to the protonated complex species in solution to form  $[\text{Ga}(\text{LH})]^+$  and  $[\text{Ga}(\text{L})(\text{LH})]^{2-}$ . The species distribution for both molar ratios is presented in **Figure 9.8**.

The titration curve with a  $\text{Ga}^{2+}$ :MSA 1:2 molar ratio shows an inflection at 0 equivalents (pH 9 - 6) since most of the ligand is bound in the  $[\text{Ga}(\text{L})_2]^{3-}$  complex (maximum 85% at pH 7.6) and the only complexes being influenced by  $\text{H}^+$  are  $[\text{Ga}(\text{L})(\text{OH})_2]^{2-}$  and  $[\text{Ga}(\text{OH})_4]^-$ .

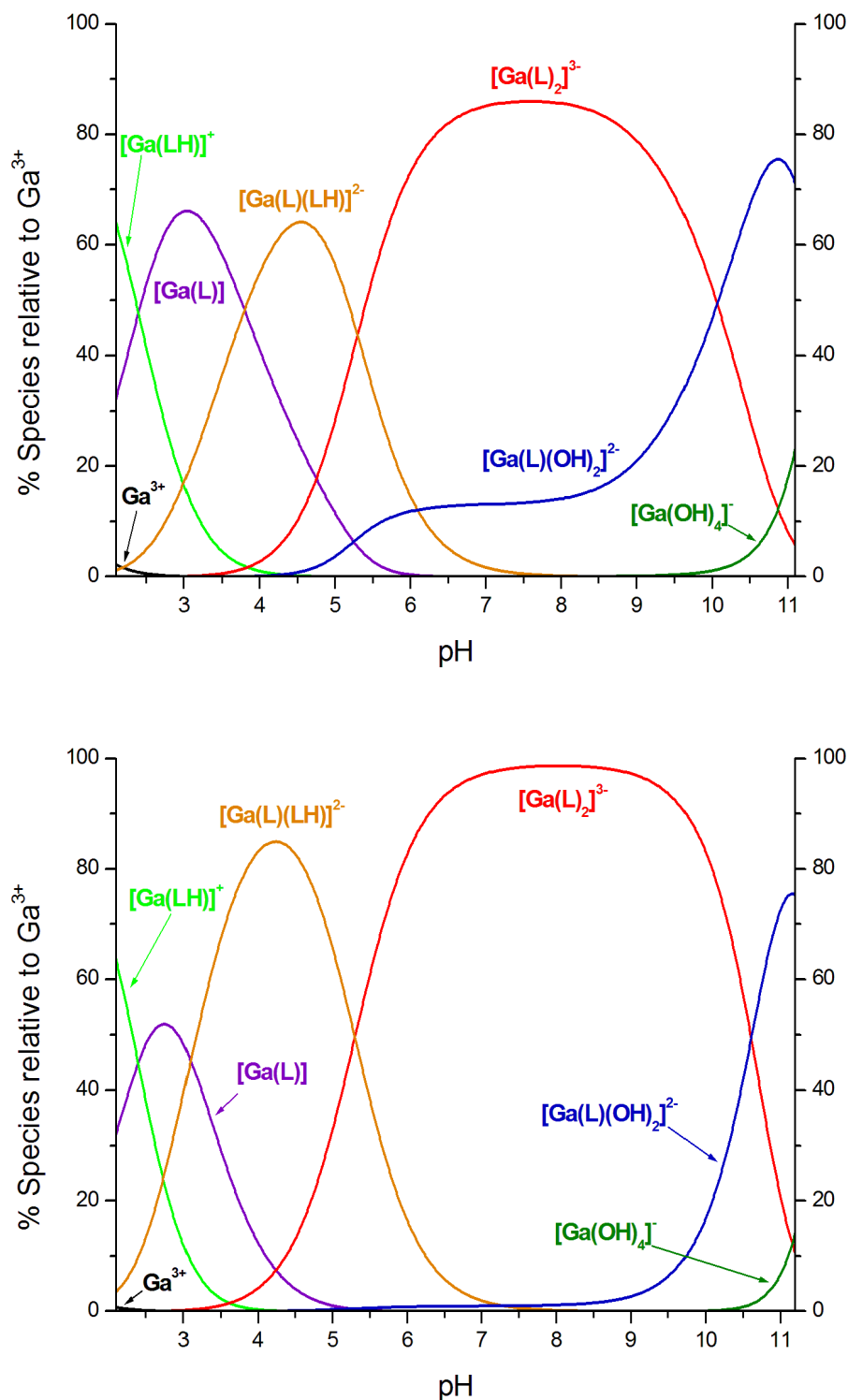


**Figure 9.8:** Species distribution diagrams as a function of pH for  $\text{Ga}^{3+}$  with the ligand MSA. Calculated for the continuous acidimetric titration performed with a 1:2 molar ratio (top) ( $[\text{Ga}^{3+}]_t = 0.50 \text{ mmol/L}$ ,  $[\text{L}]_t = 1.00 \text{ mmol/L}$ ) and 1:4 (bottom) ( $[\text{Ga}^{3+}]_t = 0.50 \text{ mmol/L}$ ,  $[\text{L}]_t = 2.00 \text{ mmol/L}$ ) in pure water,  $T = 298 \text{ K}$  and  $I = 0.1 \text{ mol/L KCl}$ . The species concentration were calculated from the equilibrium constants listed in **Table 9.11** (mean values from simultaneous evaluation of 6 titrations) with the program Hyss2006.

A very small second inflection at 0.5 equivalents (pH 5 – 4) can be assigned to the protonation of the  $[\text{Ga}(\text{L})_2]^{3-}$  complex to form  $[\text{Ga}(\text{L})(\text{LH})]^{2-}$  with a maximum concentration of 64% at pH 4.6. In acidic solution the  $[\text{Ga}(\text{L})]$  complex forms at pH 3.1 to a maximum concentration of 66%. At the end of the titration at pH 2.1 the protonated complex  $[\text{Ga}(\text{LH})]^+$  is dominant species with 63%, the  $[\text{Ga}(\text{L})]$  complex is present with 33% and the free  $\text{Ga}^{3+}$  ion with less than 5%. The species distribution shows that there is practically no free  $\text{Ga}^{3+}$  in acidic solution. However, there is 23%  $[\text{Ga}(\text{OH})_4]^-$  in alkaline solution at pH 11.1 with a known stability constants which was used as basis for the calculation of the stability constants of the  $\text{Ga}^{3+}$ -MSA system.

The titration curve in **Figure 9.7** of the 1:4 molar ratio has an inflection at 1 equivalent due to the excess ligand. Even though excess ligand was provided no species were found with more than two ligands per  $\text{Ga}^{3+}$  ion. The species distribution in **Figure 9.8** (bottom) for the 1:4 molar ratio is very similar to the 1:2 molar ratio. An exception is the formation of the  $[\text{Ga}(\text{L})(\text{OH})_2]^{2-}$  complex which appears at significant concentration in the titration range from pH 11.1 to 9 in contrast to the 1:2 molar ratio which shows significant concentrations of the  $[\text{Ga}(\text{L})(\text{OH})_2]^{2-}$  complex already in acidic solution (pH 11.1 – 5). Therefore, this complex is the main species at the beginning of the titration at pH 11.1 with 75% and the  $[\text{Ga}(\text{OH})_4]^-$  complex is present at this point with 14%.

In summary, we have been able to determine the stability constants of the  $\text{Ga}^{3+}$ -MSA system on the basis of the gallium (III) tetrahydroxo complex in pure water. Further  $\text{Ga}^{3+}$  hydroxo complexes do not appear in the species distribution. The fact that practically no free  $\text{Ga}^{3+}$  is present in acidic solution gives rise to the strong complexation of  $\text{Ga}^{3+}$  with MSA. The  $[\text{Ga}(\text{MSA})]$  complex has a  $\log\beta_{110} = 19.8(1)$  which is only 1.5 units smaller compared to the  $[\text{Fe}(\text{MSA})]$  with a  $\log\beta_{110} = 21.30(4)$ . Further the  $[\text{Ga}(\text{MSA})_2]^{3-}$  complex has a  $\log K_{120} = 14.0$  ( $\log K_{120} = [\text{ML}_2] / [\text{ML}] \times [\text{L}]$ ) in comparison to the  $[\text{Fe}(\text{MSA})_2]^{3-}$  complex with a  $\log K_{120} = 14.65$  <sup>[40]</sup>. As a result the  $\text{Fe}^{3+}$  complexes are somewhat more stable, yet the stability constants of the  $\text{Ga}^{3+}$  complexes are very close to them. Assumingly, the  $\text{Ga}^{3+}$  ion could be a potential competitor to  $\text{Fe}^{3+}$  for the complexation of the iron-chelating ligand MSA or deferasirox.

### 9.2.3 Complex formation of DSA with gallium (III) in pure water

The complex formation of the water soluble ligand DSA with  $\text{Ga}^{3+}$  was investigated. Alkaline samples prepared with potassium hydroxide for the acidimetric titrations showed absorption of  $\text{CO}_2$  and were difficult to evaluate. For this reason, the titrations were carried out alkalimetric to decrease errors in the titration experiments. The stability constants of the  $\text{Ga}^{3+}$ -DSA system were determined on the basis of the gallium (III) tetrahydroxo complex  $[\text{Ga}(\text{OH})_4]^-$  due to the strong complex formation. The titration conditions for the  $\text{Ga}^{3+}$ -DSA system are given in **Table 9.12**.

**Table 9.12:** Titration conditions for the potentiometric titration experiments of  $\text{Ga}^{3+}$  with DSA, given at  $T = 298 \text{ K}$ .

Conditions for the $\text{Ga}^{3+}$ -DSA titrations	
molar ratio of M:L	1:2
measuring method	potentiometric
method type	continuous
solvent	pure water
$[\text{M}]_t$	0.50 mmol/L
$[\text{L}]_t$	1.00 mmol/L
titration volume	50.0 mL
titrant	0.1 mol/L KOH
supporting electrolyte	0.1 mol/L KCl
electrode	Schott IoLine
$\text{p}K_w$	13.78
pH range	2.0 – 11.6
volume of data points	90
time for mixing process	600 s

Further, the titration experiments were evaluated simultaneously with the program Hyperquad2008. The gallium (III) hydroxo complexes were added to the model as constant values. The results of the evaluation are presented in **Table 9.13**.

**Table 9.13:** Mean values of the overall stability constants  $\log\beta_{xyz}$  <sup>[a]</sup> from potentiometric titrations of  $\text{Ga}^{3+}$  with DSA determined by simultaneous evaluation with Hyperquad2008 in pure water,  $T = 298 \text{ K}$  and  $I = 0.1 \text{ mol/L KCl}$ .

<b><math>\log\beta</math> values for the complexation of <math>\text{Ga}^{3+}</math>:DSA</b>	
titrations with a 1:2 molar ratio	
pH 2.0 – 11.6	
mean values by simultaneous evaluation of 7 titrations <sup>[b]</sup>	
$\sigma$ <sup>[c]</sup>	1.283
$\log\beta_{10-1}$ <sup>[d]</sup>	-2.91
$\log\beta_{10-2}$ <sup>[d]</sup>	-6.61
$\log\beta_{10-3}$ <sup>[d]</sup>	-11.01
$\log\beta_{10-4}$ <sup>[d]</sup>	-16.78
<b><math>\log\beta_{110}</math></b>	<b>21.68(6)</b>
<b><math>\log\beta_{120}</math></b>	<b>36.74(5)</b>
<b><math>\log\beta_{121}</math></b>	<b>40.7(2)</b>

<sup>[a]</sup> For the ligand L  $\log\beta_{xyz}$  is defined as:  $\beta_{xyz} = [M_xL_yH_z] \times [M]^{-x} \times [L]^{-y} \times [H]^{-z}$ .

<sup>[b]</sup> The titrations were evaluated simultaneously with the program Hyperquad2008. The deviations given in brackets correspond to the threefold standard deviation taken from Hyperquad2008.

<sup>[c]</sup> The  $\sigma$  value is taken from Hyperquad2008.

<sup>[d]</sup> The values of the gallium (III) hydroxo complexes were taken from Motekaitis and Martell and defined as constant values <sup>[143]</sup>.

The species model with the best possible fit ( $\sigma$  value of 1.283) comprehends a  $[\text{Ga}(\text{L})]^-$  (110), a  $[\text{Ga}(\text{L})_2]^{5-}$  (120) and a  $[\text{Ga}(\text{L})(\text{LH})]^{4-}$  (121) complex. The  $[\text{Ga}(\text{L})]^-$  complex has a high stability constant of  $\log\beta_{110} = 21.68(6)$ . The  $[\text{Ga}(\text{L})_2]^{5-}$  complex has an individual stability constant of  $\log K_{120} = 15.06$  ( $\log K_{120} = [\text{ML}_2] / [\text{ML}] \times [\text{L}]$ ) which gives rise to a very stable  $\text{Ga}^{3+}$ -DSA complex. The deprotonation constant of the 121 complex is quite acidic with an apparent  $\text{p}K_a = 4.0$ . In contrast to the  $\text{Ga}^{3+}$ -MSA system no mixed ligand and hydroxo complexes were found.

A very large pH range was chosen to ensure sufficient formation of  $[\text{Ga}(\text{OH})_4]^-$  in alkaline solution and to investigate if any free  $\text{Ga}^{3+}$  is still present in acidic solution. The titration curve of the  $\text{Ga}^{3+}$ -DSA system is depicted in **Figure 9.9** in comparison to the  $\text{p}K_a$  titration curve of the ligand DSA.

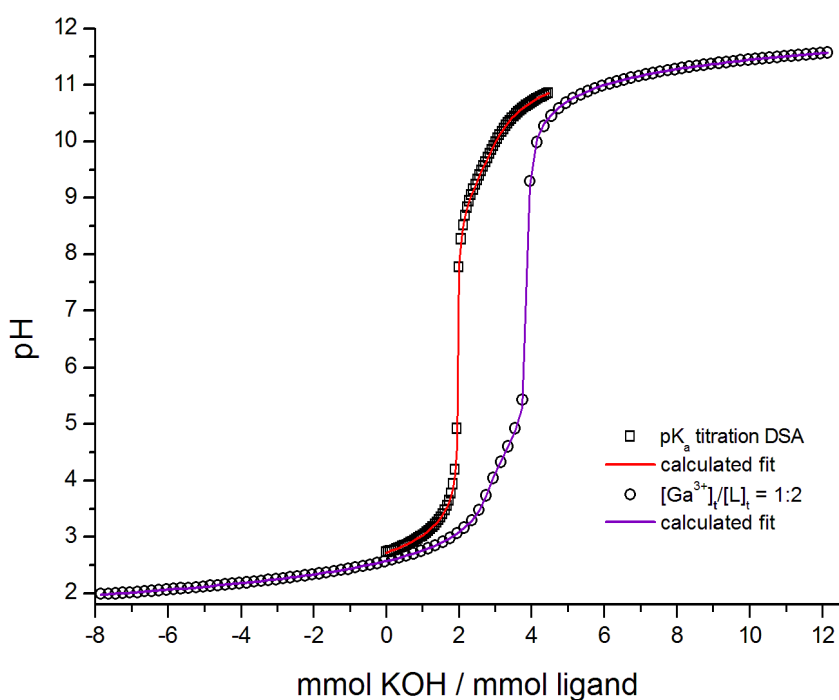


**Figure 9.9:** Potentiometric titration curves of the free ligand DSA and of  $\text{Ga}^{3+}$  with DSA with the molar ratio 1:2 ( $[\text{Ga}^{3+}]_t = 0.50 \text{ mmol/L}$ ,  $[\text{L}]_t = 1.00 \text{ mmol/L}$ ) in pure water,  $T = 298 \text{ K}$  and  $I = 0.1 \text{ mol/L KCl}$ . The open squares and circles represent experimental points and the fit (solid line) was calculated from the equilibrium constants with Hyperquad2008.

The  $\text{Ga}^{3+}$ -DSA titration curve has an obvious inflection at 4 equivalents and a small inflection at 3 equivalents. The small inflection can be assigned to the readily formed  $[\text{Ga}(\text{L})]^-$  complex in strong acidic solution which is present to

98% at pH 2.0, as illustrated in **Figure 9.10**. Only 2% free  $\text{Ga}^{3+}$  are present at the beginning of the titration at pH 2.0. The  $[\text{Ga}(\text{L})(\text{LH})]^{4-}$  complex reaches a maximum concentration of 10% at pH 4.4. From pH 5 to 11.6 the  $[\text{Ga}(\text{L})_2]^{5-}$  complex is the dominating species in solution. Its concentration reaches nearly 100% over a large pH range (about pH 6 – 10) resulting in the inflection at 4 equivalents. However, in alkaline solution (about pH > 10) the ligand DSA is exchanged by the hydroxide ions forming the  $[\text{Ga}(\text{OH})_4]^-$  complex which is present to 45% at the end of the titration (pH 11.6).

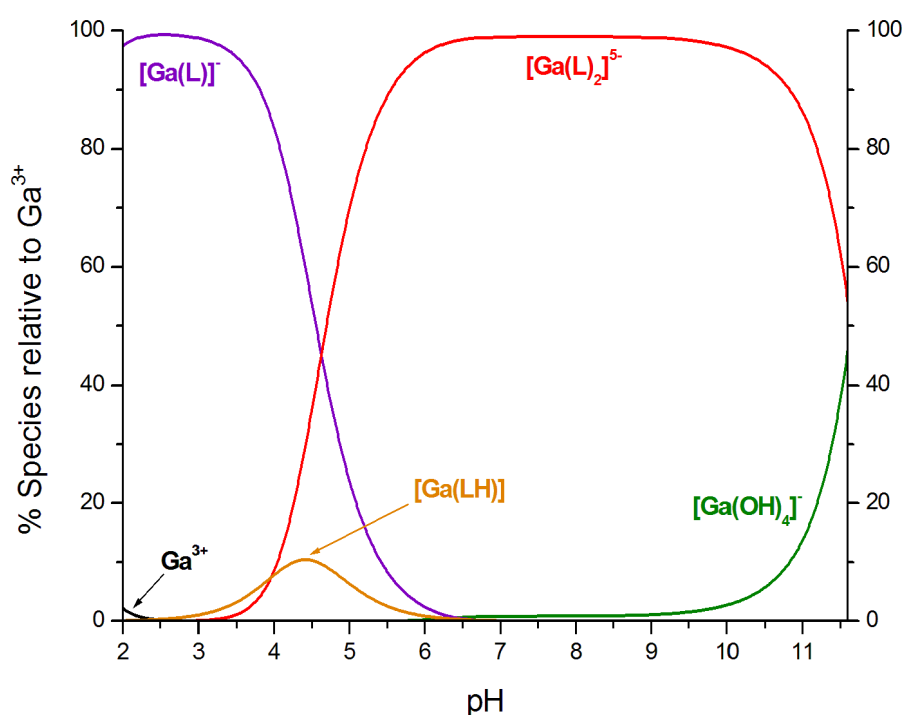


**Figure 9.10:** Species distribution diagram as a function of pH for  $\text{Ga}^{3+}$  with the ligand DSA. Calculated for the continuous potentiometric titration performed with a 1:2 molar ratio ( $[\text{Ga}^{3+}]_t = 0.50 \text{ mmol/L}$ ,  $[\text{L}]_t = 1.00 \text{ mmol/L}$ ) in pure water,  $T = 298 \text{ K}$  and  $I = 0.1 \text{ mol/L KCl}$ . The species concentration were calculated from the equilibrium constants listed in **Table 9.13** (mean values from simultaneous evaluation of 7 titrations) with the program Hyss2006.

The species distribution reveals a strong affinity of the ligand DSA to the  $\text{Ga}^{3+}$  ion with almost 100% complex formation  $[\text{Ga}(\text{DSA})]^-$  at the beginning of the titration. The complexation constants of the formed complexes could be determined in pure water by the known  $[\text{Ga}(\text{OH})_4]^-$  complex which is formed in alkaline solution from the  $[\text{Ga}(\text{DSA})_2]^{5-}$  complex.

### 9.2.4 Summary and discussion

The  $^{68}\text{Ga}^{3+}$  ion is a promising radionuclide used in complexes for PET imaging. The question arises whether the simultaneous administration of deferasirox during iron chelation therapy and a  $^{68}\text{Ga}^{3+}$  containing complex as radiopharmaceutical to a patient may cause interactions. The  $\text{Ga}^{3+}$  ion has very similar characteristics compared to the  $\text{Fe}^{3+}$  ion due to the half populated  $d^5$ -orbital of  $\text{Fe}^{3+}$  and the full populated  $d^{10}$ -orbital for  $\text{Ga}^{3+}$  and the similar ionic radius ( $\text{Ga}^{3+}$   $r = 0.620 \text{ \AA}$  (CN 6) <sup>[118]</sup> compared to  $\text{Fe}^{3+}$   $r = 0.645 \text{ \AA}$  (CN 6) <sup>[118]</sup>) which makes  $\text{Ga}^{3+}$  a possible competitive ion for deferasirox.

For this reason we investigated the complex formation of the iron-chelating ligand deferasirox and its water soluble derivatives MSA and DSA with the metal ion gallium (III) with potentiometric titration experiments. Indeed, first investigations with the ligand deferasirox in water/DMSO solution ( $x_{\text{DMSO}} = 0.20$ ) revealed a very strong affinity of  $\text{Ga}^{3+}$  to deferasirox. We observed almost 100% complex formation at the beginning of the titration. However, to be able to determine the stability constants with potentiometric titrations we need sufficient free metal ion at the beginning of the titration.

Fortunately,  $\text{Ga}^{3+}$  has the strong tendency to form hydroxo complexes in alkaline solution. On account of the known stability constants of these gallium (III) hydroxo complexes, mainly the  $[\text{Ga}(\text{OH})_4]^-$  complex, we are able to calculate the complex stability constants of the  $\text{Ga}^{3+}$ -ligand system. This method could not be applied to the water/DMSO titration evaluations since the gallium (III) hydroxo complex stability constants are not known in this medium. Additionally, the titrations were hampered by precipitate in the pH range between 3.5 and 4.5 which made it difficult to determine the stability constants. As a consequence, only some individual stability constants of the  $\text{Ga}^{3+}$ -deferasirox system were determined on the basis of the unknown  $[\text{Ga}(\text{LH})]^+$  deferasirox complex.

Of special interest was the individual stability constant of the  $[\text{Ga}(\text{L})_2]^{3-}$  complex with deferasirox in water/DMSO ( $x_{\text{DMSO}} = 0.20$ ,  $T = 298 \text{ K}$ ,  $I = 0.1 \text{ mol/L KCl}$ ) with a  $\log K_{120} = 14.8$  ( $\log K_{120} = [\text{ML}_2] / [\text{ML}] \times [\text{L}]$ ) <sup>[72]</sup>. This value reveals a strong affinity of the  $\text{Ga}^{3+}$  ion for the ligand deferasirox. In

comparison to the  $[\text{Fe}(\text{L})_2]^{3-}$  complex of the ligand deferasirox with a  $\log K_{120} = 15.23$  ( $\log K_{120} = [\text{ML}_2] / [\text{ML}] \times [\text{L}]$ ,  $x_{\text{DMSO}} = 0.20$ ,  $T = 298 \text{ K}$ ,  $I = 0.1 \text{ mol/L KNO}_3$ )<sup>[40]</sup> the affinity of deferasirox towards  $\text{Fe}^{3+}$  is still higher. The stability constants with this determination method in water/DMSO solution ( $x_{\text{DMSO}} = 0.20$ ) should be regarded as roughly determined due to the difficulties with precipitation and the evaluation without the knowledge of neither the stability constant of the readily formed  $[\text{Ga}(\text{LH})]^+$  complex nor the gallium (III) tetrahydroxo complex  $[\text{Ga}(\text{OH})_4]^-$ .

Even though deferasirox is generally poorly soluble in pure water, it is sufficiently soluble in strong alkaline solution. Consequently, a successful determination of the overall stability constant  $\log \beta_{120} = 33.8(1)$  of the  $[\text{Ga}(\text{L})_2]^{3-}$  complex in pure water was achieved. This constant was calculated on the basis of the well-known stability constant of the  $[\text{Ga}(\text{OH})_4]^-$  complex in pure water.

On account of the low solubility of deferasirox in pure water and the difficulties of the determination in water/DMSO solution we investigated the water soluble derivatives MSA and DSA with the metal ion  $\text{Ga}^{3+}$ . With the help of these investigations we have the opportunity to study this type of ligand system without precipitation in pure water. By means of comparison to deferasirox we can bring insight into the complex behaviour of the  $\text{Ga}^{3+}$ -deferasirox system.

Further, we wanted to study the possibility of metal ion exchange reactions between a  $\text{Ga}^{3+}$  radiopharmaceutical and the water soluble derivatives. A common ligand which forms strong complexes with  $\text{Ga}^{3+}$  is DOTA.  $\text{Ga}^{3+}$ -DOTA complexes are often used as compounds for new radiopharmaceuticals for PET imaging.

The stability constants of the investigated ligands deferasirox, MSA and DSA with  $\text{Ga}^{3+}$  from this work and the  $\text{Ga}^{3+}$ -DOTA system from Clarke and Martell<sup>[136]</sup> are summarised in **Table 9.14**. All stability constants were determined at  $T = 298 \text{ K}$  and  $I = 0.1 \text{ mol/L KCl}$  for comparison. Gallium (III) forms a  $[\text{Ga}(\text{DOTA-H})]$  (111) complex with  $\log \beta_{111} = 25.33$  and a  $[\text{Ga}(\text{DOTA})]^-$  (110) complex with  $\log \beta_{110} = 21.33(5)$  which were both taken into account.

**Table 9.14:** Overall stability constants  $\log\beta_{xyz}$  <sup>[a]</sup> of  $\text{Ga}^{3+}$  complexes with the listed ligands (T = 298 K, I = 0.1 mol/L KCl).

<b>Overall stability constants <math>\log\beta_{xyz}</math> <sup>[a]</sup> of <math>\text{Ga}^{3+}</math> complexes</b>				
	deferasirox	MSA	DSA	DOTA <sup>[b]</sup>
solvent	pure water	pure water	pure water	pure water
$\log\beta_{110}$	-	<b>19.8(1)</b>	<b>21.68(6)</b>	<b>21.33(5)</b>
$\log\beta_{111}$	-	22.2(3)	-	<b>25.33</b>
$\log\beta_{120}$	<b>33.8(1)</b>	<b>33.8(3)</b>	<b>36.74(5)</b>	-
$\log\beta_{121}$	-	39.1(3)	40.7(2)	-
$\log\beta_{11-2}$	-	9.3(3)	-	-

<sup>[a]</sup> For the ligand L  $\log\beta_{xyz}$  is defined as:  $\beta_{xyz} = [\text{M}_x\text{L}_y\text{H}_z] \times [\text{M}]^{-x} \times [\text{L}]^{-y} \times [\text{H}]^{-z}$ .

<sup>[b]</sup> Values taken from Clarke and Martell <sup>[136]</sup>.

The only determined overall stability constants of the  $\text{Ga}^{3+}$ -deferasirox system in pure water is for the  $[\text{Ga}(\text{L})_2]^{3-}$  (120) complex which has the same value  $\log\beta_{120} = 33.8(1)$  as the overall stability constant for the  $[\text{Ga}(\text{MSA})_2]^{3-}$  complex of the  $\text{Ga}^{3+}$ -MSA system  $\log\beta_{120} = 33.8(3)$ . This is rather uncommon, yet we do not know the value for the overall stability constant of the  $[\text{Ga}(\text{L})]$  complex for deferasirox so we cannot calculate the individual stability constant  $\log K_{120}$  ( $\log K_{120} = [\text{ML}_2] / [\text{ML}] \times [\text{L}]$ ) for deferasirox. The individual stability constant of the  $[\text{Ga}(\text{L})_2]^{3-}$  complex of deferasirox would be necessary for a significant comparison to the corresponding complex of MSA or DSA.

The stability constants of the  $\text{Ga}^{3+}$ -MSA system are somewhat smaller than those of the  $\text{Ga}^{3+}$ -DSA system. The individual stability constant of the  $[\text{Ga}(\text{MSA})_2]^{3-}$  complex is  $\log K_{120} = 14.0$  ( $\log K_{120} = [\text{ML}_2] / [\text{ML}] \times [\text{L}]$ ) which is about one unit smaller than the corresponding  $[\text{Ga}(\text{DSA})_2]^{5-}$  complex with  $\log K_{120} = 15.06$ . To display the species in solution of each one of the iron-chelating ligands MSA and DSA with DOTA the species distribution diagrams in **Figure 9.11** were calculated.

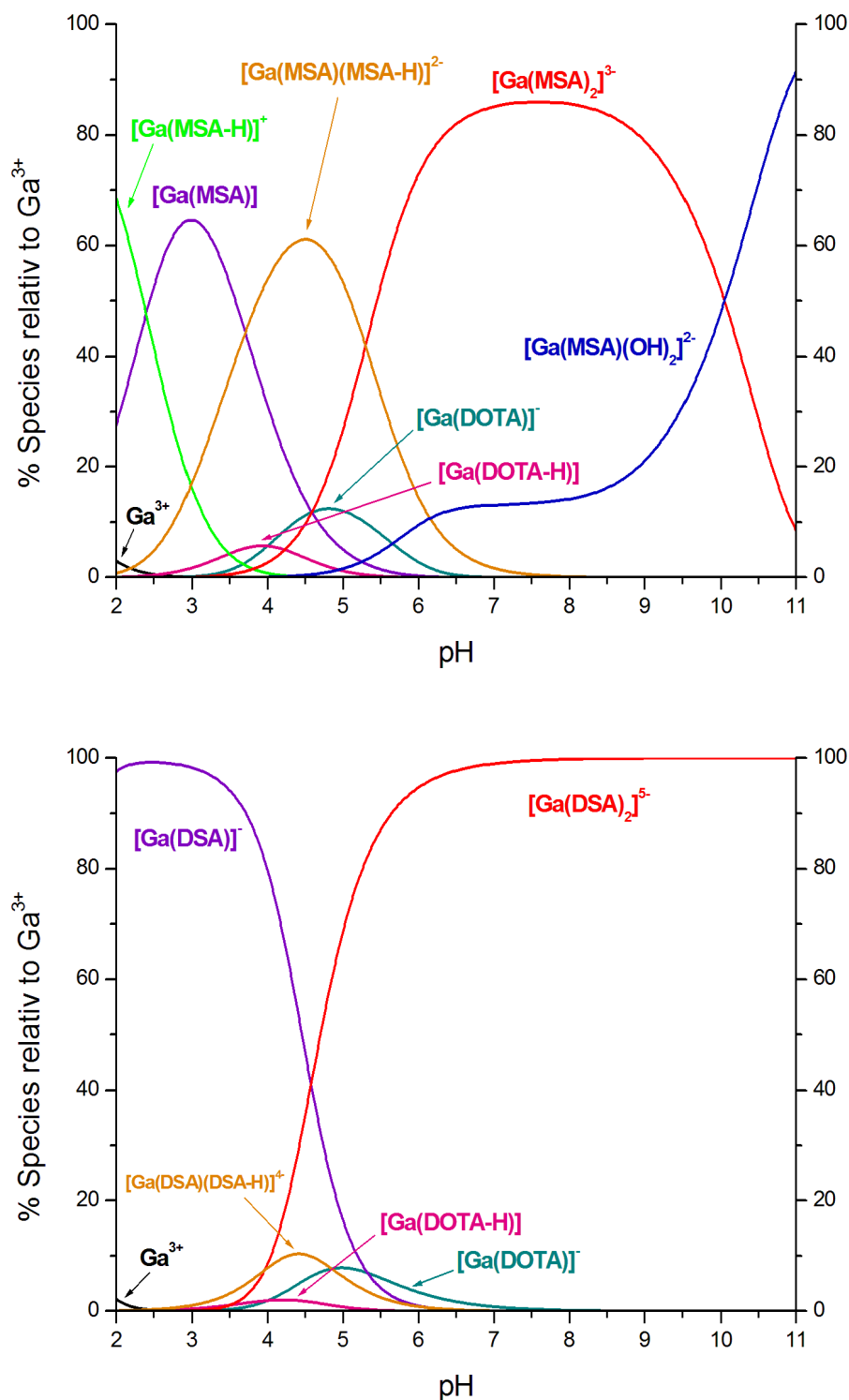


**Figure 9.11:** Species distribution diagram as a function of pH for  $Ga^{3+}$  with the ligand MSA and DOTA (top:  $[Ga^{3+}]_t = 0.50$  mmol/L,  $[DOTA]_t = 0.50$  mmol/L and  $[MSA]_t = 1.00$  mmol/L) and  $Ga^{3+}$  with the ligand DSA and DOTA (bottom:  $[Ga^{3+}]_t = 0.50$  mmol/L,  $[DOTA]_t = 0.50$  mmol/L and  $[DSA]_t = 1.00$  mmol/L) in pure water,  $T = 298$  K and  $I = 0.1$  mol/L KCl. The species concentrations were calculated from the equilibrium constants listed in **Table 9.14** with the program Hyss2006.

By comparing the  $\text{Ga}^{3+}$  110 complexes of MSA and DSA to the  $[\text{Ga}(\text{DOTA})]^-$  complex with a  $\log\beta_{110} = 21.33(5)$ , we find the order  $[\text{Ga}(\text{DSA})]^- > [\text{Ga}(\text{DOTA})]^- > [\text{Ga}(\text{MSA})]$ . Yet the values only differ by 0.35 units DSA and DOTA and by 1.53 MSA to DOTA.

In the diagram for the  $\text{Ga}^{3+}$ -MSA system (**Figure 9.11** top) the complex  $[\text{Ga}(\text{DOTA-H})]$  reaches a maximum concentration of 6% at pH 3.9 and the  $[\text{Ga}(\text{DOTA})]^-$  complex of 13% at pH 4.8. For the  $\text{Ga}^{3+}$ -DSA system (**Figure 9.11** bottom) these complexes reach even less with 2% at pH 4.2 for  $[\text{Ga}(\text{DOTA-H})]$  and 8% at pH 5.0 for  $[\text{Ga}(\text{DOTA})]^-$ . At the physiologically important pH 7.4 the  $[\text{Ga}(\text{MSA})_2]^{3-}$  complex is the dominating species with 86% next to the  $[\text{Ga}(\text{MSA})(\text{OH})_2]^{2-}$  complex with 14%. For the  $\text{Ga}^{3+}$ -DSA system the  $[\text{Ga}(\text{DSA})_2]^{5-}$  is the sole species with 100% at pH 7.4. The species diagrams of the  $\text{Ga}^{3+}$ -MSA and the  $\text{Ga}^{3+}$ -DSA system have in common that throughout the pH range the MSA and DSA containing species are clearly dominating.

We can conclude that if the ligand MSA or DSA is present in solution next to the free ligand DOTA and the metal ion  $\text{Ga}^{3+}$  is added, the ligands MSA/or DSA clearly complex the majority of the  $\text{Ga}^{3+}$  ion. Further, at physiological pH 7.4 the  $\text{Ga}^{3+}$ -DOTA complexes do not appear at all and the 120 complex of  $\text{Ga}^{3+}$ -MSA and  $\text{Ga}^{3+}$ -DSA is the dominating species. The ligands MSA and DSA are very good models for the ligand deferasirox and therefore we may draw conclusions from these ligands to deferasirox.

As a consequence, these results give room for the assumption that the simultaneous presence of  $\text{Ga}^{3+}$ -DOTA and the free ligand deferasirox, respectively MSA and DSA, could result in a ligand exchange reaction forming  $\text{Ga}^{3+}$ -deferasirox complexes. Presumably, the  $[\text{Ga}(\text{L})_2]^{3-}$  complex of deferasirox will be favoured at physiological pH 7.4. Hence, the toxic ligand DOTA will be free to form complexes with other biometal ions. Patients treated with deferasirox suffer from elevated levels of unbound  $\text{Fe}^{3+}$  in the body. The ligand DOTA also forms very stable complexes with the  $\text{Fe}^{3+}$  ion  $\log\beta_{110} = 29.4(1)$  <sup>[136]</sup>. Accordingly, a new question arises: if both deferasirox and DOTA are present in solution which ligand will preferably form complexes with the  $\text{Fe}^{3+}$  biometal ion?

To answer this question we need to take the stability constants of DOTA and the iron-chelating ligands with the  $\text{Fe}^{3+}$  ion into consideration. These overall stability constants for the  $\text{Fe}^{3+}$ -complexes of the iron-chelating ligands deferasirox, MSA and DSA as well as the stability constants of DOTA with  $\text{Fe}^{3+}$  are given in **Table 9.15**.

**Table 9.15:** Overall stability constants  $\log\beta_{xyz}$  <sup>[a]</sup> of  $\text{Fe}^{3+}$  complexes with the listed ligands (T = 298 K, I = 0.1 mol/L KCl).

Overall stability constants $\log\beta_{xyz}$ <sup>[a]</sup> of $\text{Fe}^{3+}$ complexes				
	Deferasirox <sup>[b]</sup>	MSA <sup>[c]</sup>	DSA <sup>[d]</sup>	DOTA <sup>[e]</sup>
solvent	pure water	pure water	pure water	pure water
$\log\beta_{110}$	<b>22.0</b>	<b>21.30(4)</b>	<b>24.54(4)</b>	<b>29.4(1)</b>
$\log\beta_{111}$	24.0	-	-	<b>32.63</b>
$\log\beta_{120}$	<b>36.9</b>	<b>35.95(5)</b>	<b>39.50(2)</b>	-
$\log\beta_{121}$	41.2	40.89(3)	43.67(3)	-
$\log\beta_{122}$	43.4	-	-	-

<sup>[a]</sup> For the ligand L  $\log\beta_{xyz}$  is defined as:  $\beta_{xyz} = [\text{M}_x\text{L}_y\text{H}_z] \times [\text{M}]^{-x} \times [\text{L}]^{-y} \times [\text{H}]^{-z}$ .

<sup>[b]</sup> Values extrapolated for  $x_{\text{DMSO}} = 0.00$  taken from Steinhauser <sup>[40]</sup>.

<sup>[c]</sup> Values measured by potentiometric titration taken from Steinhauser <sup>[40]</sup>.

<sup>[d]</sup> Values from this thesis section 7.2.1 and 7.2.2.

<sup>[e]</sup> Values taken from Clarke and Martell <sup>[136]</sup>.

These stability constants were used for the calculation of species distributions with the iron-chelating ligands deferasirox or DSA and DOTA in the presence of  $\text{Fe}^{3+}$  which are illustrated in **Figure 9.12**. The calculation of the species distribution diagram for the ligand deferasirox and DOTA with  $\text{Fe}^{3+}$  in pure water (**Figure 9.12**, top) is based on the stability constants of the  $\text{Fe}^{3+}$ -deferasirox system determined by extrapolation to  $x_{\text{DMSO}} = 0.00$  which has been reported previously <sup>[39-40]</sup>. The  $[\text{Fe}(\text{DOTA}-\text{H})]$  and  $[\text{Fe}(\text{DOTA})]^-$  complexes dominate clearly in acidic solution.

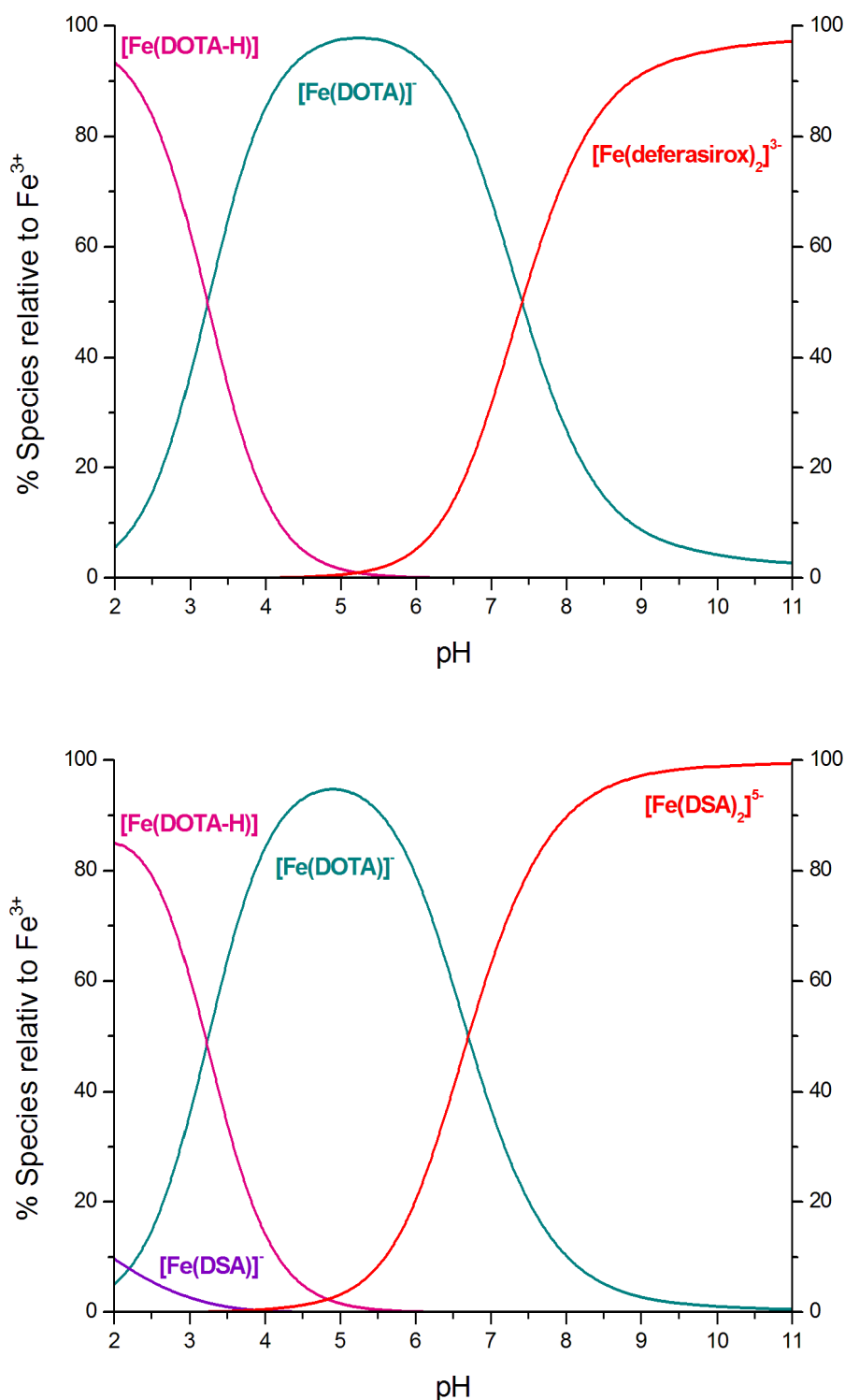


**Figure 9.12:** Species distribution diagram as a function of pH for  $\text{Fe}^{3+}$  with the ligand deferasirox and DOTA (top:  $[\text{Fe}^{3+}]_t = 0.50$  mmol/L,  $[\text{DOTA}]_t = 0.50$  mmol/L and  $[\text{deferasirox}]_t = 1.00$  mmol/L) and  $\text{Fe}^{3+}$  with the ligand DSA and DOTA (bottom:  $[\text{Fe}^{3+}]_t = 0.50$  mmol/L,  $[\text{DOTA}]_t = 0.50$  mmol/L and  $[\text{DSA}]_t = 1.00$  mmol/L) in pure water,  $T = 298$  K and  $I = 0.1$  mol/L KCl. The species concentrations were calculated from the equilibrium constants listed in **Table 9.15** with the program Hyss2006.

The  $\text{Fe}^{3+}$ -deferasirox complexes do not appear until about pH 5. At this pH the  $[\text{Fe}(\text{deferasirox})_2]^{3-}$  complex starts to form and a ligand exchange reaction is observed. The  $\text{Fe}^{3+}$  central ion which is bound to nearly 100% as  $[\text{Fe}(\text{DOTA})]^-$  complex at pH 5 starts to exchange the ligand DOTA by two ligands deferasirox forming the  $[\text{Fe}(\text{deferasirox})_2]^{3-}$  complex. At physiological pH 7.4 the exchange has taken place to 50% so that both the  $[\text{Fe}(\text{DOTA})]^-$  complex and the  $[\text{Fe}(\text{deferasirox})_2]^{3-}$  complex are present to equal amounts.

In conclusion, we suppose that if DOTA is set free by preferred complex formation of  $\text{Ga}^{3+}$  with deferasirox, DOTA will be a competitive ligand to deferasirox for the complexation of unbound  $\text{Fe}^{3+}$ .

In contrast to the  $\text{Fe}^{3+}$ -deferasirox system the species distribution diagram of DSA and DOTA with  $\text{Fe}^{3+}$  (**Figure 9.12**, bottom) shows 10% of the monocomplex  $[\text{Fe}(\text{DSA})]^-$  at pH 2. Yet, the  $[\text{Fe}(\text{DOTA-H})]$  and  $[\text{Fe}(\text{DOTA})]^-$  complexes are still clearly dominant species in acidic solution. At physiological pH 7.4 the  $[\text{Fe}(\text{DSA})_2]^{5-}$  is the dominating species with 77% and only 23% of the  $[\text{Fe}(\text{DOTA})]^-$  complex is present. This observation reveals the somewhat stronger complex behaviour of DSA with  $\text{Fe}^{3+}$  to deferasirox.

We conclude, the iron-chelators deferasirox, MSA and DSA could cause ligand exchange reactions with radiopharmaceuticals containing  $\text{Ga}^{3+}$ -complexes such as  $\text{Ga}^{3+}$ -DOTA. As a consequence, the iron-chelator is blocked by  $\text{Ga}^{3+}$  and free unbound  $\text{Fe}^{3+}$  might be complexed by DOTA. Depending on the concentrations of both deferasirox and DOTA in vivo they will be competing ligands for the  $\text{Fe}^{3+}$  ion. A simultaneous administration of the iron-chelator deferasirox and a  $^{68}\text{Ga}^{3+}$ -containing radiopharmaceutical should consider the ligand exchange reaction which might influence the targeting of PET imaging. Also chelating therapy with deferasirox might be influenced by free DOTA forming complexes with unbound  $\text{Fe}^{3+}$ .

On account of the high affinity of  $\text{Ga}^{3+}$  to deferasirox, perhaps deferasirox could function as a promising  $^{68}\text{Ga}^{3+}$ -chelator for future radiopharmaceuticals. Accordingly, the Novartis Pharma AG [CH] has patented deferasirox and the  $[\text{Ga}(\text{L})_2]^{3-}$  complex of deferasirox as “gallium uptake enhancers” for diagnostic purposes such as scintigraphy [144].

## 10 Linear free energy relation and discussion

In the past the complex behaviour of the iron-chelating ligand deferasirox and its water soluble derivative MSA has been studied with trivalent ( $\text{Fe}^{3+}$ ,  $\text{Al}^{3+}$ ) and divalent ( $\text{Cu}^{2+}$ ,  $\text{Zn}^{2+}$ ,  $\text{Mg}^{2+}$ ,  $\text{Ca}^{2+}$ ) biometal ions [37, 40]. The main difficulty of the investigations with potentiometric and spectrophotometric titrations was the poor solubility of deferasirox in pure water (0.4 g/L, pH 7.4 [38]). Hence, titration experiments were carried out in water/DMSO solution. Yet, still some titrations experiments with deferasirox especially with the divalent biometal ions  $\text{Cu}^{2+}$  and  $\text{Zn}^{2+}$  [37] and with the trivalent  $\text{Ga}^{3+}$  and  $\text{Gd}^{3+}$  ion, as shown in this work, were hampered by precipitation. Therefore, the studies on the complexation of deferasirox with these metal ions were hampered.

We developed ligands with the same structure as deferasirox only varying in the functional groups at the peripheral benzocarboxylic acid to enhance water solubility. Yet, the coordination site of the ligands is still identical to deferasirox preferring the tridentate meridional coordination mode. First the ligand MSA with one sulfonic acid instead of the carboxylic acid in deferasirox was designed and investigated [37, 40]. It was just soluble enough (0.7 g/L pure water [37]) to perform titration experiments in pure water, however still precipitation occurred during titration experiments with the metal ions  $\text{Cu}^{2+}$  and  $\text{Zn}^{2+}$ . Whereas, titrations with the ions  $\text{Ga}^{3+}$  and  $\text{Gd}^{3+}$ , in this work, showed no precipitation and investigations were successful.

To further enhance water solubility and design a ligand with sufficient water solubility to keep all complexes during titrations in solution we added a second sulfonic acid to the peripheral phenyl ring. The resulting ligand was DSA, with its two sulfonic acids it is sufficiently soluble in pure water (8 g/L) even at high concentrations. With the ligand DSA complexation with the divalent metal ions  $\text{Cu}^{2+}$ ,  $\text{Ni}^{2+}$ ,  $\text{Zn}^{2+}$  and  $\text{Cd}^{2+}$  could be investigated in detail without precipitation. Further, the trivalent metal ions  $\text{Fe}^{3+}$ ,  $\text{Al}^{3+}$ ,  $\text{Ga}^{3+}$  and  $\text{Gd}^{3+}$  have been successfully studied without difficulties as well as the electrolytes  $\text{Mg}^{2+}$  and  $\text{Ca}^{2+}$ .

By way of comparison, the complexes formed by deferasirox and DSA are in the majority of cases very similar. Usually, mononuclear complexes of

the composition  $[M(L)]^{2-}$  (110), with one ligand and one metal ion, are formed before a second ligand is bound to form bis-complexes of the composition  $[M(L)_2]^{2-}$  (120). Protonated forms of both mono-complexes and bis-complexes are observed for deferasirox and DSA depending on the type of central metal ion. These protonated complexes can differ in coordination geometry influenced by the different  $pK_a$  value of the carboxylic acid functional group of deferasirox  $pK_{a,1} = 3.65(6)$  (extrapolated to pure water,  $T = 298\text{ K}$ ,  $I = 0.1\text{ KCl}$ , see 8.1.1) in contrast to the strong acidity of the sulfonic acids, respectively the  $pK_{a,2} = 1.33(8)$  (pure water,  $T = 298\text{ K}$ ,  $I = 0.1\text{ KCl}$ , see section 7.1.1) of the triazole nitrogen of DSA. The sulfonic acids are not protonated in the investigated pH range (pH 2 - 11) and the  $pK_{a,2}$  of DSA, is also too acidic for a protonation in DSA-complexes. Therefore, DSA complexes are most likely protonated at the phenolate group coupled with a bidentate coordination mode of DSA. That is contrary to deferasirox which can form protonated complexes with a tridentate or a bidentate coordination mode with the proton found at the carboxylic acid or hydroxyphenyl ring. Nevertheless, the coordination site of both ligands is the ONO-site of the ligand.

The main complexes present in almost all investigations of deferasirox and DSA with biometal ions are the  $[M(L)]^{2-}$  and  $[M(L)_2]^{2-}$  complexes due to the favoured tridentate meridional coordination mode. These two types of complexes are especially suitable for a correlation by a linear free energy relation. Linear free energy relations for stability constants of metal-ligand complexes have been described and summarised very early by Irving and Rossotti <sup>[145]</sup>. They report on linear relationships between the stability constants of several ligands L and P, with a series of metal ions, by plotting  $\log K_{ML}$  as a function of  $\log K_{MP}$ . The linear relationships are especially promising if the ligands compared are very similar in stereochemistry, coordination properties and  $pK_a$  values. The ligands deferasirox and DSA meet these requirements very well. The  $pK_a$  values relevant for the complexation of the 110 and 120 complexes are primarily those of the hydroxyphenyl groups which have only minor differences.

Accordingly, we can correlate the stability constants of deferasirox to DSA for those complexes that were investigated without difficulties in form of a linear free energy relation. Of special interest is a linear free energy relation

between deferasirox and DSA with stability constants in pure water solution. Since stability constants of deferasirox cannot be measured in pure water, we needed to estimate them by a linear extrapolation. The results of the extrapolation to  $x_{\text{DMSO}} = 0.00$  of the stability constants of deferasirox with the metal ions  $\text{Al}^{3+}$ ,  $\text{Mg}^{2+}$  and  $\text{Ca}^{2+}$  were discussed in section 8. The main focus is on the 110 and 120 complexes. Yet a 120 complex for  $\text{Ca}^{2+}$  with deferasirox and DSA was not found. However, the 120 complex of the  $\text{Ga}^{3+}$ -deferasirox and  $\text{Ga}^{3+}$ -DSA system has been determined previously by acidimetric and alkalimetric titration in pure water (see section 9.2.1 and 9.2.3) and is added to the linear free energy relation of the 120 complexes. The values applied for the linear free energy relations are given in **Table 10.1**.

**Table 10.1:** Summary of the  $\log\beta_{xyz}$  <sup>[a]</sup> values of deferasirox and DSA with selected metal ions used for the linear free energy relation for pure water, T = 298 K and I = 0.1 mol/L KCl.

<b><math>\log\beta_{xyz}</math> values for the linear free energy relation</b>				
	<b>deferasirox</b>		<b>DSA</b>	
<b><math>\text{M}^{z+}</math></b>	<b><math>\log\beta_{110}</math></b>	<b><math>\log\beta_{120}</math></b>	<b><math>\log\beta_{110}</math> <sup>[e]</sup></b>	<b><math>\log\beta_{120}</math> <sup>[e]</sup></b>
<b><math>\text{Fe}^{3+}</math></b>	22.0 <sup>[b]</sup>	36.9 <sup>[b]</sup>	23.54(4)	39.50(2)
<b><math>\text{Al}^{3+}</math></b>	15.9(1) <sup>[c]</sup>	29.0(5) <sup>[c]</sup>	18.77(1)	32.45(1)
<b><math>\text{Ga}^{3+}</math></b>	-	33.8(1) <sup>[d]</sup>	-	36.74(5)
<b><math>\text{Mg}^{2+}</math></b>	5.31(8) <sup>[c]</sup>	7.4(6) <sup>[c]</sup>	6.74(2)	9.1(2)
<b><math>\text{Ca}^{2+}</math></b>	3.28(7) <sup>[c]</sup>	-	4.53(6)	-

<sup>[a]</sup> For the ligand L  $\log\beta_{xyz}$  is defined as:  $\beta_{xyz} = [\text{M}_x\text{L}_y\text{H}_z] \times [\text{M}]^{-x} \times [\text{L}]^{-y} \times [\text{H}]^{-z}$ .

<sup>[b]</sup> Values extrapolated for  $x_{\text{DMSO}} = 0.00$ , taken from S. Steihauser <sup>[40]</sup>.

<sup>[c]</sup> Values extrapolated for  $x_{\text{DMSO}} = 0.00$ , this thesis section 8.

<sup>[d]</sup> Value taken from the Novartis Pharma AG Final Report <sup>[72]</sup>.

<sup>[e]</sup> Values determined in this thesis.

The linear free energy relations according to Irving and Rossotti <sup>[145]</sup> are illustrated in **Figure 10.1**.

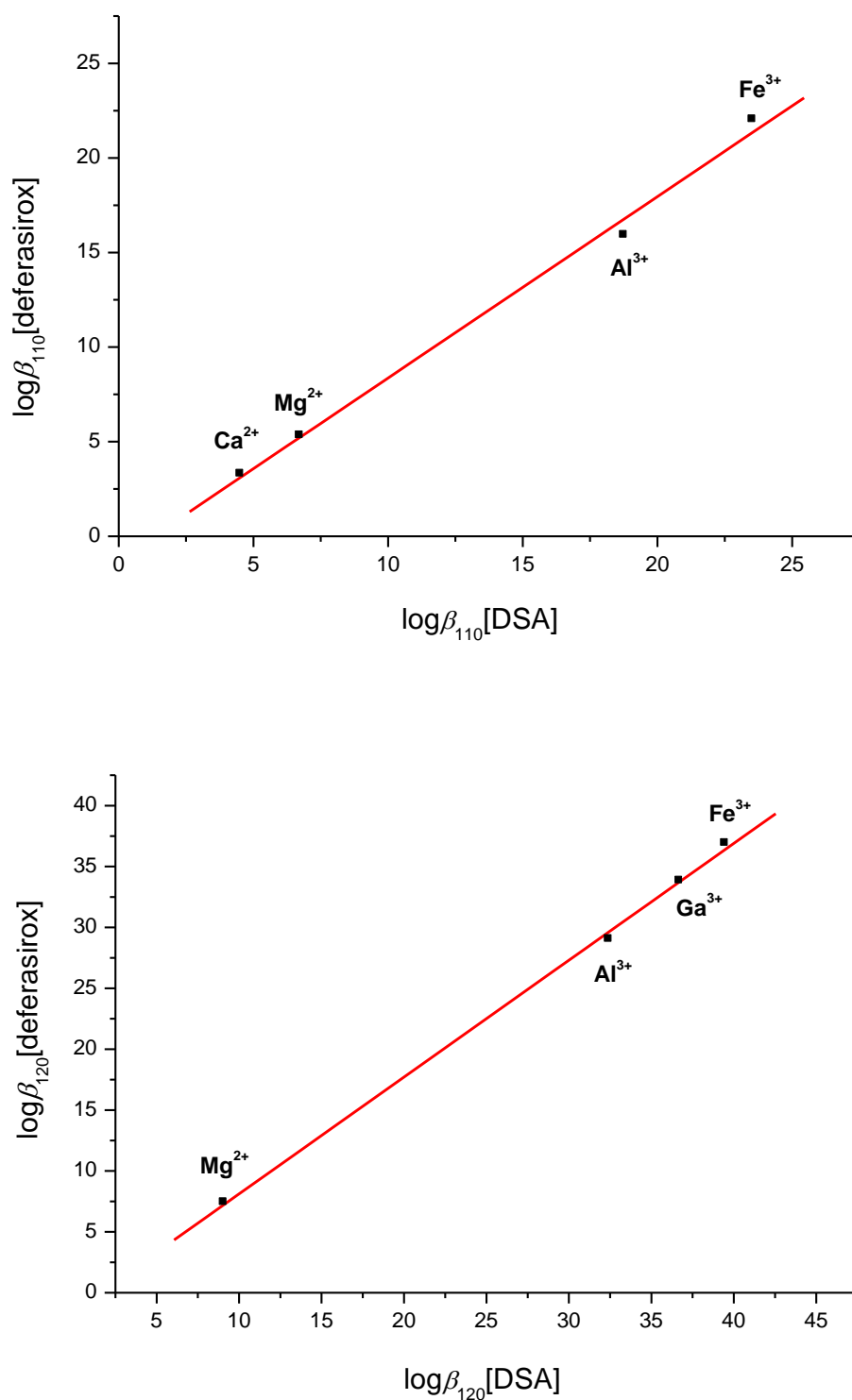


**Figure 10.1:** Linear free energy relation obtained by plotting  $\log \beta_{110}$  (top), respectively  $\log \beta_{120}$  (bottom), for complexes of deferasirox as a function of the corresponding  $\log \beta$  for complexes of DSA with selected metal ions in pure water,  $T = 298 \text{ K}$  and  $I = 0.1 \text{ mol/L KCl}$ . Values applied for the linear relationships are given in **Table 10.1**.

As the diagram in **Figure 10.1** shows, the two ligands are well correlated in form of the linear free energy relation for the 110 complex ( $R = 0.99741$ ) and the 120 complex ( $R = 0.99936$ ). The correlation is described by the calculated linear regression equations in **Table 10.2**. For each linear relationship four metal ions were applied. The linear relationship of the 110 complexes consists of the metal ions  $\text{Fe}^{3+}$ ,  $\text{Al}^{3+}$ ,  $\text{Mg}^{2+}$  and  $\text{Ca}^{2+}$ . Attributed to the absence of a 120 complex with the  $\text{Ca}^{2+}$  ion for both ligands the linear free energy relation is calculated with the 120 complex of the  $\text{Ga}^{3+}$  ion in addition to  $\text{Fe}^{3+}$ ,  $\text{Al}^{3+}$  and  $\text{Mg}^{3+}$ . Unfortunately, only the 120 complex of the  $\text{Ga}^{3+}$ -deferasirox system was determined in pure water, so that we cannot apply the  $\text{Ga}^{3+}$  ion for the linear relation of the 110 complex.

**Table 10.2:** Linear regression equations calculated for the linear free energy relations of deferasirox and DSA illustrated in **Figure 10.1** for pure water,  $T = 298 \text{ K}$  and  $I = 0.1 \text{ mol/L KCl}$ .

<b>linear free energy relation between deferasirox and DSA</b>	
<b>R</b> <sup>[a]</sup>	<b>linear regression equation</b> <sup>[b]</sup>
0.99741	$\log\beta_{110} [\text{deferasirox}] = 0.96(5) \times \log\beta_{110} [\text{DSA}] - 1.2(8)$
0.99936	$\log\beta_{120} [\text{deferasirox}] = 0.96(2) \times \log\beta_{120} [\text{DSA}] - 1.5(8)$

<sup>[a]</sup> R is the regression coefficient taken from Origin 6.0G.

<sup>[b]</sup> Linear regression equation was taken from the program Origin 6.0G.

This correlation may now be used to estimate values of stability constants of deferasirox with biometal ions that cannot be determined directly in pure water. As a result we have calculated the overall stability constants  $\log\beta_{110}$  and  $\log\beta_{120}$  for deferasirox in pure water from the determined corresponding complexes with DSA discussed in this work. The measured overall stability constants of DSA with the metal ions  $\text{M}^{z+}$  and the calculated values for deferasirox are presented in **Table 10.3**.

**Table 10.3:** Estimation of the overall stability constants  $\log\beta_{xyz}$  <sup>[a]</sup> of deferasirox with the metal ions  $M^{z+}$  by calculation from the corresponding overall stability constants of DSA with the linear regression equations of the linear free energy relation (**Table 10.2**). Conditions for the stability constants are pure water, T = 298 K and I = 0.1 mol/L KCl.

estimated $\log\beta_{xyz}$ <sup>[a]</sup> values for deferasirox in pure water				
	deferasirox		DSA	
$M^{z+}$	$\log\beta_{110}$ <sup>[b]</sup>	$\log\beta_{120}$ <sup>[b]</sup>	$\log\beta_{110}$ <sup>[d]</sup>	$\log\beta_{120}$ <sup>[d]</sup>
$Ga^{3+}$	19.6	33.8(1) <sup>[c]</sup>	21.68(6)	36.74(5)
$Gd^{3+}$	10.3	18.3	12.01(3)	20.61(2)
$Cu^{2+}$	16.0	19.4	17.93(2)	21.8(2)
$Ni^{2+}$	10.1	15.1	11.76(9)	17.24(6)
$Zn^{2+}$	9.4	13.3	11.00(1)	15.37(6)
$Cd^{2+}$	6.4	10.3	7.87(1)	12.24(3)

<sup>[a]</sup> For the ligand L  $\log\beta_{xyz}$  is defined as:  $\beta_{xyz} = [M_xL_yH_z] \times [M]^{-x} \times [L]^{-y} \times [H]^{-z}$ .

<sup>[b]</sup> Calculated values with the linear regression equations in **Table 10.2**, except  $\log\beta_{120} Ga^{3+}$ .

<sup>[c]</sup> Value taken from the Novartis Pharma AG Final Report <sup>[72]</sup>.

<sup>[d]</sup> Values determined in this thesis.

In general, the linear free energy relations illustrate that the stability constants of DSA are always somewhat higher than those of deferasirox. This can be attributed to the higher negative charge of the DSA complexes due to the higher charge of the fully deprotonated ligand  $L^{4-}$  in contrast to the fully deprotonated ligand  $L^{3-}$  deferasirox.

By means of comparison the stability constants  $\log\beta_{110}$  and  $\log\beta_{120}$  of the trivalent metal ions are in the order  $Fe^{3+} > Ga^{3+} > Al^{3+} \gg Gd^{3+}$  for both ligands. The individual stability constants for these  $[M(\text{deferasirox})_2]^{3-}$  complexes are  $\log K_{120}$  14.9 > 14.2 > 13.1 >> 8.0 ( $\log K_{120} = [ML_2] / [ML] \times [L]$ ). This  $Ga^{3+}$  complex is only 0.7 units smaller than the  $Fe^{3+}$  complex making  $Ga^{3+}$  a strong competitor for complex formation with the ligand deferasirox. This issue deserves special attention when administration of  $Ga^{3+}$  containing radiopharmaceuticals is intended for PET imaging to a patient during iron-chelation therapy with de-

ferasirox. The much lower stability constant of the  $Gd^{3+}$ -deferasirox system makes a simultaneous administration of a  $Gd^{3+}$  containing MRI contrast agent and deferasirox rather unproblematic with regard to ligand exchange reactions. The important complex at physiological pH 7.4 is usually the  $[M(L)_2]^{2-}$  complex which is present to > 95% for  $Fe^{3+}$ ,  $Ga^{3+}$  and  $Al^{3+}$  with DSA. The  $Gd^{3+}$  ion with the weakest stability in this order is found to about 75% as  $[M(L)]^{2-}$  complex and only 15%  $[M(L)_2]^{2-}$  complex at pH 7.4. The corresponding deferasirox complexes will be present at similar high concentrations.

The divalent metal ions form  $[M(L)]^{2-}$  complexes with both ligands with decreasing stability in the order  $Cu^{2+} > Ni^{2+} > Zn^{2+} > Cd^{2+} > Mg^{2+} > Ca^{2+}$ . This order is concordant with our expectations with regard to ligand-field stabilisation energy of the transition metal ions and ionic size.

The  $[Cu(L)]^{2-}$  complexes of both deferasirox and DSA most probably adopt a tridentate meridional coordination which allows the octahedral coordination geometry to distort according to the Jahn-Teller effect which is typical for the  $d^9$  electronic configuration. Through the Jahn-Teller effect the  $Cu^{2+}$  complexes gain on stability compared to the  $d^8$  electronic configuration of the  $[Ni(L)]^{2-}$  complex which is stabilised itself by ligand-field stabilisation energy. The tridentate meridional coordination mode is supported by two crystal structures obtained of the  $[Cu(DSA)(HCO_3)]^{3-}$  complex (see section 7.3.3).

In contrast,  $Zn^{2+}$  and  $Cd^{2+}$  do not experience ligand-field stabilisation energy due to the fully populated  $d^{10}$  electronic state resulting in lower values for the overall stability constants compared to the  $Cu^{2+}$  and  $Ni^{2+}$  ion complexes. The metal ion  $Cd^{2+}$  ( $\log\beta_{110} = 6.4$ ) forms a somewhat less stable 110 complex than  $Zn^{2+}$  ( $\log\beta_{110} = 9.4$ ) with the iron-chelating ligand deferasirox which is to a high extent attributed to the larger ionic radius of  $Cd^{2+}$  (CN: 6,  $r = 0.95 \text{ \AA}$  [118]) compared to  $Zn^{2+}$  (CN: 6,  $r = 0.740 \text{ \AA}$  [118]) causing higher strain [40] to the tridentate coordination mode of the iron-chelators deferasirox and DSA. However we need to note that possible chlorocomplexes of  $Cd^{2+}$ , influencing the stability constants, have not been taken into account.

In general,  $Mg^{2+}$  and  $Ca^{2+}$  ions are not dedicated to forming stable complexes with the ligands deferasirox [37-38] and DSA. The smaller  $Mg^{2+}$  ion

(CN: 6,  $r = 0.720 \text{ \AA}$  [118]) fits better into the ONO-coordination site and forms stronger complexes with the iron-chelators than the much larger  $\text{Ca}^{2+}$  ion (CN: 6,  $r = 1.00 \text{ \AA}$  [118]) [40]. The complex formation of deferasirox and DSA with these electrolytes is rather weak preferably forming the  $[\text{M}(\text{L})]^{2-}$  complex at elevated  $\text{pH} > 7$ .

The order of the individual stability constants  $\log K_{120}$  ( $\log K_{120} = [\text{ML}_2] / [\text{ML}] \times [\text{L}]$ ) of the  $[\text{M}(\text{L})_2]^{2-}$  complexes of both iron-chelating ligands deferasirox and DSA with the divalent metal ions  $\text{Ni}^{2+} > \text{Zn}^{2+} = \text{Cd}^{2+} > \text{Cu}^{2+} > \text{Mg}^{2+}$  deviates from the order of the  $[\text{M}(\text{L})]^{2-}$  complexes discussed above. Unfortunately, no bis-complexes were determined of deferasirox and DSA with the metal ion  $\text{Ca}^{2+}$ . The individual stability constant of the  $\text{Cu}^{2+}$  complex with deferasirox  $\log K_{120} = 3.4$  ( $\log K_{120} = [\text{ML}_2] / [\text{ML}] \times [\text{L}]$ ) is much smaller than the corresponding  $\text{Ni}^{2+}$  complex with  $\log K_{120} = 5.0$  and even somewhat smaller than the  $\text{Zn}^{2+}$  and  $\text{Cd}^{2+}$  complexes with both  $\log K_{120} = 3.9$ . Only the  $\text{Mg}^{2+}$  ion forms a weaker  $[\text{M}(\text{L})_2]^{2-}$  complex ( $\log K_{120} = 2.1$ ). This observation can be explained by the Jahn-Teller effect on the  $[\text{Cu}(\text{L})_2]^{2-}$  complex. Two ligands deferasirox (or DSA) in the bis-complex presumably adopt the tridentate meridional coordination mode and all four positions of the octahedron are occupied. If the octahedron follows the Jahn-Teller effect stretching the two axial bonds the ligand will also need to stretch. In this  $\text{Cu}^{2+}$  bis-complex the ligand deferasirox (or DSA) is either strained by the Jahn-Teller effect or the Jahn-Teller effect is suppressed by the ligand geometry. In either case it is obvious that the  $[\text{Cu}(\text{L})_2]^{2-}$  complex is clearly not favoured resulting in a low formation constant. The  $\text{Ni}^{2+}$ -deferasirox and -DSA systems are not distorted by the Jahn-Teller effect and accordingly the 120 complex is much more stable.

Interestingly, the two transition metal ions  $\text{Zn}^{2+}$  and  $\text{Cd}^{2+}$  with a  $d^{10}$  electronic configuration adopt the same value for the individual stability constant  $\log K_{120} = 3.9$  ( $T = 298 \text{ K}$ ,  $I = 0.1 \text{ mol/L KCl}$ ) of the  $[\text{M}(\text{L})_2]^{4-}$  complex of deferasirox. In contrast, the stability constant of the  $[\text{Cd}(\text{L})]^-$  complex of the  $\text{Cd}^{2+}$ -deferasirox system is 3.0 units smaller than the corresponding  $\text{Zn}^{2+}$ -deferasirox complex, the  $[\text{Cd}(\text{DSA})]^{2-}$  complex differs by 3.13 units from the  $[\text{Zn}(\text{DSA})]^{2-}$  complex. The determination of the stability constants of the  $\text{Cd}^{2+}$ -deferasirox system are based on the ones determined with the  $\text{Cd}^{2+}$ -DSA system which

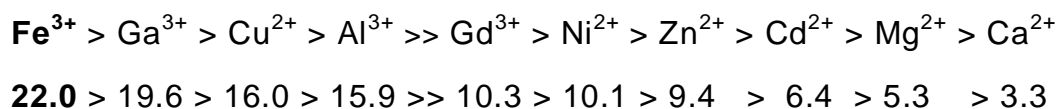
were measured in a potassium chloride medium ( $T = 298 \text{ K}$ ,  $I = 0.1 \text{ mol/L KCl}$ ). As pointed out in section 7.6 the metal ion  $\text{Cd}^{2+}$  has a stronger tendency to form chlorocomplexes ( $[\text{CdCl}]^+$  complex with  $\log K_{110} = 1.52(7)$ ,  $T = 298 \text{ K}$ ,  $I = 0.1 \text{ mol/L}$ )<sup>[55]</sup>) than for example the  $\text{Zn}^{2+}$  ion ( $[\text{ZnCl}]^+$  complex with  $\log K_{110} = 0.4(1)$ ,  $T = 298 \text{ K}$ ,  $I = 0.1 \text{ mol/L}$ )<sup>[55]</sup>). For the evaluation of the  $\text{Cd}^{2+}$ -DSA titrations the chlorocomplexes were not taken into account. Which means that possible individual formation constants  $\log K_{xyzq}$  of mixed  $\text{Cd}^{2+}$ -chloro-DSA complexes  $[\text{Cd}_x(\text{L})_y(\text{H})_z(\text{Cl})_q]$  could be included in the overall stability constants  $\log \beta_{110}$  and  $\log \beta_{120}$ . The formation constant of the  $[\text{Cd}(\text{DSA})]^{2-}$  complex is 3.13 units smaller in comparison to the  $[\text{Zn}(\text{DSA})]^{2-}$  complex. This order is in accordance with our expectations. In contrast, the stability constant of the  $[\text{Cd}(\text{DSA})_2]^{6-}$  complex  $\log K_{120} = 4.37$  ( $\log K_{120} = [\text{ML}_2] / [\text{ML}] \times [\text{L}]$ ) is obviously elevated in contrast to the corresponding  $[\text{Zn}(\text{DSA})_2]^{6-}$  complex with the same  $\log K_{120} = 4.37$  value. This result is rather unusual and may be clarified by titration experiments in a chloride free medium.

In conclusion, possible mixed DSA and chloro-complexes are assumingly responsible for the elevated  $\log \beta_{120} = 4.37$  value of the  $[\text{Cd}(\text{DSA})_2]^{6-}$  complex. Since the  $\text{Cd}^{2+}$ -deferasirox system is based on the  $\text{Cd}^{2+}$ -DSA system the elevated values calculated for  $\text{Cd}^{2+}$ -deferasirox can be explained by the same origin. For future investigations with the metal ion  $\text{Cd}^{2+}$  the stability constants of the  $\text{Cd}^{2+}$ -DSA system should be measured in a chloride free supporting electrolyte such as  $\text{KNO}_3$  to avoid chlorocomplexes.

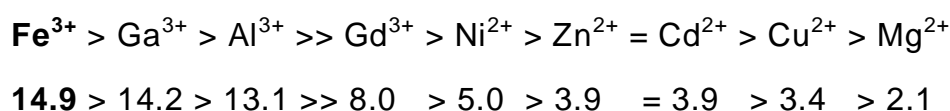
The ligand deferasirox is the active component in the pharmaceutical Exjade<sup>®</sup> applied for the treatment of iron overload. Our investigations have led to the order of the stability constants of deferasirox with the trivalent and divalent metal ions presented in **Scheme 10.1**. The order confirms that the highest stability constants of deferasirox have been found with the metal ion  $\text{Fe}^{3+}$ .

**deferasirox**

$$\log K_{110} = \log ([ML] / [M] \times [L]):$$



$$\log K_{120} = \log ([ML_2] / [ML] \times [L]):$$



**Scheme 10.1:** Descending order of the metal ion complex stability constants  $[M(L)]^{z-}$  or  $[M(L)_2]^{z-}$  of deferasirox in pure water,  $T = 298 \text{ K}$  and  $I = 0.1 \text{ mol/L KCl}$ . Values were estimated either by extrapolation for  $x_{\text{DMSO}} = 0.00$  or by calculation from the linear free energy relation based on the DSA stability constants.

However, the stability constants  $\log K_{110}$  and  $\log K_{120}$  do not reveal much about the effectiveness of the ligand deferasirox binding  $\text{Fe}^{3+}$  in contrast to the other metal ions at physiological pH 7.4. A suitable standard for comparing the affinity of a ligand for a metal ion is the pM value <sup>[146]</sup>. The pM value describes the concentration of free  $[M(\text{H}_2\text{O})_6]^{z+}$  in a solution with a total metal ion concentration  $[M]_t = 1.0 \text{ } \mu\text{mol/L}$  and a total ligand concentration  $[L]_t = 10.0 \text{ } \mu\text{mol/L}$  at the physiologically important pH 7.4. The higher the pM value the less free  $M^{z+}$  is in solution and the higher is the affinity of the ligand to forming complexes with the specific metal ion. The pM values for the ligand deferasirox and DSA with the investigated trivalent and divalent metal ions, calculated with the determined stability constants of all complexes, are given in **Table 10.4**.

**Table 10.4:** Calculated pM <sup>[a]</sup> values for the ligand deferasirox and DSA for pure water, pH = 7.4, [M]<sub>t</sub> = 1.0 μmol/L and [L]<sub>t</sub> = 10.0 μmol/L. Calculations were performed with the program Hyss2006 <sup>[147]</sup>.

estimated pM <sup>[a]</sup> values		
M <sup>z+</sup>	pM for deferasirox	pM for DSA <sup>[d]</sup>
Fe <sup>3+</sup>	22.2 <sup>[b]</sup> ; 23.5 <sup>[c]</sup>	23.6
Ga <sup>3+</sup>	19.1 <sup>[e]</sup>	20.8
Al <sup>3+</sup>	14.3 <sup>[f]</sup>	16.5
Gd <sup>3+</sup>	6.3 <sup>[e]</sup>	7.1
Cu <sup>2+</sup>	11.7 <sup>[e]</sup>	13.0
Ni <sup>2+</sup>	6.2 <sup>[e]</sup>	7.0
Zn <sup>2+</sup>	6.1 <sup>[e]</sup>	6.4
Cd <sup>2+</sup>	6.0 <sup>[e]</sup>	6.0
Mg <sup>2+</sup>	6.0 <sup>[f]</sup>	6.0
Ca <sup>2+</sup>	6.0 <sup>[f]</sup>	6.0

<sup>[a]</sup> Definition pM = -log[M<sup>z+</sup>].

<sup>[b]</sup> The pM values were calculated from the stability constants in **Table 9.15** taken from S. Steinhauser <sup>[40]</sup> and the pK<sub>a</sub> values in **Table 8.2**.

<sup>[c]</sup> Value taken from S. Steinhauser <sup>[148]</sup>. Calculated with stability constants for pure water (see also **Table 9.15**) and pK<sub>a,1</sub> = 3.7(1), pK<sub>a,2</sub> = 8.80(1) and pK<sub>a,3</sub> = 10.61(1) from S. Steinhauser <sup>[40]</sup>.

<sup>[d]</sup> The pM values were calculated from the stability constants and pK<sub>a</sub> values from this thesis.

<sup>[e]</sup> The pM values were calculated from the stability constants in **Table 10.3** and the pK<sub>a</sub> values in **Table 8.2**.

<sup>[f]</sup> The pM values were calculated from the stability constants in **Table 10.1** and the pK<sub>a</sub> values in **Table 8.2**.

The main advantage of the comparison by pM value is that all complexes are taken into account not just one complex as in **Scheme 10.1**. As we expected the pFe value is the highest pM value for both ligands deferasirox and DSA. This value shows the strong affinity of the ligand deferasirox towards the metal ion Fe<sup>3+</sup> even at low concentrations. The pFe = 22.2 is calculated with

the  $pK_a$  values for deferasirox determined in this thesis (**Table 8.2**) and the stability constants for pure water determined by extrapolation from S. Steinhauser<sup>[40]</sup>. The previously reported  $pFe = 23.5$  has been calculated by the same stability constants from S. Steinhauser<sup>[40]</sup> but with the previously in pure water determined  $pK_a$  values also from S. Steinhauser<sup>[40]</sup>. In comparison, the  $pM$  values of DSA are somewhat higher than those of deferasirox which is presumably attributed to the higher negative charge of the ligand DSA. The  $pM$  values are also strongly dependent on the  $pK_a$  values of the ligand which have been considered in the calculation. The  $pGa$ ,  $pAl$  and  $pCu$  values are also quite high, yet not as high as the  $pFe$ . A  $pM$  value of 6 for example calculated for  $Cd^{2+}$ ,  $Mg^{2+}$  and  $Ca^{2+}$  reveals that no complex has been formed at all. Other  $pM$  values somewhat higher than the value 6 such as  $Gd^{3+}$ ,  $Ni^{2+}$  and  $Zn^{2+}$  show only little complex formation.

Further, our study aimed at investigating the complex behaviour towards divalent transition metal ions in particular essential trace elements such as  $Cu^{2+}$  and  $Zn^{2+}$ . The formation of polymeric structures has first been reported by Ryabukhin for the  $Cu^{2+}$ ,  $Ni^{2+}$  and  $Co^{2+}$  complexes of the 1N-phenyl derivative of deferasirox<sup>[41]</sup>. Further, Liu and Hider<sup>[149]</sup> have applied the tendency of the 1N-phenyl derivative to form polymers on the iron-chelator deferasirox and claim it has a high affinity to  $Zn^{2+}$ . Owing to precipitation during titration experiments of  $Cu^{2+}$  and  $Zn^{2+}$  with deferasirox this assertion has not been clarified. Our titration experiments of the ligand DSA with  $Cu^{2+}$  and  $Zn^{2+}$  were not hampered by precipitation so that the complex formation was elucidated with different molar ratios in pure water.

The titration experiments with DSA and the divalent metal ions  $Cu^{2+}$ ,  $Zn^{2+}$  and  $Cd^{2+}$  gave rise to hydroxo-bridged dinuclear complexes of the composition  $[M_2(DSA)_2(OH)]^{5-}$  and  $[M_2(DSA)_2(OH)_2]^{6-}$  next to the well-known mononuclear complexes with one central metal ion. The divalent metal ion  $Ni^{2+}$  prefers a phenoxo-bridged  $[M_2(DSA)_2]^{4-}$  and a hydroxo-bridged  $[M_2(DSA)_2(OH)]^{5-}$  complex. These complexes are presumably aggregation compounds of the mononuclear complexes. A suggestion is a tridentate coordination mode of the ligand DSA with one or two hydroxo-bridges, respectively phenoxo-bridges, connecting two monomeric ligand entities. These complexes do not show any ten-

dency to form polymeric structures. Most of these complexes appear in alkaline solution and are, if present at all at physiological pH 7.4, only minor species. The dominant species in DSA solutions with the divalent metal ions  $\text{Cu}^{2+}$  and  $\text{Zn}^{2+}$  at pH 7.4 is the  $[\text{M}(\text{DSA})]^{2-}$  complex with a concentration  $> 95\%$ . An exception is the  $\text{Ni}^{2+}$ -DSA system where at pH 7.4 the  $[\text{Ni}(\text{DSA})]^{2-}$  complex appears with a concentration of  $\approx 50\%$  and the  $[\text{Ni}_2(\text{DSA})_2]^{4-}$  complex with  $\approx 45\%$ . The  $\text{Cd}^{2+}$ -DSA system only has little complex formation of mono-complexes at pH 7.4 and  $> 80\%$  free  $\text{Cd}^{2+}$  ion. The species models found with the best calculated fit for the simultaneous evaluation of the titrations with different molar ratios all show only mononuclear and dinuclear complexes. The crystal structures from an alkaline solution of  $\text{Cu}^{2+}$ -DSA also confirm the favoured tridentate coordination of the ligand DSA in the  $[\text{Cu}(\text{DSA})]^{2-}$  complex entity.

However, it needs to be mentioned that some individual titrations of the  $\text{Cu}^{2+}$ -DSA system and the  $\text{Zn}^{2+}$ -DSA system could be evaluated with a dinuclear  $[\text{Cu}_2(\text{DSA})]$  or  $[\text{Zn}_2(\text{DSA})]$  complex. This type of complex affords a bidentate coordination mode of the ligand DSA and might be a prerequisite for polymeric structures. Since these dinuclear  $[\text{Cu}_2(\text{DSA})]$  or  $[\text{Zn}_2(\text{DSA})]$  complexes could not be calculated from the simultaneous evaluations they were not taken into account for the final species models. Despite the above, we need to note that we cannot exclude the formation of a  $[\text{Cu}_2(\text{DSA})]$  or  $[\text{Zn}_2(\text{DSA})]$  complex in solution. The investigations of a frozen solution of the  $\text{Cu}^{2+}$ -DSA system at pH 2.7 with EPR spectroscopy revealed an additional half field signal assigned to the forbidden transition  $\Delta m_s = \pm 2$ . This might be evidence for a  $\text{Cu}^{2+}$ - $\text{Cu}^{2+}$  interaction as expected for the  $[\text{Cu}_2(\text{DSA})]$  complex.

The conclusion we can draw from the  $\text{Cu}^{2+}$ -DSA investigations for the  $\text{Cu}^{2+}$ -deferasirox system is that only indirect evidence for polymeric structures was found. This confirms the results of the EPR spectroscopic investigations of the green precipitate from  $\text{Cu}^{2+}$ -deferasirox titrations. Freshly precipitated solid showed a mononuclear structure in the EPR spectrum which we suggest results from the uncharged  $[\text{Cu}(\text{LH})]$  complex of deferasirox. It is not unlikely that this mononuclear uncharged complex exists over a large pH range (precipitate was observed from pH 2 – 12.5 water/DMSO  $x_{\text{DMSO}} = 0.20$ ) and finally dissolves in alkaline solution by forming the bis-complex, which is less stable due

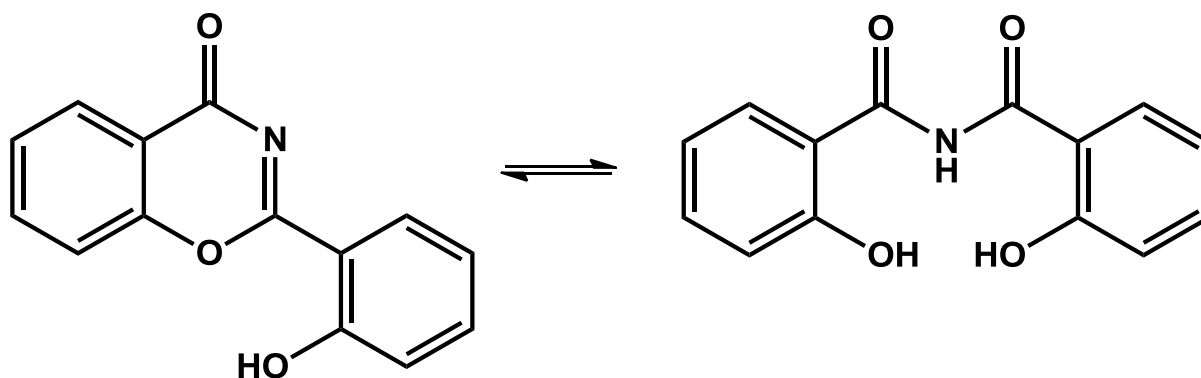
to the Jahn-Teller effect. However, evidence for a change in the structure, perhaps to a polymer, was found when the spectra of an altered probe (two months old) of the solid were recorded. Concluding, we have found little evidence for polymeric structures. The majority of our investigations on the  $M^{2+}$ -DSA/-deferasirox systems confirm the formation of only mononuclear or hydroxo-/phenoxo-bridged dinuclear complexes.

Our investigations show that the iron-chelating ligand deferasirox has the highest pFe value. Additionally, the investigations with divalent transition metal ions could not confirm the formation of polymeric structures in solution, which does not mean they do not exist. Some evidence for the possible existence of polymeric structure cannot be denied. Whereas it seems, as if the impact of polymeric structures on the complex behaviour of deferasirox with metal ions is rather negligible.

## 11 Experimental Section

### 11.1 Ligand synthesis

#### 11.1.1 Synthesis of 2-(2-hydroxyphenyl)-benzo-4*H*-[1,3]-oxazin-4-one



Salicylic acid (24.90 g, 0.18 mol) and salicylamide (20.90 g, 0.15 mol) were dissolved in 30 mL xylene (an isomeric mixture) with 1.5 mL pyridine under reflux (oil bath temperature 160°C). Over a period of 4 h, thionyl chloride (23.7 mL, 0.33 mol;  $\rho_{25^\circ\text{C}} = 1.631 \text{ g/cm}^3$ ) was added slowly under reflux to the vigorously stirred mixture. During the addition an evolution of sulphur dioxide and hydrochloric acid was observed. After completion of adding the thionyl chloride the reaction mixture was stirred for another 30 min. While the solution cooled to ambient temperature the product started to crystallize. The obtained solid was filtered and suspended in a mixture of 60 mL ethanol and 1.5 mL acetic acid. The suspension was shortly refluxed (at an oil bath temperature of 40°C) and allowed to cool to ambient temperature. The received yellow coloured precipitate had been filtered and recrystallized from 70 mL 2-methoxyethanol to give bright yellow needles of 2-(2-hydroxyphenyl)-benzo-4*H*-[1,3]-oxazin-4-one, yielding 17.59 g (73.53 mmol; 49% referring to salicylamide).

Characterisation:

**<sup>1</sup>H-NMR (D<sub>6</sub>-DMSO, TMS):**

2-(2-hydroxyphenyl)-benzo-4*H*-[1,3]-oxazin-4-one

$\delta$  (ppm) = 7.06 - 7.11 (m, 2H); 7.59 - 7.65 (m, 2H); 7.79 (d, 1H, <sup>3</sup>J = 8.3 Hz);  
7.94 (dt, 1H, <sup>3</sup>J = 8.3 Hz, <sup>4</sup>J = 1.7 Hz); 8.07 (dd, 1H, <sup>3</sup>J = 7.8 Hz, <sup>4</sup>J = 1.7 Hz);  
8.20 (dd, 1H, <sup>3</sup>J = 8.1 Hz, <sup>4</sup>J = 1.7 Hz)

**<sup>13</sup>C-NMR (D<sub>6</sub>-DMSO, TMS):**

2-(2-hydroxyphenyl)-benzo-4*H*-[1,3]-oxazin-4-one

$\delta$  (ppm) = 111.39; 117.41; 117.76; 117.91; 119.51; 126.70; 127.13; 128.92;  
135.94; 135.65; 153.81; 161.79; 163.38; 164.75

**<sup>1</sup>H-NMR (D<sub>6</sub>-DMSO, TMS):**

2-hydroxy-*N*-(2-hydroxybenzoyl)-benzamide

$\delta$  (ppm) = 6.98 (t, 2H, <sup>3</sup>J = 7.8 Hz); 7.02 (d, 2H, <sup>3</sup>J = 8.3 Hz); 7.46 (dt, 2H,  
<sup>3</sup>J = 8.3 Hz, <sup>4</sup>J = 1.7 Hz); 7.84 (dd, 2H, <sup>3</sup>J = 7.8 Hz, <sup>4</sup>J = 1.8 Hz)

**<sup>13</sup>C-NMR (D<sub>6</sub>-DMSO, TMS):**

2-hydroxy-*N*-(2-hydroxybenzoyl)-benzamide

$\delta$  (ppm) = 117.00; 118.85; 119.59; 130.56; 134.20; 156.82; 164.46

**Elemental analysis:**

of a mixture of 2-(2-hydroxyphenyl)-benzo-4*H*-[1,3]-oxazin-4-one and  
2-hydroxy-*N*-(2-hydroxybenzoyl)-benzamide

M [C<sub>14</sub>H<sub>9</sub>NO<sub>3</sub>] = 239.23 g/mol

% calculated: C: 70.29; H: 3.80; N: 5.86

% found: C: 69.51; H: 3.86; N: 5.90

**ESI-mass spectroscopy:**

2-(2-hydroxyphenyl)-benzo-4*H*-[1,3]-oxazin-4-one

ESI<sup>+</sup>-MS: [*m/z*] = 240 [LH<sub>2</sub>]<sup>+</sup>; ESI<sup>-</sup>-MS: [*m/z*] = 238 [L]<sup>-</sup>

2-hydroxy-*N*-(2-hydroxybenzoyl)-benzamide

ESI<sup>+</sup>-MS: [*m/z*] = 280 [LH<sub>3</sub> + Na]<sup>+</sup>; ESI<sup>-</sup>-MS: [*m/z*] = 256 [LH<sub>2</sub>]<sup>-</sup>

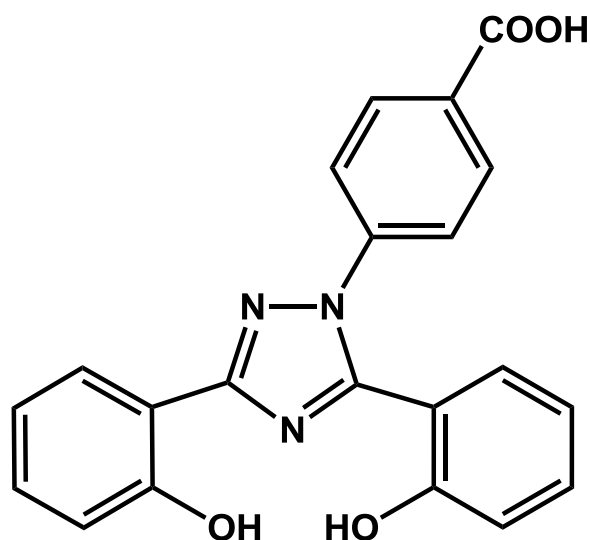
### IR-spectroscopy:

of a mixture of 2-(2-hydroxyphenyl)-benzo-4*H*-[1,3]-oxazin-4-one and 2-hydroxy-*N*-(2-hydroxybenzoyl)-benzamide

FT-IR: [cm<sup>-1</sup>] 1697; 1606; 1507; 1488; 1463; 1348; 1310; 1247; 1198; 1161; 1142; 1114; 1025; 851; 833; 748; 684

#### 11.1.2 Synthesis of 4-[3,5-bis(2-hydroxyphenyl)-1*H*-1,2,4-triazol-1-yl]benzoic acid (deferasirox)

4-Hydrazino-benzoic acid (3.35 g, 22.02 mmol) was dissolved in 200 mL ethanol and NEt<sub>3</sub> (2.92 g, 28.86 mmol, 4.0 mL, ρ<sub>20°C</sub> = 0.73 g/cm<sup>3</sup>) under reflux. To the resulting orange coloured solution 2-(2-hydroxyphenyl)-benzo-4*H*-[1,3]-oxazin-4-one (5.00 g, 20.90 mmol) was added and refluxed for another 2 h. Subsequently, the reaction mixture was cooled to ambient temperature and



precipitated by addition of hydrochloric acid (150 mL, 6.0 mol/L). Further, the suspension was concentrated to about 50% of its total volume under reduced pressure. After filtration, the resulting bright pink precipitate was dissolved in 300 mL ethanol. The product reprecipitated by addition of hydrochloric acid (200 mL, 1.0 mol/L) and water (500 mL). The rosy coloured solid was filtered and dried in vacuum to yield 6.39 g (17.11 mmol; 82 % referring to 2-(2-hydroxyphenyl)-benzo-4*H*-[1,3]-oxazin-4-one).

Characterisation:

**<sup>1</sup>H-NMR (D<sub>6</sub>-DMSO, TMS):**

δ (ppm) = 6.88 (d, 1H, <sup>3</sup>J = 8.3 Hz); 6.98 - 7.05 (m, 3H); 7.36 - 7.43 (m, 2H); 7.55 - 7.58 (m, 3H); 8.01 (d, 2H, <sup>3</sup>J = 8.3 Hz); 8.08 (dd, 1H, <sup>3</sup>J = 7.9 Hz, <sup>4</sup>J = 1.7 Hz); 10.07 (s, 1H, OH); 10.81 (s, 1H, OH)

**<sup>13</sup>C-NMR (D<sub>6</sub>-DMSO, TMS):**

δ (ppm) = 113.55; 114.30; 116.03; 116.97; 119.36; 119.60; 123.23 (2C); 126.68; 130.20 (2C); 130.44; 130.97; 131.37; 132.46; 141.10; 151.93; 155.08; 156.24; 159.80; 166.33

**Elemental analysis:**

M [C<sub>21</sub>H<sub>15</sub>N<sub>3</sub>O<sub>4</sub>] = 373.37 g/mol

% calculated: C: 67.56; H: 4.05; N: 11.26

% found: C: 67.41; H: 4.28; N: 11.13

**ESI-mass spectroscopy:**

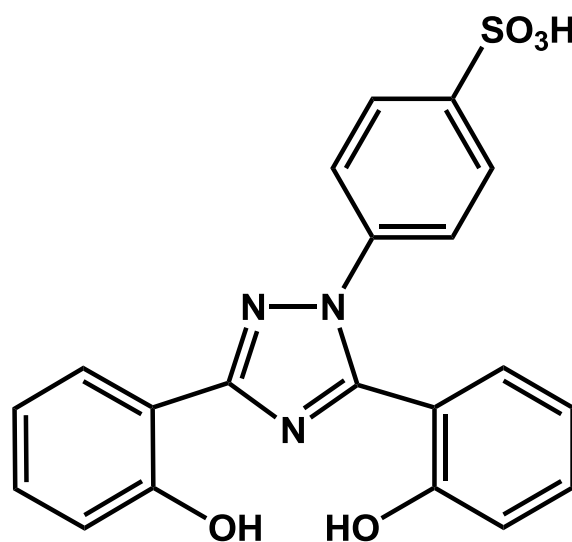
ESI<sup>+</sup>-MS: [m/z] = 374 [LH<sub>4</sub>]<sup>+</sup>; ESI<sup>-</sup>-MS: [m/z] = 372 [LH<sub>2</sub>]<sup>-</sup>

**IR-spectroscopy:**

FT-IR: [cm<sup>-1</sup>] 3316; 1678; 1607; 1585; 1517; 1495; 1479; 1451; 1431; 1416; 1351; 1278; 1223; 1155; 1037; 991; 948; 905; 852; 827; 807; 752; 705; 686; 660

### 11.1.3 Synthesis of 4-[3,5-bis(2-hydroxyphenyl)-1*H*-1,2,4-triazol-1-yl]benzenesulfonic acid (MSA)

4-Hydrazino-benzosulfonic acid hemihydrate (2.51 g, 12.75 mmol) dissolved under reflux in a solution of 300 mL ethanol with NEt<sub>3</sub> (1.29 g, 12.75 mmol, 1.77 mL,  $\rho_{20^\circ\text{C}} = 0.73 \text{ g/cm}^3$ ). Addition of 2-(2-hydroxyphenyl)-benzo-4*H*-[1,3]-oxazin-4-one (3.00 g, 12.54 mmol) to the boiling solution was followed by further reflux of the reaction mixture for 24 h. After cooling the solu-



tion to ambient temperature the crude product precipitated by addition of hydrochloric acid (80 mL, 6 mol/L). For sufficient precipitation the suspension was concentrated to about 50% of its total volume under reduced pressure. The product was filtered and washed with a small amount of cold water to result a white solid which was dried in vacuum to yield 4.27 g (9.99 mmol, 80 % referring to 2-(2-hydroxyphenyl)-benzo-4*H*-[1,3]-oxazin-4-one).

Characterisation:

#### <sup>1</sup>H-NMR (D<sub>6</sub>-DMSO, TMS):

$\delta$  (ppm) = 6.88 (d, 1H, <sup>3</sup>J = 8.1 Hz); 6.96 - 7.05 (m, 3H); 7.36 - 7.43 (m, 4H); 7.52 (dd, 1H, <sup>3</sup>J = 7.5 Hz, <sup>4</sup>J = 1.7 Hz); 7.67 (dd, 2H, <sup>3</sup>J = 7.1 Hz, <sup>4</sup>J = 1.7 Hz); 8.05 (dd, 1H, <sup>3</sup>J = 7.8 Hz, <sup>4</sup>J = 1.5 Hz)

#### <sup>13</sup>C-NMR (D<sub>6</sub>-DMSO, TMS):

$\delta$  (ppm) = 113.68; 114.23; 116.24; 117.10; 119.45; 119.79; 123.16 (2C); 126.56 (2C); 126.95; 131.16; 131.57; 132.60; 137.73; 148.23; 151.80; 155.39; 156.39; 159.31

**Elemental analysis:**

M [C<sub>20</sub>H<sub>15</sub>N<sub>3</sub>O<sub>5</sub>S · H<sub>2</sub>O] = 427.43 g/mol

% calculated: C: 56.20; H: 4.01; N: 9.83

% found: C: 56.07; H: 4.10; N: 9.69

**ESI-mass spectroscopy:**

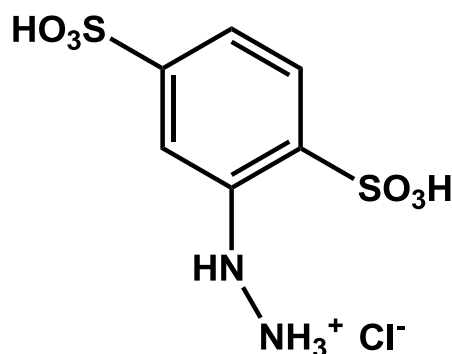
ESI<sup>+</sup>-MS: [*m/z*] = 409 [LH<sub>4</sub>]<sup>+</sup>; ESI<sup>-</sup>-MS: [*m/z*] = 410 [LH<sub>2</sub>]<sup>-</sup>

**IR-spectroscopy:**

FT-IR: [cm<sup>-1</sup>] 3198; 2901(bs); 2688; 2572; 1608; 1556; 1525; 1482; 1403; 1358; 1315; 1211; 1166; 1130; 1079; 1038; 1013; 975; 821; 768; 749; 706; 688

**11.1.4 Synthesis of 2-hydrazinylbenzene-1,4-disulfonic acid · HCl (DSH)**

Aniline-2,5-disulfonic acid (15.00 g, 59.23 mmol) was dissolved in a solution of sodium carbonate (3.14 g, 29.63 mmol) in pure water (60 mL). After filtration, the solution cooled down to 0°C in an ice bath and concentrated hydrochloric acid (1.18 g) was added. Within 15 min a solution of sodium nitrite (3.02 g, 43.77 mmol) dissolved in 20 mL pure water was slowly added to prevent the temperature from rising above 12°C. Occasionally, addition of concentrated hydrochloric acid adjusted the pH to 0, if necessary. After the complete addition of sodium nitrite and a final adjustment of the pH to 0 the solution was stirred at 0°C for an additional 30 min. The resulting precipitate was filtered and the moist pale white diazonium salt was passed on to the next step without further purification.



Sodium sulphite (20.63 g, 163.68 mmol) was dissolved in pure water (140 mL) and cooled to 0°C in an ice bath. Addition of the moist diazonium salt in portions to the vigorously stirred solution kept the temperature below 5°C. The reddish solution was stirred for an hour at 0°C. Subsequently, the tempera-

ture was allowed to rise to ambient temperature and then refluxed for an hour. After adding concentrated hydrochloric acid (52.5 mL) carefully, the mixture was again refluxed for an additional hour. The reaction mixture was cooled to ambient temperature and stirred for 12 h. Further, the suspension was concentrated to about 50% of its total volume under reduced pressure. The obtained pale white precipitate was filtered and dried for 24 h in vacuum to yield 11.22 g (32.98 mmol, 75 % relating to sodium nitrite).

Characterisation:

**$^1\text{H-NMR}$  ( $\text{D}_2\text{O}$ ,  $\text{D}_4\text{-TMPS}$ ):**

$\delta$  (ppm) = 7.49 (d, 1H,  $^4\text{J} = 1.7$  Hz); 7.56 (dd, 1H,  $^3\text{J} = 8.0$  Hz,  $^4\text{J} = 1.7$  Hz); 7.94 (d, 1H,  $^3\text{J} = 8.1$  Hz)

**$^{13}\text{C-NMR}$  ( $\text{D}_2\text{O}$ ,  $\text{D}_4\text{-TMPS}$ ):**

$\delta$  (ppm) = 113.64; 122.19; 131.92; 134.09; 144.05; 149.25

**Elemental analysis:**

$M [\text{C}_6\text{H}_8\text{N}_2\text{O}_6\text{S}_2 \cdot (\text{HCl}) \cdot (\text{Na}_2\text{SO}_4)_{1/10}] = 316.63$  g/mol

% calculated: C: 22.76; H: 2.87; N: 8.85

% found: C: 22.77; H: 2.71; N: 8.78

**ESI-mass spectroscopy:**

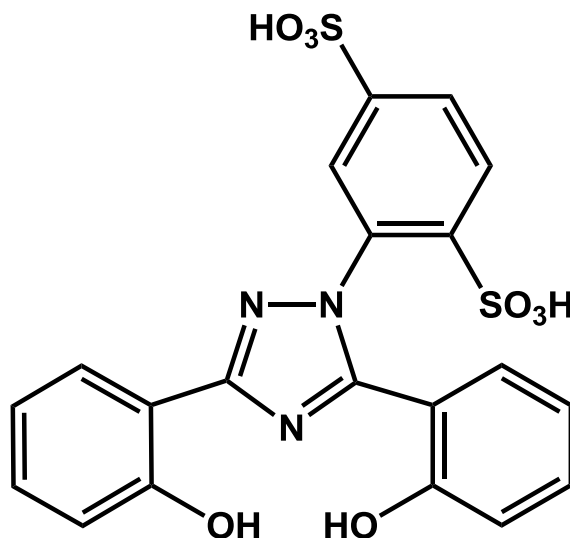
$[m/z] = 267$  (M-H)

**IR-spectroscopy:**

FT-IR:  $[\text{cm}^{-1}]$  3302; 2960; 1604; 1541; 1412; 1187; 1059; 1016; 857; 837; 663; 628; 589; 545; 519; 504

### 11.1.5 Synthesis of 2-[3,5-bis(2-hydroxyphenyl)-1*H*-1,2,4-triazol-1-yl]benzene-1,4-disulfonic acid (DSA)

To a solution mixture of  $\text{NEt}_3$  (3.74 g, 36.96 mmol, 5.12 mL,  $\rho_{20^\circ\text{C}} = 0.73 \text{ g/cm}^3$ ) in 600 mL of boiling methanol 2-hydrazinylbenzene-1,4-disulfonic acid hydrochloride (5.40 g, 17.05 mmol) was added in portions and dissolved sufficiently. A slight turbidity of the solution could be observed. To the boiling reaction mixture 2-(2-Hydroxyphenyl)-benzo-4*H*-[1,3]-oxazin-4-one (4.46 g, 18.64 mmol) was added and refluxed for 24 h. The reaction mixture was allowed to cool to ambient temperature and hydrochloric acid (500 mL, 6 mol/L) was added carefully until some white precipitate was observed. Further, the mixture was concentrated to a total volume of 50% under reduced pressure and the white precipitate was filtered off, suspended in hydrochloric acid (100 mL, 6 mol/L) and heated gently. After cooling the suspension to ambient temperature the precipitate was filtered and washed with cold hydrochloric acid (6 mol/L) and dried in vacuum for 24 h. To reprecipitate the product the white solid was added to just enough methanol to entirely dissolve it. After filtering the clear solution, ethyl acetate was added until quantitative precipitation had occurred. The product was filtered off again and dried in vacuum for 48 h. Subsequently, the product was exposed to the air for several days to achieve an equilibrium state of water absorption. The product obtained as a white solid forming the pentahydrate yielded 4.08 g (7.04 mmol, 40 % relating to 2-hydrazinylbenzene-1,4-disulfonic acid hydrochloride).



Characterisation:

**<sup>1</sup>H-NMR (D<sub>2</sub>O/NaOD, D<sub>4</sub>-TMPS):**

$\delta$  (ppm) = 6.41 (dt, 1H, <sup>3</sup>J = 8.3 Hz, <sup>4</sup>J = 1.2 Hz); 6.61 (d, 1H, <sup>3</sup>J = 7.6 Hz); 6.70 (dt, 1H, <sup>3</sup>J = 8.3 Hz, <sup>4</sup>J = 1.2 Hz); 6.80 (dd, 1H, <sup>3</sup>J = 8.3 Hz, <sup>4</sup>J = 0.9 Hz); 7.13 - 7.20 (m, 2H); 7.29 (dt, 1H, <sup>3</sup>J = 8.3 Hz, <sup>4</sup>J = 2.0 Hz); 7.69 (dd, 1H, <sup>3</sup>J = 7.6 Hz, <sup>4</sup>J = 2.0 Hz); 7.94 (d, 1H, <sup>4</sup>J = 2.0 Hz); 7.97 (dd, 1H, <sup>3</sup>J = 8.3 Hz, <sup>4</sup>J = 1.7 Hz); 8.12 (d, 1H, <sup>4</sup>J = 8.3)

**<sup>1</sup>H-NMR (D<sub>6</sub>-DMSO, TMS):**

$\delta$  (ppm) = 6.74 (dt, 1H, <sup>3</sup>J = 7.6 Hz, <sup>4</sup>J = 1.0 Hz); 6.97 (dd, 1H, <sup>3</sup>J = 8.5 Hz, <sup>4</sup>J = 1.0 Hz); 7.01 (dt, 1H, <sup>3</sup>J = 8.3 Hz, <sup>4</sup>J = 1.0 Hz); 7.05 (dd, 1H, <sup>3</sup>J = 8.3 Hz, <sup>4</sup>J = 0.9 Hz); 7.30 - 7.34 (m, 2H); 7.40 (dt, 1H, <sup>3</sup>J = 8.3 Hz, <sup>4</sup>J = 1.7 Hz); 7.63 (d, 1H, <sup>4</sup>J = 1.7 Hz); 7.79 (dd, 1H, <sup>3</sup>J = 8.3 Hz, <sup>4</sup>J = 1.7 Hz); 7.92 (d, 1H, <sup>3</sup>J = 8.3 Hz); 7.94 (dd, 1H, <sup>3</sup>J = 7.8 Hz, <sup>4</sup>J = 1.7 Hz)

**<sup>13</sup>C-NMR (D<sub>2</sub>O/NaOD, D<sub>4</sub>-TMPS):**

$\delta$  (ppm) = 115.58; 116.86; 118.98; 122.03; 122.89; 123.31; 129.73; 130.32; 132.56; 133.53; 133.84; 134.11; 134.85; 136.95; 145.11; 148.36; 159.64; 164.40; 168.10; 169.34

**<sup>13</sup>C-NMR (D<sub>6</sub>-DMSO, TMS):**

$\delta$  (ppm) = 110.36; 112.70; 116.35; 116.62; 118.66; 119.50; 125.18; 127.63; 127.77; 128.80; 130.25; 131.85; 131.91; 132.71; 144.54; 149.53; 151.36; 154.28; 155.82; 156.37

**Elemental analysis:**

M [C<sub>20</sub>H<sub>15</sub>N<sub>3</sub>O<sub>8</sub>S<sub>2</sub> · 5 H<sub>2</sub>O] = 579.56 g/mol

% calculated: C: 41.49; H: 4.35; N: 7.25

% found: C: 41.57; H: 4.50; N: 7.29

**ESI-mass spectroscopy:**

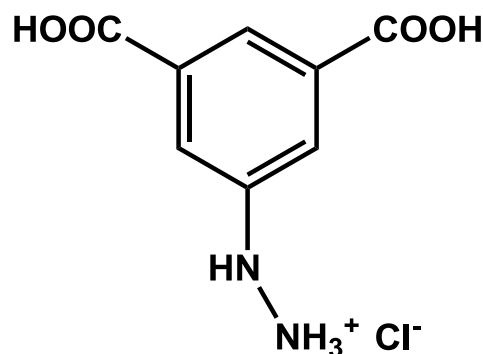
ESI<sup>+</sup>-MS: [*m/z*] = 490 [LH<sub>5</sub>]<sup>+</sup>, 512 [(LH<sub>4</sub>)Na]<sup>+</sup>; ESI<sup>-</sup>-MS: [*m/z*] = 243.6 [LH<sub>2</sub>]<sup>2-</sup>, 488 [LH<sub>3</sub>]<sup>-</sup>

**IR-spectroscopy:**

FT-IR: [cm<sup>-1</sup>] 3202; 1611; 1563; 1532; 1506; 1408; 1199; 1123; 1059; 1040; 1016; 861; 812; 767; 738; 654; 595; 548; 537; 510

**11.1.6 Synthesis of 5-hydrazinylisophthalic acid hydrochloric acid (DCH)**

5-Aminoisophthalic acid (5.00 g, 27.60 mmol) was dissolved in a solution of sodium carbonate (2.00g, 18.87 mmol) in 60 mL of pure water. After filtration, the solution was cooled in an ice bath to 0°C and 10 mL of concentrated hydrochloric acid was added to adjust to pH 0. This caused the reactant to precipitate. Within 15 min a solution of sodium nitrite (1.90 g, 27.60 mmol) in 10 mL pure water was added slowly to prevent the temperature from rising above 12°C. After the complete addition of sodium nitrite, and a final adjustment of the pH to 0, if necessary, the solution was stirred at 0°C for an additional 30 min. The resulting precipitate was filtered and the moist pale white diazonium salt was passed on to the next step without further purification.



A solution of sodium sulphite (6.88 g, 54.59 mmol) in 70 mL of pure water was cooled to 0°C in an ice bath. The moist diazonium salt was added in portions to the vigorously stirred solution to keep the temperature below 5°C. The solution was stirred for 1.5 h at 0°C. Subsequently, the temperature was allowed to rise to ambient temperature and then refluxed for 30 min. Concentrated hydrochloric acid (18.0 mL) was added carefully and the mixture was again refluxed for an additional hour. The reaction mixture was cooled to ambient temperature and stirred for 12 h. The resulting suspension was further concentrated to about 50% of its total volume under reduced pressure and the ob-

tained beige white precipitate was filtered and dried for 24 h in vacuum to yield 4.61 g (16.47 mmol, 60 % relating to sodium nitrite).

Characterisation:

**<sup>1</sup>H-NMR (D<sub>6</sub>-DMSO, TMS):**

δ (ppm) = 7.73 (s, 2H); 7.98 (s, 1H)

**<sup>13</sup>C-NMR (D<sub>6</sub>-DMSO, TMS):**

δ (ppm) = 118.33 (2C); 122.16; 131.90 (2C); 146.76; 166.74 (2C)

**Elemental analysis:**

M [C<sub>8</sub>H<sub>8</sub>N<sub>2</sub>O<sub>4</sub> · (HCl) · (Na<sub>2</sub>SO<sub>4</sub>)<sub>1/3</sub>] = 279.97 g/mol

% calculated: C: 34.32; H: 3.24; N: 10.01

% found: C: 34.08; H: 3.29; N: 9.73

**ESI-mass spectroscopy:**

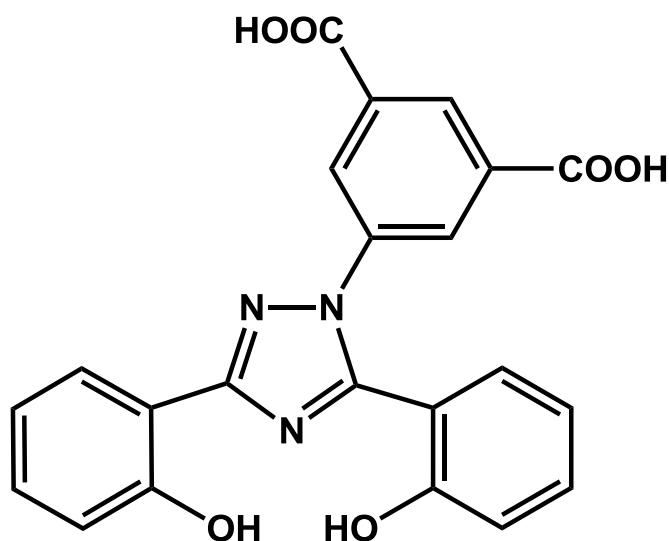
ESI<sup>+</sup>-MS: [m/z] = 197 [LH<sub>3</sub>]<sup>+</sup>; ESI<sup>-</sup>-MS: [m/z] = 195 [LH]<sup>-</sup>

**IR-spectroscopy:**

FT-IR: [cm<sup>-1</sup>] 1703; 1674; 1607; 1563; 1515; 1461; 1300; 1241; 1206; 1097; 1063; 1041; 976; 899; 831; 757; 718; 689; 668

### 11.1.7 Synthesis of 5-[3,5-bis(2-hydroxyphenyl)-1*H*-1,2,4-triazol-1-yl]isophthalic acid (DCA)

5-Hydrazinylisophthalic acid hydrochloride (2.50 g, 8.93 mmol) was dissolved in a boiling solution of 300 mL ethanol and NEt<sub>3</sub> (4.75 g, 46.89 mmol, 6.5 mL,  $\rho_{20^\circ\text{C}} = 0.73 \text{ g/cm}^3$ ). A slight turbidity of the solution could be observed. To the boiling solution 2-(2-hydroxyphenyl)-benzo-4*H*-[1,3]-oxazin-4-one (2.44 g, 10.20 mmol)



was added and the solution mixture refluxed for 24 h. The solution cooled to ambient temperature and hydrochloric acid (500 mL, 6 mol/L) was slowly added until some precipitation was observed. The mixture was concentrated to about 50 % of its total volume under reduced pressure. The beige precipitate was filtered and washed with pure water. The crude product was obtained as a beige coloured solid to yield 2.47 g (5.83 mmol, 65 % relating to 5-hydrazinylisophthalic acid hydrochloride).

For further purification 1.0 g of the crude product was passed on to preparative HPLC. The crude product was dissolved in a mixture of 22.0 mL methanol and 2.0 mL pure water and the separation was carried out with methanol and pure water, both containing 0.1% formic acid, as eluents with a flow rate of 20 mL/min. The gradient composition changed from 80% to 40% and to 90% methanol. The 90% methanol eluent mixture was kept isocratic until all ligand eluted. The ligand containing fraction was collected and the methanol evaporated under reduced pressure. The white solid was suspended in pure water, washed with pure water and filtered. After drying the product in vacuum for about 48 h a white solid was obtained with the yield 0.66 g (1.56 mmol, 66% relating to 1.0 g crude product).

Characterisation:

**<sup>1</sup>H-NMR (D<sub>6</sub>-DMSO, TMS):**

$\delta$  (ppm) = 6.87 (d, 1H, <sup>3</sup>J = 8.3 Hz); 6.99 - 7.05 (m, 3H); 6.74 (m, 2H); 7.60 (dd, 1H, <sup>3</sup>J = 7.6 Hz, <sup>4</sup>J = 1.7 Hz); 8.08 (dd, 1H, <sup>3</sup>J = 7.8 Hz, <sup>4</sup>J = 1.7 Hz); 8.20 (dd, 2H, <sup>4</sup>J = 1.7 Hz, <sup>4</sup>J = 0.8 Hz); 8.47 (dt, 1H, <sup>4</sup>J = 1.7 Hz, <sup>4</sup>J = 0.8 Hz); 10.11 (s, 1H, OH); 10.85 (s, 1H, OH)

**<sup>13</sup>C-NMR (D<sub>6</sub>-DMSO, TMS):**

$\delta$  (ppm) = 113.57; 114.06; 116.10; 117.00; 119.49; 119.63; 126.77; 127.55 (2C); 129.28; 131.01; 131.42; 132.36; 132.59; 138.39 (2C); 152.04; 154.94; 156.28; 159.88; 165.44 (2C)

**Elemental analysis:**

M [C<sub>22</sub>H<sub>15</sub>N<sub>3</sub>O<sub>6</sub> · (H<sub>2</sub>O)<sub>1/3</sub>] = 423.38 g/mol

% calculated: C: 62.41; H: 3.73; N: 9.93

% found: C: 62.33; H: 3.63; N: 9.72

**ESI-mass spectroscopy:**

ESI<sup>+</sup>-MS: [m/z] = 418 [LH<sub>5</sub>]<sup>+</sup>

**IR-spectroscopy:**

FT-IR: [cm<sup>-1</sup>] 1698; 1622; 1589; 1514; 1493; 1462; 1406; 1359; 1294; 1210; 1154; 1120; 1037; 1014; 911; 842; 822; 749; 716; 677; 660

### 11.1.8 Crystal growth of [deferasirox] · H<sub>2</sub>O

The ligand deferasirox (6.03302 g of a stock solution in DMSO  $c = 0.0091024$  mmol/g, 0.025 mmol), DMSO (41.9752 g), potassium chloride (0.81879 g, 0.10983 mmol) and potassium hydroxide (0.7 mL, 0.1 mol/L, 0.07 mmol) were given in a volumetric flask (109.83 mL) which was filled up with pure water. After one week colourless prisms were obtained which were suitable for single crystal X-ray analysis.

Elemental analysis was not possible since the crystals dissolved when dried in vacuum.

#### IR-spectroscopy:

FT-IR: [cm<sup>-1</sup>] 3310; 1677; 1607; 1584; 1516; 1495; 1479; 1450; 1431; 1416; 1351; 1277; 1222; 1154; 1037; 991; 947; 908; 851; 826; 807; 751; 704; 686; 660

### 11.1.9 Crystal growth of [DSA-H<sub>4</sub>] · 1.5 MeOH

The Ligand DSA (0,20 g, 0.35 mmol) was dissolved in 20.0 mL methanol. The solution was placed in an exsiccator filled with ethyl acetate. After about four weeks cubical shaped colourless crystals were received which could be employed for single crystal X-ray analysis.

Characterisation of the crystals was not possible. Precipitate settled on the crystals when taken out of the solution.

### 11.1.10 Crystal growth of $\text{Cs}_4[\text{DSA-H}_2]_2 \cdot (\text{H}_2\text{O})_{13/6} \cdot \text{MeOH}$

The Ligand DSA (0.050 g, 0.086 mmol) was dissolved in 4.0 mL methanol. To this stirred solution a solution of caesium hydroxide monohydrate (0.058 g, 0.345 mmol) in 4.0 mL methanol was added drop wise. The pH of the alkaline solution was adjusted to pH 5 with aqueous hydrochloric acid (0.1 mol/L). This clear solution was stored in an exsiccator filled with ethyl acetate. After four weeks colourless rhombic leaflets had grown which could be employed for single crystal X-ray analysis.

#### Elemental analysis:

$M [\text{Cs}_4(\text{C}_{20}\text{H}_{13}\text{N}_3\text{O}_8\text{S}_2)_2 \cdot (\text{H}_2\text{O})_{13/6} \cdot (\text{MeOH})] = 1577.62 \text{ g/mol}$

% calculated: C: 31.21; H: 2.20; N: 5.33

% found: C: 30.39; H: 2.32; N: 5.20

#### IR-spectroscopy:

FT-IR: [ $\text{cm}^{-1}$ ] 1623; 1589; 1495; 1470; 1370; 1297; 1207; 1143; 1120; 1064; 1042; 1024; 1000; 836; 816; 754; 702

### 11.1.11 Crystal growth of $\text{Cs}_5[\text{Fe}(\text{DSA})_2] \cdot 10.74 \text{ H}_2\text{O}$

A solution of iron(III)-acetylacetonate (0.034 g, 0.069 mmol) in 4.0 mL methanol was added drop wise to a solution of DSA (0.1 g, 0.173 mmol) in 4.0 mL methanol. The resulting dark violet solution was stirred for 30 min. Then, a solution of caesium hydroxide monohydrate (0.128 g, 0.762 mmol) in 4.0 mL pure water was added drop wise. The colour of the dark violet solution turned to bright red indicating the formation of the bis-complex with two ligands bound to one  $\text{Fe}^{3+}$  centre. The solution was stirred for 1 h and placed in an exsiccator filled with ethyl acetate. Overnight, single crystals were obtained in form of dark red prisms. These were suitable for single crystal X-ray analysis.

**Elemental analysis:** $M [\text{Cs}_5 (\text{C}_{20}\text{H}_{11}\text{N}_3\text{O}_8\text{S}_2)_2 \cdot 10.74 \text{ H}_2\text{O}] = 1884.75 \text{ g/mol}$ 

% calculated: C: 25.49; H: 2.33; N: 4.46

% found: C: 25.95; H: 2.30; N: 4.51

**IR-spectroscopy:**FT-IR: [ $\text{cm}^{-1}$ ] 1598; 1558; 1514; 1457; 1312; 1195; 1145; 1121; 1062; 1039; 1018; 989; 845; 759; 660; 590; 559; 538; 529; 501**11.1.12 Crystal growth of  $\text{Na}_3[\text{Cu}(\text{DSA})(\text{HCO}_3)] \cdot 2.5 \text{ H}_2\text{O} \cdot 1.5 \text{ MeOH}$  (violet) and  $\text{Na}_3[\text{Cu}(\text{DSA})(\text{HCO}_3)] \cdot (\text{H}_2\text{O})_{25/6} \cdot 3 \text{ MeOH}$  (green)**

A solution of copper(II)-acetylacetonate (0.011 g, 0.042 mmol) in 4.0 mL methanol was added drop wise to a solution of DSA (0.050 g, 0.086 mmol) in 4.0 mL methanol. To this mixture a solution of sodium hydroxide (0.014 g, 0.35 mmol) in 4.0 mL methanol and 1.0 mL pure water was also added drop wise causing the colour to intensify from light green to dark green. This mixture was kept in an exsiccator filled with ethyl acetate. After two weeks, green and violet rhombic plates grew from the dark green solution. Both the green and violet crystals were suitable for single crystal X-ray analysis.

**Elemental analysis:** violet crystals $M [\text{Na}_3 (\text{C}_{20}\text{H}_{11}\text{N}_3\text{O}_8\text{S}_2) \cdot (\text{HCO}_3) \cdot (\text{H}_2\text{O})_{5/2} \cdot (\text{MeOH})_{3/2}] = 772.08 \text{ g/mol}$ 

% calculated: C: 35.00; H: 3.00; N: 5.44

% found: C: 35.04; H: 3.10; N: 5.60

**Microscopic X-ray fluorescence - MXRFA:**violet and green crystals reveal the same values: Cu  $K_\alpha$  8 keV; Cu  $K_\beta$  9 keV

**Elemental analysis:** green crystals

M [Na<sub>3</sub> (C<sub>20</sub>H<sub>11</sub>N<sub>3</sub>O<sub>8</sub>S<sub>2</sub>) · (HCO<sub>3</sub>) · (H<sub>2</sub>O)<sub>25/6</sub> · (MeOH)<sub>3</sub>] = 850.22 g/mol

% calculated:        C: 33.91; H: 3.83; N: 4.94

% found:             C: 34.37; H: 3.67; N: 6.06

**IR-spectroscopy:**

a mixture of green and violet crystals, causes the following spectrum:

FT-IR: [cm<sup>-1</sup>] 1602; 1567; 1519; 1482; 1461; 1390; 1310; 1197; 1148; 1123;  
1066; 1044; 1022; 992; 844; 757; 710; 658

## 11.2 Titration experiments

Several methods based on titration experiments were used to study equilibrium constants. If possible, the titration experiment conditions were chosen very similar. In the following paragraphs conditions and procedures are described in detail.

### 11.2.1 Potentiometric titration experiments

#### Titration instrumentation

Potentiometric titrations were performed computer assisted with a piston burette 665 or 765 (dosimeter) with exchange unit 806 and pH/mV meter 713 or 780 from Metrohm AG. The exchange unit was equipped with a burette tip with antidiffusion stopper which can be immersed into the measurement solution. The titration experiment was controlled by the program Messlabor<sup>[150]</sup>.

#### pH electrodes

The pH measurements were carried out with the following single-rod measuring cell electrodes:

- SCHOTT<sup>®</sup> Instruments IoLine IL-pH-A120MF-R from SI Analytics GmbH, a double junction electrode with 3 mol/L KCl as bridge electrolyte, platinum diaphragm, iodine/iodide reference and Metrohm connector
- SenTix<sup>®</sup> 62 from WTW GmbH, a double junction electrode with 3 mol/L KCl as bridge electrolyte, platinum diaphragm, Ag/AgCl reference and BNC connector used with a Metrohm adapter, later distributed by SI Analytics GmbH as BlueLine 17 pH-R with Metrohm connector
- ROSS Ultra<sup>®</sup> pH electrode 8102 BNUWP from Orion Thermo Scientific, a double junction electrode with 3 mol/L KCl as bridge electrolyte, ceramic diaphragm, iodine/iodide reference and BNC connector with a Metrohm adapter

- Möller pH electrode, from Willi Möller AG, combined pH and reference electrode with an Ag/AgCl reference, ceramic diaphragm and Metrohm connector

### **Experimental procedure for continuous potentiometric titration experiments**

All solutions were prepared with deionised water (Millipore Synergy<sup>®</sup>, Millipore GmbH). Further, to ensure a constant ionic strength all solutions were prepared with KCl as supporting electrolyte at a concentration 0.1 mol/L KCl (puriss. p.a.  $\geq 99.5\%$ , Sigma Aldrich).

A sample of 50.0 mL (50.0 mL volumetric pipette) of the prepared solution was thermostated at 298 K (thermostat ecoline 103 or ecoline 003 from Lauda Dr. R. Wobser GmbH & CO. KG) in a double-walled glass vessel. The glass vessel was flushed with nitrogen gas that has been passed through a 0.1 mol/L KCl solution. Prior to and after all measurements the standard electrode potential  $E^\circ$  and the ionic product  $pK_w$  needed to be determined by a potentiometric titration of 50.0 mL of a 2.0 mmol/L HCl solution with 0.1 mol/L KOH (TitriPUR<sup>®</sup>, Merck KGaA) as titrant. The HCl was prepared with 0.1 mol/L HCl from a dosimeter (TitriPUR<sup>®</sup>, Merck KGaA). Both values were calculated with the program TITKURVE<sup>[151]</sup>. The mean values of  $E^\circ$  from the titrations prior to and after the actual measurement were used for the evaluation of the equilibrium constants. The ionic product was only used to monitor the electrode measurement, for further calculations the published value was used.

The sample solution was prepared in a 110 mL volumetric flask. All components were weighed in on a precision balance. If needed, the metal ion stock solution (with the concentration in mmol/g) was added to the flask first. Further, the ligand was added mostly as a solid or a stock solution. If necessary, the ligand could be well dissolved by ultrasonic treatment. In the next step, for a constant ionic strength solid KCl (puriss. p.a.  $\geq 99.5\%$ , Sigma Aldrich) was added. Some titration experiments, for example those in water/DMSO with a molar fraction  $x_{\text{DMSO}} < 0.20$ , needed to be adjusted to a specific pH prior to ti-

tration. This is carried out by adding 0.1 mol/L KOH or HCl (both TitriPUR<sup>®</sup>, Merck KGaA) to the flask with a dosimeter. The titration experiments are carried out alkalimetric with 0.1 mol/L KOH (TitriPUR<sup>®</sup>, Merck KGaA) or acidimetric with 0.1 mol/L HCl (TitriPUR<sup>®</sup>, Merck KGaA).

### 11.2.2 Potentiometric titrations in water/DMSO solution mixture

Equilibrium constants of deferasirox needed to be measured in a water/DMSO medium because of its low solubility in pure water. Titration experiments in water/DMSO solution mixtures were performed with certain molar fractions. By measuring the equilibrium constants for different molar fractions and extrapolation of the values we were able to estimate the constants for pure water. It is of importance for the preparation of all these solutions to consider the volume contraction during the mixing of DMSO with pure water since it is not an ideal solution. The DMSO volumes necessary for the preparation of 1.0 litre solution are summarized in **Table 11.1** [39]. All solutions were prepared with pure water (Millipore) that was degassed with argon prior to use.

**Table 11.1:** Partial excess molar volumes, partial molar volumes and necessary volumes of DMSO for the preparation of 1.0 litre solvent (in mL at 298 K).

$x_{DMSO}$	$\bar{V}_{DMSO}^E$	$\bar{V}_{H_2O}^E$	$\bar{V}_{DMSO}$	$\bar{V}_{H_2O}$	$V_{DMSO}$	$V_{H_2O}$	$V\%_{DMSO}$
0.06	-3.69	0.032	67.622	18.100	203.06	806.02	20.12
0.10	-3.84	0.043	67.472	18.111	309.42	705.56	30.48
0.12	-3.78	0.036	67.532	18.104	356.04	661.52	34.98
0.14	-3.67	0.019	67.642	18.087	398.95	620.93	39.11
0.16	-3.51	-0.010	67.802	18.058	438.56	583.35	42.91
0.18	-3.32	-0.052	67.992	18.016	475.21	548.49	46.42
0.20	-3.10	-0.104	68.212	17.964	509.12	515.98	49.66
0.22	-2.86	-0.169	68.452	17.899	540.60	485.62	52.68

As titrant a solution of 0.1 mol/L KOH or 0.1 mol/L HCl was used with the appropriate amount of DMSO for the desired molar ratio. First the DMSO solvent ( $\rho_{\text{DMSO}} = 1.09566 \text{ g/cm}^3$ )<sup>[37]</sup> was weighed into a 1.0 litre volumetric flask. Then KOH or HCl (both Titrisol<sup>®</sup>, Merck KGaA) was added in the presence of nitrogen. Subsequent, the flask was filled with water to the calibration mark. The warm mixture was left in the presence of nitrogen to cool to 293 K. Optimally the flask was gradually filled to the calibration mark at this temperature several times. The solution was then left to stand overnight at 293 K and filled one more time before use. A constant volume should have been achieved.

The determination of the standard electrode potential  $E^\circ$  and  $pK_w$  was also performed in the same molar fraction of DMSO as the measurement. To prepare the 2.0 mmol/L HCl solution DMSO was weighed in a 1.0 litre volumetric flask. Then 20 mL 0.1 mol/L HCl was added with a dosimeter and the needed amount of solid KCl to achieve an ionic strength of 0.1 mol/L was added to the flask. The flask was filled to the calibration mark with water. It was left to cool to 293 K which causes volume contraction. Therefore, the solution needed to be gradually filled to the calibration mark with water. After standing overnight, the solution was filled as described one last time prior to use.

The conditions described above were employed to prepare the sample solutions. If needed, first the metal ion stock solution was weighed into the 110 mL flask. Then DMSO was weighed into the flask. Further, ligand and then KCl ( $c = 0.1 \text{ mol/L}$ ) was weighed in and added to the solution mixture. As mentioned above, the ligand and KCl could well be dissolved by ultrasonic treatment. The flask was thermostated at 293 K, filled to the calibration mark several times, left to stand overnight and filled once more prior to use.

### 11.2.3 Spectrophotometric titrations

#### Continuous spectrophotometric titration experiments

Continuous spectrophotometric titrations were performed simultaneous with a continuous potentiometric titration. While the potentiometric titration was carried out as previously described in section 11.2.1 the immersion probe was dived into the sample solution. With the titration computer a trigger signal was sent to the spectrophotometer to record a spectrum just prior to the add-on of each new aliquot of titrant. Absorption data were recorded in the range  $220 < \lambda < 900$  nm, however the range  $400 < \lambda < 900$  nm was used for evaluation. Both titration experiments could be used for the determination of the equilibrium constants. These continuous titrations were studied with a total  $\text{Fe}^{3+}$  concentration of 0.48 mmol/L and 0.33 mmol/L and a total ligand concentration of 1.00 mmol/L, respectively.

#### Experimental procedure for the spectrophotometric batch titration experiments

The investigation of the  $\text{p}K_{\text{a}}$  values and the stability constant of the  $[\text{Fe}(\text{L})]$  and  $[\text{Fe}(\text{L})]^{-}$  complex of deferasirox and DSA in strong acidic solution needed to be performed as a discontinuous batch titration. For this method each sample was prepared in a 10 mL double-walled glass vessel at 298 K.

The  $\text{p}K_{\text{a}}$  batch titration of DSA was carried out with 10 samples and a total ligand concentration of 40.0 or 80.0  $\mu\text{mol/L}$ . The pH was adjusted ( $1.0 < \text{pH} < 2.0$ ) by adding the appropriate amount of 0.1 mol/L HCl solution (TitriPUR<sup>®</sup>, Merck KGaA) to a 0.1 mol/L KCl solution (prepared with solid KCl) to receive a total volume of 10.0 mL with the desired pH. The ligand was added to the 10.0 mL solution by an aliquot from a stock solution of DSA in pure water. The volume was taken into account for the total volume calculation. The absorption data were recorded ( $T = 298$  K,  $I = 0.1$  mol/L HCl/KCl) in the range  $230 < \lambda < 380$  nm. Further, the spectra were evaluated in the range  $290 < \lambda < 380$  nm for the determination of the acidity constant.

To study the stability constant of the  $[\text{Fe}(\text{DSA})]^-$  complex a batch titration was performed in the pH range  $1.00 < \text{pH} < 2.00$  with 10 samples. The pH was adjusted as previously described above for the  $\text{p}K_a$  batch titration. The total  $\text{Fe}^{3+}$  and DSA concentration was 0.2 mmol/L. For both the metal ion and ligand, a stock solution was used and an aliquot of each was added to the 10.0 mL solution. The volumes of these aliquots were taken into account for the calculation of the total volume. The absorption data were collected ( $T = 298 \text{ K}$ ,  $I = 0.1 \text{ mol/L HCl/KCl}$ ) in the range  $200 < \lambda < 1000 \text{ nm}$ . However, the spectra were evaluated in the range  $400 < \lambda < 900 \text{ nm}$ . A spectrum of a 0.2 mmol/L  $\text{Fe}^{3+}$  solution, prepared with the iron stock solution was also collected. The complexation constant was calculated with the program Specfit<sup>[152-153]</sup>.

The protonation of the ligand deferasirox was investigated in the pH range  $0 < \text{pH} < 2.0$  in water/DMSO solution. Three different molar fractions ( $x_{\text{DMSO}} = 0.06 ; 0.10 ; 0.16$ ) were chosen for examination. To adjust the pH a 1.0 mol/L KCl and a 1.0 mol/L HCl solution with the appropriate molar fraction of DMSO were necessary. The 1.0 mol/L HCl and KCl water/DMSO solutions were prepared according to the procedure described in section 11.2.2, however with Titrisol<sup>®</sup> (Merck KGaA) for HCl and solid KCl. In contrast to the other batch titrations, the 10 samples were prepared in 25 mL volumetric flasks. All solutions used were thermostated at 293 K. First, the 1.0 mol/L HCl solution (converted into  $c = \text{mmol/g}$ ) was weighed into the flask. Then, an aliquot (total ligand concentration 40.0  $\mu\text{mol/L}$ ) of a deferasirox stock solution in pure DMSO was added with a micropipette and the exact weight was noted. The flasks were filled with the 1.0 mol/L KCl solution to the calibration mark several times at 293 K, left to stand overnight and filled one last time prior to use. The absorption data were collected ( $T = 298 \text{ K}$ ,  $I = 1.0 \text{ mol/L HCl/KCl}$ ) in the range  $200 < \lambda < 1000 \text{ nm}$ . However, the spectra were evaluated in the range  $240 < \lambda < 360 \text{ nm}$ .

### Kinetic measurement of the $x_{\text{DMSO}} = 0.06$ deferasirox solution

The 10 samples of deferasirox prepared in  $x_{\text{DMSO}} = 0.06$  at pH 0.26, 0.70, 1.00 and 2.00, according to the procedure described above, were studied with a kinetic measurement over a period of 6.5 days. The measurements were carried out on a UV/VIS spectrometer Uvikon 940/941 (Kontron Instruments) with a quartz cuvette with 1.0 cm cell path length. The absorption spectra were collected ( $T = 298 \text{ K}$ ,  $I = 1.0 \text{ mol/L HCL/KCL}$ ) in the range  $190 < \lambda < 500 \text{ nm}$ . In effect, the spectra were evaluated at  $\lambda = 290 \text{ nm}$ .

#### 11.2.4 Calculation of equilibrium constants

All equilibrium constants were calculated as concentration constants. Further, the pH was defined as  $-\log[\text{H}^+]$ . The equilibrium constants were determined with the help of computer programs. For the evaluation of potentiometric titrations and spectrophotometric titrations the program Hyperquad2008<sup>[154]</sup> and Specfit<sup>[152-153]</sup> were employed, respectively.

To evaluate titration experiments with the program Hyperquad2008 the  $pK_w$ , the ionic product of water, as a constant value for the given titration conditions is required. For aqueous solution, with 0.1 mol/L KCl and 298 K, the value for the  $pK_w$  is 13.78 according to the literature<sup>[55]</sup>. For the different molar fractions used in water/DMSO solutions the  $pK_w$  ( $pK_w = -\log K_w$ ,  $K_w = [\text{H}^+] \times [\text{OH}^-]$ ) was determined by the titrations carried out prior to and after the measurements as described in section 11.2.2. The values obtained with the program TITKURVE<sup>[151]</sup> were:  $x_{\text{DMSO}} = 0.20$  with a  $pK_w$  15.58 (mean value of 34 titrations),  $x_{\text{DMSO}} = 0.18$  with a  $pK_w$  15.38 (mean value of 34 titrations),  $x_{\text{DMSO}} = 0.16$  with a  $pK_w$  15.20 (mean value of 35 titrations) and  $x_{\text{DMSO}} = 0.14$  with a  $pK_w$  15.01 (mean value of 43 titrations). These values concur with those obtained from the literature<sup>[122-123]</sup>. The  $E^\circ$ ,  $pK_w$  and the total concentrations of the ligand and metal ion were ascertained as fixed values. Furthermore, when refining complex formation constants the  $pK_a$  values previously determined are also defined as fixed values.

Equilibrium constants investigated with spectrophotometric titration experiments were calculated with the program Specfit<sup>[152-153]</sup>. For the determination of  $pK_a$  values the pH was calculated and the total concentrations were ascertained as fixed

values. The ligand species were all defined as coloured species. For the determination of complex formation constants a spectrum of the  $\text{Fe}^{3+}$  stock solution was collected (the conditions were described above in section 11.2.3, batch titration experiments) and defined in the program as a known spectrum and a coloured species. All metal-containing species were defined as coloured species. In contrast, the ligand and its protonation products were treated as non-coloured species.

Species distributions for all titration experiments were calculated with the program Hyss2006 <sup>[147]</sup>.

### 11.2.5 NMR-titration experiments

The protonation of deferasirox in the range  $0 \leq \text{pD} \leq 1.0$  was studied by an NMR-titration experiment in  $\text{D}_2\text{O}$ -DCI/ $\text{D}_6$ -DMSO with a molar fraction of  $x_{\text{DMSO}} = 0.20$ . The study was carried out dependent on pD <sup>[155-156]</sup>. The samples were prepared without an inert supporting electrolyte by mixing the appropriate amount of DCI (stock solution 20% in  $\text{D}_2\text{O}$ ) and  $\text{D}_2\text{O}$  to adjust the pD. The total volume of  $\text{D}_2\text{O}$ -DCI and  $\text{D}_6$ -DMSO were obtained from **Table 11.1**. The ligand (0.005 g) was dissolved in the necessary volume of  $\text{D}_6$ -DMSO and then  $\text{D}_2\text{O}$  and last DCI was added. The samples were left to stand overnight. Subsequently, the NMR spectra were recorded with TMS as internal standard at  $294 \pm 2$  K. The  $\text{p}K_{\text{a}}^{\text{D}}$  value was calculated with the program NMR-Tit <sup>[126]</sup>.

## 11.3 Instrumentation

The following instruments were employed for analytical measurements reported in this thesis.

### 11.3.1 NMR-spectroscopy

The NMR spectra were performed on a Bruker Avance Ultrashield 400 with a resonance frequency of 400.13 MHz for  $^1\text{H}$ -NMR spectra and 100.6 MHz for  $^{13}\text{C}$ -NMR spectra. The measurements were carried out at 294 K, if not stated differently. As deuterated solvents  $\text{D}_6$ -DMSO with tetramethylsilan (TMS) as internal standard and  $\text{D}_2\text{O}$  with 3-(trimethylsilyl)propionic-2,2,3,3- $\text{D}_4$  acid sodium salt ( $\text{D}_4$ -TMPS) were used. The unit for the chemical shift  $\delta$  is ppm referring to the internal standard. Further, the solvent employed for each particular NMR is remarked in brackets. The multiplicities are abbreviated as follows: s = singlet, d = doublet, t = triplet, dd = double doublet, dt = double triplet and m = multiplet. Moreover, the unit for the coupling constant  $J$  is Hz.

### 11.3.2 Elemental analysis (C,H,N)

The elemental analyses were performed on a Vario EL elemental analyzer from Elementar Analysensysteme GmbH (instrument belongs to the research group of Prof. D. Volmer, Saarland University; formerly Prof. C. Huber, University of Salzburg) by A. Zschka (research group of Prof. K. Hegetschweiler) or S. Harling (research group of Prof. G. Kickelbick, Saarland University; formerly research group of senior Prof. M. Veith, Saarland University).

### 11.3.3 UV-VIS-spectroscopy

Spectrophotometric titration experiments were carried out on a Tidas UV-NIR/100-1 or Tidas 100 diode array spectrophotometer from J&M Analytik AG at 298 K. The instrument was equipped with an immersion probe from HELIMA GmbH & Co.KG, with 1 cm cell path length.

The kinetic measurements were performed on a double-beam UV/VIS spectrometer Uvikon 940/941 (Kontron Instruments) with a quartz cuvette with 1.0 cm cell path length.

#### **11.3.4 IR-spectroscopy**

IR-spectra were collected on a FT-IR spectrometer Vector 22 MIR with a golden-gate ATR-unit from Bruker. The spectra were generated with OPUS NT 3.1 software. The signal band positions are stated in the unit  $\text{cm}^{-1}$ .

#### **11.3.5 ESI-mass spectroscopy**

ESI-mass spectra were performed by Dr. Mathias Großer (magrochem, Saarland University) on a Micromass ZQ-4000 ESI-mass spectrometer (single-quadrupole) from Waters GmbH.

#### **11.3.6 Preparative HPLC**

Purification of the ligand DCA was performed on a preparative HPLC from Gilson Inc. equipped with a Valvemate<sup>®</sup> II Valve Actuator, high pressure pumps 306, 333 and 334 and a PrepFC<sup>™</sup> fraction collector. A UV/VIS-155 detector from Gilson Inc. was applied to observe the separation. The separation was monitored by the TRILUTION<sup>®</sup> LC Software v2.1 (Gilson Inc.). The reversed phase chromatographic column Sep Tech ST60-10 C18 (Dynamax 250 x 41.4 mm) from Varian Inc. was used as preparative HPLC column.

#### **11.3.7 EPR-spectroscopy**

The EPR experiments were carried out by Prof. P. Strauch at the University of Potsdam in his research group for Inorganic Material Chemistry on an EPR-Spectrometer ELEXSYS E500 CW-EPR-Series for X-band and S-band from Bruker BioSpin GmbH. The EPR-spectra were recorded with X-band with the frequency 9 - 10 GHz and a field strength of 0.34 tesla ( $g = 2$ ).

### 11.3.8 ICP-OES spectroscopy

The determination of the exact concentration of metal ion stock solutions was performed on an Optical Emission Spectrometer Optima 2000 DV from Perkin Elmer by T. Allgayer in the research group for Inorganic and Analytic Chemistry of senior Prof. H.P. Beck, Saarland University.

### 11.3.9 Microscopic X-ray fluorescence - MXRFA

The  $\mu$ XRF spectra of the green and violet crystals of  $\text{Na}_3[\text{Cu}(\text{DSA})(\text{HCO}_3)] \cdot 2.5\text{H}_2\text{O} \cdot 1.5\text{MeOH}$  and  $\text{Na}_3[\text{Cu}(\text{DSA})(\text{HCO}_3)] \cdot (\text{H}_2\text{O})_{25/6} \cdot 3\text{MeOH}$  were investigated on a Micro-RFA model Eagle from the company Röntgenanalytik, Taunusstein Germany. The instrument was equipped with a polycapillary lense for very high resolution, to achieve spatial resolution of up to 30  $\mu\text{m}$  and a Si(Li)-semiconductor detector with 165 eV energy resolution. The recording of the spectra was carried out by Dr. R. Haberkorn in the research group for Inorganic and Analytic Chemistry of senior Prof. H.P. Beck, Saarland University.

### 11.3.10 Crystal structure determination

X-ray diffraction data were collected on a Bruker X8 Apex or a Stoe IPDS diffractometer by Dr. Volker Huch (research group of senior Prof. M. Veith, Saarland University). The data sets were solved and refined with the programs SHELXS-97<sup>[157]</sup> and SHELXL-97<sup>[158]</sup>. Residual electron density was subtracted and revised with the Squeeze option of the program Platon<sup>[56-57]</sup>, if necessary. The program Diamond 3.2f<sup>[159]</sup> was used for the presentation of the crystal structures as ORTEP-plots.

### 11.3.11 Cyclic voltammetry

Cyclic voltammetric studies were performed on a 797 VA Computrace from Metrohm AG. A platinum pin was used as counter electrode and an Ag/AgCl electrode as reference electrode with a potential versus normal hydrogen electrode of 208.7 mV ( $T = 298\text{ K}$ , determined by Metrohm AG) or the po-

tential was determined with the help of an iron(III/II)-hexacyanoferrate solution ( $E^\circ = 0.46$  V,  $c([\text{K}_4(\text{Fe}(\text{CN})_6)] = 10.0$  mmol/L in 0.01 mol/L NaOH,  $T = 298$  K and  $I = 0.1$  mol/L KCl) [63]. For measurements in acidic solution a gold electrode was applied as working electrode. Hence, a hanging mercury drop electrode (HMDE) as working electrode was needed for measurements in alkaline solution. The cyclic voltammograms were recorded in water, using 0.5 mol/L KCl as supporting electrolyte and a  $\text{Fe}^{3+}$  and DSA concentration of 2.3 mmol/L and 5.0 mmol/L, respectively. The pH of the sample solutions was adjusted with a SenTix® 62 pH electrode from WTW GmbH and a 780 pH/mV meter from Metrohm AG. The pH electrode was calibrated prior to use with three standard buffer solutions (pH = 4.0, 7.0 and 10.0 from Fluka AG).

## 11.4 Chemicals and preparation of stock solutions

### Chemicals

Chemicals applied for syntheses were commercially available products of reagent grade quality and were used as obtained from the following suppliers: Sigma-Aldrich, Fluka, Acros, Merck and Alfa-Aesar. Solvents were obtained from the mentioned suppliers and from the central chemical depot of the Saarland University and employed as received.

The DMSO used for titration experiments was analytical reagent grade from Fisher Scientific and stored under nitrogen once opened. Potassium chloride for titration experiments was of puriss p.a. grade  $\geq 99.5\%$  from Sigma-Aldrich.

Water used for synthesis and titrations was deionised and purified with a Millipore Synergy® from Millipore GmbH.

Metal salts for crystal synthesis and stock solutions were obtained of highest available quality.

The deuterated solvents for NMR-spectroscopy  $\text{D}_6$ -DMSO (99.9 atom %D) and  $\text{D}_2\text{O}$  (99.90 atom %D) were obtained from Aldrich and Euriso-top,

respectively. Internal standards were added separately D<sub>4</sub>-TMPS (99 atom %D, ABCR GmbH & Co. KG) and TMS (99.9+% NMR grade, Fluka).

### Stock solutions

The metal ion stock solutions used for titration experiments were prepared differently and additional acid added to the stock solutions to prevent hydrolysis needed to be determined prior to use. The density of the stock solutions was determined at 293 K and the concentration was stated in mmol/g.

Preparation of the stock solutions:

- For the Fe<sup>3+</sup>, Mg<sup>2+</sup> and Ca<sup>2+</sup> stock solutions the protons in solution were determined by potentiometric titration with EDTA (Titrisol<sup>®</sup>, Merck KGaA).
- The Al<sup>3+</sup> stock solution did not contain protons and was prepared with an ampoule of hydrochloric acid (Titrisol<sup>®</sup>, Merck KGaA) for a 0.1 mol/L solution.
- The protons in the Zn<sup>2+</sup> solution needed to be determined with potentiometric titrations with ethylenediamine prior to use.
- The metal ion stock solutions of Cu<sup>2+</sup>, Ni<sup>2+</sup> and Cd<sup>2+</sup> were employed without any further analysis.
- The stock solutions of Ga<sup>3+</sup> and Gd<sup>3+</sup> were prepared by dissolving the metal salts GdCl<sub>3</sub> · 6H<sub>2</sub>O (Aldrich) and GaCl<sub>3</sub> (ultra dry 99.999% ampoule, Sigma-Aldrich) in pure water. The exact concentration was analysed by ICP-OES spectroscopy with the help of a calibration curve prepared with standard solution for AAS of the metal ion obtained from Aldrich. The Ga<sup>3+</sup> solution was acidified to 0.5 mol/L HCl with Titrisol<sup>®</sup> (Merck KGaA) and Gd<sup>3+</sup> to 0.02 mol/L HCl by addition of 0.1 mol/L HCl from a dosimeter.
- Stock solutions of the ligand deferasirox were prepared in DMSO (analytical reagent grade, Fisher scientific).
- Stock solutions of the ligand DSA were prepared in pure water.

## 12 Appendix

### Electrode tests

First potentiometric titrations were carried out with the Möller pH electrode. Soon we noticed difficulties during titration experiments. The difficulties were due to large changes in the standard potential  $E^0$  of the electrode during titration experiments and strong deviations in alkaline solution from the calculated fit with Hyperquad2008. As a consequence, these titrations were not easy to evaluate and often could not be evaluated at all. There was a need for an appropriate electrode to carry out long term potentiometric titration experiments. Fourteen electrodes were tested with respect to the following criteria:

- equilibrium: acidimetric and alkalimetric titrations with HCl, MSA ( $pK_a$  titration) and the Fe(EDTA) system
- $\Delta E^0$  [MV]: changes in standard potential should be  $\Delta E^0 < 2$  otherwise they were defined as bad
- electrolyte loss: bridging electrolyte should need to be refilled only once a week
- evaluation: the evaluation of the MSA and Fe(EDTA) system should be good and the values in the expected range
- alkaline: evaluations should not deviate from the titration curve in alkaline solution

Some of the electrode tests were performed by T. Nicolai, under my supervision, during his studies.

The following table lists the electrodes tested and their characteristics.

electrode	company	type	reference	diaphragm	pH range	electrolyte	conditioning	connector
Möller pH electrode	Willi Möller AG	single-rod	Ag/AgCl	ceramic	0-14	3 mol/L KCl	3 mol/L KCl	Lemo (Metrohm)
CA85/2-SC pH electrode	Willi Möller AG	single-rod double junction	Ag/AgCl	glass grinding	0-14	3 mol/L KCl	3 mol/L KCl	Lemo (Metrohm)
DGI112-Pro	Mettler Toledo	double junction	ARGENTHAL	flexible teflon	0-14	3 mol/L KCl	0.5 mol/L KCl	Lemo (Metrohm)
Ref DX200	Mettler Toledo	double junction	Ag/AgCl	glass grinding	-	3 mol/L KCl	-	banana
Glas DG300-SC	Mettler Toledo	glass electrode	-	-	0-13	-	0.5 mol/L KCl	Lemo (Metrohm)
InLab Routine	Mettler Toledo	single-rod	InLab	ceramic	0-14	3 mol/L KCl	none	Lemo (Metrohm)
InLab Mono	Mettler Toledo	glass electrode	InLab	-	0-14	-	none	Lemo (Metrohm)
InLab Reference	Mettler Toledo	reference electrode	InLab	ceramic	-	3 mol/L KCl	-	banana
Ross Ultra 8102BNUWP	Orion Thermo Scientific	single-rod double junction	Ross® iodine/iodide	ceramic	0-14	3 mol/L KCl	3 mol/L KCl	BNC with adapter
Ross 8101BNWP	Orion	glass electrode	Ross®	-	-	-	storage solution	BNC with adapter
Ross 800500u	Thermo Scientific	reference electrode double junction	Ross® iodine/iodide	ceramic	0-14	3 mol/L KCl	-	Pintip with adapter
Sen Tix 62	WTW	single-rod	Ag/AgCl	platinum	0-14	3 mol/L KCl	none	BNC with adapter
pHC2011	Radiometer analytical	single-rod	Red-Rod	porous pin	0-14 alkaline	saturated KCl with KCl crystals	none	BNC with adapter
pHG211-8	Radiometer	glass electrode	Red-Rod	-	0-14 alkaline	-	none	BNC with adapter
REF201	analytical	reference electrode	Red-Rod	porous pin	0-14 alkaline	saturated KCl with KCl crystals	-	banana
KCW11/NH/Gel	Russell Thermo Scientific	single-rod double junction	K-Series K-Polymer	ceramic	0-14	gel no refill	none	BNC with adapter
KR5/Gel	Russell	reference electrode double junction	K-Series	ceramic	0-14	gel no refill	none	banana
Ross 8101BNWP	Orion Thermo Scientific	glass electrode	Ross® iodine/iodide	-	-	-	storage solution	BNC
IoLine IL-pH-A120MF-R	SI -Analytics	single-rod double junction	iodine/iodide	platinum	0-14	3 mol/L KCl	storage solution	Lemo (Metrohm)

The following table presents an overview of the test results. At first the SenTix 62 electrode and the Ross Ultra 8102BNUWP were quite good and used for titrations experiments while still searching for an even better electrode. Finally, a new electrode was developed by SI-Analytics, the SCHOTT® Instruments IoLine electrode, which turned out to be an excellent combination of the SenTix 62 and the Ross Ultra. It combines the precise iodine/iodide reference system with a platinum diaphragm. This electrode was the best electrode for performing potentiometric titration experiments.

electrode	company	equilibrium	$\Delta E^0$ [mV]	electrolyte loss	evaluation	alkaline
Möller pH electrode	Willi Möller AG	good	bad	good	bad	bad
CA85/2-SC pH electrode	Willi Möller AG	good	bad	bad	bad	bad
DGI112-Pro	Mettler Toledo	good	bad	bad	bad	good
Ref DX200	Mettler Toledo	good	good	bad	bad	-
Glas DG300-SC	Mettler Toledo					
InLab Routine	Mettler Toledo	good	good	good	bad	bad
InLab Mono	Mettler Toledo	good	good	good	bad	bad
InLab Reference						
Ross Ultra 8102BNUWP	Orion Thermo Scientific	good	bad	good	good	bad
Ross 8101BNWP	Orion	good	bad	good	bad	bad
Ross 800500u	Thermo Scientific					
Sen Tix 62	WTW	good	good	bad	good	good
pHC2011	Radiometer analytical	good	bad	good	bad	good
pHG211-8	Radiometer	bad	bad	good	bad	good
REF201	analytical					
KCW11/NH/Gel	Russell Thermo Scientific	good	bad	good	bad	bad
KR5/Gel	Russell	bad	bad	good	-	-
Ross 8101BNWP	Orion Thermo Scientific					
IoLine IL-pH-A120MF-R	SI-Analytics, Schott	good	good	good	good	good

**Crystallographic data** (further information on CD)**Crystal structure [DSA-H<sub>4</sub>] · 1.5 MeOH**

Operator	Dr. Volker Huch	
Diffractometer	Bruker X8 Apex	
Identification code	sh2725a	
Empirical formula	C <sub>21.50</sub> H <sub>21</sub> N <sub>3</sub> O <sub>9.50</sub> S <sub>2</sub>	
Formula weight	537.53 g/mol	
Temperature	100(2) K	
Wavelength	0.71073 Å	
Crystal system	monoclinic	
Space group	C2/c	
Unit cell dimensions	a = 16.181(5) Å	α = 90°
	b = 16.416(5) Å	β = 91.782(18)°
	c = 21.898(7) Å	γ = 90°
Volume	5814(3) Å <sup>3</sup>	
Z	8	
Density (calculated)	1.228 mg/m <sup>3</sup>	
Absorption coefficient	0.233 mm <sup>-1</sup>	
F(000)	2232	
Crystal size	0.2 x 0.3 x 0.4 mm <sup>3</sup>	
Theta range for data collection	1.77 to 26.00°	
Index ranges	-19 ≤ h ≤ 19, -20 ≤ k ≤ 20, -26 ≤ l ≤ 26	
Reflections collected	48374	
Independent reflections	5699 [R(int) = 0.0480]	
Completeness to theta = 26.00°	99.8 %	
Absorption correction	Semi-empirical from equivalents	
Refinement method	Full-matrix least-squares on F <sup>2</sup>	
Data / restraints / parameters	5699 / 7 / 348	
Goodness-of-fit on F <sup>2</sup>	1.075	
Final R indices [I > 2σ(I)]	R <sub>1</sub> = 0.0674, wR <sub>2</sub> = 0.2021	
R indices (all data)	R <sub>1</sub> = 0.0764, wR <sub>2</sub> = 0.2104	
Largest diff. peak and hole	1.360 and -0.609 e.Å <sup>-3</sup>	

**Crystal structure Cs<sub>4</sub>[DSA-H<sub>2</sub>]<sub>2</sub> · (H<sub>2</sub>O)<sub>13/6</sub> · MeOH**

Operator	Dr. Volker Huch	
Diffractometer	Bruker X8 Apex	
Identification code	sh3040	
Empirical formula	C <sub>20.50</sub> H <sub>17.17</sub> Cs <sub>2</sub> N <sub>3</sub> O <sub>9.58</sub> S <sub>2</sub>	
Formula weight	788.80 g/mol	
Temperature	100(2) K	
Wavelength	0.71073 Å	
Crystal system	Triclinic	
Space group	P-1	
Unit cell dimensions	a = 10.8806(6) Å	α = 91.971(3)°
	b = 16.1975(9) Å	β = 106.856(3)°
	c = 16.3259(9) Å	γ = 96.096(3)°
Volume	2731.6(3) Å <sup>3</sup>	
Z	4	
Density (calculated)	1.918 mg/m <sup>3</sup>	
Absorption coefficient	2.876 mm <sup>-1</sup>	
F(000)	1519	
Crystal size	0.22 x 0.11 x 0.04 mm <sup>3</sup>	
Theta range for data collection	1.97 to 30.00°	
Index ranges	-15 ≤ h ≤ 15, -22 ≤ k ≤ 22, -22 ≤ l ≤ 22	
Reflections collected	60393	
Independent reflections	15842 [R(int) = 0.0959]	
Completeness to theta = 30.00°	99.6 %	
Absorption correction	Semi-empirical from equivalents	
Max. and min. transmission	0.8936 and 0.5703	
Refinement method	Full-matrix least-squares on F <sup>2</sup>	
Data / restraints / parameters	15842 / 0 / 633	
Goodness-of-fit on F <sup>2</sup>	0.883	
Final R indices [I > σ <sub>2</sub> (I)]	R <sub>1</sub> = 0.0543, wR <sub>2</sub> = 0.1045	
R indices (all data)	R <sub>1</sub> = 0.1103, wR <sub>2</sub> = 0.1183	
Largest diff. peak and hole	2.191 and -1.801 e.Å <sup>-3</sup>	

**Crystal structure Cs<sub>5</sub>[Fe(DSA)<sub>2</sub>] · 10.74 H<sub>2</sub>O**

Operator	Dr. Volker Huch	
Diffractometer	Bruker X8 Area	
Identification code	sh2862a	
Empirical formula	C <sub>40</sub> H <sub>43.48</sub> Cs <sub>5</sub> Fe N <sub>6</sub> O <sub>26.74</sub> S <sub>4</sub>	
Formula weight	1884.77 g/mol	
Temperature	133(2) K	
Wavelength	0.71073 Å	
Crystal system	monoclinic	
Space group	C2/c	
Unit cell dimensions	a = 21.0813(6) Å	α = 90°
	b = 11.2287(4) Å	β = 98.059(2)°
	c = 26.4674(8) Å	γ = 90°
Volume	6203.4(3) Å <sup>3</sup>	
Z	4	
Density (calculated)	2.018 mg/m <sup>3</sup>	
Absorption coefficient	3.352 mm <sup>-1</sup>	
F(000)	3618	
Crystal size	0.59 x 0.23 x 0.19 mm <sup>3</sup>	
Theta range for data collection	1.55 to 26.00°	
Index ranges	-26 ≤ h ≤ 26, -13 ≤ k ≤ 13, -32 ≤ l ≤ 32	
Reflections collected	44730	
Independent reflections	6104 [R(int) = 0.0322]	
Completeness to theta = 26.00°	100.0 %	
Absorption correction	Semi-empirical from equivalents	
Max. and min. transmission	0.5684 and 0.2445	
Refinement method	Full-matrix least-squares on F <sup>2</sup>	
Data / restraints / parameters	6104 / 0 / 420	
Goodness-of-fit on F <sup>2</sup>	1.256	
Final R indices [I > 2 σ (I)]	R <sub>1</sub> = 0.0682, wR <sub>2</sub> = 0.1524	
R indices (all data)	R <sub>1</sub> = 0.0778, wR <sub>2</sub> = 0.1588	
Largest diff. peak and hole	1.896 and -1.060 e.Å <sup>-3</sup>	

**Crystal structure Na<sub>3</sub>[Cu(DSA)(HCO<sub>3</sub>)] · 2.5 H<sub>2</sub>O · 1.5 MeOH**

Operator	Dr. Volker Huch	
Diffractometer	Stoe IPDS	
Identification code	sh2986	
Empirical formula	C <sub>22.50</sub> H <sub>22</sub> Cu N <sub>3</sub> Na <sub>3</sub> O <sub>15</sub> S <sub>2</sub>	
Formula weight	771.06 g/mol	
Temperature	213(2) K	
Wavelength	0.71073 Å	
Crystal system	triclinic	
Space group	P-1	
Unit cell dimensions	a = 10.343(4) Å	α = 71.75(7)°
	b = 10.962(8) Å	β = 74.37(5)°
	c = 14.304(7) Å	γ = 76.27(7)°
Volume	1462.4(14) Å <sup>3</sup>	
Z	2	
Density (calculated)	1.751 mg/m <sup>3</sup>	
Absorption coefficient	1.014 mm <sup>-1</sup>	
F(000)	784	
Crystal size	0.39 x 0.22 x 0.09 mm <sup>3</sup>	
Theta range for data collection	2.30 to 27.00°	
Index ranges	-13 ≤ h ≤ 13, -14 ≤ k ≤ 14, -18 ≤ l ≤ 18	
Reflections collected	16103	
Independent reflections	5929 [R(int) = 0.0881]	
Completeness to theta = 27.00°	93.0 %	
Absorption correction	None	
Refinement method	Full-matrix least-squares on F <sup>2</sup>	
Data / restraints / parameters	5929 / 0 / 431	
Goodness-of-fit on F <sup>2</sup>	0.945	
Final R indices [I > 2σ(I)]	R <sub>1</sub> = 0.0575, wR <sub>2</sub> = 0.1449	
R indices (all data)	R <sub>1</sub> = 0.0870, wR <sub>2</sub> = 0.1589	
Largest diff. peak and hole	1.254 and -0.811 e.Å <sup>-3</sup>	

**Crystal structure Na<sub>3</sub>[Cu(DSA)(HCO<sub>3</sub>)] · (H<sub>2</sub>O)<sub>25/6</sub> · 3 MeOH**

Operator	Dr. Volker Huch	
Diffractometer	Bruker X8 Area	
Identification code	sh3031	
Empirical formula	C <sub>24</sub> H <sub>32.33</sub> Cu N <sub>3</sub> Na <sub>3</sub> O <sub>18.17</sub> S <sub>2</sub>	
Formula weight	850.17 g/mol	
Temperature	100(2) K	
Wavelength	0.71073 Å	
Crystal system	monoclinic	
Space group	P2(1)/c	
Unit cell dimensions	a = 11.9315(7) Å	α = 90°
	b = 21.6062(12) Å	β = 105.147(2)°
	c = 14.9654(8) Å	γ = 90°
Volume	3724.0(4) Å <sup>3</sup>	
Z	4	
Density (calculated)	1.516 mg/m <sup>3</sup>	
Absorption coefficient	0.810 mm <sup>-1</sup>	
F(000)	1747	
Crystal size	0.29 x 0.19 x 0.19 mm <sup>3</sup>	
Theta range for data collection	1.77 to 27.00°	
Index ranges	-15 ≤ h ≤ 14, -26 ≤ k ≤ 27, -16 ≤ l ≤ 19	
Reflections collected	32384	
Independent reflections	8119 [R(int) = 0.0504]	
Completeness to theta = 27.00°	99.9 %	
Absorption correction	Semi-empirical from equivalents	
Max. and min. transmission	0.8614 and 0.7991	
Refinement method	Full-matrix least-squares on F <sup>2</sup>	
Data / restraints / parameters	8119 / 2 / 466	
Goodness-of-fit on F <sup>2</sup>	1.025	
Final R indices [I > 2σ(I)]	R <sub>1</sub> = 0.0750, wR <sub>2</sub> = 0.2131	
R indices (all data)	R <sub>1</sub> = 0.1021, wR <sub>2</sub> = 0.2372	
Largest diff. peak and hole	2.555 and -0.780 e.Å <sup>-3</sup>	

## 13 References

- [1] R. Crichton, *Inorganic Biochemistry of Iron Metabolism*, 2. ed., John Wiley & Sons, Chichester, **2001**.
- [2] D. T. Richens, *The chemistry of aqua ions*, John Wiley & Sons, Chichester, **1997**.
- [3] F. Bou-Abdallah, *BBA-GEN Subjects* **2010**, 1800, 719-731.
- [4] G. Löffler, P. E. Petrides, *Biochemie und Pathobiochemie*, 6. ed., Springer-Verlag, Berlin, **1998**.
- [5] N. C. Andrews, P. J. Schmidt, *Annu. Rev. Physiol.* **2007**, 69, 69-85.
- [6] A. L. Schade, R. W. Reinhard, H. Levy, *Arch. Biochem. Biophys.* **1949**, 20, 170-172.
- [7] H. Z. Sun, H. Y. Li, P. J. Sadler, *Chem. Rev.* **1999**, 99, 2817-2842.
- [8] H. A. Huebers, C. A. Finch, *Physiol. Rev.* **1987**, 67, 520-582.
- [9] U. Schwertmann, J. Friedl, H. Stanjek, *J. Colloid Interf. Sci.* **1999**, 209, 215-223.
- [10] P. M. Harrison, P. Arosio, *BBA-Bioenergetics* **1996**, 1275, 161-203.
- [11] W. Wang, M. A. Knovich, L. G. Coffman, F. M. Torti, S. V. Torti, *BBA-GEN Subjects* **2010**, 1800, 760-769.
- [12] X. F. Liu, E. C. Theil, *Accounts Chem. Res.* **2005**, 38, 167-175.
- [13] M. Uchida, S. Kang, C. Reichhardt, K. Harlen, T. Douglas, *BBA-GEN Subjects* **2010**, 1800, 834-845.
- [14] R. J. Ward, M. H. Ramsey, D. P. E. Dickson, A. Florence, R. R. Crichton, T. J. Peters, S. Mann, *Eur. J. Biochem.* **1992**, 209, 847-850.
- [15] R. J. Ward, R. Legssyer, C. Henry, R. R. Crichton, *J. Inorg. Biochem.* **2000**, 79, 311-317.
- [16] J. E. Huheey, E. A. Keiter, R. L. Keiter, *Anorganische Chemie, Prinzipien von Struktur und Reaktivität*, 3. ed., Walter de Gruyter, Berlin, **2003**.
- [17] E. C. Theil, M. Matzapetakis, X. F. Liu, *J. Biol. Inorg. Chem.* **2006**, 11, 803-810.
- [18] R. R. Crichton, F. Roman, F. Roland, *Febs Lett.* **1980**, 110, 271-274.
- [19] O. Kakhlon, Z. I. Cabantchik, *Free Radical Bio. Med.* **2002**, 33, 1037-1046.
- [20] F. Petrat, H. de Groot, R. Sustmann, U. Rauen, *Biol. Chem.* **2002**, 383, 489-502.
- [21] J. A. Wang, K. Pantopoulos, *Biochem. J.* **2011**, 434, 365-381.
- [22] A. Taher, M. D. Cappellini, *Ther. Clin. Risk Manag.* **2009**, 5, 857-868.
- [23] A. Pietrangelo, *Annu. Rev. Nutr.* **2006**, 26, 251-270.
- [24] [http://www.exjade.com/Videos/exjade\\_moa\\_chapter\\_two.jsp](http://www.exjade.com/Videos/exjade_moa_chapter_two.jsp), Exjade international website, Iron Toxicity, **14.07.2011**.
- [25] H. Nick, *Curr. Opin. Chem. Biol.* **2007**, 11, 419-423.
- [26] M. D. Cappellini, A. Taher, *Acta Haematol.* **2009**, 122, 165-173.
- [27] R. Galanello, R. Origa, *Orphanet J. Rare Dis.* **2010**, 5.
- [28] H. Nick, P. Acklin, R. Lattmann, P. Buehlmayer, S. Hauffe, J. Schupp, D. Alberti, *Curr. Med. Chem.* **2003**, 10, 1065-1076.
- [29] D. S. Kalinowski, D. R. Richardson, *Pharmacol. Rev.* **2005**, 57, 547-583.
- [30] M. D. Cappellini, P. Pattoneri, *Annu. Rev. Med.* **2009**, 60, 25-38.

- [31] E. Vichinsky, *Am. J. Hematol.* **2008**, *83*, 398-402.
- [32] A. V. Hoffbrand, *Best Pract. Res. Clin. Ha.* **2005**, *18*, 299-317.
- [33] E. Jabbour, G. Garcia-Manero, A. Taher, H. M. Kantarjian, *Oncologist* **2009**, *14*, 489-496.
- [34] E. Vichinsky, O. Onyekwere, J. Porter, P. Swerdlow, J. Eckman, P. Lane, B. Files, K. Hassell, P. Kelly, F. Wilson, F. Bernaudin, G. L. Forni, I. Okpala, C. Ressayre-Djaffer, D. Alberti, J. Holland, P. Marks, E. Fung, R. Fischer, B. U. Mueller, T. Coates, I. Deferasirox Sickle Cell, *Brit. J. Haematol.* **2007**, *136*, 501-508.
- [35] A. Pietrangelo, P. Brissot, H. Bonkovsky, C. Niederau, L. Rojkaer, R. Weitzman, P. Williamson, O. Schoenborn-Kellenberger, P. Phatak, *J. Hepatol.* **2009**, *50*, S24-S24.
- [36] H. Glickstein, R. Ben El, M. Shvartsman, Z. I. Cabantchik, *Blood* **2005**, *106*, 3242-3250.
- [37] U. Heinz, Doctoral Thesis, Saarland University (Saarbrücken), **2001**.
- [38] U. Heinz, K. Hegetschweiler, P. Acklin, B. Faller, R. Lattmann, H. P. Schnebli, *Angew. Chem. Int. Ed.* **1999**, *38*, 2568-2570.
- [39] S. Steinhauser, Doctoral Thesis, Saarland University (Saarbrücken), **2005**.
- [40] S. Steinhauser, U. Heinz, M. Bartholomä, T. Weyermüller, H. Nick, K. Hegetschweiler, *Eur. J. Inorg. Chem.* **2004**, 4177-4192.
- [41] Y. I. Ryabukhin, N. V. Shibaeva, A. S. Kuzharov, V. G. Korobkova, A. V. Khokhlov, A. D. Garnovskii, *Sov. J. Coord. Chem.* **1987**, *13*, 493-498.
- [42] Y. I. Ryabukhin, L. N. Faleeva, V. G. Korobkova, *Chem. Heter. Com. (Engl. Trans.)* **1983**, *19*, 332-336.
- [43] T. Eicher, S. Hauptmann, *Chemie der Heterocyclen, Struktur, Reaktionen und Synthesen*, Thieme, Stuttgart, **1994**.
- [44] J. Houben, E. Müller, H. Kropf, K. H. Büchel, T. Weyl, *Methoden der Organischen Chemie, Vol. 10/2 Stickstoffverbindungen I, Methoden zur Herstellung und Umwandlung von Arylhydrazinen und Arylhydrazonen*, Thieme, Stuttgart, **1967**.
- [45] G. Heinzemann, *Justus Liebigs Ann. Chem.* **1878**, *190*, 222-228.
- [46] O. Zander, *Justus Liebigs Ann. Chem.* **1879**, *198*, 1-29.
- [47] C. Hulme, T. E. V. Jr., T. Nixey, B. Chenera, V. Gore, M. D. Bartberger, Y. Sun, *Molecular Diversity* **2003**, *7*, 161-164.
- [48] A. E. Martell, R. J. Motekaitis, *Determination and Use of Stability Constants*, VCH Verlagsgesellschaft mbH, Weinheim, **1988**.
- [49] F. Teucke, Staatsexamensarbeit, Saarland University (Saarbrücken), **2008**.
- [50] H. Cerfontain, B. W. Schnitger, *Recl. Trav. Chim. Pays-Bas* **1972**, *91*, 199-208.
- [51] H. Cerfontain, A. Koeberg-Telder, *J. Chem. Soc., Perkin Trans. 2* **1975**, 226-229.
- [52] D. S. Crumrine, J. M. Shankweiler, R. V. Hoffman, *J. Org. Chem.* **1986**, *51*, 5013-5015.
- [53] D. S. Crumrine, D. C. French, *J. Org. Chem.* **1990**, *55*, 5494-5496.
- [54] R. L. Benoit, M. Frechette, D. Boulet, *Can. J. Chem.* **1989**, *67*, 2148-2152.

- [55] R. M. Smith, A. E. Martell, R. J. Motekaitis, K. Hegetschweiler, S. Stucky, *Critically Selected Stability Constants of Metal Complexes*, NIST Standard Reference Database 46 (Version 9.0), Saarland University, Saarbrücken, **2009**.
- [56] A. L. Spek, *PLATON*, Utrecht University, Netherlands, **2006**.
- [57] P. v. d. Sluis, A. L. Spek, *Acta Cryst.* **1990**, *A46*, 194-201.
- [58] T. Nicolai, Staatsexamensarbeit, Saarland University (Saarbrücken), **2009**.
- [59] S. Stucky, *unpublished results* **2007**.
- [60] P. T. Lieu, M. Heiskala, P. A. Peterson, Y. Yang, *Mol. Aspects Med.* **2001**, *22*, 1-87.
- [61] B. Halliwell, J. M. C. Gutteridge, *Arch. Biochem. Biophys* **1986**, *246*, 501-514.
- [62] E. Fibach, E. A. Rachmilewitz, *Ann. N. Y. Acad. Sci.* **2010**, *1202*, 10-16.
- [63] D. R. Lide, *Handbook of Chemistry and Physics*, 74<sup>th</sup> Edition, CRC Press Inc., Boca Raton, Florida, **1993 - 1994**.
- [64] P. Sharp, *P. Nutr. Soc.* **2004**, *63*, 563-569.
- [65] D. Huster, H.-J. Hühn, J. Mössner, K. Caca, *Der Internist* **2005**, *46*, 731-740.
- [66] P. J. M. W. L. Birker, H. C. Freeman, *J. Am. Chem. Soc.* **1977**, *99*, 6890-6899.
- [67] M. S. Haddad, D. N. Hendrickson, *Inorg. Chim. Acta* **1978**, *28*, L121-L122.
- [68] V. Pérez, I. Monsalvo, P. Demare, V. Gómez-Vidales, I. Regla, I. Castillo, *Inorg. Chem. Commun.* **2011**, *14*, 389-391.
- [69] S. Iglesias, O. Castillo, A. Luque, P. Roman, *Inorg. Chim. Acta* **2003**, *349*, 273-278.
- [70] A. Prescimone, J. Sanchez-Benitez, K. K. Kamenev, S. A. Moggach, J. E. Warren, A. R. Lennie, M. Murrie, S. Parsons, E. K. Brechin, *Dalton Trans.* **2010**, *39*, 113-123.
- [71] R. Kirmse, J. Stach, *ESR-Spektroskopie Anwendung in der Chemie*, Akademie-Verlag, Berlin, **1985**.
- [72] S. Stucky, N. J. Koch, K. Hegetschweiler, *Complex formation of ICL670 and related ligands with Fe<sup>III</sup>, Ga<sup>III</sup>, Gd<sup>III</sup> and Cu<sup>II</sup>*, Novartis Pharma AG Final Report, Saarbrücken, **2008**.
- [73] C. H. Lee, S. T. Wong, T. S. Lin, C. Y. Mou, *J. Phys. Chem. B* **2005**, *109*, 775-784.
- [74] S. Kawata, M. Iwaizumi, H. Kosugi, H. Yokoi, *Chem. Lett.* **1987**, 2321-2324.
- [75] S. Noro, H. Miyasaka, S. Kitagawa, T. Wada, T. Okubo, M. Yamashita, T. Mitani, *Inorg. Chem.* **2005**, *44*, 133-146.
- [76] X. Wang, *Acta Cryst.* **2009**, *E65*, m1658.
- [77] S. Hazra, R. Koner, M. Nayak, H. A. Sparkes, J. A. K. Howard, S. Dutta, S. Mohanta, *Eur. J. Inorg. Chem.* **2009**, 4887-4894.
- [78] P. DeBurgomaster, J. Zubieta, *Acta Cryst.* **2010**, *E66*, m1350-m1351.
- [79] M. A. Ali, A. H. Mirza, F. H. Bujang, M. H. S. A. Hamid, P. V. Bernhardt, *Polyhedron* **2006**, *25*, 3245-3252.
- [80] D. Petrovic, T. Bannenber, S. Randoll, P. G. Jones, M. Tamm, *Dalton Trans.* **2007**, 2812-2822.

- [81] Z. W. Mao, G. Liehr, R. van Eldik, *J. Am. Chem. Soc.* **2000**, *122*, 4839-4840.
- [82] E. Denkhaus, K. Salnikow, *Crit. Rev. Oncol. Hemat.* **2002**, *42*, 35-56.
- [83] R. P. Hausinger, *Sci. Total Environ.* **1994**, *148*, 157-166.
- [84] S. B. Mulrooney, R. P. Hausinger, *Fems Microbiology Reviews* **2003**, *27*, 239-261.
- [85] J. Kuchar, R. P. Hausinger, *Chem. Rev.* **2004**, *104*, 509-525.
- [86] C. S. A. Baltazar, M. C. Marques, C. M. Soares, A. M. DeLacey, I. A. C. Pereira, P. M. Matias, *Eur. J. Inorg. Chem.* **2011**, 948-962.
- [87] S. E. Schram, E. M. Warshaw, A. Laumann, *Int. J. Dermatol.* **2010**, *49*, 115-125.
- [88] M. Costa, K. Salnikow, J. E. Sutherland, L. Broday, W. Peng, Q. W. Zhang, T. Kluz, *Mol. Cell. Biochem.* **2002**, *234*, 265-275.
- [89] C. Y. Chen, Y. F. Wang, W. R. Huang, Y. T. Huang, *Toxicol. Appl. Pharm.* **2003**, *189*, 153-159.
- [90] R. F. M. Herber, *Int. Arch. Occ. Env. Hea.* **1999**, *72*, 279-283.
- [91] H. Elias, D. Hess, H. Paulus, *Z. anorg. allg. Chem.* **1990**, *589*, 101-114.
- [92] H. Liu, H. Wang, D. Niu, Z. Lu, *Synth. React. Inorg. M.* **2005**, *35*, 233-236.
- [93] Y. Gultneh, A. R. Khan, B. Ahvazi, R. J. Butcher, *Polyhedron* **1998**, *17*, 3351-3360.
- [94] B. L. Vallee, D. S. Auld, *Acc. Chem. Res.* **1993**, *26*, 543-551.
- [95] W. N. Lipscomb, N. Strater, *Chem. Rev.* **1996**, *96*, 2375-2433.
- [96] J. E. Coleman, *Curr. Opin. Chem. Biol.* **1998**, *2*, 222-234.
- [97] C. Bergquist, T. Fillebeen, M. M. Morlok, G. Parkin, *J. Am. Chem. Soc.* **2003**, *125*, 6189-6199.
- [98] M. Subat, K. Woinaroschy, S. Anthofer, B. Malterer, B. Konig, *Inorg. Chem.* **2007**, *46*, 4336-4356.
- [99] A. Mondal, G. Mostafa, A. Ghosh, N. R. Chaudhuri, W. T. Wong, *Polyhedron* **1998**, *17*, 1217-1221.
- [100] S.-Y. Wan, Y.-Z. Li, T.-a. Okamura, J. Fan, W.-Y. Sun, N. Ueyama, *Eur. J. Inorg. Chem.* **2003**, 3783-3789.
- [101] D. Anselmo, E. C. Escudero-Adan, J. Benet-Buchholz, A. W. Kleij, *Dalton Trans.* **2010**, *39*, 8733-8740.
- [102] P. Chaudhuri, C. Stockheim, K. Wieghardt, W. Deck, R. Gregorzik, H. Vahrenkamp, B. Nuber, J. Weiss, *Inorg. Chem.* **1992**, *31*, 1451-1457.
- [103] M. D. Hannant, M. Schormann, D. L. Hughes, M. Bochmann, *Inorg. Chim. Acta* **2005**, *358*, 1683-1691.
- [104] N. N. Murthy, K. D. Karlin, *J. Chem. Soc., Chem. Commun.* **1993**, 1236-1238.
- [105] K. Selmeczi, C. Michel, A. Milet, I. Gautier-Luneau, C. Philouze, J.-L. Pierre, D. Schnieders, A. Rompel, C. Belle, *Chem. Eur. J.* **2007**, *13*.
- [106] R. R. Buchholz, M. E. Etienne, A. Dorgelo, R. E. Mirams, S. J. Smith, S. Y. Chow, L. R. Hanton, G. B. Jameson, G. Schenk, L. R. Gahan, *Dalton Trans.* **2008**, 6045-6054.
- [107] A. Hartwig, *Biometals* **2010**, *23*, 951-960.
- [108] R. A. Goyer, *Annu. Rev. Nutr.* **1997**, *17*, 37-50.
- [109] G. Kazantzis, *Biometals* **2004**, *17*, 493-498.
- [110] H. Strasdeit, *Angew. Chem. Int. Ed.* **2001**, *40*, 707-709.

- [111] T. W. Lane, F. M. M. Morel, *Proc. Natl. Acad. Sci. USA* **2000**, *97*, 4627-4631.
- [112] A. S. Saljooghi, S. J. A. Fatemi, *Biometals* **2010**, *23*, 707-712.
- [113] R. A. Allred, L. H. McAlexander, A. M. Arif, L. M. Berreau, *Inorg. Chem.* **2002**, *41*, 6790-6801.
- [114] R. A. Allred, S. A. Huefner, K. Rudzka, A. M. Arif, L. M. Berreau, *Dalton Trans.* **2007**, 351-357.
- [115] S. V. Perry, *Biochem. Bioph. Res. Co.* **2008**, *369*, 43-48.
- [116] M. Kawahara, K. Konoha, T. Nagata, Y. Sadakane, *Biomed. Res. Trace Elements* **2007**, *18*, 211-220.
- [117] A. Becaria, A. Campbell, S. C. Bondy, *Toxicol. Ind. Health* **2002**, *18*, 309-320.
- [118] R. D. Shannon, *Acta Cryst.* **1976**, *A32*, 751-767.
- [119] C. M. Reinke, J. Breitreutz, H. Leuenberger, *Drug Safety* **2003**, *26*, 1011-1025.
- [120] A. I. Arief, *Environ. Geochem. Health* **1999**, *12*, 89-93.
- [121] C. F. Baes, R. E. Mesmer, *The Hydrolysis of Cations*, Wiley-Interscience, New York, **1976**.
- [122] P. Fiordiponti, F. Rallo, F. Rodante, *Z. Phys. Chem. Neue Folge* **1974**, *88*, 149-159.
- [123] E. M. Woolley, L. G. Hepler, *Analytical Chemistry* **1972**, *44*, 1520-1523.
- [124] D. Martin, A. Weise, H.-J. Niclas, *Angew. Chem.* **1967**, *8*, 340-357.
- [125] S. Stucky, N. J. Koch, U. Heinz, K. Hegetschweiler, *Chemical Papers* **2008**, *62*, 388-397.
- [126] A. Ries, K. Hegetschweiler, *NMR-Tit, Program for the Simulation of pH Dependent Shifts in NMR Spectra*, Version 2.0, Saarbrücken, **1999**.
- [127] M. Schaefer, *Met Based Drugs* **1997**, *4*, 159-171.
- [128] S. Aime, W. Dastru, S. G. Crich, E. Gianolio, V. Mainero, *Biopolymers* **2002**, *66*, 419-428.
- [129] A. J. L. Villaraza, A. Bumb, M. W. Brechbiel, *Chem. Rev.* **2010**, *110*, 2921-2959.
- [130] P. Caravan, J. J. Ellison, T. J. McMurry, R. B. Lauffer, *Chem. Rev.* **1999**, *99*, 2293-2352.
- [131] S. K. Morcos, *Eur. J. Radiol.* **2008**, *66*, 175-179.
- [132] J. M. Idee, M. Port, I. Raynal, M. Schaefer, S. Le Greneur, C. Corot, *Fundam. Clin. Pharm.* **2006**, *20*, 563-576.
- [133] S. Laurent, L. V. Elst, F. Copoix, R. N. Muller, *Invest. Radiol.* **2001**, *36*, 115-122.
- [134] Z. L. Cheng, D. L. J. Thorek, A. Tsourkas, *Angew. Chem. Int. Ed.* **2010**, *49*, 346-350.
- [135] Z. Kotkova, J. Kotek, D. Jirak, P. Jendelova, V. Herynek, Z. Berkova, P. Hermann, I. Lukes, *Chem. Eur. J.* **2010**, *16*, 10094-10102.
- [136] E. T. Clarke, A. E. Martell, *Inorg. Chim. Acta* **1991**, *190*, 37-46.
- [137] W. Wadsak, M. Mitterhauser, *Eur. J. Radiol.* **2010**, *73*, 461-469.
- [138] T. J. Wadas, E. H. Wong, G. R. Weisman, C. J. Anderson, *Chem. Rev.* **2010**, *110*, 2858-2902.
- [139] D. E. Reichert, J. S. Lewis, C. J. Anderson, *Coord. Chem. Rev.* **1999**, *184*, 3-66.

- 
- [140] M. Fani, J. P. Andre, H. R. Maecke, *Contrast Media Mol. Imaging* **2008**, 3, 53-63.
- [141] W. R. Harris, V. L. Pecoraro, *Biochemistry* **1983**, 22, 292-299.
- [142] A. Heppeler, S. Froidevaux, A. N. Eberle, H. R. Maecke, *Curr. Med. Chem.* **2000**, 7, 971-994.
- [143] R. J. Motekaitis, A. E. Martell, *Inorg. Chem.* **1980**, 19, 1646-1651.
- [144] H. Nick, R. Lattmann, Novartis AG [CH], Novartis Pharma GmbH [AT], WO 2007/051773 A1, **2007**.
- [145] H. Irving, H. Rossotti, *Acta Chem. Scand.* **1956**, 10, 72-93.
- [146] W. R. Harris, K. N. Raymond, F. L. Weigl, *J. Am. Chem. Soc.* **1981**, 103, 2667-2675.
- [147] P. Gans, L. Alderighi, A. Ienco, D. Peters, A. Sabatini, A. Vacca, *Coord. Chem. Rev.* **1999**, 184, 311-318.
- [148] S. Steinhauser, U. Heinz, M. Bartholoma, T. Weyhermuller, H. Nick, K. Hegetschweiler, *Eur. J. Inorg. Chem.* **2005**, 2262-2262.
- [149] Z. D. Liu, R. C. Hider, *Med. Res. Rev.* **2002**, 22, 26-64.
- [150] *MESLABOR, a computer program for the control of potentiometric and spectrophotometric titrations*, Scientec GmbH, Saarbrücken, **2002**.
- [151] K. Hegetschweiler, *TITKURVE*, Version 1.1, **1993**.
- [152] R. A. Binstead, B. Jung, A. D. Zuberbühler, *SPECFIT/32, Version 3.0*, Spectrum Software Associates, Marlborough, MA 01752, USA, **2000**.
- [153] H. Gampp, M. Maeder, C. J. Meyer, A. D. Zuberbühler, *Talanta* **1985**, 32, 1133-1139.
- [154] P. Gans, A. Sabatini, A. Vacca, *Talanta* **1996**, 43, 1739-1753.
- [155] R. Lumry, E. L. Smith, R. R. Glantz, *J. Am. Soc.* **1951**, 73, 4330-4340.
- [156] R. Delgado, J. J. R. F. D. Silva, M. T. S. Amorim, M. F. Cabral, S. Chaves, J. Costa, *Anal. Chim. Acta* **1991**, 245, 271-282.
- [157] G. M. Sheldrick, *Program for Crystal Structure Solution*, SHELXS-97, Version 2, Göttingen, **1997**.
- [158] G. M. Sheldrick, *Program for Crystal Structure Refinement*, SHELXL-97, Version 2, Göttingen, **1997**.
- [159] *Diamond, Program for Crystal and Molecular Structure Visualisation*, Crystal Impact GbR, Version 3.2 f, Bonn, **2010**.